THE UNIVERSITY
of LIVERPOOL

Suspended Sediment Transport Modelling in Simple Tidal Conditions

Thesis submitted in accordance with the requirements of
The University of Liverpool for the degree of
Doctor in Philosophy

By

Stuart Gardiner

B.Sc, M.Sc

April 2004

Abstract

Sedimentation and scour can be problematic for a number of engineering and environmental projects. Suspended sediment transport rates are hugely influential in these processes and as such it is essential that both accurate and cost effective engineering models are available.

Although many such models exist in the literature, they can become expensive to use when applied to large areas or for long periods of time, since these situations often require a large number of computation points. A new approach to suspended sediment transport modelling has been shown by O'Connor et al (2001) to improve upon the efficiency of conventional methods. It is the aim of this thesis to present the details of this method and to perform a preliminary investigation into the viability of incorporating a parametric approach.

The parametric approach is based on a Fourier series approximation to 1DV suspended sediment transport rates in the presence of tidal currents, the coefficients of which are the subject of the parameterisation.

A conventional 2DV model for predicting tidal suspended sediment transport rates is used to assess the efficiency of both the parametric and non-parametric versions of the new method. Although only simplified situations are considered, it is shown that the new approach of O'Connor et al (2001) requires only 72% of the computation time used by the conventional approach whilst maintaining the same level of accuracy. The parametric approach improves on efficiency still further, requiring only 60% of the computation time; however, this is offset by an incurred error of the order 5%.

It is concluded therefore that both parameterised and non-parameterised versions of the new approach offer much more efficient methods for calculating tidal suspended sediment transport rates.

Acknowledgements

The author wishes to take this opportunity to thank his supervisor, Professor B.A. O'Connor, for his assistance during the course of this study. Thanks also to Dr. K.H.M. Ali for helping out since Professor O'Connor's retirement.

The author is also grateful to Dr J. Nicholson, Mr M. Li and Dr C.P Rose for their patience and advice throughout the project. Thanks also to the External and Internal Examiners, Professor D.M. McDowell and Eur.Ing. T.S. Hedges, for their helpful technical comments.

The author would also like to acknowledge the financial support of the EPSRC who were responsible for the funding of the project. Thanks also to Welfare and Advisory Services at The University of Liverpool for providing significant financial assistance towards the end of the project.

Thanks are also due to Neil, Chris, Mike, Ste, Greg, Ken and the rest of the Civil Engineering department for making my time at Liverpool University an enjoyable one. Thanks also to the chemistry mob and those at Carnatic halls of residence, in particular Professor D.J. Dutton for his assistance over the past few years.

Huge thanks must go to my family; Mum, Dad, Mike and the hounds. Their tireless support and encouragement has been inspiring since day one of the project.

Finally, the author would like to say a special thanks to the staff of The Birmingham Royal Orthopaedic Hospital, the Oncology staff at The Bristol Children's Hospital, the staff of the North Devon District Hospital, members of C.L.I.C and Dr R.G. Ford. Without the dedication and care of these people, it is likely that none of this would have been possible.

Table of Contents

List of Tables

List of Figures

List of Symbols

a	Reference level	(m)
	Chapter 3: Constant	
a_n	Mean Fourier coefficient	($kgm^{-2}s^{-1}$)
A	Chapter 4: Constant	
	Chapter 4: Algebraic expression for 1DV numerics	
A_*	Constant	
b	Constant	
b_n	Lag Fourier Coefficient	($kgm^{-2}s^{-1}$)
B	Algebraic expression for 1DV numerics	
c	Sediment concentration	(kgm^{-3})
c_1	Constant	
c_2	Constant	
c_3	Constant	
c_4	Constant	
c_d	Drag coefficient	(N/D)
C	Chezy coefficient	($m^{0.5}s^{-1}$)
C'	Grain related Chezy coefficient	($m^{0.5}s^{-1}$)
d_i	i-th percentile grain diameter	(m)
d_{50}	Median grain diameter	(m)
d_s	Van Rijn representative grain diameter	(m)
D_*	Van Rijn particle parameter	(N/D)
E_s	Non-dimensional reference concentration	(N/D)
f_d	Fluid drag on a particle	($kgms^{-2}$)
f_g	Gravitational force on a particle	($kgms^{-2}$)
Fr	Froude number	(N/D)
g	Acceleration due to gravity	(ms^{-2})
h	Water depth	(m)

h_m	Mean tidal water depth	(m)
i	Vertical step counter	
ii	Number of vertical computation points	
i_b	Proportion of ϕ-size grains in the bed	
k	Horizontal grid counter	
	Chapter 4: Kinetic energy	(m^2s^{-2})
kk	Number of horizontal grids	
k_s	Roughness height	(m)
k_s'	Grain-related roughness	(m)
k_s''	Form-related roughness	(m)
l	Characteristic eddy size	(m)
l_d	Length scale of turbulence	(m)
m	Exponent used in parameterisation of lag transport	(N/D)
n	Surface level indicator for vertical step counter	
	Chapter 4: Constant	
	Chapter 7: Constant	
p	Probability that the particles in a single layer of the bed are transported as bed-load	
q	Turbulent fluctuation	(ms^{-1})
$q_{s,c}$	Volumetric suspended load transport	(m^2s^{-1})
q_*	Dimensionless bed-load transport rate	(N/D)
r	Tidal range	(m)
	Chapter 4, Radius of a sphere	(cm)
r_x	Advection proportionality variable	(N/D)
R	Non-dimensional group	(N/D)
Re	Reynolds number	(N/D)
s	Relative density of sediment particles	(N/D)
t	Time	(s)
t_1, t_2	Times for which tidal velocity is equal	(s)
t_*	Tidal growth period	(s)
tp	Tidal period	(s)

T	Van Rijn's excess shear-stress parameter	(N/D)
	Chapter 7: Period of Fourier Series	(s)
	Chapter 7: Time	(s)
T_{diff}	Diffusive transport	($kgm^{-2}s^{-1}$)
T_{dm}	Suspended sediment transport due to depth-mean values	($kgm^{-2}s^{-1}$)
T_m	Suspended sediment transport at maximum tidal velocity	($kgm^{-2}s^{-1}$)
T_s	Suspended sediment transport	($kgm^{-2}s^{-1}$)
$\overline{T}_s$	Mean tidal suspended sediment transport	($kgm^{-2}s^{-1}$)
T_{disp}	Transport due to fluctuations from depth-mean values	($kgm^{-2}s^{-1}$)
T_*	Dimensionless transport rate	(N/D)
u	Longitudinal flow velocity	(ms^{-1})
up	Twice the duration of the flood stage of the tide	(s)
u_*	Longitudinal bed-shear velocity	(ms^{-1})
U_+	Dimensionless velocity group	(N/D)
v	Lateral flow velocity	(ms^{-1})
w	Vertical flow velocity	(ms^{-1})
w_f	Particle fall velocity	(ms^{-1})
$w_{f,m}$	Particle fall velocity in sediment laden flow	(ms^{-1})
x	Longitudinal co-ordinate	(m)
X	Grain size Reynolds Number	(N/D)
	Chapter 7: Tidal stage indicator	(N/D)
y	Lateral co-ordinate	(m)
Y	Grain Froude Number	(N/D)
	Chapter 7: Lag transport variable	($kgm^{-2}s^{-1}$)
z	Vertical co-ordinate	(m)
z_*	Transformed vertical co-ordinate	(N/D)
z_0	Zero velocity level	(m)
Z	Ratio of water depth to sediment grain size	(N/D)

	Chapter 4: Standardised Normal variable	
	Chapter 6: Non-dimensional group	(N/D)
Z_n	Non-dimensional group	(N/D)
α	Ratio of diffusive transport to actual transport	(N/D)
	Chapter 7: constant used in 1DV parameterisation	(N/D)
	Chapter 8: constant used in 1DV parameterisation for the 2DV situation	(N/D)
α_r	Tidal ratio	(N/D)
β	Ratio of sediment diffusion to fluid diffusion	(N/D)
β_i	Chapter 7: Constant used in 1DV parameterisation	(N/D)
	Chapter 8: constant used in 1DV parameterisation for the 2DV situation	(N/D)
ε	Dissipation of turbulent energy	(m^2s^{-3})
ε_c	Curvature component of the sediment diffusion coefficient	(m^2s^{-1})
ε_t	Tangential component of the sediment diffusion coefficient	(m^2s^{-1})
ε_f	Fluid diffusion/mixing coefficient	(m^2s^{-1})
ε_s	Sediment diffusion/mixing coefficient	(m^2s^{-1})
ϕ	Chapter 3: Tidal group	(N/D)
	Chapter 4: Damping of turbulence due to the presence of sediment	(N/D)
	Chapter 4: ϕ-scale for sediment grain size distribution	(ϕ)
γ	Bed form shape factor	(N/D)
γ_s	Gravitational factor	$(kgm^{-2}s^{-2})$
γ_0	Constant	
η	Vertical coordinate transformation variable	(N/D)
λ	Bed form wavelength	(m)
λ_b	Linear concentration at the bed	(kgm^{-3})

μ	Dynamic viscosity	($kgm^{-1}s^{-1}$)
	Chapter 4: Mean grain size	(m)
μ_ϕ	Mean grain size using the ϕ-scale	(m)
κ	Von Karman's constant (= 0.4)	(N/D)
ν	Kinematic viscosity	(m^2s^{-1})
ν_t	Eddy viscosity	(m^2s^{-1})
θ	Mobility/Shields parameter	(N/D)
ρ	Density of water	(kgm^{-3})
ρ_s	Density of sediment	(kgm^{-3})
σ	Standard deviation of sediment grain size distribution	(N/D)
σ_ϕ	Standard deviation of sediment grain size distribution using the ϕ-scale	(N/D)
σ_D	Constant	
τ	Shear stress	($kgm^{-1}s^{-2}$)
τ_b'	Effective/grain shear stress	($kgm^{-1}s^{-2}$)
τ_s^*	Dimensionless grain bed-shear stress	(N/D)
ω	Frequency of Fourier series	(s^{-1})
ξ	Vertical coordinate transformation variable	(N/D)
Δt	Size of time step for numerical solution	(s)
ΔT_s	Lag suspended sediment transport	(kgm^2s^{-1})
Δx	Size of Longitudinal step for numerical solution	(m)
Δz_*	Size of vertical step for numerical solution	(N/D)
Δ	Bed form height	(m)
	Chapter 7: submerged relative density of grains	(N/D)
Π_i	Non-dimensional group of parameters	(N/D)

Subscripts (Unless defined above):-

a	Value at reference level
b	Value at bed level
cr	Value at initiation of motion

d	Dune related
e	Equilibrium values
h	Value at water surface level
m	Value at maximum tidal velocity
r	Ripple related
s	Sand wave related
x	Value taken in the longitudinal direction
y	Value taken in the lateral direction
z	Value taken in the vertical direction

Superscripts (Unless defined above):-

$\bar{x}$	Time average value or depth-average value (see text)
x'	Fluctuation from time average value or deviation from depth-average value (see text)

Graphs:-

VR = $\sqrt{\rho\gamma_s d_{50}}$

Prefix P denotes the parameterised version of the variable.

Chapter 1

Introduction

1.1 General Background

Sediment transport has been important from an engineering perspective for centuries and perhaps never more so than now. The fear of global warming and the rising sea levels that it will bring suggest that the need for accurate and efficient models for predicting morphological changes will be very much in demand in the future.

Rising sea levels mean that flood prevention is an area of major concern. Coastlines are often protected by naturally occurring structures such as near-shore sandbars; these structures dissipate wave energy before they reach the shore. Monitoring of such structures is essential in preventing both flooding and coastal erosion.

Beach migration is another problem associated with coastal erosion. The changing environment not only affects wildlife, it can also have a devastating impact on the local economy. Many seaside communities rely on revenue gained from tourism and leisure industries based on the availability of sandy beaches or the presence of rare wildlife.

In the present climate of environmental awareness, engineering models are often used to assess the impact of structures on areas of special interest, such as tidal mud flats, which may be the home of rare flora and/or fauna. Such is the case when choosing the site for a new power station, which relies on a local source of water for cooling purposes. This also highlights a problem associated with

sediment carried in suspension since this can cause blockages and possible damage to the cooling system of the power station.

A more traditional use for sediment transport models is their application to the problem of dredging. Busy harbours and ports often require navigation channels to allow access to larger vessels. Such channels must be maintained by regular dredging, the frequency of which is dictated by the rate at which they refill. This in turn depends upon the sediment transport rate.

Harbours and ports also require sea defences such as sea walls. The use of such structures alters the flow field in the region; this in turn can alter sediment transport rates, which will then have an impact on the neighbouring coastline.

Sediment transport is also important for offshore structures such as oilrigs. Scouring can cause instability to the foundations of these offshore platforms and hence threaten the safety of workers.

Knowledge of sediment transport can also be economically beneficial. Consider the case of deep-sea pipelines; these need to be covered with enough sediment so that they are not snagged by deep-sea trawlers. Instead of spending much time, effort and money on engineering projects to cover the pipelines, it is often possible to allow nature to perform the task.

It can be seen that sediment transport plays an important role for a variety of applications. It is essential therefore, that there exist accurate and efficient engineering models capable of predicting sediment transport rates.

1.2 Scope of the Present Study

Sediment transport comprises two separate physical processes, bed-load sediment transport and suspended sediment transport. Bed-load is considered to represent those grains that maintain contact with the bed whilst moving with the flow. Suspended sediment transport concerns those grains that are carried up

from the bed and held in suspension whilst moving with the flow. This thesis concerns suspended sediment transport only.

There are many different models used to predict suspended sediment transport rates. The complex processes involved in predicting suspended sediment transport means that assumptions are often made to allow simplification. This obviously limits the area of application for such a model but is seen as a necessary evil until techniques improve sufficiently.

If large sediment grains are studied then it is often assumed that adjustments to local flow conditions are instantaneous and therefore negates the need for time dependence in the mathematical model. However, if the grain size is small, then time dependency must be retained.

If the area of study is horizontally uniform then the number of dimensions considered in the model is reduced. Only a one-dimensional vertical (1DV) model is required for this situation. However, if the uniformity is in one horizontal direction only, then it is necessary to consider a two-dimensional vertical (2DV) model. If there is no uniformity at all in the system then it is necessary to use a fully three-dimensional (3D) model.

It is also possible to use a depth-average model for some applications, this requires either a one-dimensional horizontal (1DH) model or a two-dimensional horizontal (2DH) model.

Unfortunately, models that are applied to a large area, or consider a long period of time, often require a large number of computation points. Such models are very expensive to run. Even with the rapid advancement of computer processor speeds, it is necessary to seek out new methods that reduce computational costs but retain accuracy.

This objective formed the main aim of the EPSRC funded COSMOD project (grant number: GR/L96967/01) involving the maritime research group at Liverpool University; headed by Professor O'Connor. The project evaluates a

new approach to suspended sediment transport modelling based on a Predictor-Corrector method derived by using a splitting technique on the original concentration equation.

The objective is now to further improve upon the COSMOD project by undertaking a preliminary study into the viability of a parametric approach. As such, the parameterisation considers the more simplistic 2DV situation for fine grains where only tidal currents are present, it being assumed that the effect of waves and the expansion to three-dimensions will form the basis for further research projects, should the initial parameterisation prove viable.

The aims of this thesis are therefore:-

1) To present the details of a new theory proposed by O'Connor (1999) for a Predictor-Corrector method for calculating tidal suspended sediment transport rates.
2) To produce a parameterised 1DV model that can be used in place of a numerical 1DV model in the new Corrector method.
3) To investigate the accuracy and computational cost of the new parameterised Corrector method.

1.3 Structure of the Thesis

Chapter 2 begins by deriving the three-dimensional advection-diffusion equation since this forms the basis for most suspended sediment transport models. The chapter then proceeds by describing the conventional approach to 2DV suspended sediment transport modelling. The full mathematical derivation of the new method proposed by O'Connor (1999) is then presented so that the theory of both methods can be compared.

A major problem associated with suspended sediment transport modelling is the prediction of bed form dimensions and hence roughness. The bed form dimensions can also be used to define the reference level for concentration

calculations and as such have a large influence in determining transport rates. Chapter 3 therefore presents a discussion on available bed form models and describes the model used in subsequent chapters.

Chapter 4 then describes the 1DV tidal suspended sediment transport model used in the new Corrector method. The chapter discusses all components of the model, presenting various methods found in the literature for the particle fall velocity, vertical diffusion coefficient and boundary conditions. The chapter also presents models for both the vertical and longitudinal flow velocities. The model includes a coordinate transform to increase the accuracy of the numerical solution, details of which are also given in chapter 4. The chapter concludes by performing tests to assess the validity of the proposed model.

The thesis then proceeds to chapter 5 where details are given of how the 1DV model is incorporated into the new Corrector method. Details are also given of the boundary conditions imposed on the model and the numerical schemes used to solve it.

A conventional 2DV suspended sediment transport model is then constructed in chapter 6 so that it can be used to test the relative accuracy and computational cost of the new Corrector method. The chapter includes details of the construction of the conventional model and also describes an analytical test used to prove the suitability of the model.

Chapter 7 then presents a parametric approach to 1DV suspended sediment transport modelling. The parameterisation is based on the coefficients of the Fourier series approximation to the 1DV tidal transport rates. The coefficients are parameterised by relating them to non-dimensional groups obtained from the set of characteristic parameters defining the system. The chapter gives details of the regression analysis used to fit the parameter groups and also tests the parameterised model against results from the numerical 1DV model.

Chapter 8 then proceeds to explain how the numerical 1DV model is replaced by the parameterised 1DV model in the new Corrector method. The chapter

describes how the parameterised 1DV model must first be modified for the 2DV system before it can be used in the new Corrector method. It is also shown that parameterisations for both the depth-average concentration and the transport due to fluctuations from depth-average values are required if the 1DV parameterised model is used in the new Corrector method. Details for both parameterisations are given in chapter 8.

Chapter 9 then discusses both the accuracy and computational cost of the new Corrector method and the parameterised Corrector method relative to the conventional 2DV model.

Chapter 9 also brings the thesis to its conclusion by providing recommendations for further research.

Chapter 2

Sediment Transport Theory

2.1 Introduction

The main aim of this thesis is to test the speed and accuracy of a parametric version of a new approach to suspended sediment transport modelling first proposed by O'Connor (1999). Before the parameterisation can be attempted, it is important to understand how the new approach differs from conventional models. The present chapter therefore presents the theoretical derivation of the new approach.

If the model is shown to be quicker for a 2DV situation, then it is assumed that the method must be quicker still for a full three-dimensional model; this would need further investigation but is not within the scope of this thesis. Therefore only the 2DV situation is described herein.

However, it is important to establish the fundamental equations upon which the theory is based, therefore the derivation of the 3D advection-diffusion equation for sediment concentration is given. This forms a foundation for the modelling theory presented later in the chapter.

After presenting a brief description of dimensional modelling, details are given of the conventional approach to 2DV sediment transport modelling.

Attention then turns to the derivation of the new approach. The new model is constructed from the three-dimensional advection-diffusion equation for sediment concentration. After first omitting the lateral dimension, the advection-diffusion equation is split into two equations so that the vertical and longitudinal

dimensions are separated. The vertical dimension is then coupled with a flow model to give 1DV transport rates at a series of spatial points. The longitudinal equation is then manipulated so that it becomes an equation with transport as the dependent variable rather than the sediment concentration. Essentially, the longitudinal equation is multiplied through by the depth-mean longitudinal flow velocity, then integrated over the water depth. The manipulated longitudinal equation is then used at all spatial points to correct the 1DV results for longitudinal effects.

Only the theory is presented in this chapter; chapter 5 describes the method of solution whilst chapter 6 compares the new Corrector method with a conventional 2DV model.

2.2 Derivation of the Advection-Diffusion Equation

A brief derivation of the three-dimensional advection-diffusion equation is given below; for more details see Ippen (1966), also McDowell and O'Connor (1977).

The derivation assumes that the substance concerned is a continuum, i.e. it has a continuous structure. This implies that molecular diffusion is negligible relative to the macroscopic effects of the turbulent mixing in the system. The derivation is then based on the principle of continuity applied to a fluid element when a mass is introduced into the system.

Consider a small fluid element with dimensions dx, dy and dz. Consider first the longitudinal dimension. A mass, with density ρ and concentration c, is introduced into the system where the longitudinal flow is assumed steady and has velocity u, as shown in figure 2.2.1.

The flux across the exit wall of the fluid element is given by applying Taylor's series expansion:-

$$flux\ out = \left(\rho cu + \frac{\partial}{\partial x}(\rho cu)dx \right) dydz \qquad (2.2.1)$$

The net flux, equal to the rate of change of mass, is then given by:-

$$\frac{\partial}{\partial t}(\rho c)dxdydz = \rho cudydz - \left(\rho cu + \frac{\partial}{\partial x}(\rho cu)dx\right)dydz$$

$$\frac{\partial}{\partial t}(\rho c)dxdydz = -\frac{\partial}{\partial x}(\rho cu)dydzdx \qquad (2.2.2)$$

Since the argument described above can be applied equally to the lateral (y) and vertical (z) directions, then the full three-dimensional net flux is given by:-

$$\frac{\partial}{\partial t}(\rho c)+\frac{\partial}{\partial x}(\rho cu)+\frac{\partial}{\partial y}(\rho c\mathrm{v})+\frac{\partial}{\partial z}(\rho c\mathrm{w})=0 \qquad (2.2.3)$$

where,

v -Lateral flow velocity

w -Vertical flow velocity

If the density gradients are neglected with respect to the concentration gradients then the density is eliminated from equation (2.2.3) to give:-

$$\frac{\partial c}{\partial t}+\frac{\partial}{\partial x}(cu)+\frac{\partial}{\partial y}(c\mathrm{v})+\frac{\partial}{\partial z}(c\mathrm{w})=0 \qquad (2.2.4)$$

The instantaneous concentration and fluid flow velocity can be expressed as a combination of their time-average (overbar) and fluctuating (prime) components, i.e.:-

$$c = \bar{c} + c'$$

$$u = \bar{u} + u'$$

$$\mathrm{v} = \bar{\mathrm{v}} + \mathrm{v}'$$

$$\mathrm{w} = \bar{\mathrm{w}} + \mathrm{w}'$$

Substitution of these expressions into equation (2.2.4) and then taking the time-average value of each term gives:-

$$\frac{\partial\overline{(\bar{c}+c')}}{\partial t}+\frac{\partial}{\partial x}\overline{[(\bar{c}+c')(\bar{u}+u')]}+\frac{\partial}{\partial y}\overline{[(\bar{c}+c')(\bar{v}+v')]}+\frac{\partial}{\partial z}\overline{[(\bar{c}+c')(\bar{w}+w')]}=0 \tag{2.2.5}$$

Equation (2.2.5) can be simplified by considering that the time-average of a fluctuating term is zero, also, the time-average of the product of a time-average and fluctuating term is zero. Thus, equation (2.2.5) becomes:-

$$\frac{\partial\bar{c}}{\partial t}+\frac{\partial}{\partial x}\bar{u}\,\bar{c}+\frac{\partial}{\partial y}\bar{v}\,\bar{c}+\frac{\partial}{\partial z}\bar{w}\,\bar{c}+\frac{\partial}{\partial x}\overline{u'c'}+\frac{\partial}{\partial y}\overline{v'c'}+\frac{\partial}{\partial z}\overline{w'c'}=0 \tag{2.2.6}$$

The product of fluctuating terms can be modelled using an analogy with Fick's law of diffusion. The mass flux is proportional to the mean concentration gradient such that:-

$$\overline{u'c'}=-\varepsilon_{f,x}\frac{\partial\bar{c}}{\partial x}$$

$$\overline{v'c'}=-\varepsilon_{f,y}\frac{\partial\bar{c}}{\partial y}$$

$$\overline{w'c'}=-\varepsilon_{f,z}\frac{\partial\bar{c}}{\partial z}$$

where,

$\varepsilon_{f,x}$ -Longitudinal fluid diffusion coefficient

$\varepsilon_{f,y}$ -Lateral fluid diffusion coefficient

$\varepsilon_{f,z}$ -Vertical fluid diffusion coefficient

McDowell and O'Connor (1977) suggest that if the mass concerned is sediment, then the diffusion model must be modified. This is achieved by using a sediment

diffusion coefficient, $\varepsilon_{s,i}$, which can be expressed in terms of the fluid diffusion coefficient via a proportionality coefficient, β. Details are given in chapter 4.

Thus, equation (2.2.6) becomes:-

$$\frac{\partial \bar{c}}{\partial t}+\frac{\partial}{\partial x}\bar{u}\,\bar{c}+\frac{\partial}{\partial y}\bar{\mathrm{v}}\,\bar{c}+\frac{\partial}{\partial z}\bar{\mathrm{w}}\,\bar{c}=\frac{\partial}{\partial x}\left(\varepsilon_{s,x}\frac{\partial \bar{c}}{\partial x}\right)+\frac{\partial}{\partial y}\left(\varepsilon_{s,y}\frac{\partial \bar{c}}{\partial y}\right)+\frac{\partial}{\partial z}\left(\varepsilon_{s,z}\frac{\partial \bar{c}}{\partial z}\right) \tag{2.2.7}$$

The sediment is assumed to travel with the same velocity as the flow in both the longitudinal and lateral directions. However, the particle velocity in the vertical direction must be modified for gravitational effects. This is achieved by incorporating the particle fall velocity, w_f. Hence, dropping the overbar notation, the three-dimensional advection-diffusion equation for sediment concentration can be written as:-

$$\frac{\partial c}{\partial t}+\frac{\partial}{\partial x}(cu)+\frac{\partial}{\partial y}(c\mathrm{v})+\frac{\partial}{\partial z}\left(c\{\mathrm{w}-w_f\}\right)=\frac{\partial}{\partial x}\left(\varepsilon_{s,x}\frac{\partial c}{\partial x}\right)+\frac{\partial}{\partial y}\left(\varepsilon_{s,y}\frac{\partial c}{\partial y}\right)+\frac{\partial}{\partial z}\left(\varepsilon_{s,z}\frac{\partial c}{\partial z}\right) \tag{2.2.8}$$

2.3 Conventional 2DV Model

2.3.1 Introduction

The three-dimensional advection-diffusion equation, equation (2.2.8), can be used in conjunction with a model for the velocity flow field to yield sediment transport rates for the full three-dimensional situation. However, it is not always necessary to consider all three dimensions. There are four main dimensional models for calculating the sediment concentration:-

3D -Fully three-dimensional

2DV -Vertical and longitudinal

2DH -Longitudinal and lateral

1DV -Vertical only

The number of dimensions required is dependent on the region of application. For example, if the region is considered horizontally uniform then only a 1DV model is required. However, if there is non-uniformity in one of the horizontal directions then a 2DV model must be used. There have been numerous models proposed for each of the dimensional categories; see Van Rijn (1993) for an extensive review.

2.3.2 Standard Solution Approach

If the lateral dimension of equation (2.2.8) is omitted, then the 2DV advection-diffusion equation for sediment concentration is given by:-

$$\frac{\partial c}{\partial t}+\frac{\partial}{\partial x}(cu)+\frac{\partial}{\partial z}(c\{w-w_f\})=\frac{\partial}{\partial x}\left(\varepsilon_{s,x}\frac{\partial c}{\partial x}\right)+\frac{\partial}{\partial z}\left(\varepsilon_{s,z}\frac{\partial c}{\partial z}\right) \qquad (2.3.1)$$

Following the operator splitting technique of O'Connor (1971), see also Verboom (1975), equation (2.3.1) can be replaced by two equations so that the dimensions are separated, see O'Connor and Nicholson (1997); i.e.:-

$$\frac{\partial c}{\partial t}+\frac{\partial}{\partial z}(w-w_f)c=\frac{\partial}{\partial z}\left(\varepsilon_{s,z}\frac{\partial c}{\partial z}\right) \qquad (2.3.2)$$

$$\frac{\partial c}{\partial t}+\frac{\partial uc}{\partial x}=\frac{\partial}{\partial x}\left(\varepsilon_{s,x}\frac{\partial c}{\partial x}\right) \qquad (2.3.3)$$

Equations (2.3.2) and (2.3.3) can now be solved by any appropriate numerical approach. The method of solution proceeds by first solving equation (2.3.2). This gives concentration values at an intermediate time step that are then used as the values for the previous time step in the solution of equation (2.3.3). This results in the solution of the 2DV sediment concentration field. Transport rates are then found by coupling the concentration field to the velocity flow field.

2.3.3 Boundary Conditions

Equations (2.3.2) and (2.3.3) must be solved subject to surface, bed and lateral boundary conditions.

Surface Boundary

A simple zero concentration condition is applied at the water surface for reasons explained later in section 2.4.2.

Bed Boundary

One ingredient common to all models for sediment transport is their need for bed form information. In order to calculate the transport value, the sediment concentration equation must be solved and then coupled to the flow field. The flow field requires roughness values for its calculation. These roughness values are dependent on the bed forms present for the given regime.

For those models involving the vertical dimension, the solution of the sediment concentration equation also requires a reference concentration, c_a; this in turn depends on the given reference level, a, from which the calculations begin. This reference level also depends upon the dimensions of the bed forms present for the given regime, as will be seen in chapter 4.

Lateral Boundary

The condition applied at each lateral boundary, both inflow and outflow, is based on the assumption that the region of interest is such that longitudinal effects are influential. It is assumed therefore that both the inflow and outflow boundaries are such that only 1DV effects are present.

2.4 New Corrector Method

2.4.1 Introduction

Although the conventional 2DV model can be used to predict suspended sediment transport rates, it can require vast amounts of computation time if the

model is applied over a large area with a large number of computational points. This often means that it is impractical to use in such conditions. The model described in the next section is designed so that the amount of computation is reduced and hence, crucially, the computational time is also reduced.

2.4.2 Theory

As with the conventional 2DV method, the advection-diffusion equation is split using the operator splitting technique to again give equation (2.3.2) and equation (2.3.3). However, instead of solving equation (2.3.2) and equation (2.3.3) in sequence, to give the concentration field, as in the conventional method, equation (2.3.2) is solved first but is then combined with the flow field to give 1DV suspended sediment transport values. The aim now is to manipulate equation (2.3.3) so that the 1DV transport values can be used instead of the concentration values.

Consider equation (2.3.3). Multiply through by the depth-mean longitudinal flow velocity and then integrate over the water column, i.e.:-

$$\underbrace{\int_a^h \bar{u}\frac{\partial c}{\partial t}dz}_{(i)} + \underbrace{\int_a^h \bar{u}\frac{\partial uc}{\partial x}dz}_{(ii)} = \underbrace{\int_a^h \bar{u}\frac{\partial}{\partial x}\left(\varepsilon_{s,x}\frac{\partial c}{\partial x}\right)dz}_{(iii)} \qquad (2.4.1)$$

Now consider just the first component of equation (2.4.1), i.e. part (i).

$$\int_a^h \bar{u}\frac{\partial c}{\partial t}dz = \bar{u}\int_a^h \frac{\partial c}{\partial t}dz \qquad (2.4.2)$$

Applying Leibnitz's Theorem to the right hand side of the above equation then gives:-

$$\int_a^h \bar{u}\frac{\partial c}{\partial t}dz = \bar{u}\left[\frac{\partial}{\partial t}\int_a^h c dz - \frac{\partial h}{\partial t}c_h + \frac{\partial a}{\partial t}c_a\right] \qquad (2.4.3)$$

If the sediment concentration at the surface, c_h, is assumed zero and the reference level is independent of time; equation (2.4.3) then becomes:-

$$\int_a^h \bar{u}\frac{\partial c}{\partial t}dz = \bar{u}\frac{\partial}{\partial t}\int_a^h cdz \qquad (2.4.4)$$

Now writing the sediment concentration in terms of its depth-mean and fluctuating/dispersive components:-

$$\int_a^h \bar{u}\frac{\partial c}{\partial t}dz = \bar{u}\frac{\partial}{\partial t}\int_a^h (\bar{c}+c')dz \qquad (2.4.5)$$

Since the integral of the fluctuating component of the sediment concentration is zero, then:-

$$\int_a^h \bar{u}\frac{\partial c}{\partial t}dz = \bar{u}\frac{\partial}{\partial t}\int_a^h \bar{c}dz$$

$$\int_a^h \bar{u}\frac{\partial c}{\partial t}dz = \bar{u}\frac{\partial}{\partial t}(h-a)\bar{c} \qquad (2.4.6)$$

[Aside: Consider the transport rate:-

$$T_{s,x} = \int_a^h ucdz$$

Split the velocity and sediment concentration into depth-mean and fluctuating components:-

$$T_{s,x} = \int_a^h \bar{u}\bar{c}dz + \int_a^h u'c'dz$$

$$T_{s,x} = (h-a)\overline{u}\,\overline{c} + T_{disp,x} \qquad (2.4.7)$$

where,

$T_{disp,x} = \int_a^h u'c'dz$ -Dispersive transport

Now differentiate with respect to time:-

$$\frac{\partial T_{s,x}}{\partial t} = \frac{\partial}{\partial t}(h-a)\overline{u}\,\overline{c} + \frac{\partial T_{disp,x}}{\partial t}$$

$$\frac{\partial T_{s,x}}{\partial t} = \overline{u}\frac{\partial}{\partial t}(h-a)\overline{c} + (h-a)\overline{c}\frac{\partial \overline{u}}{\partial t} + \frac{\partial T_{disp,x}}{\partial t}$$

This can now be used in equation (2.4.6)]

Equation (2.4.6) can now be expressed as:-

$$\overline{u}\frac{\partial}{\partial t}(h-a)\overline{c} = \frac{\partial T_{s,x}}{\partial t} - (h-a)\overline{c}\frac{\partial \overline{u}}{\partial t} - \frac{\partial T_{disp,x}}{\partial t} \qquad (2.4.8)$$

Now consider part (ii) of equation (2.4.1); applying Leibnitz's Theorem gives:-

$$\int_a^h \overline{u}\frac{\partial uc}{\partial x}dz = \overline{u}\left[\frac{\partial}{\partial x}\int_a^h ucdz - \frac{\partial h}{\partial x}c_h u_h + \frac{\partial a}{\partial x}c_a u_a\right] \qquad (2.4.9)$$

Again, the sediment concentration at the surface is assumed zero. The reference level is assumed constant in the longitudinal direction. Therefore equation (2.4.9) simplifies to:-

$$\int_a^h \overline{u}\frac{\partial uc}{\partial x}dz = \overline{u}\frac{\partial}{\partial x}\int_a^h ucdz \qquad (2.4.10)$$

It can be seen that the integral on the right hand side of equation (2.4.10) is simply that of transport; this leads to the following equation:-

$$\int_a^h \bar{u}\frac{\partial uc}{\partial x}dz = \bar{u}\frac{\partial T_{s,x}}{\partial x} \qquad (2.4.11)$$

Now consider the final part of equation (2.4.1), i.e. part (iii). Applying Leibnitz's Theorem:-

$$\int_a^h \bar{u}\frac{\partial}{\partial x}\left(\varepsilon_{s,x}\frac{\partial c}{\partial x}\right)dz = \bar{u}\left[\frac{\partial}{\partial x}\int_a^h \varepsilon_{s,x}\frac{\partial c}{\partial x}dz - \frac{\partial h}{\partial x}\left(\varepsilon_{s,x}\frac{\partial c}{\partial x}\right)_h + \frac{\partial a}{\partial x}\left(\varepsilon_{s,x}\frac{\partial c}{\partial x}\right)_a\right] \qquad (2.4.12)$$

The sediment diffusion/mixing coefficient in the longitudinal direction is zero at the surface since the sediment concentration is assumed zero at the surface. Equation (2.4.12) therefore simplifies to:-

$$\int_a^h \bar{u}\frac{\partial}{\partial x}\left(\varepsilon_{s,x}\frac{\partial c}{\partial x}\right)dz = \bar{u}\frac{\partial}{\partial x}\int_a^h \varepsilon_{s,x}\frac{\partial c}{\partial x}dz \qquad (2.4.13)$$

The integrand on the right hand side of equation (2.4.13) has the same dimensions as transport. Since it contains the longitudinal sediment diffusion/mixing coefficient, it can be thought of as diffusive transport.

$$\text{i.e.} \qquad T_{diff,x} = -\int_a^h \varepsilon_{s,x}\frac{\partial c}{\partial x}dz \qquad (2.4.14)$$

Thus, equation (2.4.13) can be written as:-

$$\int_a^h \bar{u}\frac{\partial}{\partial x}\left(\varepsilon_{s,x}\frac{\partial c}{\partial x}\right)dz = -\bar{u}\frac{\partial T_{diff,x}}{\partial x} \qquad (2.4.15)$$

Collecting the new expressions for parts (i) - (iii), i.e. equations (2.4.8), (2.4.11) & (2.4.14), equation (2.4.1) can be written as:-

$$\frac{\partial T_{s,x}}{\partial t}+\overline{u}\frac{\partial}{\partial x}\left(\{1+\alpha\}T_{s,x}\right)=\overline{c}(h-a)\frac{\partial \overline{u}}{\partial t}+\frac{\partial T_{disp,x}}{\partial t} \qquad (2.4.16)$$

where,

$$\alpha=\frac{T_{diff,x}}{T_{s,x}}$$

It can be seen that the equation is now written in terms of transport rather than concentration. Equation (2.4.16) defines the Corrector method.

As stated earlier, the new Corrector method has been designed so that the required amount of computation, and hence time, is likely to be reduced. However, testing is needed to determine the efficiency of the method.

Conventional 2DV models work by first calculating the concentration at each vertical point and then performing calculations over the entire spatial plane for each of these vertical points in turn. The new Corrector method however, uses the transport value instead of the concentration and therefore has only one calculation over the spatial plane. This is perhaps best explained by use of a diagram, see figures 2.4.1 and 2.4.2.

Figure 2.4.1 describes the sequence followed by the conventional 2DV method for calculating the concentration field. If the z-axis is divided into n equally spaced grid points, then equation (2.3.2) is solved so that the 1DV concentration is found at each vertical grid point $i=1...n$; shown by the left hand side of figure 2.4.1. The right hand side of figure 2.4.1 shows the solution of equation (2.3.3). The solution procedure starts at $i=1$ and solves equation (2.3.3) for all grid points on the plane shown in figure 2.4.1. Having now calculated the 2DV concentration values for $i=1$, the procedure then moves to $i=2$ where the method is repeated. This process is repeated for all vertical points $i=1...n$.

The procedure for the Corrector method begins with the same step as that used by the conventional method. The left hand side of figure 2.4.2 shows the solution of equation (2.3.2) to give 1DV concentration values. Instead of proceeding to the solution of equation (2.3.3), the Corrector method couples the 1DV concentration values with a flow velocity model so that 1DV transport values are obtained. The right hand side of figure 2.4.2 then shows the solution of equation (2.4.16). Since the transport involves the integral of the concentration values for $i = 1 \ldots n$, there is only one calculation on the right hand side of figure 2.4.2.

It can be seen therefore, that the Corrector method requires only one calculation to obtain the 2DV transport values from the 1DV values, whereas the conventional method requires $n-2$ calculations (since the concentration is assumed zero at the surface, i.e. $i = n$, and the reference concentration is given, i.e. $c = c_a$ at $i = 1$). This reduction in calculation steps is designed to reduce the amount of time required for computation.

2.5 Summary

The basic mathematical equations used for modelling suspended sediment transport have been presented. The conventional approach to 2DV sediment transport has been described and the equations given.

Since conventional 2DV models are expensive to run for large spatial domains, in terms of computer run time, a new method proposed by O'Connor (1999) has been described which has been designed to reduce the number of calculations required and hence reduce the computational time. This new method is constructed so that 1DV transport values are first calculated, then fed into an equation which corrects them for longitudinal effects.

It is therefore necessary to first construct a 1DV sediment transport model. As stated in section 2.3.3, the 1DV model requires bed form information; the next chapter therefore describes the bed form model used in the 1DV model.

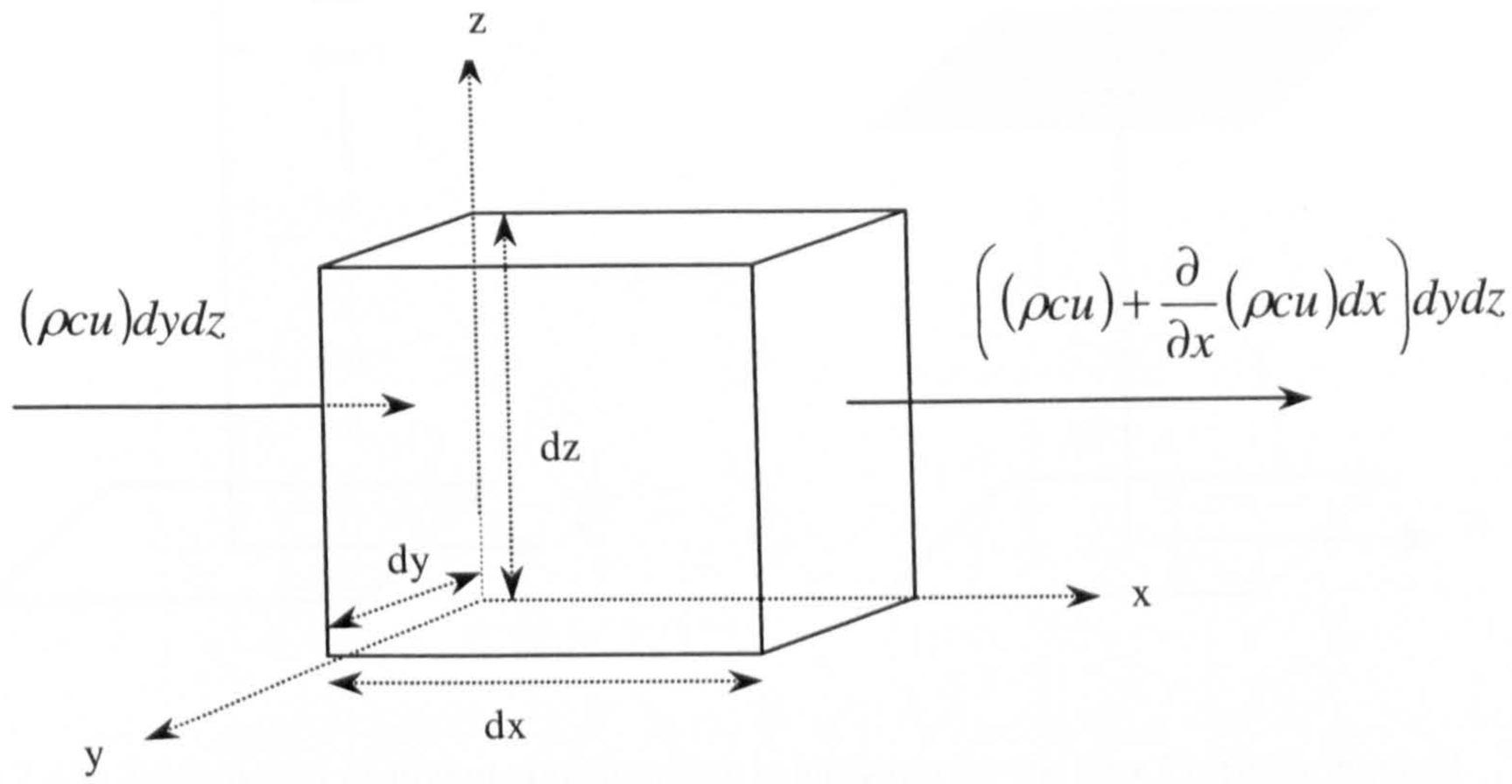

Figure 2.2.1: Conservation of mass for a small fluid element

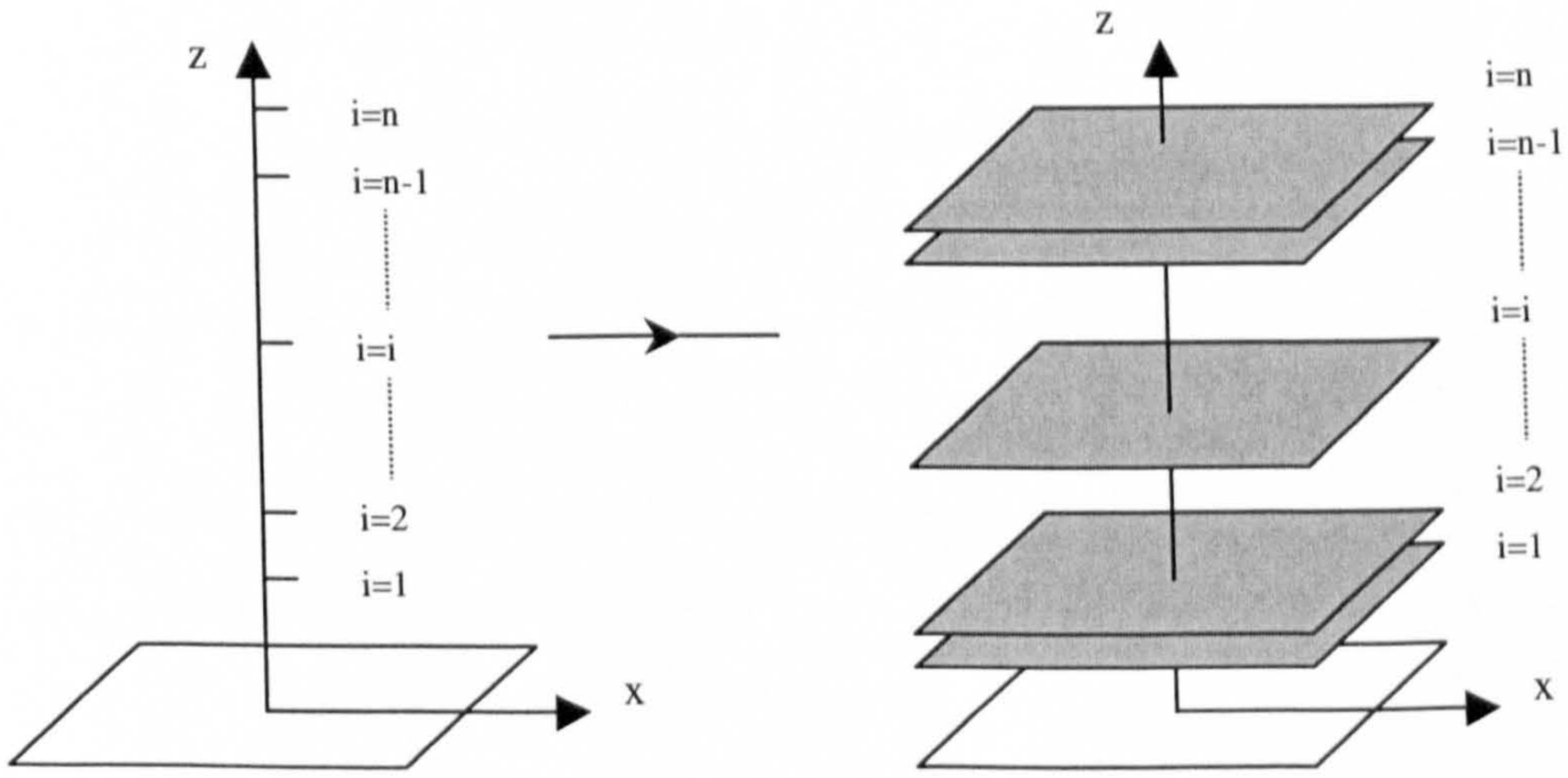

Figure 2.4.1: Sequence of sediment concentration calculation for the conventional 2DV method

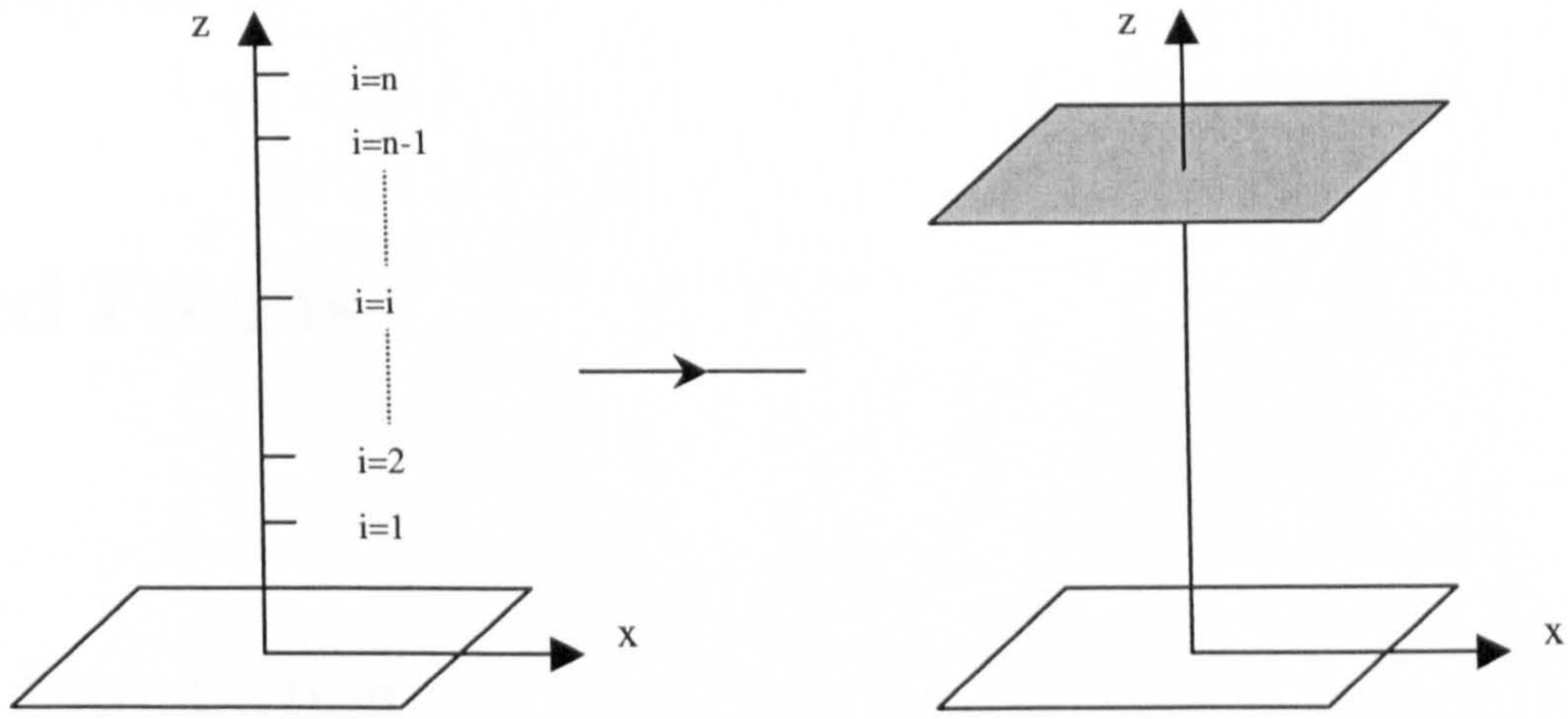

Figure 2.4.2: Sequence of sediment concentration calculation for the new Corrector method

Chapter 3

Bed Forms

3.1 Introduction

Bed forms are of paramount importance for sediment transport calculations since they greatly affect not only the roughness of the flow, but also influence the bed boundary condition, as stated in section 2.3.3.

There are numerous types of bed forms that can be present at any given time; it is therefore necessary to first define those that are important in sediment transport calculations; this is done in section 3.2.

Section 3.3 discusses the generation of each class of bed form. It is shown that the type of bed form present is dependent upon the local conditions, dictated, primarily, by longitudinal flow velocity and grain size. Using these values, it is possible to make distinctions between different bed form types. Section 3.4.1 describes methods found in the literature.

Having established which bed forms are present for the given conditions, it is possible to then find both the height and wavelength of the bed form. Section 3.4.2 describes methods for determining dimensions of bed forms in steady flow, which assume the bed forms are in equilibrium, whilst section 3.5 discusses the limiting effect on the bed form dimensions due to tidal flow.

The height of the bed form can then be used to determine the reference level for sediment transport calculations. Effective roughness values can also be determined form the bed form dimensions so that both initiation of motion and the longitudinal flow velocity profile can be determined.

3.2 Definitions

A search through the literature reveals many terms that are used to describe bed forms. In essence, a bed form is any sedimentary deviation from a flat bed. These deviations come in many different shapes and sizes, from very small mini-ripples to large sand waves.

The literature can be misleading however, since some authors use the term sand wave to describe any bed form, including ripples, mega-ripples, dunes, anti-dunes and larger structures. Yalin (1977) distinguishes between ripples, dunes and anti-dunes, stating that further classification causes confusion.

The term dune can be used to describe any feature larger than a ripple; some authors describe mega-ripples as dunes, only of different length and height characteristics. As a general rule, ripples are those bed forms whose length is very much smaller than the local water depth whereas dunes have a length scale of the same order or larger than the local water depth.

Bed forms may be described as either transverse or longitudinal. The former describes those bed forms whose crests lie perpendicular to the direction of the flow, whilst the latter describes those bed forms whose crests are parallel to the direction of the flow. Examples of longitudinal bed forms are notably ridges and ribbons. Transverse bed forms tend to be more diverse; classification often depends on individual authors. In general, transverse bed forms include ripples, mega-ripples, dunes, anti-dunes and sand waves.

Each of these classes can be separated into different sub-classes. Ripples can be classified as straight, sinuous, catenary, linguoid or lunate, depending on the shape of their crest line. See Simons and Richardson (1961) for examples of different types of bed forms.

3.3 Generation of Bed Forms

3.3.1 Ripples

It would appear to be widely accepted that ripples are only dependent on sediment properties and are totally independent of the hydraulic conditions. Yalin (1977) suggests that ripples are caused by a discontinuity in the bed's surface, this induces an instability, which grows into the form of ripples.

3.3.2 Dunes

Unlike ripples, dunes are strongly dependent on the hydraulic conditions. According to studies by Velikanov (1955,1958), the presence of dunes is due to turbulence producing eddies that are of the same order as the flow depth. Using these studies Yalin (1977) explains that a discontinuity in the bed can lead to the disturbance of the turbulence structure which then produces the dune.

3.3.3 Anti-dunes

Yalin (1977) argues that the mechanism behind the formation of anti-dunes is the existence of a wave on the free surface caused by an original discontinuity in the bed. This leads to a change in the water depth along the free surface wave. Since the laws of continuity must be obeyed, this implies that the flow under the trough of the wave must be faster than that under the crest, since the depth is greater. Since the flow is faster, there is more erosion on the bed at this point. This leads to the formation of an anti-dune that is in phase, if not with the same amplitude, as the free surface wave.

3.4 Bed Forms in Steady Flow

3.4.1 Classification

The first step towards the inclusion of a bed form model in sediment transport calculations is to determine which bed forms are present for the given conditions.

Fredsøe and Diegaard (1992) offer the following classification. At low flow velocities there is a small viscous sublayer above the bed. If this sublayer is larger than the diameter of the bed material then the hydraulic conditions are described as smooth, otherwise they are hydraulically rough. If the flow is hydraulically smooth at the moment when the critical velocity for motion of the sediment particles is reached then, according to Simons and Richardson (1961), ripples will be produced. If it is rough, then dunes will form.

Yalin (1977) gives another classification where the type of bed form present is dependent on the Froude number. It is suggested that if the Froude number is less than one, then both ripples and dunes will be present; if the Froude number is greater than one then only anti-dunes are present.

Yalin (1977) also discusses the possibility of different bed form classes existing together. It is argued that since the wavelength for dunes and anti-dunes are similar in magnitude, then it is not possible for them to coexist.

On the possibility of the co-existence of ripples and anti-dunes, Yalin states that the two have never been observed together. It is therefore assumed that the two bed form types do not coexist.

Ripples and dunes may coexist however, since there must be a transition period when ripples become dunes. After extensive experimental analysis, including data sets from numerous other authors, Yalin (1977) is able to define regions where each bed form can be said to exist. His classification is determined by the

value of the grain size Reynolds number, denoted by X, and the ratio of water depth to sediment diameter, denoted by Z.

i.e. $$X = \frac{u_* d_{50}}{\nu} \tag{3.4.1}$$

$$Z = \frac{h}{d_{50}} \tag{3.4.2}$$

where,

u_* -Bed shear velocity

d_{50} -Median grain diameter

ν -Kinematic viscosity

h -Water depth

The classification is given by:-

If $X \leq 8$ then ripples are present

If $8 \leq X \leq 24$ then $\begin{cases} \text{If } Z \text{ is large } (\geq 1000) \text{ then ripples and dunes are present} \\ \text{If } Z \text{ is small } (\leq 700) \text{ then ripples or dunes are present} \end{cases}$

Yalin admits that the limiting values of 1000 and 700 are only rough guides. It is also unclear as to which bed forms exist between these values.

Van Rijn (1993) offers an alternative classification based on field and flume data. A non-dimensional bed-shear stress, T, and a non-dimensional grain parameter, D_*, are used to classify bed forms rather than the Froude number. The bed form classification of Van Rijn (1993) is shown in table 3.4.1.

The symbols used in table 3.4.1 can be defined as follows,

$$T = \frac{\tau_b' - \tau_{b,cr}}{\tau_{b,cr}} \tag{3.4.3}$$

$$D_* = d_{50}\left[\frac{(s-1)g}{\nu^2}\right]^3 \tag{3.4.4}$$

τ_b' -Effective/grain-related bed-shear stress

$\tau_{b,cr}$ -Critical bed-shear stress

d_{50} -Median grain diameter

s -Relative density of the grain

g -Acceleration due to gravity

ν -Kinematic viscosity

At low values of both the dimensionless parameters T and D_*, only ripples are present. Van Rijn (1993) defines these ripples as mini-ripples; these are equivalent to the ripples described by Yalin (1977). As the bed-shear stress parameter increases these ripples become ripples defined as mega-ripples; their dimensions are slightly larger than those of mini-ripples. Unlike mini-ripples, which are a function of grain size only, mega-ripples are affected by the properties of the flow.

During this period dunes also start to form. Dunes reach their maximum height relatively quickly then start to decay until they completely disappear in the transitional stage at which point sand waves take over as the dominating bed form.

It can be seen that as the grain size increases then, even at small values of the bed-shear stress parameter, there are no ripples present

3.4.2 Dimensions

There are numerous different methods found in the literature for calculating bed form height and length. The models of Tsubaki and Shinohara (1954), Gill (1971), Yalin (1977), Ranga Raju and Soni (1976), Allen (1968) and Fredsøe (1982) are reviewed by Van Rijn (1993) who also describes a new bed form

model. The new model presents formulae for each of the bed form classes; namely ripples, mega-ripples, dunes and sand waves.

The dimensions of ripples are given by the formula used by Yalin (1985):-

$$\Delta_r = 50 - 200 d_{50} \tag{3.4.5}$$

$$\lambda_r = 500 - 1000 d_{50} \tag{3.4.6}$$

where,

Δ_r -Ripple height

λ_r -Ripple wavelength

This would seem to be roughly equivalent to the model of Yalin (1977) which gives the ripple dimensions as:-

$$\Delta_r = 750 d_{50} \tag{3.4.7}$$

$$\lambda_r = 1000 d_{50} \tag{3.4.8}$$

Van Rijn (1993) gives the following formulae for determining the dimensions of mega-ripples:-

$$\frac{\Delta_r}{h} = 0.02\left(1 - e^{-0.1T}\right)(10 - T) \tag{3.4.9}$$

$$\lambda_r = 0.5h \tag{3.4.10}$$

The dimensions of dunes are given by:-

$$\frac{\Delta_d}{h} = 0.11\left(\frac{d_{50}}{h}\right)^{0.3}\left(1 - e^{-0.5T}\right)(25 - T) \tag{3.4.11}$$

$$\lambda_d = 7.3h \tag{3.4.12}$$

where,

Δ_d -Dune height

λ_d -Dune wavelength

Finally, the dimensions of sand waves are given by:-

$$\frac{\Delta_s}{h} = 0.15\left(1 - e^{-0.5(T-15)}\right)\left(1 - Fr^2\right) \quad (3.4.13)$$

$$\lambda_s = 10h \quad (3.4.14)$$

where,

Δ_s -Sand wave height

λ_s -Sand wave wavelength

Fr -Froude number

Van Rijn (1993) compares the new model with those listed at the beginning of the section. It is shown that the models of Ranga Raju and Soni (1976), Tsubaki and Shinohara (1959) and Fredsøe (1980) all show an increasing bed form height as the mean velocity is increased whereas the model of Van Rijn shows a more realistic decreasing trend.

Van Rijn (1993) also compares equations (3.4.9) and (3.4.11) with field data. It is concluded that the formulae given are tentative at best. This would suggest that more work is needed in this area.

3.5 Tidal Bed Forms

It is widely recognised that although large bed forms are present in tidal flows, they are generally smaller than their steady flow counterparts. The problem is primarily with tidal dunes since ripples adjust instantaneously to a change in flow, as shown by Terwindt (1971). Due to the reversing nature of tidal flows, bed forms do not reach their equilibrium (steady flow) dimensions. The flood

and ebb of the tide allows not only for growth of the bed form but also erosion; this must be taken into account when including a bed form model for tidal systems.

O'Connor and Duckett (1989) present a model that accounts for tidal flow in a bed form prediction model for dunes. Using the suggestion of Jain and Kennedy (1971) that sand waves approach their equilibrium wavelength exponentially, the following model for the bed form wavelength is presented.

$$\frac{\lambda}{\lambda_e} = 1 - \exp(-a\phi) \qquad (3.5.1)$$

where,

λ -Bed form wavelength

λ_e -Equilibrium/steady flow bed form wavelength

$$\phi = \frac{\overline{u}_m t_*}{h_m}$$

$$a = 10^b$$

$$b = 1.29 \log_{10}\left(\frac{X^2}{Y}\right) - 7.13$$

$\overline{u}_m$ -Maximum tidal depth-average velocity

t_* -Tidal growth period

h_m -Tidal mean water depth

$X = \frac{u_* d_{50}}{\nu}$ -Grain Reynolds Number

$Y = \frac{u_*^2}{sgd_{50}}$ -Grain Froude Number

u_* -Bed-shear velocity

d_{50} -Median grain diameter

g -Acceleration due to gravity

s -Submerged relative density of grains

ν -Viscosity

The expression for the parameter a was obtained by fitting equation (3.5.1) to field data, see Duckett (1984).

The tidal growth period is defined as the time during a flood period for which the critical velocity for initiation of motion is exceeded, as shown in figure 3.5.1.

This is expressed mathematically by the formula given below:-

$$t_* = \frac{tp}{2} - 2t_{cr} \qquad (3.5.2)$$

where,

$$t_{cr} = \frac{tp}{2\pi}\sin^{-1}\left(\frac{\overline{u}_{cr}}{\overline{u}_m}\right)$$

$\overline{u}_{cr}$ -Longitudinal tidal depth-average flow velocity at initiation of motion

$\overline{u}_m$ -Maximum tidal longitudinal flow velocity

tp -Tidal period

O'Connor and Duckett (1989) suggest that the wavelength of the bed form is dictated by the properties of the Spring tide since this has the largest growth period. The height is then dependent on preceding tides in the Spring-Neap cycle. Equation (3.5.1) should therefore use values from the Spring tide to obtain bed form dimensions.

The model is tested against data from two field sites and is shown to produce reasonable predictions for tidal bed form dimensions.

3.6 Effective Roughness

3.6.1 Introduction

By using the bed form dimensions, it is possible to determine the effective roughness, k_s.

The effective roughness consists of two components, the first is the contribution made by the grain roughness generated by skin friction; the second is the contribution made by the form roughness generated by the presence of bed forms. The form roughness is the combined effect of the roughness due to the different types of bed forms present, which, in turn, depends upon the dimensions of each bed form. The effective roughness is therefore determined by:-

$$k_s = k_s' + k_s'' \qquad (3.6.1)$$

where,

k_s -Effective roughness height

k_s' -Grain-related effective roughness

k_s'' -Form-related effective roughness

Once calculated, the effective roughness is used to predict bed-shear velocity, which is then used to determine the initiation of motion and the longitudinal flow velocity profile.

3.6.2 Grain Roughness

Van Rijn (1993) presents a review of existing techniques incorporating the work of Lyn (1991), Aguirre-Pe and Fuentes (1990), Kamphuis (1974), Gladki (1975), Hey (1979), Mahmood (1971), Wilson (1988,1989), Einstein and Chien (1955) and Winterwerp et al (1990). All models are based on a multiple of a grain percentile representing the top layer of the bed, either d_{84} or d_{90}.

Based on the work by those authors listed above and also the data of Van Rijn (1982), Van Rijn (1993) proposes the following formulae to determine grain roughness:-

$$k_s' = \begin{cases} 3d_{90} & ;\theta < 1 \\ 3\theta d_{90} & ;\theta \geq 1 \end{cases} \qquad (3.6.2)$$

where,

k_s' -Grain-related effective roughness

$\theta = \dfrac{u_*^2}{((s-1)gd_{50})}$ -Mobility/Shields parameter

$u_* = \dfrac{\sqrt{g}}{C}\bar{u}$ -Bed-shear velocity

$C = 18\log\left(\dfrac{12h}{k_s}\right)$ -Chezy Coefficient

$\bar{u}$ -Depth-average longitudinal flow velocity

g -Acceleration due to gravity

s -Relative density of the sediment particles

d_{50} -Median grain diameter

h -Water depth

k_s -Effective roughness height

It can be seen that the grain roughness is a function of the overall roughness, which in turn is a function of the grain roughness. It therefore requires an iterative solution process where the initial guess is taken as $k_s' = 3d_{90}$.

3.6.3 Form Roughness

According to Van Rijn (1993), the form-related roughness can be expressed in terms of bed height, steepness and shape. It is also proposed that the overall form roughness is simply a summation of effects due to the different bed form types present, i.e.:-

$$k_s'' = k_{s,r}'' + k_{s,d}'' + k_{s,s}'' \qquad (3.6.3)$$

where,

$k''_{s,r}$ -Form-related roughness due to ripples

$k''_{s,d}$ -Form-related roughness due to dunes

$k''_{s,s}$ -Form-related roughness due to sand waves

Ripples

Based on analysis of field data, Van Rijn (1993) proposes the following formula to calculate the form-related roughness due to ripples:-

$$k''_{s,r} = 20\gamma_r \Delta_r \left(\frac{\Delta_r}{\lambda_r}\right) \qquad (3.6.4)$$

where,

$k''_{s,r}$ -Form-related roughness due to ripples

γ_r -Ripple shape factor ($=1$ for ripples only, $=0.7$ for ripples superimposed on dunes)

Δ_r -Ripple height

λ_r -Ripple wavelength

It is assumed that equation (3.6.4) is valid for both ripples and mega-ripples.

Dunes

Van Rijn (1993) also proposes the following formula for the prediction of form-related roughness due to dunes:-

$$k''_{s,d} = 1.1\gamma_d \Delta_d \left(1 - e^{-25\left(\frac{\Delta_d}{\lambda_d}\right)}\right) \qquad (3.6.5)$$

where,

$k''_{s,d}$ -Form-related roughness due to dunes

$\gamma_d = 0.7$ -Dune shape factor

Δ_d -Dune height

λ_d -Dune wavelength

Sand waves

Van Rijn (1993) argues that since the length of a sand wave is much greater that its height, then the slope is relatively mild and hence will not invoke flow separation. It is concluded therefore that there is no contribution to the roughness by a sand wave, i.e.:-

$$k''_{s,s} = 0 \qquad (3.6.6)$$

3.6.4 Conclusion

Van Rijn (1993) uses the method described above to predict Chezy values based on dune dimensions. The results are then compared against the models of Engelund and Hansen (1967) and White et al (1979) for numerous field and flume data. It should be noted that the dune shape factor is set as unity for these tests. It is shown that the model of Engelund and Hansen produces better results for the flume tests whereas the model of Van Rijn is best for field data.

It is concluded therefore, that the model of Van Rijn will be used herein to calculate the effective roughness.

3.7 Summary

By using the classification of bed forms as used by Van Rijn (1993), shown in table 3.4.1, it is possible to determine which bed forms are present for any given situation.

Equations (3.4.7) - (3.4.14) are then used to calculate the height and wavelength of the bed form. However, these are steady-state dimensions that must then be modified via equation (3.5.1) to account for the limiting action of the flood and ebb of the tide.

Once the height of the bed form is calculated, it is then possible to determine a reference level for the sediment concentration calculations, as suggested in section 2.3.3.

The effective roughness can then be calculated from the bed form dimensions via equation (3.6.1), thus allowing the longitudinal flow velocity profile to be determined. The effective roughness also enables calculations of the bed-shear velocity, and hence initiation of motion.

The details of both the longitudinal flow velocity and the reference level for sediment concentration calculations are discussed in more detail in the next chapter, which describes the 1DV tidal sediment transport model.

Transport regime		Particle size	
		$1 \le D_* \le 10$	$D_* > 10$
Lower	$0 \le T \le 3$	Mini-ripples	Dunes
	$3 < T \le 10$	Mega-ripples and dunes	Dunes
	$10 < T \le 15$	Dunes	Dunes
Transition	$15 < T < 25$	Washed-out dunes, sand waves	
Upper	$T \ge 25$, $Fr < 0.8$	(symmetrical) sand waves	
	$T \ge 25$, $Fr \ge 0.8$	Plane bed and/or anti-dunes	

Table 3.4.1: Classification of bed forms according to Van Rijn (1993)

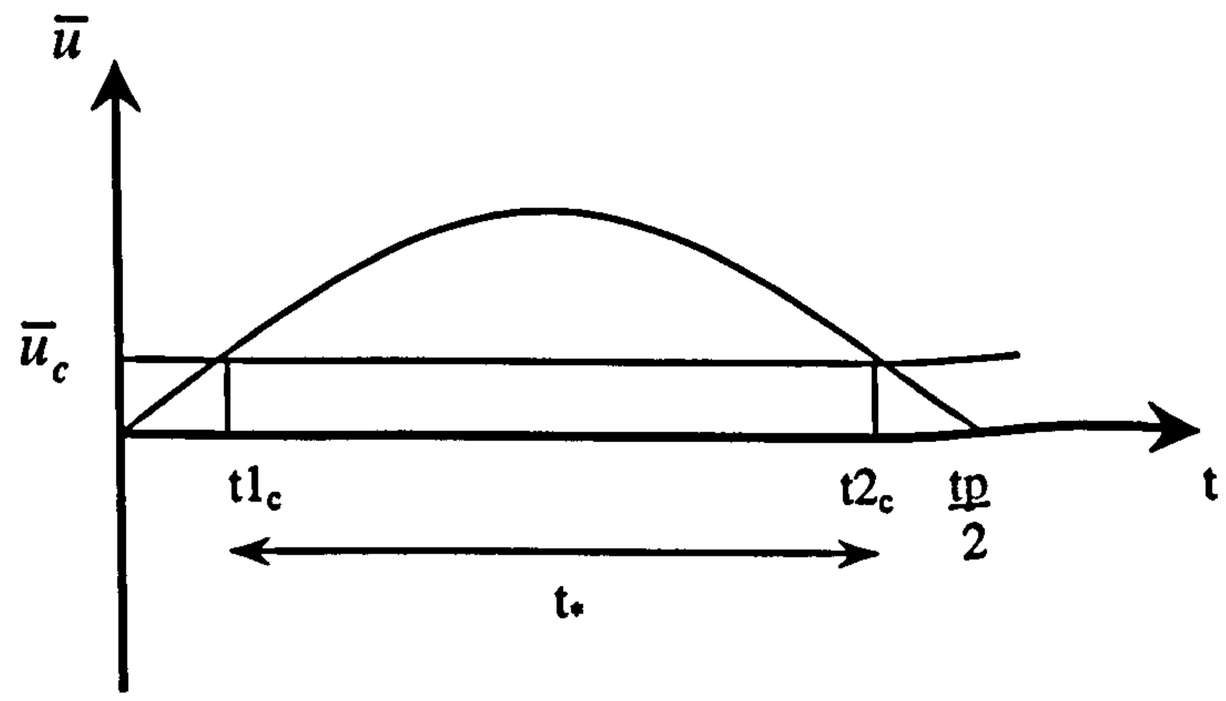

Figure 3.5.1: Growth period on the flood stage of the tide

Chapter 4

1DV Transport Model

4.1 Introduction

Chapter 2 described how the new Corrector method corrects 1DV sediment transport values for longitudinal effects. Although this should reduce computational time, the method can be improved still further by using a parameterised version of the 1DV sediment transport model. It can be seen that the 1DV model is essential therefore in achieving the aim of the project. The present chapter gives details of the proposed 1DV suspended sediment transport model.

The model uses bed form information, given by the model described in the previous chapter, to determine concentration and velocity profiles.

The concentration profile is found by solving the vertical split of the three-dimensional advection-diffusion equation. This is done via finite difference techniques once expressions have been determined for the sediment fall velocity, sediment diffusion coefficient and vertical flow velocity. The numerical approximation also requires boundary conditions before it can be solved, details of which are also presented.

The longitudinal flow velocity profile is then described by a logarithmic profile that can easily be solved analytically.

Tidal conditions are approximated by varying both the water depth and the depth-averaged longitudinal flow velocity with time.

The whole system is then transformed in the vertical coordinate so that more computational points will be in the near-bed region thus improving the accuracy of the numerical schemes.

Transport rates are then calculated by using either the method of grain size fractions or by the use of a representative grain size. The actual transport integral is approximated by Simpson's rule for numerical quadrature.

The 1DV sediment transport model is then compared to that of O'Connor and Nicholson (1997) for three data sets.

4.2 Sediment Concentration Model

As described in chapter 2, the sediment concentration can be modelled by the 3-D advection-diffusion equation. Considering only the vertical and longitudinal dimensions and applying the operator splitting technique given by O'Connor (1971), the 1DV concentration equation is given by:-

$$\frac{\partial c}{\partial t}+\frac{\partial}{\partial z}(\mathrm{w}-w_f)c=\frac{\partial}{\partial z}\left(\varepsilon_{s,z}\frac{\partial c}{\partial z}\right) \qquad (2.3.2)$$

If the vertical flow gradient is assumed negligible, i.e. slowly changing tidal velocity, and the particle fall velocity is independent of depth, then equation (2.3.2) reduces to:-

$$\frac{\partial c}{\partial t}=\varepsilon_{s,z}\frac{\partial^2 c}{\partial z^2}+\left(\frac{\partial \varepsilon_{s,z}}{\partial z}-\mathrm{w}+w_f\right)\frac{\partial c}{\partial z} \qquad (4.2.1)$$

4.2.1 Boundary Conditions

Two boundary conditions are necessary for the 1DV model, one prescribed at the water surface and one at a reference level located near the bed.

Surface Boundary

A simple zero concentration condition is preferred at the water surface; this then allows the simplifications to Leibnitz's theorem used in the derivation of the new Corrector method as described in section 2.4. This is also consistent with the parabolic sediment diffusion coefficient described later in section 4.4.

Bed Boundary

The condition imposed on the bed boundary is more complex than that at the water surface. The first step is to establish the location of the bed boundary. This is defined as the reference level, from which sediment concentration calculations begin. Determining this reference level requires knowledge of the bed forms present, details are given later in section 4.6.2.

Once the reference level has been determined then a reference concentration is imposed which assumes local equilibrium conditions. The choice of condition at the reference level is discussed in detail within section 4.6.3.

4.3 Particle Fall Velocity

4.3.1 Introduction

When deriving the three-dimensional advection-diffusion equation in chapter 2, it was assumed that the sediment traveled with the same velocity as that of the fluid in the horizontal plane. It was also stated that this is not the case for the vertical dimension. A sediment grain carried into suspension feels the effect of gravitational forces that tend to bring the grain back to the bed. Other forces, such as drag, will oppose this motion. These effects are combined to describe the settling velocity of the grain, also known as the fall velocity.

4.3.2 Spherical Grains

A first principles approach is used by Van Rijn (1993) to determine an expression for the fall velocity of a spherical particle in a still fluid. Consider the fluid drag as given by Stokes Law, f_d, and the gravitational force, f_g, on the particle:-

$$f_d = \frac{1}{2}\left(c_d \rho w_f^2\right)\frac{1}{4}\left(\pi d^2\right)$$

$$f_g = \frac{1}{6}(\rho_s - \rho)gd^3$$

where,

w_f -Fall velocity

c_d -Drag coefficient

ρ -Density of the fluid

ρ_s -Density of the sediment

d -Diameter of the grain

g -Acceleration due to gravity

Equating gives the following expression for the particle fall velocity:-

$$w_f = \left[\frac{4(s-1)gd}{3c_d}\right]^{0.5} \qquad (4.3.1)$$

where,

$$s = \frac{\rho_s}{\rho}$$

Van Rijn (1993) suggests the following relationship between the drag coefficient and the Reynolds number, Re:-

$$c_d = \frac{24}{\mathrm{Re}}$$

where,

$$\mathrm{Re} = \frac{w_f d}{\nu}$$

ν -Viscosity of the fluid

Equation (4.3.1) then becomes:-

$$w_f = \frac{(s-1)gd^2}{18\nu}\text{; Stokes region (Re<1)} \qquad (4.3.2)$$

Gibbs et al (1971) describe extensive experimental analysis of the settling velocity for glass spheres of differing densities. The effects of temperature, salinity and sphere diameter on the settling velocity are considered. The results of these experiments lead to the construction of an empirical formula for the settling velocity of a sphere in water, given below.

$$w_f = \frac{-3\nu + \sqrt{9\nu^2 + gr^2\rho(\rho_s - \rho)(0.015476 + 0.1984r)}}{\rho(0..011607 + 0.14881r)} \qquad (4.3.3)$$

where,

r -Radius of the sphere

N.B: all units are in centimetres, grams and seconds.

4.3.3 Non-spherical Grains

Whilst the spherical approximation for the grain shape is adequate for small grains, it becomes less accurate for larger grains whose shape becomes more irregular.

Van Rijn (1993) presents the following formula for non-spherical particles:-

$$w_f = \begin{cases} \dfrac{(s-1)gd^2}{18\nu} & ; 1 < d \le 100\mu m \\ \dfrac{10\nu}{d}\left[\left(1 + \dfrac{0.01(s-1)gd^3}{\nu^2}\right)^{0.5} - 1\right] & ; 100 < d < 1000\mu m \\ 1.1[(s-1)gd]^{0.5} & ; d \ge 1000\mu m \end{cases} \qquad (4.3.4)$$

The models of Gibbs (1971) and Van Rijn (1993) are compared by Soulsby (1994) using 115 measurements of fall velocity for both natural sands and irregular shaped lightweight grains. The comparison also includes a model proposed by Hallermeier (1981) and a new empirical model determined by considering both viscous and bluff body drag. The new model proposed by Soulsby (1994) is shown below.

$$w_f = \frac{\nu}{d_{50}}\left[\left(10.36^2 + 1.049 D_*^3\right)^{0.5} - 10.36\right] \qquad (4.3.5)$$

where,

$$D_* = \left(\frac{\{s-1\}g}{\nu^2}\right)^{1/3} d_{50}$$

The models of Van Rijn and Hallermeier are shown to give good agreement with the test data. However, the model of Soulsby is shown to give the best agreement.

4.3.4 Hindered Settling

When considering flows containing high concentrations of sediment, the interaction between the sediment grains should be included in the particle fall velocity.

Due to the high concentration there will be many grains occupying a small space, each of which creates a drag. Since the grains are so close to each other, the drag caused by one grain will be felt by all nearby grains. This will lead to each grain experiencing an increase in drag that will slow its motion; this is known as hindered settling.

Soulsby (1994) accounts for hindered settling by modifying the existing model for sediment fall velocity, i.e.:-

$$w_f = \frac{\nu}{d_{50}}\left[\left(10.36^2 + 1.049(1-c)^{4.7} D_*^3\right)^{0.5} - 10.36\right] \qquad (4.3.6)$$

Van Rijn (1993) considers the model for hindered settling suggested by Richardson and Zaki (1954),

$$w_{f,m} = (1-c)^{\gamma} w_f \qquad (4.3.7)$$

where,

$w_{f,m}$ -Grain fall velocity in a suspension

w_f -Grain fall velocity in a clear fluid

c -Volumetric concentration

γ -Coefficient

For grains in the range 50 - 500 μm, Van Rijn uses $\gamma = 4$.

However, when Van Rijn compares the model with that of Oliver (1961), he concludes that the model of Oliver shows better agreement with experimental data than the model of Richardson and Zaki over the full test range. The model of Oliver is shown below:-

$$w_{f,m} = (1-2.15)\left(1-0.75c^{0.33}\right)w_f \qquad (4.3.8)$$

4.3.5 Conclusion

For the sake of simplicity, the effect of hindered settling is omitted from the 1DV model. However, any future work should look in more detail at the significance of the effect on the sediment concentration.

Although fine sediments are considered in the present project, the results of Soulsby (1994) suggest that the spherical approximation for the particle shape may be too simplistic. It is concluded therefore that the fall velocity of the sediment particles is given by equation (4.3.5).

4.4 Vertical Diffusion Modelling

4.4.1 Introduction

Sediment diffusion is often modelled by relating it to the fluid diffusion, which describes the turbulence of the flow field. This in turn can be modelled by a number of different methods, the most common of which are the models based on kinetic energy and those that use a Fickian diffusion analogy. This section gives a brief description of the aforementioned methods so that an appropriate model for the vertical sediment diffusion coefficient may be determined. For a more detailed discussion, see Fredsøe and Deigaard (1992).

4.4.2 Kinetic Energy Models

k-Models

The one equation approach, known as the k-model involves the use of a transport equation for the kinetic energy, k, of the system. The kinetic energy is defined to be,

$$k=\frac{1}{2}\left(\overline{u'}^2+\overline{v'}^2+\overline{w'}^2\right) \tag{4.4.1}$$

where $\overline{u'}$, $\overline{v'}$ and $\overline{w'}$ are the time-averaged velocity fluctuations in the x,y and z directions respectively.

The transport of the kinetic energy is defined by,

$$\frac{\partial k}{\partial t}=\underbrace{\frac{\partial}{\partial z}\left(\nu_t\frac{\partial k}{\partial t}\right)}_{diffusion}+\underbrace{\nu_t\left(\frac{\partial u}{\partial t}\right)^2}_{production}-\underbrace{c_2\frac{k^{3/2}}{l_d}}_{dissipation} \tag{4.4.2}$$

where,

$c_2 \approx 0.08$

$l_d = \kappa c_2^{0.25} z \approx 0.213z$ (length scale of turbulence)

ν_t -Eddy viscosity

The Kolmogorov-Prandtl model is used to represent the eddy viscosity,

$$\nu_t = l_d \sqrt{k} \tag{4.4.3}$$

The boundary conditions for the system are given as:-

$$u\left(\frac{k_n}{30}, t\right) = 0 \quad ; \quad \frac{\partial u}{\partial z} \to 0 \text{ as } z \to \infty$$

$$k = \frac{1}{\sqrt{c_1}} \nu_t \frac{\partial u}{\partial z} \quad ; \quad \text{for } z = \frac{k_n}{30} \quad \text{(i.e. local equilibrium)}$$

$$\frac{\partial k}{\partial z} = 0 \quad ; \quad \text{as } z \to \infty \quad \text{(i.e. no flux at the upper boundary)}$$

k-ε Models

The two equation k-ε approach is an extension of the one equation k-model; the mixing length is now considered to be a function of both space and time. To ensure closure for this model it is necessary to include an equation that describes the transport of the dissipation, ε. Thus the k model described previously is used in conjunction with the following equation for the dissipation,

$$\frac{\partial \varepsilon}{\partial t} = \frac{\partial}{\partial z}\left(\frac{\nu_t}{\sigma_D} \frac{\partial \varepsilon}{\partial z}\right) + c_3 \varepsilon \frac{\nu_t}{k} \left(\frac{\partial u}{\partial z}\right)^2 - c_4 \frac{\varepsilon^2}{k} \tag{4.4.4}$$

where σ_D, c_3, c_4, are experimentally obtained constants.

The boundary conditions are given as:-

$$\varepsilon = c_2^{3/4} \frac{k^{3/2}}{\kappa z} \quad \text{for} \quad z \to \frac{k_n}{30}$$

$$\frac{\partial \varepsilon}{\partial z} = 0 \quad \text{for} \quad z \to \infty$$

4.4.3 Fickian Diffusion

It is also possible to model the time-averaged fluid turbulent fluctuation terms by using Fick's Law of diffusion. Simply stated, Fick's Law reads,

Flux of solute mass in a given direction	$\propto$	Gradient of solute concentration in that direction

This concept is expressed mathematically by the introduction of a diffusion coefficient, $\varepsilon_{f,i}$; i.e.:-

$$\overline{c'u_i'} = -\varepsilon_{f,i}\frac{\partial c}{\partial x_i} \tag{4.4.5}$$

The negative sign indicates that the mass travels from regions of high concentration to regions of low concentration (i.e. sediment is transported upwards from the bed). The fluid diffusion coefficient has dimensions m^2s^{-1}, thus representing a characteristic velocity given by the shear stress, and a characteristic length given by the mixing length.

For equation (4.4.5) to be valid, the fluctuating terms are assumed to act in a random manner. The particles collide so frequently due to the concentration that each particle quickly loses the memory of its previous motion, i.e. each particle follows a random path.

4.4.4 Form of the Fluid Diffusion Coefficient

The form of the fluid diffusion coefficient can be determined by considering Prandtl's mixing length theory. A brief discussion is given below; see Fredsøe and Deigaard (1992) for more details.

Consider an eddy, of characteristic size l, travelling up through the water column. As it travels there is an exchange of fluid and hence there is also an exchange of momentum. Continuity argues that the same amount of fluid

transported upwards must be transported downwards. The fluid discharge in each direction is given by ρq, where q can be seen as a typical value of the turbulent fluctuation.

When the fluid particles reach a new height in the water column they adapt to the new flow velocity,

$$\text{Change in velocity} \approx l\frac{du}{dz}$$

Consider the total momentum exchange per unit area, i.e.,

$$\rho q l \frac{du}{dz} = \tau$$

where τ is an equivalent shear stress.

Continuity also implies that q has the same magnitude as the horizontal velocity fluctuations. This in turn is related to the change in velocity to give the following,

$$q \approx l\frac{du}{dz}$$

Thus,

$$\tau = \rho l^2 \frac{du}{dz}\left|\frac{du}{dz}\right| \rho\varepsilon_f \frac{du}{dz} \qquad (4.4.6)$$

where,

ε_f -Fluid momentum/diffusion coefficient

(It must be noted that molecular terms have been neglected in the derivation of this term.)

Assuming a logarithmic velocity profile, i.e.:-

$$\frac{du}{dz}=\frac{u_*}{\kappa z} \tag{4.4.7}$$

Also, from Reynolds' equations,

$$\tau=\rho u_*^2\left(1-\frac{z}{h}\right) \tag{4.4.8}$$

Substituting gives,

$$\varepsilon_f=\kappa z u_*\left(1-\frac{z}{h}\right) \tag{4.4.9}$$

Thus, following from the hydrodynamics, a parabolic distribution for the fluid diffusion coefficient is obtained.

Although the use of a linear shear stress and a logarithmic velocity profile suggest a parabolic distribution for the fluid diffusion coefficient, Kerssens et al (1979) suggests the use of a parabolic-constant distribution. Based on the river data of Coleman (1970), the fluid diffusion in the lower half of the water column is modelled by the parabolic expression given by equation (4.4.9) whilst the upper half is described by a constant value, i.e.:-

$$\varepsilon_f=\begin{cases}\kappa u_* h\dfrac{z}{h}\left(1-\dfrac{z}{h}\right) & ;\ \dfrac{z}{h}<0.5\\ 0.25\kappa u_* h & ;\ \dfrac{z}{h}\geq 0.5\end{cases} \tag{4.4.10}$$

4.4.5 Sediment Diffusion Coefficient

Equation (4.4.5) assumes that all quantities behave as momentum. However, McDowell and O'Connor (1977) suggest that this is not the case for sediment since sediment particles have greater inertia than fluid particles. It is suggested

that the sediment diffusion coefficient can be obtained from the fluid diffusion coefficient via a proportionality coefficient, β.

Van Rijn (1984) includes the β coefficient and also introduces a factor that accounts for the damping of the turbulence due to the presence of the sediment, ϕ. The formula is given below.

$$\varepsilon_s=\beta\phi\varepsilon_f \tag{4.4.11}$$

According to Van Rijn (1984), β represents the difference between the diffusion of a fluid particle and a discrete sediment particle. A value for β is obtained by considering the ratio of the maximum values for the sediment and fluid diffusion coefficients,

$$\beta=\frac{\varepsilon_{s,\max}}{\varepsilon_{f,\max}}$$

To calculate $\varepsilon_{s.\max}$, Van Rijn uses data taken from a study of the Enoree river by Coleman (1970). The average value of ε_s in the upper half of the flow is used to represent the maximum value of the sediment diffusion coefficient. This gives the following empirical form for β,

$$\beta=1+2\left(\frac{w_f}{u_*}\right)^2 \;;\; 0.1<\frac{w_f}{u_*}<1 \tag{4.4.12}$$

Carstens (1952) argues that β should be less than unity since sediment particles do not respond fully to turbulent fluctuations. However, Singamsetti (1966) argues that β should actually be greater than unity since the centrifugal force for sediment particles is greater than that for the fluid particles and are therefore thrown further outwards from the centre of the eddy. This in turn increases their mixing length; i.e. diffusivity is increased.

To investigate these claims, Jobson and Sayre (1970) try to combine both concepts in one model. Both the velocity and the sediment diffusion coefficient are split into two components. The first component is taken as the tangent to the pathlines of the fluid particles in the immediate neighbourhood of the sediment particles. The second is the radial component, which is normal to the pathlines. By using this split it is possible to express the sediment diffusion coefficient as,

$$\varepsilon_s = \varepsilon_c + \varepsilon_t$$

where,

ε_c -Component relating to the curvature of the pathlines, i.e. a measure of the centrifugal force. (Singametti)

ε_t -Component relating to the tangential component of the velocity fluctuations. (Carstens)

It is argued that ε_t is similar to ε_f therefore the original equation, $\varepsilon_s = \beta\varepsilon_f$, is valid when ε_c is negligible, i.e. when turbulence is uniform over the entire flow field. Since ε_s is always less than or equal to ε_f, if $\varepsilon_c = 0$ then this would suggest that $\beta < 1$.

If, however, there are large eddies present then the turbulence cannot be assumed to be uniform. In this situation ε_c becomes large which implies that $\beta > 1$.

Jobson and Sayre conclude that the value of β is dependent on the conditions of the system. If strong vortices are present then $\beta > 1$, if not then $\beta < 1$.

The ϕ term in equation (4.4.11) expresses the damping of the turbulence by the presence of the sediment particles. A more detailed explanation is given by Van Rijn (1984) where it is described as a (free) fit-parameter that depends on the local concentration. If there is no turbulence damping, i.e. the sediment concentration is not large enough, then the ϕ-factor is set equal to unity.

4.4.6 Conclusions

The kinetic energy models require the solution of partial differential equations; this can be problematic in itself. It is therefore concluded that a profile model based on a Fickian diffusion analogy shall be used in the present study.

For the simple situations considered within this thesis it will be assumed that the effect of damping on the sediment diffusion is negligible. Also, since the sediments to be considered are fine particles, the sediment diffusion is assumed to be congruent with the fluid diffusion so that the sediment diffusion coefficient is given by,

$$\varepsilon_s = \kappa z u_* \left(1 - \frac{z}{h}\right) \tag{4.4.13}$$

4.5 Vertical Flow Velocity

Having now found expressions for the sediment fall velocity and the sediment diffusion coefficient, the only term remaining in Equation (4.2.1) is that of the vertical flow velocity. A simple formula is used that relates the vertical flow velocity to the rate of change of the water depth and the position in the water column from the zero velocity level, z_0, i.e.:-

$$w = \frac{\partial h}{\partial t}\left(\frac{z}{h} - \frac{z_0}{h}\right) \tag{4.5.1}$$

The precise nature of this term is not considered important since the term is relatively small.

4.6 Bed Boundary

4.6.1 Introduction

To ensure closure on the mathematical system, a boundary condition must be applied at the bed. However, the location of this boundary is somewhat

ambiguous. It would appear from the literature that two common methods exist for defining the reference level at which the bed boundary is located. The first method relates the reference level to the diameter of some percentile grain particle in the non-uniform distribution. The second relates to the bed forms present in the system. A brief description of some of those methods employed in the literature is presented in the next sub-section.

Once the reference level has been established, it is then necessary to impose some condition at this boundary. Several methods for calculating the reference concentration are found in the literature, these are discussed in sub-section 4.6.3.

4.6.2 Reference Level

As stated earlier, the bed boundary condition must be applied at a given reference level, a. The literature reveals numerous methods for determining the reference level. An early approach, adopted by Einstein (1950), defines the reference level at a height of twice the diameter of the thirty-fifth percentile grain particle, i.e.:-

$$a = 2d_{35}$$

Engelund and Fredsøe (1976) also base their reference level on grain size. Here the reference level is defined at a height of twice the median grain diameter, i.e.:-

$$a = 2d_{50}$$

Smith and McLean (1977) define the reference level by,

$$a = 3d_{90}$$

Winyu and Shibayama (1994) use a value of one hundred times the grain diameter for the situation of uniformly distributed grains.

An alternative method uses bed form height rather than grain diameter to determine the reference level. Nielsen (1986) defines the reference level to be at

the same level as the ripple crests. This can be seen to be similar to the method of Van Rijn (1984) who defines the reference level at a height that is equal to half the bed form height above the mean bed level.

Van Rijn (1984) also notes that using a reference level that is too low can result in large errors in the concentration profile. After some experimental analysis, Van Rijn (1984) concludes that a minimum reference level should be imposed. The expression given relates the reference level to the water depth, h, i.e.:-

$$a_{\min} = 0.01h$$

4.6.3 Reference Concentration

Once the reference level has been determined, it is then possible to prescribe a concentration value at the bed boundary. There are many formulae found in the literature for determining the reference concentration, all of which assume equilibrium conditions at the reference level such that the flux upwards is equal to the flux downwards; i.e.:-

$$\varepsilon_s \frac{\partial c_a}{\partial z} = w_f c_a \qquad (4.6.1)$$

where,

c_a -Reference concentration given at the reference level a

It is possible to determine the reference concentration for suspended sediment by considering the reference level to be at the edge of the bed-load region. The reference concentration is then given by the bed-load concentration, c_b.

Einstein (1950) relates the bed-load concentration to a dimensionless bed-load transport rate. The relationship is described by the following formula,

$$c_b = \frac{1}{23.2} \frac{q_*}{\sqrt{\tau_s^*}} \qquad (4.6.2)$$

where,

q_* -Dimensionless bed-load transport rate

τ_s^* -Dimensionless bed-shear stress associated with skin friction due to the grains

Sternberg et al (1988) describes a model that considers excess Shields stress and is also related to the bed volume concentration. The model is also capable of considering non-uniform grain size since it divides the grain distribution into grain size fractions.

$$c_a = \frac{\gamma_0 i_b c_b T}{1+\gamma_0 T} \tag{4.6.3}$$

i_b -Proportion of ϕ-size grains in the bed sediment

c_b -Bed volume concentration (= 1-porosity)

γ_0 -Empirical constant

$T = \frac{\tau' - \tau_{cr}}{\tau_{cr}}$ -Excess bed-shear stress

τ' -Effective/grain shear stress

τ_{cr} -Critical shear stress

By using linear regression on experimental data, Sternberg et al simplify equation (4.6.3) to give:-

$$\frac{c_a}{i_b c_b} = 2.53\times10^{-7} T^2 + 3.63\times10^{-6} \tag{4.6.4}$$

It is noted that this formula may over predict for cases of thermal stratification.

Engelund and Fredsøe (1976) adopt a probabilistic approach. The method relates the concentration at the bed layer to the Shields parameter via the linear concentration at the bed, λ_b.

It must be noted that the reference level is defined at a distance above the bed equal to twice the grain diameter, i.e. the edge of the bed load region as described by Einstein (1950).

The concentration at the reference level is given by,

$$c_b = \frac{0.65}{\left(1+\frac{1}{\lambda_b}\right)^3} \tag{4.6.5}$$

The linear concentration is related to the Shields parameter via the following equation,

$$\theta = \theta_{cr} + \frac{\pi}{6}\beta p + 0.027 s \theta \lambda_b^2$$

where,

θ –Shields parameter

θ_{cr} -Critical value of Shields parameter

β -Dynamic friction factor

s -Relative density of sediment

p -Probability that the particles in a single layer of the bed are transported as bed load

Van Rijn (1984) highlights some of the difficulties associated with using bed load values to predict a reference level concentration. It has the obvious disadvantage of predicting zero concentration at the reference level when there is no bed load transport when, in reality, this is not necessarily the case since sediment may still be held in suspension.

An alternative method is proposed by Van Rijn (1984) that describes an empirically derived formula for the value of the concentration at the bed reference level. The formula relates the reference concentration to both a non-

dimensional shear-stress parameter and a non-dimensional grain parameter. The expression given by Van Rijn (1984) is shown below:-

$$c_a = 0.015 \frac{d_{50}}{a} \frac{T^{1.5}}{D_*^{0.3}} \tag{4.6.6}$$

where,

$D_* = d_{50}\left(\frac{(s-1)g}{\nu^2}\right)^{1/3}$ -Dimensionless particle parameter

$T = \frac{\tau_b' - \tau_{b,cr}}{\tau_{b,cr}}$ -Dimensionless bed-shear stress parameter

a -Reference level

d_{50} -Median grain size

$\tau_b' = \rho g\left(\frac{\bar{u}}{C'}\right)^2$ -Effective/grain bed-shear stress

$\tau_{b,cr} = (\rho_s - \rho) g d_{50} \theta_{cr}$ -Critical bed-shear stress according to Shields

$C' = 18\log\left(\frac{12h}{3d_{90}}\right)$ -Grain-related Chezy coefficient

$\theta_{cr} = \frac{u_{*,cr}^2}{(s-1)gd_{50}}$ -Critical Shields value

$u_{*,cr} = \frac{\sqrt{g}}{C}\bar{u}_{cr}$ -Critical bed-shear velocity

$C = 18\log\left(\frac{12h}{k_s}\right)$ -Chezy coefficient

k_s -Roughness height

It must be noted that the expression for the reference level concentration, c_a, was obtained from analysis of equilibrium profiles which relies upon the assumption that the concentration at the bed adapts instantaneously to equilibrium conditions.

Garcia and Parker (1991) provide a useful comparison of several different methods of calculating the reference concentration. Predicted values from models by Einstein (1950), Engelund and Fredsøe (1976), Smith and McLean (1977), Itakura and Kishi (1980), Van Rijn (1984), Celik and Rodi (1984), also Akiyama and Fukushima (1986) are compared with experimental data. The analysis performed by Garcia and Parker shows that the model of Smith and McLean and also that of Van Rijn produce the best agreement with the test data.

It must be noted that the comparison tests were carried out using a reference level of $a = 0.05h$. This is not consistent with the reference level used in the original construction of each model.

Garcia and Parker (1991) also propose a new empirical model based on the data used in the previous comparison. The model relates to grain shear velocity, particle fall velocity and the particle Reynolds number via the relationship,

$$E_s = \frac{AZ_u^5}{1+\frac{A}{0.3}Z_u^5} \qquad (4.6.7)$$

where,

$$Z_u = \frac{u'_*}{w_f} R_p^n$$

$A = 1.3\text{x}10^{-7}$

$u'_* = \sqrt{\tau'_b (s-1) g d_{50}}$ -Grain shear velocity

w_f -Fall velocity

R_p -Particle Reynolds number

$n = 0.6$

It is shown that this model gives better agreement to the observed data than the other models compared earlier. The authors do note however that this should be expected since this data was used to derive the new model.

4.6.4 Conclusion

Since the present study concerns tidal currents, which can produce large tidal dunes, it seems reasonable to adopt the bed form reference level of Van Rijn (1984). This also avoids the complication associated with the trough region of the bed form considered when using a reference level of only a few grain diameters. The bed form level of Van Rijn (1984) is therefore used herein as the reference level for the 1DV model.

The work of Garcia and Parker (1991) indicates that the model of Van Rijn (1984) provides the best method for calculating the reference concentration and hence is used herein.

4.7 Longitudinal Flow Velocity

Having now established expressions for all terms in equation (4.2.1) and defined the boundary conditions, it is possible to determine the concentration field. To enable sediment transport rates to be calculated, it is first necessary to determine the flow field. Since this project is only concerned with the 2DV situation, only a longitudinal velocity profile is required.

Section 4.4.4 described how a linear shear-stress and a logarithmic velocity profile lead to a parabolic distribution for the fluid, and hence sediment, diffusion coefficient; the longitudinal flow velocity is therefore described by the following logarithmic profile:-

$$u = \frac{u_*}{\kappa} \ln\left(\frac{z}{z_0}\right) \tag{4.7.1}$$

where,

u -Longitudinal flow velocity

u_* -Bed-shear velocity

κ -von Karman's constant ($= 0.4$)

$z_0 = \frac{k_s}{30}$ -Zero velocity level

z -Vertical coordinate

4.8 Tidal Conditions

4.8.1 Introduction

In order to simulate tidal conditions, the 1DV model must be slightly modified.

First, the depth-average longitudinal flow velocity is given a sinusoidal variation over a tidal period of 12.42 hours. In fact, if the flood and ebb stages of the tide are treated separately, then the variation is considered to be over only the flood stage. The ebb stage of the tide can then be modelled by a similar expression but with a slightly different period to allow for flood or ebb dominated tides.

Second, the water depth is allowed to vary over a tidal period such that low tide is experienced at the start of the tidal cycle and high tide at the end of the flood stage.

The reference level for the sediment concentration calculations must also be modified to allow for the change in bed form height during the tidal cycle.

Since the depth-average longitudinal flow velocity now varies sinusoidally, it is also necessary to establish the conditions for initiation of motion.

Each modification is discussed in the following sub-sections.

4.8.2 Tidal Velocity

For simplicity, the tidal depth mean velocity is assumed to vary sinusoidally over the tidal period. This can be described by the following equation.

$$\overline{u} = \overline{u}_m \sin\left(\frac{2\pi}{up} t\right) \qquad (4.8.1)$$

where,

$\bar{u}$ -Depth-mean longitudinal tidal flow velocity

$\bar{u}_m$ -Maximum depth-mean longitudinal tidal flow velocity

up -Twice the duration of the flood stage of the tide

t -Time

The period of the function is taken as twice the duration of the flood stage of the tide (up) rather than the actual tidal period. This allows the model to cope with either flood or ebb dominated situations.

It should be noted that if there is no bias towards either flood or ebb stage of the tide, then the velocity period for the flood stage is equal to the actual tidal period.

4.8.3 Tidal Water Depth

If low tide occurs at time zero, high tide at half the velocity period, then the variation in the tidal water depth can be described by the following trigonometric function:-

$$h = h_m - \frac{r}{2}\cos\left(\frac{2\pi}{up}t\right) \qquad (4.8.2)$$

where,

h_m -Mean tidal water depth

r -Tidal range

up -Twice the duration of the flood stage of the tide

4.8.4 Tidal Reference Level

The reference level chosen in section 4.6 is defined at half of the bed form height above the mean bed level. During a tidal period, the bed form height, predicted by the method described in chapter 3, will change since the shear stress parameter will vary throughout the tidal cycle. This in turn leads to a different reference level at each stage of the tide; however, this can cause complications to

the assumptions made in simplifying the Corrector method as discussed in chapter 2. It is therefore preferable to use a constant reference level based on the maximum bed form height achieved over the tidal cycle.

This is also more realistic since the dimensions of tidal dunes are set by the Spring tide conditions and do not change significantly during any individual tide during the Spring-Neap cycle, see chapter 3.

4.8.5 Initiation of Motion

Since the longitudinal flow velocity has a sinusoidal variation over the flood period, a note must be made concerning the initiation of motion. If the tidal velocity starts from zero and slowly increases towards its maximum value at 25% of the flood period, then there will be no sediment concentration in suspension until the critical value for the velocity is reached, i.e.:-

$$\overline{u} \geq \overline{u}_{cr}$$

where,

$\overline{u}$ -Depth-average longitudinal tidal flow velocity

$\overline{u}_{cr}$ -Critical depth-average longitudinal tidal flow velocity

This condition can be translated to the equivalent expression:-

$$\theta \geq \theta_{cr} \tag{4.8.3}$$

where,

$\theta = \dfrac{u_*^2}{(s-1)gd_{50}}$ -Mobility/Shields value

θ_{cr} -Critical mobility/Shields parameter

$u_* = \dfrac{\sqrt{g}}{C}\overline{u}$ -Critical bed-shear velocity

$C = 18\log\left(\frac{12h}{k_s}\right)$ -Chezy coefficient

k_s -Roughness height

The value of the critical mobility/Shields parameter can be determined via the parameterised equations of Van Rijn (1993), shown below.

$$\begin{aligned}
\theta_{cr} &= 0.24D_*^{-1} && \text{for} && 1 < D_* \leq 4 \\
\theta_{cr} &= 0.14D_*^{-0.64} && \text{for} && 4 < D_* \leq 10 \\
\theta_{cr} &= 0.04D_*^{-0.1} && \text{for} && 10 < D_* \leq 20 \\
\theta_{cr} &= 0.013D_*^{0.29} && \text{for} && 20 < D_* \leq 150 \\
\theta_{cr} &= 0.055 && \text{for} && D_* > 150
\end{aligned} \qquad (4.8.4)$$

4.9 Coordinate Transform

Before sediment transport rates are calculated, the vertical coordinate, z, is first transformed. By transforming the coordinate system, it is possible to concentrate calculations in regions that are more significant, i.e. the near-bed region. This concentration improves the accuracy of the numerical approximation since distances between computation points in the z coordinate are reduced near the bed, whilst step sizes in the transformed coordinate remain constant.

The transform used here is essentially that of O'Connor and Nicholson (1997). The transform suggested is based on a logarithmic function and is applied to a 1DV suspended sediment transport model used to model tidal conditions. It should be noted that O'Connor and Nicholson (1997) include a transform on the sediment concentration; this has been omitted from the present study.

The transform is given by:-

$$z_* = 1 - \frac{\xi}{\xi_b} \quad ; \quad \xi = -\ln\left(\frac{1}{\eta}\right) \quad ; \quad \eta = \frac{z}{h}$$

$$\xi_a = -\ln\left(\frac{1}{\eta_a}\right) \quad ; \qquad \eta_a = \frac{a}{h} \tag{4.9.1}$$

where,

z -Vertical coordinate

h -Water depth

a -Tidal reference level

Applying this to equation (4.2.1) gives:-

$$\frac{\partial c}{\partial t} = A\frac{\partial^2 c}{\partial z_*^{\,2}} + B\frac{\partial c}{\partial z_*} \tag{4.9.2}$$

where,

$$A = \frac{\varepsilon_{s,z}}{\xi_a^2 \eta^2 h^2}$$

$$B = \frac{\varepsilon_{s,z}}{\xi_a h^2 \eta^2} - \left(\frac{\frac{\partial \varepsilon_{s,z}}{\partial z} - \mathrm{w} + w_f + \eta z_* \frac{\partial h}{\partial t}}{\xi_a \eta h} \right)$$

The corresponding boundary conditions are now:-

Surface: $c = 0$ at $z_* = 1$ (4.9.3)

Bed: $c = c_a$ at $z_* = 0$ (4.9.4)

4.10 Numerical Solution

The transformed sediment concentration equation, equation (4.9.2), together with the boundary conditions given by (4.9.3) and (4.9.4), are solved by first discretising the partial differentials using finite difference approximations.

The approximations for the first and second order spatial derivatives are given by an implicit Crank-Nicholson scheme using central differences. The vertical

dimension is divided by 33 equally spaced nodes, as suggested by O'Connor and Nicholson (1997). The vertical step size is therefore given by:-

$$\Delta z_* = \frac{1}{ii-1} = \frac{1}{32} = 0.03125 \qquad (4.10.1)$$

where,

ii -Number of vertical nodes ($=33$)

The temporal derivative is approximated by the weighted finite difference scheme proposed by Stone and Brian (1963). The difference between values at the present and previous time steps are weighted such that the current spatial step contributes two thirds of the overall value. A weight of one sixth is then assigned to both forward and backward spatial steps.

The temporal step size is also taken from O'Connor and Nicholson (1997), i.e.:-

$$\Delta t = 0.1$$

The number of iterations required is dependent on the duration of the flood stage, up. If the tide is neither flood nor ebb dominated then the model is run for half a tidal period, i.e. 6.21 hours, which requires 223561 iterations.

The application of the finite difference approximations to equation (4.9.2) leads to a tri-diagonal solution matrix; this is solved using Gaussian Elimination.

More details of the application and solution of the finite difference approximations to equation (4.9.2) can be found in Appendix B.

4.11 Sediment Transport Rates

The sediment transport rates in the longitudinal direction are given by:-

$$T_{s,x} = \int_a^h ucdz \tag{4.11.1}$$

Applying the coordinate transform described in section 4.9 gives:-

$$T_{s,x} = -h\xi_a \int_0^1 \eta_a^{\,1-z_*} ucdz_* \tag{4.11.2}$$

Since the z_* coordinate is divided into equally spaced intervals, it is possible to use numerical quadrature to approximate the integral in equation (4.11.2).

Let $F = \eta_a^{\,1-z_*} uc$

Now, using Simpson's Rule for numerical quadrature:-

$$\int_0^1 F dz_* \approx \frac{\Delta z_*}{3}\left[F_{i=1} + F_{i=n} + 4\left(F_{i=2} + F_{i=4} + \cdots + F_{i=n-2}\right) + 2\left(F_{i=3} + F_{i=5} + \cdots + F_{i=n-1}\right)\right] \tag{4.11.3}$$

where i is used as the vertical step counter such that:-

$$F_{i=1} = \eta_a^{\,1-0} uc = \eta_a uc$$

$$F_{i=2} = \eta_a^{\,1-\Delta z_*} uc$$

$$\vdots$$

$$F_{i=l} = \eta_a^{\,1-(i-1)\Delta z_*} uc$$

$$\vdots$$

$$F_{i=n-1} = \eta_a^{\,1-(n-2)\Delta z_*} uc$$

$$F_{i=n} = \eta_a^{\,1-(n-1)\Delta z_*} uc = uc$$

Therefore, by using numerical quadrature, it is possible to calculate sediment transport rates for the 1DV model.

4.12 Non-uniform Grain Distribution

4.12.1 Introduction

In actual field situations, it is usual for the bed material to consist of a mixture of grain sizes; this can prove problematic when calculating sediment transport rates.

The literature reveals two methods for calculating sediment transport rates for non-uniform bed material; the first involves dividing the grain distribution into fractions, represented by d_i where $i\%$ of the material has a smaller diameter. The sediment transport rate is then found by combining the contributions made by each grain size fraction.

The second method is that proposed by Van Rijn (1993); it is based on finding a representative particle size for the grain distribution. The sediment transport rate is then found by running the model once only using the representative particle size for the suspended sediment.

Both methods are described in the following sub-sections.

4.12.2 Distribution of Grain Size

In practical situations the distribution of material is usually determined by sieve methods. The material is fed through a series of sieves with ever decreasing mesh diameter. In such a manner the amount of each grain diameter can be calculated and hence the distribution found.

Van Rijn (1993) suggests that, ideally, the distribution of grain sizes should follow that of a normal distribution when first converted to the ϕ-scale. The ϕ-scale is defined by,

$$\phi = -\log_2(d) \tag{4.12.1}$$

where d is the diameter of the grain measured in millimetres.

Thus, if the median diameter (d_{50}) and the standard deviation (σ) of the grains are known, then the distribution is given by:-

$$\phi \sim N(\mu_\phi, \sigma_\phi^2) \tag{4.12.2}$$

where,

$\mu_\phi = -\log_2(\mu)$

$\sigma_\phi = -\log_2(\sigma)$

$\sigma = 0.5\left(\frac{d_{50}}{d_{16}} + \frac{d_{84}}{d_{50}}\right)$

$\mu = d_{50}$ (since ϕ is normally distributed)

Let Z be a variable such that it has the standardised Normal Distribution:-

$$Z = \frac{\phi - \mu_\phi}{\sigma_\phi} \sim N(0,1) \tag{4.12.3}$$

The probability of d_i is defined by:-

$$P(Z \le d_i) = \frac{i}{100} \tag{4.12.4}$$

The value for Z can be found from statistical tables; say $Z = a$, then,

$$Z = \frac{\phi - \mu_\phi}{\sigma_\phi} = a \tag{4.12.5}$$

$$\frac{-\log_2(d_i) + \log_2(d_{50})}{-\log_2(\sigma)} = a$$

$$d_i = \sigma^a d_{50} \tag{4.12.6}$$

Hence, if $Z = a$ can be found from the statistical tables, then the diameter of any grain can be calculated.

Having established the distribution of the non-uniform bed material, it is now possible to calculate the transport rates for each fraction.

4.12.3 Representative Grain Size

Computing the transport rate for each grain size fraction can be very time-consuming if a large number of fractions are used. Van Rijn (1993) proposes the use of a representative grain diameter, which would replace the method of fractions. Instead of running a model for all fractions, the model would be run once only, using the representative grain size for the suspended sediment; thus saving much computer run-time.

The representative grain size is derived by considering equilibrium transport rates in steady uniform currents. Two different bed material distributions were considered, $d_{50} = 250$ μm with $\sigma = 1.5$ and 2.5, in mean flow velocities of $0.5 ms^{-1}$ and $1.5 ms^{-1}$ and a flow depth of 10m.

Based on these conditions, Van Rijn (1993) proposed the following equation for the representative particle size.

$$d_s = \begin{cases} [1 + 0.011(\sigma - 1)(T - 25)]d_{50} & ; \quad 0 < T < 25 \\ d_{50} & ; \quad T \geq 25 \end{cases} \qquad (4.12.7)$$

where,

d_s -Representative grain size of suspended sediment

d_{50} -Median grain size of bed material

σ -Geometric standard deviation of bed material

T -Dimensionless bed-shear stress parameter

Van Rijn (1993) also suggests that d_s can be approximated by $0.8d_{50}$.

4.13 Validation

4.13.1 Introduction

Before the 1DV model can be used in the Corrector method, it must first be tested and validated. Since no field data were available, the 1DV model was compared with the model of O'Connor and Nicholson (1997).

4.13.2 Test Model

The transport calculations given in the model of O'Connor and Nicholson (1997) use bed form data originally obtained from the bed form model of O'Connor (1992). These data take the form of Chezy values at different velocities during a tidal cycle. Since the aim is to test the validity of the numerical schemes used in the 1DV transport model rather than the bed form component, the 1DV model is modified so that it uses the same Chezy data and hence predicts the same bed form dimensions as O'Connor (1992).

The Chezy data used by O'Connor and Nicholson (1997) is given at varying velocities during a tidal cycle; it was necessary therefore to interpolate between the given values so that values at each time step in the 1DV model could be determined. A simple linear interpolation scheme was used, the error being small since the time step of the model is only 0.1 seconds.

O'Connor and Nicholson (1997) use the formula of Muir Wood and Fleming (1981) to determine the particle fall velocity; this formula is therefore also adopted in the 1DV model for the test cases.

4.13.3 Test Data

Table 4.13.1 gives the data sets taken from O'Connor and Nicholson (1997). Values for the tidal range (r), mean tidal water depth (h_m), maximum depth-average tidal longitudinal flow velocity ($\overline{u}_m$), median grain diameter (d_{50}), standard deviation for the grain distribution (σ) and the time given as twice the duration of the flood stage of the tide (up) are all shown.

Table 4.13.2 gives values for the variation of Chezy values through the tidal cycle as given by O'Connor and Nicholson (1997).

The data is used to test both the method of fractions and the use of the representative particle size suggested by Van Rijn (1993). The method of fractions uses ten grain size fractions where each fractional grain diameter is given by:-

$$d_5 = d_{50}\sigma^{-1.6449}$$

$$d_{15} = d_{50}\sigma^{-1.0364}$$

$$d_{25} = d_{50}\sigma^{-0.6745}$$

$$d_{35} = d_{50}\sigma^{-0.3853}$$

$$d_{45} = d_{50}\sigma^{-0.1257}$$

$$d_{55} = d_{50}\sigma^{0.1257}$$

$$d_{65} = d_{50}\sigma^{0.3853}$$

$$d_{75} = d_{50}\sigma^{0.6745}$$

$$d_{85} = d_{50}\sigma^{1.0364}$$

$$d_{95} = d_{50}\sigma^{1.6449}$$

It is assumed that no grain size is smaller than 60 μm.

The overall sediment transport rate is then given by:-

$$T_{s,x} = 0.1\sum_{i=1} T_{s,x,i} \qquad (4.13.1)$$

where,

$T_{s,x,i}$ -Transport rate given by the ith grain size fraction

4.13.4 Results

It should be noted that the 1DV model has been coded using FORTRAN 90 and is run via The University of Liverpool's UNIX system. The model of O'Connor and Nicholson (1997) however, is run via a stand alone PC with 500MHz processor speed and 64Mb of memory, using a DOS based Quick Basic code. It is therefore expected that some computational differences may exist between the two codes.

Figure 4.13.1 shows the comparison between the three models. It can be seen that the 1DV model shows an excellent agreement with the model of O'Connor and Nicholson (1997). The representative grain size method seems to give a reasonable first approximation but is somewhat inaccurate.

The good agreement shown in all three test cases would seem to validate the 1DV model when calculated via the method of grain size fractions. It is seen that although the method of representative grain size is much faster computationally, since the model is run once only, the loss in accuracy is unacceptable. It is acknowledged that this could provide a faster approach to non-uniform sediment transport rates but requires further research.

4.14 Summary

A 1DV sediment transport model has been constructed that can now be used in the new Corrector method described in chapter 2.

Having chosen a logarithmic profile for the longitudinal flow velocity, a parabolic sediment diffusion coefficient is used to ensure theoretical consistency.

A simple model based on the rate of change of the water depth is used to determine the vertical flow velocity.

The fall velocity of the sediment particles is determined using the empirical formula of Soulsby (1994), which is based on experimental data for both natural sands and irregular shaped lightweight grains.

The reference level is taken at a height of half the bed form height above the mean bed level, as given by Van Rijn (1993). An empirical formula, also proposed by Van Rijn (1993), is used to prescribe the reference concentration at the bed boundary. This boundary concentration assumes that local equilibrium conditions prevail. A zero concentration is imposed on the surface boundary to ensure consistency with the simplifications to the Corrector method.

The concentration field is solved by first transforming the vertical coordinate. The resulting system is then solved numerically by using a Crank-Nicholson implicit scheme for the spatial derivatives and the spatially weighted scheme of Stone and Brian (1963) for the temporal derivative.

Tidal sediment transport rates are approximated by using Simpson's rule for numerical quadrature after first using ten grain size fractions to represent the non-uniform nature of the bed material.

It can be seen that the 1DV sediment transport model described above has been validated by the good agreement shown with the model of O'Connor and Nicholson (1997).

The next chapter describes how the 1DV sediment transport model is used in the new Corrector method.

Set	r (m)	h_m (m)	$\overline{u}_m$ (ms^{-1})	d_{50} (μm)	σ	up (s)
4	3	10	2	200	1.7044	44712
5	3	20	2	200	1.7044	44712
6	9	10	2	200	1.7044	44712

Table 4.13.1: Data sets used to compare the 1DV model with the model of O'Connor and Nicholson (1997)

$\overline{u}$ (ms^{-1})	Data Set 4	
	Chezy (accelerating) ($m^{0.5}s^{-1}$)	Chezy (decelerating) ($m^{0.5}s^{-1}$)
0	50.3	50.3
0.4	49.4	51.2
0.6	55.3	56.5
0.8	64.3	65.0
1.0	75.3	75.7
1.2	84.5	85.2
1.4	84.6	85.7
1.6	84.7	85.6
1.8	85.0	85.4
2.0	85.10	85.10

Table 4.13.2a: Chezy values from O'Connor and Nicholson (1997) for tidal set 4

$\overline{u}$ (ms^{-1})	Data Set 5	
	Chezy (accelerating) ($m^{0.5}s^{-1}$)	Chezy (decelerating) ($m^{0.5}s^{-1}$)
0	55.3	55.3
0.4	54.8	55.8
0.6	59.0	59.7
0.8	66.8	67.2
1.0	76.9	77.1
1.2	88.5	88.6
1.4	91.1	91.7
1.6	91.2	91.6
1.8	91.3	92.5
2.0	91.4	91.5

Table 4.13.2b: Chezy values from O'Connor and Nicholson (1997) for tidal set 5

$\overline{u}$ (ms^{-1})	Data Set 6	
	Chezy (accelerating) ($m^{0.5}s^{-1}$)	Chezy (decelerating) ($m^{0.5}s^{-1}$)
0	50.3	50.3
0.4	46.9	52.6
0.6	53.8	57.4
0.8	63.5	65.5
1.0	74.9	76.0
1.2	82.9	85.8
1.4	83.3	86.5
1.6	83.6	86.3
1.8	84.1	86.0
2.0	85.1	85.1

Table 4.13.2c: Chezy values from O'Connor and Nicholson (1997) for tidal set 6

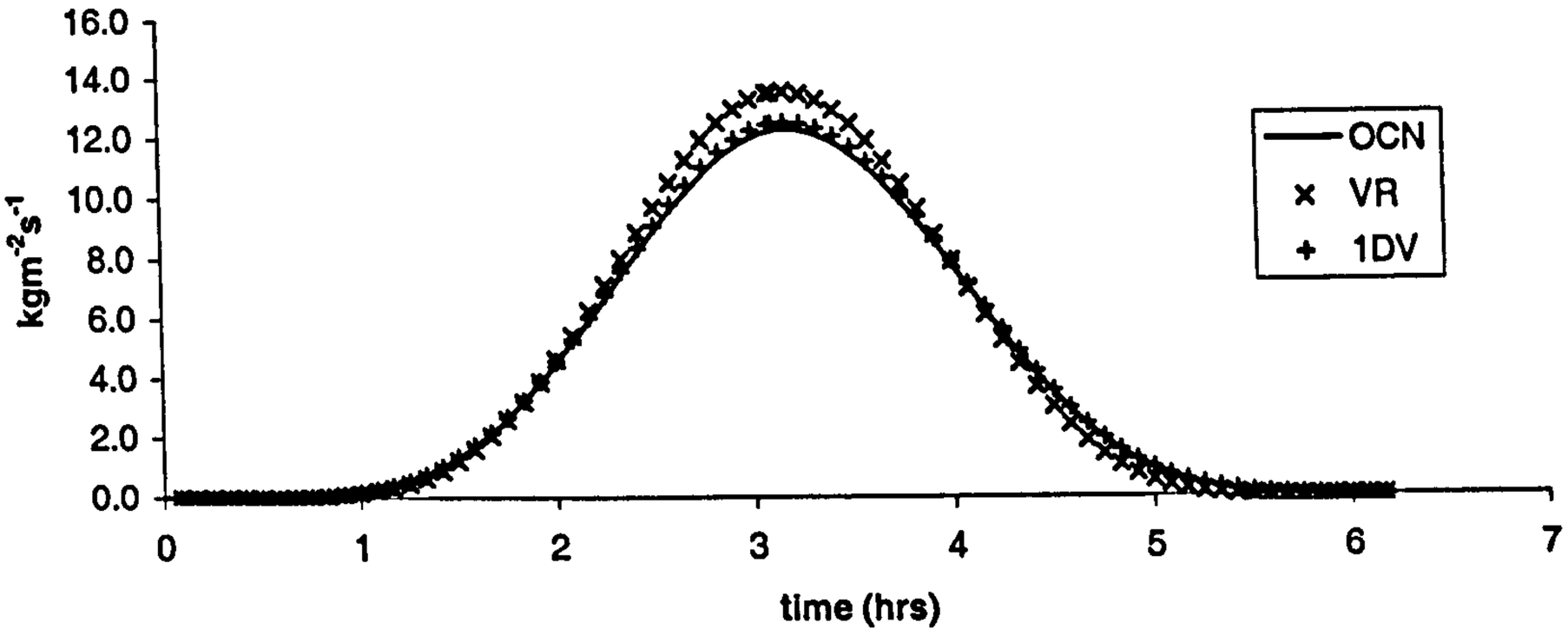

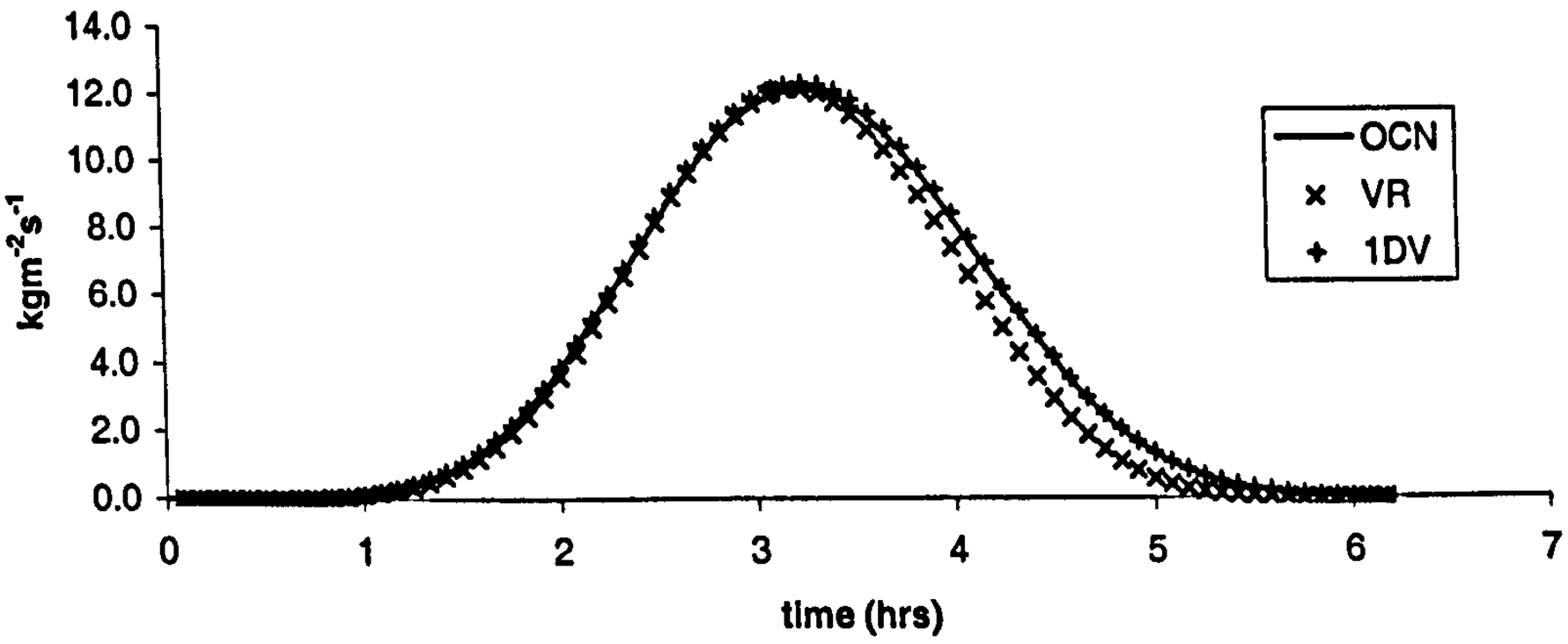

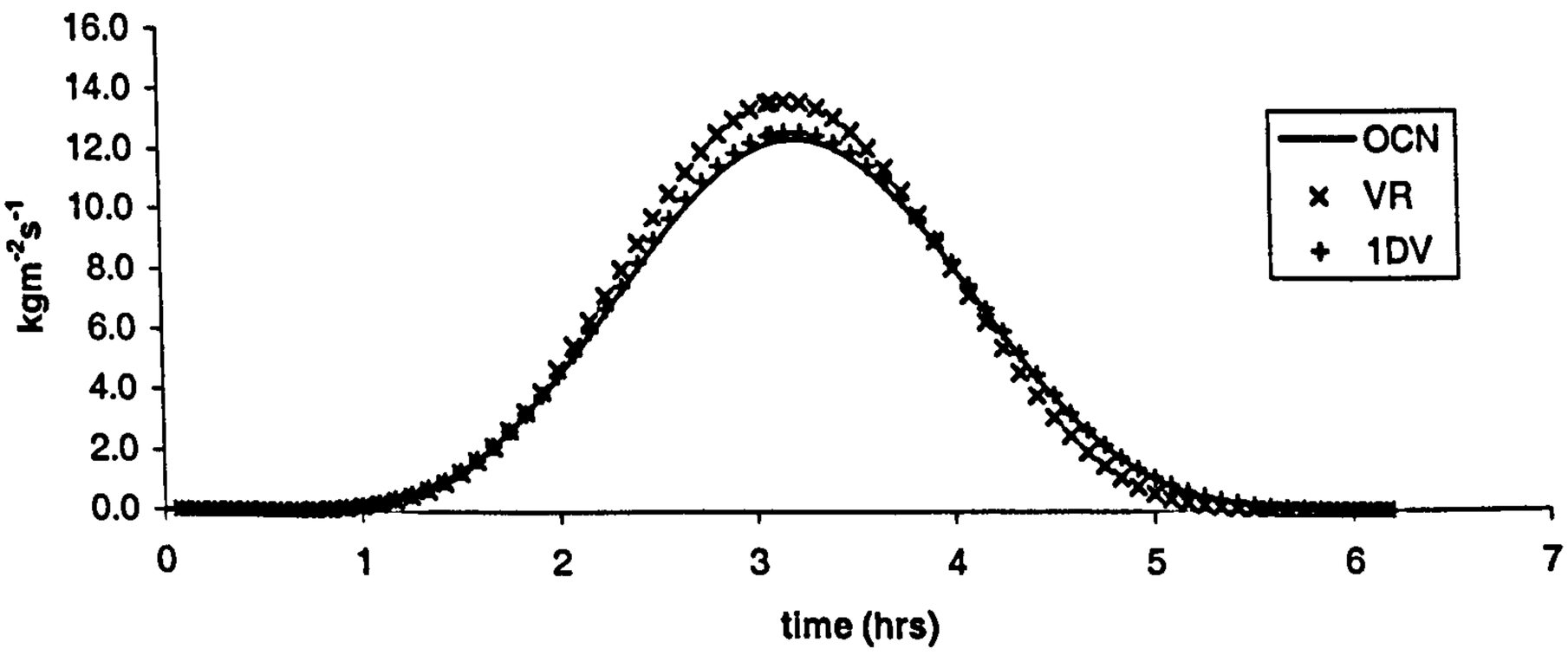

Figure 4.13.1 a-c: Comparison of 1DV model with the model of O'Connor and Nicholson (1997) (OCN) and the representative grain size of van Rijn (1993) (VR)

Chapter 5

New Corrector Method

5.1 Introduction

The aim of this chapter is to expand upon the mathematical theory presented in chapter 2, which gave the derivation of the new Corrector method proposed by O'Connor (1999). The new method works by first solving the 1DV model, then modifying these results using a spatial corrector. Unfortunately, this means that numerical error is introduced into the overall technique by the result of the 1DV computation. This method has already been tested by O'Connor et al (2001) and shown to improve upon the efficiency of conventional methods.

An alternative approach is to use a parameterised version of the 1DV model in the hope that the efficiency may be improved still further. However, this is the subject of chapter 8; the present chapter is concerned with the details of the first approach. It is designed more as a practical guide to implementing the Corrector method; it describes how the results from the 1DV model from chapter 4 are used to produce a 2DV model.

Recall that the new Corrector method is given by:-

$$\frac{\partial T_{s,x}}{\partial t}+\bar{u}\frac{\partial}{\partial x}\left(\{1+\alpha\}T_{s,x}\right)=\bar{c}(h-a)\frac{\partial \bar{u}}{\partial t}+\frac{\partial T_{disp,x}}{\partial t} \qquad (2.4.16)$$

where,

$$\alpha=\frac{T_{diff,x}}{T_{s,x}}$$

Essentially, the 1DV tidal sediment transport rates are fed into equation (2.4.16) so that they are then corrected for longitudinal effects; hence the name "Corrector method".

To be able to implement the Corrector method, it is first necessary to understand how each term in equation (2.4.16) is obtained. The most important terms are detailed below.

For more details see appendix A, which contains a diagram detailing the structure of the computer code.

5.2 Depth-mean Concentration

Chapter 4 describes how the 1DV model first calculates the sediment concentration profile when considering tidal transport rates. From this, it is quite easy to find the contributions to the profile of both the depth-mean and dispersive/fluctuating components of the sediment concentration. By using Simpson's rule for numerical integration, as described in chapter 4, the depth-mean concentration can be obtained from the equation described below.

$$\bar{c} = \frac{1}{(h-a)} \int_a^h c\,dz \qquad (5.2.1)$$

5.3 Dispersive Transport

Now that the depth-mean concentration has been determined, it is simple to find the transport due to depth-mean values, T_{dm}.

Consider:-

$$T_{dm} = \int_a^h \bar{u}\,\bar{c}\,dz$$

$$T_{dm} = \overline{u}\,\overline{c}(h-a)$$

This is easily calculated since the depth-mean longitudinal flow velocity is given by the simple sinusoidal equation (4.8.1).

From equation (2.4.7) it can be seen that the dispersive transport is then given by:-

$$T_{disp,x} = T_{s,x} - T_{dm} \tag{5.3.1}$$

where $T_{s,x}$ is the transport value obtained by the 1DV model.

5.4 Diffusive Transport

Recall from chapter 2 that the diffusive transport is defined by:-

$$T_{diff,x} = -\int_a^h \varepsilon_{s,x} \frac{\partial c}{\partial x} dz \tag{2.4.14}$$

Since the sediment concentration profile is calculated by the 1DV model at each longitudinal grid point, the sediment concentration gradient in the longitudinal direction can be found by finite difference approximations. It only remains to determine a value for the sediment diffusion/mixing coefficient, $\varepsilon_{s,x}$.

5.4.1 Longitudinal Sediment Diffusion Coefficient

The literature reveals three main methods for dealing with the longitudinal sediment diffusion coefficient. The most common of these is to neglect the term altogether, it being argued that the variation in the concentration in the longitudinal direction is over a much larger length scale to those in the vertical, see Katopodi and Ribberink (1992).

O'Connor and Nicholson (1988) performed analytical and laboratory tests on a three-dimensional sediment transport model. They suggest that the flow field dominates the spreading process and therefore the values for the horizontal sediment diffusion coefficient are less important than modelling of the advection process. Use was made of both longitudinal and lateral diffusive coefficients, each set equal to depth-average values.

Lin and Falconer (1997) use a similar argument when considering large estuaries. Since the vertical scale is much smaller than the horizontal scale, they suggest that the vertical sediment diffusion coefficient is an order of magnitude larger than its horizontal counterpart. Even so, they employ a method that sets the longitudinal sediment diffusion coefficient equal to a constant value over the water depth. This constant is set equal to the depth-average vertical sediment diffusion coefficient.

Kim (1993) uses a third method that sets the horizontal sediment diffusion coefficient equal to the vertical sediment diffusion coefficient at each computational point when considering three-dimensional sediment transport.

The influence of the longitudinal sediment diffusion coefficient is investigated by Van Rijn (1993) by means of scale analysis performed on the 2DV sediment concentration equation (equation (2.3.1)). Using a scale of 10m for the vertical distance, 100m for the longitudinal distance, $1ms^{-1}$ for the velocity, $0.1ms^{-1}$ for the fall velocity, $0.1m^2s^{-1}$ for both the vertical and longitudinal diffusion coefficients and 10000s for the time scale, Van Rijn obtains the following order of magnitude for each term in the equation:-

$$\frac{\partial c}{\partial t} \approx O(10^{-1})$$

$$u\frac{\partial c}{\partial x} \approx O(10)$$

$$w\frac{\partial c}{\partial z} \approx O(10)$$

$$\frac{\partial}{\partial x}\left(\varepsilon_{s,x}\frac{\partial c}{\partial x}\right) \approx O\left(10^{-2}\right)$$

$$\frac{\partial}{\partial z}\left(\varepsilon_{s,z}\frac{\partial c}{\partial z}\right) \approx O\left(10^{0}\right)$$

From the analysis of Van Rijn, it can be seen that the contribution of the longitudinal sediment diffusion coefficient is negligible compared with the other components of the equation.

Although the method of O'Connor and Nicholson and that of Kim are both valid, Van Rijn's scale analysis shows that the longitudinal diffusive transport is negligible and is therefore omitted from subsequent calculations. Equation (2.4.16) then simplifies to:-

$$\frac{\partial T_{s,x}}{\partial t} + \overline{u}\frac{\partial T_{s,x}}{\partial x} = \overline{c}(h-a)\frac{\partial \overline{u}}{\partial t} + \frac{\partial T_{disp,x}}{\partial t} \qquad (5.4.1)$$

5.5 Boundary Conditions

5.5.1 Introduction

Before the boundary conditions can be discussed, it is important to first establish the structure of the solution domain.

The bed is divided into $k = 1 \ldots kk$ grids in the longitudinal direction, each of equal length. Each grid contains sediment with different characteristics. Since the median grain diameter is different for each grid, it follows that the bed form dimensions, and hence roughness, will also be different for each grid.

The size of the longitudinal grid is defined by the wavelength of the bed form given by the conditions within the first grid. The longitudinal direction is then non-dimensionalised by dividing through by the total length of all kk grids.

5.5.2 Surface Boundary

Again, a zero concentration is assumed at the water surface.

5.5.3 Bed Forms

Although the topography of the system is complicated by the addition of the longitudinal dimension, the calculations for the bed form dimensions remain the same as those described in chapter 3.

Each grid is considered independent of the others so that the bed form dimensions and roughness only depend upon the sediment and flow characteristics of the individual grid.

5.5.4 Reference Level

Since the bed form height differs for each grid, it is necessary to reconsider the reference level for the sediment calculations. In chapter three, the reference level was only considered at one spatial point in a tidal cycle; now there are kk spatial points each producing different bed forms. Previously, the reference level was defined at a height of half the bed form height above the mean bed level; this was based on the maximum height that the bed form achieved over the tidal cycle. This is extended so that the maximum bed form height over the tidal period is found for each grid; the mean bed level over all kk grids is then used in determining the reference level, see figure 5.5.1.

$$\text{i.e.} \qquad a = \frac{\sum_{k=1}^{kk} a_k}{kk}$$

5.5.5 Inflow Boundary

The inflow boundary, $k = 1$, is positioned so that it has the same sediment and flow characteristics as the upstream grid. This means that the 1DV transport rates for the inflow boundary are the same as those given in the previous grid.

5.5.6 Outflow Boundary

The condition imposed on the outflow boundary, $k = kk$, is similar to that at the inflow boundary. Here the sediment and flow characteristics for grid $k = kk$ are the same as those for the downstream grid. Again, this means that the 1DV transport rates are the same for the two grids.

5.6 Numerical Solution

Equation (5.4.1) is split into two parts by using the operator splitting technique, see O'Connor (1971) and Verboom (1975).

$$\frac{\partial T_{s,x}}{\partial t} + \bar{u}\frac{\partial T_{s,x}}{\partial x} = 0 \qquad (5.6.1)$$

$$\frac{\partial T_{s,x}}{\partial t} = \bar{c}(h-a)\frac{\partial \bar{u}}{\partial t} + \frac{\partial T_{disp,x}}{\partial t} \qquad (5.6.2)$$

This enables different numerical techniques to be used for each component of the split. Equation (5.6.1) is solved using the method of characteristic projection described by Yotsukura and Fiering (1964), see also O'Connor (1971), whilst equation (5.6.2) is solved using standard finite difference techniques.

5.6.1 Commutability

Since the Corrector method now involves two applications of the operator splitting technique, a note must be made on the commutability of the scheme. Nicholson (1983) discusses the commutability of the operator splitting technique

when applied to the 3D advection-diffusion equation for sediment concentration. He concludes that although the scheme does not satisfy the commutability condition, the error incurred is assumed negligible if the model can be verified satisfactorily. For this reason, no attempt has been made to rectify the error caused in using the operator splitting technique in the Corrector method.

Hence, the Corrector method is implemented by first solving the 1DV model as given by equation (4.2.1), then solving equation (5.6.1) and finally by solving equation (5.6.2).

5.6.2 Method of Characteristic Projection

Characteristic Solution

The solution of equation (5.6.1) can be found by first determining the characteristic solution. This is, essentially, the solution of an ordinary differential equation (o.d.e) determined by the original partial differential equation (p.d.e). The solutions of the o.d.e form characteristic curves, each determined by a unique initial condition (known as the Cauchy data). If the initial condition is known then the solution to the o.d.e, and hence the p.d.e, can be found, see Smith (1998).

The characteristic solution for equation (5.6.1) is given by:-

$$x = \bar{u}t$$

Projection

The transport rate at each grid point is given by projecting backwards along the characteristic solution, into the matrix of solutions for the previous time step. Effectively, the advection process is reversed. The transport is projected backwards in the longitudinal direction by a distance defined by the time step of the computer code, Δt, and the depth-average longitudinal flow velocity. The transport rate is then found by using linear interpolation on the known transport values during the previous time step. It is acknowledged that the use of a linear

interpolation scheme may be less accurate than a higher order scheme. However, since the aim is to test the relative accuracy the different methods, it is assumed that, being common to both models, a linear scheme will suffice.

The boundary conditions for the system are easy to implement since the 1DV values across the boundary are the same.

The details of the interpolation are given in appendix C.

5.6.3 Finite Difference Scheme

Since equation (5.6.2) contains only time derivatives, a Stone and Brian (1963) finite difference scheme is used as an approximation.

The boundary conditions for the finite difference scheme are more complex than those used in the projection method since these are no longer 1DV values. A weighted-average is introduced which gives a 70% bias towards values obtained from the grid with the same sediment and flow characteristics.

This results in a tri-diagonal matrix that is solved using Gaussian Elimination. Again, details can be found in appendix C.

5.7 Summary

Details of how the new Corrector method uses the 1DV model described in chapter 4 to give 2DV suspended sediment transport rates have been presented.

The chapter has also presented details of how each component of the new corrector method can be obtained. Methods for calculating the depth-mean concentration, dispersive transport and diffusive transport are all given.

It has also been argued that the contribution of the diffusive transport is negligible and is therefore omitted from the calculations of 2DV suspended sediment transport rates.

The boundary conditions for the new Corrector method have been presented and are such that the same conditions used for the 1DV model are imposed at the surface and bed, whilst a weighted-average approach is used at both the inflow and outflow boundary.

Having established the equations and boundary conditions for the 2DV system, details have then been given of the numerical techniques used in the calculation of the transport rates.

Before the model can be tested, it is first necessary to establish the transport rates produced by the conventional approach, see section 2.3.2. This requires the construction of a conventional 2DV model; the next chapter describes such a model and presents a comparison between the two 2DV methods.

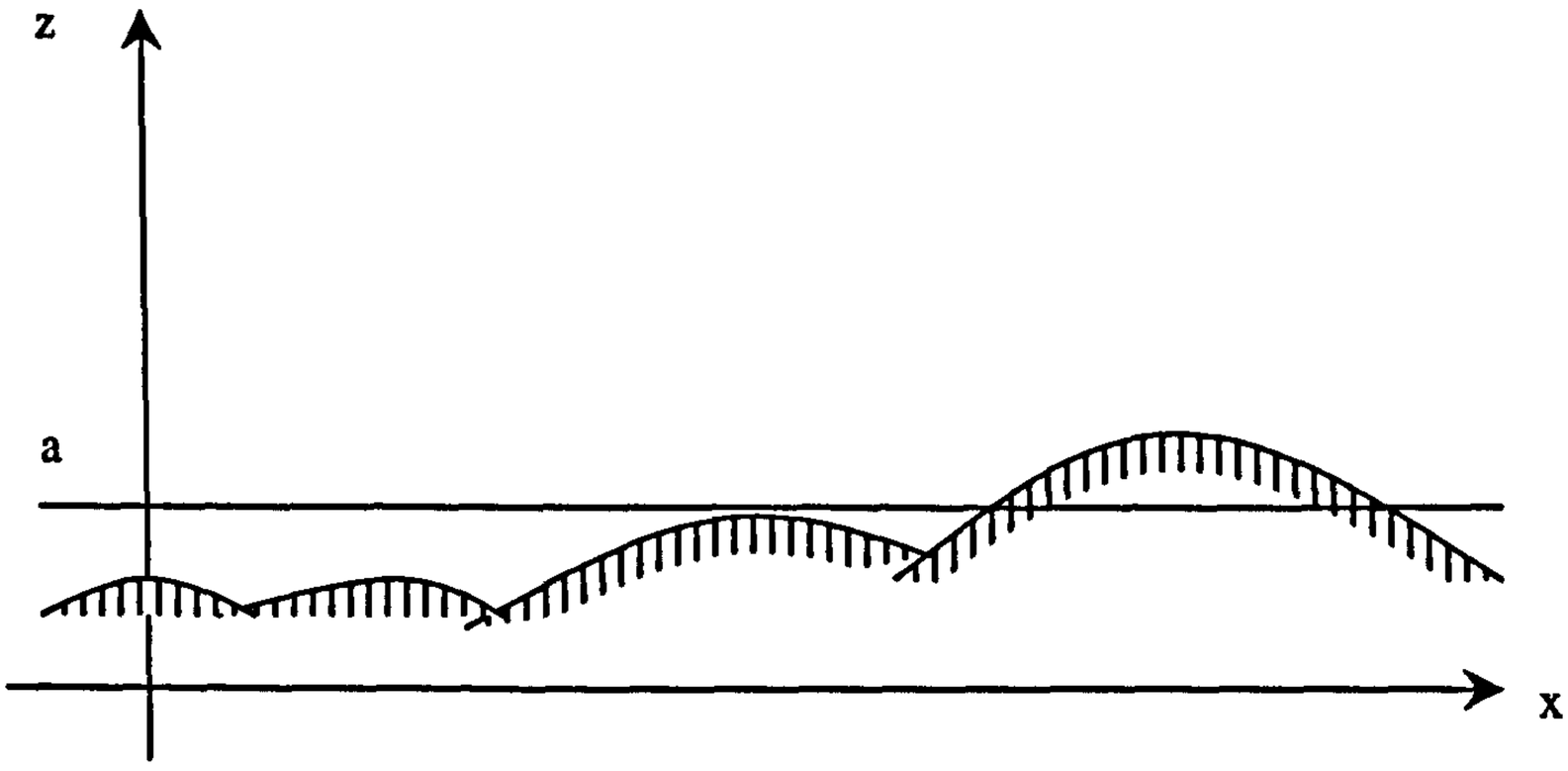

Figure 5.5.1: Reference level for the Corrector method

Chapter 6

Validation of the Corrector Method

6.1 Introduction

Chapter 5 described a new approach for calculating 2DV tidal sediment transport rates; this chapter describes the methods used to test the new method.

It is first necessary to construct a conventional 2DV model. Section 6.2 describes the theory by which the conventional model is derived. Essentially, by neglecting the lateral dimension, the three-dimensional advection-diffusion equation can then be split to produce a 1DV model and a 1DH model. When solved in sequence, these models produce 2DV values. Section 6.2 also discusses the numerical methods used to solve the conventional 2DV model.

The hydrodynamics are then discussed so that the transport rates can be determined. These transport rates are then tested against the analytical model of Mei (1969) in order to validate the model.

Once the conventional 2DV model has been validated, it is then used to test the new Corrector method. Section 6.5 discusses the accuracy and the computational time required for two test cases.

6.2 Theory

As described in chapter 2, if the lateral dimension of the three-dimensional advection-diffusion equation for sediment concentration, equation (2.2.8), is

omitted, then the 2DV advection-diffusion equation for sediment concentration is given by:-

$$\frac{\partial c}{\partial t}+\frac{\partial}{\partial x}(cu)+\frac{\partial}{\partial z}(c\{w-w_f\})=\frac{\partial}{\partial x}\left(\varepsilon_{s,x}\frac{\partial c}{\partial x}\right)+\frac{\partial}{\partial z}\left(\varepsilon_{s,z}\frac{\partial c}{\partial z}\right) \qquad (2.3.1)$$

However, if the continuity equation is applied to the three-dimensional advection-diffusion equation before the lateral dimension is omitted, then the 2DV version becomes:-

$$\frac{\partial c}{\partial t}+u\frac{\partial c}{\partial x}+(w-w_f)\frac{\partial c}{\partial z}=\frac{\partial}{\partial x}\left(\varepsilon_{s,x}\frac{\partial c}{\partial x}\right)+\frac{\partial}{\partial z}\left(\varepsilon_{s,z}\frac{\partial c}{\partial z}\right) \qquad (6.2.1)$$

The operator splitting technique described by O'Connor (1971), see also Verboom (1975), is then applied to equation (6.2.1) so that the dimensions are separated, i.e.:-

$$\frac{\partial c}{\partial t}+(w-w_f)\frac{\partial c}{\partial z}=\frac{\partial}{\partial z}\left(\varepsilon_{s,z}\frac{\partial c}{\partial z}\right) \qquad (6.2.2)$$

$$\frac{\partial c}{\partial t}+u\frac{\partial c}{\partial x}=\frac{\partial}{\partial x}\left(\varepsilon_{s,x}\frac{\partial c}{\partial x}\right) \qquad (6.2.3)$$

It can be seen that the solution of equation (6.2.2) gives 1DV concentration values, whilst the solution of equation (6.2.3) gives 1DH concentration values. However, solved in sequence, they produce 2DV values.

6.2.1 1DV Model

The solution procedure starts with equation (6.2.2). This can be simplified to give equation (4.2.1) and therefore is solved by the same methods, as described in chapter 4.

Essentially, the equation is first transformed by using a modified version of the coordinate transform proposed by O'Connor and Nicholson (1997); this allows greater accuracy in the near bed region where the concentration is prevalent. The expressions given in chapter 4 for the particle fall velocity, vertical fluid velocity and vertical sediment diffusion coefficient are again used here.

Applying a zero concentration at the water surface and using Van Rijn's reference level and reference concentration, the system is then solved using the numerical scheme proposed by Stone and Brian (1963) for the temporal derivative and an implicit Crank-Nicholson scheme based on central differences for the spatial derivatives.

The solution of equation (6.2.2) gives a 1DV sediment concentration profile that accounts for vertical advection, vertical diffusion and particle settling.

6.2.2 1DH Model

Equation (6.2.3) is now split using the operator splitting technique so that the process of advection can be considered separately to that of diffusion, i.e.:-

$$\frac{\partial c}{\partial t}+u\frac{\partial c}{\partial x}=0 \qquad (6.2.4)$$

$$\frac{\partial c}{\partial t}=\frac{\partial}{\partial x}\left(\varepsilon_{s,x}\frac{\partial c}{\partial x}\right) \qquad (6.2.5)$$

Advection

Since equation (6.2.4) is purely advection, it can be solved by the method of characteristic projection. This is of the same form as equation (5.6.1) and so has a similar characteristic solution, i.e.:-

$$x=ut \qquad (6.2.6)$$

Note that this time the actual longitudinal flow velocity is required rather than the depth-average value.

The interpolation method used to solve equation (6.2.4) is the same as that used in the solution of the new Corrector method, i.e.:-

$$c_{i,k}^{n} = c_{i,k-1}^{n-1} + r_x\left(c_{i,k}^{n-1} - c_{i,k-1}^{n-1}\right) \tag{6.2.7}$$

For more details, see appendix C. It should be noted however, that the interpolation method for equation (6.2.4) must be applied at each vertical step, i.e. $i = 2 \ldots ii-1$.

The inflow boundary condition remains the same, i.e. since the 1DV values are the same at $k = 0$ and $k = 1$ then:-

$$c_{i,1}^{n} = c_{i,0}^{n-1} + r_x\left(c_{i,1}^{n-1} - c_{i,0}^{n-1}\right)$$

$$\text{i.e.} \qquad c_{i,1}^{n} = c_{i,0}^{n-1} = c_{i,1}^{n-1} \tag{6.2.8}$$

As with the Corrector method, the outflow boundary does not cause a problem and is therefore given by:-

$$c_{i,kk}^{n} = c_{i,kk-1}^{n-1} + r_x\left(c_{i,kk}^{n-1} - c_{i,kk-1}^{n-1}\right) \tag{6.2.9}$$

Again, the interpolation method described can only be used if the following condition is satisfied:-

$$u < \frac{\Delta x}{\Delta t} \tag{6.2.10}$$

where,

u -Longitudinal flow velocity

Δx -Longitudinal step size for numerical solution

Δt -Temporal step size for numerical solution

Diffusion

By the arguments presented in section 5.4.1, the longitudinal sediment diffusion coefficient is assumed to be negligible; equation (6.2.5) is therefore omitted from the model.

The 2DV concentration is therefore given by the solution of equation (4.2.1) and equation (6.2.4).

6.3 Transport

Having now obtained the sediment concentration field, it only remains to calculate the flow velocity in order to calculate the suspended sediment transport. The same logarithmic profile as described in chapter 4 is used for the longitudinal flow velocity, i.e.:-

$$u = \frac{u_*}{\kappa} \ln\left(\frac{z}{z_0}\right) \qquad (4.7.1)$$

Also, so that the tidal suspended sediment transport rates may be found, the depth-average longitudinal flow velocity is again given by the following sinusoidal expression:-

$$\bar{u} = \bar{u}_m \sin\left(\frac{2\pi}{up} t\right) \qquad (4.8.1)$$

The 2DV concentration value is then multiplied by the corresponding longitudinal velocity value at each vertical step. The transport is then found by using Simpson's rule for numerical integration, as described in chapter 4.

6.4 Analytical Test

6.4.1 Introduction

Although the theory for the conventional 2DV model has been presented and the numerical solution described, it is important that the model be verified before it can be trusted. Unfortunately, no field data were available so a theoretical test is used instead. To enable an analytical solution, only simple situations can be considered using present techniques. Although these simple situations do not truly describe the field, they do, nonetheless, provide a useful guide to the verification of the numerical model. It is proposed therefore that the 2DV conventional model be tested against the analytic solution of the simplified 2DV sediment concentration equation as given by Mei (1969).

6.4.2 Method of Mei

The technique described by Mei (1969) is used to find an analytical solution to the model proposed by Apman and Rumer (1967). The concentration of sediment in a region of transition from an immobile bed to a sediment-laden bed is modelled by the steady-state version of the 2DV advection-diffusion equation. The bed is assumed to be always flat and horizontal. The flow depth is assumed independent of longitudinal distance. The flow is considered two-dimensional and steady. The second order derivative of the longitudinal sediment diffusion coefficient is assumed negligible. Hence, the 2DV advection-diffusion equation is now reduced to the following equation:-

$$u\frac{\partial c}{\partial x} - w_f \frac{\partial c}{\partial z} = \frac{\partial \varepsilon_{s,x}}{\partial x}\frac{\partial c}{\partial x} + \frac{\partial \varepsilon_{s,z}}{\partial z}\frac{\partial c}{\partial z} + \varepsilon_{s,z}\frac{\partial^2 c}{\partial z^2}$$

It is then assumed that both the velocity and sediment diffusivity are constant, thus allowing the further reduction:-

$$u\frac{\partial c}{\partial x} - w_f \frac{\partial c}{\partial z} = \varepsilon_s \frac{\partial^2 c}{\partial z^2}$$

Now, normalising the sediment concentration with the reference concentration, the x and z coordinates with the water depth, the equation becomes:-

$$\frac{\partial^2 c'}{\partial z'^2} + Z\frac{\partial c'}{\partial z'} = R\frac{\partial c'}{\partial x'} \qquad (6.4.1)$$

where,

$$Z = \frac{w_f h}{\varepsilon_s} \quad ; \quad R = \frac{uh}{\varepsilon_s} \quad ; \quad z' = \frac{z}{h} \quad ; \quad x' = \frac{x}{h}$$

$$c' = \frac{c}{c_a}$$

The boundary conditions are such that the concentration is equal to the reference concentration at the bed boundary and a no-flux condition is imposed at the surface boundary, i.e.:-

Bed: $$c' = 1 \qquad ; x' > 0, z' = 0 \qquad (6.4.2)$$

Surface: $$\frac{\partial c'}{\partial z'} + Zc' = 0 \qquad ; x > 0, z = 1 \qquad (6.4.3)$$

Since the bed moves from a rigid bottom to a sediment-laden bottom, the following initial condition also applies:-

Initial condition: $$c' = 0 \qquad ; x = 0 \qquad (6.4.4)$$

Equation (6.4.1), together with conditions (6.4.2)-(6.4.4), is then solved by the use of a Laplace transform to give the following analytical solution:-

$$c' = \frac{1}{2} erfc\left(\frac{z'}{2}\sqrt{\frac{R}{x'}} + \frac{Z}{2}\sqrt{\frac{x}{R}}\right) + \frac{1}{2} e^{-Zz'} erfc\left(\frac{z'}{2}\sqrt{\frac{R}{x'}} - \frac{Z}{2}\sqrt{\frac{x}{R}}\right) \qquad (6.4.5)$$

It should be noted that equation (6.4.5) is only an approximation of the Laplace transform for small $\frac{x'}{R}$, i.e. within 10 -20 water depths from $x = 0$.

Results from equation (6.4.5) were compared by Mei to the numerical results of Apman and Rumer and were shown to be almost identical.

Unfortunately, due to the simplifications to allow an analytical solution, some modifications must be made to the conventional model described in section 6.2 in order to verify it with the analytical method. The modifications made are described in the next sub-section.

6.4.3 Modified 2DV Model for Analytical Test

Sediment Diffusion

The analytical solution requires a constant value for the sediment diffusivity. The value used is therefore the depth-average value of the original parabolic distribution.

Flow Velocity

Again, the analytical method requires a constant value for the longitudinal flow velocity. The depth-average value from the logarithmic profile originally used is therefore used at each vertical step.

The vertical flow velocity, w, is set equal to zero.

Surface Boundary

The conventional 2DV model described in section 6.2 uses a zero concentration condition at the surface; this must now be changed to a no-flux condition. Using the transform described in chapter 4, condition (6.4.3) can be written as:-

$$\frac{\partial c}{\partial z_*} - \left(\frac{w_f y_b h}{\varepsilon_s} \right) c = 0$$

A simple backward difference approximation is used for the concentration gradient in the vertical direction, i.e.:-

$$\frac{\partial c}{\partial z_*} = \frac{c_{ii} - c_{ii-1}}{\Delta z_*}$$

The concentration at the surface is now given by the following equation:-

$$c_{ii} = \frac{c_{ii-1}}{1 - \frac{w_f y_b h \Delta z_*}{\varepsilon_s}} \qquad (6.4.6)$$

Obviously the solution matrix must be altered to accommodate this modification. The iterative process now works from $i = 2 \ldots ii$ rather than $i = 2 \ldots ii - 1$.

Time dependence

Since only the steady state is considered for the analytical solution, the tidal model is altered by considering values at maximum tidal velocity only.

It must be noted that since the 1DV solution uses an implicit finite difference scheme in its solution, an iterative procedure must be used in order to find the steady state solution.

Flow Depth

Since the method of Mei does not include bed forms, a slight modification of the vertical coordinate is also necessary. The vertical coordinate, z, is simply shifted downwards by the value of the reference level.

6.4.4 Results

The modified version of the 2DV conventional model was coded into a FORTRAN 90 program. This was then run for two different tidal input sets, given in table 6.4.1.

The analytical model of Mei requires values for the complimentary error function; these were obtained by using the built-in function from Microsoft Excel 97. These values were then read into a FORTRAN 90 code so that the analytical sediment concentration profile could be determined at each horizontal grid point.

It can be seen from figure 6.4.1 that the modified conventional 2DV model shows good agreement with the analytical solution for data set 501. The slight inaccuracy shown at steps $k=2$ and $k=3$ could be due to the simplistic interpolation scheme used for the solution of the advection component. This could also be due to the implicit nature of the finite difference scheme used in the solution of the 1DV component. In either case, the difference is considered negligible.

Figure 6.4.2 shows that the two models also agree well for data set 502. The discrepancy shown for $k=3$ is greatest near the surface where the concentration is much smaller and is therefore seen as negligible.

The good agreement shown for both data sets validates the modified conventional 2DV model; it is therefore assumed that the original version of the conventional 2DV model is also validated. It is now possible to compare the conventional approach to 2DV sediment transport modelling with the new Corrector method.

6.5 Comparison with the new Corrector Method

6.5.1 Introduction

Since the aim of the project is to produce a faster method for calculating 2DV sediment transport rates via the new Corrector method and subsequent parameterisation, it is necessary to first compare the speed and accuracy of the new Corrector method with the conventional approach to 2DV sediment transport modelling.

The first test must be to ensure that the 2DV effects are actually significant, i.e. significantly different to the 1DV values. Since only simple hydrodynamic situations are considered, this is achieved by varying the grain size distribution in the longitudinal direction.

Having established that the 2DV results are different to the 1DV results, the conventional 2DV approach can then be tested against the new Corrector method to assess both the speed and accuracy of the new approach.

6.5.2 Comparison with 1DV Results

The first step in testing any new theory must be to apply it to a basic situation. Once proven to be acceptable, then testing may proceed to more complicated situations. Therefore, only a simple situation is considered here. It is assumed that the longitudinal depth-average tidal velocity does not alter in the longitudinal direction. The generation of horizontal effects is given through a variation in the median grain diameter and standard deviation of grain size distribution between longitudinal grid points. Again, the data sets used are those shown in table 6.4.1.

Although nine grid points were used in total, the variation in grain size and standard deviation is such that the 2DV effects are only significant when there is a sudden increase in the median grain size between neighbouring grid points.

Figure 6.5.1 shows the region of interest for data set 805. It can be seen that there is little difference between 1DV and 2DV sediment transport rates for the grid $k=3$, this is because the preceding grids contain the same grain distribution. Again, there is little difference at grid $k=5$ since this has the same grain distribution as its predecessor. However, there is a difference at grid $k=4$; this is due to the sudden jump from a distribution with median grain size of 150 microns with standard deviation of 1.7044, to a median grain size of 250 microns with a standard deviation of 1.5. This is seen more clearly in figure 6.5.3a. Here, the difference between the 1DV and 2DV rates is plotted as a percentage for the

mid-tidal region, i.e. from 2hrs to 4hrs. It can be seen that there is a difference between the two models ranging between 2.5% and 4% during this time.

Although this may not be considered to be a significant amount, it is sufficient to show that the 2DV effects, i.e. longitudinal advection, are contributing to the transport rates.

The difference between 1DV and 2DV transport rates for data set 807 is shown in figure 6.5.2. There is little difference shown for the grid $k = 1$; this is due to the boundary condition, which gives a bias towards 1DV values at the inflow grid. Grid $k = 3$ also shows little difference; this is because it has the same grain distribution as the preceding grid. However, there is a difference shown for grid $k = 2$. Figure 6.5.3b shows the percentage difference between the 1DV and 2DV rates during the mid-tide stage. It can be seen that the difference for this stage ranges between 3% and 7%. Again, this is sufficient to show that the longitudinal advection contributes to the transport rate.

6.5.3 Comparison of 2DV Methods

Accuracy

Both the conventional 2DV model and the new Corrector model are run using the data sets given in table 6.4.1. Both models are coded using FORTRAN 90, and are run on The University of Liverpool UNIX system. The system uses four 400MHz CPU's with 4Mb cache and 1Gb memory.

Figure 6.5.4 shows the same computational grids as used for the comparison of 1DV and 2DV values for data set 805. It can clearly be seen that both of the models give almost identical results for all grid points. Figure 6.5.5 shows that this is also the case for data set 807.

The excellent agreement is better shown by considering the percentage difference between the two methods during the mid-tide stage. Figure 6.5.6 shows that the percentage difference for data set 805 is remarkably low. This should be

expected for grid points $k=3$ and $k=5$ since these are effectively 1DV values. However, grid $k=4$ also shows excellent agreement, with only 0.05% maximum difference during the mid-tide stage.

Data set 807 shows similar results, as shown in figure 6.5.7. Again the agreement is extremely good for $k=1$ and $k=3$ since these are effectively 1DV values. However, the agreement remains extremely good for grid $k=2$, showing a maximum percentage difference of just 0.14% during the mid-tide stage.

It is therefore concluded that the new Corrector method is sufficiently accurate that it may be used instead of the conventional 2DV model.

Computational Speed

Having examined the accuracy of the new Corrector method, it only remains to test the computational speed. Again the data sets given in table 6.4.1 are used. The time taken to complete the computation over half of the flood period for the nine longitudinal grid points is given in table 6.5.1. [The efficiency is defined as the ratio of the Corrector Method over the conventional method, expressed as a percentage.]

It can clearly be seen that the new Corrector method requires only 72% of the time used by the conventional 2DV model. This is significant in itself. However, if the model was applied to a much larger area, including the lateral dimension, then it is clear that the time saved by using the new Corrector method would be considerable.

6.5.4 Conclusion

By considering only a simple hydrodynamic situation where 2DV effects are given by a variation in grain size distribution in the longitudinal direction, it has been possible to examine the accuracy and computational speed of a new method for calculating tidal sediment transport rates.

For the two data sets used in the comparison, the difference between transport values predicted by the two methods is of the order of 0.1% during the mid-tide stage of the flood section of the tide. The difference between the two methods is therefore considered negligible.

The new Corrector method requires only 72% of the time needed by the conventional 2DV model to calculate sediment transport rates for nine longitudinal computation points over half of a tidal cycle. If the area of application is increased, the lateral dimension included and the full tidal cycle considered, then the reduction in computation time will be dramatic.

It is therefore concluded that the new Corrector method provides a much quicker method for calculating 2DV sediment transport rates without significant loss in accuracy.

6.6 Summary

The first part of this chapter concerned the construction of a conventional model for calculating 2DV tidal transport rates. The theory presented showed how the conventional model is based on the three-dimensional advection-diffusion equation. The 2DV model is obtained by first solving the 1DV model described in chapter 4, then solving for longitudinal effects, namely advection since the longitudinal diffusion is assumed negligible.

The conventional 2DV tidal sediment transport model was then tested against the analytical model of Mei (1969). Some modifications were necessary since the analytical expression is only valid for certain simple situations. The conventional 2DV model showed good agreement with the analytical expression, thus providing validation for the numerical model.

Once validated, the conventional 2DV tidal sediment transport model was then used to test the new Corrector method. Both models were run for two different tidal data sets that generated longitudinal effects by varying the grain distribution

in neighbouring longitudinal computation grids. The difference in predicted values was remarkably small, of the order of 0.1%. It was also shown that the computational time required for the new Corrector method was only 72% of that used by the conventional 2DV approach.

This chapter has therefore shown that the new Corrector method is capable of predicting 2DV tidal sediment transport rates to the same degree of accuracy as the conventional approach but requires much less time to do so.

The next chapter uses a parameterised version of the 1DV model so that the computation time is reduced further still.

Set	r (m)	h_m (m)	$\overline{u}_m$ (ms^{-1})	up (s)
501	3	20	1	44712
502	3	10	1	44712
805	3	10	2	44712
807	3	20	2	44712

Table 6.4.1a: Tidal information used in the validation of the conventional 2DV model

Set	d_{50} (μm)			σ		
	k=1	k=2	k=3	k=1	k=2	k=3
501	220	220	220	2.0	2.0	2.0
502	180	180	180	1.5	1.5	1.5

Table 6.4.1b: Spatial information used in the analytical test of Mei (1969)

Set	d_{50} (μm)									σ								
	k=1	k=2	k=3	k=4	k=5	k=6	k=7	k=8	k=9	k=1	k=2	k=3	k=4	k=5	k=6	k=7	k=8	k=9
805	150	150	150	250	250	250	250	250	250	1.7044	1.7044	1.7044	1.5	1.5	1.5	1.5	1.5	1.5
807	150	250	250	250	250	250	250	250	250	1.7044	1.5	1.5	1.5	1.5	1.5	1.5	1.5	1.5

Table 6.4.1c: Spatial information for the data sets used to compare the Corrector method with the conventional 2DV model

Input Set	Conventional 2DV Hrs:min:s	Corrector Method Hrs:min:s	Efficiency (%)
805	1:29:26.25	1:04:35.16	72
807	1:29:09.26	1:04:25.99	72

Table 6.5.1: Comparison of computational time required for the 2DV methods

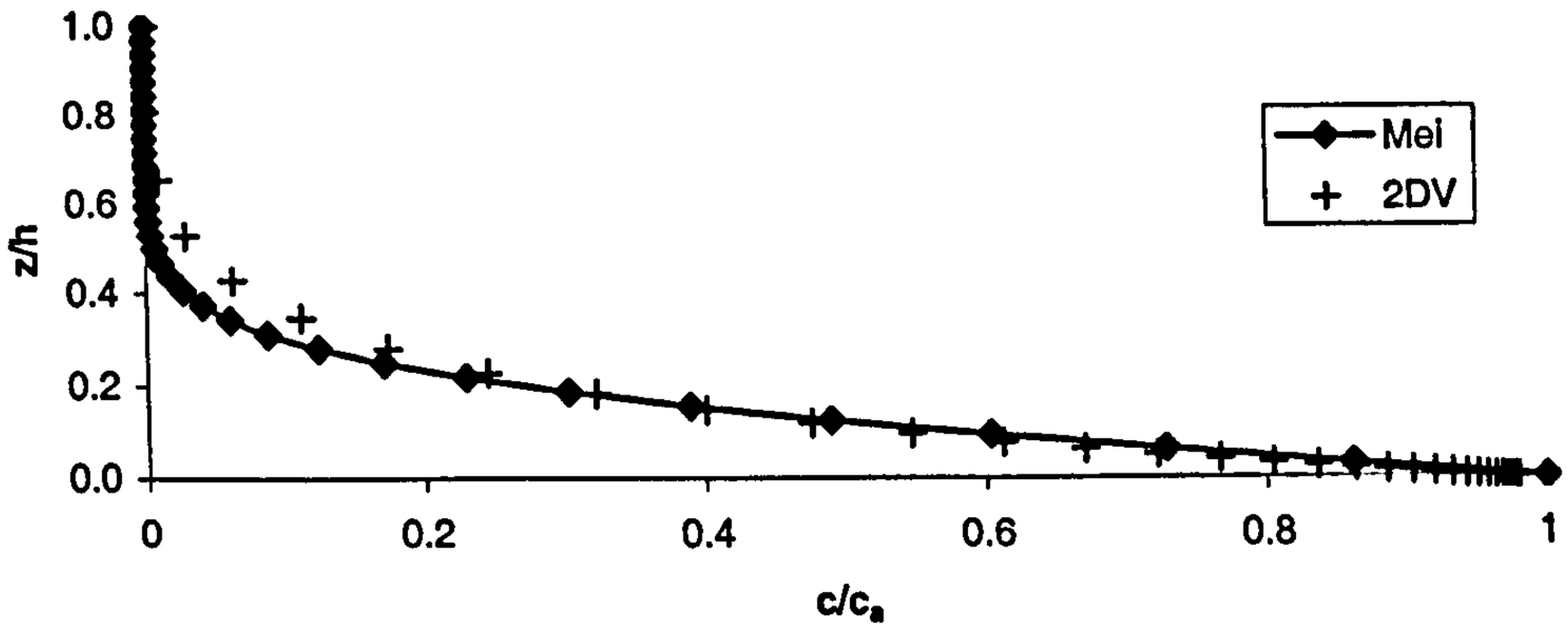

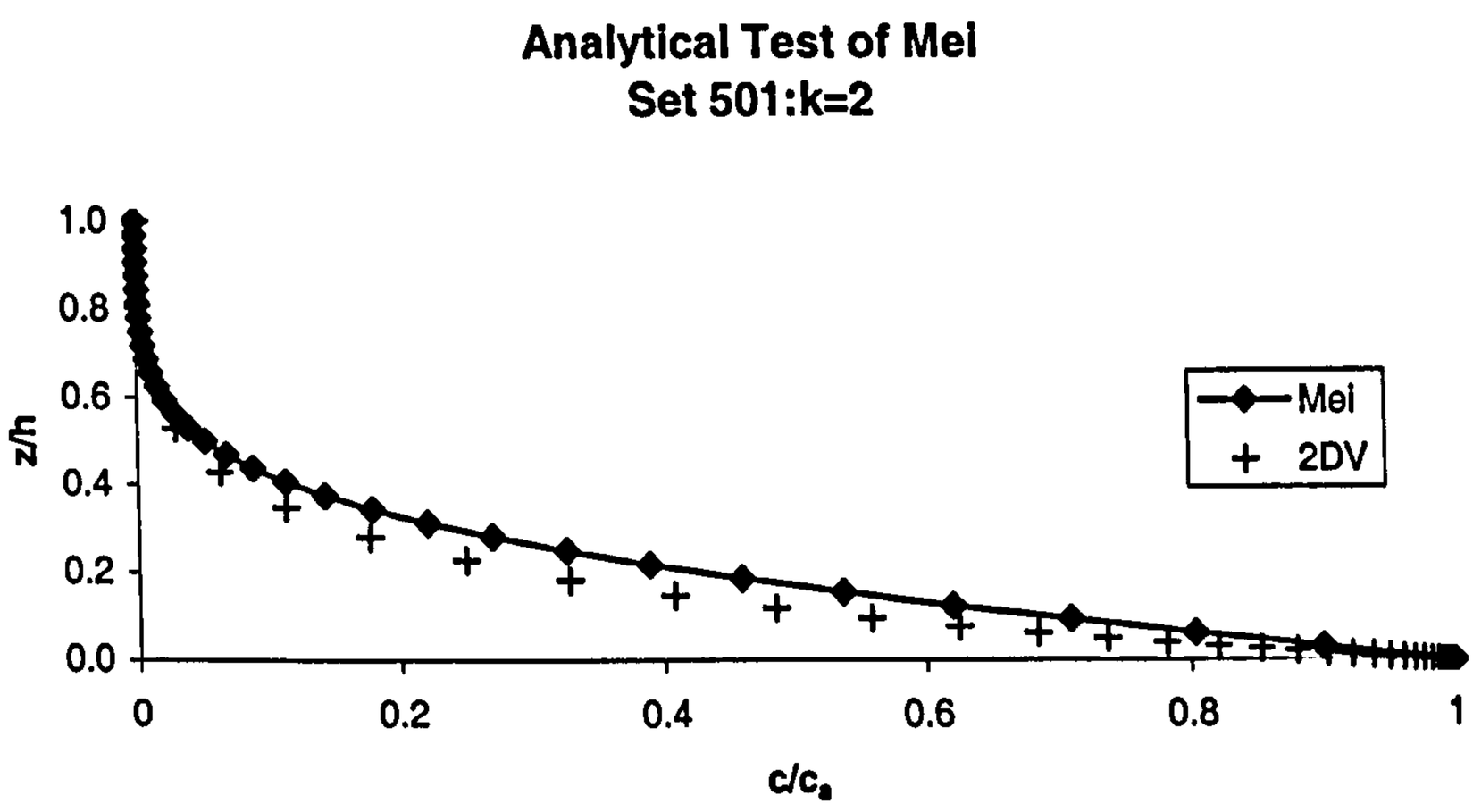

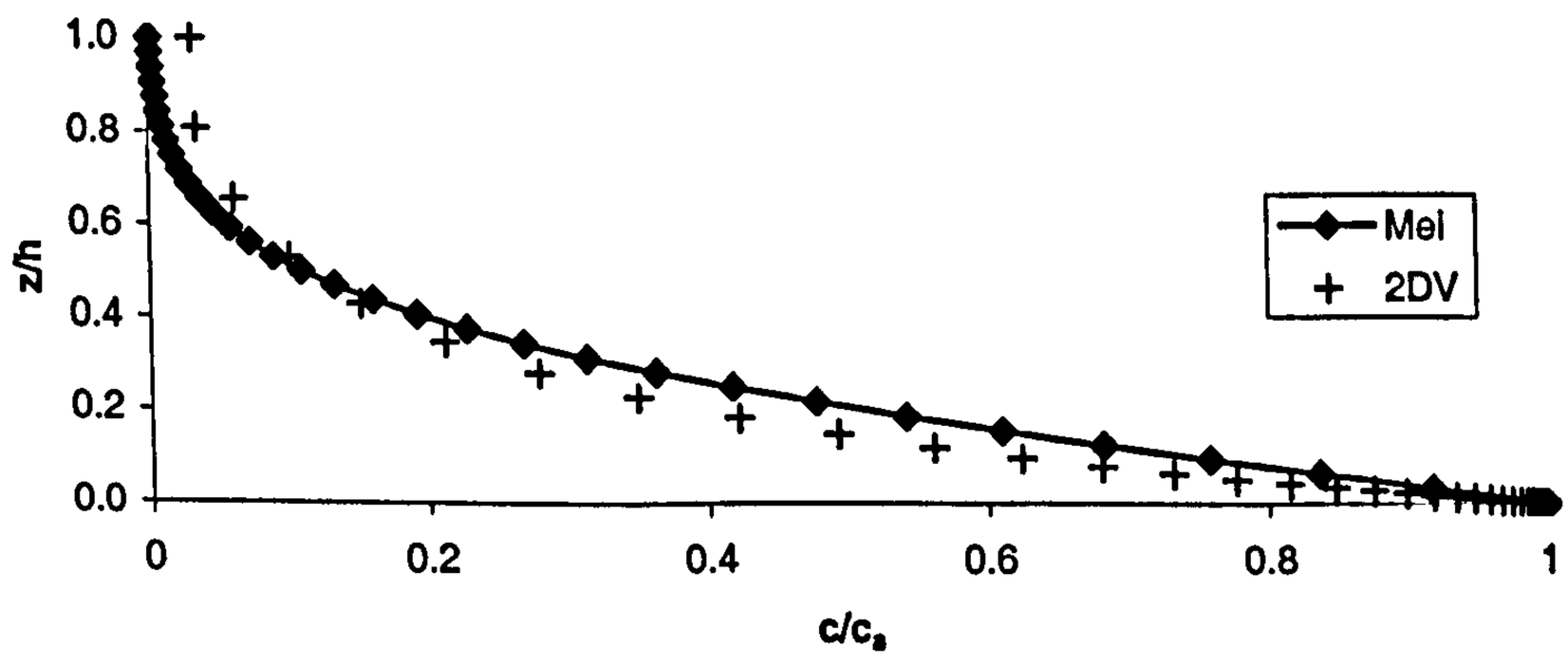

Figure 6.4.1a-c: Comparison of concentration profiles produced by the conventional 2DV model and the analytical method of Mei (1969)

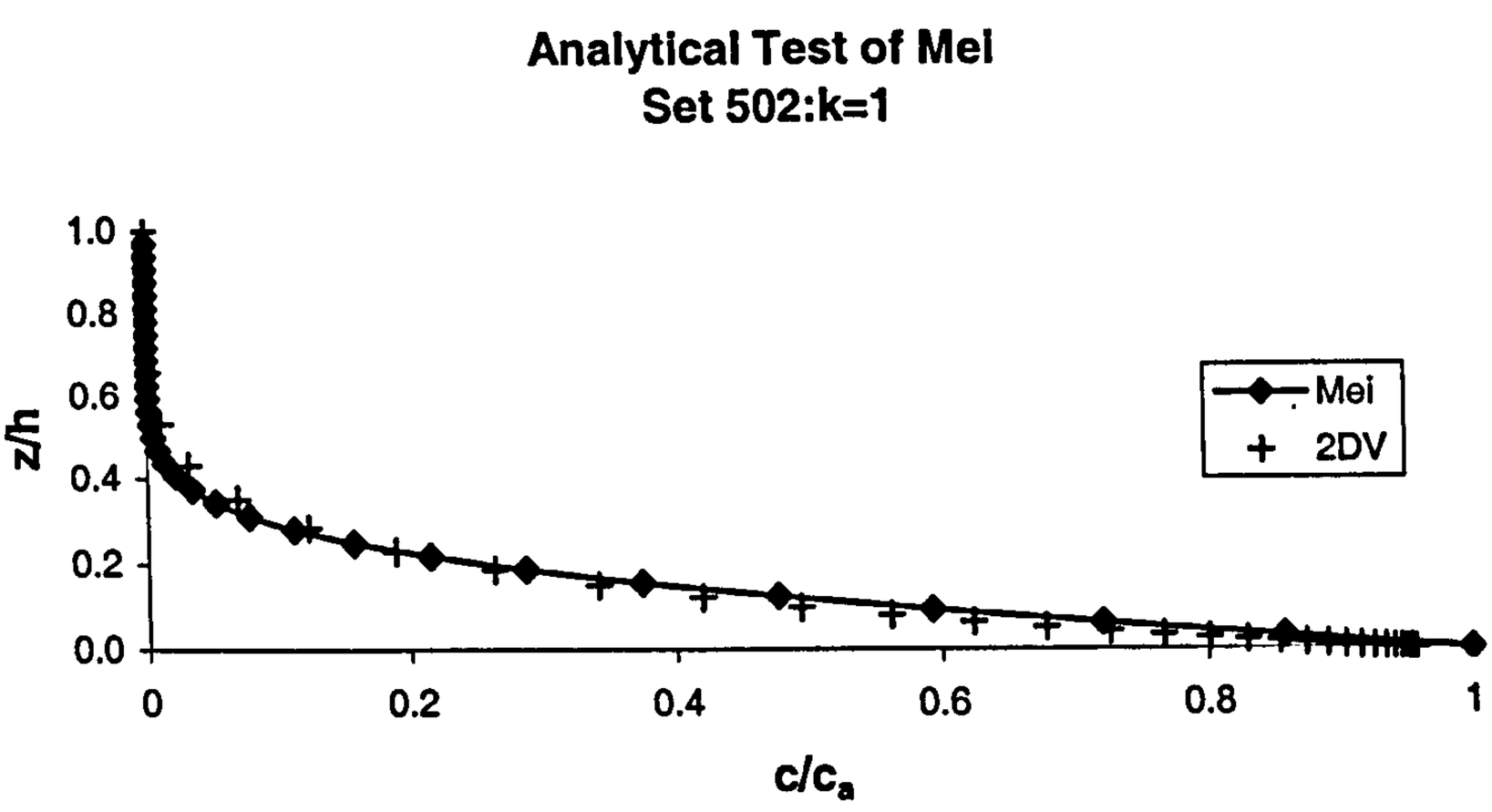

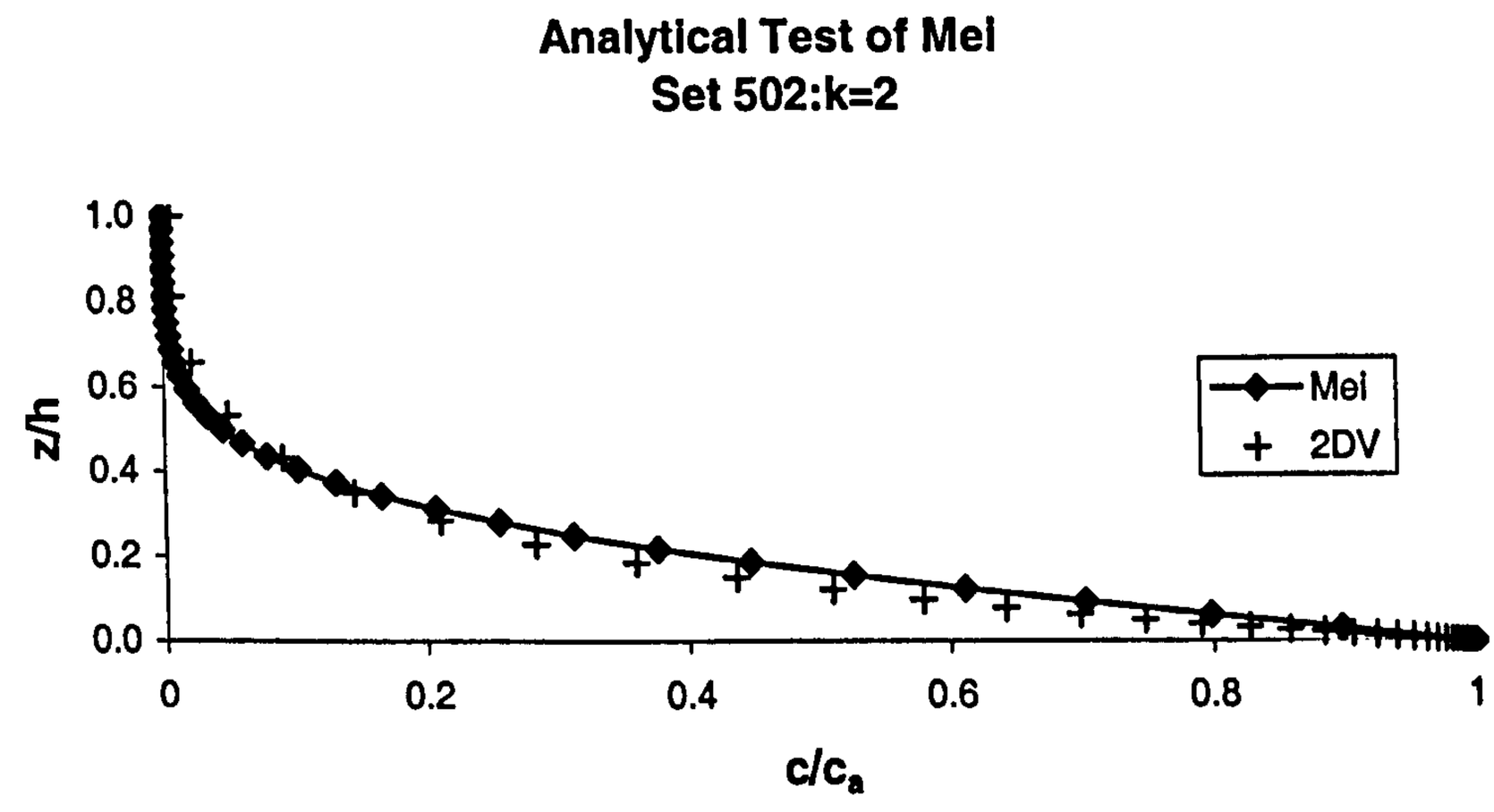

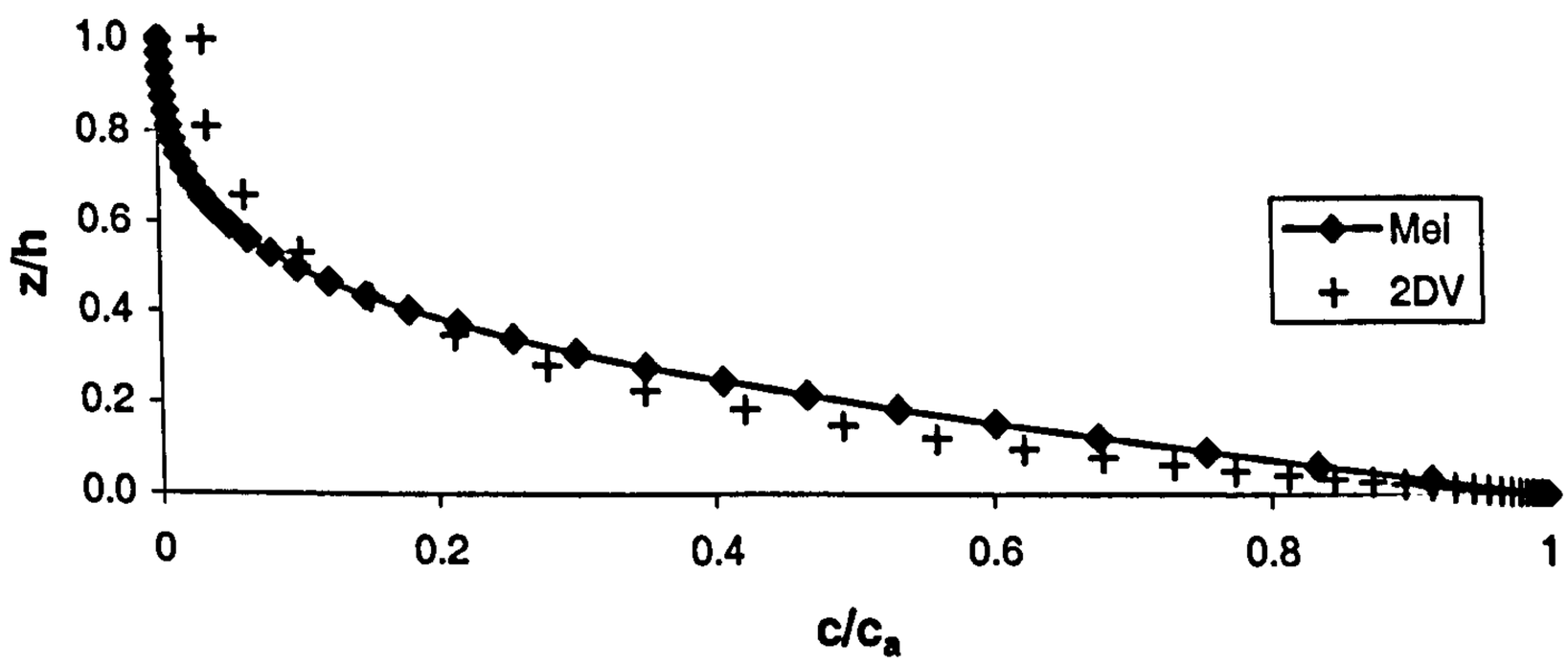

Figure 6.4.2a-c: Comparison of concentration profiles produced by the conventional 2DV model and the analytical method of Mei (1969)

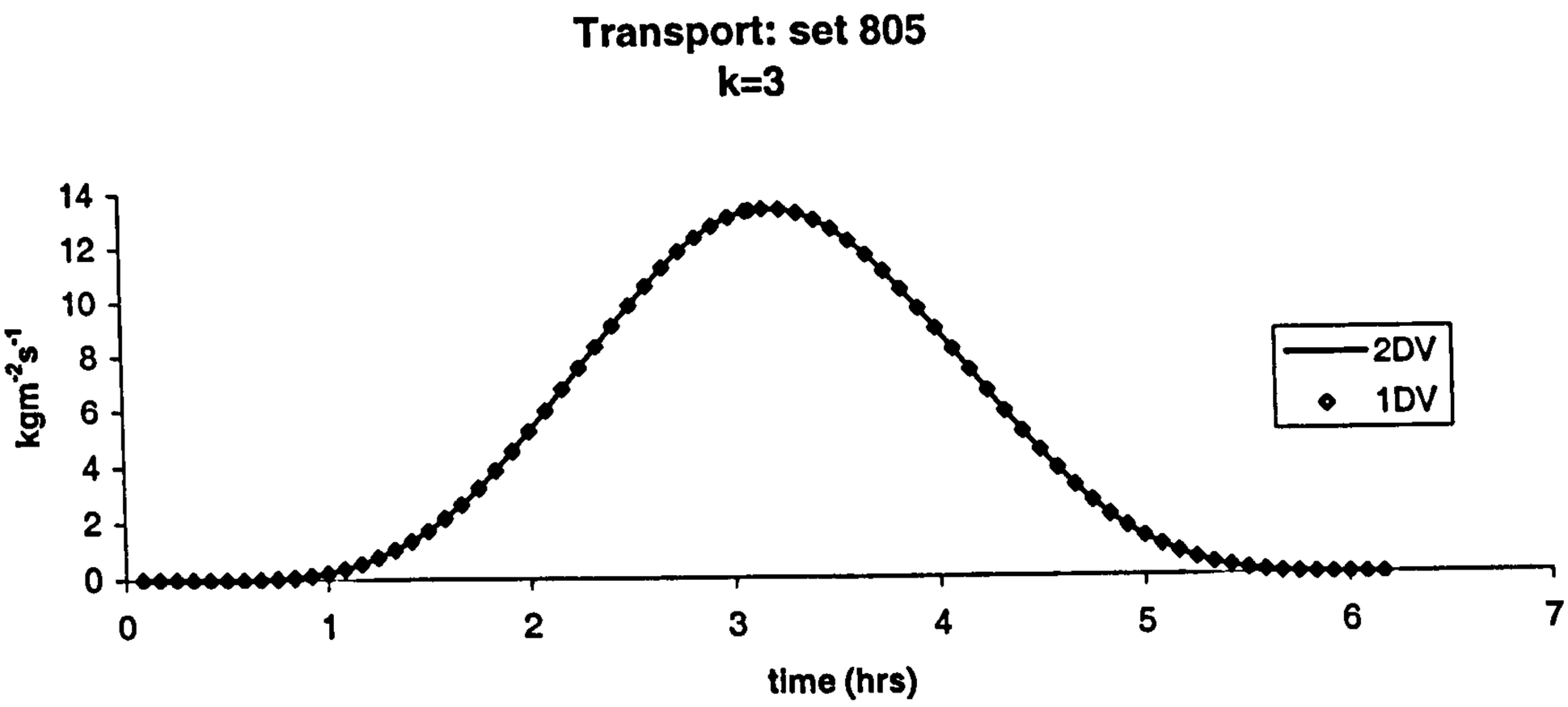

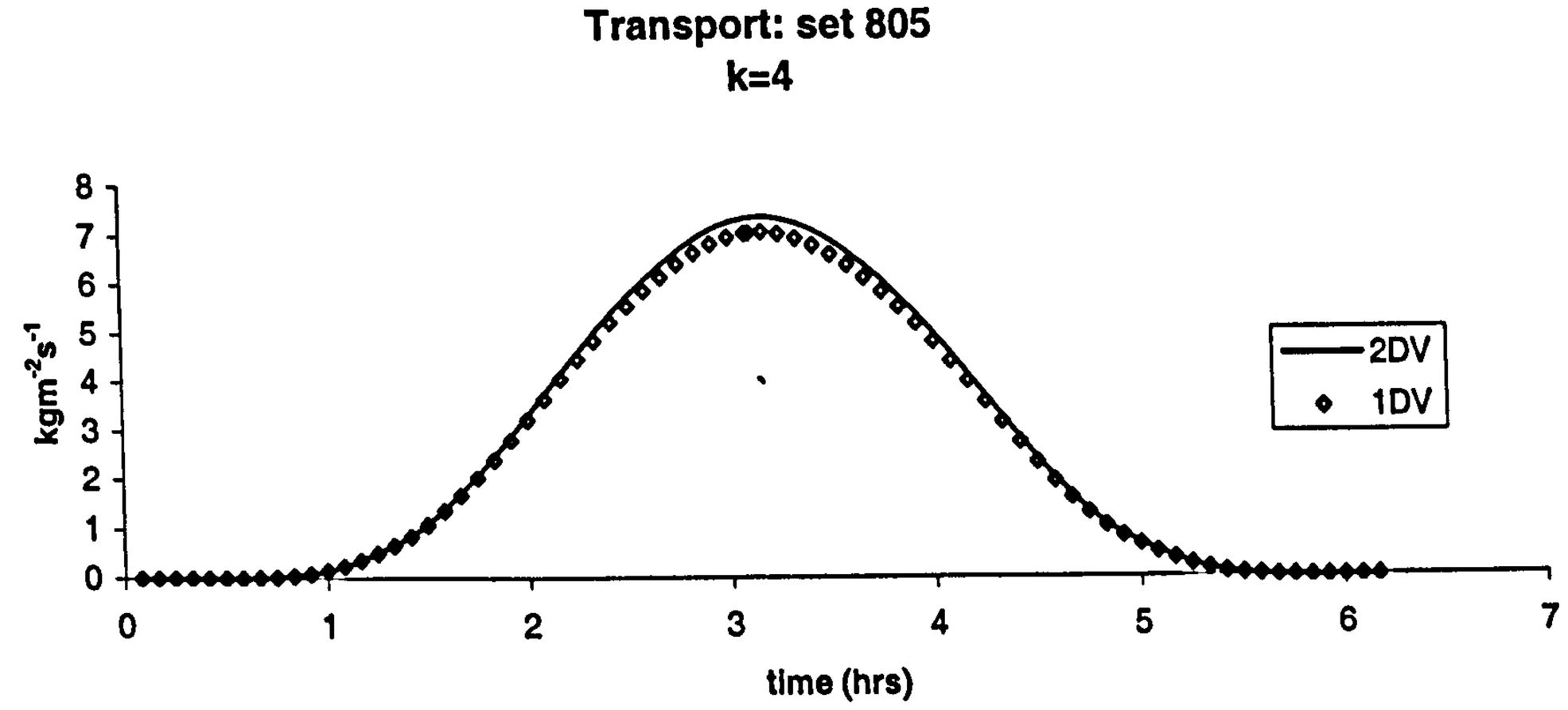

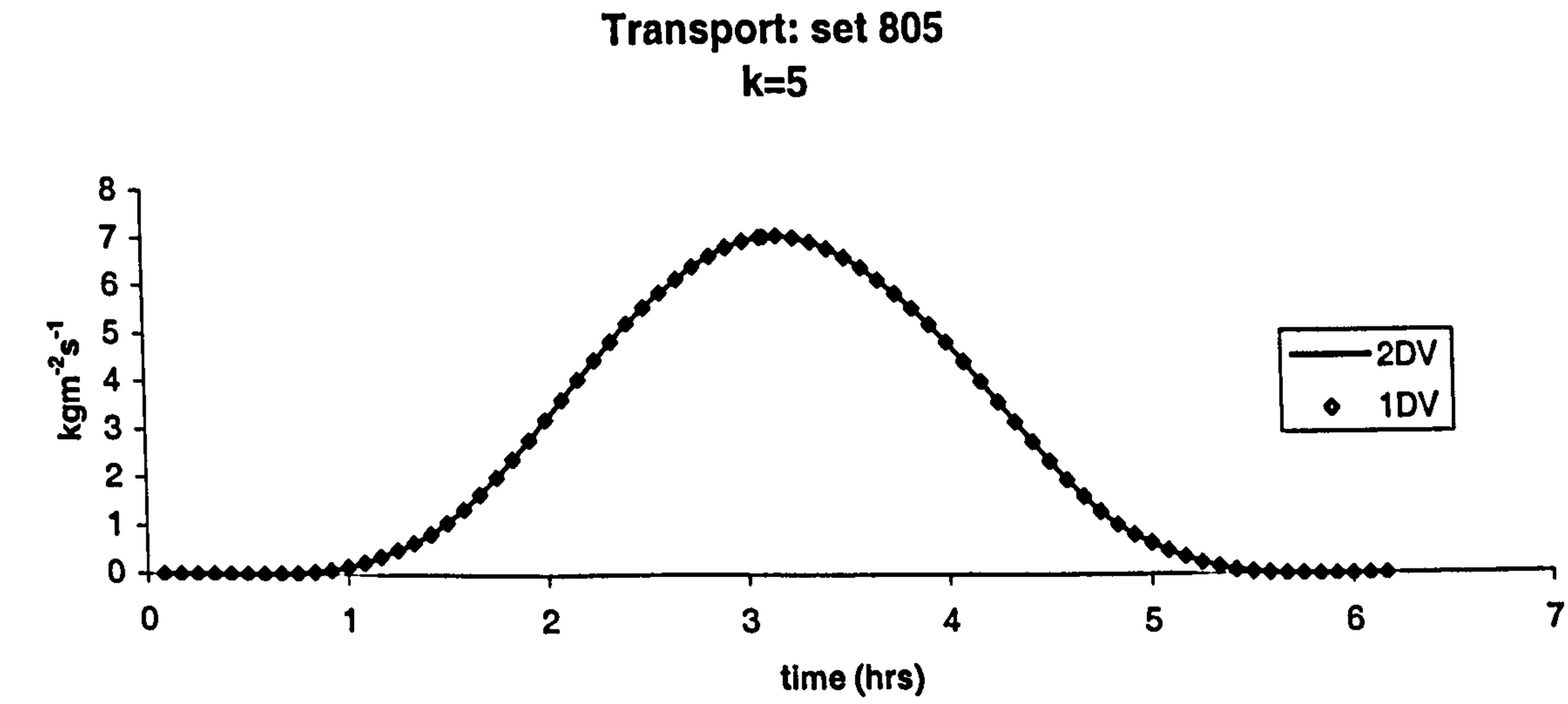

Figure 6.5.1a-c: Effect of longitudinal advection on the 1DV model

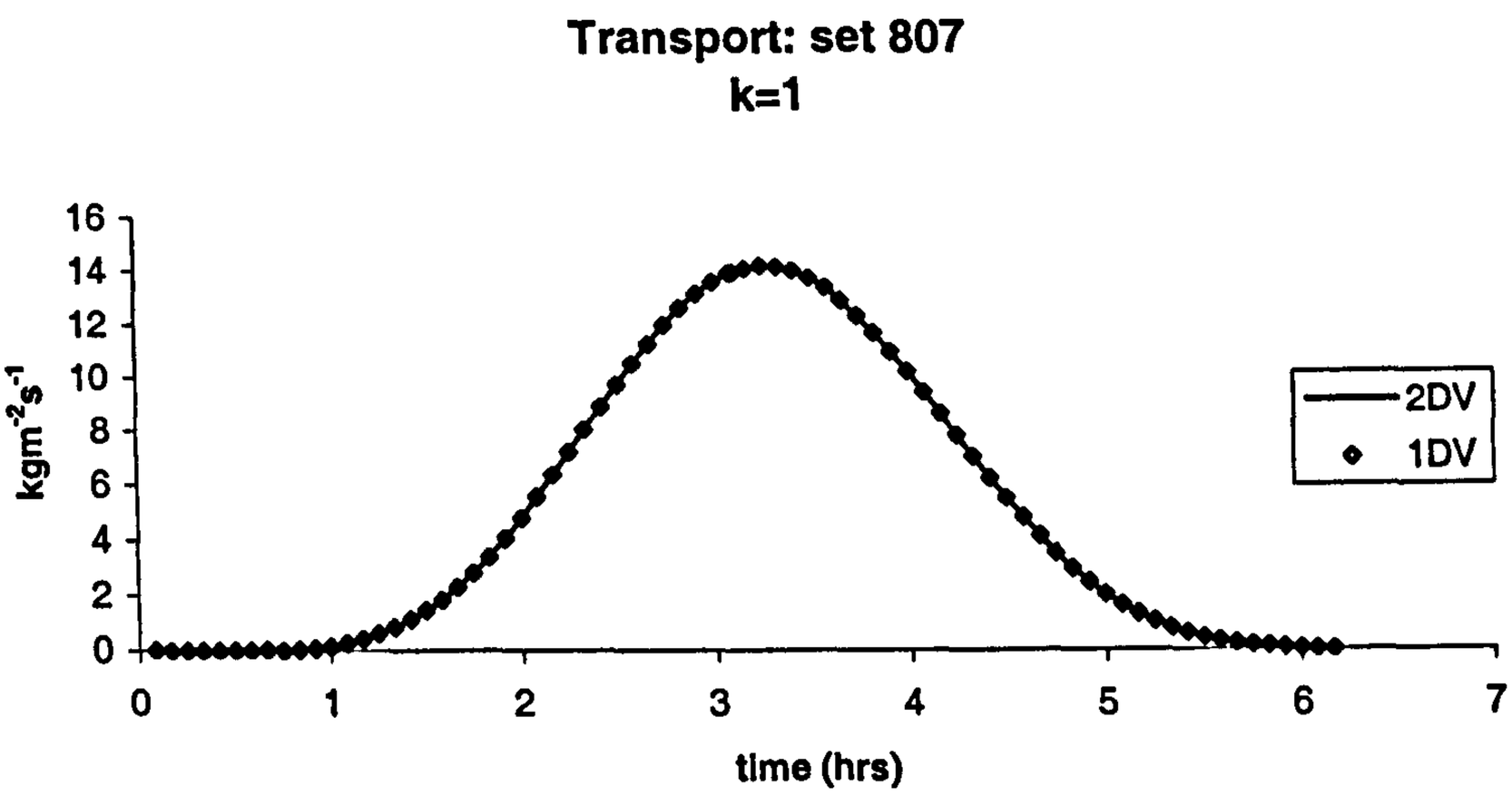

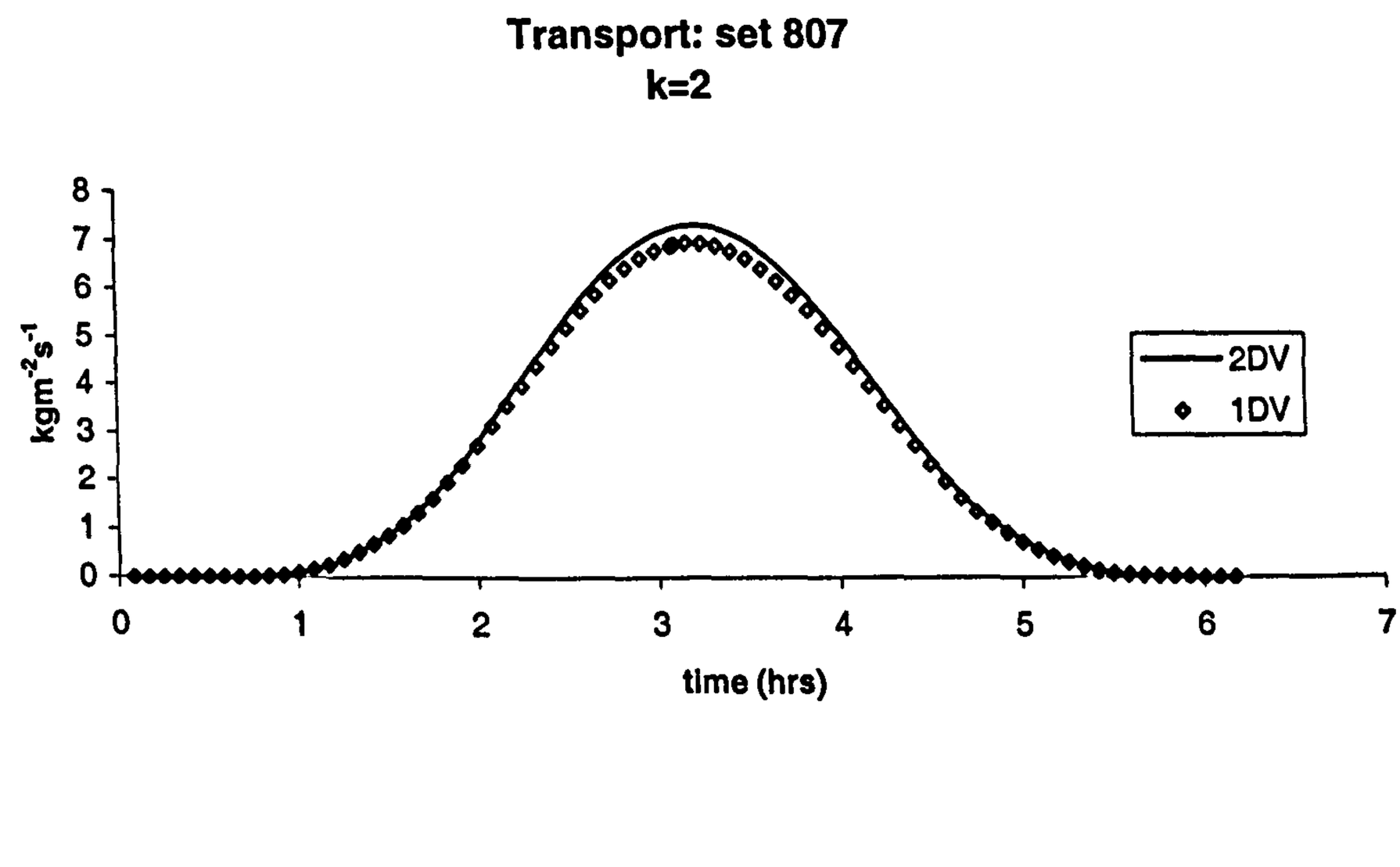

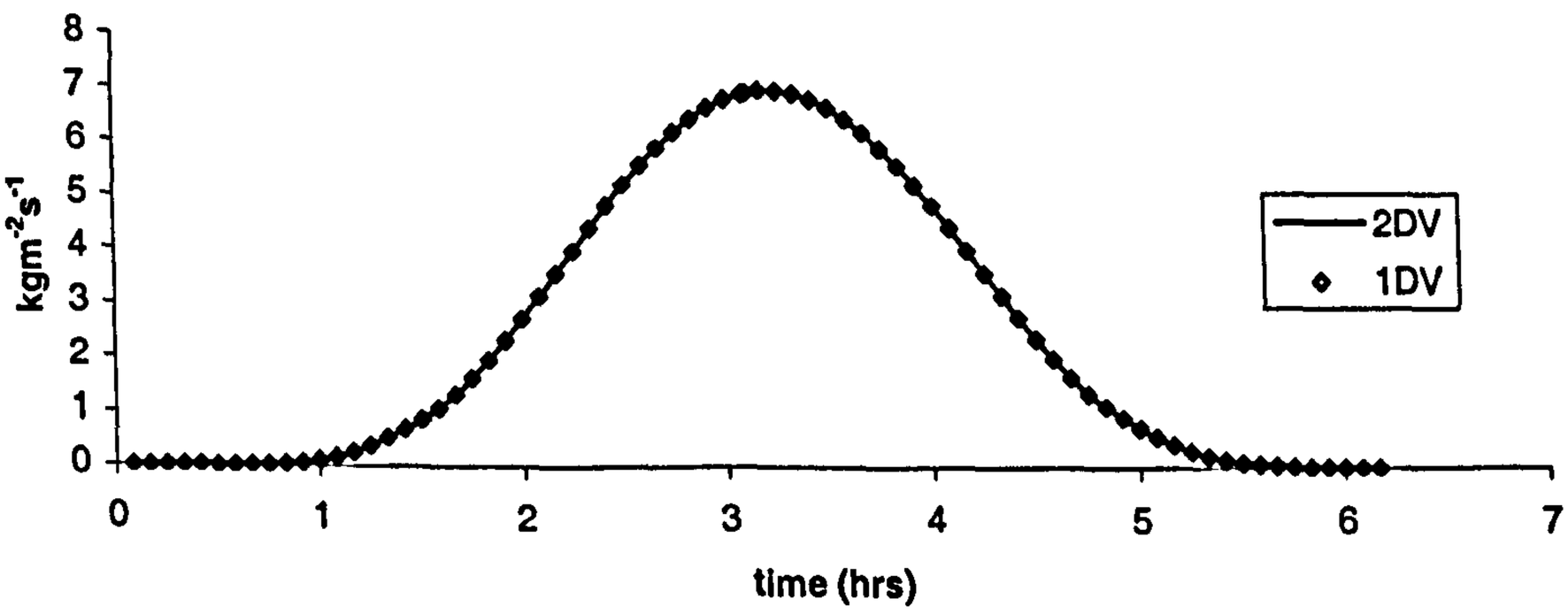

Figure 6.5.2a-c: Effect of longitudinal advection on the 1DV model

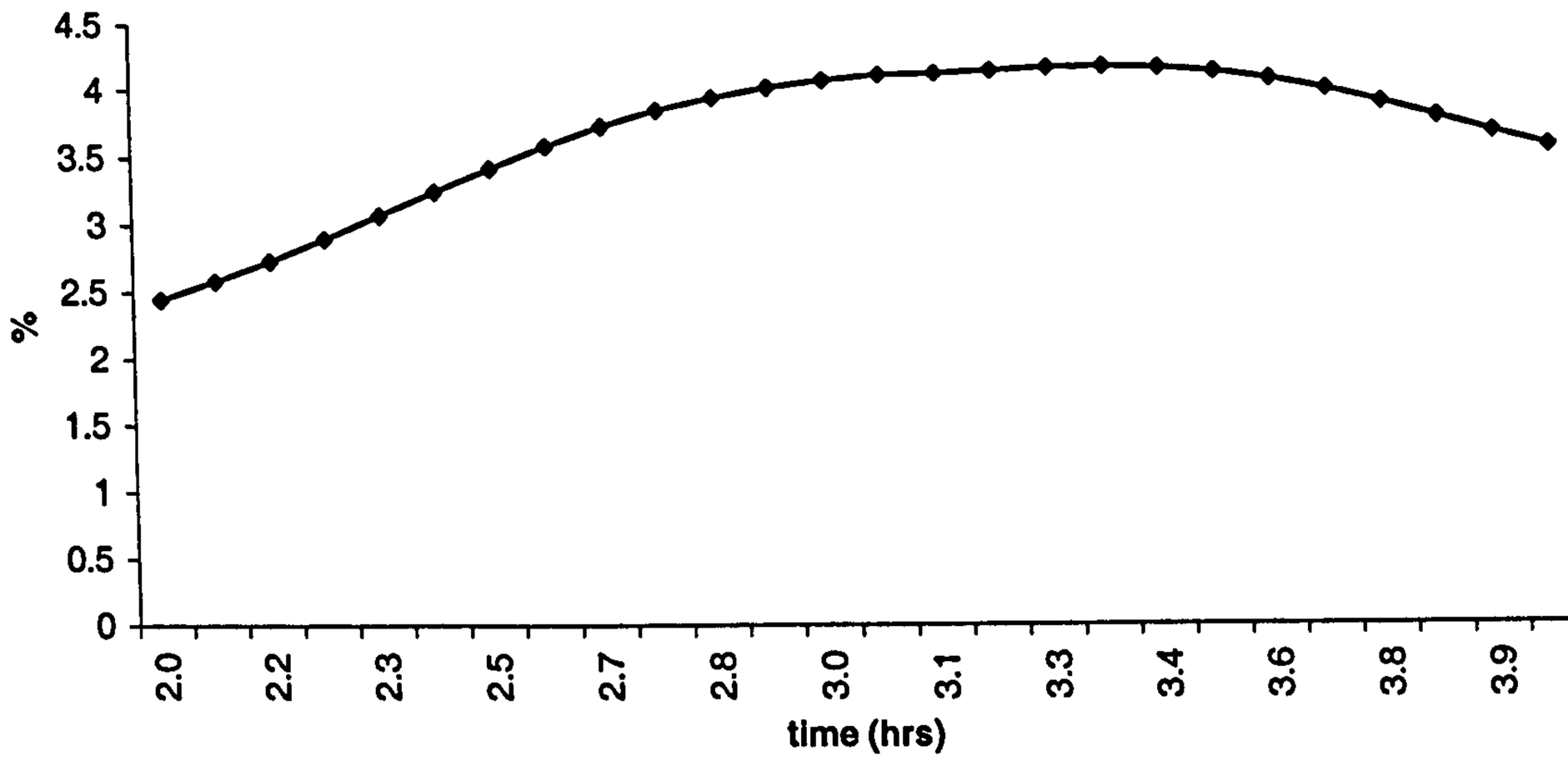

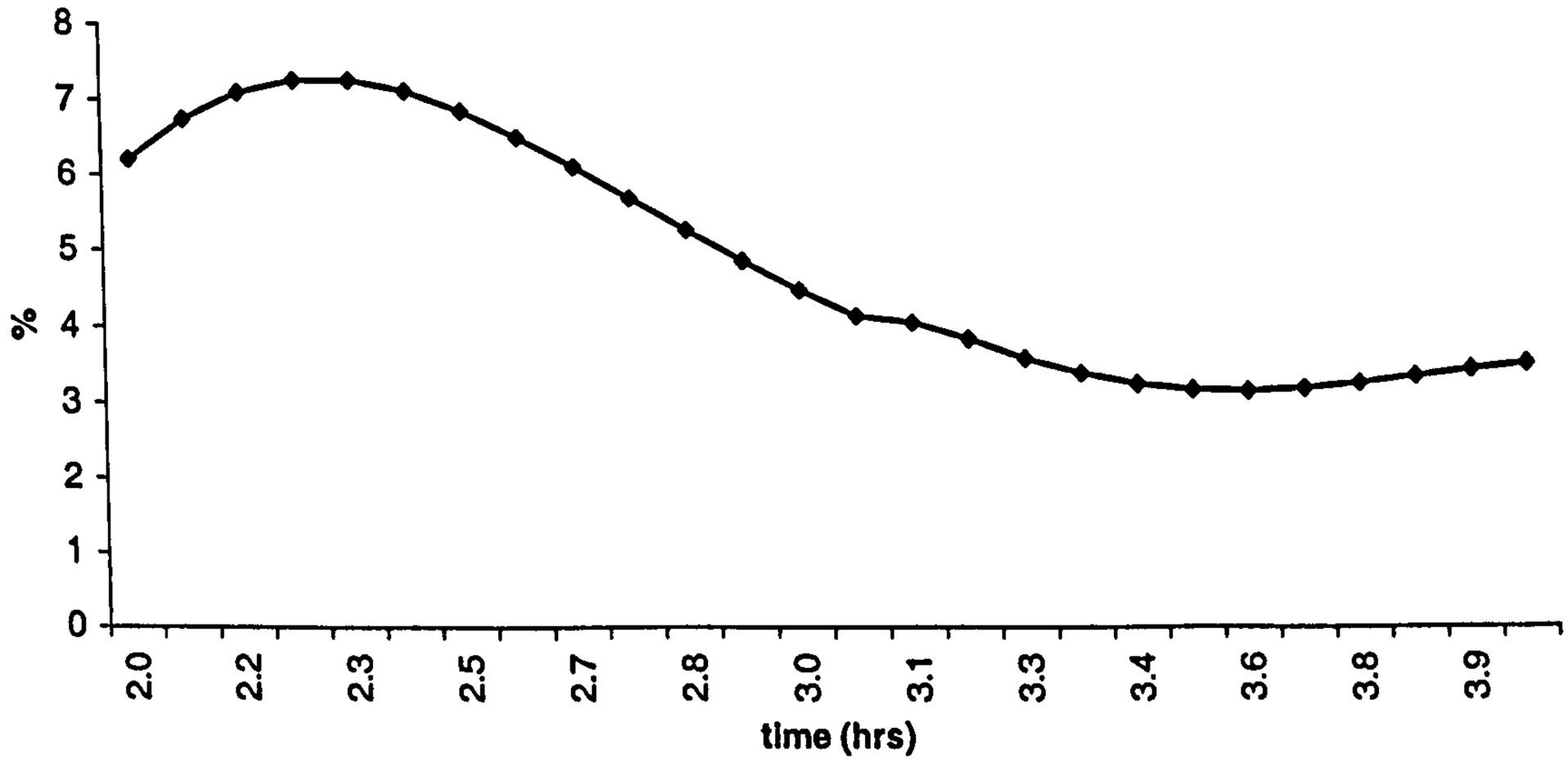

Figure 6.5.3a&b: Mid-tide difference to show the effect of longitudinal advection on the 1DV model

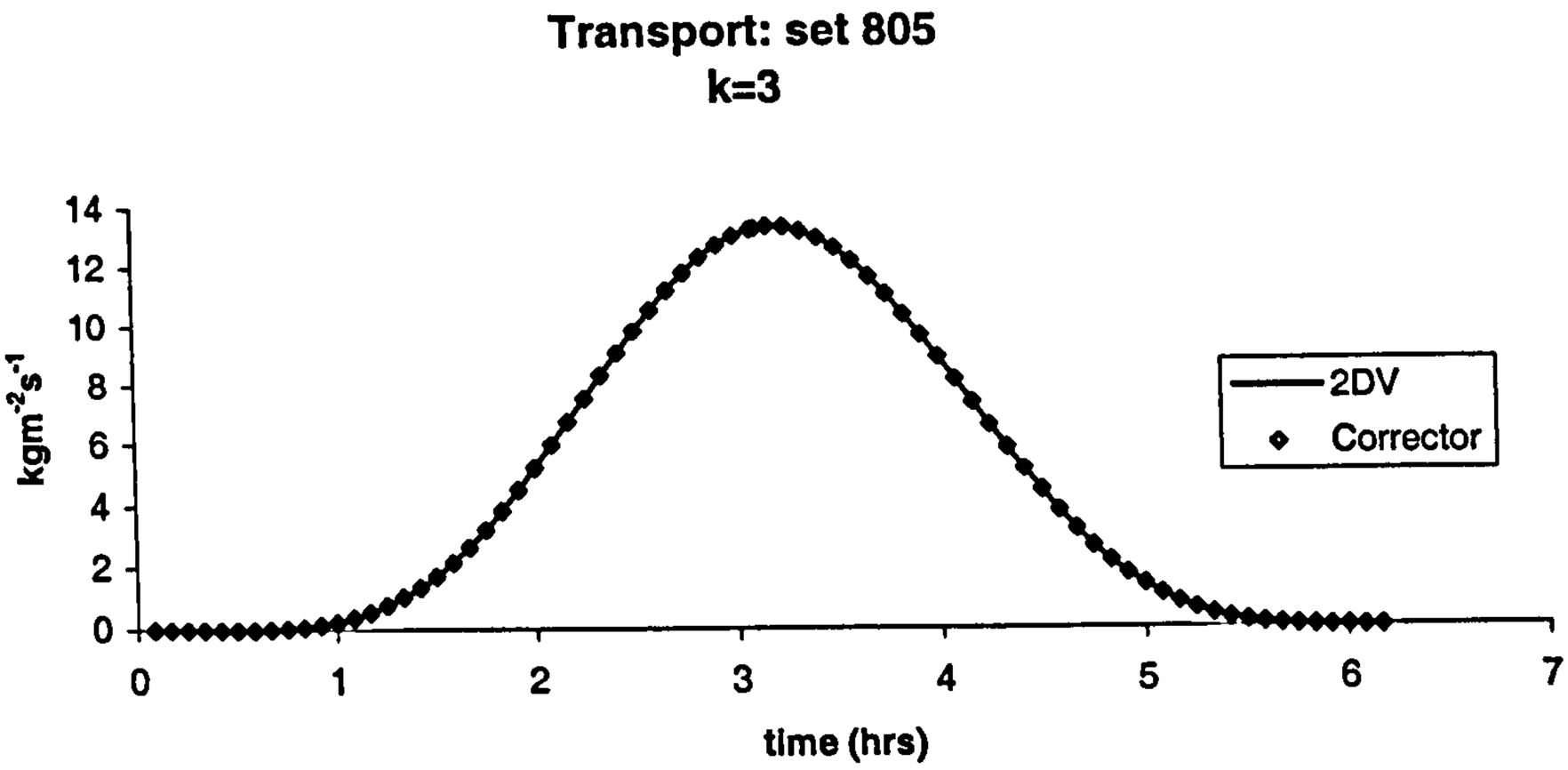

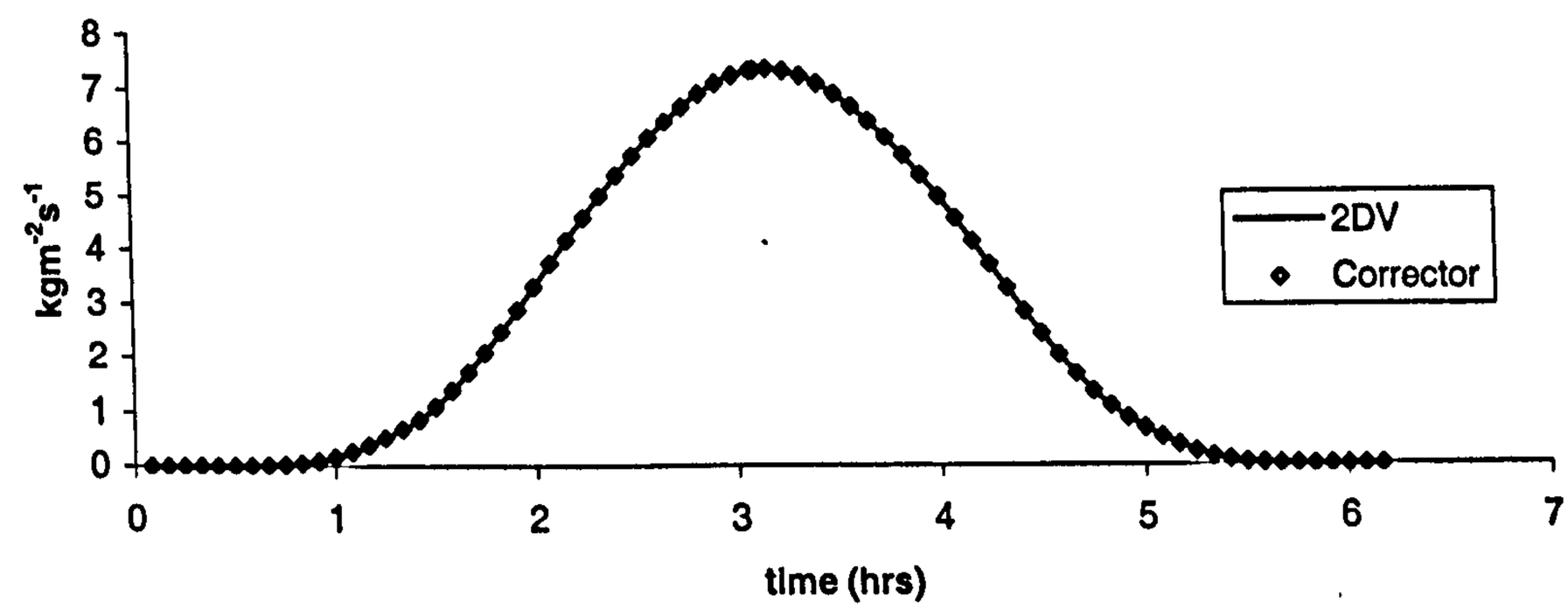

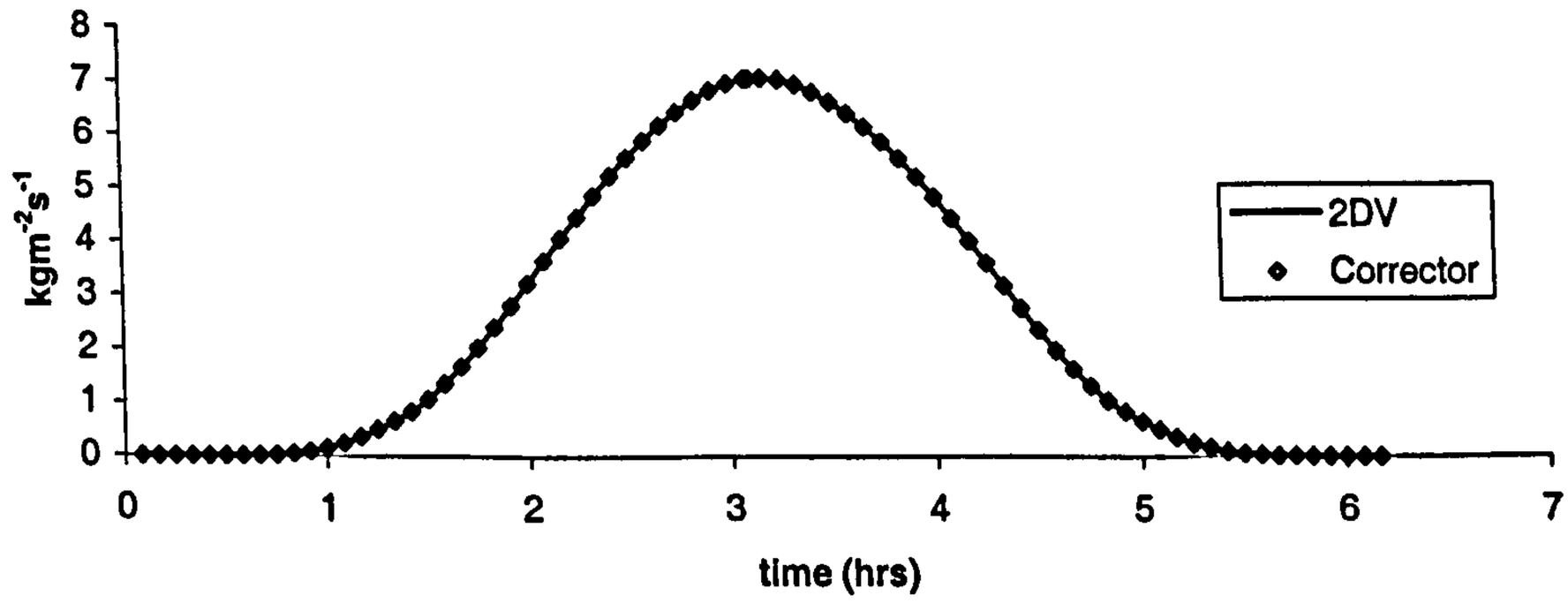

Figure 6.5.4a-c: Comparison of conventional 2DV model with the new Corrector method

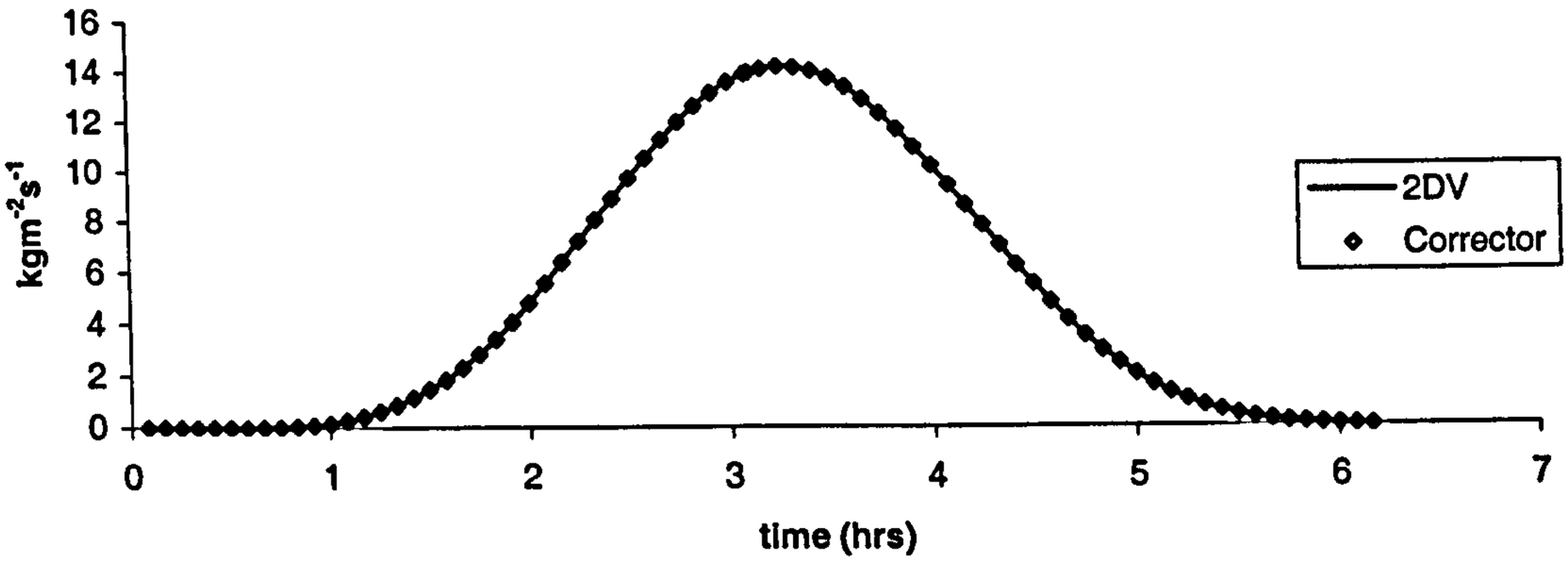

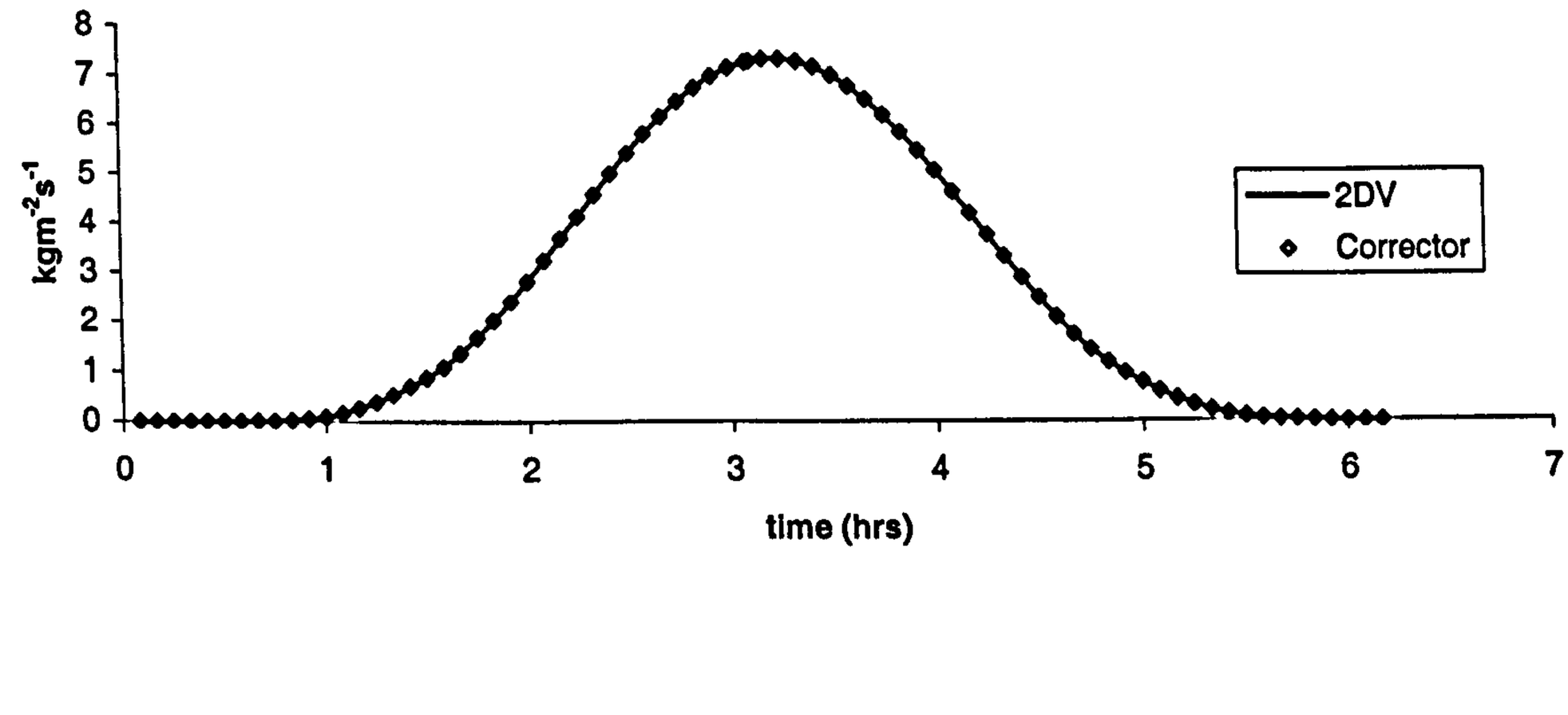

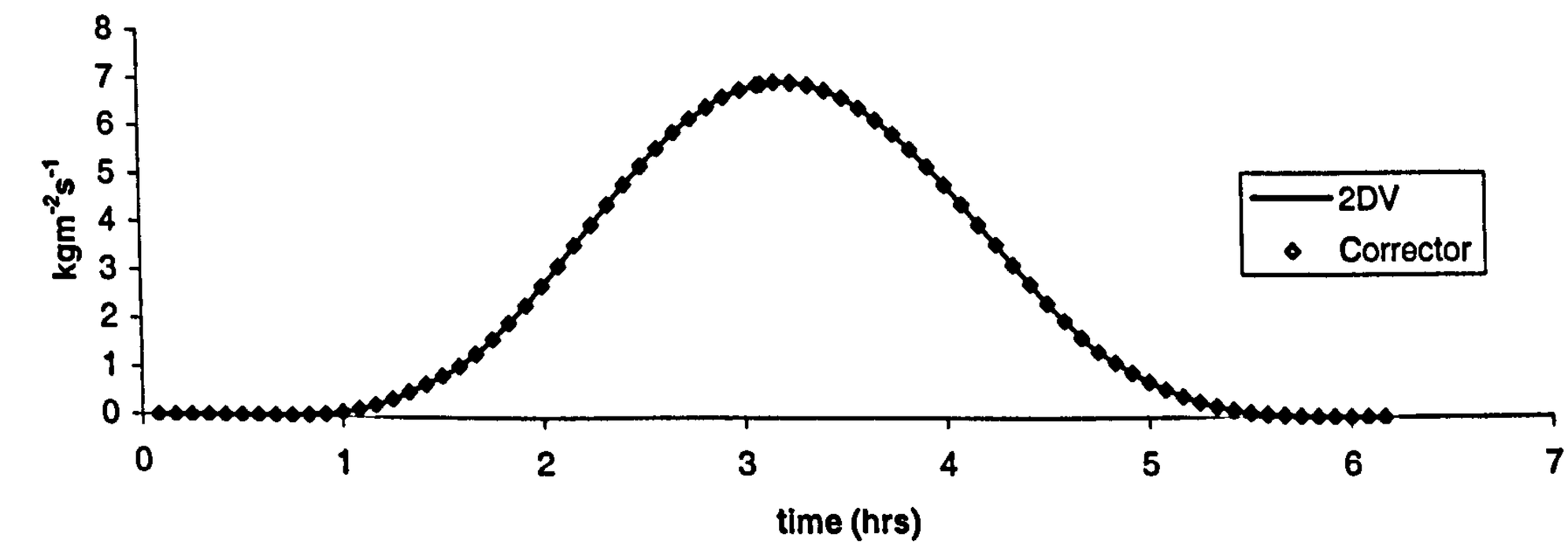

Figure 6.5.5a-c: Comparison of conventional 2DV model with the new Corrector method

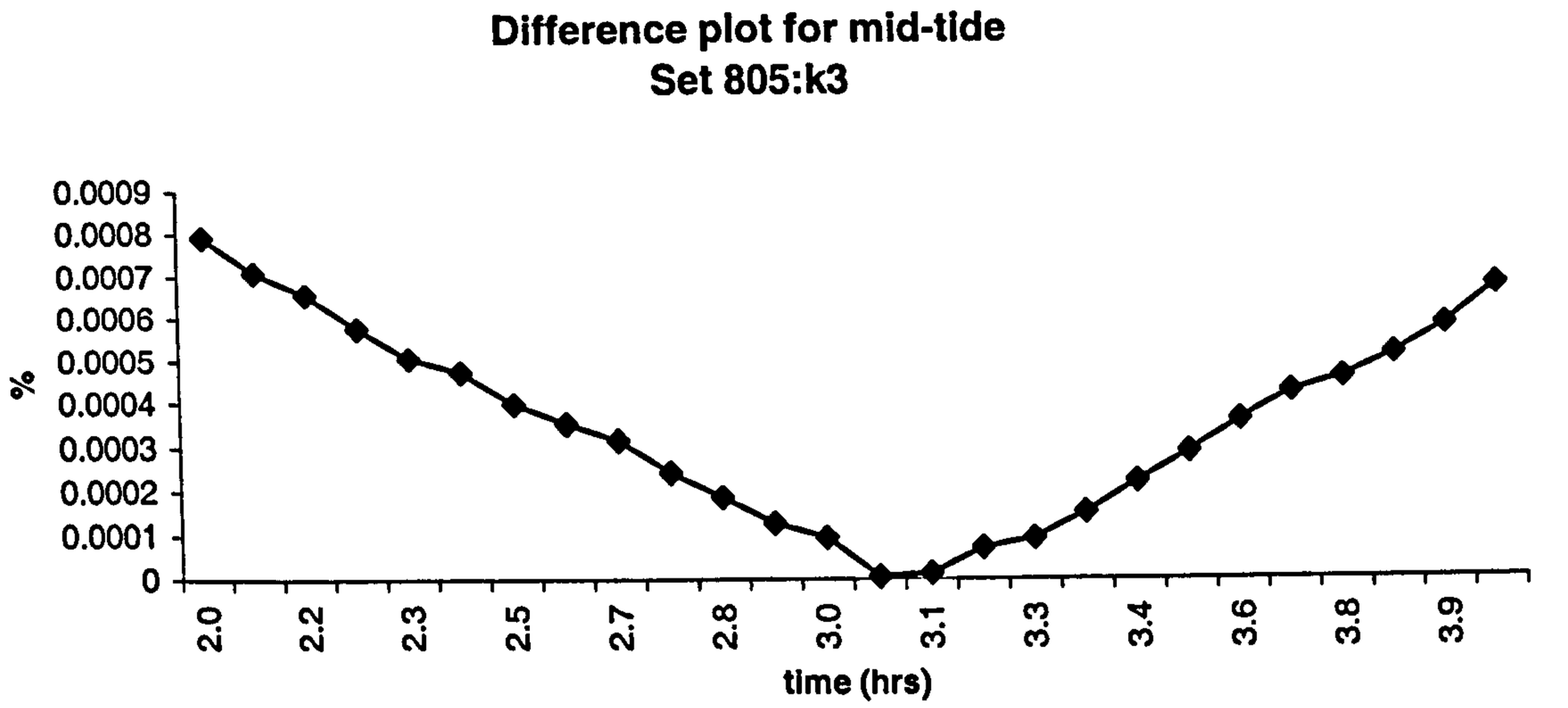

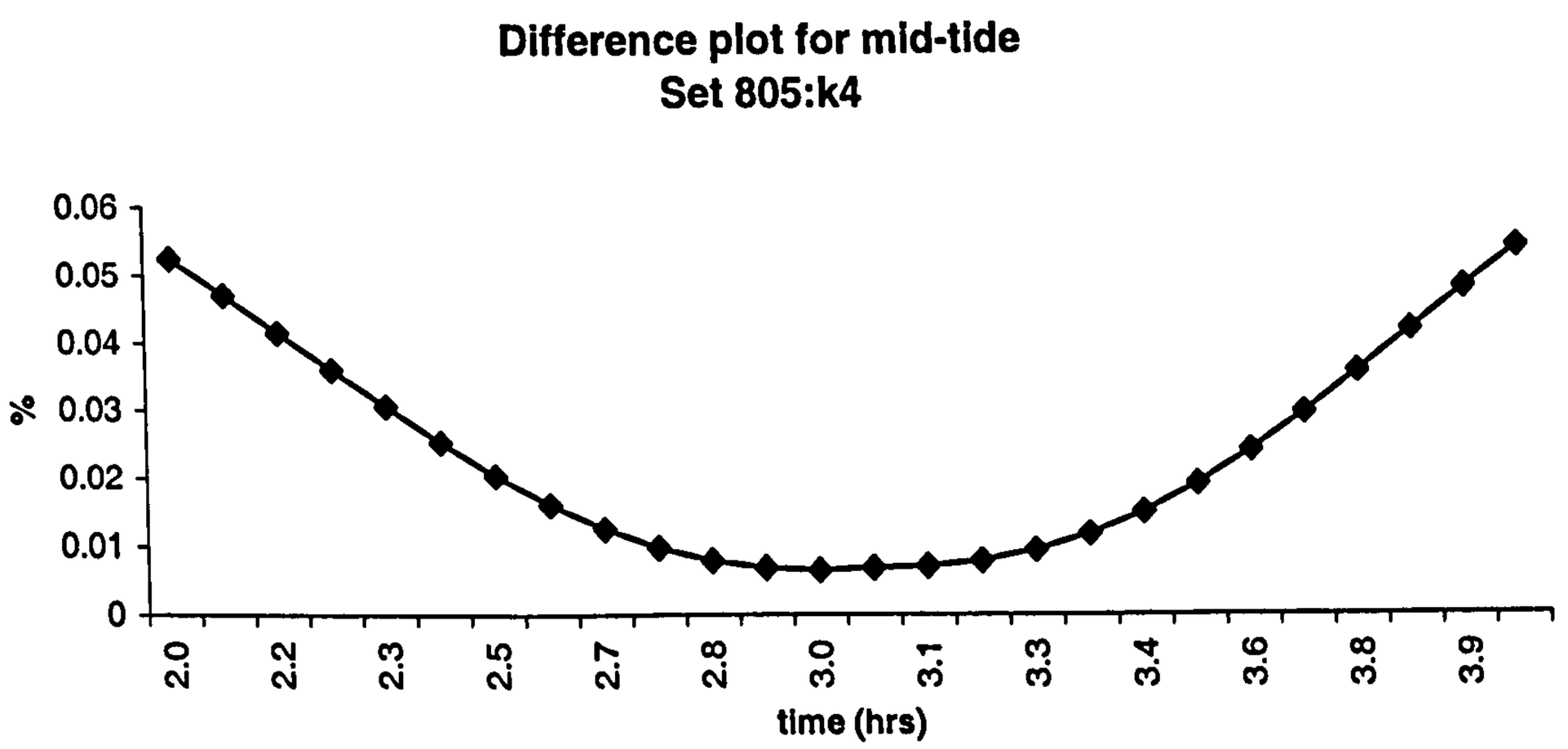

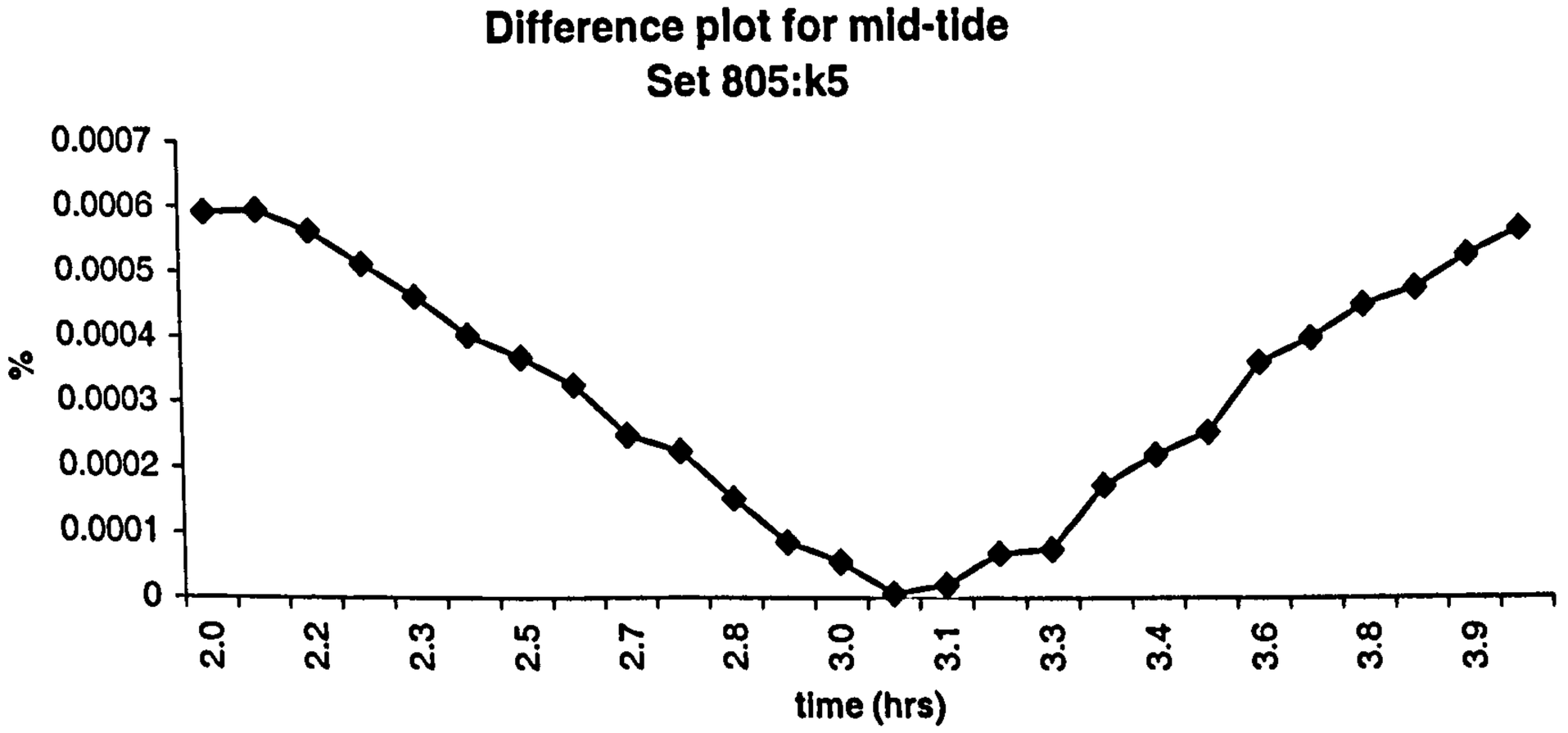

Figure 6.5.6a-c: Difference between conventional 2DV method and Corrector method during the mid-tide phase.

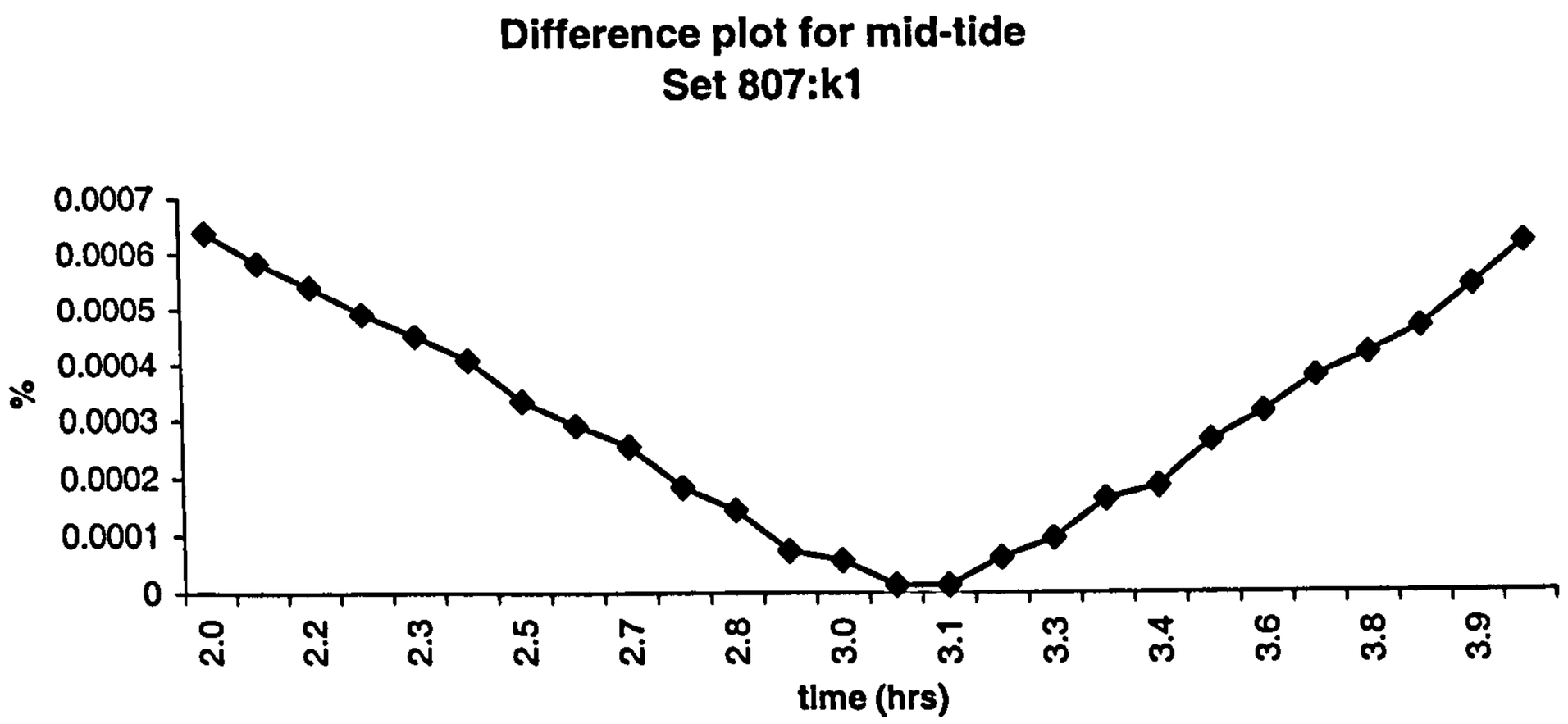

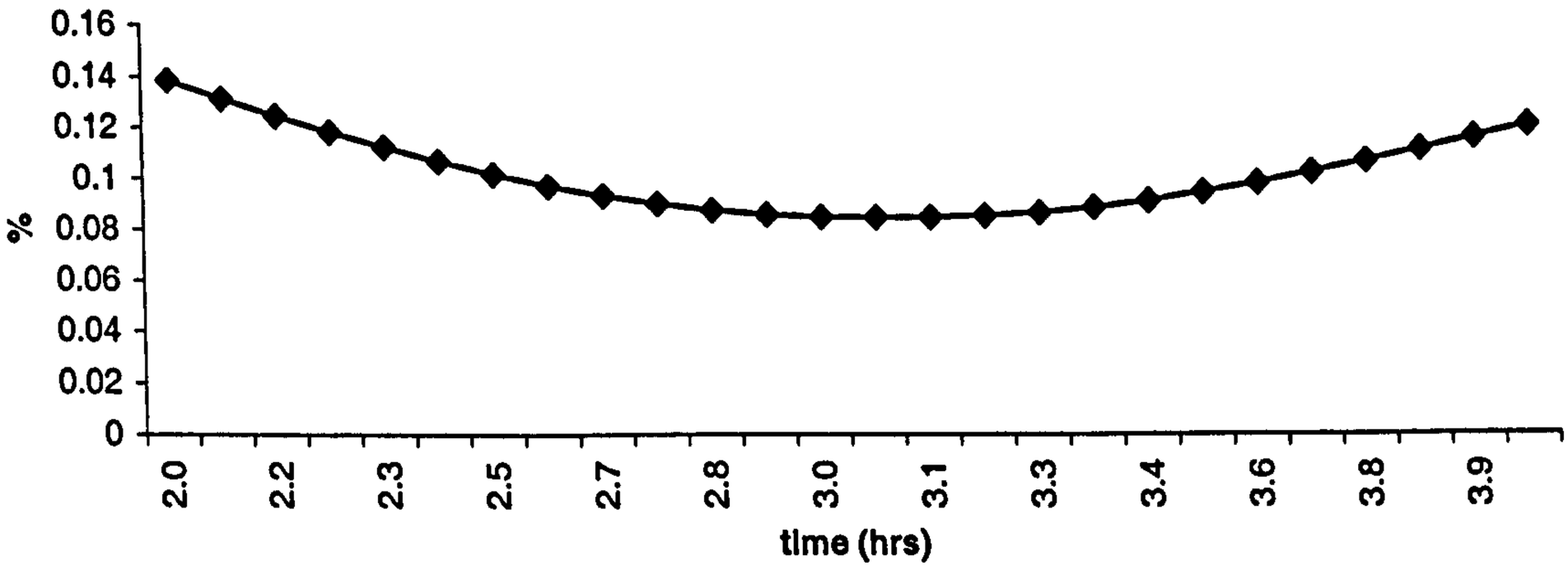

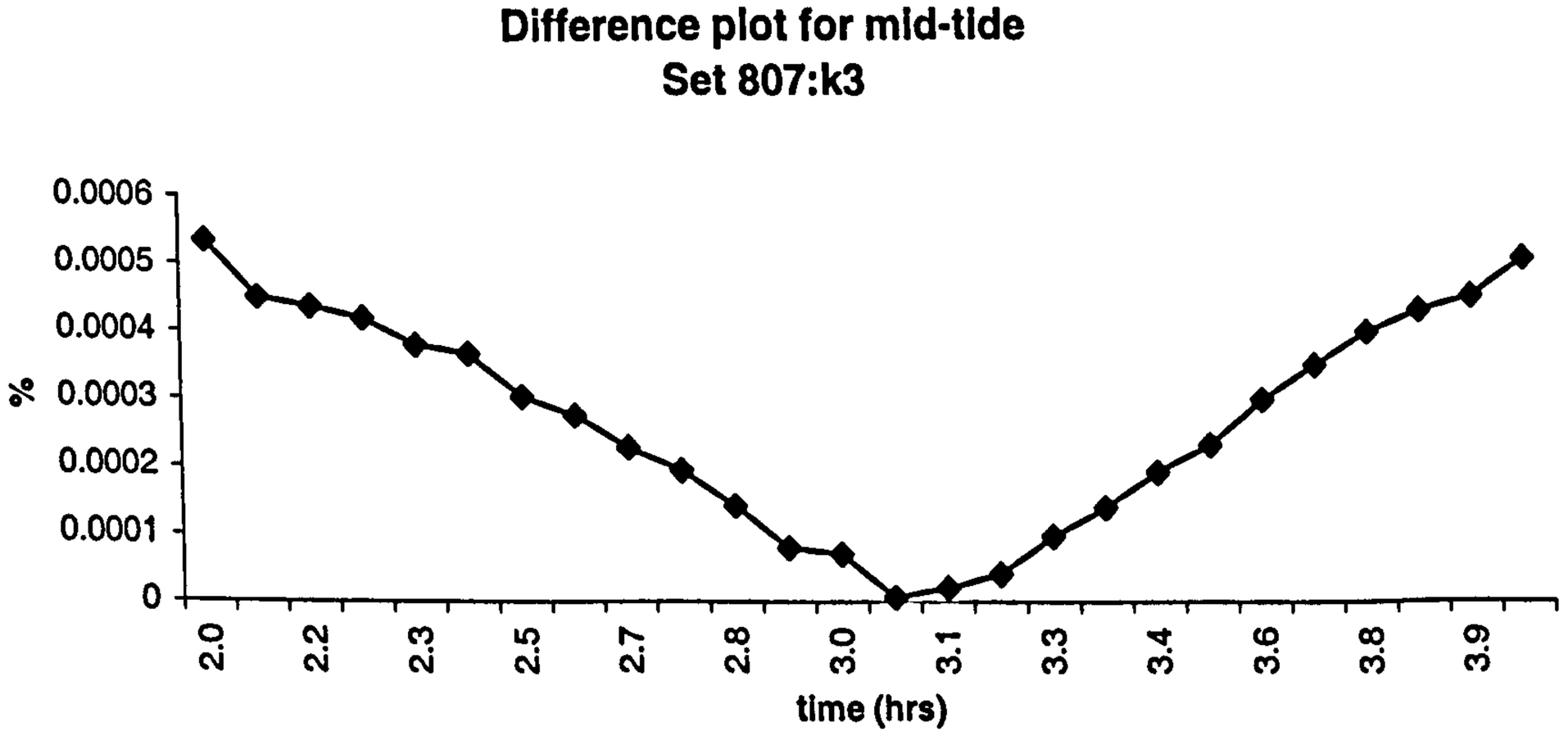

Figure 6.5.7a-c: Difference between conventional 2DV method and Corrector method during the mid-tide phase.

Chapter 7

Parameterisation of the 1DV Model

7.1 Introduction

The new Corrector method, described in chapter 5, has produced a much quicker way of calculating suspended sediment transport rates without significant loss of accuracy; however, it may be possible to improve the method still further. By employing a parameterised version of the 1DV model, it is hoped that the computation time for the new Corrector method will be further reduced. It is also important to assess the impact of the parameterisation on the accuracy of the model. This chapter therefore presents a preliminary investigation into the accuracy of a parametric version of the numerical 1DV model.

The method of parameterisation replaces the complex system of governing equations by simple algebraic formulae. These formulae are based on non-dimensional parameter groups suggested by the physical properties of the system. By choosing an appropriate functional form for these parameter groups the physical properties of the system are retained. Thus, a system of equations requiring numerical methods for its solution can be reduced to a series of algebraic equations that can be solved analytically.

Section 7.2 discusses available parametric models that are based on assuming a power law relation. However, since tidal sediment transport is periodic, it seems reasonable to assume the functional form of the parameterisation to be based on a Fourier Series approximation, details of which are given in section 7.3. The parameterisation is then concerned with replacing the coefficients of the Fourier series with formulae based on the non-dimensional parameter groups.

The functional form of each parameterisation is tested using regression analysis. The parameterised 1DV model is then tested against the numerical 1DV model for seven different tidal input sets.

7.2 Power Law

One of the main problems associated with parameterisation is determining the functional form that the parameterisation should take. Obviously the function should adhere to the same physical properties as the more complicated system, as far as possible. Properties such as maxima and limiting values shown by the system of equations should be replicated by the function used in the parameterisation.

Van Rijn (1993) uses a simple power law function to parameterise the volumetric suspended load transport in rivers for steady flow. Van Rijn also states that this model is capable of giving a first estimate; this calls into question its accuracy for actual field application. The model is described by the formula given below.

$$\frac{q_{s,c}}{\bar{u}h} = 0.012\left(\frac{\bar{u}-\bar{u}_{cr}}{\sqrt{\{s-1\}gd_{50}}}\right)^{2.4}\left(\frac{d_{50}}{h}\right)\left(\frac{1}{D_*}\right)^{0.6} \qquad (7.2.1)$$

where,

$q_{s,c}$ -Volumetric suspended load transport (m^2s^{-1})

$\bar{u}_{cr}$ -Critical depth-averaged velocity

h -Water depth

$\bar{u}$ -Depth-average velocity

$D_* = \left(\frac{(s-1)g}{\nu^2}\right)^{1/3} d_{50}$ - Van Rijn particle parameter

s - Relative density of the sediment particles

g -Acceleration due to gravity

d_{50} -Median grain size

ν -Kinematic Viscosity

O'Connor and Nicholson (1997) also use a power law concept to produce a parameterisation for current influenced estuaries. The suspended sediment transport rate (T_s) is first split into mean transport ($\overline{T}_s$) and lag transport (ΔT_s):-

$$T_s = \overline{T}_s\left(1 \pm \frac{\Delta T_s}{2}\right) \tag{7.2.2}$$

The parameterisation for the lag component is given as:-

$$Y = \frac{\Delta T_s}{2}$$

$$Y = 1 \qquad \text{for} \quad X < X_c'$$

$$\ln(Y) = \ln(Y_1)\left(\frac{X - X_c'}{1 - X_c'}\right) \qquad \text{for} \quad X_c' \le X < X_0 \tag{7.2.3}$$

$$Y = Y_0\left(\frac{1 - X}{1 - X_0}\right)^m \qquad \text{for} \quad X \ge X_0$$

where,

$X = \dfrac{\overline{u}}{\overline{u}_m}$ -Tidal stage defined in terms of velocity

X_c' -X value at initiation of motion

Y_0 -Value of equation 7.2.3 when $X = X_0$

Y_1 -Value of Y when $X = 1$ (i.e. at maximum velocity)

Further parameterisations are presented for Y_1, X_c', X_0 and m in terms of non-dimensional groups, each raised to a power.

The parameterisation of the mean transport is given as:-

$$T_* = A_* U_*^{\,n} \tag{7.2.4}$$

where,

$$T_* = \frac{\overline{T}_s}{\left(\sqrt{\Delta g} d_{50}^{3/2} \rho_s\right)}$$

$$A_* = \exp(\gamma)$$

$$\gamma = -5.5 \ln(E)$$

$$U_+ = \frac{\overline{u}}{\sqrt{\Delta g d_{50}}}$$

$$E = d_{50}\left[\frac{\Delta g}{\nu^2}\right]^{1/3}$$

Δ -Submerged relative density of the grains

ρ_s -Density of the sediment particle

A value of $n = 3.5$ is given for the particular field application considered. The model is shown to agree with analytical solutions and also produces good agreement with actual field data.

It can be seen that the model is based on that of Van Rijn but has been modified to allow for tidal lag.

Although the model produces good agreement with field data, O'Connor (1999) suggests that a better parameterisation may be found by using a Fourier Series approximation for tidal sediment transport rates.

7.3 Fourier Analysis

7.3.1 Theory

By considering tidal sediment transport, one physical property is immediately obvious, i.e. the periodicity of the tide. One method used to approximate periodic functions is that of the Fourier Series. The Fourier Series uses an infinite sum of the trigonometric functions cos and sin, each with different amplitude and phase.

The Fourier Series approximation to a time dependent function F, which has frequency ω and period T, is given below.

$$F(t) = 0.5a_0 + \sum_{n=1}^{\infty} a_n \cos(n\omega t) + \sum_{n=1}^{\infty} b_n \sin(n\omega t) \qquad (7.3.1)$$

where the Fourier coefficients a_0, a_n and b_n are defined by:-

$$a_0 = \frac{2}{T}\int_0^T F(t)dt$$

$$a_n = \frac{2}{T}\int_0^T F(t)\cos(n\omega t)dt \quad ; \quad n = 1,2,.....$$

$$b_n = \frac{2}{T}\int_0^T F(t)\sin(n\omega t)dt \quad ; \quad n = 1,2,.....$$

7.3.2 Tidal Application

The idea of using Fourier series to approximate tidal suspended sediment transport rates was proposed by O'Connor (1999). However, before a Fourier approximation can be determined, it is first necessary to make some basic assumptions.

If flow reversal effects are ignored then the flood and ebb stages of the tide can be considered separately. In practice, the model is only run for the flood stage. If the flood stage is repeated, figure 7.3.1, so that it covers the entire tidal period, then equation (7.3.1) can be simplified. For this situation, only the even Fourier coefficients are present, James (1992). Again, the model is only run for the original flood period.

.

The defining equations are now given by:-

$$F(t) = 0.5a_0 + \sum_{n=1}^{\infty} a_{2n} \cos(2n\omega t) + \sum_{n=1}^{\infty} b_{2n} \sin(2n\omega t) \qquad (7.3.2)$$

with,

$$a_{2n} = \frac{4}{T}\int_0^{T/2} F(t)\cos(n\omega t)dt \quad ; \quad n = 0,1,2,.....$$

$$b_{2n} = \frac{4}{T}\int_0^{T/2} F(t)\sin(n\omega t)dt \quad ; \quad n = 1,2,.....$$

Since tides can be flood or ebb dominated, the time for the crossover is not always half of the tidal period. To allow the model to cope with this situation, twice the duration of the flood stage of the tide, up, is used as the period of the Fourier approximation.

[N.B: $up = tp$ for neither flood nor ebb dominated tides]

The Fourier approximation to the tidal sediment transport rates during the flood stage of the tide is now given by:-

$$T_s(t) = 0.5a_0 + \sum_{n=1}^{\infty} a_{2n}\cos(2n\omega t) + \sum_{n=1}^{\infty} b_{2n}\sin(2n\omega t) \qquad (7.3.3)$$

$$a_{2n} = \frac{4}{up}\int_0^{up/2} T_s(t)\cos(n\omega t)dt \quad ; \quad n = 0,1,2,.....$$

$$b_{2n} = \frac{4}{up}\int_0^{up/2} T_s(t)\sin(n\omega t)dt \quad ; \quad n = 1,2,.....$$

where,

$$\omega = \frac{2\pi}{up}$$

Further simplifications can be achieved by considering the sediment transport rate when the depth-average tidal velocity during the flood stage is at its maximum, i.e. at time $t_m = \frac{up}{4}$.

$$T_m = 0.5a_0 + \sum_{n=1}^{\infty} a_{2n}\cos(2n\omega t_m) + \sum_{n=1}^{\infty} b_{2n}\sin(2n\omega t_m) \qquad (7.3.4)$$

Simple manipulation gives an expression for a_0 :-

$$0.5a_0 = T_m - \sum_{n=1}^{\infty} a_{2n}\cos(2n\omega t_m) - \sum_{n=1}^{\infty} b_{2n}\sin(2n\omega t_m)$$

Substituting this expression back into equation (7.3.3) gives:-

$$T_s(t) = T_m + \sum_{n=1}^{\infty} a_{2n}\{\cos(2n\omega t) - \cos(2n\omega t_m)\} + \sum_{n=1}^{\infty} b_{2n}\{\sin(2n\omega t) - \sin(2n\omega t_m)\}$$

Now,

$$2n\omega t_m = 2n\frac{2\pi}{up}\frac{up}{4} = n\pi$$

$$\sin(n\pi) = 0 \quad \forall \; n$$

$$\cos(n\pi) = \begin{cases} -1 & ; \quad n\ odd \\ +1 & ; \quad n\ even \end{cases}$$

Thus, the Fourier approximation for tidal sediment transport takes the form:-

$$T_s(t) = T_m + \sum_{n=1}^{\infty} a_{2n}\{\cos(2n\omega t) + (-1)^{n-1}\} + \sum_{n=1}^{\infty} b_{2n}\sin(2n\omega t) \qquad (7.3.5)$$

7.3.3 Mean and Lag Transport

O'Connor (1999) proposed that there are certain properties of the Fourier Series that support its use in the approximation for tidal sediment transport.

Consider the mean transport rate ($\overline{T}_s(t)$). This is the average value of the transport rates given at the same velocity; t_1 is during the accelerating flood stage and t_2 during the decelerating stage; figure 7.3.2.

$$\text{i.e.} \qquad \overline{T}_s(t) = \frac{T_s(t_1) + T_s(t_2)}{2} \tag{7.3.6}$$

Now substitute for $T_s(t_1)$ and $T_s(t_2)$:-

$$\overline{T}_s(t) = T_m + 0.5\sum_{n=1}^{\infty} a_{2n}\left\{\cos(2n\omega t_1) + 2(-1)^{n-1} + \cos(2n\omega t_2)\right\}$$

$$+ 0.5\sum_{n=1}^{\infty} b_{2n}\left\{\sin(2n\omega t_1) + \sin(2n\omega t_2)\right\}$$

If the flood stage is assumed symmetrical (i.e. no bias towards either accelerating or decelerating phase) then:-

$$t_2 = \frac{up}{2} - t_1$$

Now,

$$\cos(2n\omega t_2) = \cos\left\{2n\omega\left(\frac{up}{2} - t_1\right)\right\}$$

$$= \cos(2n\pi)\cos\left(4\frac{n\pi}{up}t_1\right) + \sin(2n\pi)\sin\left(4\frac{n\pi}{up}t_1\right)$$

But,

$$\cos(2n\pi) = 1 \quad \forall n$$

$$\sin(2n\pi) = 0 \quad \forall n$$

$$\rightarrow \quad \cos(2n\omega t_2) = \cos(2n\omega t_1)$$

Similarly,

$$\sin(2n\omega t_2) = -\sin(2n\omega t_1)$$

Hence,

$$\overline{T}_s(t) = T_m + \sum_{n=1}^{\infty} a_{2n}\left\{\cos(2n\omega t_1) + (-1)^{n-1}\right\} \tag{7.3.7}$$

Now consider the lag. This is defined as the difference between transport rates at the same velocity, i.e.:-

$$\Delta T_s = T_s(t_2) - T_s(t_1) \tag{7.3.8}$$

By a similar argument as the mean transport, the following equation is obtained for the lag:-

$$\Delta T_s = -2\sum_{n=1}^{\infty} b_{2n}\sin(2n\omega t_1) \tag{7.3.9}$$

It is interesting to note that the mean transport is determined solely by the 'a' Fourier coefficients whilst the lag solely by the 'b' coefficients. This would seem to suggest that the Fourier Series shares the properties of the physical system and hence supports its use for predicting tidal sediment transport rates.

Having shown that a Fourier Series can be used to predict sediment transport rates, it will be seen later that if $T_m, a_2, a_4, a_6, b_2, b_4$, and b_6 are parameterised, then the Fourier series approach can be used instead of the numerical 1DV model.

7.4 Characteristic Parameters

Having now established which terms require parameterisation, the next step is to determine which parameters should be used. Yalin (1977) suggests that these characteristic parameters are determined by the components defining the system.

Yalin considers the case of a stationary, uniform, two-dimensional, two-phase flow for cohesionless grains of a specified geometry. The components defining the system are given as:-

(i) Fluid : defined by its density, ρ, and dynamic viscosity, μ.

(ii) Grains : defined by their density, ρ_s, and diameter, d.

(iii) Flow : defined by the flow depth, h, gravitational factor, γ_s, and bed-shear velocity, u_*.

where,

$$\gamma_s = g(\rho_s - \rho)$$

g -Acceleration due to gravity

N.B: Here, it is preferred that the kinematic viscosity, ν, is used instead of the dynamic viscosity.

The characteristic parameters for this situation are therefore given as:-

$$\rho, \nu, \rho_s, d, h, \gamma_s, u_* \qquad (7.4.1)$$

Consider the situation where the grain is no longer of a specified geometry but is instead described by a sediment grain size distribution. The median grain diameter, d_{50}, must now be used instead of the parameter d. The geometric standard deviation of the grain size distribution, σ, must also be added to ensure that the distribution is described in full. The set of characteristic parameters (7.4.1) now becomes:-

$$\rho, \nu, \rho_s, d_{50}, \sigma, h, \gamma_s, u_* \qquad (7.4.2)$$

Now, applying the above to a tidal situation requires the addition of parameters that define the tidal conditions, i.e.:-

r -Tidal range

h_m -Mean water depth

$\overline{u}_m$ -Maximum depth-average longitudinal tidal velocity

up -Twice the duration of the flood stage of the tide

Since the water depth, h, is already part of the characteristic set, it must be replaced by h_m to allow for tidal conditions. Similarly, since the flow is defined, in part, by the bed shear stress, the value at maximum tidal velocity is used for the tidal situation. However, the bed shear velocity is influenced by many factors; this makes the control of any group containing this parameter virtually impossible in the coded model. It is therefore proposed that the maximum depth-average longitudinal tidal velocity be used as the characteristic parameter instead. The new, and final, set of characteristic parameters is therefore given by:-

$$\rho, \nu, \rho_s, d_{50}, \sigma, h_m, \gamma_s, \overline{u}_m, r, up \qquad (7.4.3)$$

Although the characteristic parameters have now been determined, it is more useful to parameterise in terms of non-dimensional groups since these are independent of units and they show the relative importance of the various parameters. The next section describes how these groups are formed.

7.5 Parameter Groups

Consider the quantity A, which must be determined for a given system. The value of A is given as a function of the characteristic parameters, i.e.:-

$$A = f_A(\rho, \nu, \rho_s, d_{50}, \sigma, h_m, \gamma_s, \overline{u}_m, r, up) \qquad (7.5.1)$$

Since there are ten characteristic parameters and only three dimensions (mass (M), length (L) and time (T)), Buckingham's Pi Theorem states that there are seven non-dimensional groups that can be formed, i.e.:-

$$A = \Psi_A(\Pi_1, \Pi_2, \ldots, \Pi_7) \qquad (7.5.2)$$

The seven non-dimensional groups are by no means unique but are determined by the choice of the three basic quantities. The basic quantities chosen for the characteristic set (7.4.3) are:-

$$\rho, \gamma_s, d_{50} \tag{7.5.3}$$

These are the same basic quantities as those used by Van Rijn (1993) in equation (7.2.1) and Yalin (1977) for steady flow conditions.

Now, using the basic quantities (7.5.3), the base dimensions can be expressed as:-

$$\begin{aligned} M &= \rho d_{50}^3 \\ L &= d_{50} \\ T &= \rho^{1/2} d_{50}^{1/2} \gamma_s^{-1/2} \end{aligned} \tag{7.5.4}$$

The seven non-dimensional groups are then found by non-dimensionalising the remaining seven characteristic parameters, i.e.:-

$$\nu \quad \rightarrow \quad \Pi_1 = \frac{\nu^2 \rho}{d_{50}^3 \gamma_s}$$

$$\rho_s \quad \rightarrow \quad \Pi_2 = \frac{\rho_s}{\rho}$$

$$\sigma \quad \rightarrow \quad \Pi_3 = \sigma$$

$$h_m \quad \rightarrow \quad \Pi_4 = \frac{h_m}{d_{50}}$$

$$\bar{u}_m \quad \rightarrow \quad \Pi_5 = \frac{\bar{u}_m^2 \rho}{d_{50} \gamma_s}$$

$$up \quad \rightarrow \quad \Pi_6 = \frac{up^2 \gamma_s}{\rho d_{50}}$$

$$r \quad \rightarrow \quad \Pi_7 = \frac{r}{d_{50}}$$

If the density ratio described by the third group is assumed to take the constant value 2.6 for all cases considered, then this group can be omitted from further analysis. After some simple manipulation and renumbering, the new set of groups becomes:-

$$\nu \quad \rightarrow \quad \Pi_1 = d_{50}\left(\frac{(s-1)g}{\nu^2}\right)^{1/3} \tag{7.5.5}$$

$$\sigma \quad \rightarrow \quad \Pi_2 = \sigma \tag{7.5.6}$$

$$h_m \quad \rightarrow \quad \Pi_3 = \frac{d_{50}}{h_m} \tag{7.5.7}$$

$$\bar{u}_m \quad \rightarrow \quad \Pi_4 = \frac{\bar{u}_m}{\sqrt{d_{50}g(s-1)}} \tag{7.5.8}$$

$$up \quad \rightarrow \quad \Pi_5 = \frac{up^2\gamma_s}{\rho d_{50}} \tag{7.5.9}$$

$$r \quad \rightarrow \quad \Pi_6 = \frac{r}{d_{50}} \tag{7.5.10}$$

[Aside: It should be noted that Π_1, Π_3 and Π_4 are essentially the same groups as used by Van Rijn in equation (7.2.1).]

7.6 Parameterisation Functions

7.6.1 Introduction

The form for each of the parameterisation functions is first estimated by considering the results of the numerical 1DV model. A database consisting of one hundred and eighty-nine data sets, each describing typical tidal conditions, is used to observe the effect of each of the six non-dimensional parameter groups on the chosen quantities $T_m, a_2, a_4, a_6, b_2, b_4$, and b_6. The data sets are formed into sets of twenty-seven; each of these is then broken down into three sets of nine. These sets of nine are chosen such that the value of one of the groups varies

whilst the other five remain constant, thus clearly showing the effect of each non-dimensional group on each quantity to be parameterised.

A functional form is then suggested based on both the observations and certain theoretical criteria, such as limits and maxima.

The functional form is then tested using regression analysis by way of a least-squares estimator.

7.6.2 Data

The data sets cover a wide range of tidal conditions, summarised below.

Tidal range (m):	$1 \le r \le 9$
Mean water level (m):	$9 \le h_m \le 20$
Maximum depth-average tidal velocity (ms^{-1}):	$1 \le \overline{u}_m \le 2$
Median grain diameter (μm):	$150 \le d_{50} \le 250$
Velocity period (s):	$3500 \le up \le 44712$
Standard deviation of grain size distribution:	$1.4 \le \sigma \le 2.2$
Kinematic viscosity (m^2s^{-1}):	$\nu = 1.39 \times 10^{-6}$

Table 7.6.1 gives full details of each of the one hundred and eighty-nine data sets used.

Table 7.6.2 contains values for all of the quantities to be parameterised.

The values of the six non-dimensional parameter groups for each data set are given in table 7.6.3.

7.6.3 Functional Form

Since the seven parameter groups are non-dimensional, the chosen quantities must also be non-dimensional. Several variations were tried; the best results were

obtained by non-dimensionalising T_m, a_2, and a_4 with their equilibrium values, as suggested by O'Connor (1999), and a_6, b_2, b_4, and b_6 with the basic quantities given by (7.5.3). All relevant equilibrium values are given in table 7.6.4.

Using equilibrium values has the advantage that limiting values are immediately apparent, i.e. T_m, a_2, and a_4 should tend to their equilibrium values as time tends to positive infinity. This suggests that the functional form could be based on an exponential function.

Figures 7.6.1 - 7.6.7 show the effect of each of the six parameter groups on the non-dimensional quantities to be parameterised. It can be seen from figure 7.6.1 that the ratio of transport at maximum tidal velocity, T_m, and equilibrium transport at maximum tidal velocity, T_{me}, shows a possible correlation with Π_1, Π_2 and Π_3. The effect of the other groups seems negligible since the graph shows little change in the ordinate compared with the range of values shown on the abscissa. The same argument applies to both a_2 and a_4 when non-dimensionalised by their respective equilibrium values; as can be seen from figures 7.6.2 and 7.6.3.

Figure 7.6.4 suggests that a_6 non-dimensionalised by the chosen basic quantities may be correlated with Π_1, Π_3 and Π_4.

Figure 7.6.5 suggests that b_2 non-dimensionalised by the chosen basic quantities can be correlated with all groups save Π_6; this group seems to have little effect. The same argument applies to b_4 when non-dimensionalised by the chosen basic quantities, as can be seen from figure 7.6.6.

Figure 7.6.7 shows that b_6 non-dimensionalised by the chosen basic quantities can be correlated with Π_1, Π_3, Π_4 and Π_5

Having now established which groups are influential for each parameterisation, it only remains to chose a functional form for these groups to take. In order to use the same functional form for each group in each parameterisation it is first necessary to manipulate one of the groups, i.e.:-

$$\Pi_2 = \sigma \qquad \rightarrow \qquad \Pi_2 = \frac{1}{\ln \sigma} \tag{7.6.1}$$

Using this new definition of Π_2, it is proposed that the following functional forms should be used:-

$$\frac{PT_m}{T_{me}} = 1 - \exp\left\{\alpha \Pi_1^{\beta_1} \Pi_2^{\beta_2} \Pi_3^{\beta_3}\right\} \tag{7.6.2}$$

$$\frac{Pa_2}{a_{2e}} = 1 - \exp\left\{\alpha \Pi_1^{\beta_1} \Pi_2^{\beta_2} \Pi_3^{\beta_3}\right\} \tag{7.6.3}$$

$$\frac{Pa_4}{a_{4e}} = 1 - \exp\left\{\alpha \Pi_1^{\beta_1} \Pi_2^{\beta_2} \Pi_3^{\beta_3}\right\} \tag{7.6.4}$$

$$\frac{-Pa_6}{\sqrt{\rho \gamma_s d_{50}}} = \alpha \Pi_1^{\beta_1} \Pi_3^{\beta_3} \Pi_4^{\beta_4} \tag{7.6.5}$$

$$\frac{-Pb_2}{\sqrt{\rho \gamma_s d_{50}}} = \alpha \Pi_1^{\beta_1} \Pi_2^{\beta_2} \Pi_3^{\beta_3} \Pi_4^{\beta_4} \Pi_5^{\beta_5} \tag{7.6.6}$$

$$\frac{Pb_4}{\sqrt{\rho \gamma_s d_{50}}} = \alpha \Pi_1^{\beta_1} \Pi_2^{\beta_2} \Pi_3^{\beta_3} \Pi_4^{\beta_4} \Pi_5^{\beta_5} \tag{7.6.7}$$

$$\frac{-Pb_6}{\sqrt{\rho \gamma_s d_{50}}} = \alpha \Pi_1^{\beta_1} \Pi_3^{\beta_3} \Pi_4^{\beta_4} \Pi_5^{\beta_5} \tag{7.6.8}$$

where subscript e denotes the equilibrium value of the variable and prefix P denotes the parameterised version of the variable. It should also be noted that the value for each α and β is different for each parameterisation, i.e. each of equations (7.6.2) - (7.6.8).

7.6.4 Estimation

The α's and β's in equations (7.6.2 - 7.6.8) are evaluated by using regression analysis with a least squares estimator on the output of the one hundred and eighty-nine different tidal data sets.

Regression analysis cannot be performed on the parameterisation functions in their present state; some simple manipulation is required first.

For example, consider the parameterisation of the transport at maximum velocity:-

$$\frac{PT_m}{T_{me}} = 1 - \exp\left\{\alpha \Pi_1^{\beta_1} \Pi_2^{\beta_2} \Pi_3^{\beta_3}\right\} \qquad (7.6.2)$$

$$\rightarrow \qquad 1 - \frac{PT_m}{T_{me}} = \exp\left\{\alpha \Pi_1^{\beta_1} \Pi_2^{\beta_2} \Pi_3^{\beta_3}\right\}$$

$$\rightarrow \qquad \ln\left[1 - \frac{PT_m}{T_{me}}\right] = \alpha \Pi_1^{\beta_1} \Pi_2^{\beta_2} \Pi_3^{\beta_3}$$

$$\rightarrow \qquad \ln\left\{\ln\left[1 - \frac{PT_m}{T_{me}}\right]\right\} = \ln\left[\alpha \Pi_1^{\beta_1} \Pi_2^{\beta_2} \Pi_3^{\beta_3}\right]$$

$$\rightarrow \qquad \ln\left\{\ln\left[1 - \frac{PT_m}{T_{me}}\right]\right\} = \ln[\alpha] + \beta_1 \ln[\Pi_1] + \beta_2 \ln[\Pi_2] + \beta_3 \ln[\Pi_3]$$

This is now in a form that allows multiple-linear regression analysis using a least squares estimator. A similar method is used for the other parameterisation functions.

7.7 1DV Parameterisation

7.7.1 Analysis Variables

The values obtained for the α's and β's are shown in table 7.7.1. The table also includes values for several analysis variables; namely, r^2, F-obs, mean % error, max % error, mean diff and max diff.

The % error term for a variable x is defined by:-

$$\%error = 100 \times \left| \frac{x - px}{x} \right|$$

where px is the value given by the parameterisation of x.

The mean % error is therefore the average value of % error for all one hundred and eighty-nine data sets. Similarly, the maximum error for the one hundred and eighty-nine sets is given by max % error.

The absolute difference between the actual value of variable x and its parameterised value has the units of transport and is defined by:-

$$diff = |x - px|$$

Again the terms mean and max refer to the one hundred and eighty-nine data sets used in the regression analysis.

The correlation between the data and the proposed parameterisation function is described by the r^2 term. If the parameterisation function is a good representation of the actual relationship, i.e. good correlation, then the r^2 value will be close to 1 ($0 \leq r^2 \geq 1$).

It is possible that a high r^2 value could be produced by chance. This can be determined by considering the single tailed F-distribution. The regression analysis returns a value for F-obs (observed); if the good agreement is not due to chance then this must be greater than the critical F value (F_{cr}). Statistical tables provide a value for F_{cr} once the degrees of freedom have been determined.

Let k = the number of independent variables (number of different groups)

n = the number of data sets used (=189)

Then the F-distribution has degrees of freedom given by:-

$$\nu_1 = k$$

$$\nu_2 = n-(k+1)$$

The critical F value for each of the parameterisations is therefore:-

$F_{cr} \approx 2.68$ for T_m, a_2, a_4 and a_6

$F_{cr} \approx 2.29$ for the parameterisation of b_2 and b_4

$F_{cr} \approx 2.45$ for the parameterisation of b_6

[It should be noted that the values stated above are actually for $\nu_2 = 120$ since this was the largest value available from statistical tables. This gives a slightly higher critical F value than for the cases considered here. However, if it can be shown that the observed F value is significantly greater than this value, it follows that it will also be greater for a smaller value.]

7.7.2 Results of Regression Analysis

During the regression analysis, it became evident that slightly better results were obtained when the critical value of the depth-average longitudinal flow velocity, $\bar{u}_c$, was introduced into Π_4 as used by Van Rijn in equation (7.2.1); i.e.:-

$$\Pi_4 = \frac{\bar{u}_m - \bar{u}_c}{\sqrt{d_{50} g (s-1)}} \qquad (7.7.1)$$

Table 7.7.2 gives the values for the critical depth-average longitudinal flow velocity and equation (7.7.1) for each of the sets used in the analysis detailed below.

The following regression analysis is therefore performed on the functional forms given by equations (7.6.2) - (7.6.8), using the non-dimensional groups defined by equations (7.5.5), (7.6.1), (7.5.7), (7.7.1) and (7.5.9).

Figure 7.7.1 shows the parameterised quantities plotted against the actual values from the numerical 1DV model. The bold line denotes a perfect agreement.

The regression analysis of the parameterisation of the transport at maximum velocity, T_m, returns a high value for both r^2 and F-obs (table 7.7.1b), 0.952 and 1234.7 respectively. This suggests that the parameterisation function chosen is a good representation of the actual relationship as supported by the low values for the % error and difference terms. In fact, the maximum difference in actual transport terms is only 0.066199 $kgm^{-2}s^{-1}$.

Good agreement is also shown for a_2. Again the r^2 value is close to 1 and the F-obs value well above the critical. The max diff term is again very small, only 0.06602 $kgm^{-2}s^{-1}$.

The parameterisation of a_4 is only slightly worse. The r^2 value is close to 1, the F-obs value, although less than before, is still well above the critical value. Again the maximum difference in terms of transport is very small, only 0.09923 $kgm^{-2}s^{-1}$.

The r^2 value for a_6 is a little lower than that for the previous parameterisations but is still relatively high. The F-obs value is much smaller than previous values mentioned, although it is still much greater than the critical value. However, the

error variables suggest that the parameterisation may need further improvement. The high value for max % error is somewhat misleading since the maximum difference in terms of actual transport is only 0.002946 $kgm^{-2}s^{-1}$. It must also be considered that the contribution made by a_6 is relatively small compared to the contribution of the other mean Fourier coefficients and transport at maximum tidal velocity, as can be seen from table 7.6.2.

When analysing the lag coefficients it must be considered that T_m and a_2 are the main contributors to the overall transport. This said, the parameterisation of b_2 is still remarkably good. An r^2 value of 0.976 and F-obs of 1493.7 would seem to suggest that the model used is a valid one. This is supported by the low % error variables and max diff value of only 0.011463 $kgm^{-2}s^{-1}$.

Again, the r^2 value for the parameterisation of b_4 is high, as is the F-obs value. The parameterisation is shown to produce good results by the low value for the analysis variables; the maximum difference between the predicted and approximated values is only 0.004305 $kgm^{-2}s^{-1}$.

The parameterisation for b_6 is similar to that of a_6 in that the r^2 value is relatively high but the F-obs value is much lower than for the other parameterisations, although still much greater than the critical value. The relatively high values for the % error variables would seem to suggest that the function used in the parameterisation might be improved upon. However, the difference variables suggest that the model does produce reasonable results.

One further test of the regression analysis is to look for patterns in the residual plots. The residual is defined as the observed value minus the predicted value. Consider the parameterisation of the transport at maximum tidal velocity:-

$$\frac{PT_m}{T_{me}} = 1 - \exp\left\{\alpha \Pi_1^{\beta_1} \Pi_2^{\beta_2} \Pi_3^{\beta_3}\right\} \qquad (7.6.2)$$

The regression analysis is actually performed on the transformed version, i.e.:-

$$\ln\left\{\ln\left[1-\frac{PT_m}{T_{me}}\right]\right\}=\ln[\alpha]+\beta_1\ln[\Pi_1]+\beta_2\ln[\Pi_2]+\beta_3\ln[\Pi_3]$$

The residual is therefore defined by:-

$$residual=\ln\left\{\ln\left[1-\frac{T_m}{T_{me}}\right]\right\}-(\ln[\alpha]+\beta_1\ln[\Pi_1]+\beta_2\ln[\Pi_2]+\beta_3\ln[\Pi_3]) \qquad (7.7.2)$$

Figures 7.7.2 - 7.7.8 show the residual plots for all seven parameterisations. The absence of any obvious patterns in the residual plots suggests that the assumption of normality inherent in using multi-linear regression is valid for the analysis performed above.

Although the regression analysis has produced models that appear to approximate the actual relationships, they must be tested against independent data sets that were not used in the regression analysis. Seven such data sets are given in table 7.6.1b. The corresponding values of the quantities to be parameterised are given in table 7.7.3, non-dimensional group values in table 7.7.4 and equilibrium values in table 7.7.5.

Table 7.7.6 shows the results of using the parameterised expressions suggested above for the seven independent data sets.

Although all values for the analysis variables are slightly higher for the independent sets, the parameterisations would appear to provide a good approximation for their respective variables.

As stated earlier, it is preferable for the parameterisation to replicate the properties of the original system as far as possible. Consider the parameterisation of the transport due to depth-average values:-

$$\frac{PT_m}{T_{me}} = 1 - \exp\left\{\alpha \Pi_1^{\beta_1} \Pi_2^{\beta_3} \Pi_3^{\beta_3}\right\} \qquad (7.6.2)$$

where,

$\alpha = -1.388$; $\beta_1 = 1.183$

$\beta_2 = 0.832$

$\beta_3 = 0.206$

Consider:-

$d_{50} \to \infty$ i.e. $\Pi_1 , \Pi_3 \to \infty$

$$\therefore \quad \frac{PT_m}{T_{me}} \to 1 - \exp\{-\infty\}$$

i.e. $$\frac{PT_m}{T_{me}} \to 1$$

This simply states that as the median grain size increases, the parameterised transport at maximum velocity will tend towards its equilibrium value. This is to be expected since larger particles are assumed to adjust instantaneously to flow conditions. It is a simple task to show that this is also the case for the parameterisations of a_2 and a_4.

Consider now the power law function for a_6:-

$$\frac{-Pa_6}{\sqrt{\rho \gamma_s d_{50}}} = \alpha \Pi_1^{\beta_1} \Pi_3^{\beta_3} \Pi_4^{\beta_4} \qquad (7.6.5)$$

where,

$\alpha = 5.523e-11$; $\beta_1 = -3.188$

$\beta_3 = -1.408$

$\beta_4 = 1.925$

Now, if $d_{50} \rightarrow \infty$ then:-

L.H.S of (7.6.5): $$\frac{-Pa_6}{\sqrt{\rho\gamma_s d_{50}}} \rightarrow 0$$

R.H.S of (7.6.5): $$\alpha\Pi_1^{\beta_1}\Pi_3^{\beta_3}\Pi_4^{\beta_4} \rightarrow 0$$

Essentially, as the grain size becomes infinitely large, there is no transport since the flow velocity is not sufficient to initiate motion. It is a simple exercise to show that the parameterisations for b_2, b_4 and b_6 share the same property.

Combining the parameterisations for the Fourier coefficients and the transport at maximum velocity, an approximation for the tidal suspended sediment transport rate ($PT_s(t)$) is given by the model described below.

$$PT_s(t) \approx PT_m + \sum_{n=1}^{3} Pa_{2n}\left\{\cos(2n\omega t) + (-1)^{n-1}\right\} + \sum_{n=1}^{3} Pb_{2n}\sin(2n\omega t) \quad (7.7.3)$$

7.7.3 Model Test

Figure 7.7.9 shows a comparison between the numerical 1DV model and the parameterised version, equation (7.7.3), for six of the seven independent data sets. As can be seen, the parameterisation produces a good approximation for all sets.

Figures 7.7.10 and 7.7.11 show the difference in accuracy between the mean and lag parameterisations respectively. They also show the difference in magnitude of the contributions to the overall transport value by the mean and lag. It can be seen that although the lag seems slightly inaccurate, the actual magnitude means that the difference is insignificant.

7.8 Summary

It has been shown that tidal suspended sediment transport rates can be accurately approximated using a Fourier series consisting of the first four mean coefficients and first three lag coefficients.

These mean and lag coefficients have been parameterised using non-dimensional groups based on ten characteristic parameters obtained from the physical properties of the system.

By carrying out regression analysis and performing comparison tests against independent sets, it is shown that the parameterisations for the variables $T_m, a_2, a_4, a_6, b_2, b_4$, and b_6 sufficiently reproduce the actual relationships.

Comparison tests against output from the numerical 1DV model show that the parameterised model produces reasonable results. It is now possible to replace the 1DV model with the more simplistic parameterised version, i.e. equation (7.7.3).

The next chapter describes how the 1DV parameterised model can be used to replace the 1DV model in the Corrector method.

Set	r (m)	h_m (m)	$\overline{u}_m$ (ms^{-1})	d_{50} (m)	up (s)	σ
100	3	10	1	0.00015	44712	1.5
101	3	10	1	0.00016	44712	1.5
102	3	10	1	0.00017	44712	1.5
103	3	10	1	0.00018	44712	1.5
104	3	10	1	0.00019	44712	1.5
105	3	10	1	0.0002	44712	1.5
106	3	10	1	0.00021	44712	1.5
107	3	10	1	0.00022	44712	1.5
108	3	10	1	0.00023	44712	1.5
109	6	15	1.5	0.00017	44712	1.7044
110	6	15	1.5	0.00018	44712	1.7044
111	6	15	1.5	0.00019	44712	1.7044
112	6	15	1.5	0.0002	44712	1.7044
113	6	15	1.5	0.00021	44712	1.7044
114	6	15	1.5	0.00022	44712	1.7044
115	6	15	1.5	0.00023	44712	1.7044
116	6	15	1.5	0.00024	44712	1.7044
117	6	15	1.5	0.00025	44712	1.7044
118	9	20	2	0.00021	44712	2
119	9	20	2	0.000215	44712	2
120	9	20	2	0.00022	44712	2
121	9	20	2	0.000225	44712	2
122	9	20	2	0.00023	44712	2
123	9	20	2	0.000235	44712	2
124	9	20	2	0.00024	44712	2
125	9	20	2	0.000245	44712	2
126	9	20	2	0.00025	44712	2
127	4	9	1.2	0.00022	44000	1.4
128	4	9	1.2	0.00022	44000	1.5
129	4	9	1.2	0.00022	44000	1.6
130	4	9	1.2	0.00022	44000	1.7
131	4	9	1.2	0.00022	44000	1.8
132	4	9	1.2	0.00022	44000	1.9
133	4	9	1.2	0.00022	44000	2
134	4	9	1.2	0.00022	44000	2.1
135	4	9	1.2	0.00022	44000	2.2
136	7	16	1.7	0.00025	43000	1.4
137	7	16	1.7	0.00025	43000	1.5
138	7	16	1.7	0.00025	43000	1.6
139	7	16	1.7	0.00025	43000	1.7
140	7	16	1.7	0.00025	43000	1.8
141	7	16	1.7	0.00025	43000	1.9
142	7	16	1.7	0.00025	43000	2
143	7	16	1.7	0.00025	43000	2.1
144	7	16	1.7	0.00025	43000	2.2
145	8	19	1.9	0.00023	38000	1.4
146	8	19	1.9	0.00023	38000	1.5
147	8	19	1.9	0.00023	38000	1.6
148	8	19	1.9	0.00023	38000	1.7
149	8	19	1.9	0.00023	38000	1.8
150	8	19	1.9	0.00023	38000	1.9

Table 7.6.1a: Data sets used in the regression analysis for the 1DV parameterisations

Set	r (m)	h_m (m)	$\overline{u}_m$ (ms^{-1})	d_{50} (m)	up (s)	σ
151	8	19	1.9	0.00023	38000	2
152	8	19	1.9	0.00023	38000	2.1
153	8	19	1.9	0.00023	38000	2.2
154	5	11	1	0.00015	44712	1.7044
155	5	11	1.1	0.00015	44712	1.7044
156	5	11	1.2	0.00015	44712	1.7044
157	5	11	1.3	0.00015	44712	1.7044
158	5	11	1.4	0.00015	44712	1.7044
159	5	11	1.5	0.00015	44712	1.7044
160	5	11	1.6	0.00015	44712	1.7044
161	5	11	1.7	0.00015	44712	1.7044
162	5	11	1.8	0.00015	44712	1.7044
163	3	18	1.1	0.0002	39000	1.9
164	3	18	1.2	0.0002	39000	1.9
165	3	18	1.3	0.0002	39000	1.9
166	3	18	1.4	0.0002	39000	1.9
167	3	18	1.5	0.0002	39000	1.9
168	3	18	1.6	0.0002	39000	1.9
169	3	18	1.7	0.0002	39000	1.9
170	3	18	1.8	0.0002	39000	1.9
171	3	18	1.9	0.0002	39000	1.9
172	8	14	1	0.00022	36000	1.6
173	8	14	1.1	0.00022	36000	1.6
174	8	14	1.2	0.00022	36000	1.6
175	8	14	1.3	0.00022	36000	1.6
176	8	14	1.4	0.00022	36000	1.6
177	8	14	1.5	0.00022	36000	1.6
178	8	14	1.6	0.00022	36000	1.6
179	8	14	1.7	0.00022	36000	1.6
180	8	14	1.8	0.00022	36000	1.6
181	4	10	1.2	0.00017	37000	1.5
182	4	11	1.2	0.00017	37000	1.5
183	4	12	1.2	0.00017	37000	1.5
184	4	13	1.2	0.00017	37000	1.5
185	4	14	1.2	0.00017	37000	1.5
186	4	15	1.2	0.00017	37000	1.5
187	4	16	1.2	0.00017	37000	1.5
188	4	17	1.2	0.00017	37000	1.5
189	4	18	1.2	0.00017	37000	1.5
190	6	11	1.6	0.00019	42000	1.8
191	6	12	1.6	0.00019	42000	1.8
192	6	13	1.6	0.00019	42000	1.8
193	6	14	1.6	0.00019	42000	1.8
194	6	15	1.6	0.00019	42000	1.8
195	6	16	1.6	0.00019	42000	1.8
196	6	17	1.6	0.00019	42000	1.8
197	6	18	1.6	0.00019	42000	1.8
198	6	19	1.6	0.00019	42000	1.8
199	8	12	1.9	0.00021	44712	2
200	8	13	1.9	0.00021	44712	2
201	8	14	1.9	0.00021	44712	2
202	8	15	1.9	0.00021	44712	2

Table 7.6.1a contd.: Data sets used in the regression analysis for the 1DV parameterisations

Set	r (m)	h_m (m)	$\overline{u}_m$ (ms^{-1})	d_{50} (m)	up (s)	σ
203	8	16	1.9	0.00021	44712	2
204	8	17	1.9	0.00021	44712	2
205	8	18	1.9	0.00021	44712	2
206	8	19	1.9	0.00021	44712	2
207	8	20	1.9	0.00021	44712	2
208	3	10	1	0.00016	35000	1.6
209	3	10	1	0.00016	36000	1.6
210	3	10	1	0.00016	37000	1.6
211	3	10	1	0.00016	38000	1.6
212	3	10	1	0.00016	39000	1.6
213	3	10	1	0.00016	40000	1.6
214	3	10	1	0.00016	41000	1.6
215	3	10	1	0.00016	42000	1.6
216	3	10	1	0.00016	43000	1.6
217	6	14	1.4	0.0002	36000	1.8
218	6	14	1.4	0.0002	37000	1.8
219	6	14	1.4	0.0002	38000	1.8
220	6	14	1.4	0.0002	39000	1.8
221	6	14	1.4	0.0002	40000	1.8
222	6	14	1.4	0.0002	41000	1.8
223	6	14	1.4	0.0002	42000	1.8
224	6	14	1.4	0.0002	43000	1.8
225	6	14	1.4	0.0002	44712	1.8
226	8	19	2	0.00023	36000	1.7044
227	8	19	2	0.00023	37000	1.7044
228	8	19	2	0.00023	38000	1.7044
229	8	19	2	0.00023	39000	1.7044
230	8	19	2	0.00023	40000	1.7044
231	8	19	2	0.00023	41000	1.7044
232	8	19	2	0.00023	42000	1.7044
233	8	19	2	0.00023	43000	1.7044
234	8	19	2	0.00023	44712	1.7044
235	1	10	1	0.00015	44712	1.7044
236	2	10	1	0.00015	44712	1.7044
237	3	10	1	0.00015	44712	1.7044
238	4	10	1	0.00015	44712	1.7044
239	5	10	1	0.00015	44712	1.7044
240	6	10	1	0.00015	44712	1.7044
241	7	10	1	0.00015	44712	1.7044
242	8	10	1	0.00015	44712	1.7044
243	9	10	1	0.00015	44712	1.7044
244	1	15	1.5	0.0002	40000	1.6
245	2	15	1.5	0.0002	40000	1.6
246	3	15	1.5	0.0002	40000	1.6
247	4	15	1.5	0.0002	40000	1.6
248	5	15	1.5	0.0002	40000	1.6
249	6	15	1.5	0.0002	40000	1.6
250	7	15	1.5	0.0002	40000	1.6
251	8	15	1.5	0.0002	40000	1.6
252	9	15	1.5	0.0002	40000	1.6
253	1	20	2	0.00022	38000	2.1
254	2	20	2	0.00022	38000	2.1

Table 7.6.1a contd.: Data sets used in the regression analysis for the 1DV parameterisations

Set	r (m)	h_m (m)	$\overline{u}_m$ (ms^{-1})	d_{50} (m)	up (s)	σ
255	3	20	2	0.00022	38000	2.1
256	4	20	2	0.00022	38000	2.1
257	5	20	2	0.00022	38000	2.1
258	6	20	2	0.00022	38000	2.1
259	7	20	2	0.00022	38000	2.1
260	8	20	2	0.00022	38000	2.1
261	9	20	2	0.00022	38000	2.1
262	3	10	1	0.00015	36000	1.7044
263	3.2	10.66667	1.032796	0.00016	37180.64	1.7044
264	3.4	11.33333	1.064581	0.00017	38324.93	1.7044
265	3.6	12	1.095445	0.00018	39436.02	1.7044
266	3.8	12.66667	1.125463	0.00019	40516.66	1.7044
267	4	13.33333	1.154701	0.0002	41569.22	1.7044
268	4.2	14	1.183216	0.00021	42595.77	1.7044
269	4.4	14.66667	1.21106	0.00022	43598.16	1.7044
270	4.6	15.33333	1.238278	0.00023	44578.02	1.7044
271	5	12	1.5	0.00017	35000	1.4
272	5.294118	12.70588	1.543487	0.00018	36014.7	1.4
273	5.588235	13.41176	1.585782	0.00019	37001.59	1.4
274	5.882353	14.11765	1.626978	0.0002	37962.83	1.4
275	6.176471	14.82353	1.667157	0.00021	38900.32	1.4
276	6.470588	15.52941	1.706389	0.00022	39815.75	1.4
277	6.764706	16.23529	1.74474	0.00023	40710.6	1.4
278	7.058824	16.94118	1.782266	0.00024	41586.2	1.4
279	7.352941	17.64706	1.819017	0.00025	42443.73	1.4
280	4	11	1.6	0.00015	35500	1.6
281	4.266667	11.73333	1.652473	0.00016	36664.24	1.6
282	4.533333	12.46667	1.70333	0.00017	37792.64	1.6
283	4.8	13.2	1.752712	0.00018	38888.3	1.6
284	5.066667	13.93333	1.800741	0.00019	39953.93	1.6
285	5.333333	14.66667	1.847521	0.0002	40991.87	1.6
286	5.6	15.4	1.893146	0.00021	42004.16	1.6
287	5.866667	16.13333	1.937696	0.00022	42992.64	1.6
288	6.133333	16.86667	1.981245	0.00023	43958.88	1.6

Table 7.6.1a contd.: Data sets used in the regression analysis for the 1DV parameterisations

Set	r (m)	h_m (m)	$\overline{u}_m$ (ms^{-1})	d_{50} (m)	up (s)	σ
1	3	10	1	0.00015	44712	1.7044
2	3	10	1	0.0002	44712	1.7044
3	3	10	1	0.00025	44712	1.7044
4	3	10	2	0.0002	44712	1.7044
5	3	20	2	0.0002	44712	1.7044
6	9	10	2	0.0002	44712	1.7044
7	3	20	1	0.0002	44712	1.7044

Table 7.6.1b: Independent data sets used to test the 1DV parameterisations

Set	T_m ($kgm^{-2}s^{-1}$)	a_2 ($kgm^{-2}s^{-1}$)	a_4 ($kgm^{-2}s^{-1}$)	a_6 ($kgm^{-2}s^{-1}$)	b_2 ($kgm^{-2}s^{-1}$)	b_4 ($kgm^{-2}s^{-1}$)	b_6 ($kgm^{-2}s^{-1}$)
100	1.961664	-0.92395	0.339873	-0.0531	-0.15942	0.109212	-0.02422
101	1.707595	-0.80148	0.303178	-0.05019	-0.13039	0.092189	-0.02144
102	1.342942	-0.62881	0.243711	-0.04181	-0.09479	0.068961	-0.01657
103	1.066194	-0.49827	0.197349	-0.03474	-0.06924	0.051765	-0.0128
104	0.860981	-0.40169	0.162202	-0.0291	-0.05125	0.039335	-0.00998
105	0.748629	-0.34977	0.143086	-0.02545	-0.04087	0.032035	-0.00807
106	0.606958	-0.28299	0.117652	-0.02127	-0.03008	0.024188	-0.00633
107	0.499561	-0.23245	0.098089	-0.01801	-0.02238	0.018457	-0.00501
108	0.417098	-0.19372	0.082863	-0.01543	-0.01683	0.014228	-0.00402
109	13.25444	-6.43836	1.890275	-0.14847	-1.40395	0.741294	-0.06312
110	10.70578	-5.20066	1.540444	-0.12021	-1.07475	0.572471	-0.04934
111	8.775844	-4.26361	1.273673	-0.09909	-0.8337	0.447969	-0.03907
112	7.673777	-3.72583	1.127035	-0.09531	-0.69027	0.376078	-0.0367
113	6.305061	-3.06244	0.931844	-0.07611	-0.53439	0.292983	-0.02768
114	5.248482	-2.5502	0.780179	-0.06147	-0.4186	0.230901	-0.021
115	4.421979	-2.14941	0.660763	-0.05014	-0.33144	0.18391	-0.01601
116	3.767589	-1.83201	0.565661	-0.04125	-0.26506	0.147928	-0.01223
117	3.243699	-1.57783	0.489059	-0.03418	-0.21392	0.120062	-0.00936
118	19.6325	-9.61352	2.652985	-0.17078	-2.02201	0.996517	-0.05683
119	18.0669	-8.85776	2.442271	-0.14699	-1.81978	0.89796	-0.04889
120	16.67006	-8.18326	2.254112	-0.1261	-1.64181	0.811056	-0.04197
121	15.42079	-7.57982	2.085711	-0.10777	-1.48484	0.734265	-0.03595
122	14.30051	-7.03843	1.934672	-0.09171	-1.34597	0.666245	-0.03071
123	13.29397	-6.55165	1.799013	-0.07769	-1.22287	0.605933	-0.02621
124	12.38749	-6.11309	1.67686	-0.06545	-1.1135	0.552308	-0.02236
125	11.56928	-5.71659	1.566646	-0.05479	-1.01607	0.504531	-0.01905
126	10.82924	-5.3577	1.46701	-0.04552	-0.9291	0.461893	-0.01624
127	0.978306	-0.47912	0.17885	-0.0118	-0.03288	0.025297	-0.0035
128	1.205763	-0.59359	0.21233	-0.01076	-0.05063	0.035957	-0.0035

Table 7.6.2: Transport at maximum velocity and Fourier coefficients used in regression analysis

Set	T_m ($kgm^{-2}s^{-1}$)	A_2 ($kgm^{-2}s^{-1}$)	a_4 ($kgm^{-2}s^{-1}$)	a_6 ($kgm^{-2}s^{-1}$)	b_2 ($kgm^{-2}s^{-1}$)	b_4 ($kgm^{-2}s^{-1}$)	b_6 ($kgm^{-2}s^{-1}$)
129	1.440919	-0.71187	0.245368	-0.00966	-0.07045	0.046873	-0.00329
130	1.675226	-0.82956	0.277171	-0.00862	-0.09119	0.057572	-0.00301
131	1.903768	-0.94425	0.307421	-0.00767	-0.11204	0.067835	-0.00274
132	2.124166	-1.05458	0.336085	-0.00684	-0.13254	0.077597	-0.00251
133	2.335579	-1.16028	0.363213	-0.00614	-0.15243	0.086859	-0.00233
134	2.537953	-1.26128	0.38891	-0.00558	-0.1716	0.095655	-0.00221
135	2.731675	-1.35775	0.413351	-0.00517	-0.19002	0.104013	-0.00215
136	3.470399	-1.67373	0.571548	-0.06541	-0.14798	0.096492	-0.01542
137	4.230735	-2.05073	0.674634	-0.06874	-0.22555	0.138794	-0.01874
138	5.021997	-2.44367	0.777623	-0.07102	-0.31264	0.183321	-0.02145
139	5.813828	-2.83718	0.87761	-0.07254	-0.40409	0.227901	-0.02361
140	6.588383	-3.22201	0.973306	-0.07354	-0.49632	0.271359	-0.02535
141	7.33626	-3.59372	1.064237	-0.0742	-0.58715	0.31313	-0.02674
142	7.826517	-3.83915	1.118324	-0.0723	-0.65214	0.340921	-0.02682
143	8.141854	-3.99833	1.148858	-0.06932	-0.6977	0.358902	-0.02621
144	8.436554	-4.14683	1.177829	-0.06685	-0.7395	0.37537	-0.02563
145	6.660921	-3.25124	1.042785	-0.08672	-0.43507	0.262731	-0.02958
146	7.800437	-3.81699	1.175462	-0.08829	-0.59888	0.34024	-0.03133
147	8.931701	-4.37742	1.30275	-0.09016	-0.76848	0.416186	-0.03246
148	10.02393	-4.91765	1.422994	-0.09239	-0.93621	0.488501	-0.03324
149	11.06395	-5.43113	1.535976	-0.09498	-1.09798	0.556499	-0.03382
150	12.048	-5.91648	1.642091	-0.09794	-1.25201	0.620092	-0.0343
151	12.97784	-6.37417	1.742016	-0.10128	-1.39788	0.679589	-0.03476
152	13.85641	-6.80619	1.836357	-0.10495	-1.53567	0.735296	-0.03521
153	14.68833	-7.21457	1.925746	-0.1089	-1.6659	0.787592	-0.03566
154	2.77061	-1.32179	0.443522	-0.05768	-0.29911	0.182525	-0.03275
155	4.796635	-2.30566	0.771685	-0.09335	-0.49756	0.301865	-0.04413
156	7.289089	-3.55167	1.143755	-0.09637	-0.73125	0.426147	-0.03831
157	9.856009	-4.87274	1.472601	-0.05151	-0.96237	0.529678	-0.01607

Table 7.6.2 contd.: Transport at maximum velocity and Fourier coefficients used in regression analysis

Set	T_m ($kgm^{-2}s^{-1}$)	a_2 ($kgm^{-2}s^{-1}$)	a_4 ($kgm^{-2}s^{-1}$)	a_6 ($kgm^{-2}s^{-1}$)	b_2 ($kgm^{-2}s^{-1}$)	b_4 ($kgm^{-2}s^{-1}$)	b_6 ($kgm^{-2}s^{-1}$)
158	13.44449	-6.56933	1.956582	-0.09888	-1.2458	0.677068	-0.0352
159	18.2235	-8.84808	2.692752	-0.22612	-1.60755	0.890176	-0.08277
160	24.08823	-11.6896	3.601762	-0.33907	-2.03927	1.141211	-0.11836
161	31.17074	-15.1433	4.68518	-0.43797	-2.54305	1.427652	-0.14358
162	29.18194	-14.2059	4.381104	-0.38163	-2.22872	1.247682	-0.11431
163	3.080302	-1.47739	0.453535	-0.05941	-0.47804	0.260286	-0.03182
164	4.493426	-2.18383	0.64589	-0.06015	-0.65996	0.341122	-0.02053
165	6.065731	-2.99283	0.827191	-0.03278	-0.85307	0.408476	0.006157
166	8.327596	-4.06782	1.119492	-0.06385	-1.107	0.535878	-0.02178
167	11.32005	-5.50204	1.548845	-0.12811	-1.43614	0.720353	-0.06416
168	15.02532	-7.29584	2.086073	-0.19255	-1.82939	0.935957	-0.09333
169	16.07021	-7.81622	2.255078	-0.20334	-1.8339	0.94383	-0.08491
170	16.29605	-7.94473	2.298407	-0.1915	-1.7306	0.888946	-0.06625
171	19.14277	-9.34113	2.701587	-0.21342	-1.94073	0.993924	-0.06424
172	0.686618	-0.32326	0.118925	-0.01988	-0.07086	0.047743	-0.01072
173	1.152432	-0.5505	0.196227	-0.02684	-0.11601	0.07534	-0.01271
174	1.731349	-0.84441	0.281379	-0.02311	-0.17099	0.103514	-0.00942
175	2.364361	-1.17864	0.354707	-0.00237	-0.23046	0.126199	0.001094
176	3.337711	-1.63045	0.48356	-0.02026	-0.30679	0.164702	-0.00527
177	4.670996	-2.26402	0.6913	-0.06093	-0.41008	0.226402	-0.02182
178	6.33438	-3.07153	0.950383	-0.09393	-0.53781	0.301953	-0.03502
179	8.335907	-4.05769	1.251956	-0.11385	-0.68962	0.388173	-0.04268
180	8.54902	-4.18624	1.270238	-0.09168	-0.65823	0.367193	-0.03358
181	3.529104	-1.71242	0.596261	-0.05765	-0.29346	0.189373	-0.02156
182	3.663405	-1.77275	0.615869	-0.06446	-0.3322	0.212545	-0.02525
183	3.783654	-1.82662	0.631803	-0.07049	-0.37179	0.235959	-0.02937
184	3.891033	-1.87462	0.644313	-0.07573	-0.41189	0.259311	-0.03378
185	3.986632	-1.91739	0.653737	-0.0802	-0.4522	0.282338	-0.03835
186	4.071431	-1.9554	0.660376	-0.08395	-0.49246	0.30482	-0.04297

Table 7.6.2 contd.: Transport at maximum velocity and Fourier coefficients used in regression analysis

Set	T_m ($kgm^{-2}s^{-1}$)	a_2 ($kgm^{-2}s^{-1}$)	a_4 ($kgm^{-2}s^{-1}$)	a_6 ($kgm^{-2}s^{-1}$)	b_2 ($kgm^{-2}s^{-1}$)	b_4 ($kgm^{-2}s^{-1}$)	b_6 ($kgm^{-2}s^{-1}$)
187	4.146419	-1.98901	0.664517	-0.08704	-0.53247	0.326605	-0.04756
188	4.212378	-2.01871	0.666456	-0.08953	-0.57204	0.347559	-0.05203
189	4.270178	-2.04472	0.666424	-0.0915	-0.611	0.36759	-0.05635
190	11.48533	-5.60104	1.700964	-0.13895	-0.89763	0.499253	-0.04959
191	12.01846	-5.85496	1.768607	-0.14889	-1.00686	0.552096	-0.05459
192	12.51738	-6.09248	1.828289	-0.15774	-1.1212	0.607033	-0.06017
193	12.98445	-6.3148	1.880672	-0.16553	-1.23985	0.663458	-0.06616
194	13.4217	-6.52334	1.926026	-0.17226	-1.36212	0.720876	-0.07243
195	13.83105	-6.71836	1.964832	-0.17799	-1.48736	0.778789	-0.07881
196	14.2139	-6.9012	1.997486	-0.18277	-1.61494	0.83676	-0.0852
197	14.57208	-7.07247	2.02426	-0.18667	-1.74433	0.894413	-0.0915
198	14.90667	-7.23262	2.045676	-0.18977	-1.87494	0.951421	-0.09759
199	13.74184	-6.77244	1.922685	-0.08082	-0.98054	0.530302	-0.03881
200	14.16041	-6.97621	1.978339	-0.08772	-1.06284	0.564847	-0.03794
201	14.55418	-7.16676	2.029157	-0.09531	-1.14967	0.601877	-0.03764
202	14.92519	-7.34486	2.075279	-0.10331	-1.2404	0.641025	-0.03795
203	15.27514	-7.51165	2.116921	-0.11151	-1.33454	0.681953	-0.03888
204	15.60564	-7.66846	2.154111	-0.11976	-1.43163	0.72432	-0.04041
205	15.9181	-7.81613	2.187114	-0.12793	-1.53129	0.767865	-0.0425
206	16.21399	-7.95524	2.216316	-0.13593	-1.63313	0.812325	-0.04514
207	16.49439	-8.08668	2.241645	-0.14368	-1.73687	0.857433	-0.04825
208	1.958304	-0.92819	0.322018	-0.04755	-0.20636	0.131161	-0.02636
209	1.971676	-0.93419	0.326338	-0.04836	-0.2024	0.129549	-0.0261
210	1.984522	-0.93999	0.330472	-0.04914	-0.19859	0.127964	-0.02585
211	1.996897	-0.9455	0.334438	-0.04989	-0.19491	0.126389	-0.02558
212	2.00878	-0.95085	0.338263	-0.05061	-0.19135	0.124838	-0.02531
213	2.020224	-0.95599	0.341926	-0.0513	-0.18793	0.123309	-0.02504
214	2.031264	-0.96096	0.345468	-0.05196	-0.18461	0.121807	-0.02477
215	2.041926	-0.96577	0.348868	-0.0526	-0.18142	0.120329	-0.02451

Table 7.6.2 contd.: Transport at maximum velocity and Fourier coefficients used in regression analysis

Set	T_m ($kgm^{-2}s^{-1}$)	a_2 ($kgm^{-2}s^{-1}$)	a_4 ($kgm^{-2}s^{-1}$)	a_6 ($kgm^{-2}s^{-1}$)	b_2 ($kgm^{-2}s^{-1}$)	b_4 ($kgm^{-2}s^{-1}$)	b_6 ($kgm^{-2}s^{-1}$)
216	2.052231	-0.97042	0.352171	-0.05321	-0.17833	0.118882	-0.02424
217	6.817064	-3.32485	0.942497	-0.05788	-0.78551	0.39527	-0.02276
218	6.731271	-3.28362	0.935684	-0.05636	-0.75537	0.382279	-0.02182
219	6.64808	-3.24374	0.928751	-0.05489	-0.72702	0.369942	-0.02095
220	6.56743	-3.20494	0.921751	-0.05349	-0.70033	0.358224	-0.02014
221	6.48926	-3.16731	0.914682	-0.05213	-0.67519	0.347091	-0.01937
222	6.413405	-3.13082	0.907619	-0.05084	-0.65145	0.336499	-0.01866
223	6.339803	-3.09539	0.90056	-0.04959	-0.62904	0.326424	-0.01798
224	6.2684	-3.06095	0.893504	-0.04839	-0.60785	0.316832	-0.01736
225	6.150898	-3.00428	0.881545	-0.04644	-0.57417	0.301449	-0.01637
226	12.27754	-6.0278	1.710492	-0.09891	-1.1717	0.599278	-0.03344
227	12.12052	-5.95387	1.694209	-0.09498	-1.12595	0.578414	-0.03173
228	11.96871	-5.88242	1.678001	-0.09121	-1.08301	0.558699	-0.03017
229	11.82189	-5.81327	1.661994	-0.08759	-1.04266	0.540043	-0.02872
230	11.67984	-5.7462	1.646116	-0.08411	-1.0047	0.522379	-0.0274
231	11.54228	-5.68137	1.630432	-0.08077	-0.96896	0.505649	-0.02618
232	11.40915	-5.61854	1.615011	-0.07756	-0.93524	0.489784	-0.02506
233	11.28018	-5.55744	1.599771	-0.07448	-0.90345	0.474738	-0.02402
234	11.06851	-5.4573	1.574219	-0.06947	-0.85298	0.450699	-0.02243
235	2.695377	-1.28022	0.455732	-0.0633	-0.2364	0.151792	-0.02643
236	2.703651	-1.28582	0.452547	-0.06173	-0.24497	0.15606	-0.02749
237	2.711989	-1.29144	0.449358	-0.06026	-0.25367	0.160332	-0.02858
238	2.720394	-1.29689	0.446164	-0.05889	-0.26249	0.164623	-0.0297
239	2.728872	-1.3023	0.44296	-0.05762	-0.27144	0.168935	-0.03084
240	2.737422	-1.30766	0.439749	-0.05647	-0.28052	0.173277	-0.03201
241	2.746049	-1.31295	0.436528	-0.05543	-0.28975	0.177657	-0.03319
242	2.75476	-1.31817	0.433318	-0.05451	-0.29912	0.182078	-0.03439
243	2.763561	-1.32334	0.430134	-0.05372	-0.30865	0.186552	-0.0356
244	7.156678	-3.45643	1.098178	-0.1051	-0.60135	0.345908	-0.04004

Table 7.6.2 contd.: Transport at maximum velocity and Fourier coefficients used in regression analysis

Set	T_m ($kgm^{-2}s^{-1}$)	a_2 ($kgm^{-2}s^{-1}$)	a_4 ($kgm^{-2}s^{-1}$)	a_6 ($kgm^{-2}s^{-1}$)	b_2 ($kgm^{-2}s^{-1}$)	b_4 ($kgm^{-2}s^{-1}$)	b_6 ($kgm^{-2}s^{-1}$)
245	7.097136	-3.42943	1.08154	-0.10253	-0.60897	0.347579	-0.03937
246	7.039808	-3.40348	1.065405	-0.1001	-0.61661	0.349254	-0.03875
247	6.984628	-3.37833	1.049773	-0.09782	-0.62424	0.350919	-0.03817
248	6.931383	-3.35415	1.03457	-0.09568	-0.63188	0.352584	-0.03762
249	6.880041	-3.33064	1.019799	-0.09366	-0.63953	0.354256	-0.03711
250	6.830407	-3.30795	1.005423	-0.09178	-0.64717	0.355925	-0.03663
251	6.782409	-3.2859	0.991444	-0.09001	-0.65483	0.3576	-0.03618
252	6.735983	-3.26453	0.977807	-0.08836	-0.66249	0.35928	-0.03575
253	19.69544	-9.61704	2.724932	-0.20318	-2.02754	1.01199	-0.0559
254	19.69374	-9.61936	2.704571	-0.19861	-2.06501	1.023058	-0.05592
255	19.67883	-9.61519	2.682464	-0.19406	-2.10086	1.03325	-0.05597
256	19.65488	-9.6063	2.659282	-0.18958	-2.13553	1.042795	-0.05606
257	19.6246	-9.59428	2.635414	-0.1852	-2.16935	1.051864	-0.0562
258	19.58971	-9.57966	2.611084	-0.18096	-2.20251	1.060576	-0.0564
259	19.55137	-9.56332	2.586399	-0.17685	-2.23512	1.068977	-0.05666
260	19.51055	-9.54562	2.561552	-0.17291	-2.26731	1.077153	-0.05698
261	19.46759	-9.52669	2.536645	-0.16912	-2.29911	1.085133	-0.05737
262	2.594206	-1.23753	0.409947	-0.05386	-0.29669	0.178483	-0.03162
263	2.875555	-1.37081	0.463582	-0.06436	-0.32226	0.197175	-0.03434
264	2.970016	-1.41773	0.485676	-0.06701	-0.3238	0.199747	-0.03244
265	2.761481	-1.32211	0.455765	-0.05974	-0.28923	0.178635	-0.02596
266	2.575522	-1.23802	0.426952	-0.05151	-0.25889	0.159352	-0.02004
267	2.516363	-1.22028	0.412798	-0.04005	-0.24396	0.146784	-0.013
268	2.303174	-1.12171	0.377861	-0.03199	-0.21364	0.12785	-0.00897
269	2.118247	-1.03651	0.34679	-0.02458	-0.18788	0.111614	-0.00559
270	1.956946	-0.96246	0.319051	-0.0178	-0.16588	0.097638	-0.00276
271	8.673954	-4.16943	1.34688	-0.1393	-0.74058	0.442728	-0.05284
272	7.91678	-3.79848	1.247446	-0.14386	-0.63124	0.384349	-0.05347
273	7.284117	-3.49355	1.162287	-0.14165	-0.54189	0.335218	-0.05095

Table 7.6.2 contd.: Transport at maximum velocity and Fourier coefficients used in regression analysis

Set	T_m ($kgm^{-2}s^{-1}$)	a_2 ($kgm^{-2}s^{-1}$)	a_4 ($kgm^{-2}s^{-1}$)	a_6 ($kgm^{-2}s^{-1}$)	b_2 ($kgm^{-2}s^{-1}$)	b_4 ($kgm^{-2}s^{-1}$)	b_6 ($kgm^{-2}s^{-1}$)
274	7.060554	-3.39142	1.141295	-0.14165	-0.48956	0.307849	-0.04948
275	6.444243	-3.10037	1.046708	-0.12696	-0.41584	0.263407	-0.04224
276	5.931755	-2.8594	0.966433	-0.11319	-0.35575	0.226585	-0.03585
277	5.50275	-2.65888	0.897817	-0.10031	-0.30634	0.195839	-0.03022
278	4.790029	-2.3226	0.778462	-0.08001	-0.24212	0.154553	-0.02263
279	4.315719	-2.1001	0.698069	-0.06527	-0.19893	0.126705	-0.01746
280	25.42198	-12.2776	3.812317	-0.41245	-2.47626	1.387791	-0.16131
281	23.07451	-11.1533	3.482494	-0.37505	-2.15568	1.216468	-0.14308
282	21.08387	-10.2061	3.19555	-0.33436	-1.88804	1.070494	-0.12372
283	16.37001	-7.9454	2.482572	-0.24148	-1.371	0.77765	-0.08444
284	13.67743	-6.65813	2.070814	-0.18353	-1.075	0.609063	-0.06095
285	12.32409	-6.02525	1.85004	-0.13792	-0.91298	0.513155	-0.04313
286	11.15963	-5.47243	1.666547	-0.10778	-0.78285	0.438433	-0.03258
287	10.20951	-5.02314	1.513903	-0.08118	-0.67819	0.377785	-0.02382
288	9.417628	-4.64937	1.383886	-0.05732	-0.59229	0.327565	-0.01644

Table 7.6.2 contd.: Transport at maximum velocity and Fourier coefficients used in regression analysis

Set	Π_1	Π_2	Π_3	Π_4	Π_5	Π_6
100	3.015396	2.466303	0.000015	20.60914	2.09192E+14	20000
101	3.216423	2.466303	0.000016	19.95471	1.96118E+14	18750
102	3.417449	2.466303	0.000017	19.35892	1.84582E+14	17647.06
103	3.618475	2.466303	0.000018	18.81349	1.74327E+14	16666.67
104	3.819502	2.466303	0.000019	18.3117	1.65152E+14	15789.47
105	4.020528	2.466303	0.00002	17.84804	1.56894E+14	15000
106	4.221555	2.466303	0.000021	17.4179	1.49423E+14	14285.71
107	4.422581	2.466303	0.000022	17.01744	1.42631E+14	13636.36
108	4.623608	2.466303	0.000023	16.64338	1.3643E+14	13043.48
109	3.417449	1.875423	1.13E-05	29.03837	1.84582E+14	35294.12
110	3.618475	1.875423	0.000012	28.22023	1.74327E+14	33333.33
111	3.819502	1.875423	1.27E-05	27.46755	1.65152E+14	31578.95
112	4.020528	1.875423	1.33E-05	26.77206	1.56894E+14	30000
113	4.221555	1.875423	0.000014	26.12685	1.49423E+14	28571.43
114	4.422581	1.875423	1.47E-05	25.52616	1.42631E+14	27272.73
115	4.623608	1.875423	1.53E-05	24.96507	1.3643E+14	26086.96
116	4.824634	1.875423	0.000016	24.43943	1.30745E+14	25000
117	5.02566	1.875423	1.67E-05	23.94566	1.25515E+14	24000
118	4.221555	1.442695	1.05E-05	34.83581	1.49423E+14	42857.14
119	4.322068	1.442695	1.08E-05	34.42835	1.45948E+14	41860.47
120	4.422581	1.442695	0.000011	34.03488	1.42631E+14	40909.09
121	4.523094	1.442695	1.13E-05	33.65459	1.39462E+14	40000
122	4.623608	1.442695	1.15E-05	33.28676	1.3643E+14	39130.43
123	4.724121	1.442695	1.18E-05	32.93075	1.33527E+14	38297.87
124	4.824634	1.442695	0.000012	32.58591	1.30745E+14	37500
125	4.925147	1.442695	1.23E-05	32.25169	1.28077E+14	36734.69
126	5.02566	1.442695	1.25E-05	31.92754	1.25515E+14	36000
127	4.422581	2.972013	2.44E-05	20.42093	1.38125E+14	18181.82

Table 7.6.3: Values of the non-dimensional groups for each set used in the regression analysis

Set	Π_1	Π_2	Π_3	Π_4	Π_5	Π_6
128	4.422581	2.466303	2.44E-05	20.42093	1.38125E+14	18181.82
129	4.422581	2.127643	2.44E-05	20.42093	1.38125E+14	18181.82
130	4.422581	1.884559	2.44E-05	20.42093	1.38125E+14	18181.82
131	4.422581	1.701298	2.44E-05	20.42093	1.38125E+14	18181.82
132	4.422581	1.557987	2.44E-05	20.42093	1.38125E+14	18181.82
133	4.422581	1.442695	2.44E-05	20.42093	1.38125E+14	18181.82
134	4.422581	1.347823	2.44E-05	20.42093	1.38125E+14	18181.82
135	4.422581	1.268299	2.44E-05	20.42093	1.38125E+14	18181.82
136	5.02566	2.972013	1.56E-05	27.13841	1.16088E+14	28000
137	5.02566	2.466303	1.56E-05	27.13841	1.16088E+14	28000
138	5.02566	2.127643	1.56E-05	27.13841	1.16088E+14	28000
139	5.02566	1.884559	1.56E-05	27.13841	1.16088E+14	28000
140	5.02566	1.701298	1.56E-05	27.13841	1.16088E+14	28000
141	5.02566	1.557987	1.56E-05	27.13841	1.16088E+14	28000
142	5.02566	1.442695	1.56E-05	27.13841	1.16088E+14	28000
143	5.02566	1.347823	1.56E-05	27.13841	1.16088E+14	28000
144	5.02566	1.268299	1.56E-05	27.13841	1.16088E+14	28000
145	4.623608	2.972013	1.21E-05	31.62243	9.85436E+13	34782.61
146	4.623608	2.466303	1.21E-05	31.62243	9.85436E+13	34782.61
147	4.623608	2.127643	1.21E-05	31.62243	9.85436E+13	34782.61
148	4.623608	1.884559	1.21E-05	31.62243	9.85436E+13	34782.61
149	4.623608	1.701298	1.21E-05	31.62243	9.85436E+13	34782.61
150	4.623608	1.557987	1.21E-05	31.62243	9.85436E+13	34782.61
151	4.623608	1.442695	1.21E-05	31.62243	9.85436E+13	34782.61
152	4.623608	1.347823	1.21E-05	31.62243	9.85436E+13	34782.61
153	4.623608	1.268299	1.21E-05	31.62243	9.85436E+13	34782.61
154	3.015396	1.875423	1.36E-05	20.60914	2.09192E+14	33333.33
155	3.015396	1.875423	1.36E-05	22.67005	2.09192E+14	33333.33
156	3.015396	1.875423	1.36E-05	24.73097	2.09192E+14	33333.33

Table 7.6.3 contd.: Values of the non-dimensional groups for each set used in the regression analysis

Set	Π_1	Π_2	Π_3	Π_4	Π_5	Π_6
157	3.015396	1.875423	1.36E-05	26.79188	2.09192E+14	33333.33
158	3.015396	1.875423	1.36E-05	28.8528	2.09192E+14	33333.33
159	3.015396	1.875423	1.36E-05	30.91371	2.09192E+14	33333.33
160	3.015396	1.875423	1.36E-05	32.97462	2.09192E+14	33333.33
161	3.015396	1.875423	1.36E-05	35.03554	2.09192E+14	33333.33
162	3.015396	1.875423	1.36E-05	37.09645	2.09192E+14	33333.33
163	4.020528	1.557987	1.11E-05	19.63284	1.19368E+14	15000
164	4.020528	1.557987	1.11E-05	21.41765	1.19368E+14	15000
165	4.020528	1.557987	1.11E-05	23.20245	1.19368E+14	15000
166	4.020528	1.557987	1.11E-05	24.98725	1.19368E+14	15000
167	4.020528	1.557987	1.11E-05	26.77206	1.19368E+14	15000
168	4.020528	1.557987	1.11E-05	28.55686	1.19368E+14	15000
169	4.020528	1.557987	1.11E-05	30.34167	1.19368E+14	15000
170	4.020528	1.557987	1.11E-05	32.12647	1.19368E+14	15000
171	4.020528	1.557987	1.11E-05	33.91127	1.19368E+14	15000
172	4.422581	2.127643	1.57E-05	17.01744	9.24637E+13	36363.64
173	4.422581	2.127643	1.57E-05	18.71918	9.24637E+13	36363.64
174	4.422581	2.127643	1.57E-05	20.42093	9.24637E+13	36363.64
175	4.422581	2.127643	1.57E-05	22.12267	9.24637E+13	36363.64
176	4.422581	2.127643	1.57E-05	23.82441	9.24637E+13	36363.64
177	4.422581	2.127643	1.57E-05	25.52616	9.24637E+13	36363.64
178	4.422581	2.127643	1.57E-05	27.2279	9.24637E+13	36363.64
179	4.422581	2.127643	1.57E-05	28.92964	9.24637E+13	36363.64
180	4.422581	2.127643	1.57E-05	30.63139	9.24637E+13	36363.64
181	3.417449	2.466303	0.000017	23.2307	1.26399E+14	23529.41
182	3.417449	2.466303	1.55E-05	23.2307	1.26399E+14	23529.41
183	3.417449	2.466303	1.42E-05	23.2307	1.26399E+14	23529.41
184	3.417449	2.466303	1.31E-05	23.2307	1.26399E+14	23529.41

Table 7.6.3 contd.: Values of the non-dimensional groups for each set used in the regression analysis

Set	Π_1	Π_2	Π_3	Π_4	Π_5	Π_6
185	3.417449	2.466303	1.21E-05	23.2307	1.26399E+14	23529.41
186	3.417449	2.466303	1.13E-05	23.2307	1.26399E+14	23529.41
187	3.417449	2.466303	1.06E-05	23.2307	1.26399E+14	23529.41
188	3.417449	2.466303	0.00001	23.2307	1.26399E+14	23529.41
189	3.417449	2.466303	9.44E-06	23.2307	1.26399E+14	23529.41
190	3.819502	1.701298	1.73E-05	29.29872	1.45725E+14	31578.95
191	3.819502	1.701298	1.58E-05	29.29872	1.45725E+14	31578.95
192	3.819502	1.701298	1.46E-05	29.29872	1.45725E+14	31578.95
193	3.819502	1.701298	1.36E-05	29.29872	1.45725E+14	31578.95
194	3.819502	1.701298	1.27E-05	29.29872	1.45725E+14	31578.95
195	3.819502	1.701298	1.19E-05	29.29872	1.45725E+14	31578.95
196	3.819502	1.701298	1.12E-05	29.29872	1.45725E+14	31578.95
197	3.819502	1.701298	1.06E-05	29.29872	1.45725E+14	31578.95
198	3.819502	1.701298	0.00001	29.29872	1.45725E+14	31578.95
199	4.221555	1.442695	1.75E-05	33.09401	1.49423E+14	38095.24
200	4.221555	1.442695	1.62E-05	33.09401	1.49423E+14	38095.24
201	4.221555	1.442695	0.000015	33.09401	1.49423E+14	38095.24
202	4.221555	1.442695	0.000014	33.09401	1.49423E+14	38095.24
203	4.221555	1.442695	1.31E-05	33.09401	1.49423E+14	38095.24
204	4.221555	1.442695	1.24E-05	33.09401	1.49423E+14	38095.24
205	4.221555	1.442695	1.17E-05	33.09401	1.49423E+14	38095.24
206	4.221555	1.442695	1.11E-05	33.09401	1.49423E+14	38095.24
207	4.221555	1.442695	1.05E-05	33.09401	1.49423E+14	38095.24
208	3.216423	2.127643	0.000016	19.95471	1.20173E+14	18750
209	3.216423	2.127643	0.000016	19.95471	1.27138E+14	18750
210	3.216423	2.127643	0.000016	19.95471	1.34299E+14	18750
211	3.216423	2.127643	0.000016	19.95471	1.41656E+14	18750
212	3.216423	2.127643	0.000016	19.95471	1.4921E+14	18750
213	3.216423	2.127643	0.000016	19.95471	1.5696E+14	18750

Table 7.6.3 contd.: Values of the non-dimensional groups for each set used in the regression analysis

Set	Π_1	Π_2	Π_3	Π_4	Π_5	Π_6
214	3.216423	2.127643	0.000016	19.95471	1.64906E+14	18750
215	3.216423	2.127643	0.000016	19.95471	1.73048E+14	18750
216	3.216423	2.127643	0.000016	19.95471	1.81387E+14	18750
217	4.020528	1.701298	1.43E-05	24.98725	1.0171E+14	30000
218	4.020528	1.701298	1.43E-05	24.98725	1.07439E+14	30000
219	4.020528	1.701298	1.43E-05	24.98725	1.13325E+14	30000
220	4.020528	1.701298	1.43E-05	24.98725	1.19368E+14	30000
221	4.020528	1.701298	1.43E-05	24.98725	1.25568E+14	30000
222	4.020528	1.701298	1.43E-05	24.98725	1.31925E+14	30000
223	4.020528	1.701298	1.43E-05	24.98725	1.38439E+14	30000
224	4.020528	1.701298	1.43E-05	24.98725	1.4511E+14	30000
225	4.020528	1.701298	1.43E-05	24.98725	1.56894E+14	30000
226	4.623608	1.875423	1.21E-05	33.28676	8.84435E+13	34782.61
227	4.623608	1.875423	1.21E-05	33.28676	9.34253E+13	34782.61
228	4.623608	1.875423	1.21E-05	33.28676	9.85436E+13	34782.61
229	4.623608	1.875423	1.21E-05	33.28676	1.03798E+14	34782.61
230	4.623608	1.875423	1.21E-05	33.28676	1.0919E+14	34782.61
231	4.623608	1.875423	1.21E-05	33.28676	1.14717E+14	34782.61
232	4.623608	1.875423	1.21E-05	33.28676	1.20381E+14	34782.61
233	4.623608	1.875423	1.21E-05	33.28676	1.26182E+14	34782.61
234	4.623608	1.875423	1.21E-05	33.28676	1.3643E+14	34782.61
235	3.015396	1.875423	0.000015	20.60914	2.09192E+14	6666.667
236	3.015396	1.875423	0.000015	20.60914	2.09192E+14	13333.33
237	3.015396	1.875423	0.000015	20.60914	2.09192E+14	20000
238	3.015396	1.875423	0.000015	20.60914	2.09192E+14	26666.67
239	3.015396	1.875423	0.000015	20.60914	2.09192E+14	33333.33
240	3.015396	1.875423	0.000015	20.60914	2.09192E+14	40000
241	3.015396	1.875423	0.000015	20.60914	2.09192E+14	46666.67

Table 7.6.3 contd.: Values of the non-dimensional groups for each set used in the regression analysis

Set	Π_1	Π_2	Π_3	Π_4	Π_5	Π_6
242	3.015396	1.875423	0.000015	20.60914	2.09192E+14	53333.33
243	3.015396	1.875423	0.000015	20.60914	2.09192E+14	60000
244	4.020528	2.127643	1.33E-05	26.77206	1.25568E+14	5000
245	4.020528	2.127643	1.33E-05	26.77206	1.25568E+14	10000
246	4.020528	2.127643	1.33E-05	26.77206	1.25568E+14	15000
247	4.020528	2.127643	1.33E-05	26.77206	1.25568E+14	20000
248	4.020528	2.127643	1.33E-05	26.77206	1.25568E+14	25000
249	4.020528	2.127643	1.33E-05	26.77206	1.25568E+14	30000
250	4.020528	2.127643	1.33E-05	26.77206	1.25568E+14	35000
251	4.020528	2.127643	1.33E-05	26.77206	1.25568E+14	40000
252	4.020528	2.127643	1.33E-05	26.77206	1.25568E+14	45000
253	4.422581	1.347823	0.000011	34.03488	1.03023E+14	4545.455
254	4.422581	1.347823	0.000011	34.03488	1.03023E+14	9090.909
255	4.422581	1.347823	0.000011	34.03488	1.03023E+14	13636.36
256	4.422581	1.347823	0.000011	34.03488	1.03023E+14	18181.82
257	4.422581	1.347823	0.000011	34.03488	1.03023E+14	22727.27
258	4.422581	1.347823	0.000011	34.03488	1.03023E+14	27272.73
259	4.422581	1.347823	0.000011	34.03488	1.03023E+14	31818.18
260	4.422581	1.347823	0.000011	34.03488	1.03023E+14	36363.64
261	4.422581	1.347823	0.000011	34.03488	1.03023E+14	40909.09
262	3.015396	1.875423	0.000015	20.60914	1.35613E+14	20000
263	3.216423	1.875423	1.5E-05	20.60915	1.35613E+14	20000
264	3.417449	1.875423	1.5E-05	20.60913	1.35613E+14	20000
265	3.618475	1.875423	0.000015	20.60914	1.35613E+14	20000
266	3.819502	1.875423	1.5E-05	20.60914	1.35613E+14	20000
267	4.020528	1.875423	1.5E-05	20.60915	1.35613E+14	20000
268	4.221555	1.875423	0.000015	20.60914	1.35613E+14	20000
269	4.422581	1.875423	1.5E-05	20.60914	1.35613E+14	20000

Table 7.6.3 contd.: Values of the non-dimensional groups for each set used in the regression analysis

Set	Π_1	Π_2	Π_3	Π_4	Π_5	Π_6
270	4.623608	1.875423	1.5E-05	20.60913	1.35613E+14	20000
271	3.417449	2.972013	1.42E-05	29.03837	1.13104E+14	29411.76
272	3.618475	2.972013	1.42E-05	29.03837	1.13104E+14	29411.77
273	3.819502	2.972013	1.42E-05	29.03837	1.13104E+14	29411.76
274	4.020528	2.972013	1.42E-05	29.03837	1.13104E+14	29411.77
275	4.221555	2.972013	1.42E-05	29.03838	1.13104E+14	29411.77
276	4.422581	2.972013	1.42E-05	29.03837	1.13104E+14	29411.76
277	4.623608	2.972013	1.42E-05	29.03837	1.13104E+14	29411.77
278	4.824634	2.972013	1.42E-05	29.03838	1.13104E+14	29411.77
279	5.02566	2.972013	1.42E-05	29.03837	1.13104E+14	29411.76
280	3.015396	2.127643	1.36E-05	32.97462	1.31873E+14	26666.67
281	3.216423	2.127643	1.36E-05	32.97463	1.31873E+14	26666.67
282	3.417449	2.127643	1.36E-05	32.97462	1.31873E+14	26666.66
283	3.618475	2.127643	1.36E-05	32.97462	1.31873E+14	26666.67
284	3.819502	2.127643	1.36E-05	32.97463	1.31873E+14	26666.67
285	4.020528	2.127643	1.36E-05	32.97463	1.31873E+14	26666.67
286	4.221555	2.127643	1.36E-05	32.97463	1.31873E+14	26666.67
287	4.422581	2.127643	1.36E-05	32.97462	1.31873E+14	26666.67
288	4.623608	2.127643	1.36E-05	32.97462	1.31873E+14	26666.67

Table 7.6.3 contd.: Values of the non-dimensional groups for each set used in the regression analysis

Set	T_{me} ($kgm^{-2}s^{-1}$)	a_{2e} ($kgm^{-2}s^{-1}$)	a_{4e} ($kgm^{-2}s^{-1}$)
100	2.864754	-1.32386	0.546523
101	2.412122	-1.11078	0.468989
102	1.822025	-0.83753	0.359595
103	1.393602	-0.63981	0.278614
104	1.088004	-0.49911	0.219941
105	0.916325	-0.42167	0.186914
106	0.72351	-0.33244	0.148672
107	0.58165	-0.2669	0.120313
108	0.475573	-0.21798	0.098952
109	21.49324	-10.352	3.51653
110	16.67213	-8.0314	2.725976
111	13.15964	-6.34108	2.151023
112	11.08951	-5.34012	1.822673
113	8.823102	-4.25155	1.446571
114	7.128315	-3.43715	1.165928
115	5.841696	-2.81865	0.953274
116	4.851264	-2.34227	0.789832
117	4.079032	-1.97068	0.662615
118	30.0645	-14.667	4.681702
119	27.24828	-13.313	4.226326
120	24.7721	-12.1227	3.827291
121	22.58886	-11.0719	3.476874
122	20.65841	-10.1424	3.168052
123	18.94697	-9.3177	2.895268
124	17.4259	-8.58382	2.653728
125	16.07056	-7.9288	2.43929
126	14.86001	-7.34344	2.24852
127	1.078861	-0.5264	0.205589

Set	T_{me} ($kgm^{-2}s^{-1}$)	a_{2e} ($kgm^{-2}s^{-1}$)	a_{4e} ($kgm^{-2}s^{-1}$)
128	1.400625	-0.68739	0.260048
129	1.765498	-0.87042	0.319666
130	2.159559	-1.06838	0.38208
131	2.570734	-1.27497	0.445487
132	2.989583	-1.48532	0.508657
133	3.409301	-1.69592	0.570814
134	3.825257	-1.90441	0.631501
135	4.234531	-2.10901	0.690514
136	3.78087	-1.81009	0.654858
137	4.83989	-2.32848	0.824195
138	6.048903	-2.92302	1.012766
139	7.362115	-3.57113	1.213105
140	8.73822	-4.25208	1.419102
141	10.14387	-4.94916	1.626275
142	11.18404	-5.46921	1.771665
143	11.94355	-5.85177	1.871946
144	12.66015	-6.21262	1.9661
145	7.526225	-3.64863	1.288544
146	9.298034	-4.52219	1.561142
147	11.22343	-5.47303	1.850518
148	13.22927	-6.46471	2.146076
149	15.25991	-7.46903	2.440557
150	17.2764	-8.46646	2.72944
151	19.25387	-9.44435	3.010069
152	21.17699	-10.3952	3.281081
153	23.03851	-11.315	3.54202
154	4.666095	-2.18871	0.866685
155	8.151014	-3.8743	1.516374

Table 7.6.4: Equilibrium values for each data set used in the regression analysis

Set	T_{me} ($kgm^{-2}s^{-1}$)	a_{2e} ($kgm^{-2}s^{-1}$)	a_{4e} ($kgm^{-2}s^{-1}$)
156	12.37044	-5.99832	2.229582
157	16.54713	-8.18469	2.812639
158	22.64869	-10.993	3.688898
159	30.77154	-14.8177	5.065176
160	40.74382	-19.6104	6.76872
161	52.80243	-25.4508	8.794469
162	47.79727	-23.0981	7.901285
163	5.480268	-2.61688	1.030762
164	7.822156	-3.82425	1.403072
165	10.33796	-5.16402	1.716384
166	14.26972	-6.95005	2.275852
167	19.31128	-9.3465	3.116718
168	25.50292	-12.3358	4.151379
169	26.43354	-12.8254	4.29454
170	25.84878	-12.5825	4.161051
171	29.9788	-14.6041	4.784264
172	0.887065	-0.40579	0.181542
173	1.4921	-0.69979	0.299259
174	2.227048	-1.07834	0.424625
175	3.001463	-1.4997	0.524425
176	4.279109	-2.07116	0.705612
177	6.015136	-2.88348	1.007226
178	8.177833	-3.92424	1.384839
179	10.77208	-5.19674	1.822433
180	10.78894	-5.24735	1.789743
181	4.87555	-2.34867	0.923352
182	5.125556	-2.46103	0.977928
183	5.362713	-2.56712	1.029838

Set	T_{me} ($kgm^{-2}s^{-1}$)	a_{2e} ($kgm^{-2}s^{-1}$)	a_{4e} ($kgm^{-2}s^{-1}$)
184	5.588499	-2.6677	1.079326
185	5.804197	-2.76349	1.126692
186	6.010866	-2.85503	1.17212
187	6.209401	-2.94267	1.215794
188	6.400507	-3.02682	1.257853
189	6.584917	-3.10787	1.298467
190	17.33683	-8.39723	2.832461
191	18.36912	-8.88856	3.005254
192	19.36748	-9.36338	3.171693
193	20.3355	-9.82398	3.332436
194	21.27632	-10.2714	3.487907
195	22.19269	-10.7074	3.638759
196	23.0864	-11.1328	3.7853
197	23.95981	-11.5488	3.927912
198	24.81398	-11.9559	4.066587
199	19.73104	-9.68276	3.019312
200	20.52968	-10.0731	3.153908
201	21.30041	-10.4489	3.284428
202	22.04654	-10.8111	3.411161
203	22.77078	-11.1617	3.534443
204	23.47586	-11.5024	3.654471
205	24.16413	-11.8339	3.771847
206	24.83802	-12.1586	3.886893
207	25.49934	-12.4763	3.999684
208	3.020778	-1.4039	0.571426
209	3.03438	-1.41027	0.574739
210	3.047722	-1.41652	0.577993
211	3.060804	-1.42266	0.581181

Table 7.6.4 contd.: Equilibrium values for each data set used in the regression analysis

Set	T_{me} ($kgm^{-2}s^{-1}$)	a_{2e} ($kgm^{-2}s^{-1}$)	a_{4e} ($kgm^{-2}s^{-1}$)
212	3.073645	-1.42867	0.584304
213	3.086242	-1.43457	0.58737
214	3.098623	-1.44037	0.590383
215	3.110785	-1.44608	0.593341
216	3.122738	-1.45168	0.59625
217	10.53813	-5.10615	1.707567
218	10.36153	-5.02203	1.677043
219	10.19273	-4.94149	1.647925
220	10.03127	-4.8644	1.620102
221	9.876732	-4.79059	1.593503
222	9.7285	-4.71978	1.568025
223	9.586249	-4.65189	1.543603
224	9.449652	-4.58669	1.520203
225	9.227731	-4.48055	1.48218
226	16.24508	-7.94276	2.595683
227	15.97832	-7.81736	2.547699
228	15.72358	-7.69756	2.501988
229	15.48002	-7.58309	2.458347
230	15.24686	-7.47346	2.416644
231	15.02332	-7.36816	2.376753
232	14.80899	-7.26721	2.338556
233	14.60316	-7.17033	2.301901
234	14.26902	-7.01281	2.242622
235	4.527637	-2.12692	0.839952
236	4.528575	-2.12718	0.840331
237	4.529573	-2.12742	0.840805
238	4.530617	-2.12761	0.841413
239	4.531726	-2.12778	0.842117

Set	T_{me} ($kgm^{-2}s^{-1}$)	a_{2e} ($kgm^{-2}s^{-1}$)	a_{4e} ($kgm^{-2}s^{-1}$)
240	4.532905	-2.12786	0.842963
241	4.534157	-2.12793	0.843922
242	4.535497	-2.12791	0.845008
243	4.536944	-2.12791	0.846225
244	10.01262	-4.79444	1.677409
245	9.897188	-4.73954	1.6577
246	9.785769	-4.68654	1.638759
247	9.678182	-4.63531	1.620506
248	9.574093	-4.58573	1.602912
249	9.473427	-4.53762	1.585968
250	9.375867	-4.49096	1.569628
251	9.281252	-4.4457	1.553828
252	9.189485	-4.40173	1.538564
253	31.52434	-15.3921	4.880782
254	31.4568	-15.3592	4.870327
255	31.3649	-15.3141	4.856263
256	31.2567	-15.2609	4.839832
257	31.13721	-15.2022	4.821801
258	31.00965	-15.1395	4.802715
259	30.87627	-15.0739	4.782799
260	30.73882	-15.0062	4.762444
261	30.59796	-14.9368	4.741746
262	4.404161	-2.06805	0.810508
263	4.782888	-2.24747	0.898549
264	4.810108	-2.26739	0.914483
265	4.311173	-2.04273	0.822491
266	3.882356	-1.85124	0.739328
267	3.651667	-1.76401	0.684311

Table 7.6.4 contd.: Equilibrium values for each data set used in the regression analysis

Set	T_{me} ($kgm^{-2}s^{-1}$)	a_{2e} ($kgm^{-2}s^{-1}$)	a_{4e} ($kgm^{-2}s^{-1}$)
268	3.240888	-1.57514	0.603116
269	2.894834	-1.41616	0.533881
270	2.601253	-1.2813	0.474483
271	11.49189	-5.44184	1.992587
272	10.14905	-4.79946	1.772105
273	9.061525	-4.28729	1.590897
274	8.527319	-4.04614	1.508127
275	7.599314	-3.61583	1.341018
276	6.846628	-3.26806	1.203945
277	6.230908	-2.9848	1.090477
278	5.307526	-2.55515	0.918535
279	4.699225	-2.27326	0.804307
280	42.08814	-20.1199	7.173185
281	36.67471	-17.5559	6.256396
282	32.24812	-15.4699	5.49475
283	23.70652	-11.4158	4.007276
284	18.92954	-9.15217	3.16989
285	16.3423	-7.94597	2.695341
286	14.3634	-7.01159	2.34172
287	12.78719	-6.26842	2.057323
288	11.50512	-5.66399	1.823369

Table 7.6.4 contd.: Equilibrium values for each data set used in the regression analysis

	α	β_1	β_2	β_3	β_4	β_5
T_m	-1.388	1.183	0.832	0.206	----------	----------
a_2	-1.537	1.165	0.870	0.214	----------	----------
a_4	-6.418	1.164	0.785	0.358	----------	----------
a_6	5.523e-11	-3.188	----------	-1.408	1.925	----------
b_2	369.084	-3.614	-1.512	-1.291	2.478	-0.808
b_4	35.84	-3.541	-1.200	-1.159	2.321	-0.704
b_6	0.02124	-4.326	----------	-1.605	1.595	-0.627

Table 7.7.1a: Results of parameterisation

	r^2	F-obs	mean % error	max % error	mean diff ($kgm^{-2}s^{-1}$)	max diff ($kgm^{-2}s^{-1}$)
T_m	0.952	1234.7	2.254	11.778	0.015182	0.066199
a_2	0.951	1199.9	2.299	11.694	0.015563	0.06602
a_4	0.913	644.6	3.457	22.552	0.02057	0.09923
a_6	0.793	236.9	34.603	1249.454	0.000409	0.002946
b_2	0.976	1493.7	14.174	49.392	0.002224	0.011463
b_4	0.979	1669.6	12.118	39.104	0.001013	0.004305
b_6	0.836	231.9	28.697	288.346	0.000148	0.000955

Table 7.7.1b: Analysis of parameterisation

Set	$\bar{u}_c$	Π_4
100	0.40382	12.28676
101	0.401608	11.94074
102	0.399535	11.62435
103	0.397576	11.33369
104	0.395718	11.06543
105	0.38651	10.94959
106	0.388272	10.65502
107	0.389955	10.3814
108	0.391572	10.1263
109	0.405466	21.18899
110	0.403497	20.62904
111	0.40165	20.11266
112	0.39234	19.76956
113	0.39415	19.26159
114	0.395879	18.78931
115	0.397546	18.34856
116	0.399131	17.93641
117	0.400654	17.54971
118	0.396119	27.93624
119	0.397001	27.59431
120	0.397854	27.26442
121	0.398708	26.94541
122	0.399534	26.63717
123	0.400333	26.33911
124	0.401132	26.05029
125	0.401903	25.77066
126	0.402673	25.49936
127	0.386658	13.841
128	0.383623	13.89264
129	0.380796	13.94075
130	0.378146	13.98585
131	0.375641	14.02848
132	0.373264	14.06893
133	0.371016	14.10718
134	0.368881	14.14352
135	0.366842	14.17821
136	0.41119	20.57427
137	0.408104	20.62353
138	0.405209	20.66975
139	0.402483	20.71326
140	0.399924	20.75412
141	0.397509	20.79267
142	0.395214	20.82931
143	0.39304	20.86401
144	0.390937	20.89758
145	0.414135	24.72982
146	0.411099	24.78035
147	0.408246	24.82783
148	0.405576	24.87227
149	0.403059	24.91416
150	0.400664	24.95402

Set	$\bar{u}_c$	Π_4
151	0.398422	24.99134
152	0.396241	25.02764
153	0.394213	25.06139
154	0.398788	12.39046
155	0.398646	14.4543
156	0.398533	16.51755
157	0.398454	18.58009
158	0.398376	20.64261
159	0.398338	22.70431
160	0.398278	24.76646
161	0.398251	26.82793
162	0.39823	28.88927
163	0.398602	12.51858
164	0.398563	14.30408
165	0.398534	16.0894
166	0.398508	17.87467
167	0.398489	19.65981
168	0.398478	21.44481
169	0.398481	23.22956
170	0.398457	25.01479
171	0.398475	26.79928
172	0.393541	10.32038
173	0.393362	12.02517
174	0.393216	13.7294
175	0.393102	15.43308
176	0.393004	17.13649
177	0.39293	18.83949
178	0.392898	20.54178
179	0.392846	22.24441
180	0.392811	23.94675
181	0.397692	15.53181
182	0.401669	15.45482
183	0.405239	15.38571
184	0.40846	15.32336
185	0.411409	15.26627
186	0.414126	15.21367
187	0.41665	15.16481
188	0.41898	15.1197
189	0.421176	15.07719
190	0.385813	22.23383
191	0.389807	22.16069
192	0.393381	22.09525
193	0.396605	22.03621
194	0.39955	21.98228
195	0.402284	21.93222
196	0.404785	21.88642
197	0.407147	21.84317
198	0.409323	21.80332
199	0.373879	26.58183
200	0.377831	26.51299
201	0.381363	26.45147

Table 7.7.2: Extra data used in regression analysis

Set	$\bar{u}_c$	Π_4
202	0.384579	26.39546
203	0.387507	26.34446
204	0.390199	26.29757
205	0.392681	26.25434
206	0.395006	26.21384
207	0.397173	26.17609
208	0.399025	11.99228
209	0.399037	11.99204
210	0.399033	11.99212
211	0.399029	11.9922
212	0.399025	11.99228
213	0.399036	11.99206
214	0.399032	11.99214
215	0.399028	11.99222
216	0.399024	11.9923
217	0.387466	18.07175
218	0.387482	18.07146
219	0.387474	18.0716
220	0.387468	18.07171
221	0.387482	18.07146
222	0.387475	18.07159
223	0.387469	18.07169
224	0.387483	18.07144
225	0.387481	18.07148
226	0.405438	26.5389
227	0.405442	26.53884
228	0.405445	26.53879
229	0.405448	26.53874
230	0.405452	26.53867
231	0.405425	26.53912
232	0.405428	26.53907
233	0.405431	26.53902
234	0.405426	26.5391
235	0.401917	12.32598
236	0.400243	12.36048
237	0.398465	12.39712
238	0.396596	12.43564
239	0.394608	12.47661
240	0.39249	12.52026
241	0.390227	12.5669
242	0.387806	12.61679
243	0.385188	12.67075
244	0.401488	19.60629
245	0.400353	19.62654

Set	$\bar{u}_c$	Π_4
246	0.399172	19.64762
247	0.397968	19.66911
248	0.396696	19.69181
249	0.3954	19.71494
250	0.394037	19.73927
251	0.392604	19.76485
252	0.391126	19.79123
253	0.403372	27.17052
254	0.402498	27.18539
255	0.401623	27.20028
256	0.400716	27.21572
257	0.399776	27.23171
258	0.398804	27.24825
259	0.3978	27.26534
260	0.396795	27.28244
261	0.395725	27.30065
262	0.398461	12.3972
263	0.398442	12.65835
264	0.398414	12.89627
265	0.398377	13.11428
266	0.39836	13.31449
267	0.390811	13.63394
268	0.394246	13.7422
269	0.397546	13.84392
270	0.400729	13.93965
271	0.406448	21.16998
272	0.406421	21.39217
273	0.406415	21.59622
274	0.398712	21.92214
275	0.402227	22.03243
276	0.4056	22.1361
277	0.40886	22.23356
278	0.411981	22.32599
279	0.415015	22.41317
280	0.402949	24.67019
281	0.40292	24.93447
282	0.402913	25.17466
283	0.402906	25.39455
284	0.402876	25.59729
285	0.395278	25.91969
286	0.398747	26.0293
287	0.402097	26.13196
288	0.40533	26.22856

Table 7.7.2contd: Extra data used in regression analysis

Set	T_m ($kgm^{-2}s^{-1}$)	a_2 ($kgm^{-2}s^{-1}$)	a_4 ($kgm^{-2}s^{-1}$)	a_6 ($kgm^{-2}s^{-1}$)	b_2 ($kgm^{-2}s^{-1}$)	b_4 ($kgm^{-2}s^{-1}$)	b_6 ($kgm^{-2}s^{-1}$)
1	2.733338	-1.30174	0.45254	-0.06059	-0.25621	0.161639	-0.02868
2	1.143613	-0.54292	0.204655	-0.02971	-0.08084	0.05543	-0.00973
3	0.478348	-0.22554	0.091151	-0.01417	-0.02349	0.017781	-0.00355
4	16.00282	-7.77014	2.390988	-0.18196	-0.71124	0.408212	-0.03709
5	18.89108	-9.20842	2.754808	-0.21945	-1.65428	0.888671	-0.06509
6	15.16021	-7.37523	2.194236	-0.15904	-0.9126	0.536369	-0.05569
7	1.346637	-0.63657	0.214849	-0.0349	-0.19418	0.119489	-0.0232

Table 7.7.3: Transport at maximum velocity and Fourier coefficients for independent sets

Set	Π_1	Π_2	Π_3	Π_4	Π_5	Π_6	$\overline{u}_c$
1	3.02E+00	1.875423	0.000015	12.40402	2.09192E+14	20000	0.39813
2	4.02E+00	1.875423	0.00002	11.04919	1.56894E+14	15000	0.38093
3	5.03E+00	1.875423	0.000025	9.757425	1.25515E+14	12000	0.388777
4	4.02E+00	1.875423	0.00002	28.90317	1.56894E+14	15000	0.380597
5	4.02E+00	1.875423	0.00001	28.43841	1.56894E+14	15000	0.406637
6	4.02E+00	1.875423	0.00002	29.15696	1.56894E+14	45000	0.366378
7	4.02E+00	1.875423	0.00001	10.58767	1.56894E+14	15000	0.406788

Table 7.7.4: Values of the non-dimensional groups and critical depth-average flow velocity for each independent set

Set	T_{me} ($kgm^{-2}s^{-1}$)	a_{2e} ($kgm^{-2}s^{-1}$)	a_{4e} ($kgm^{-2}s^{-1}$)	a_{6e} ($kgm^{-2}s^{-1}$)
1	4.580468	-2.15219	0.849715	-0.13361
2	1.59695	-0.74914	0.312104	-0.05191
3	0.585025	-0.27261	0.118503	-0.02094
4	21.39508	-10.3204	3.342453	-0.29481
5	27.10905	-13.1566	4.379759	-0.37357
6	19.9682	-9.62894	3.129845	-0.28173
7	2.146879	-0.99042	0.428676	-0.08294

Table 7.7.5: Equilibrium values for each independent data set

	Mean % error	Max % error	Mean diff ($kgm^{-2}s^{-1}$)	Max diff ($kgm^{-2}s^{-1}$)
T_m	3.305	7.919	0.022788	0.049675
a_2	2.848	6.027	0.019911	0.03874
a_4	6.168	15.359	0.037261	0.076979
a_6	31.961	65.595	0.00052	0.001492
b_2	11.855	20.1596	0.001493	0.005952
b_4	10.994	16.986	0.00077	0.002471
b_6	32.055	53.638	0.000169	0.000502

Table 7.7.6: Effect of parameterisation on independent sets

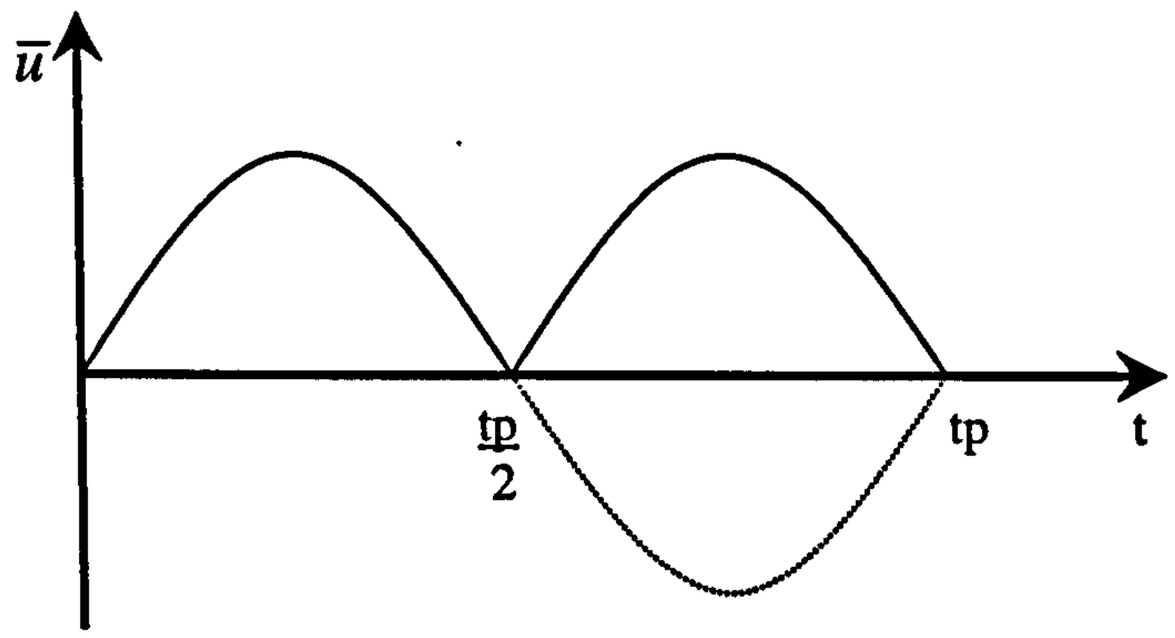

Figure 7.3.1: Period of the Fourier approximation

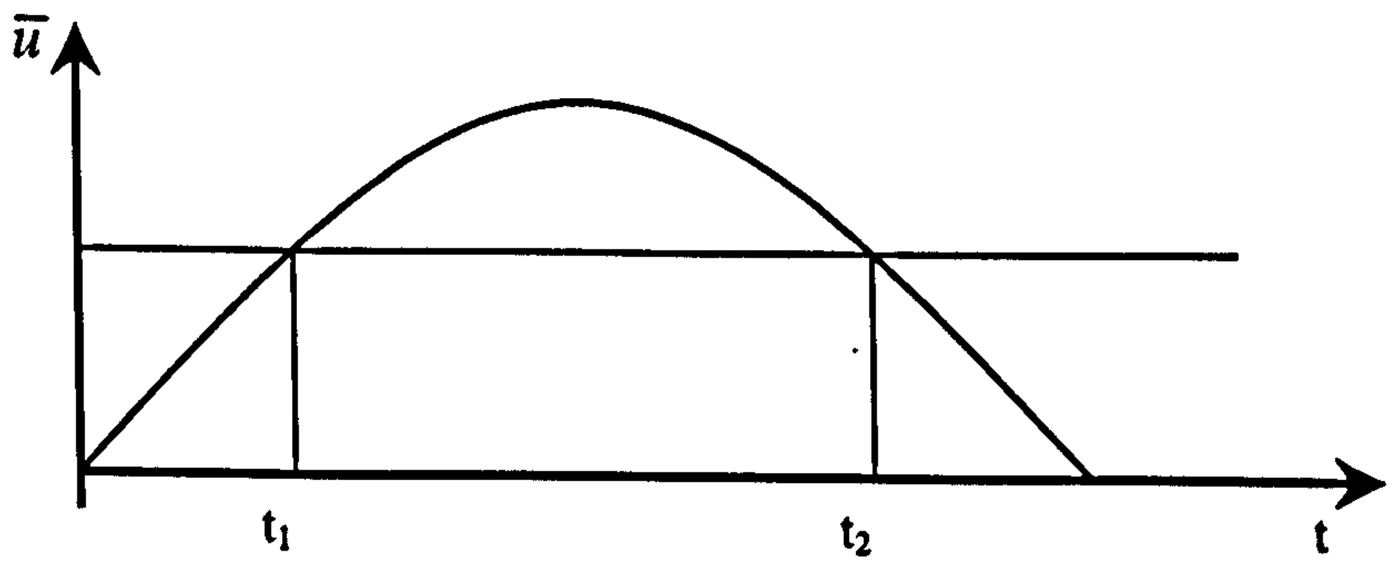

Figure 7.3.2: Time at equal depth-average velocity

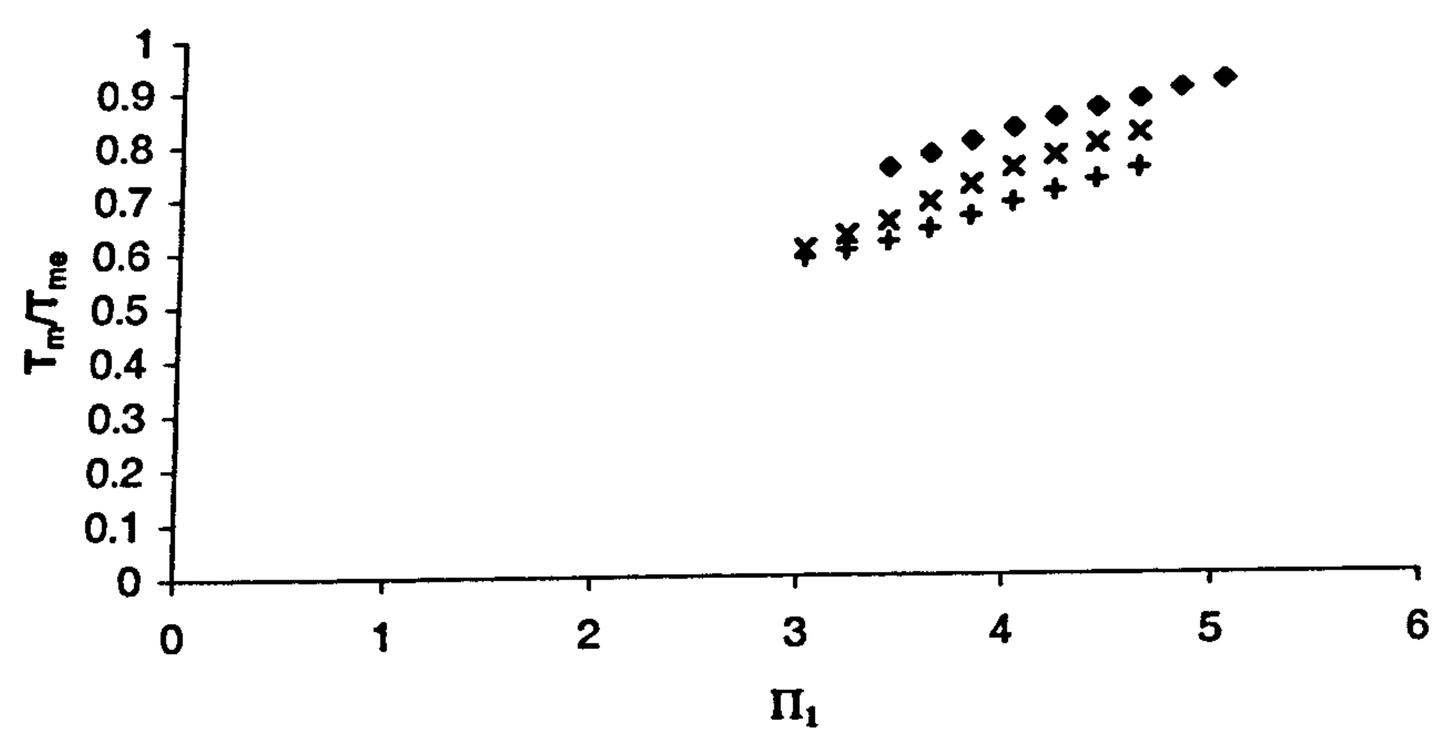

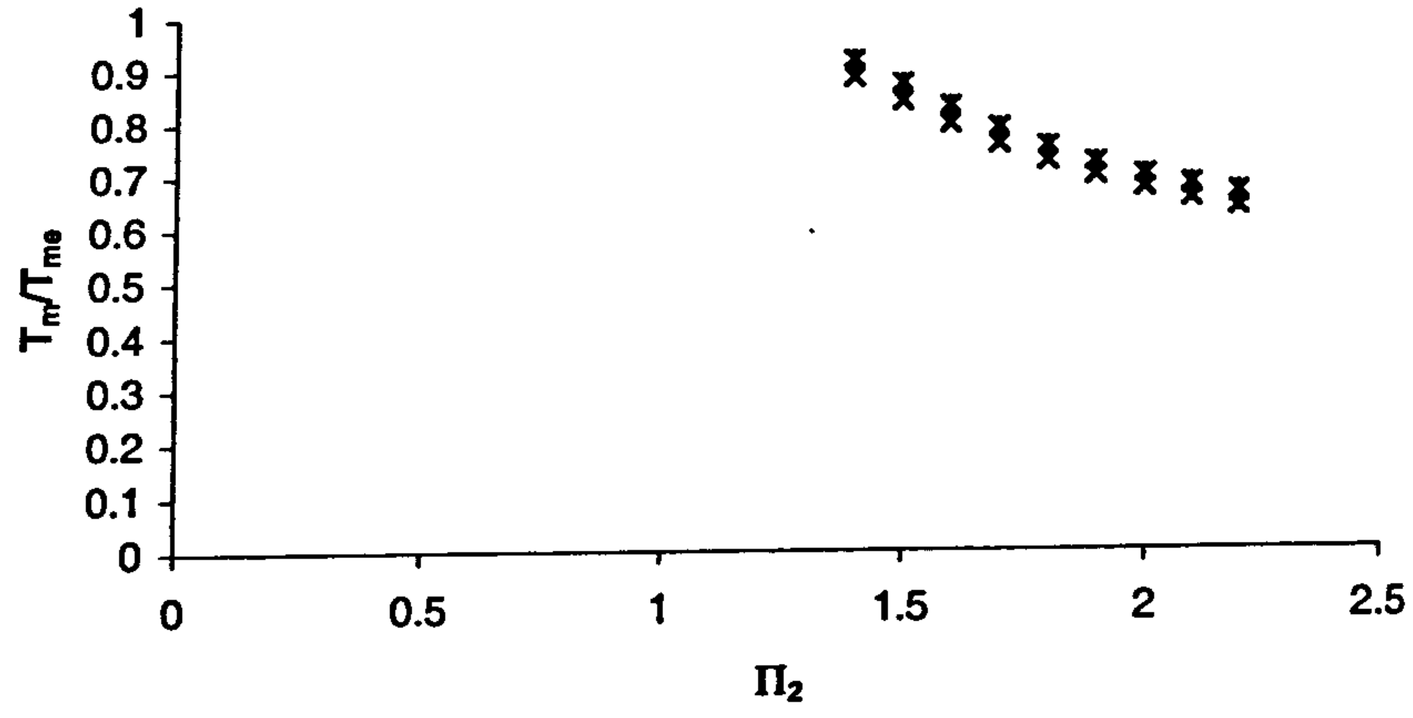

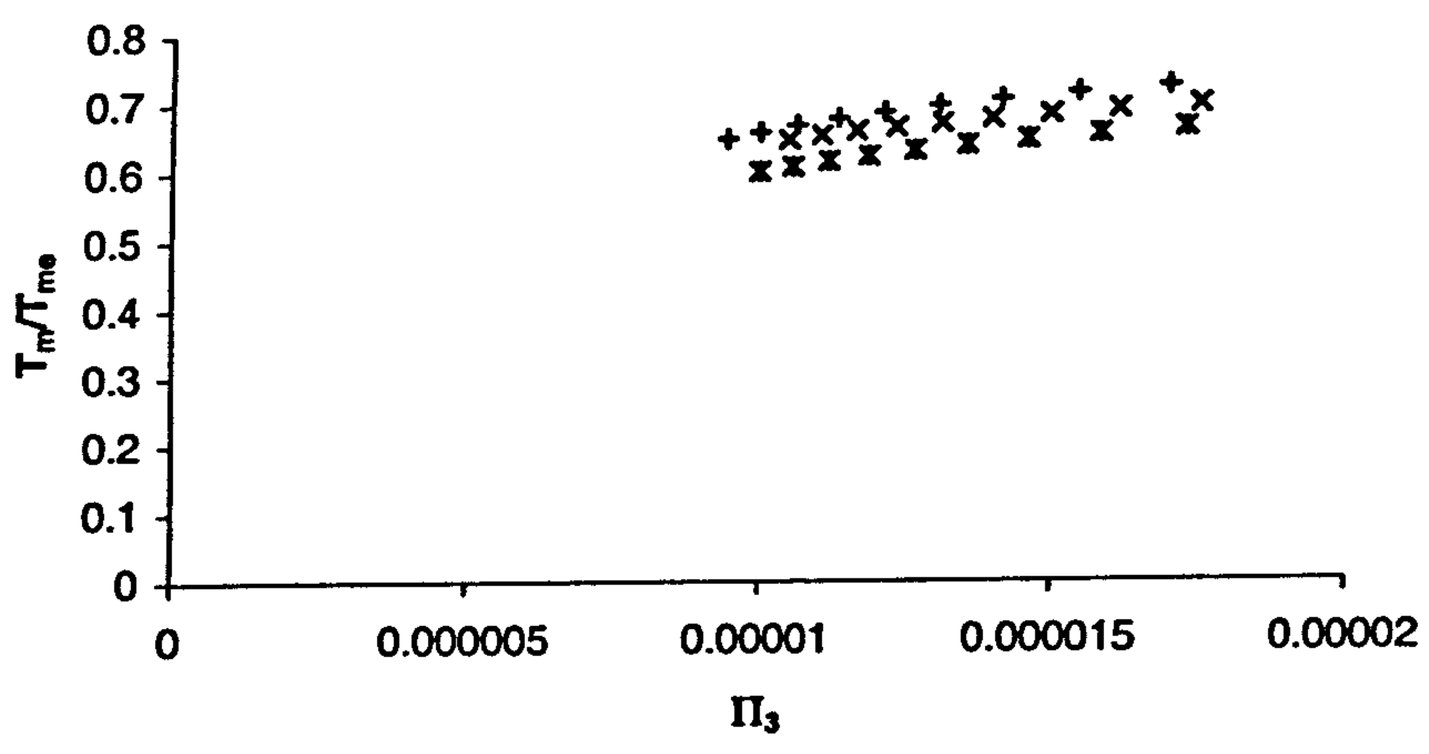

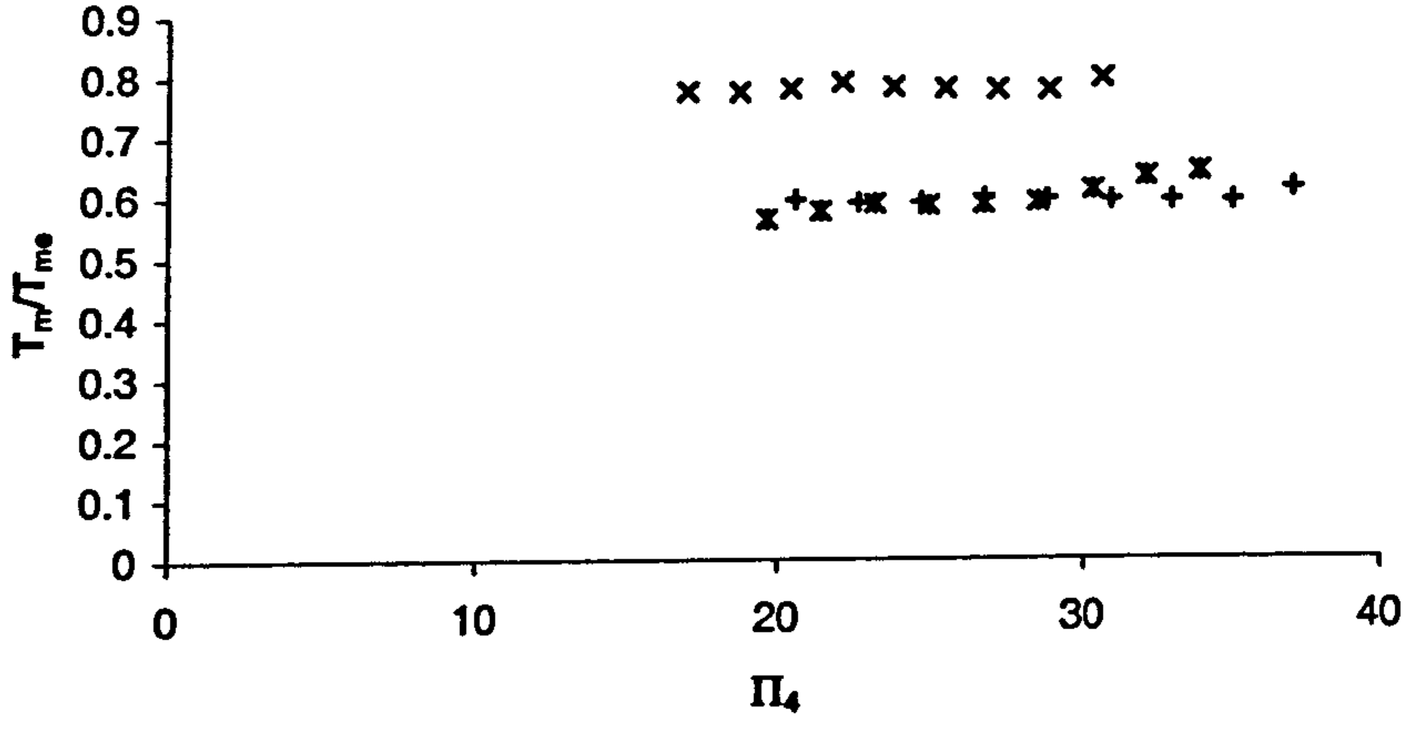

Figure 7.6.1a-d: Parameterisation quantity versus non-dimensional group values for the data sets used in the regression analysis
(Symbols represent the three sets of nine for each group)

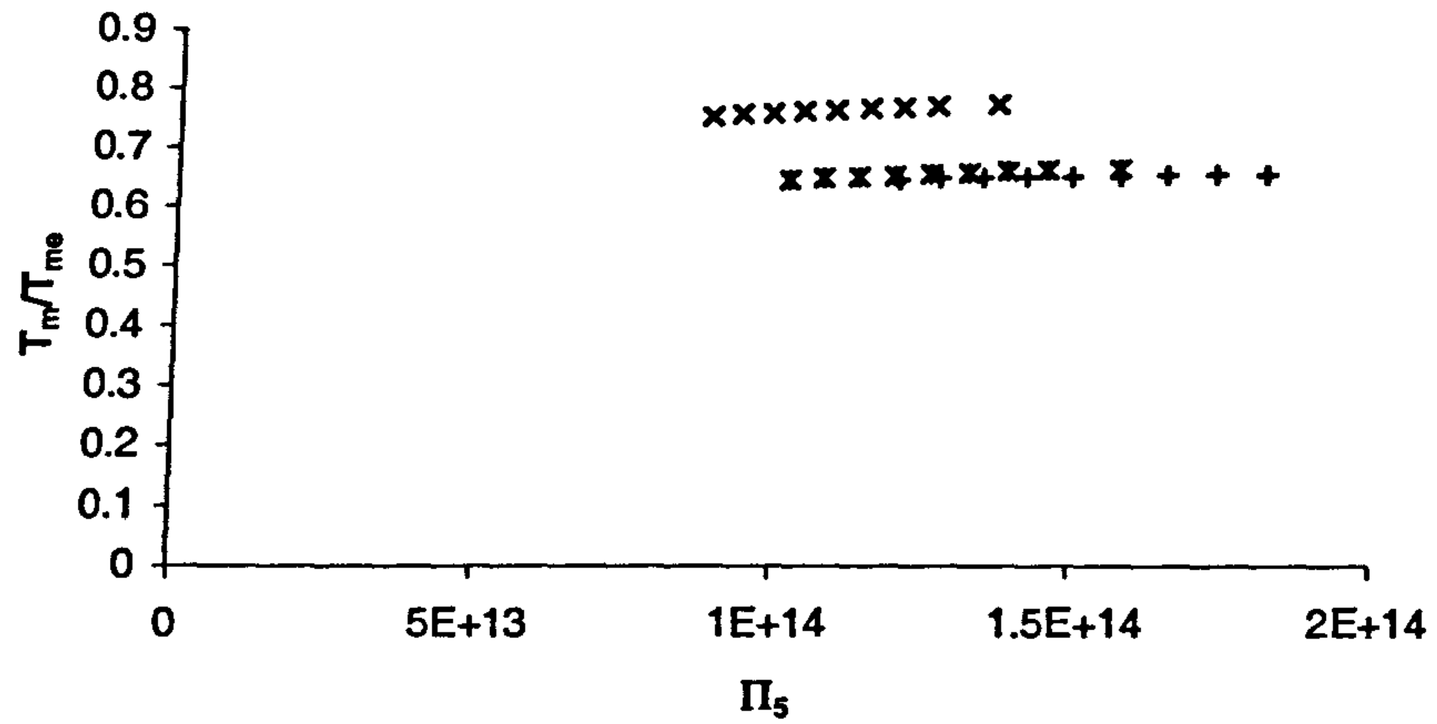

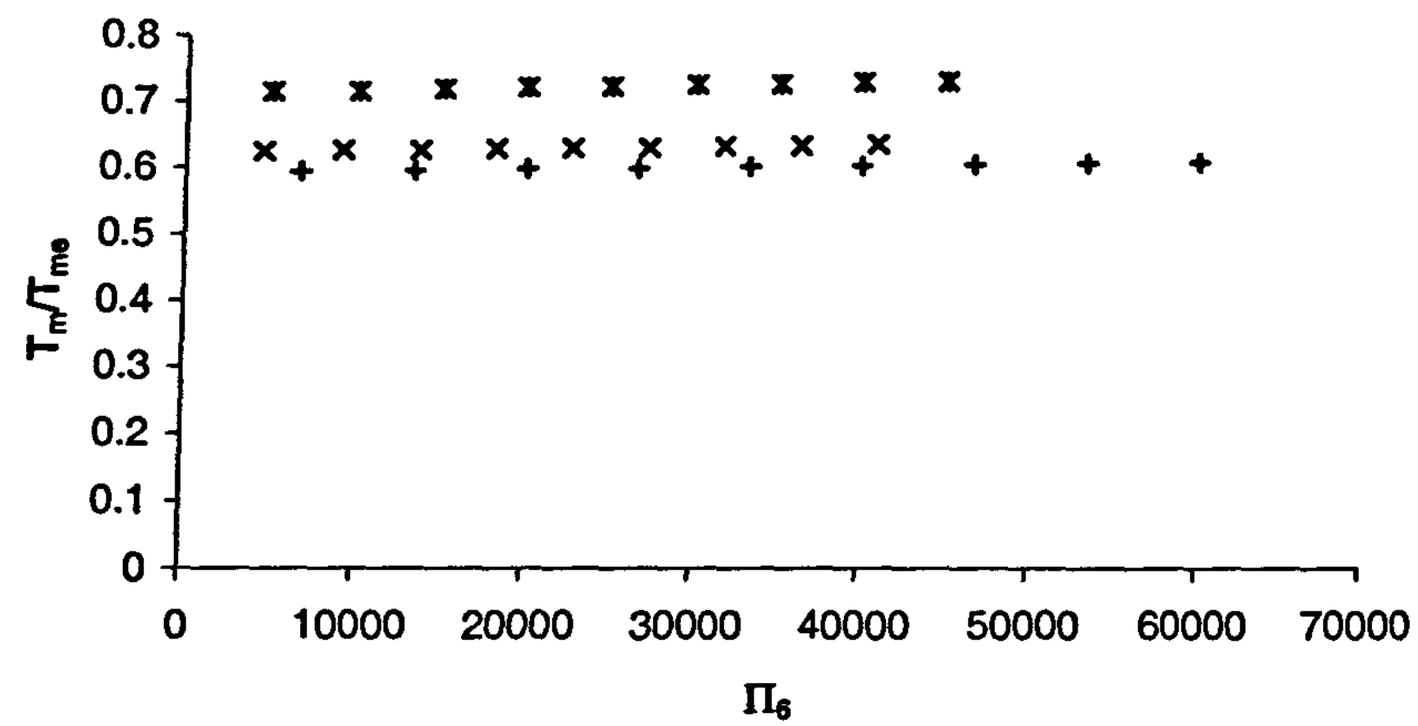

Figure 7.6.1e-f: Parameterisation quantity versus non-dimensional group values for the data sets used in the regression analysis
(Symbols represent the three sets of nine for each group)

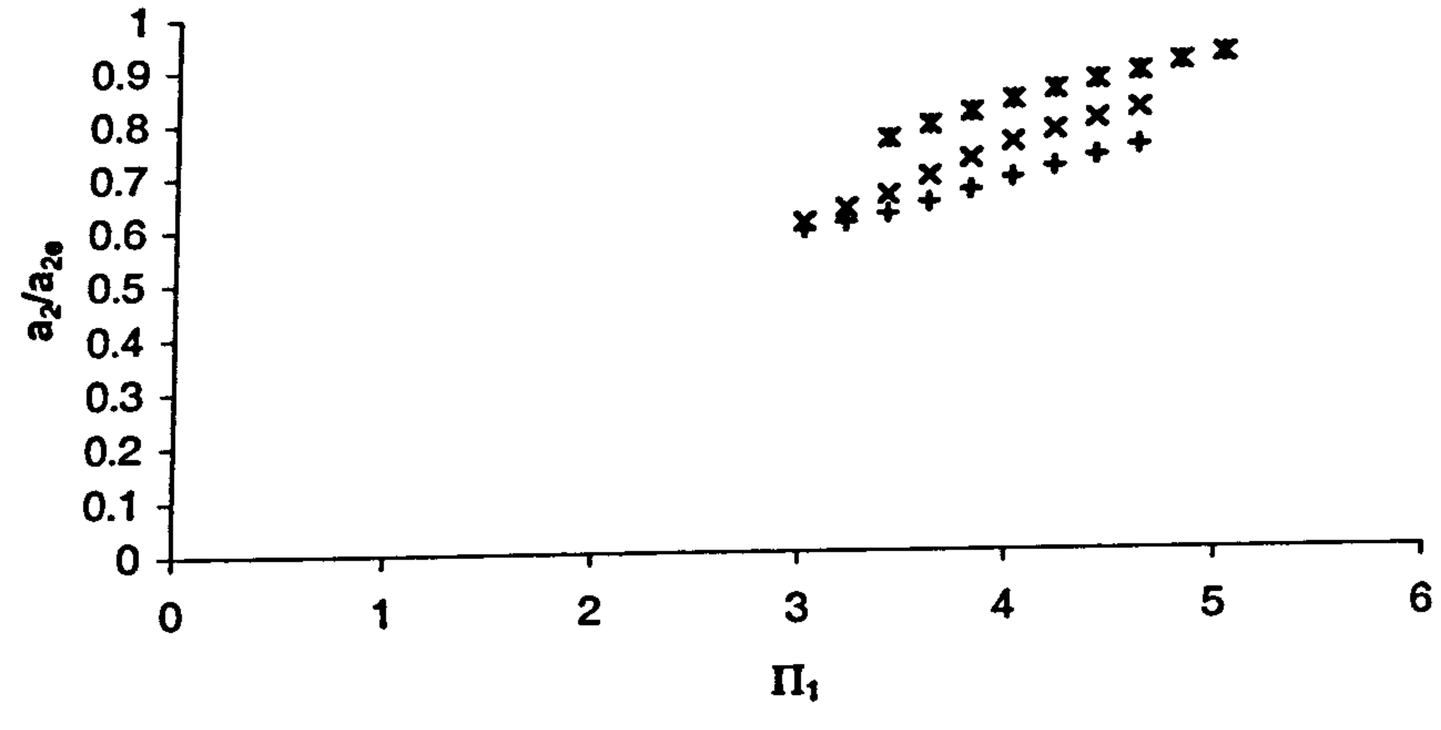

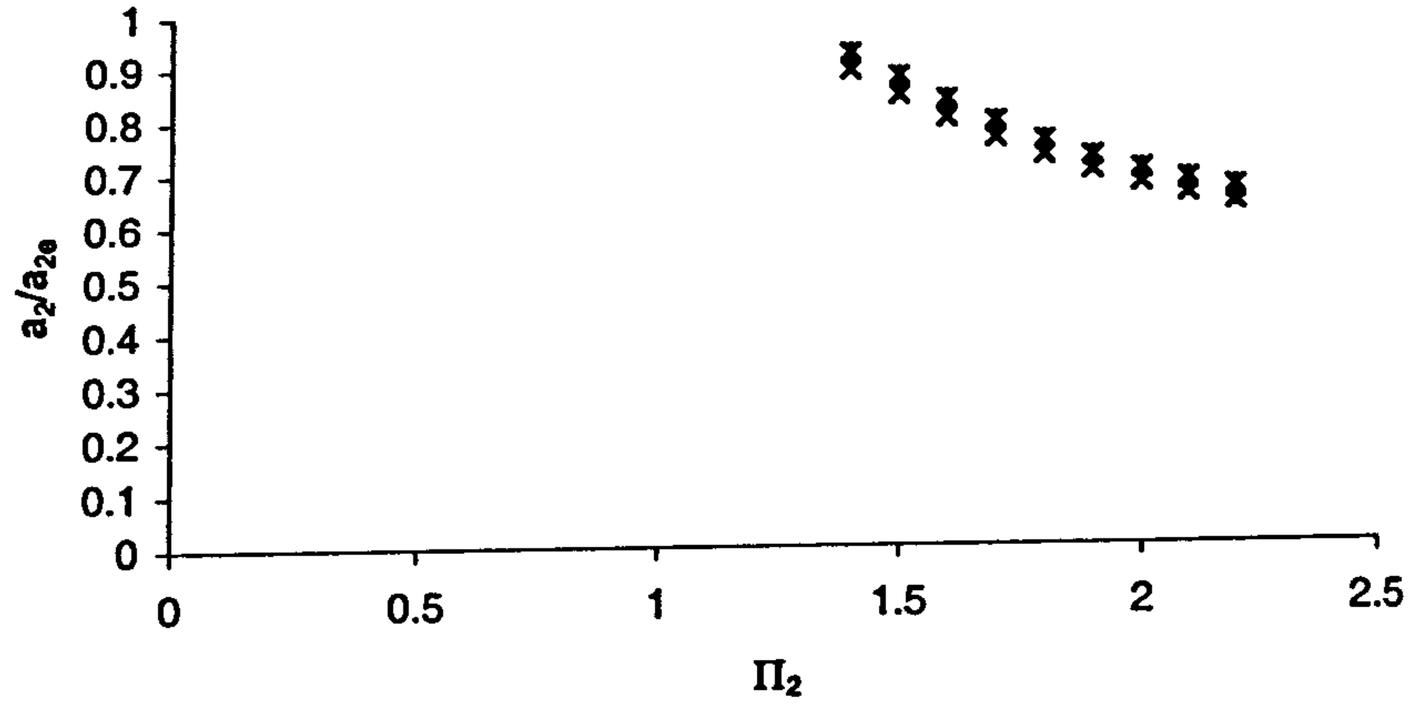

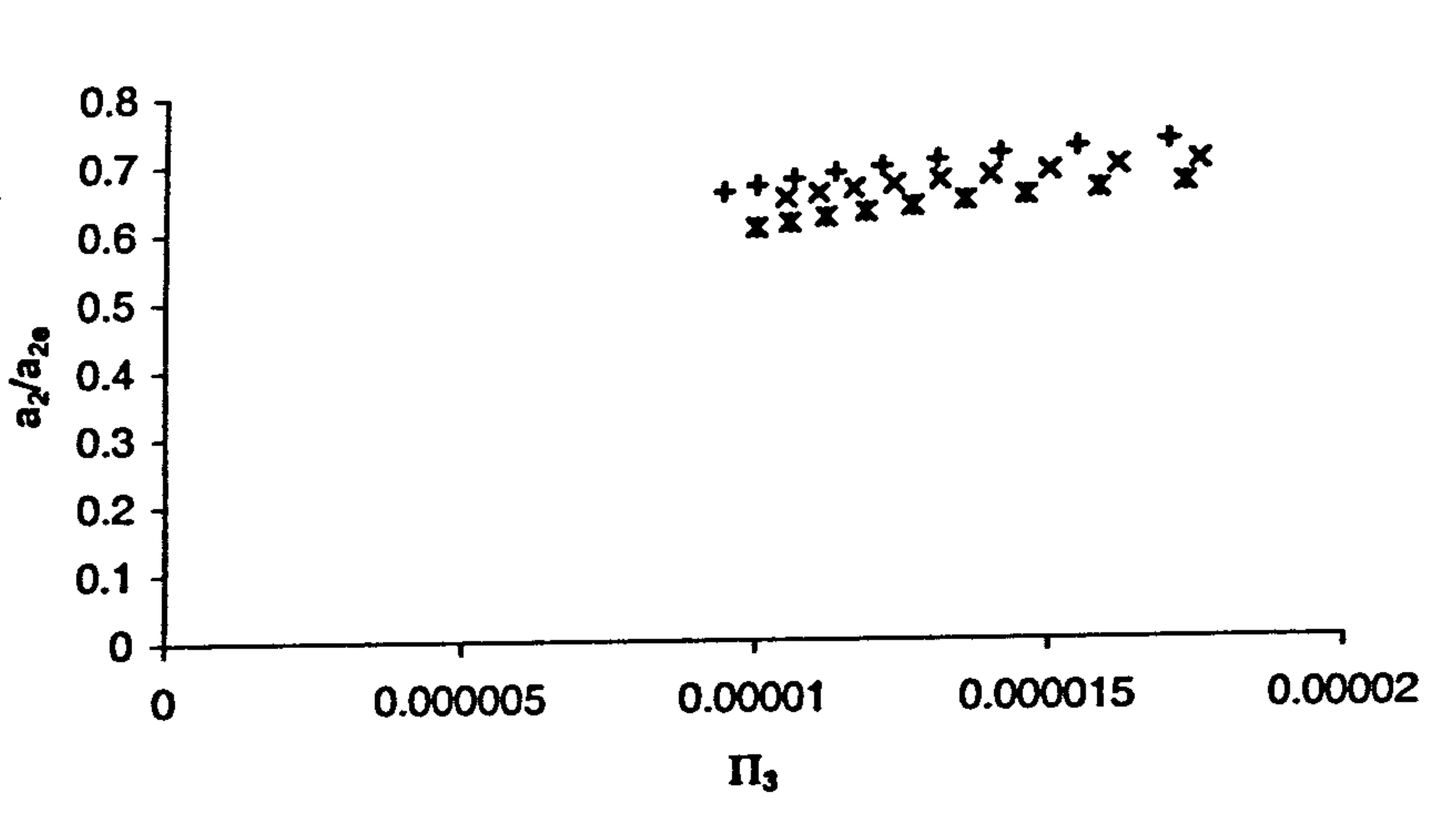

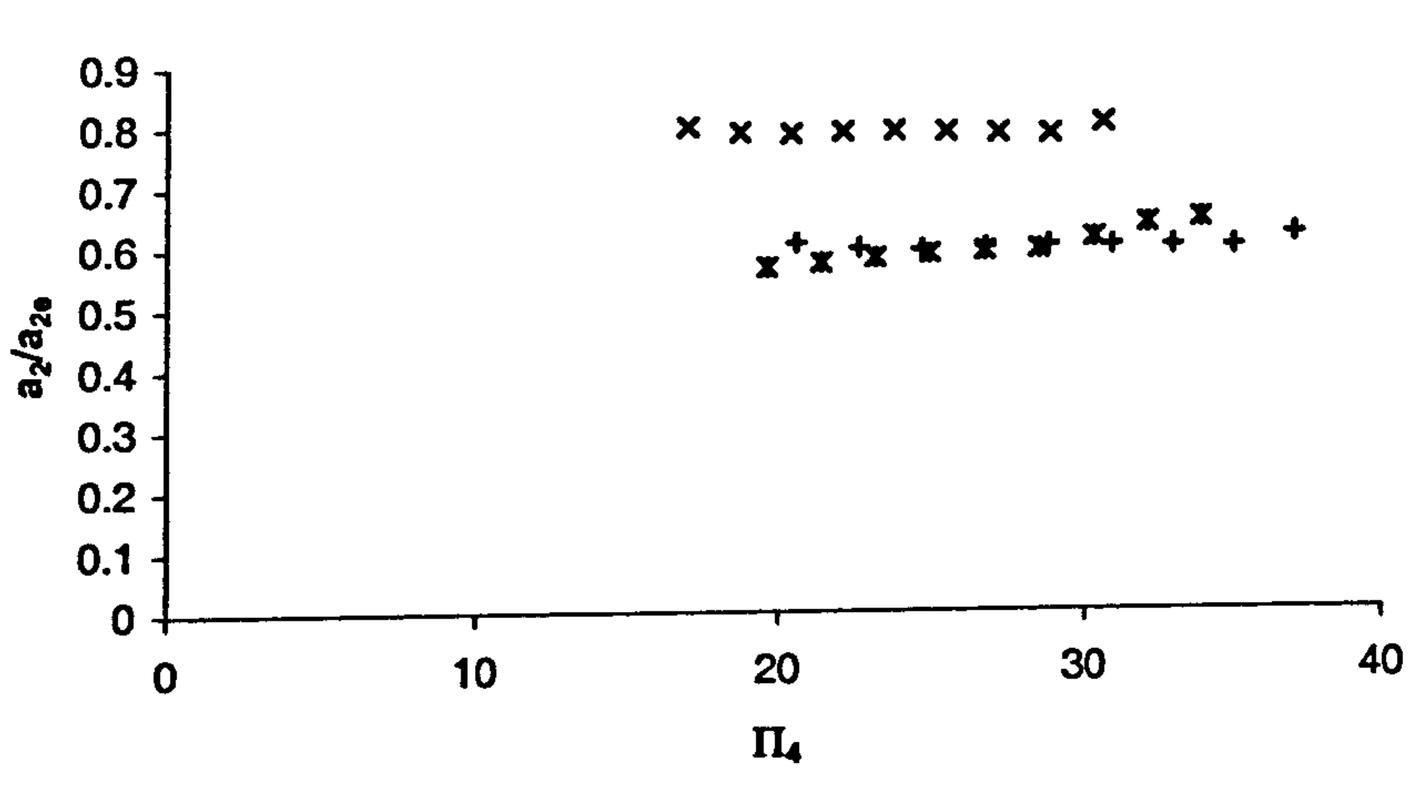

Figure 7.6.2a-d: Parameterisation quantity versus non-dimensional group values for the data sets used in the regression analysis
(Symbols represent the three sets of nine for each group)

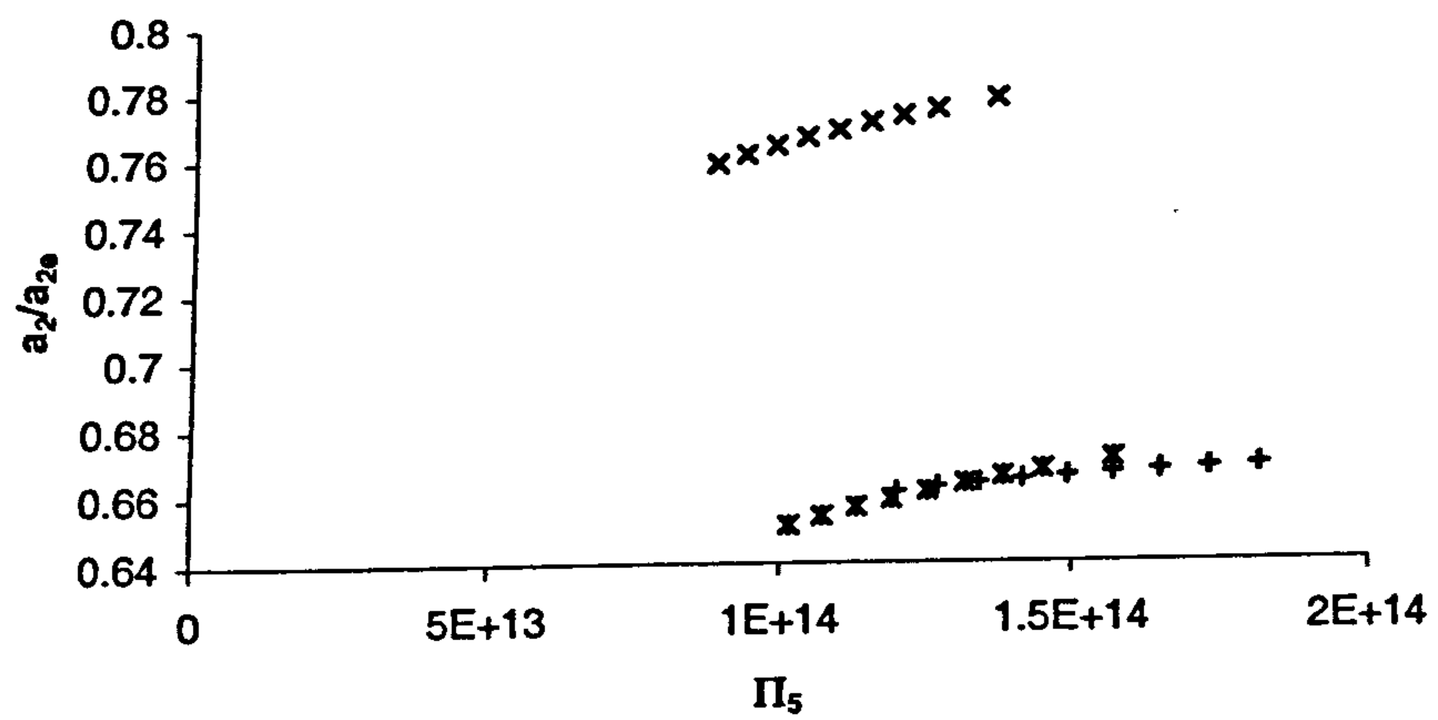

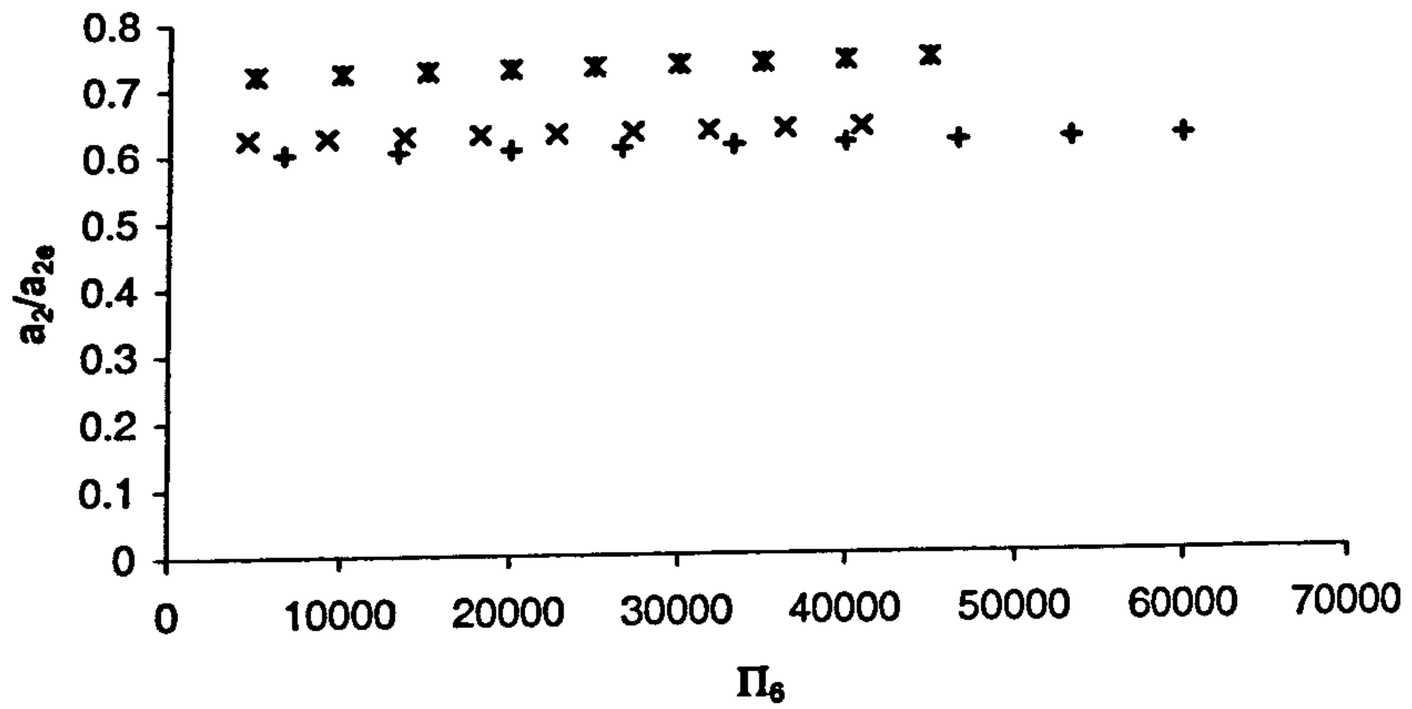

Figure 7.6.2e-f: Parameterisation quantity versus non-dimensional group values for the data sets used in the regression analysis
(Symbols represent the three sets of nine for each group)

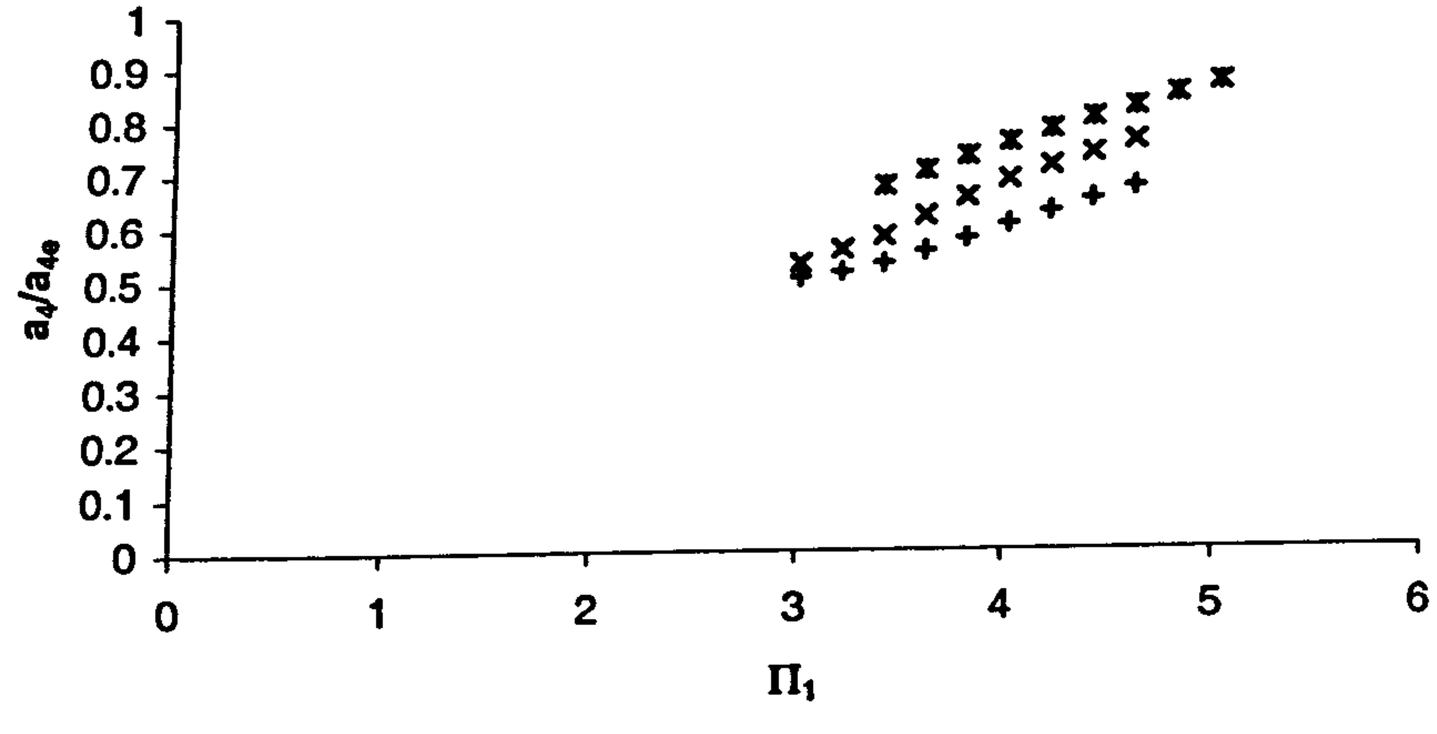

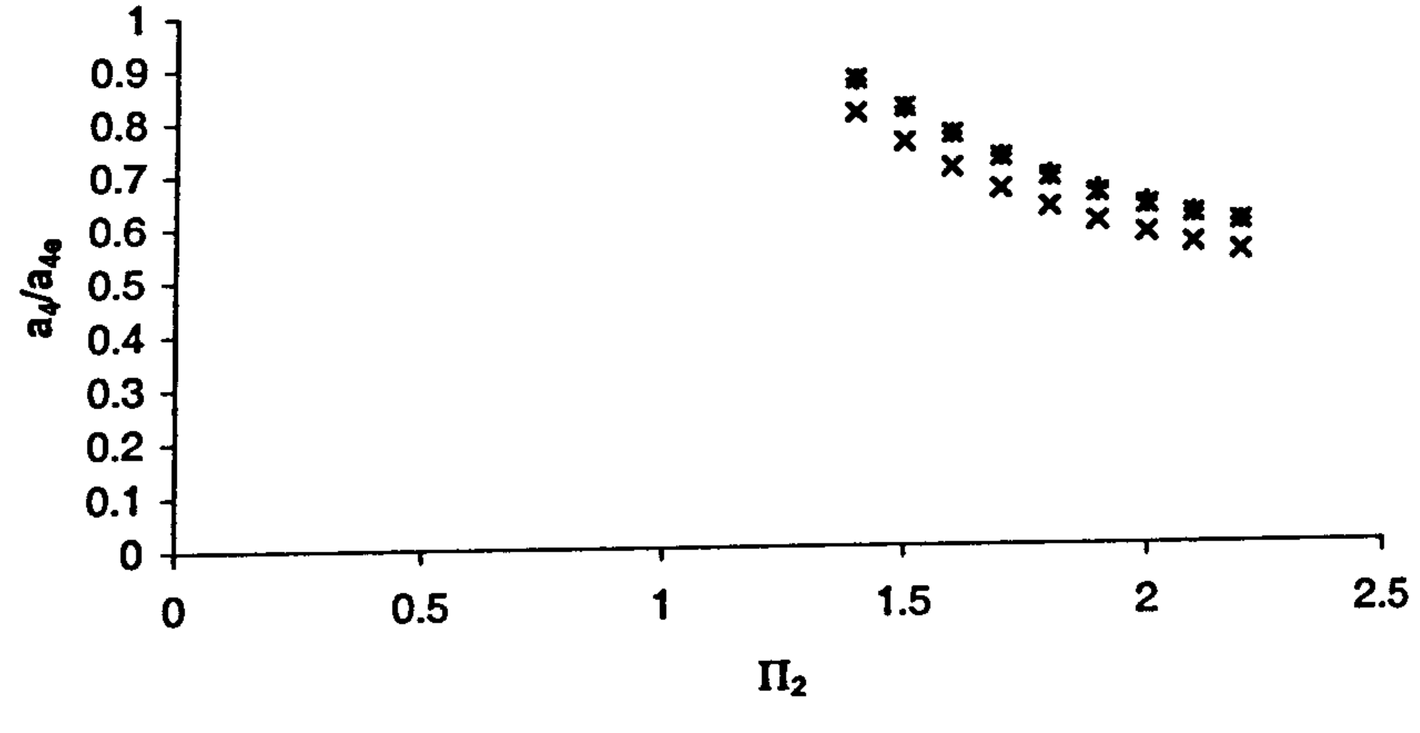

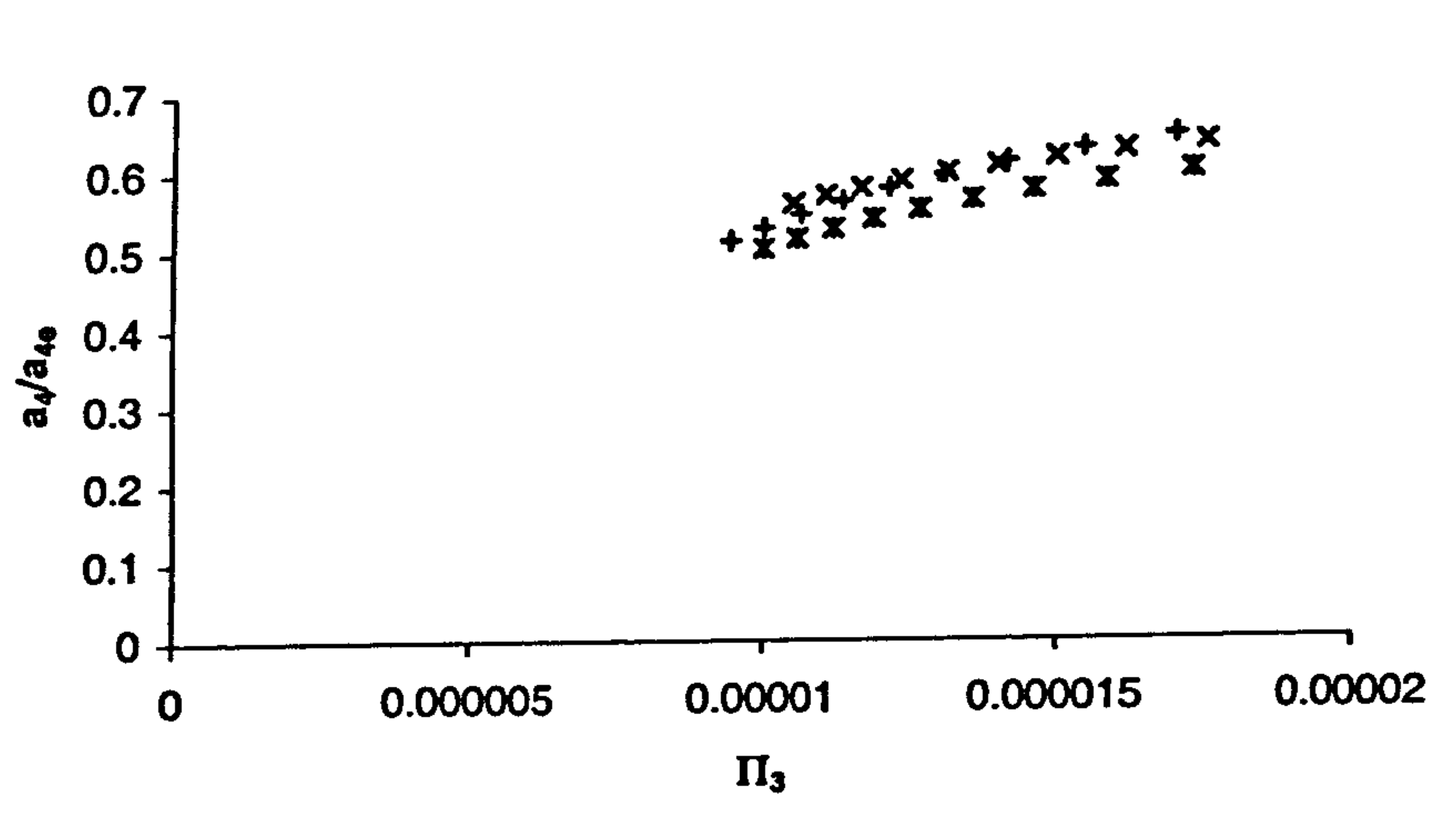

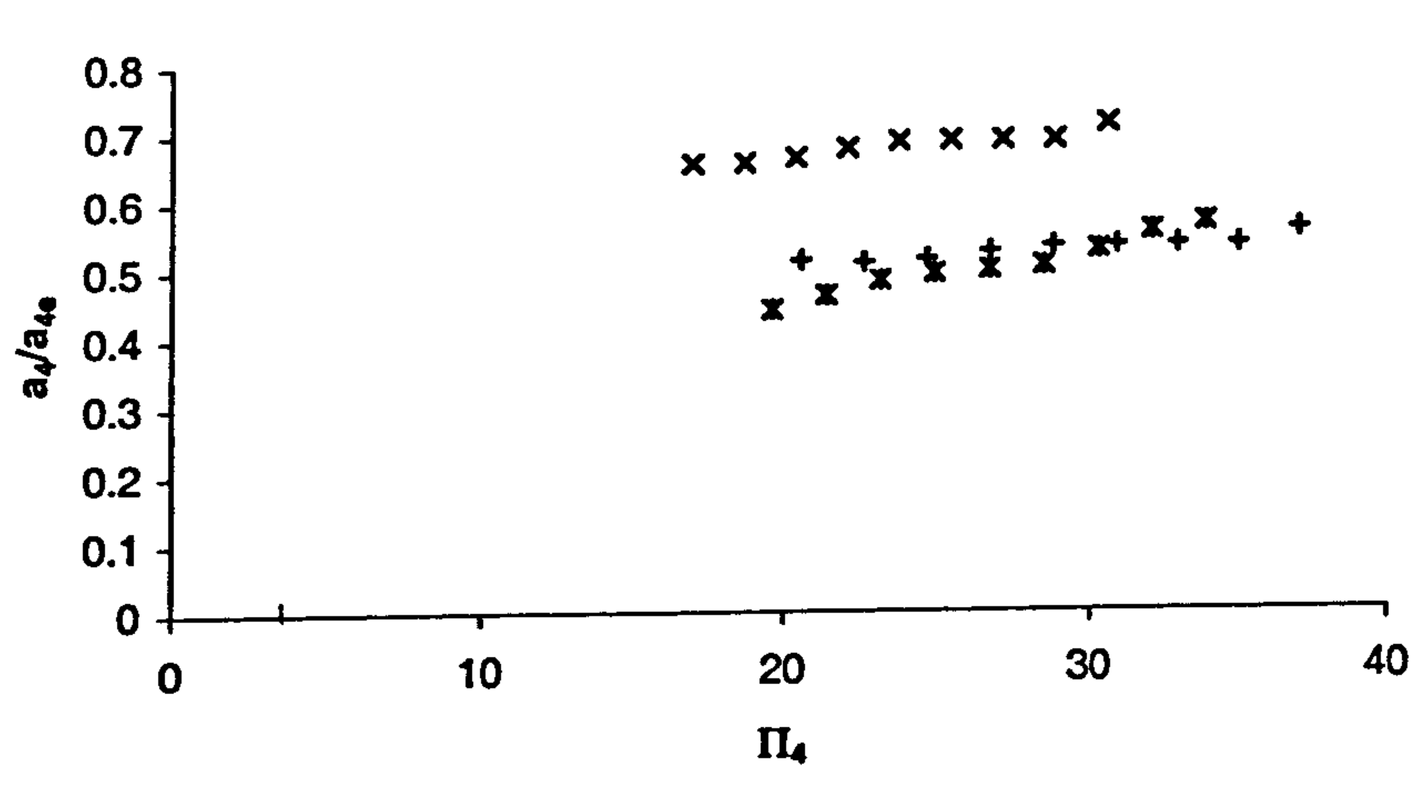

Figure 7.6.3a-d: Parameterisation quantity versus non-dimensional group values for the data sets used in the regression analysis
(Symbols represent the three sets of nine for each group)

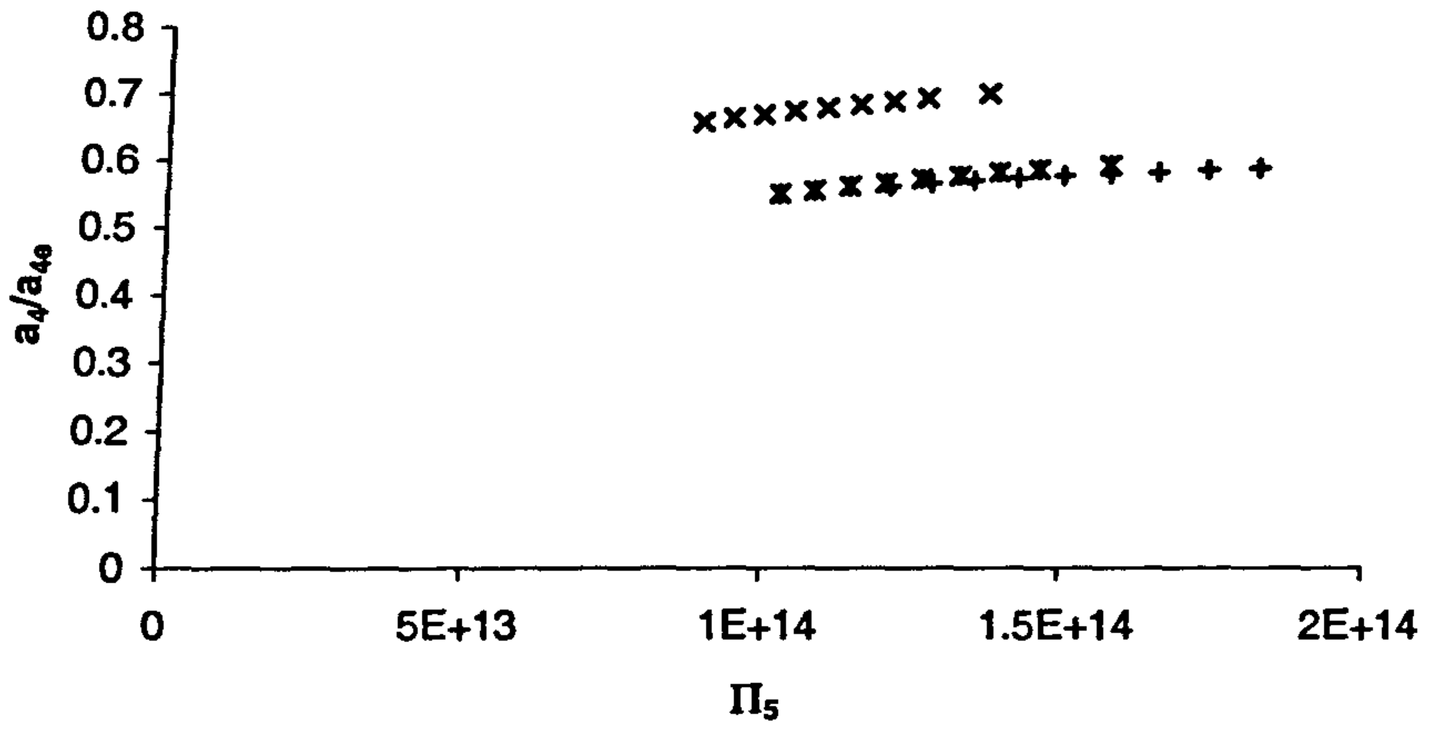

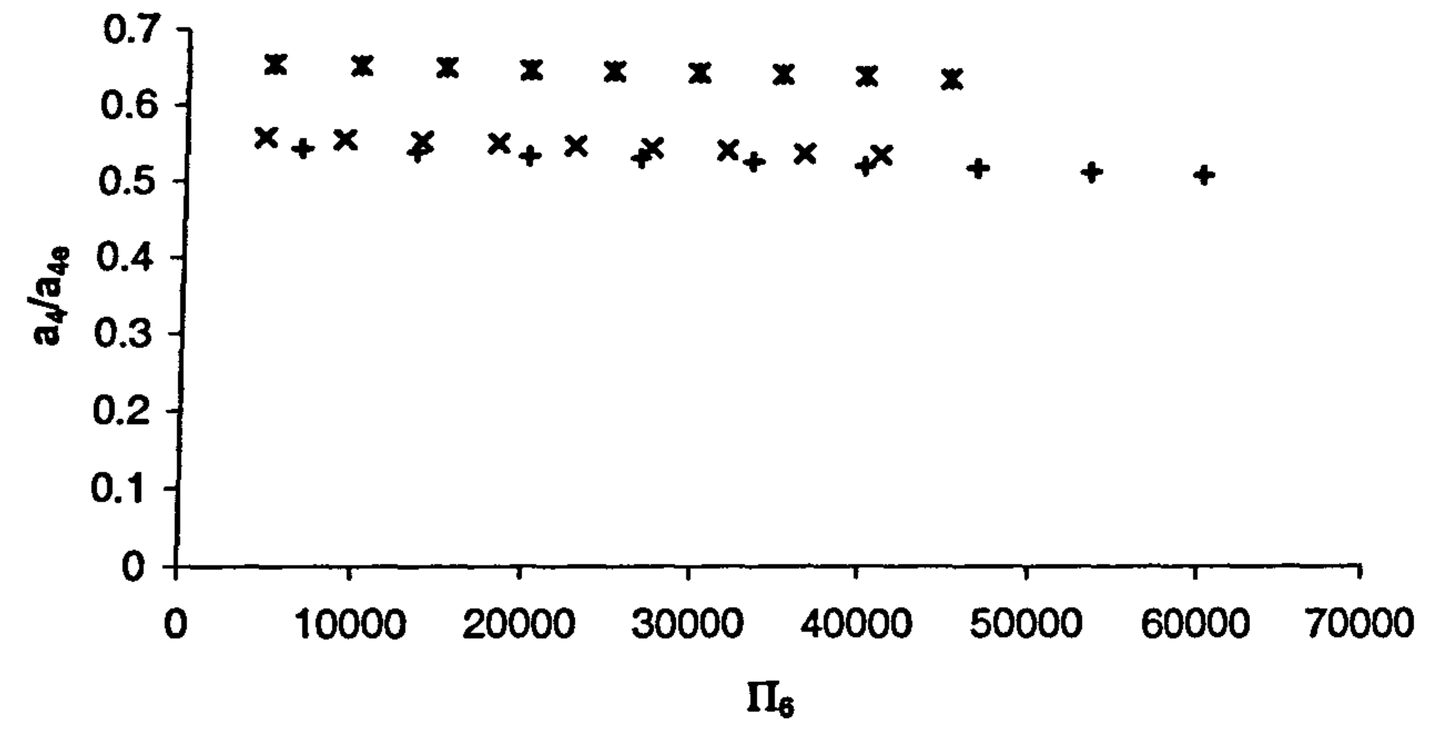

Figure 7.6.3e-f: Parameterisation quantity versus non-dimensional group values for the data sets used in the regression analysis
(Symbols represent the three sets of nine for each group)

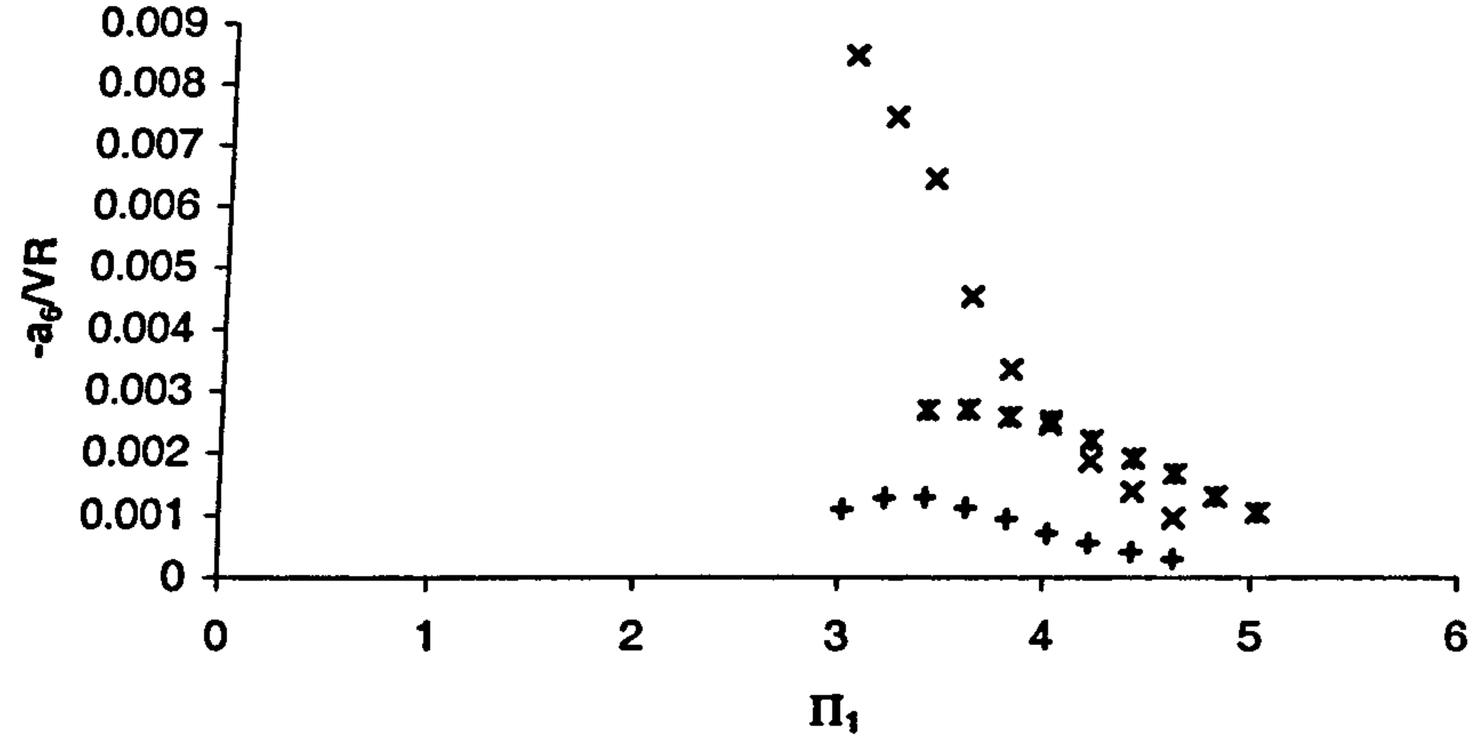

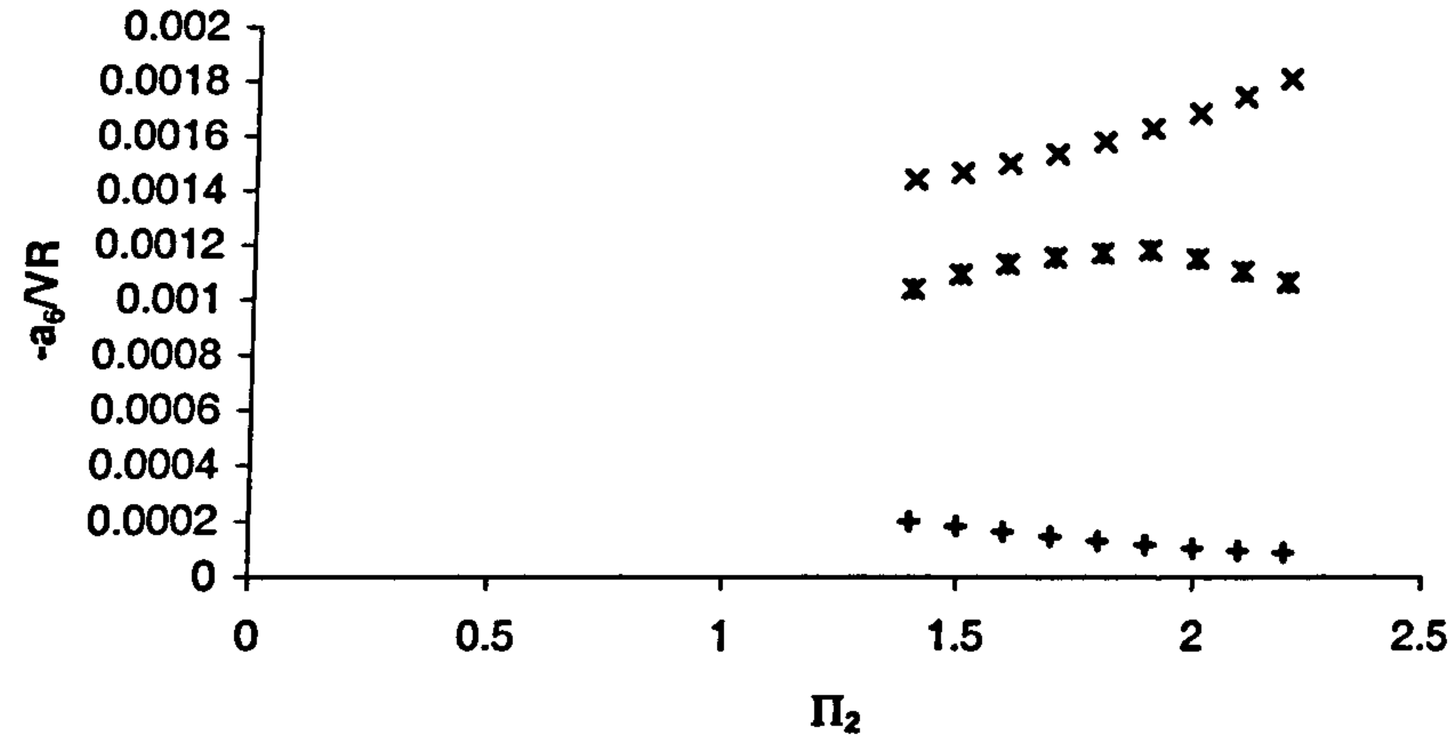

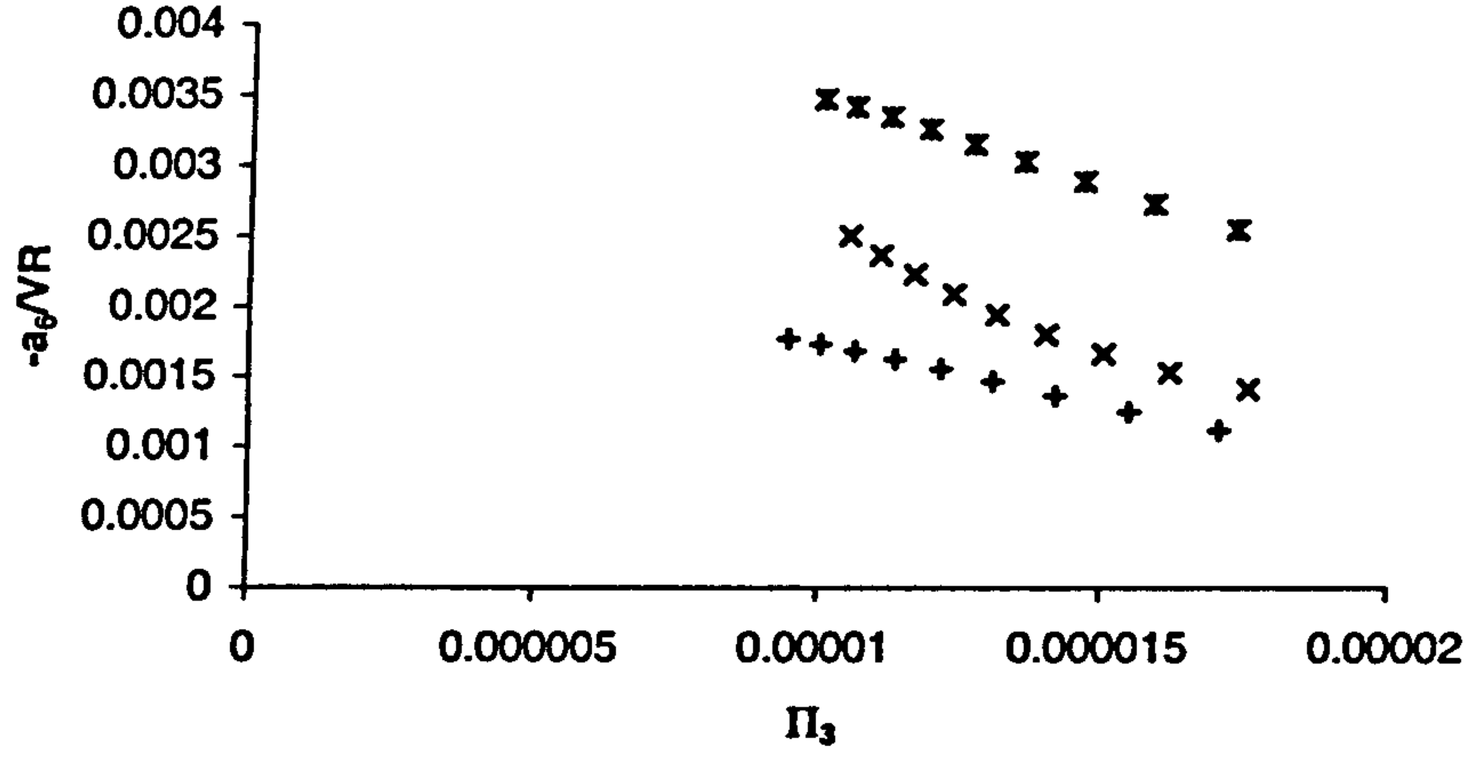

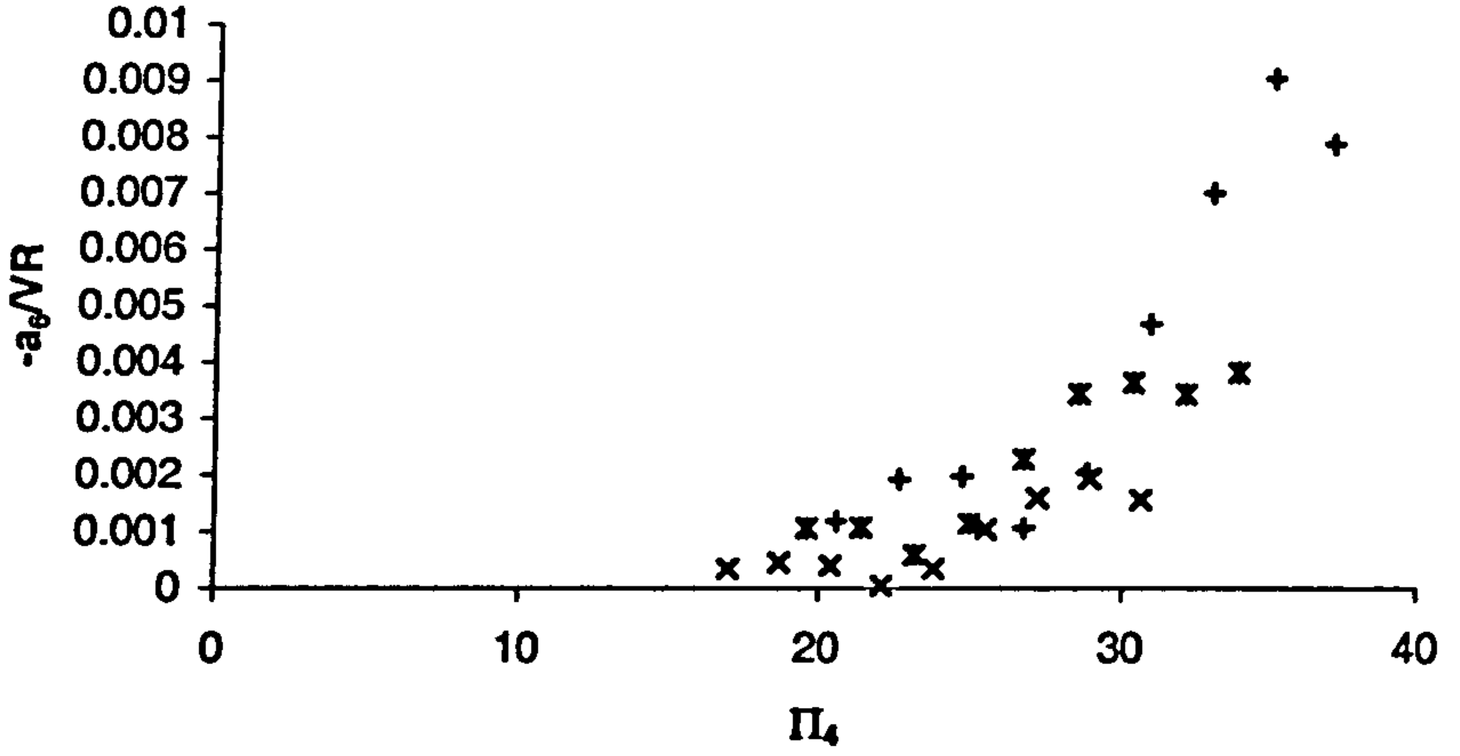

Figure 7.6.4a-d: Parameterisation quantity versus non-dimensional group values for the data sets used in the regression analysis
(Symbols represent the three sets of nine for each group)

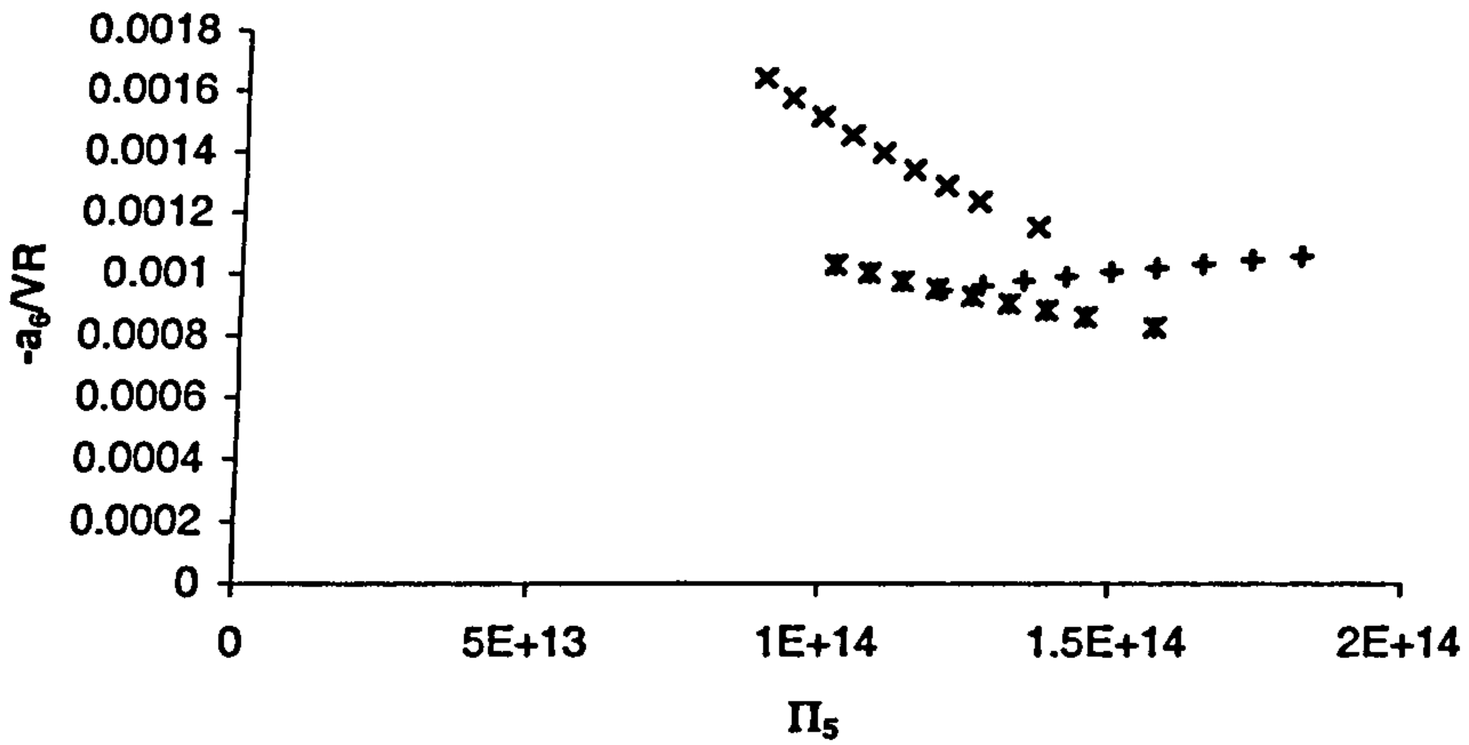

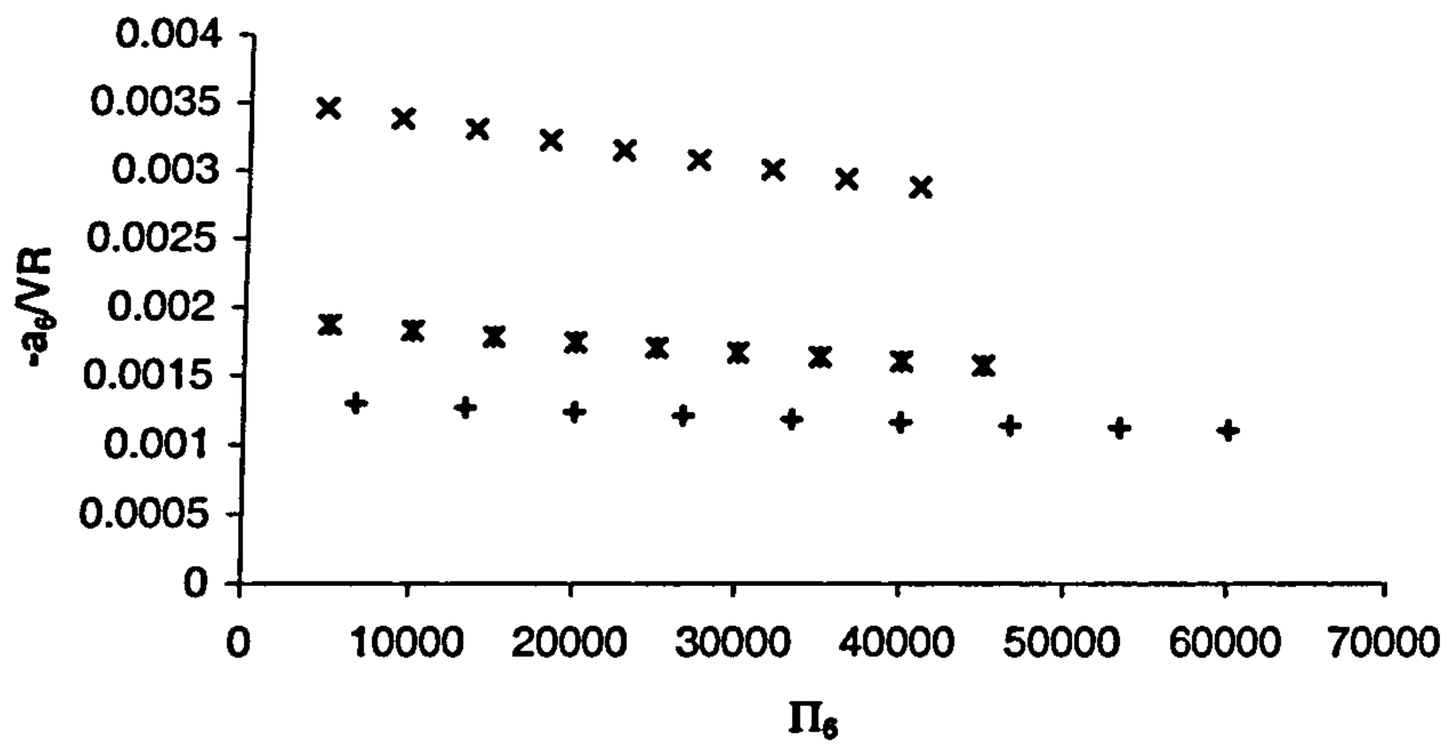

Figure 7.6.4e-f: Parameterisation quantity versus non-dimensional group values for the data sets used in the regression analysis
(Symbols represent the three sets of nine for each group)

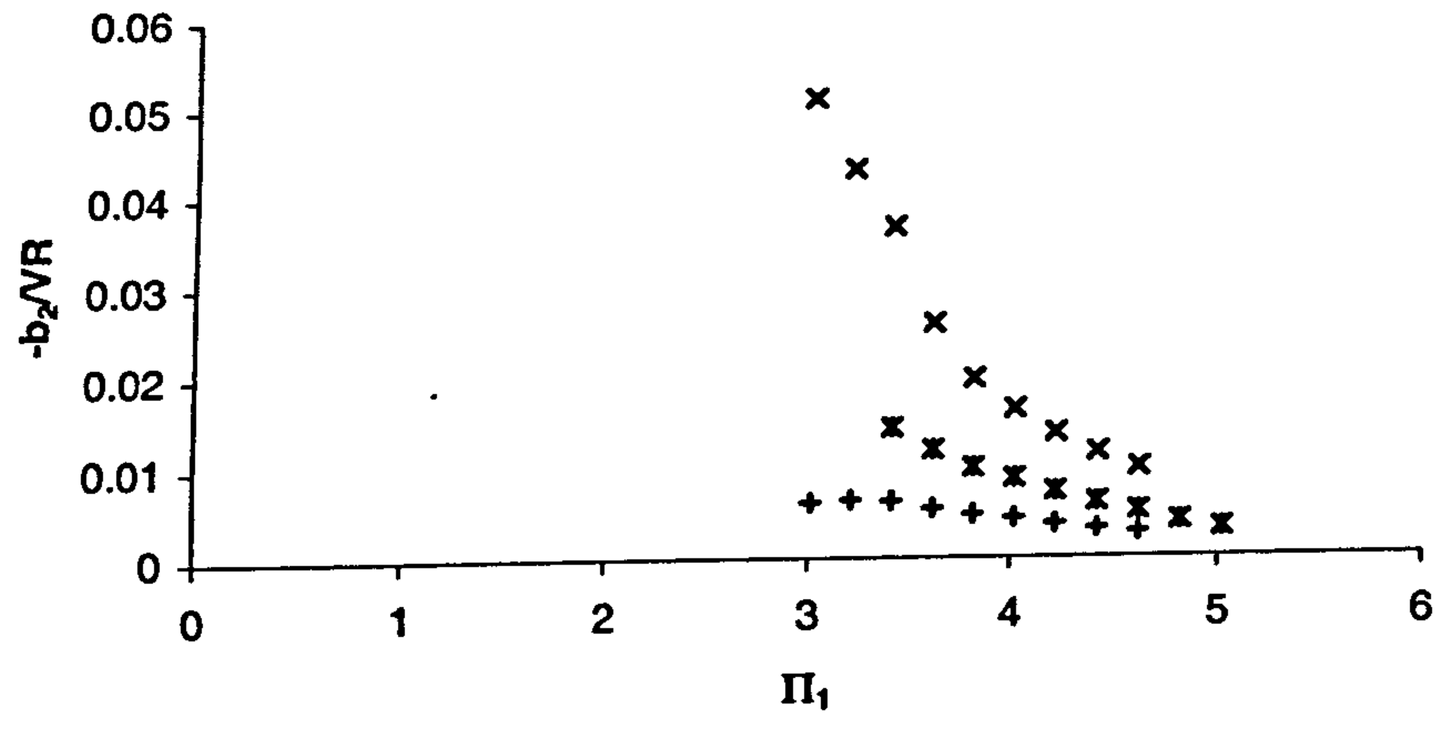

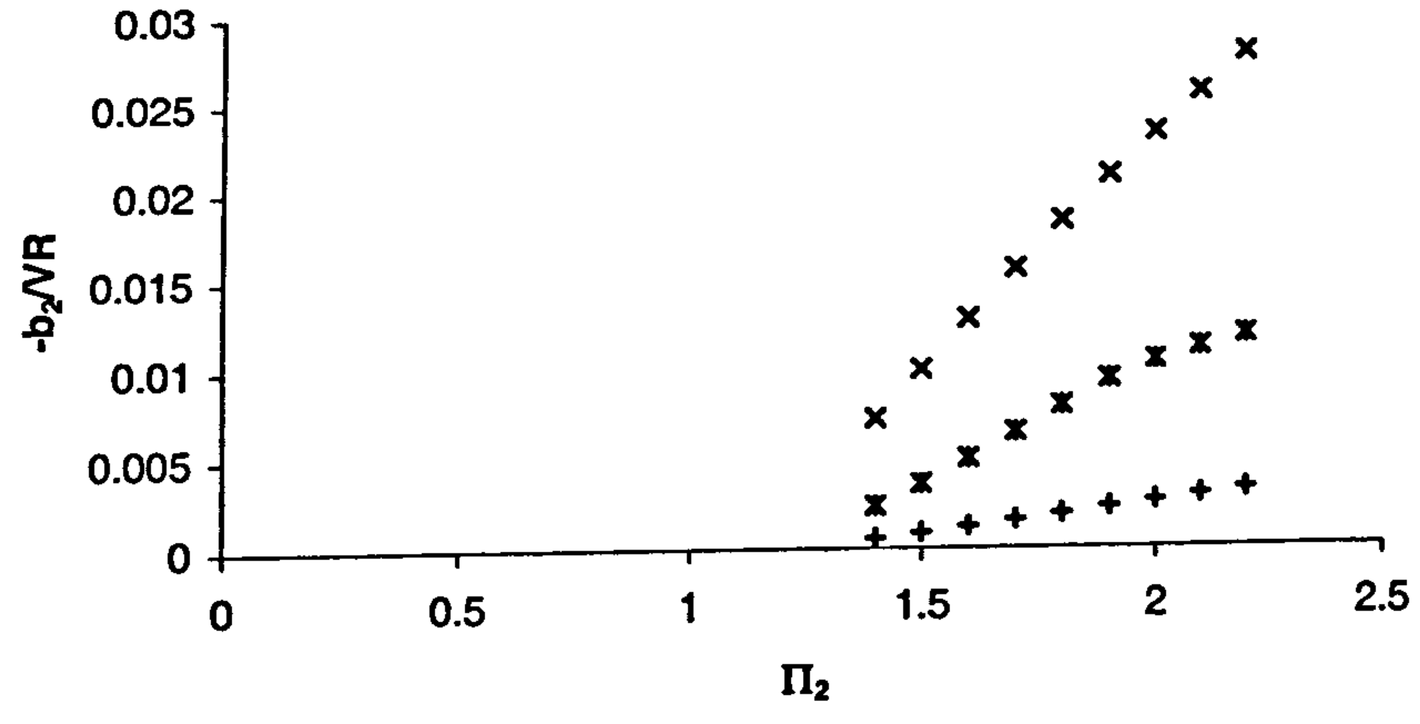

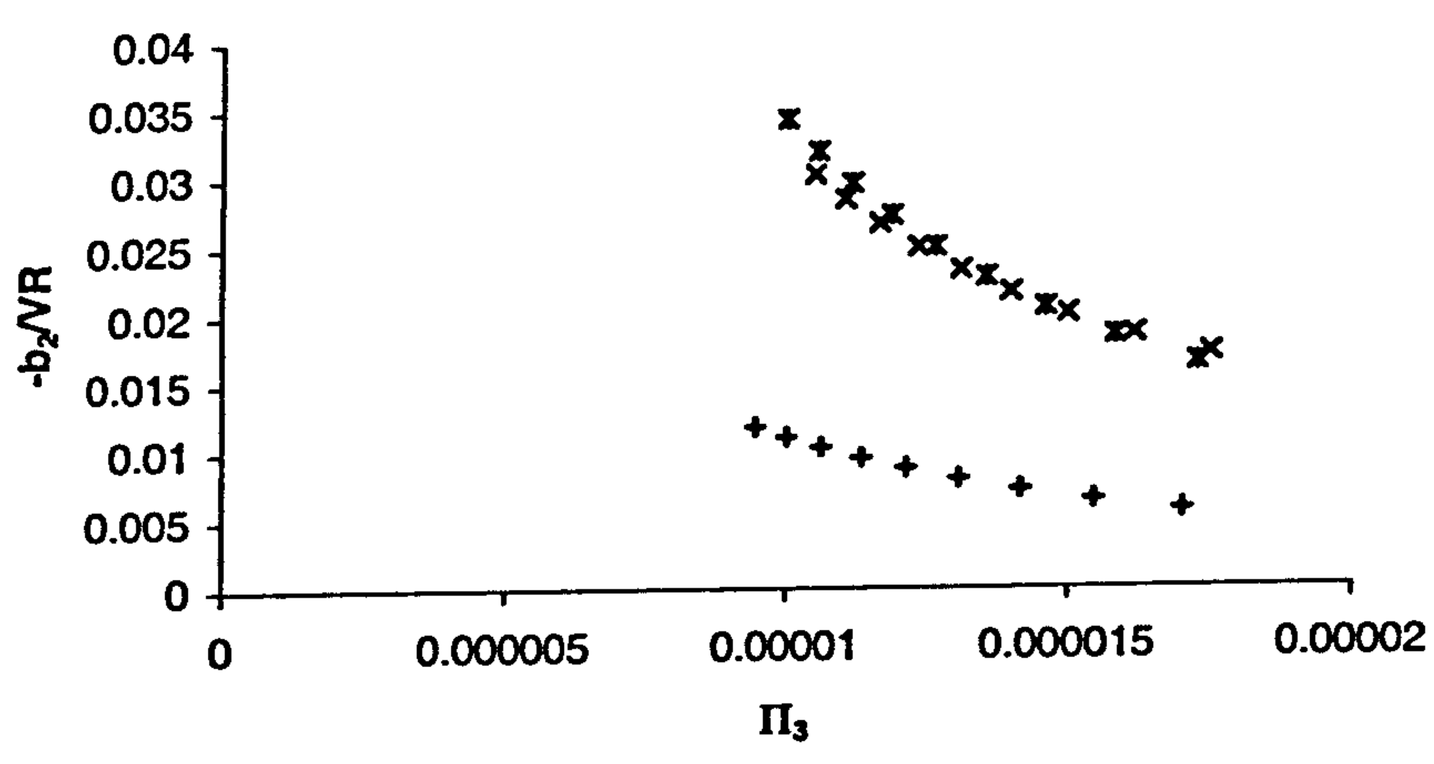

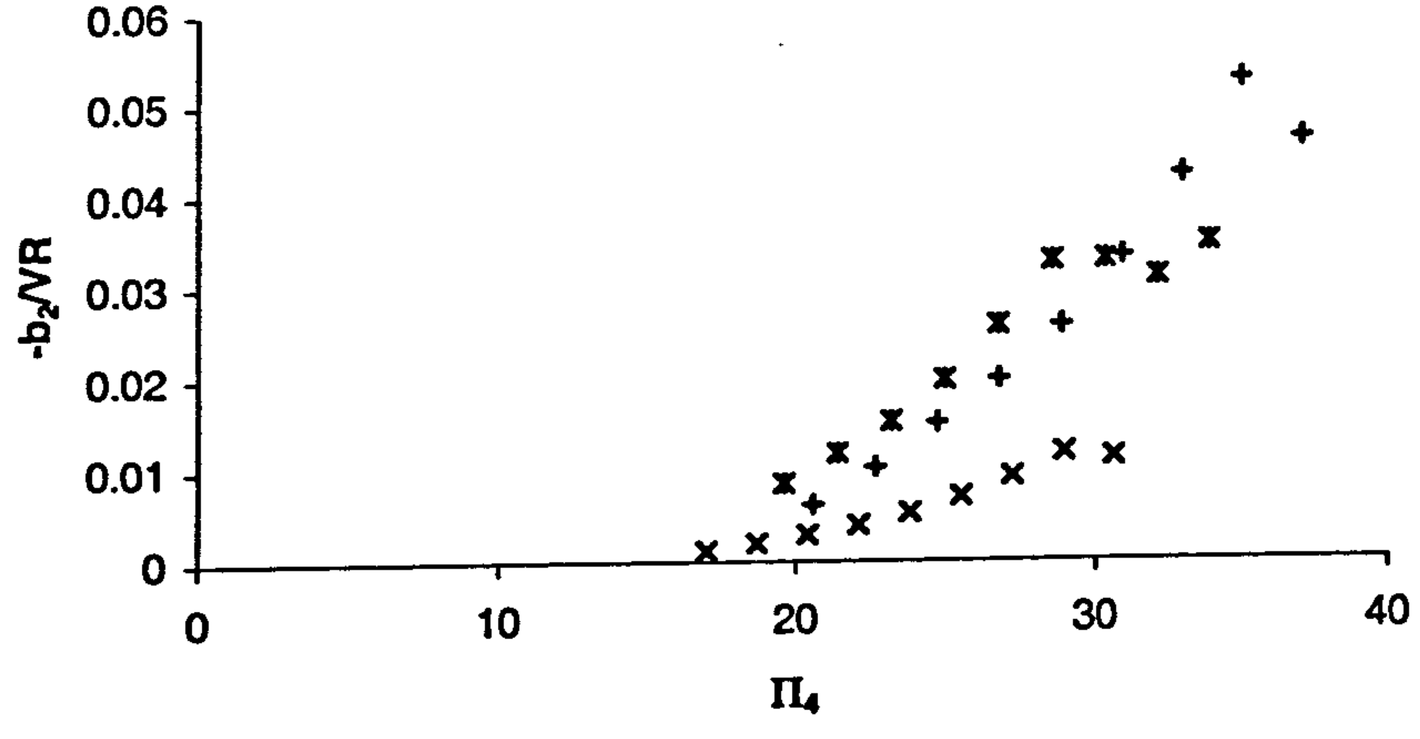

Figure 7.6.5a-d: Parameterisation quantity versus non-dimensional group values for the data sets used in the regression analysis
(Symbols represent the three sets of nine for each group)

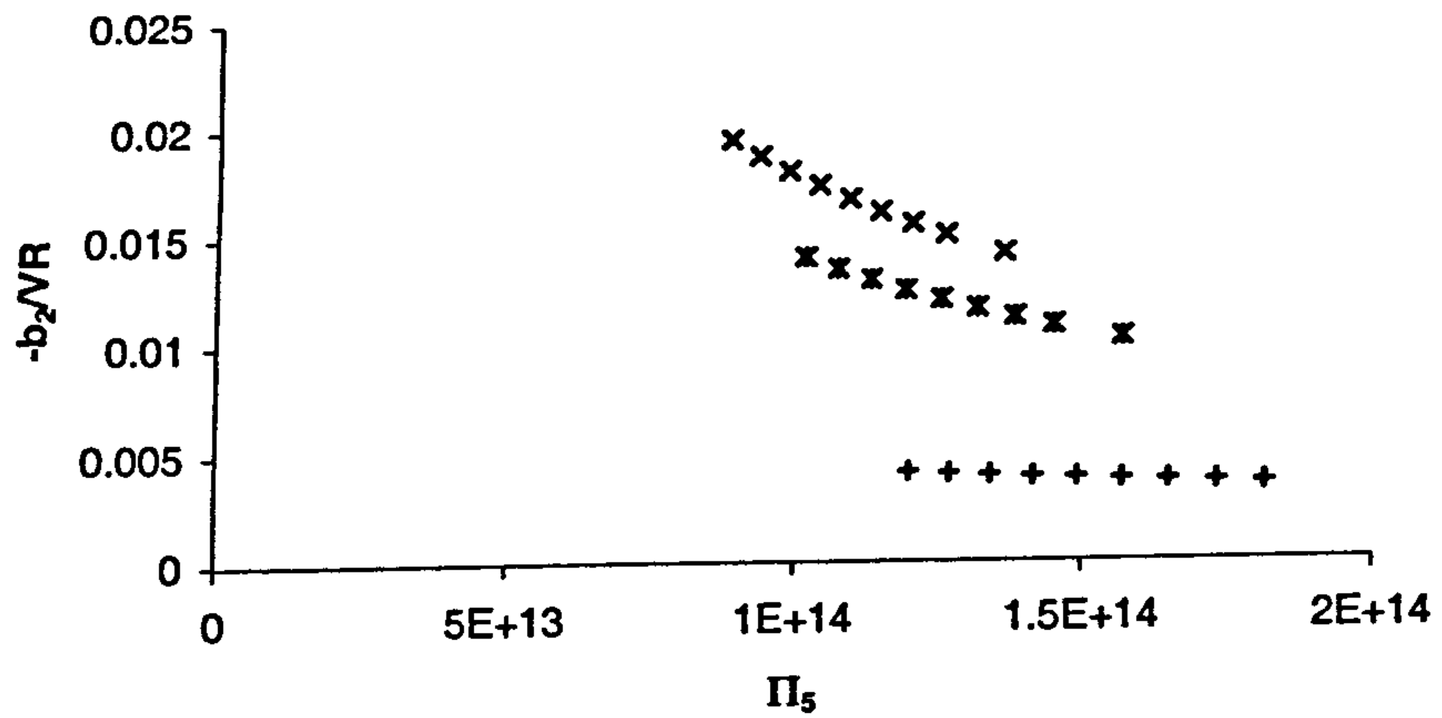

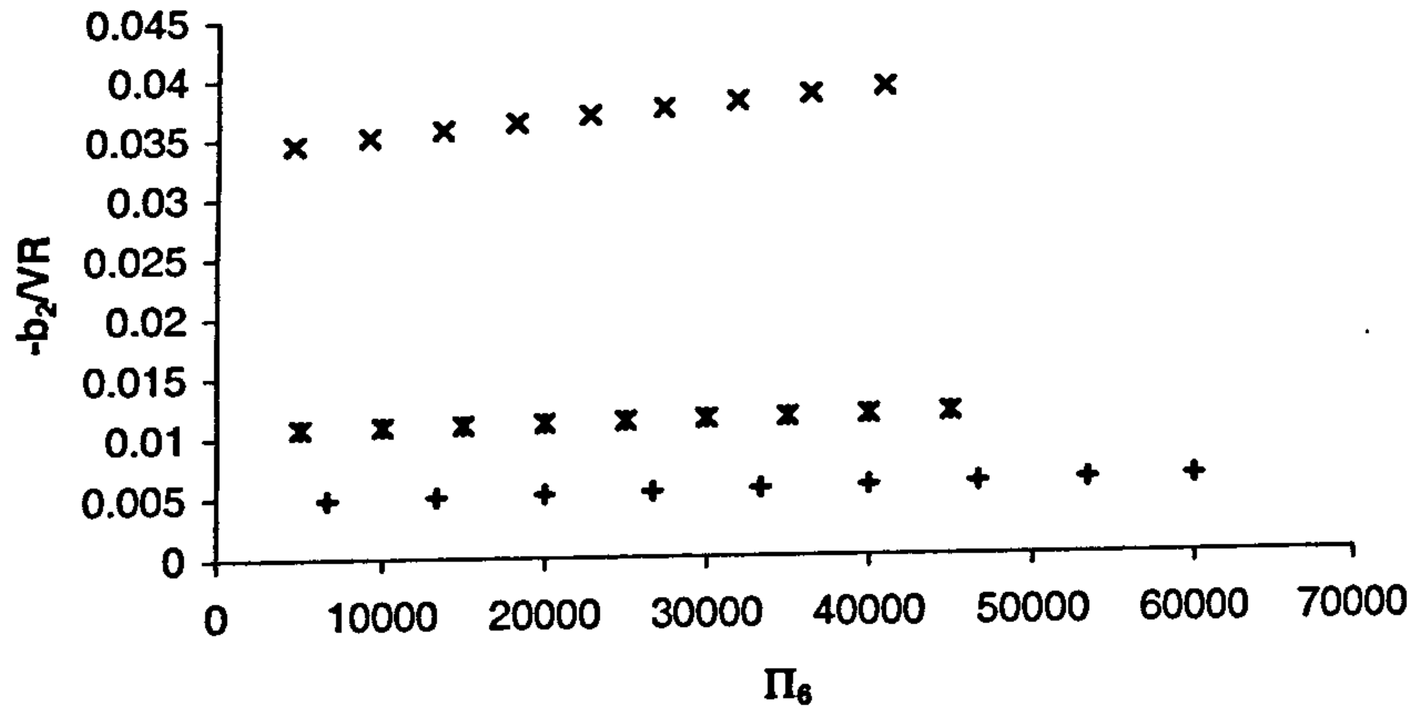

Figure 7.6.5e-f: Parameterisation quantity versus non-dimensional group values for the data sets used in the regression analysis
(Symbols represent the three sets of nine for each group)

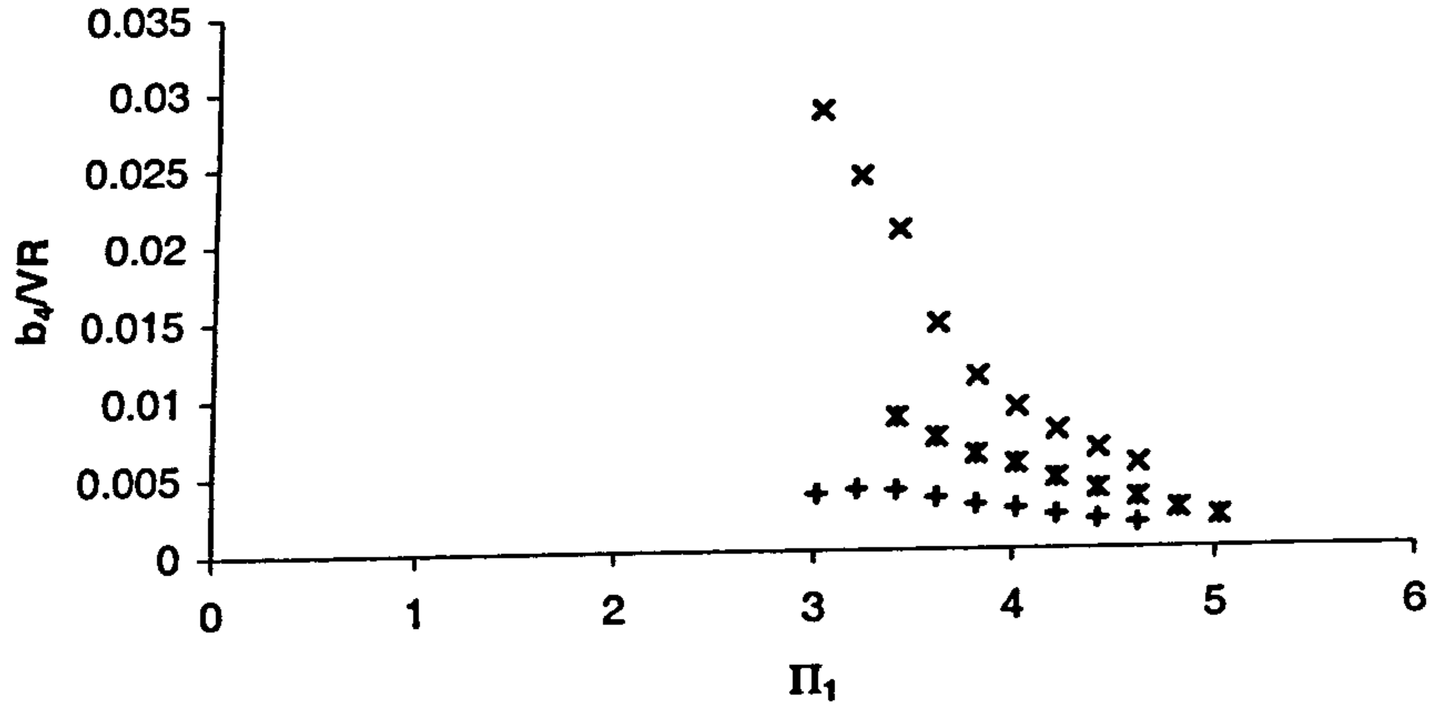

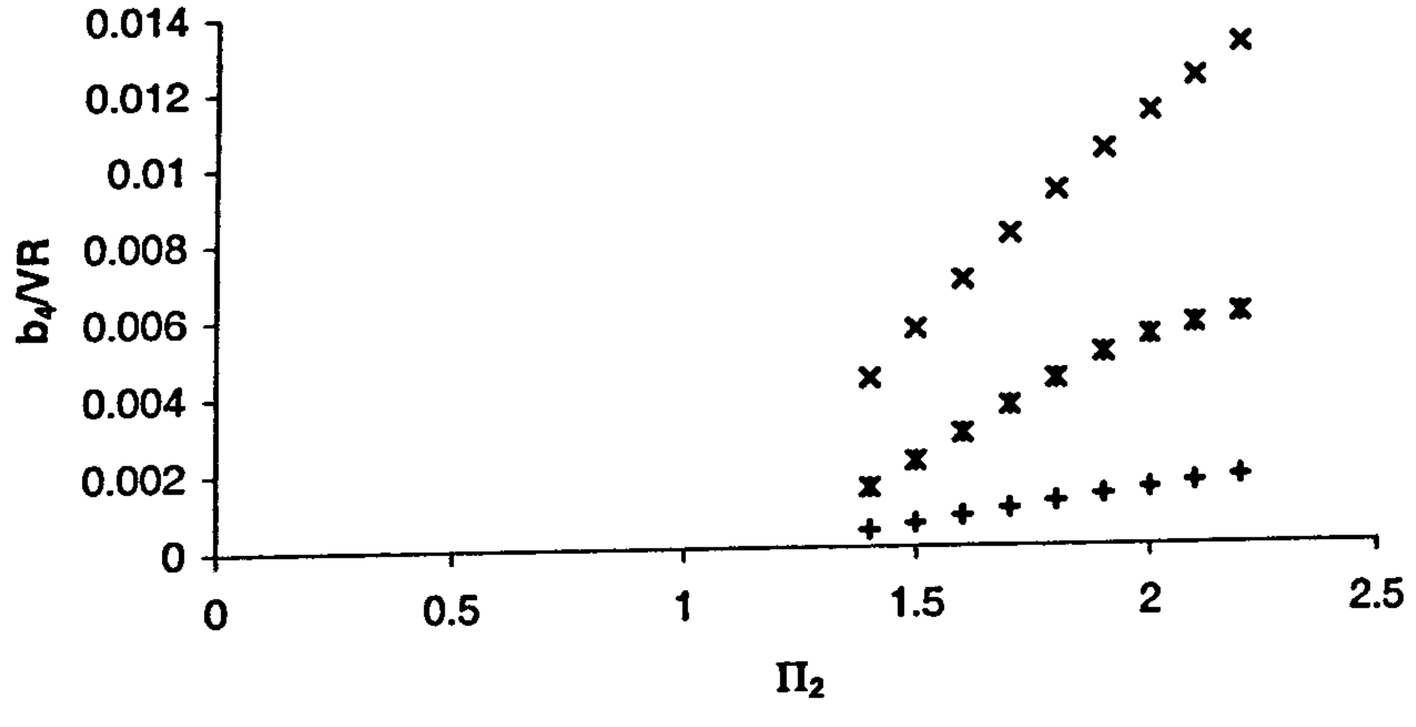

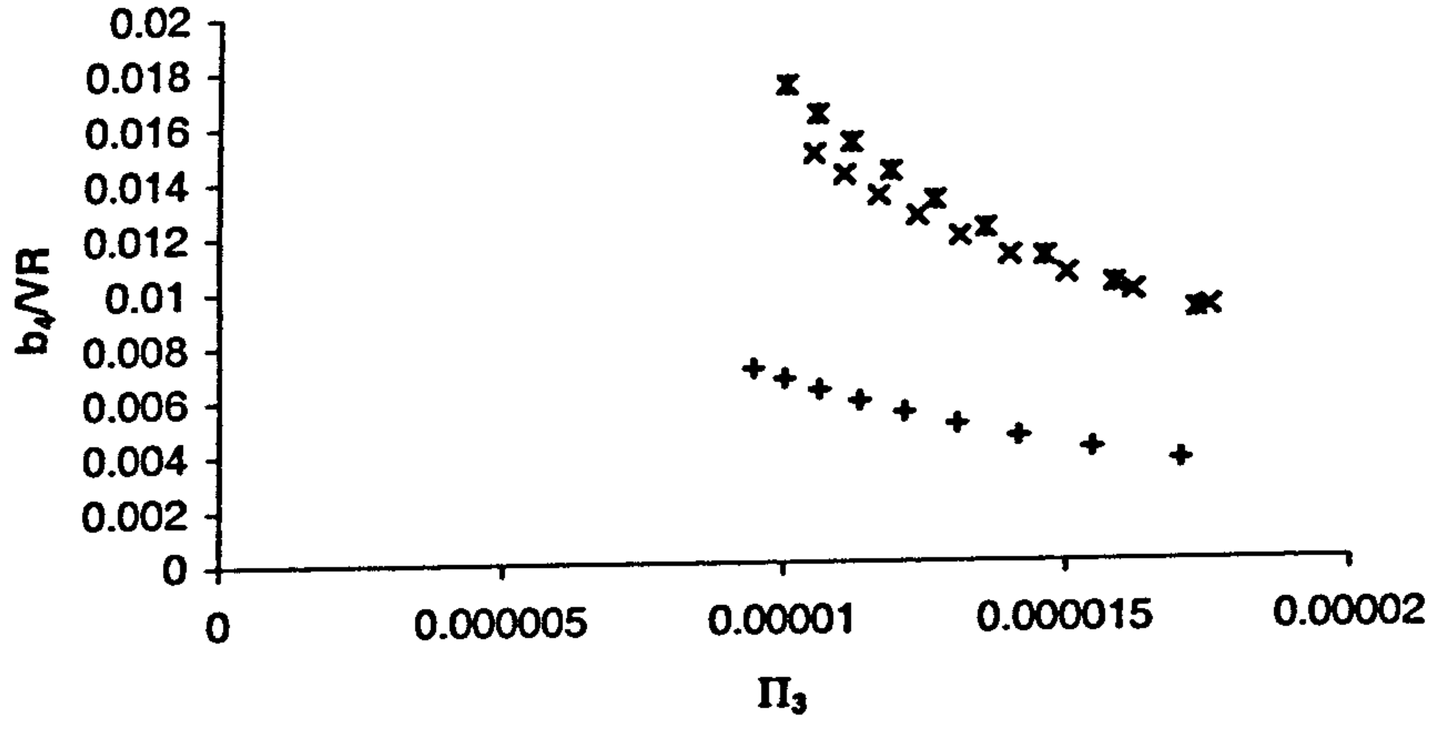

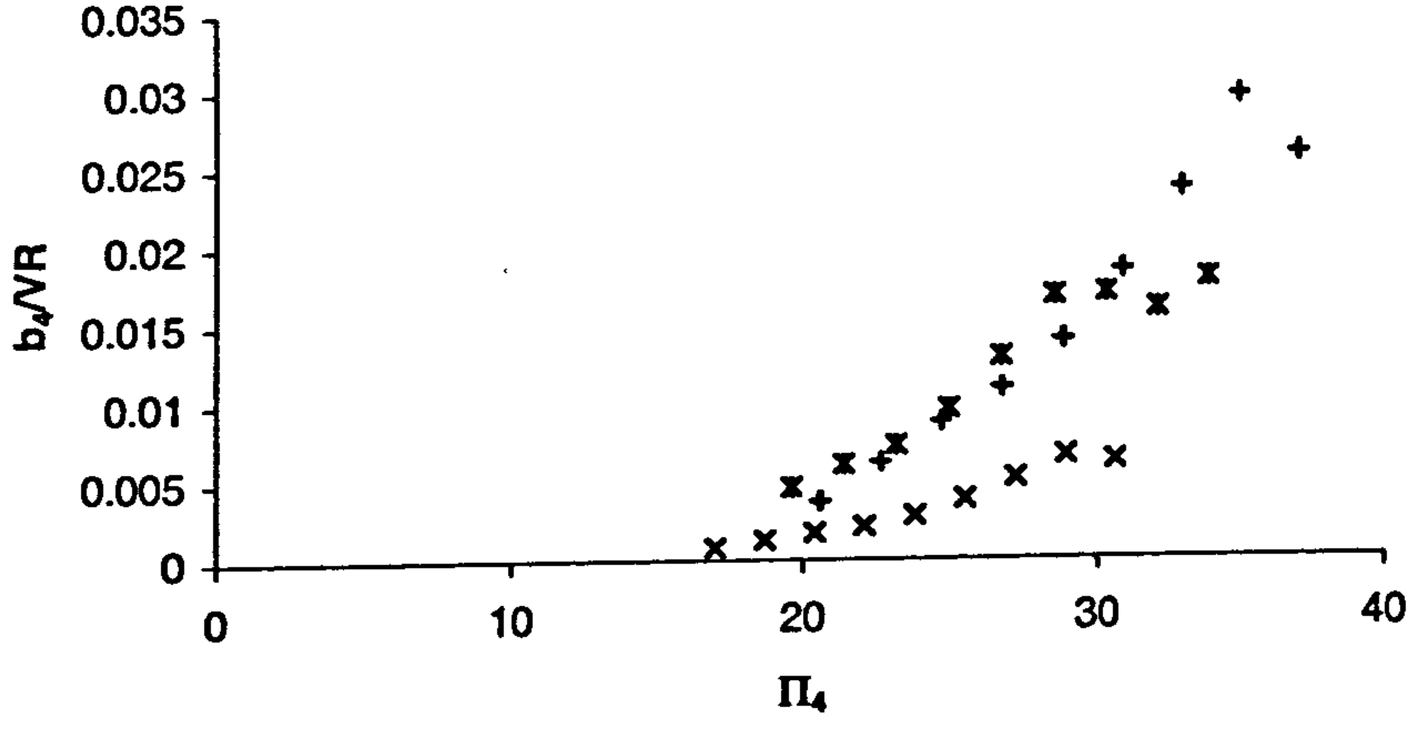

Figure 7.6.6a-d: Parameterisation quantity versus non-dimensional group values for the data sets used in the regression analysis
(Symbols represent the three sets of nine for each group)

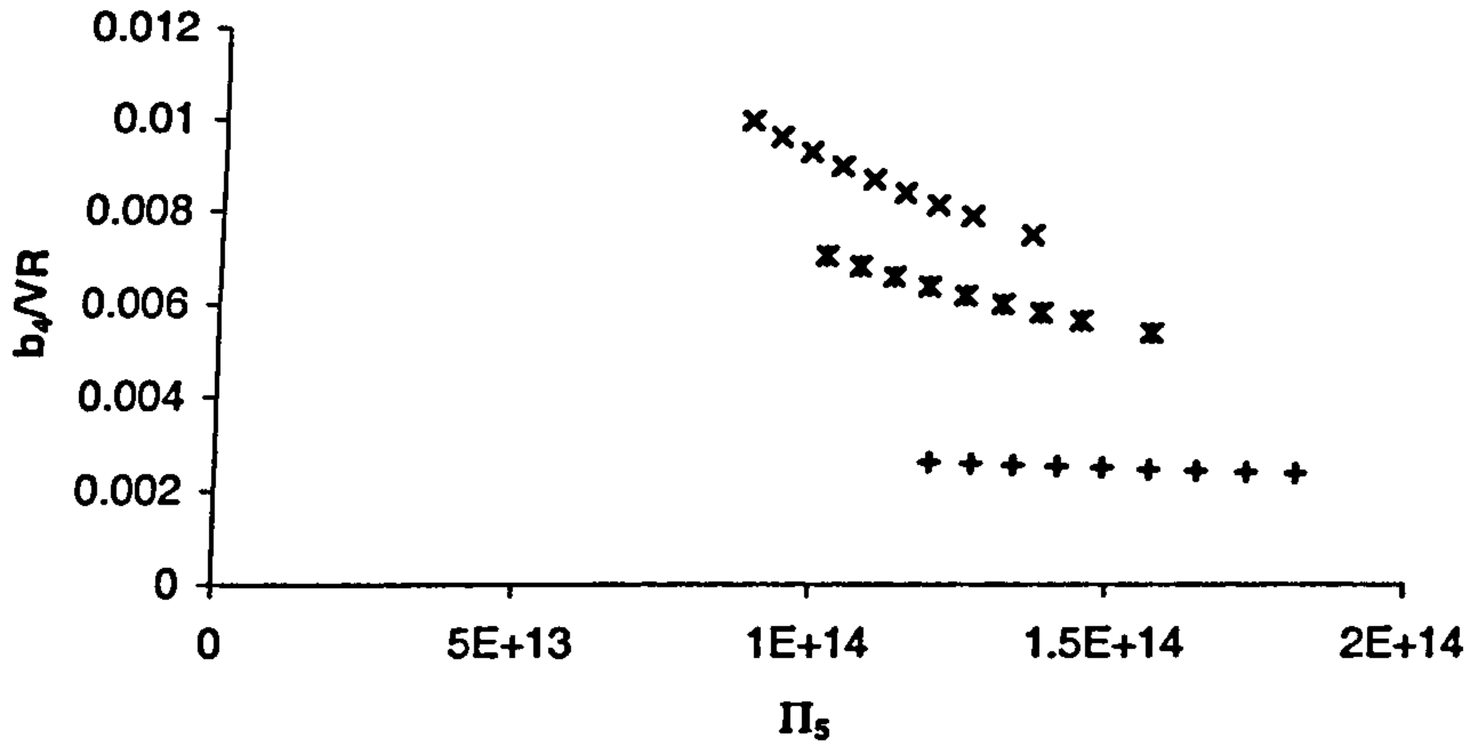

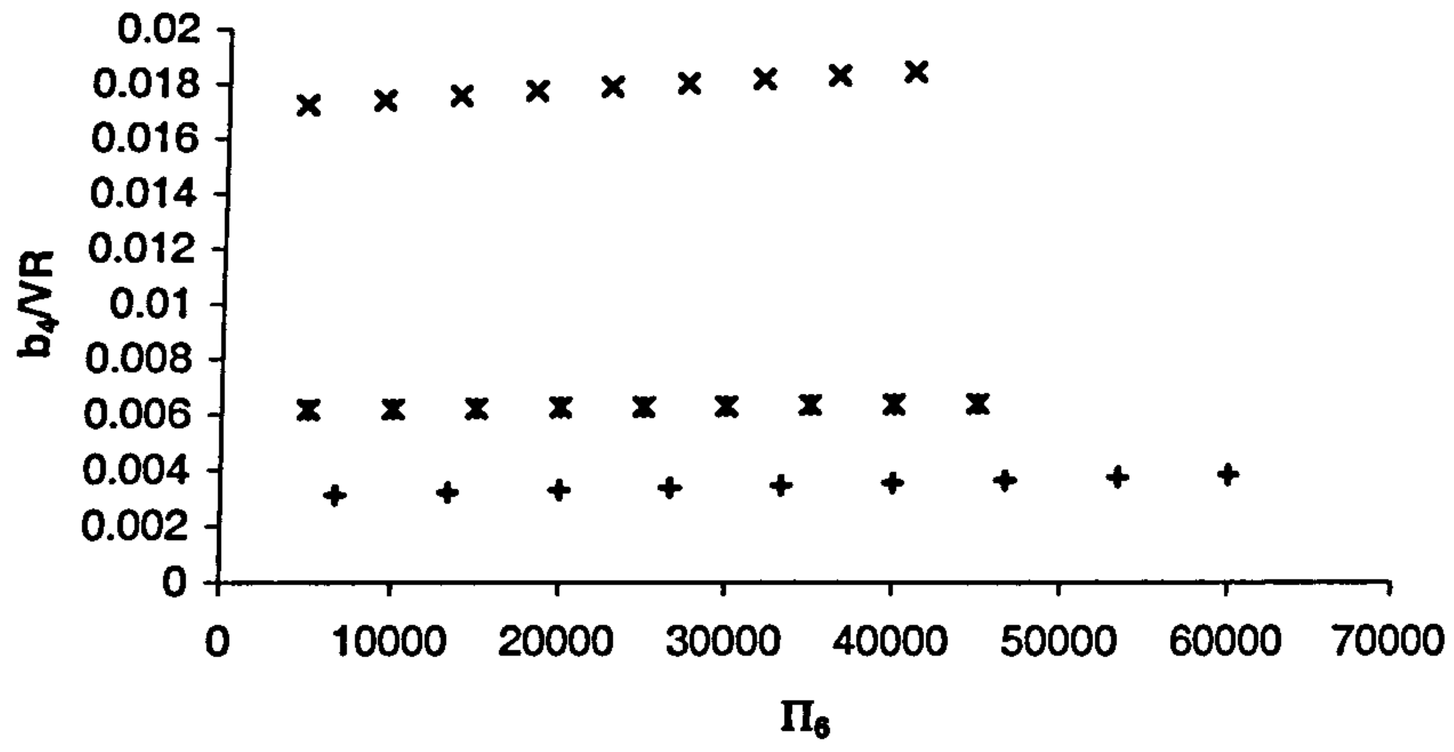

Figure 7.6.6e-f: Parameterisation quantity versus non-dimensional group values for the data sets used in the regression analysis
(Symbols represent the three sets of nine for each group)

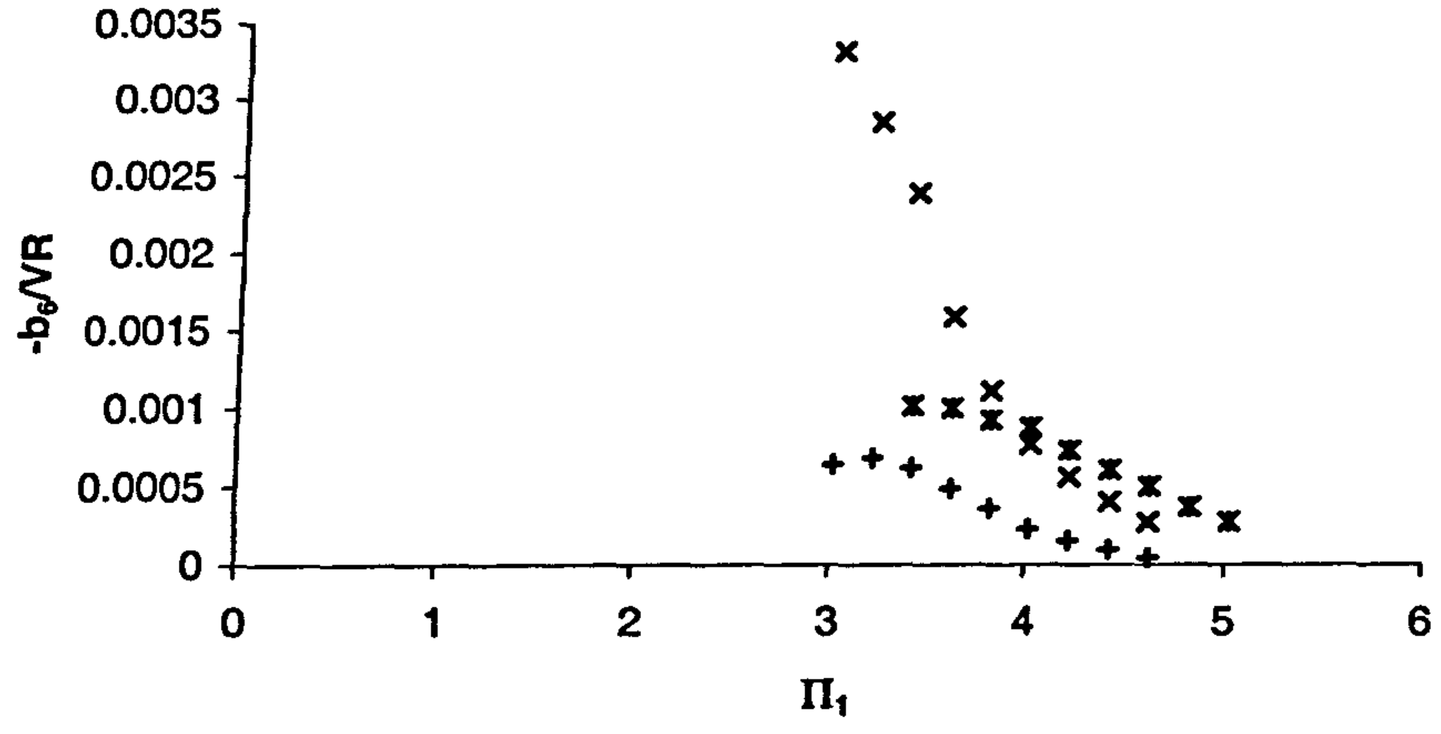

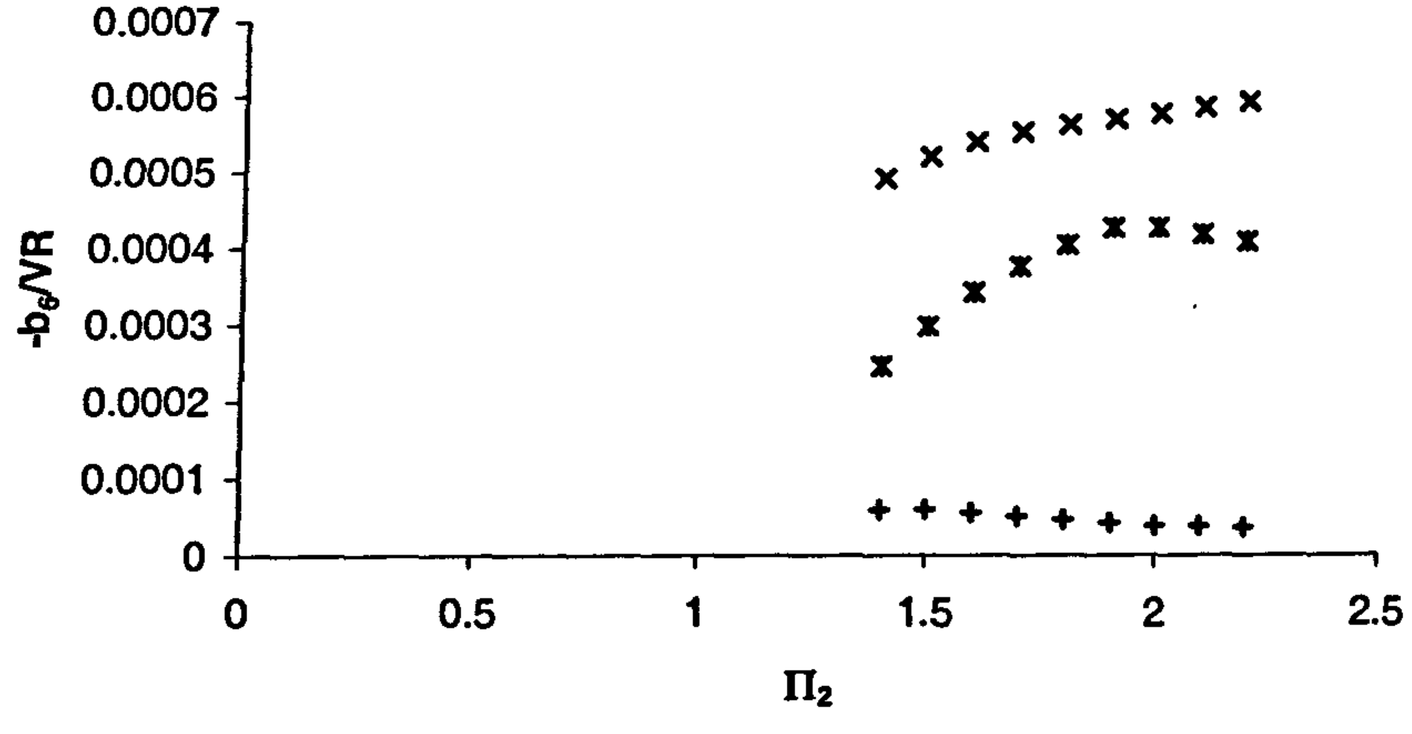

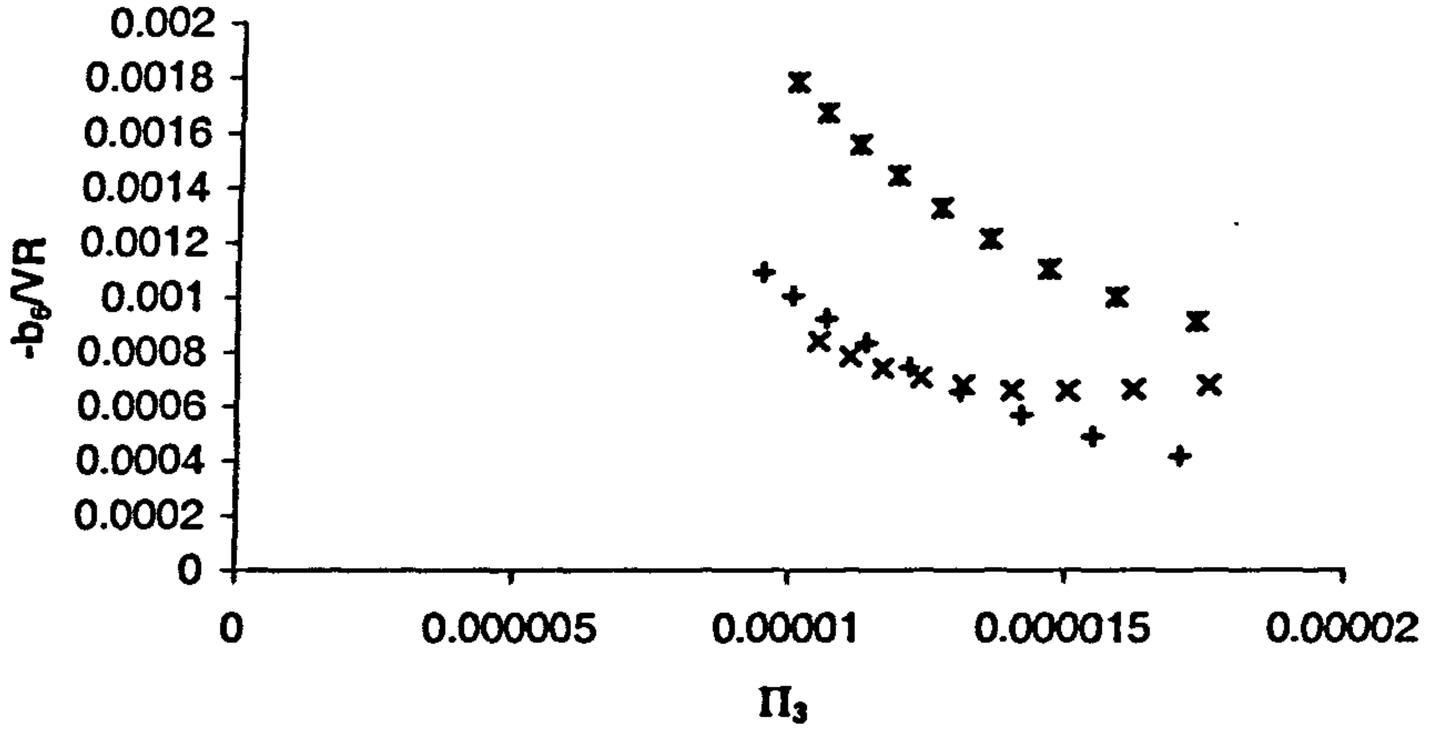

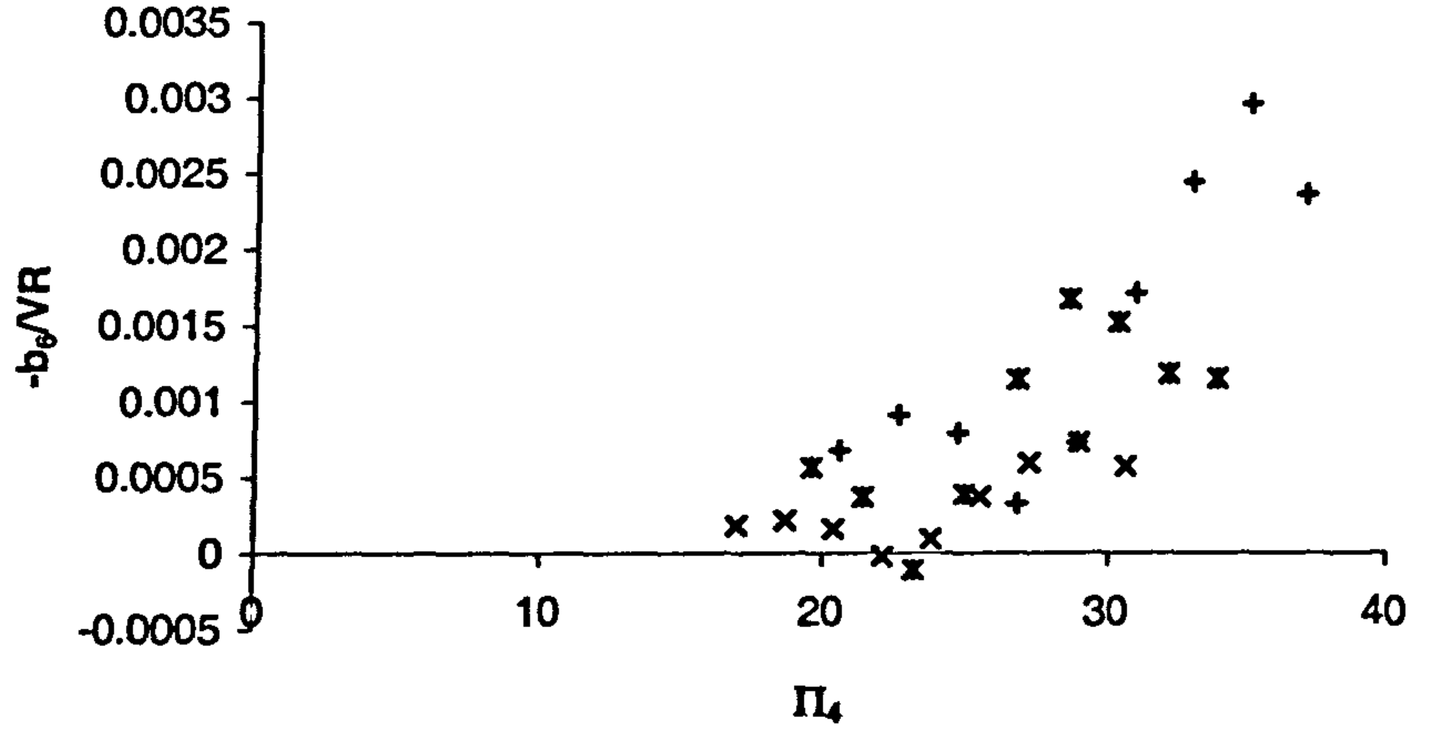

Figure 7.6.7a-d: Parameterisation quantity versus non-dimensional group values for the data sets used in the regression analysis
(Symbols represent the three sets of nine for each group)

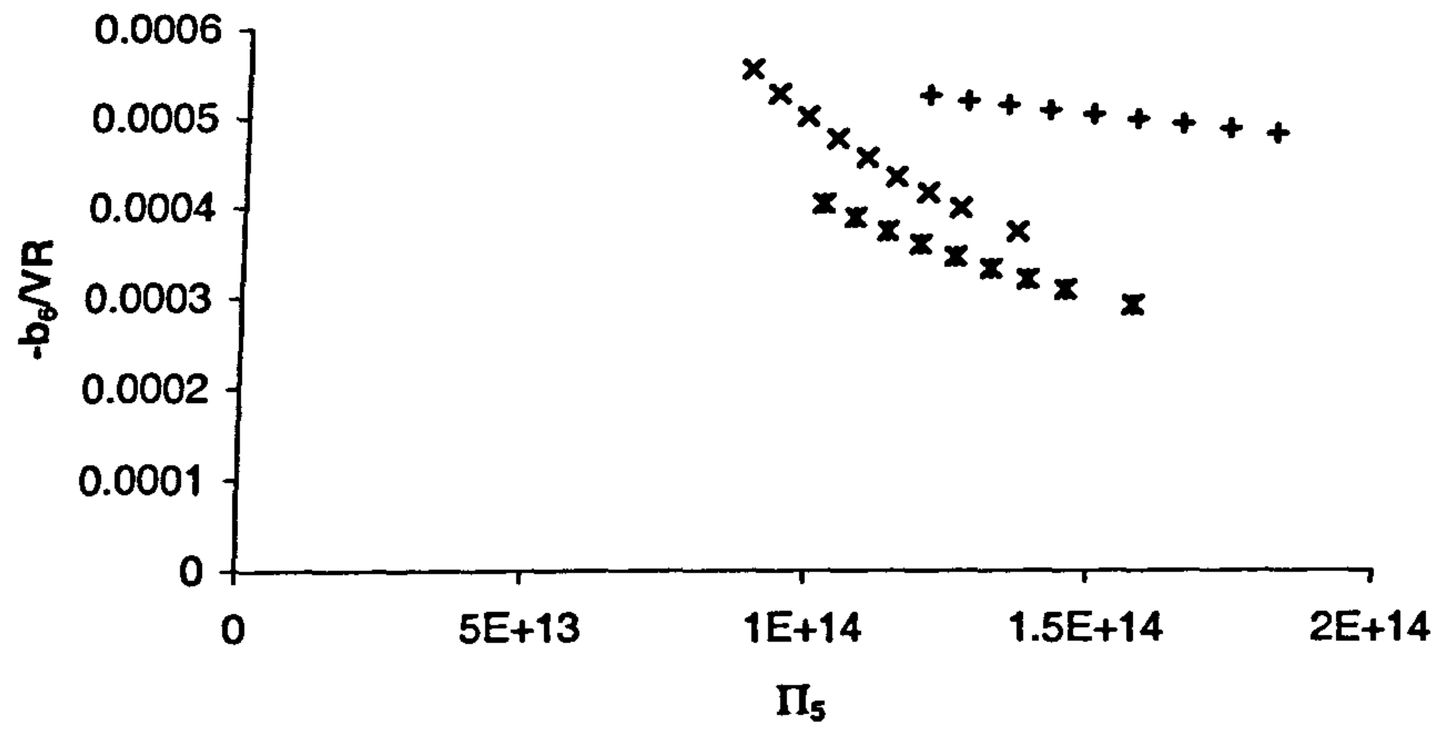

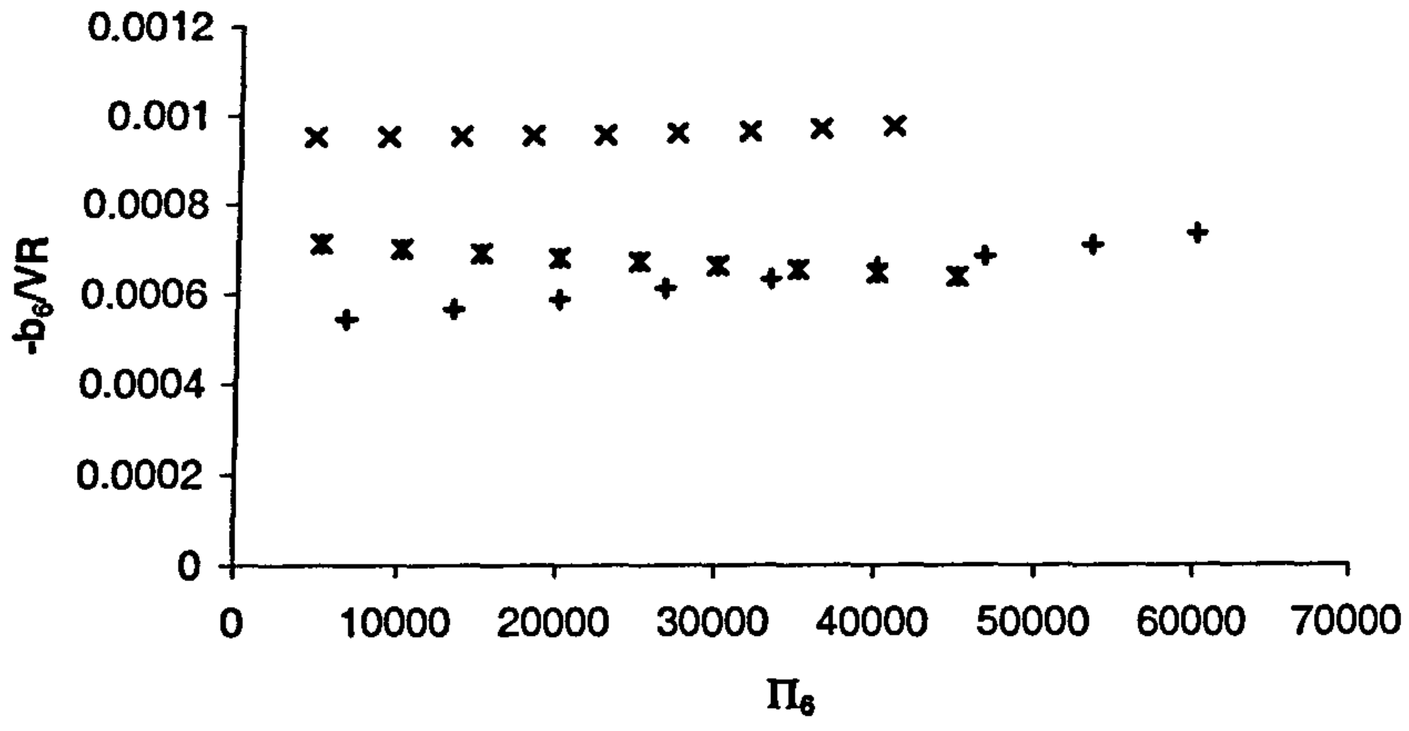

Figure 7.6.7e-f: Parameterisation quantity versus non-dimensional group values for the data sets used in the regression analysis
(Symbols represent the three sets of nine for each group)

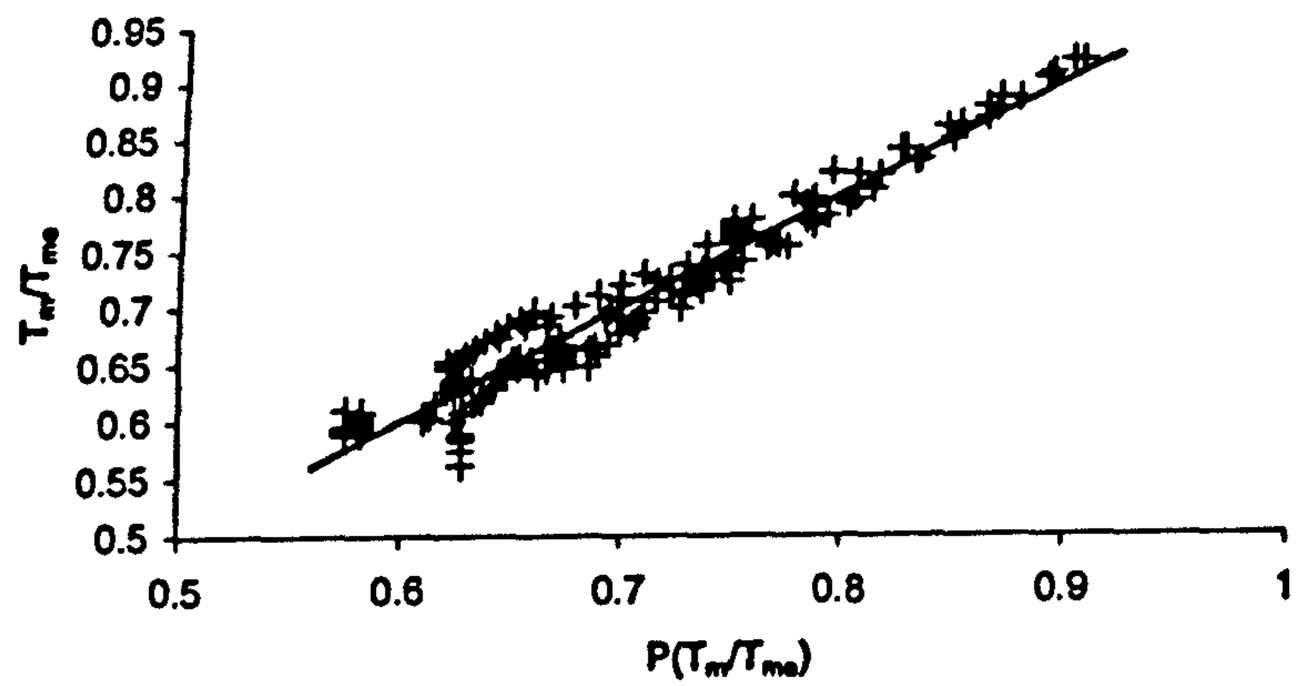

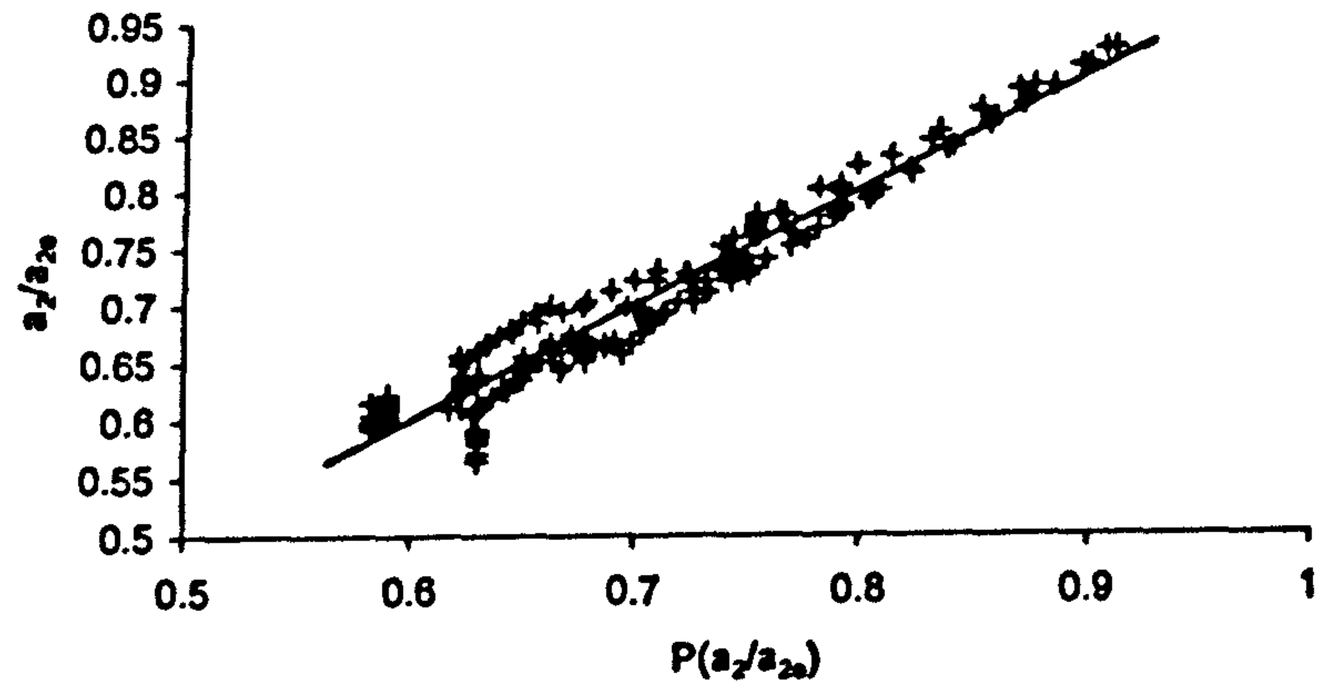

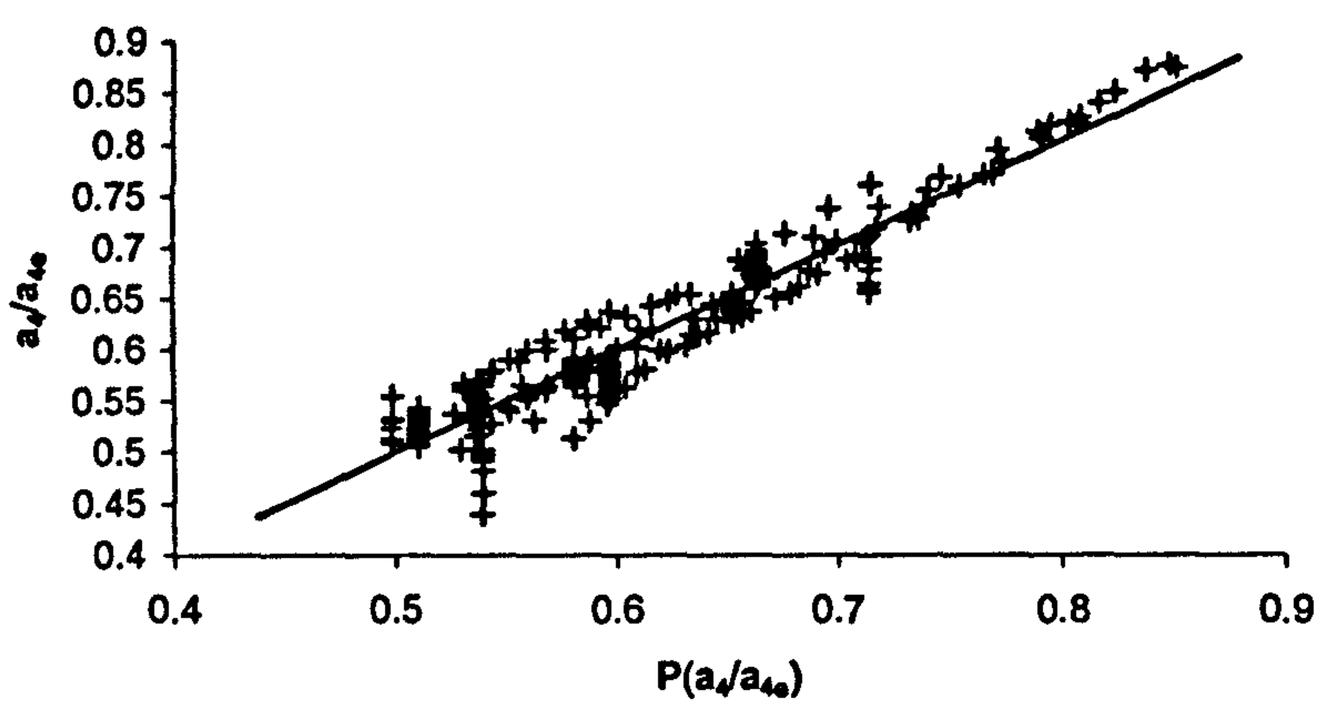

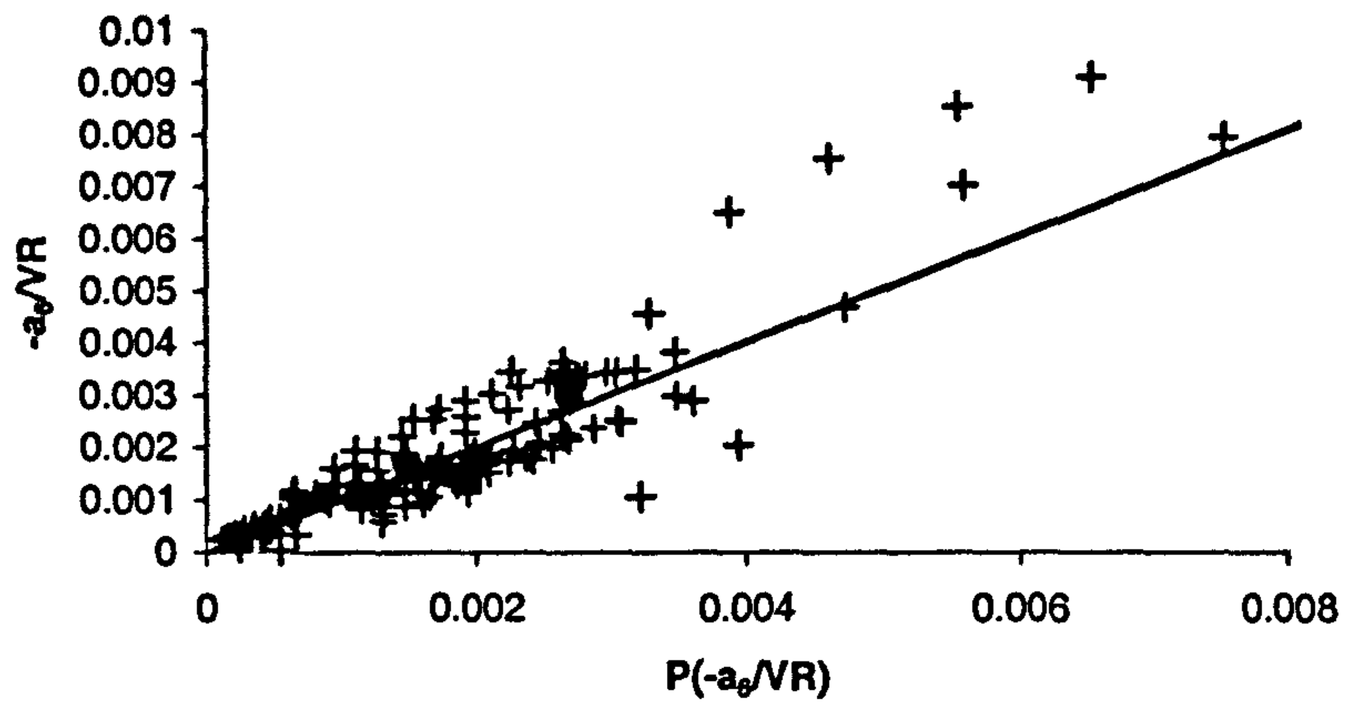

Figure 7.7.1a-d: Parameterised 1DV quantities versus values from the numerical 1DV model

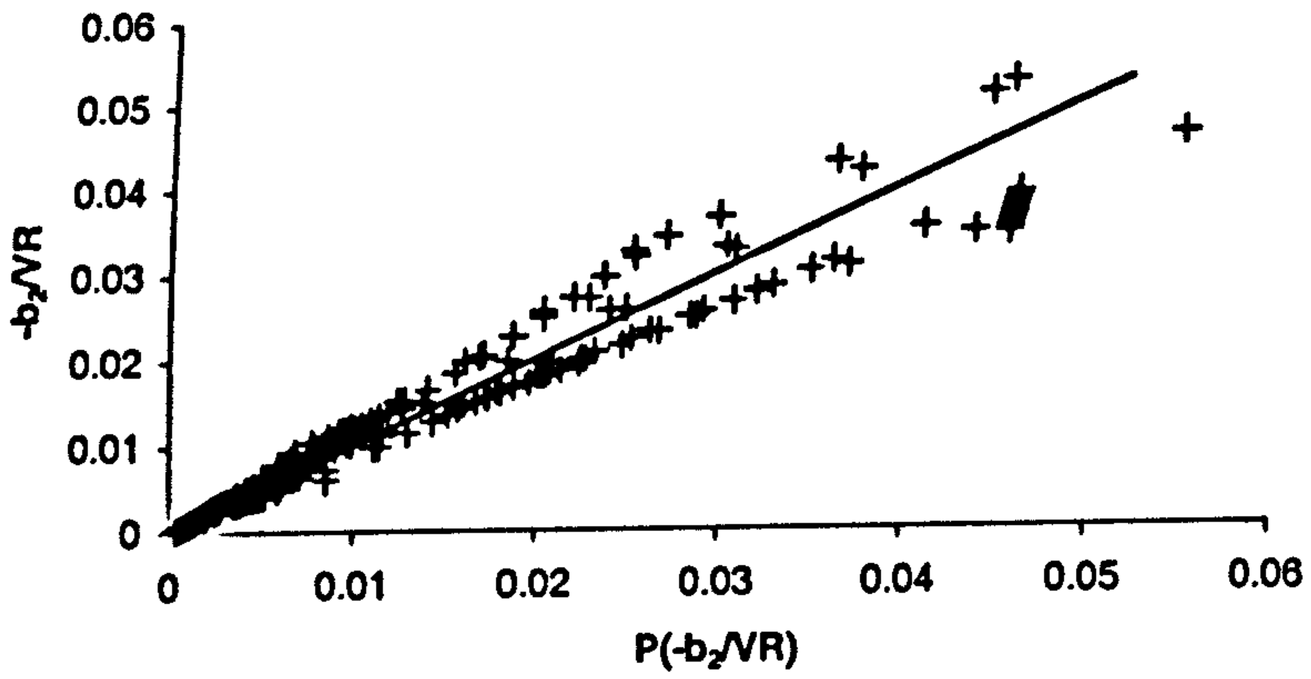

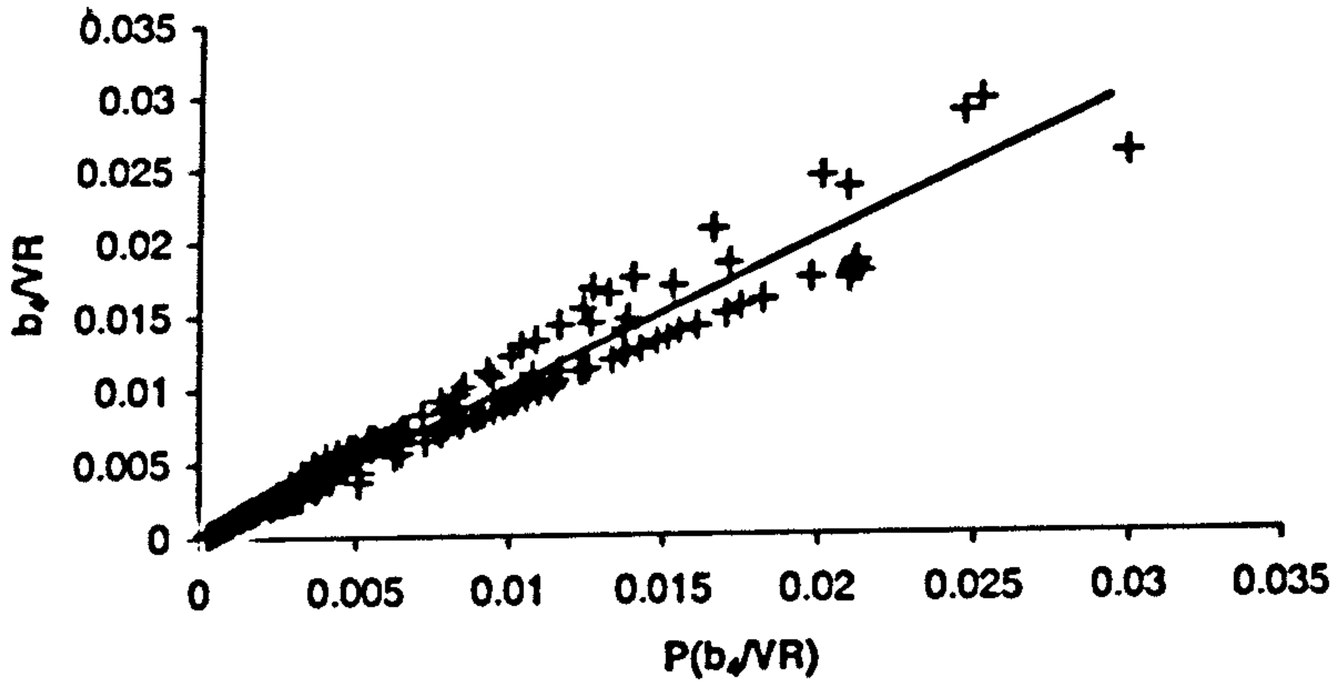

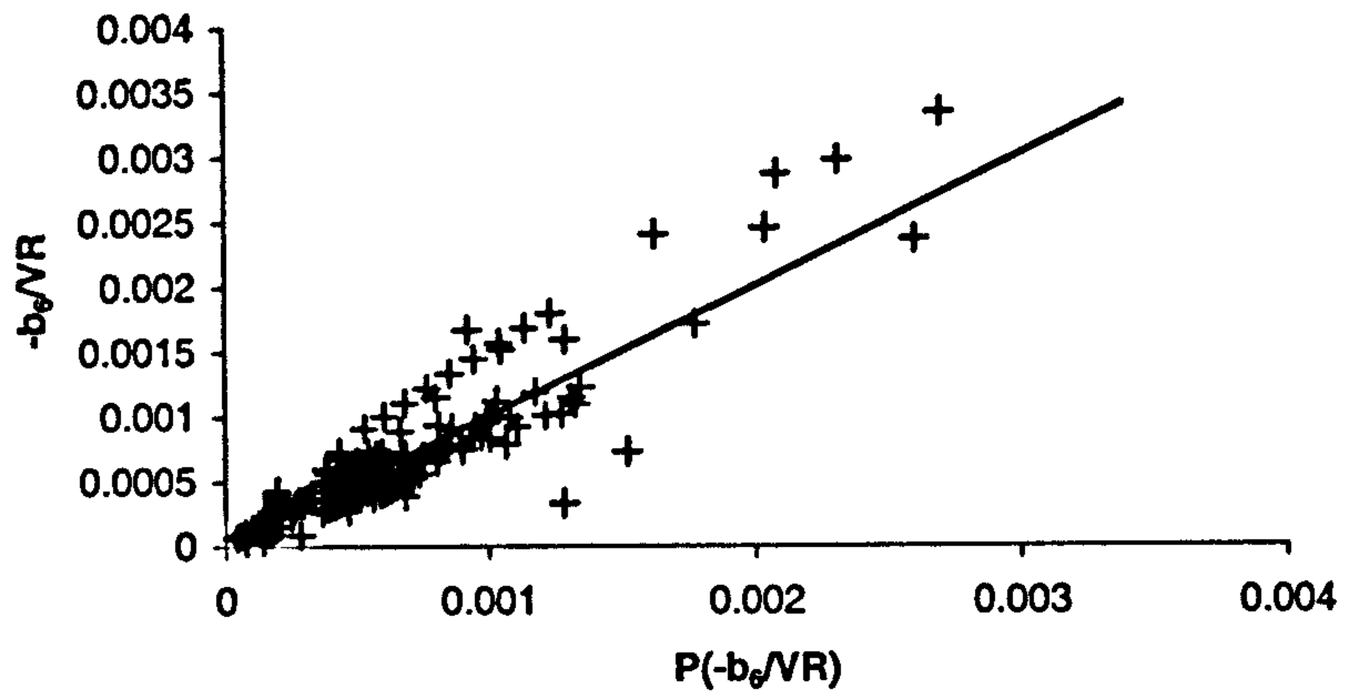

Figure 7.7.1e-g: Parameterised 1DV quantities versus values from the numerical 1DV model

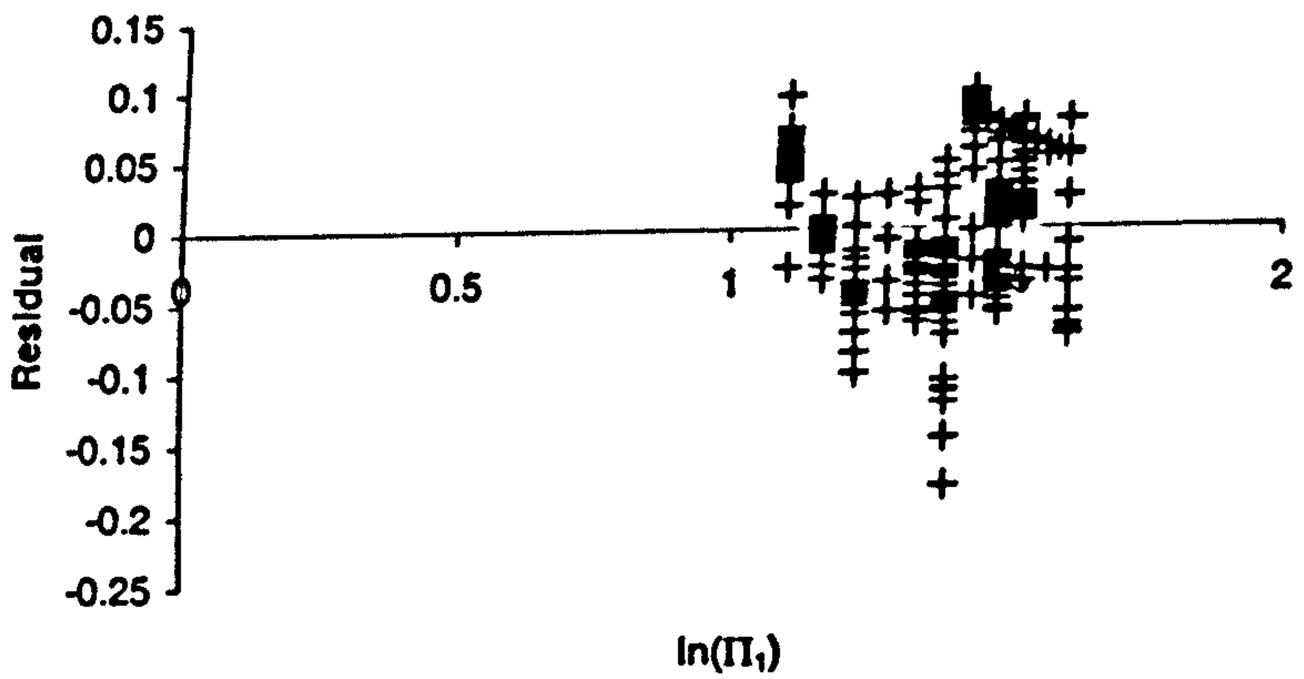

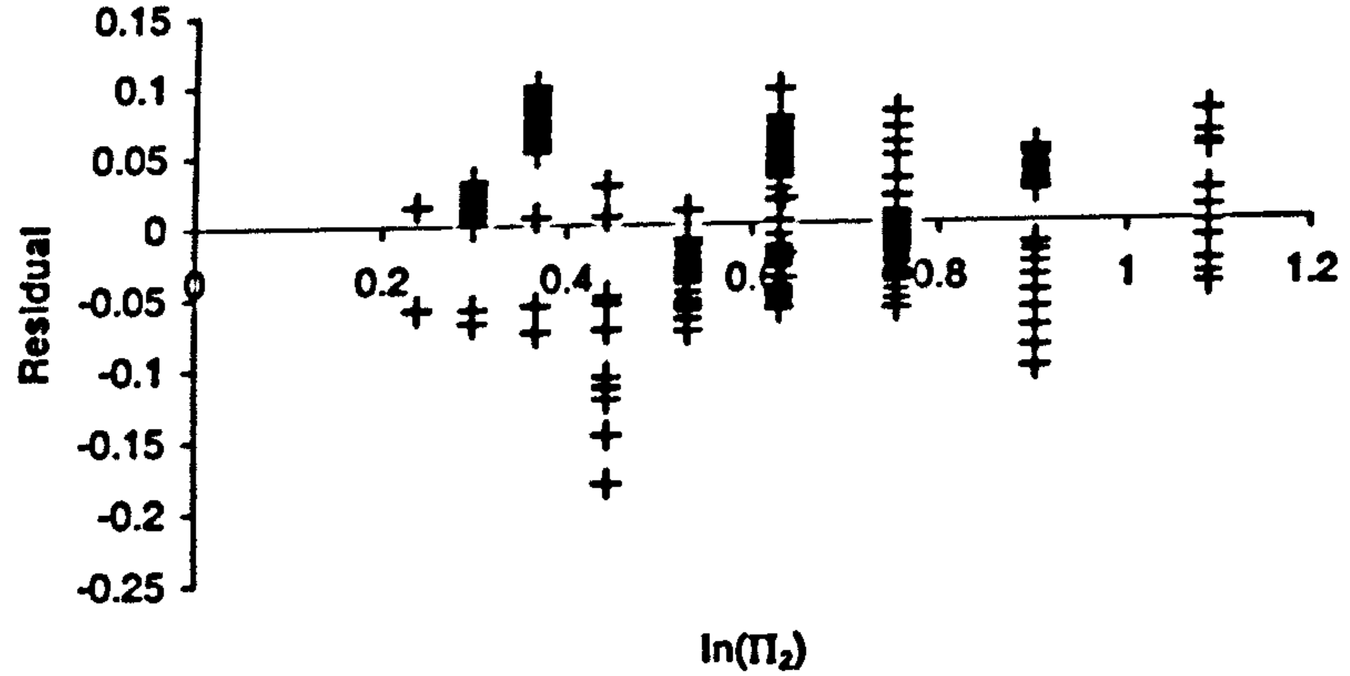

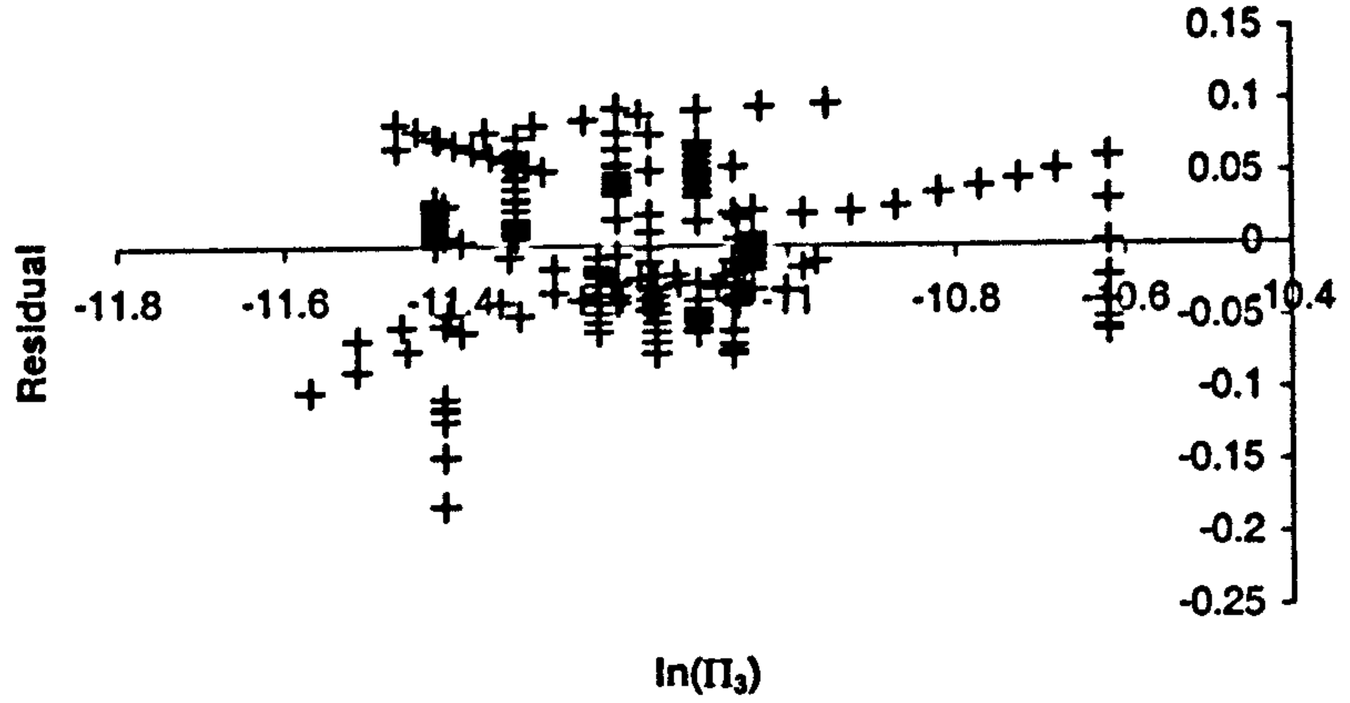

Figure 7.7.2a-c: Residual plots for the parameterisation of T_m

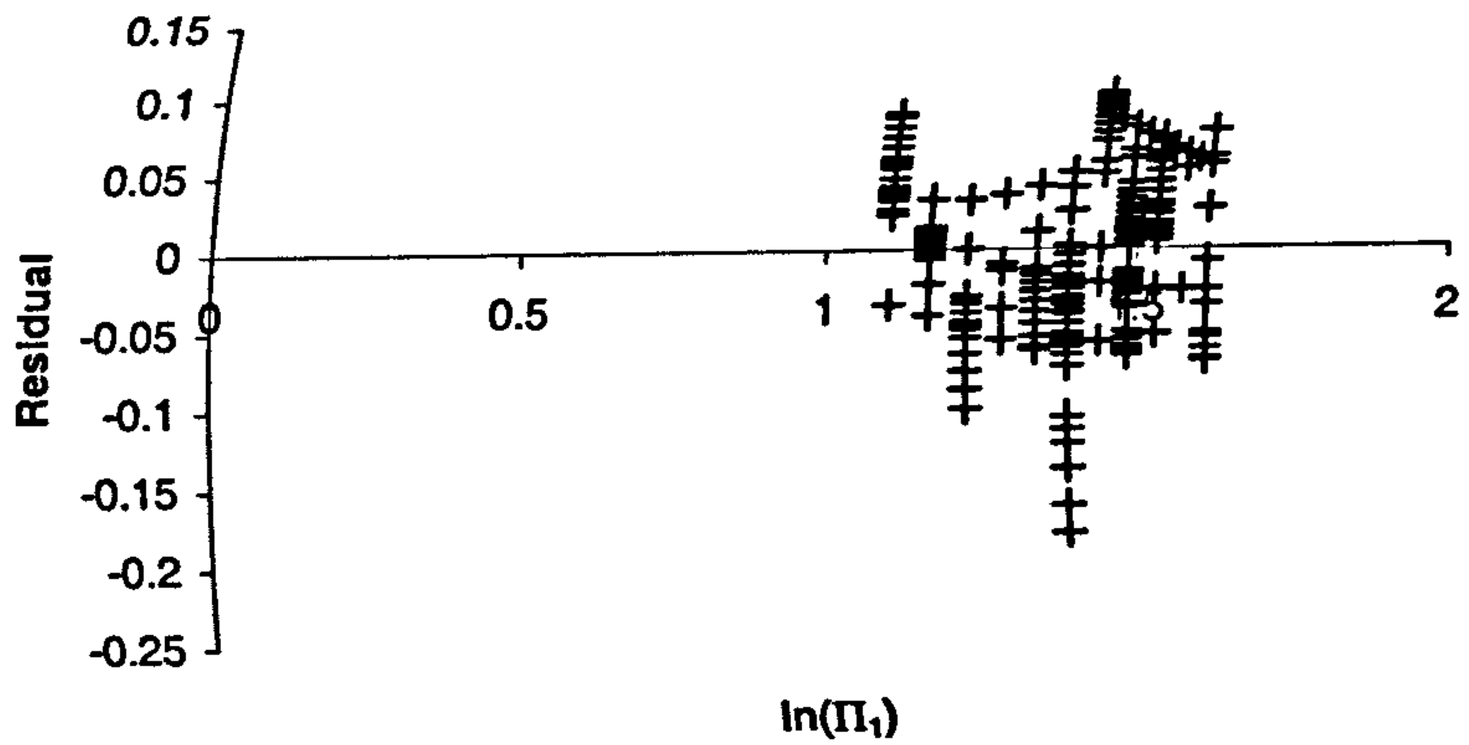

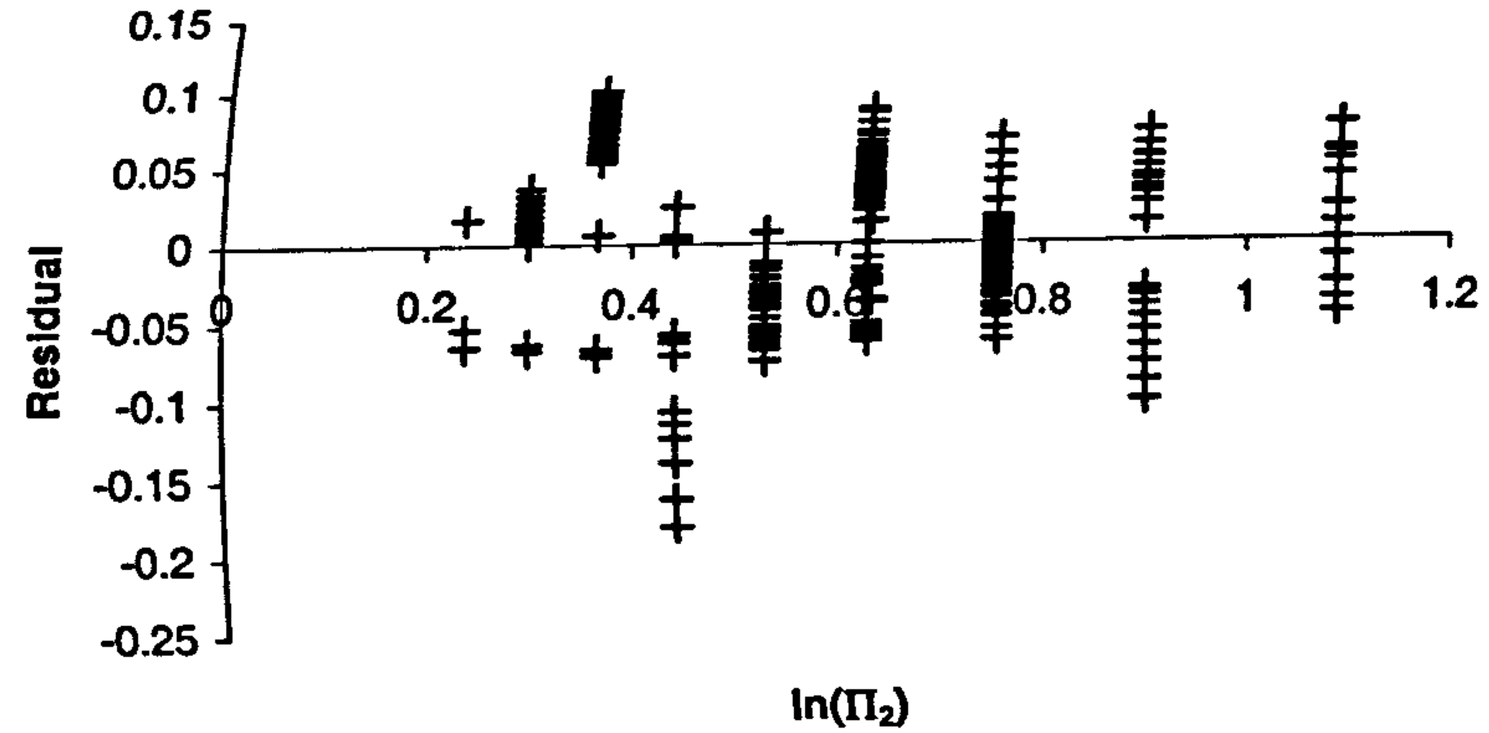

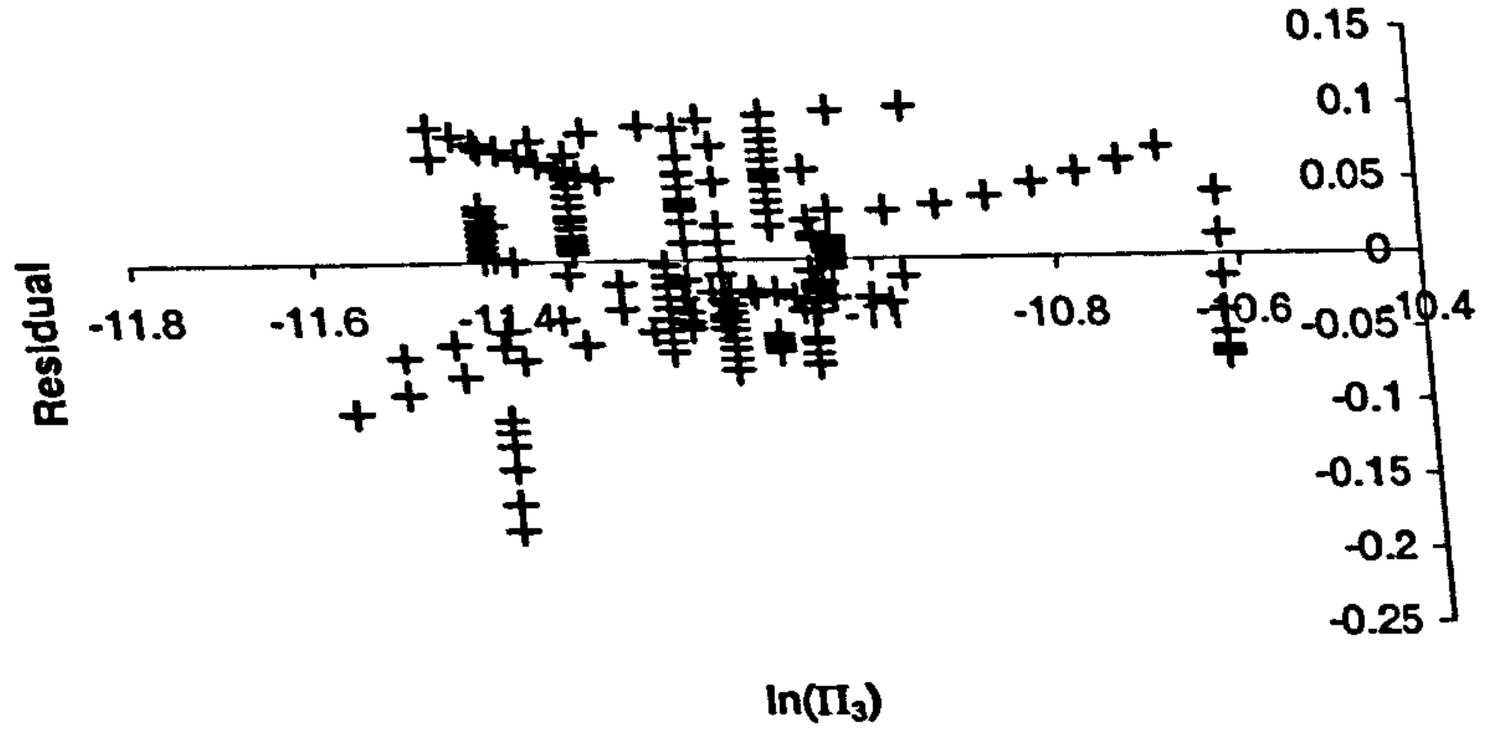

Figure 7.7.3a-c: Residual plots for the parameterisation of a_2

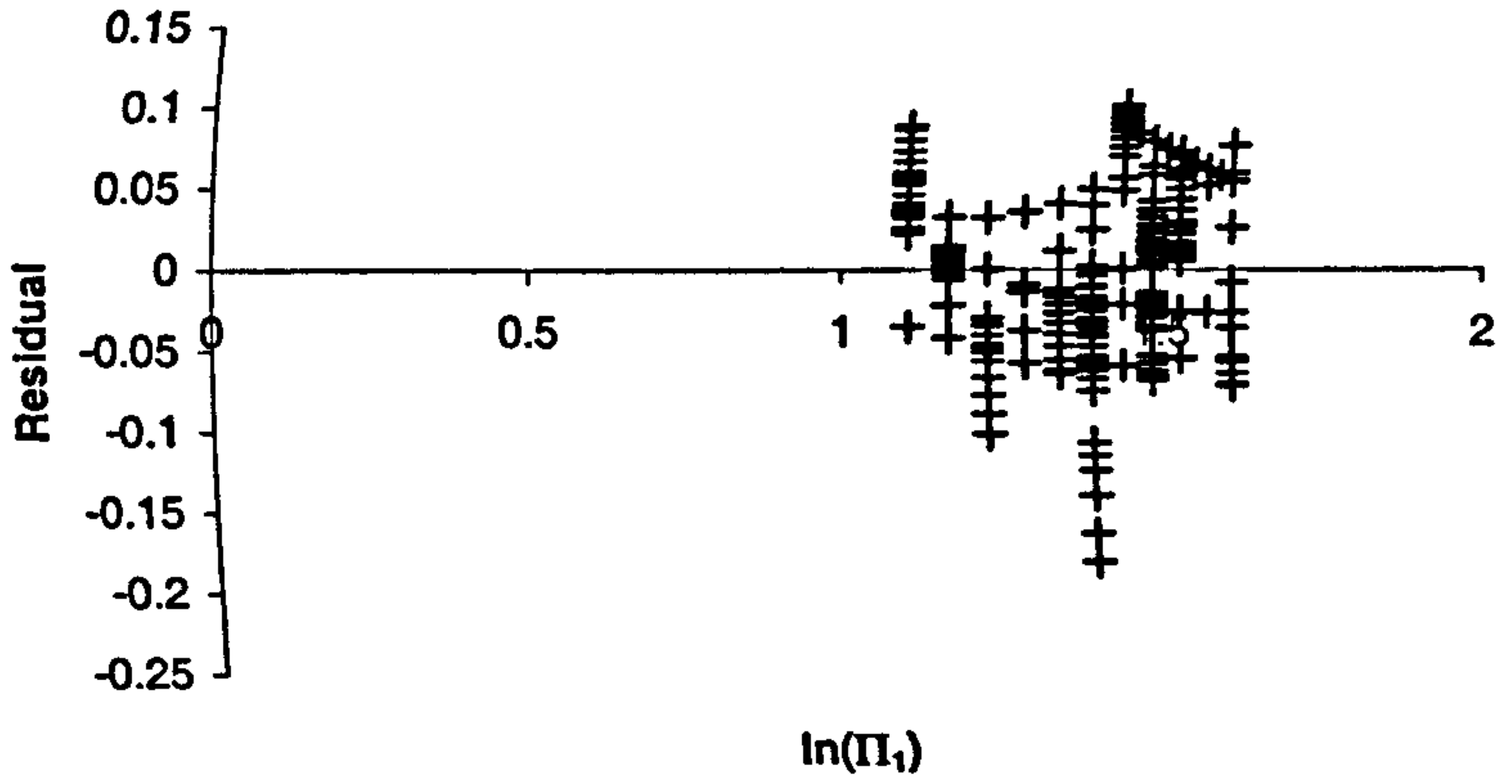

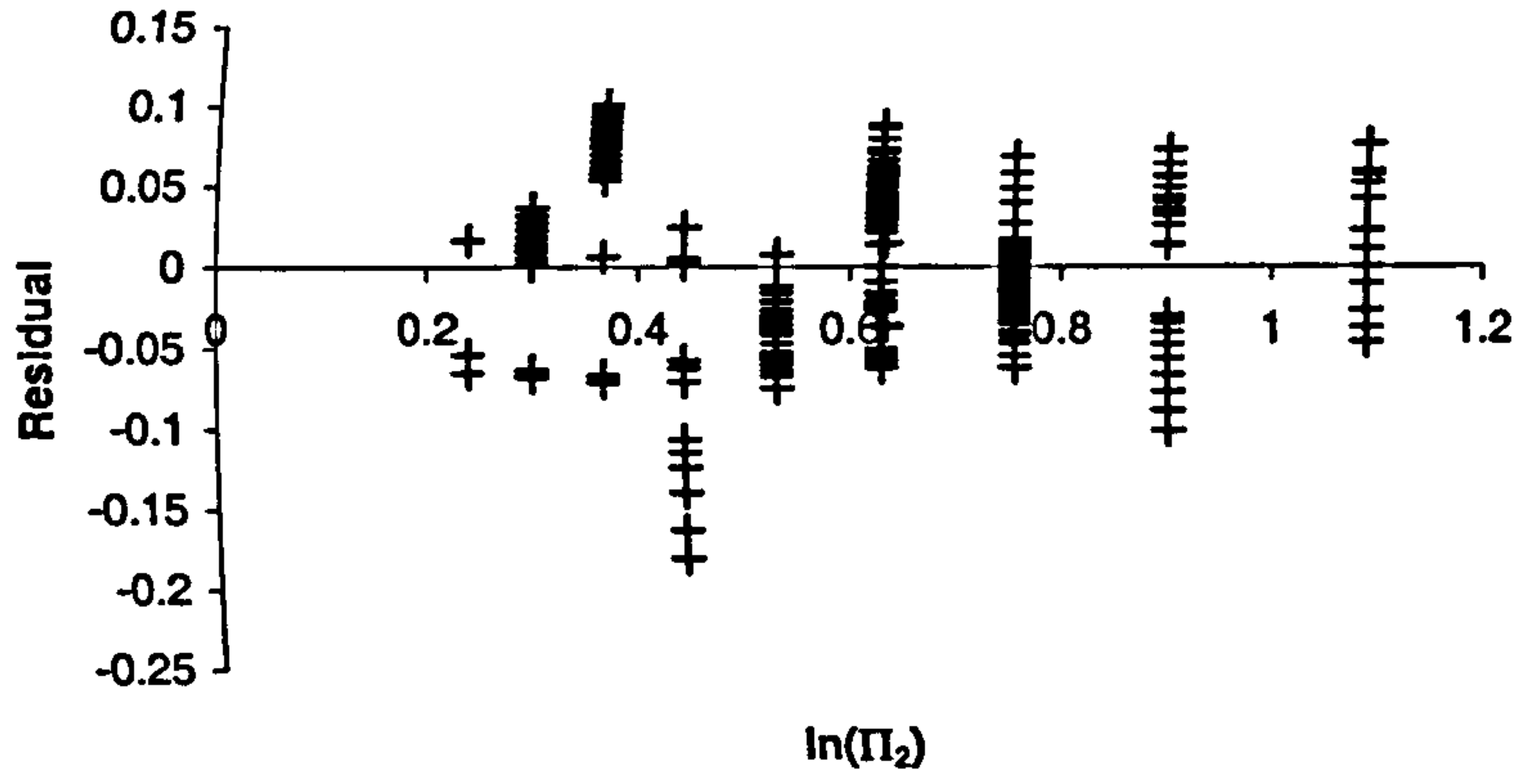

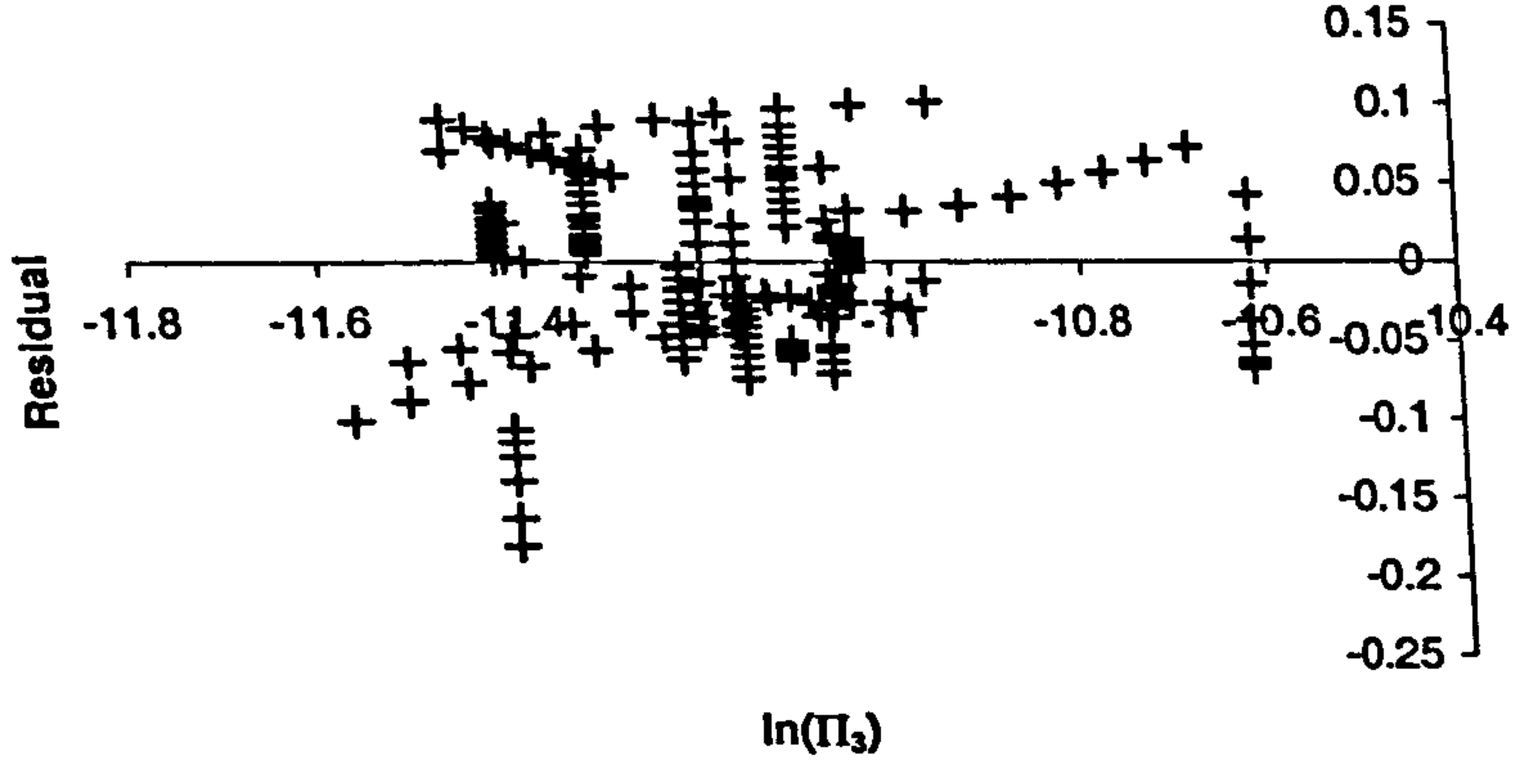

Figure 7.7.3a-c: Residual plots for the parameterisation of a_2

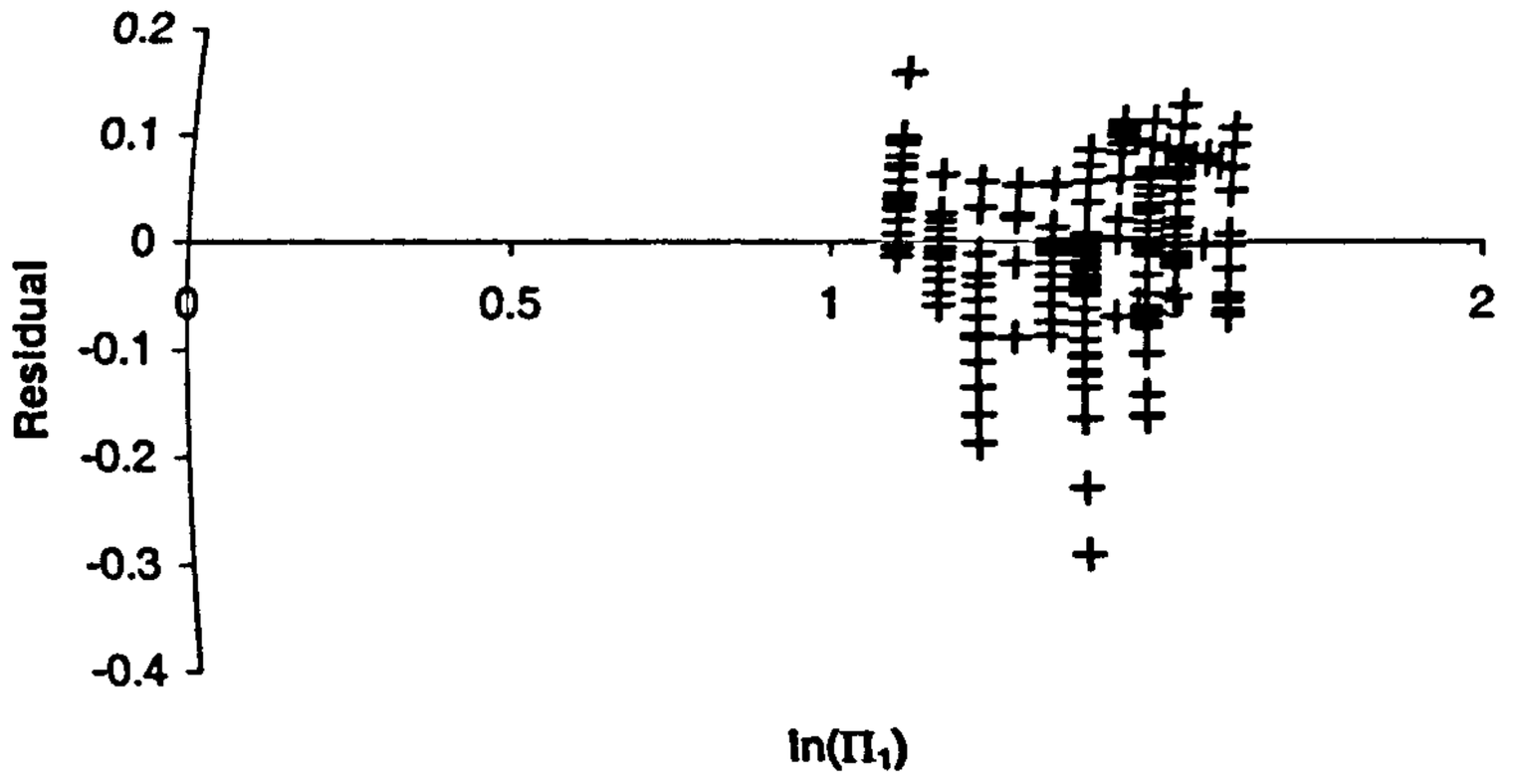

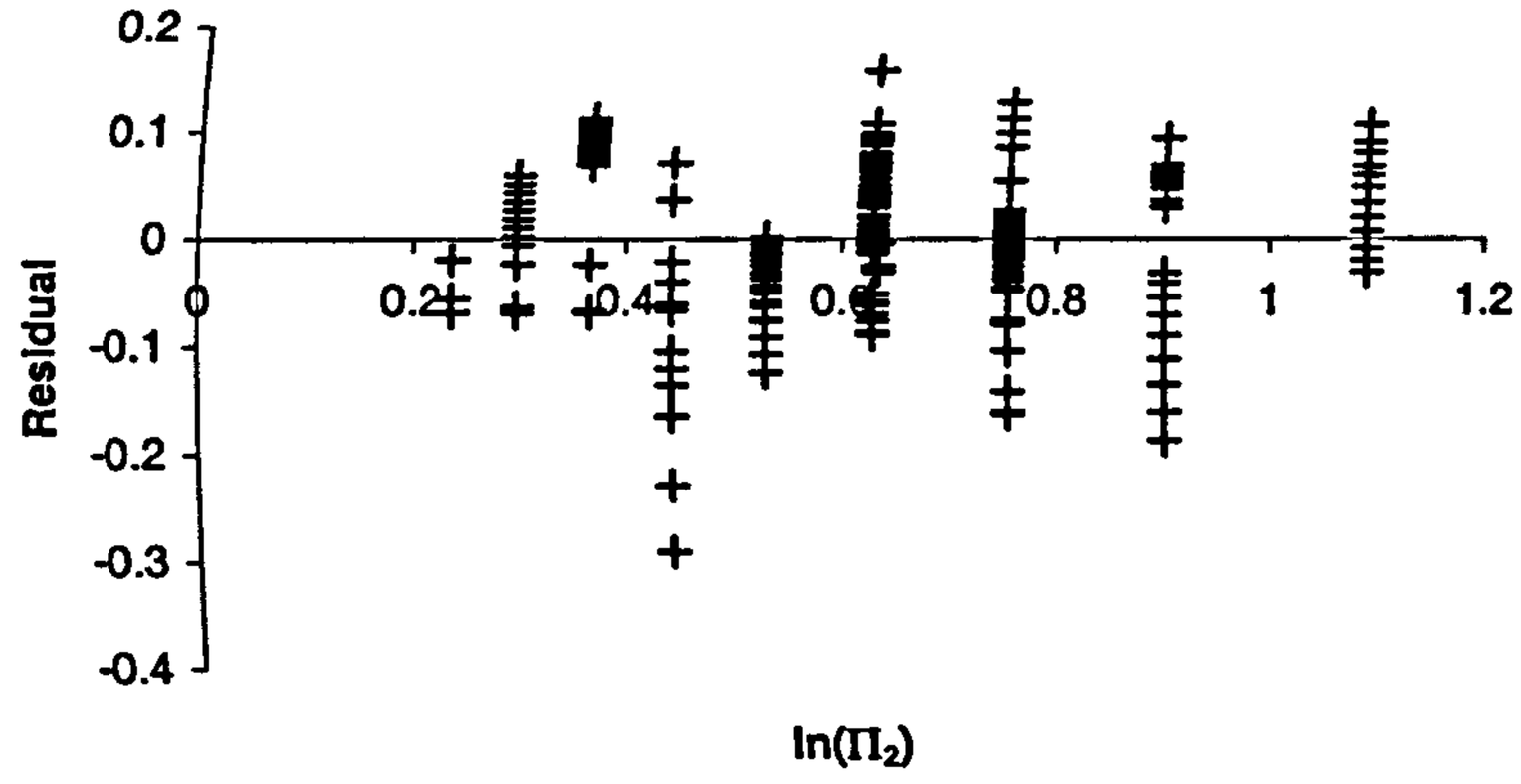

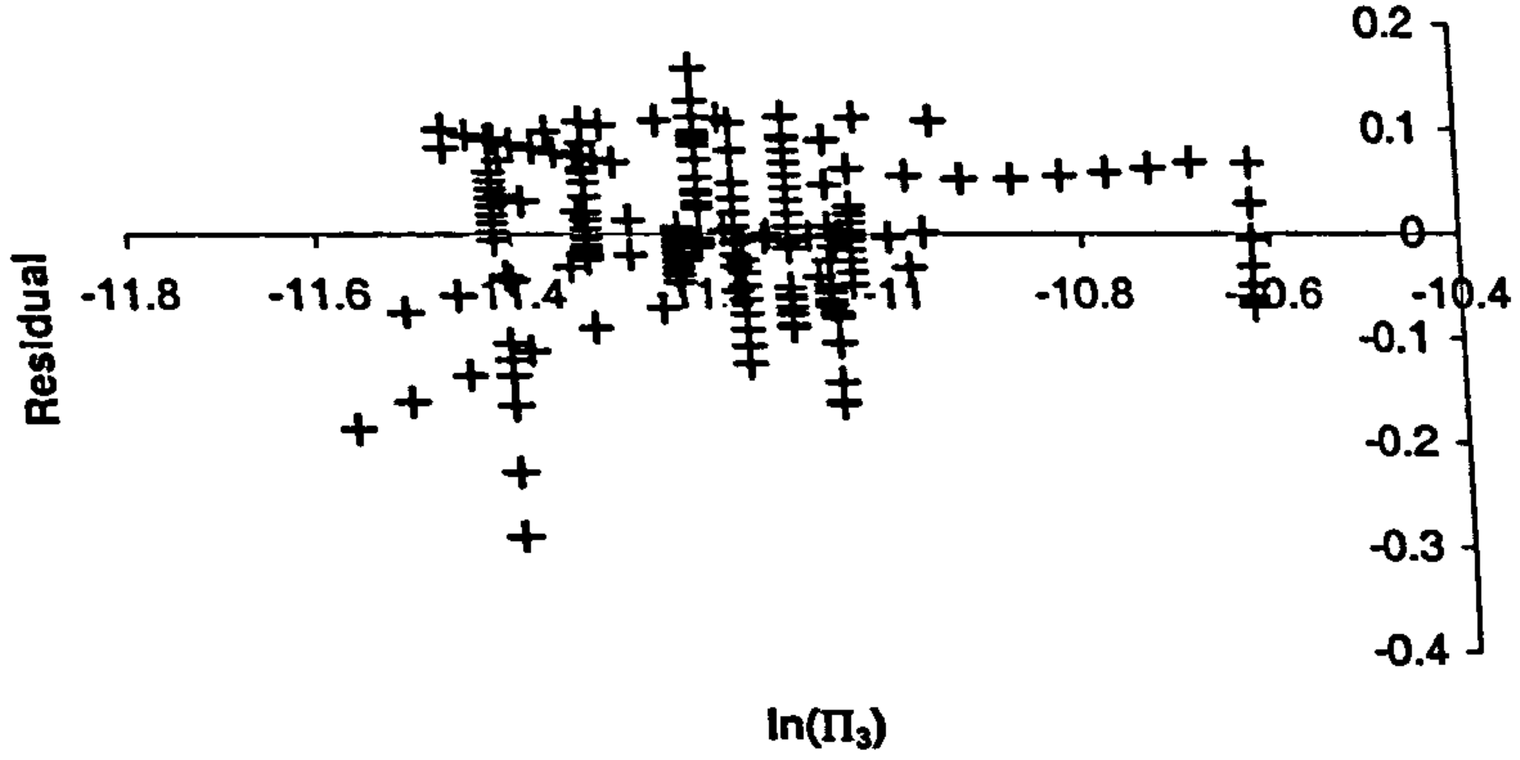

Figure 7.7.4a-c: Residual plots for the parameterisation of a_4

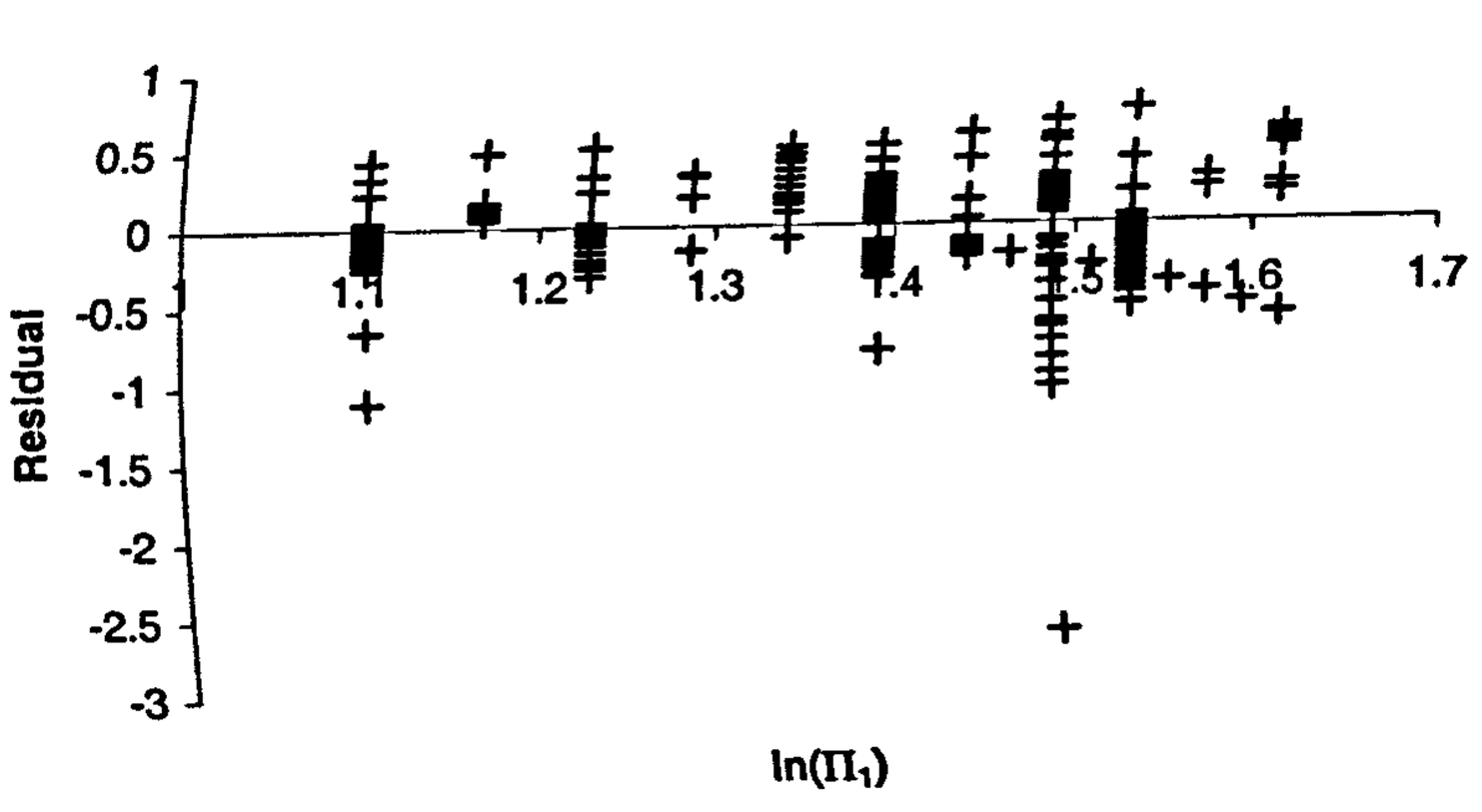

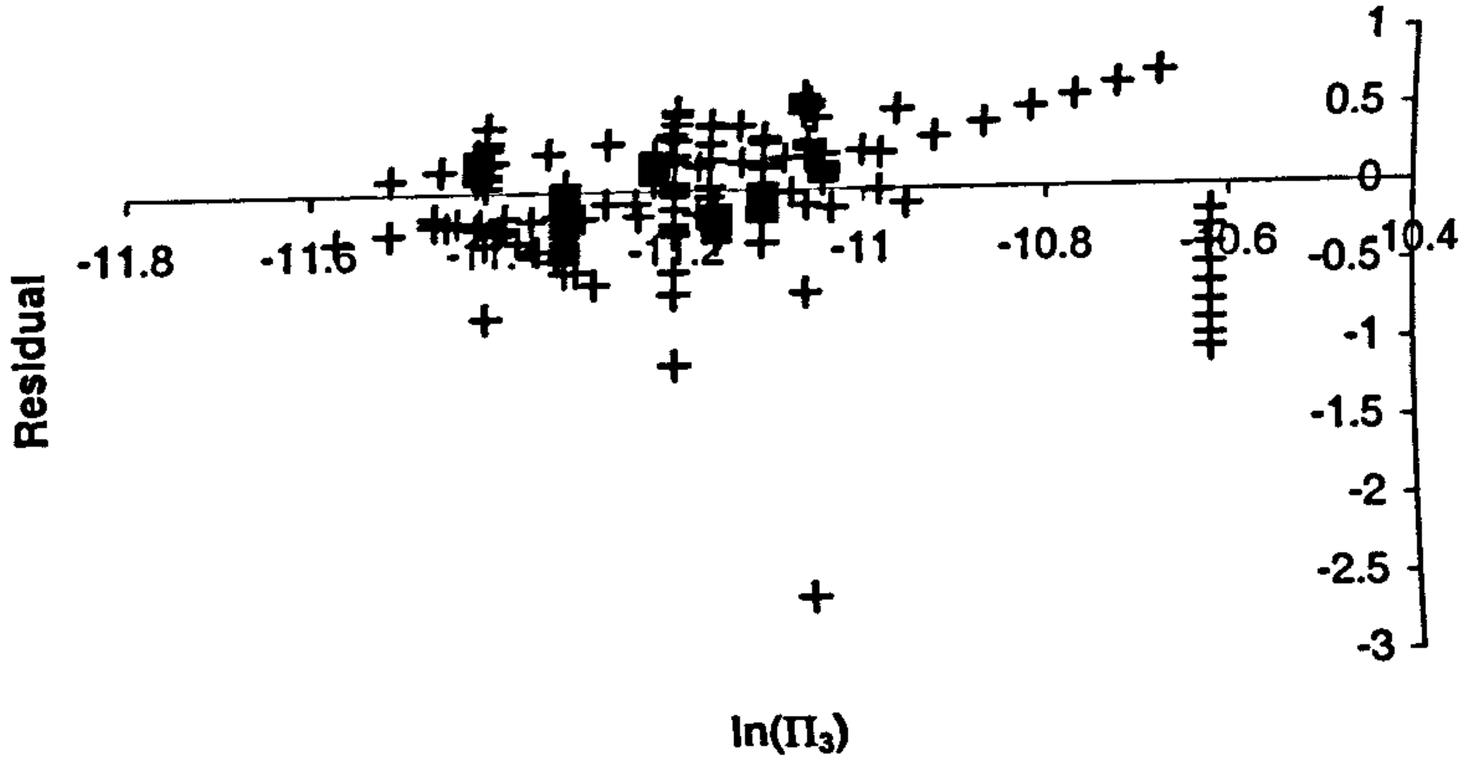

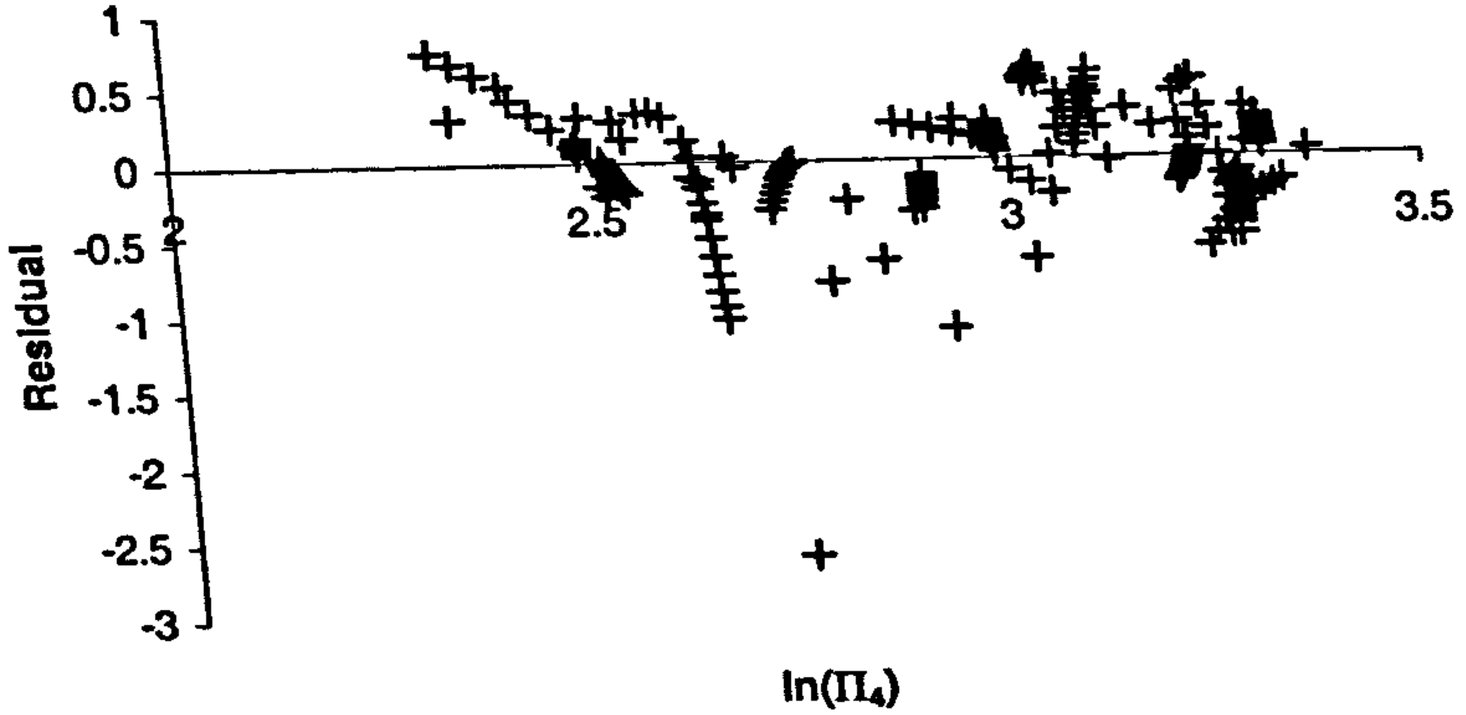

Figure 7.7.5a-c: Residual plots for the parameterisation of a_6

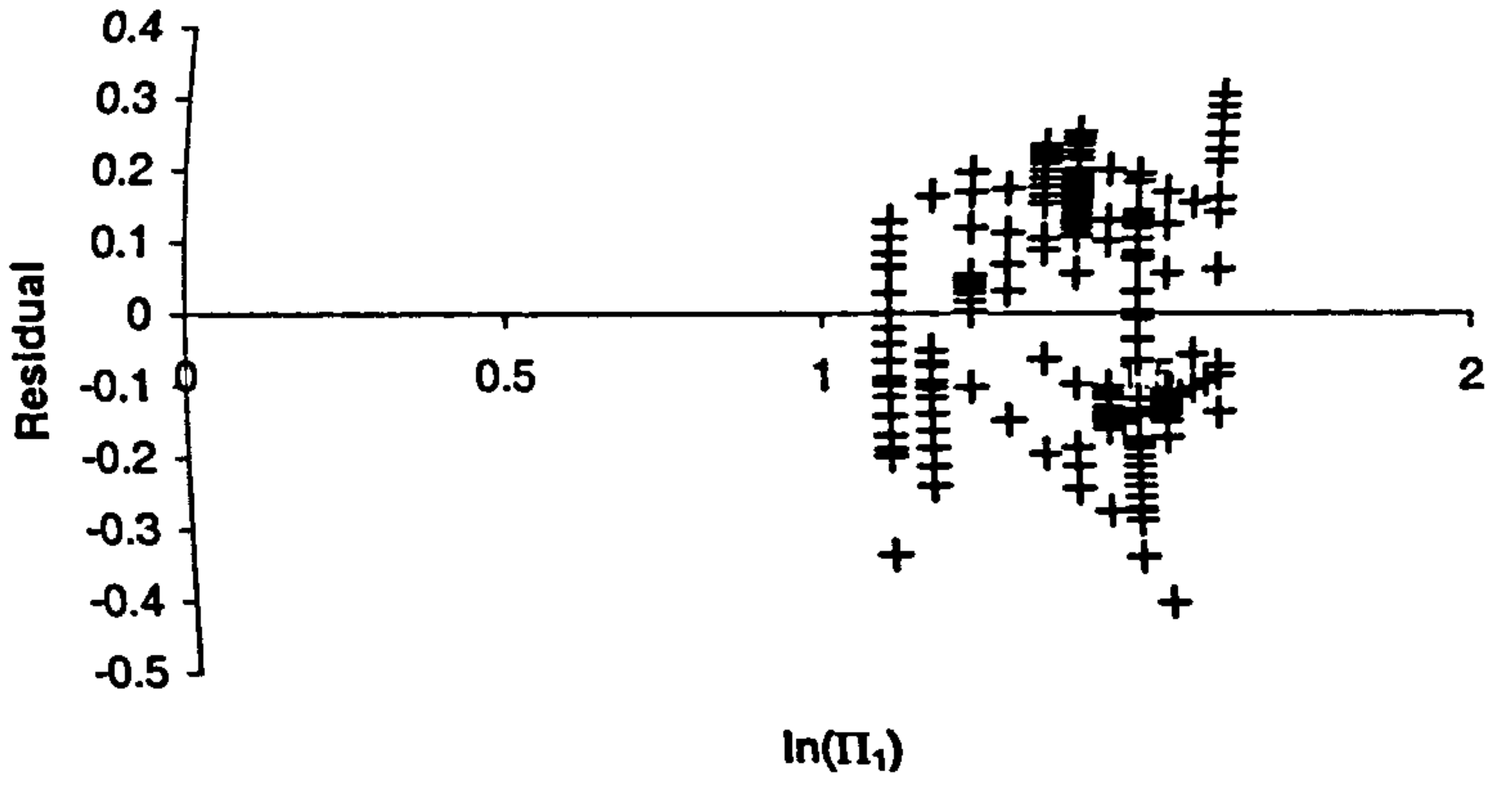

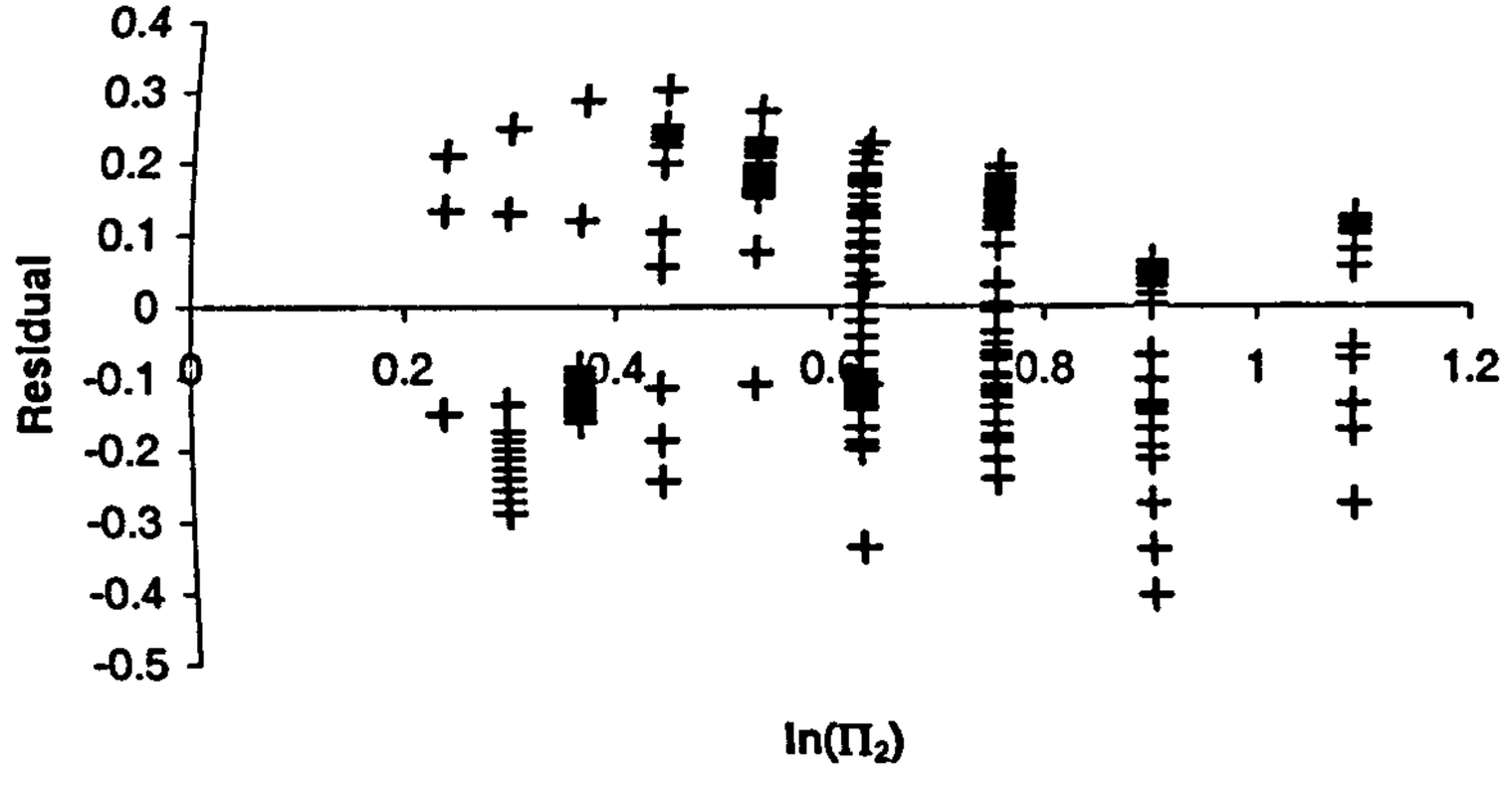

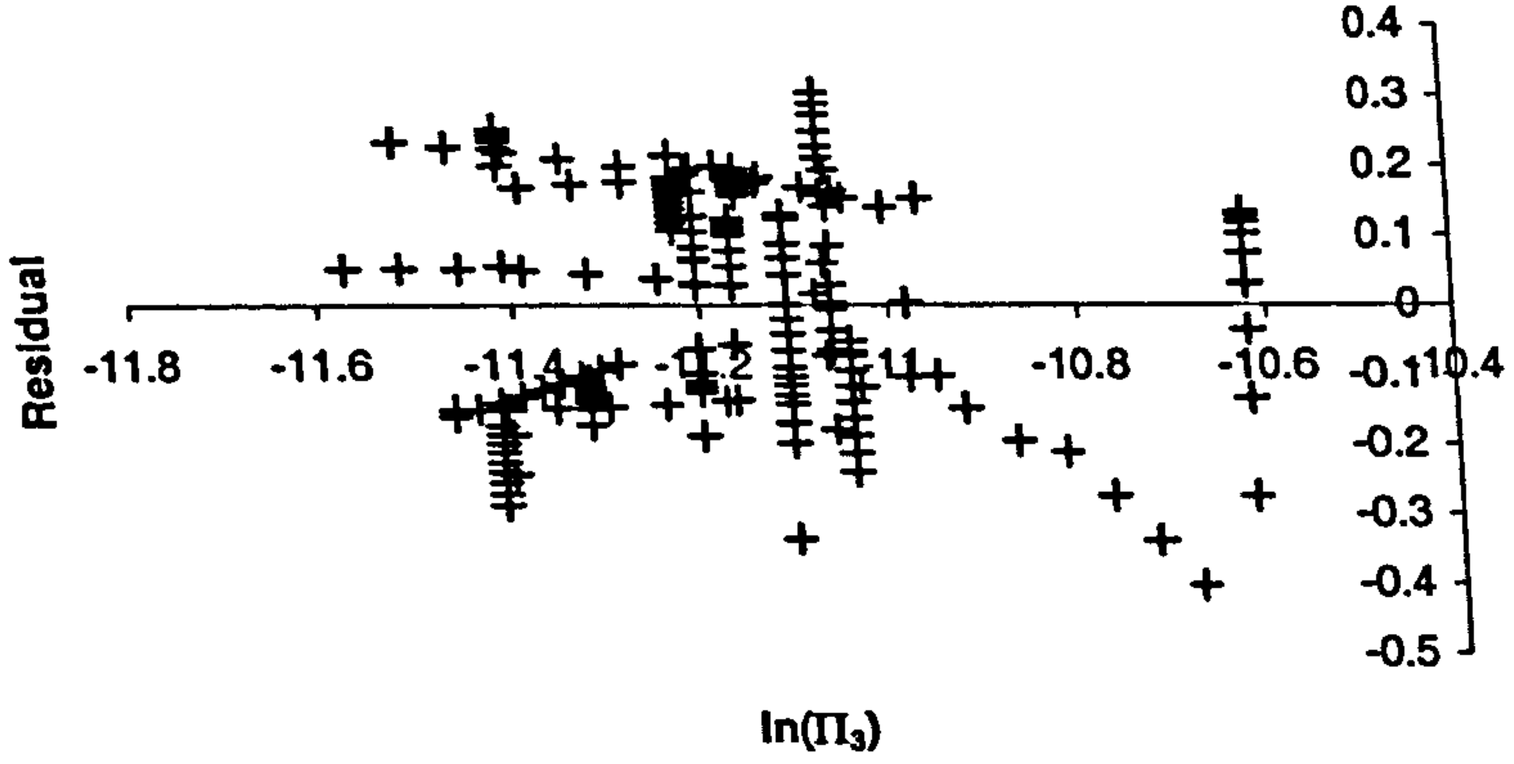

Figure 7.7.6a-c: Residual plots for the parameterisation of b_2

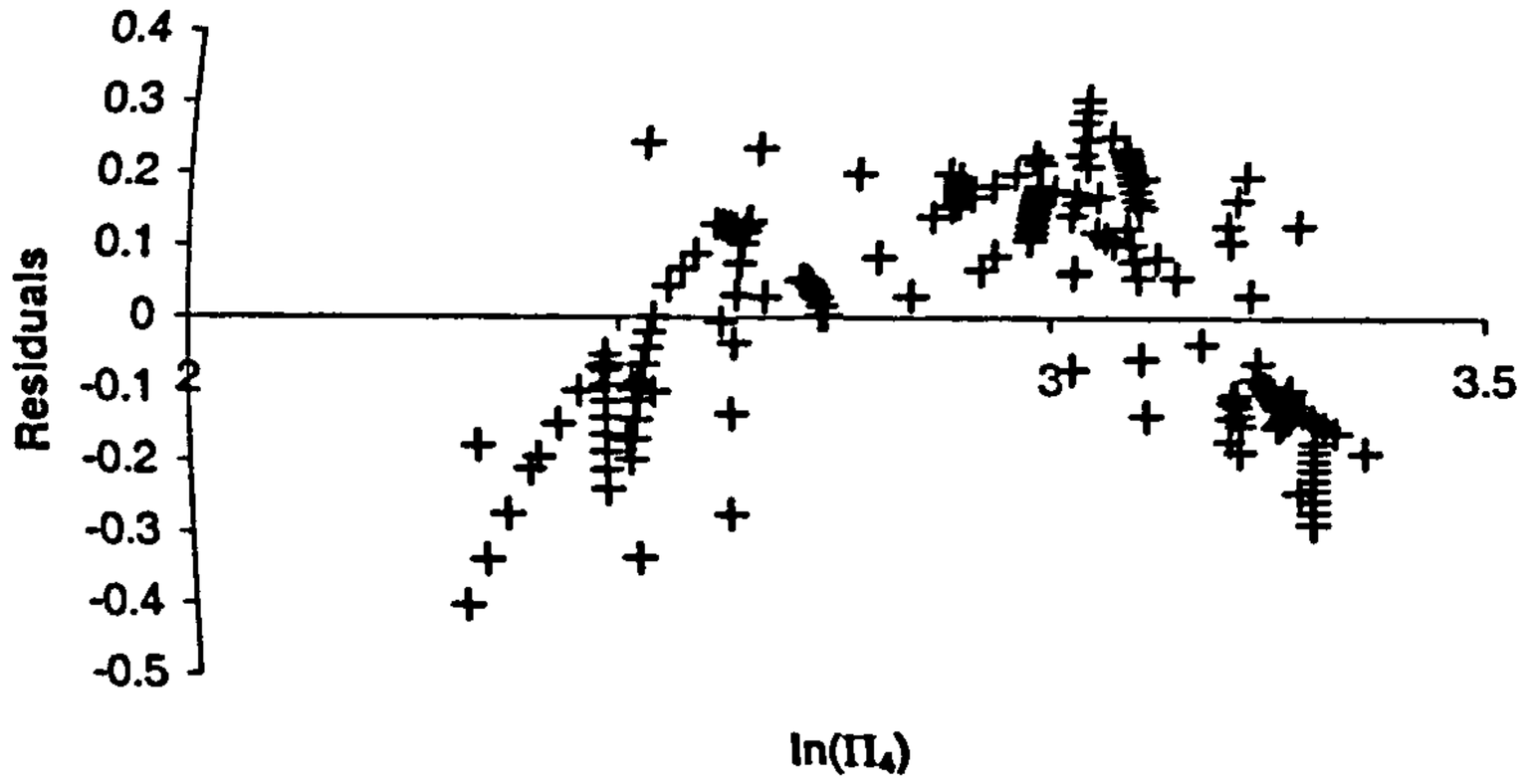

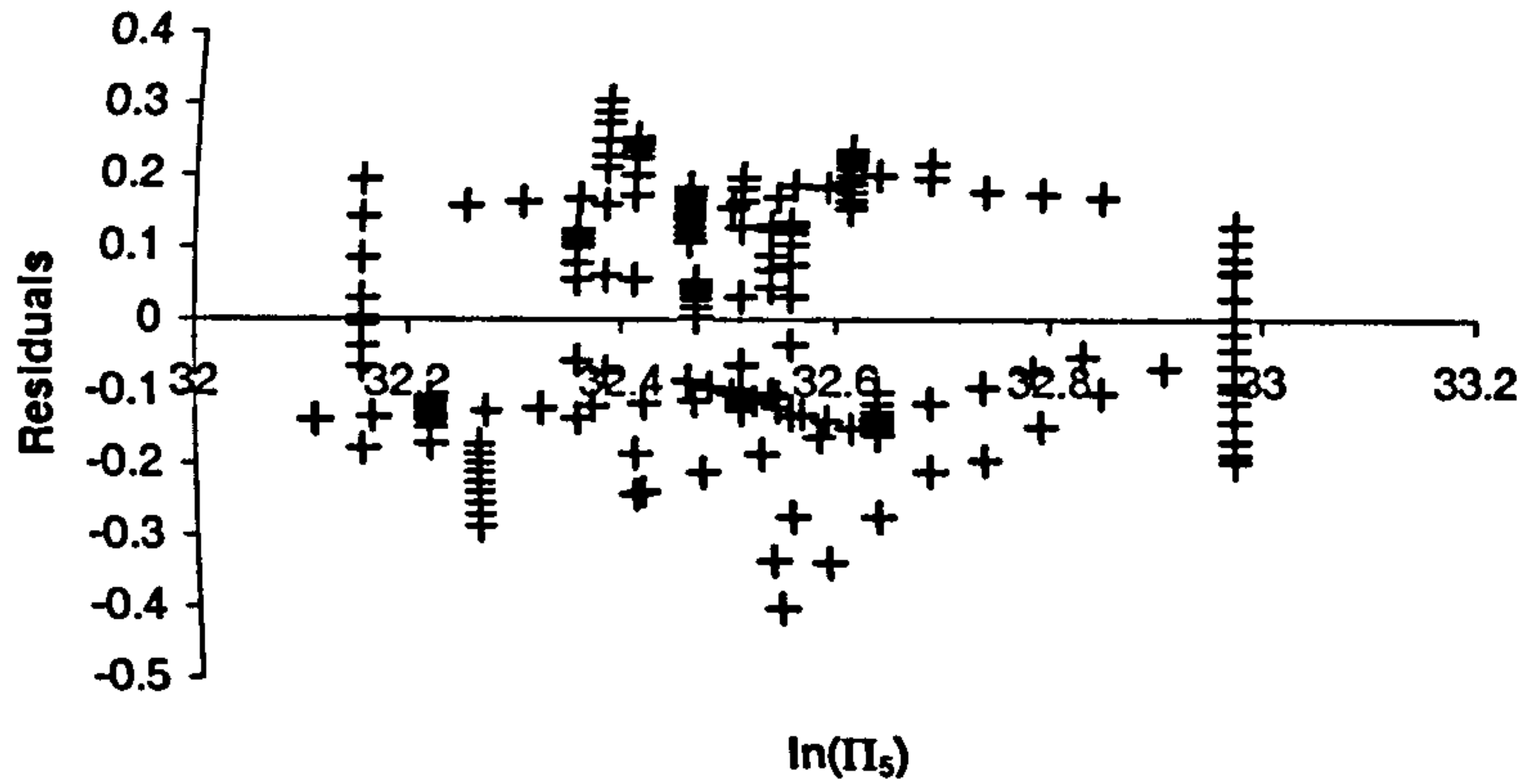

Figure 7.7.6d-e: Residual plots for the parameterisation of b_2

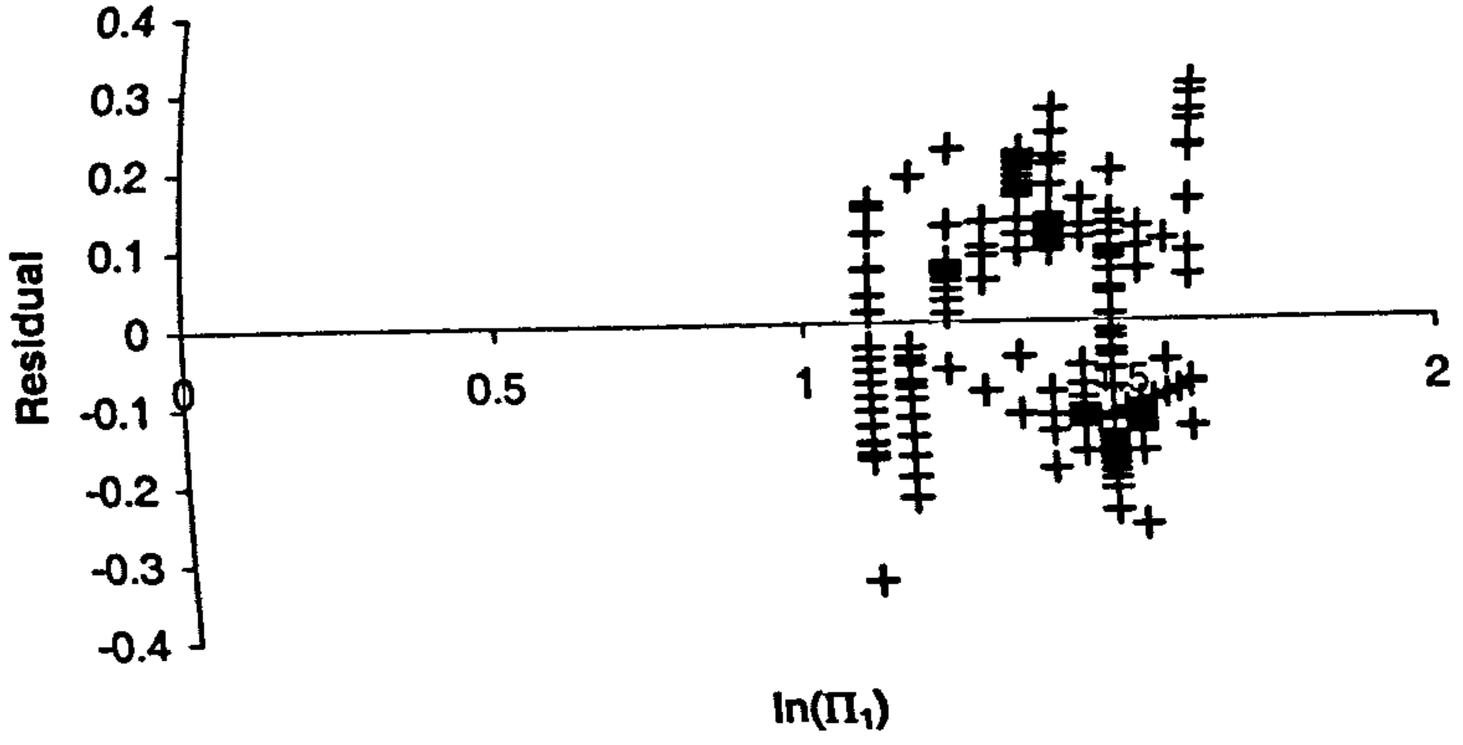

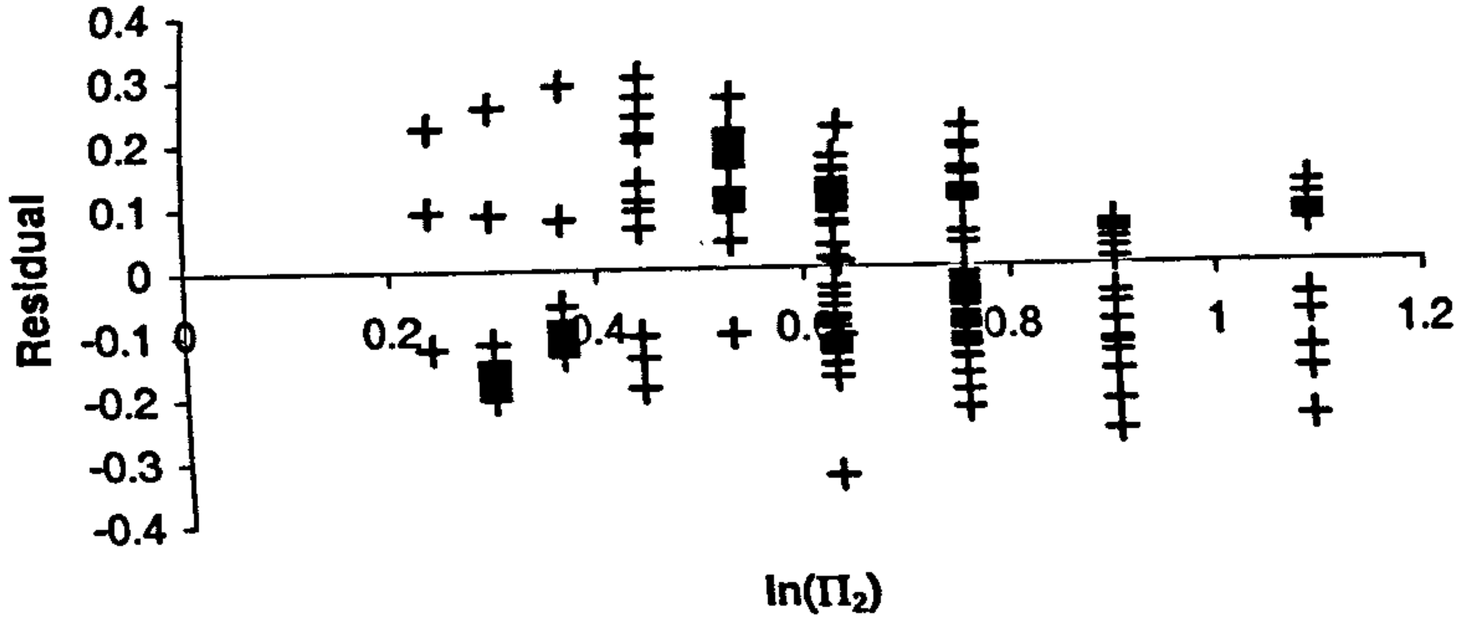

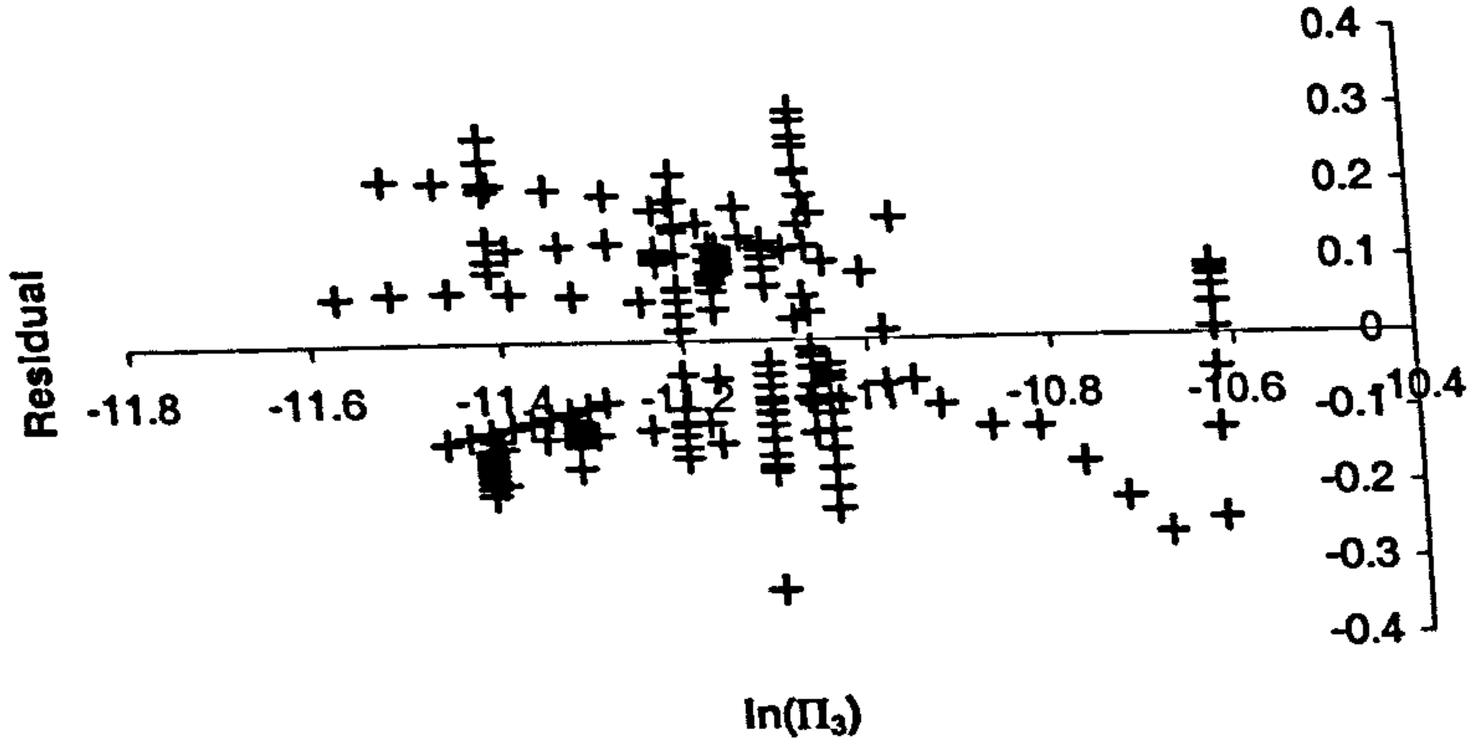

Figure 7.7.7a-c: Residual plots for the parameterisation of b_4

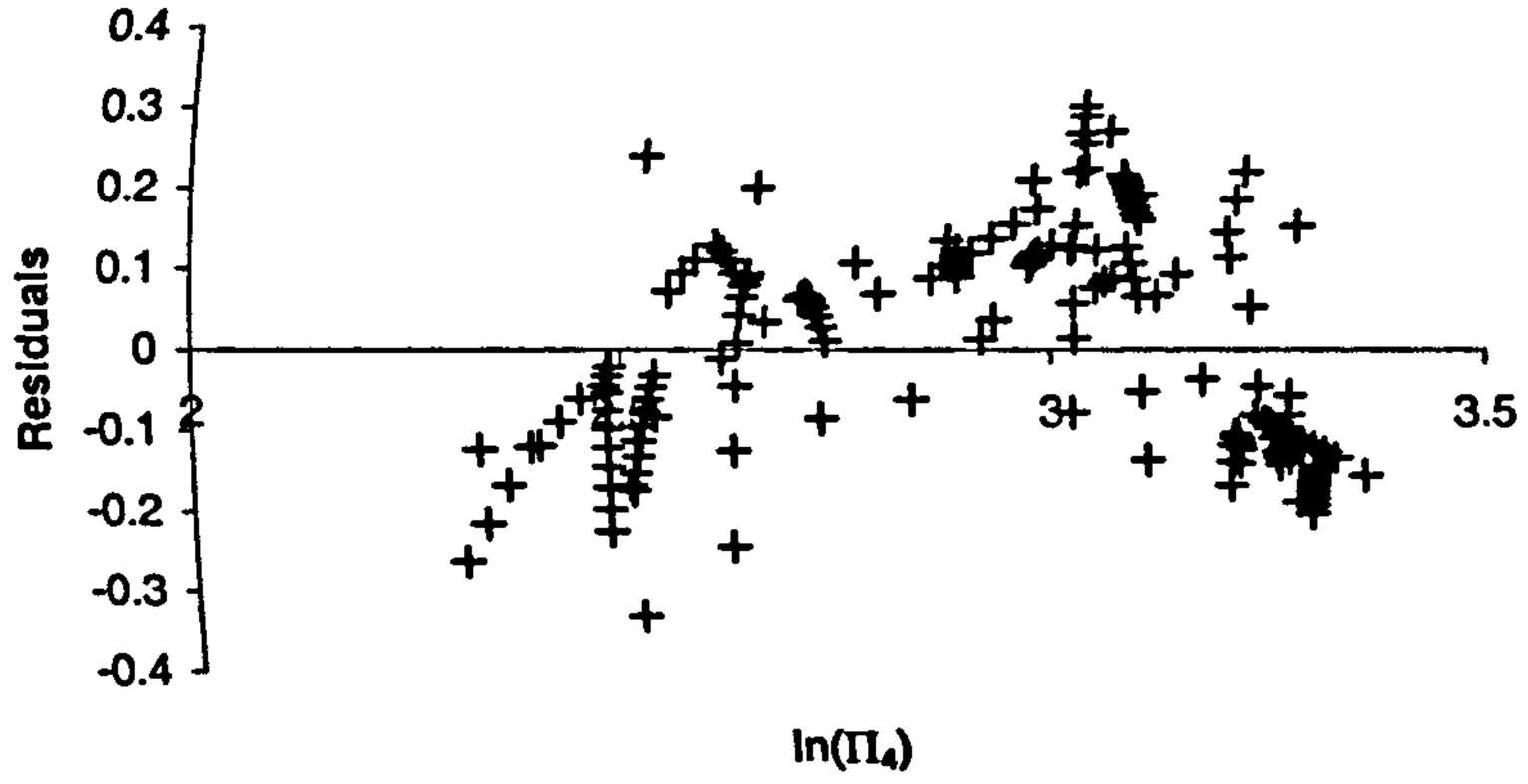

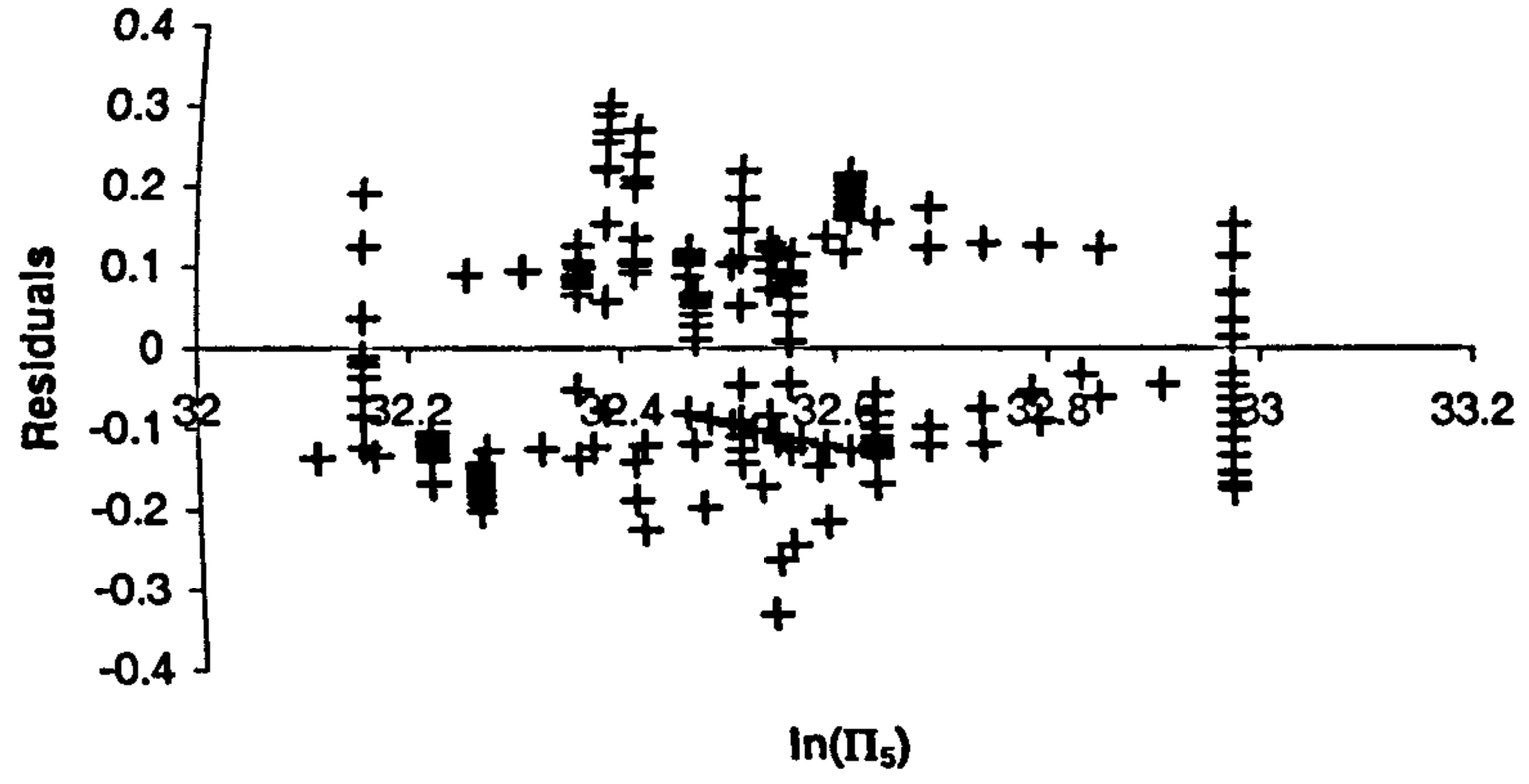

Figure 7.7.7d-e: Residual plots for the parameterisation of b_4

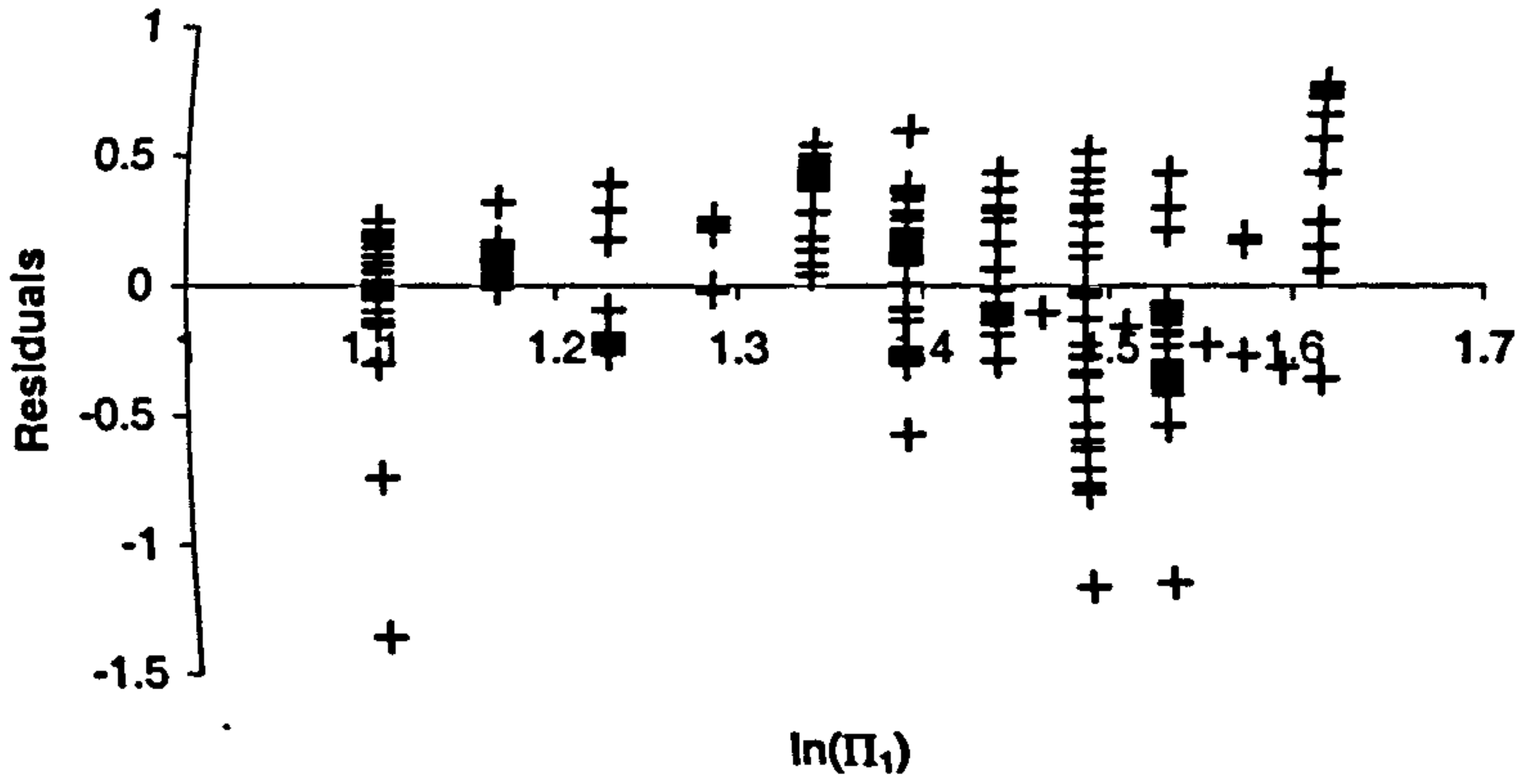

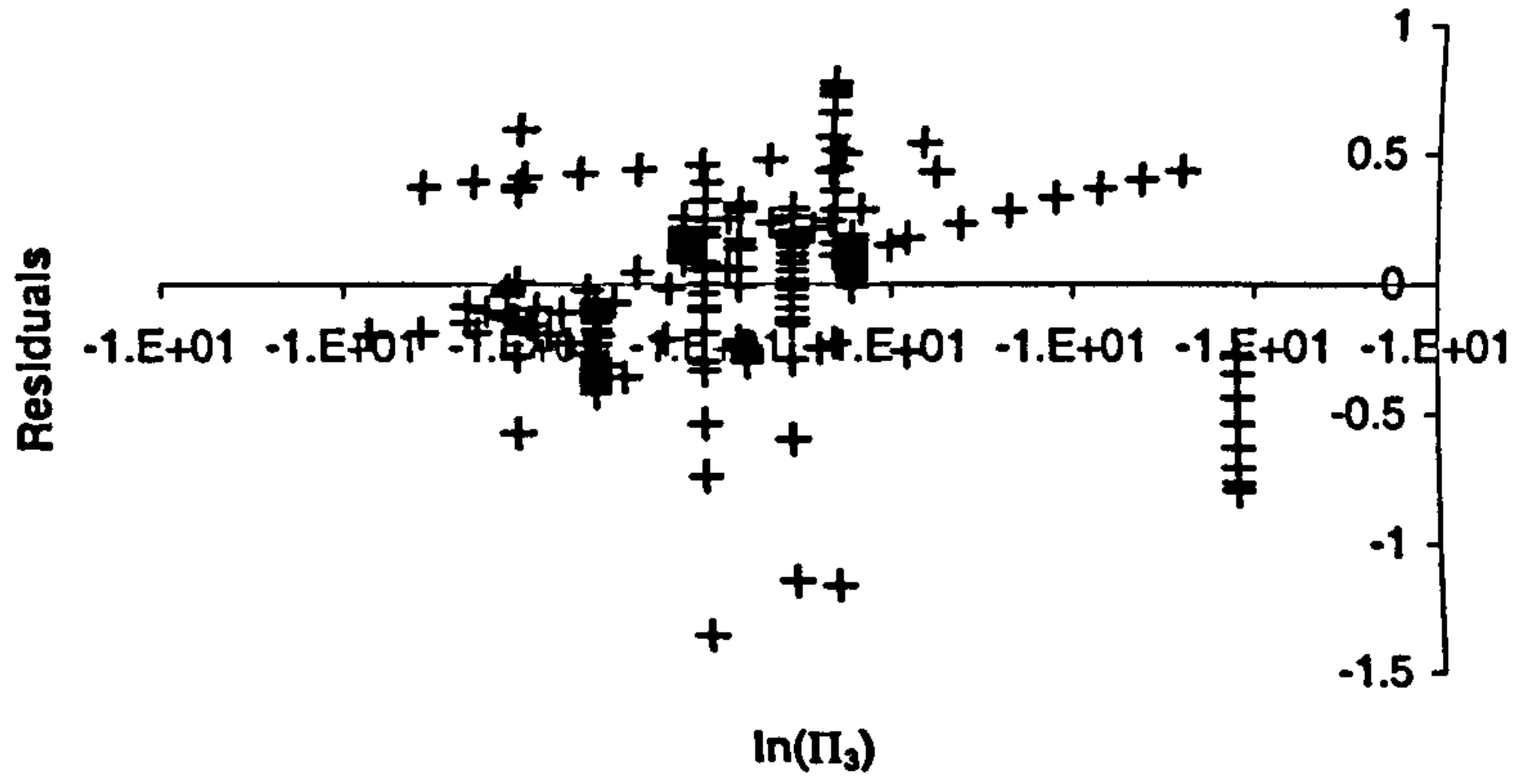

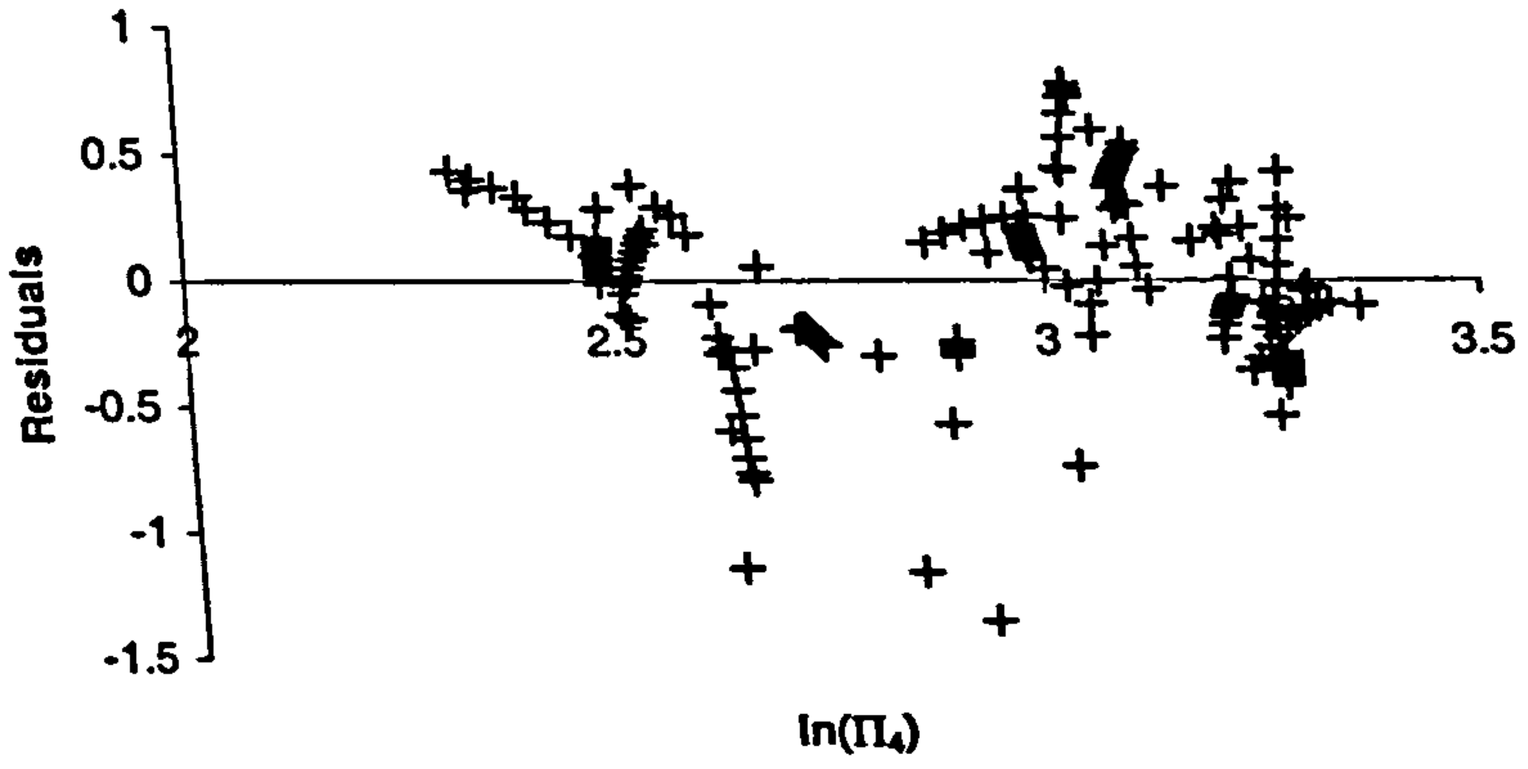

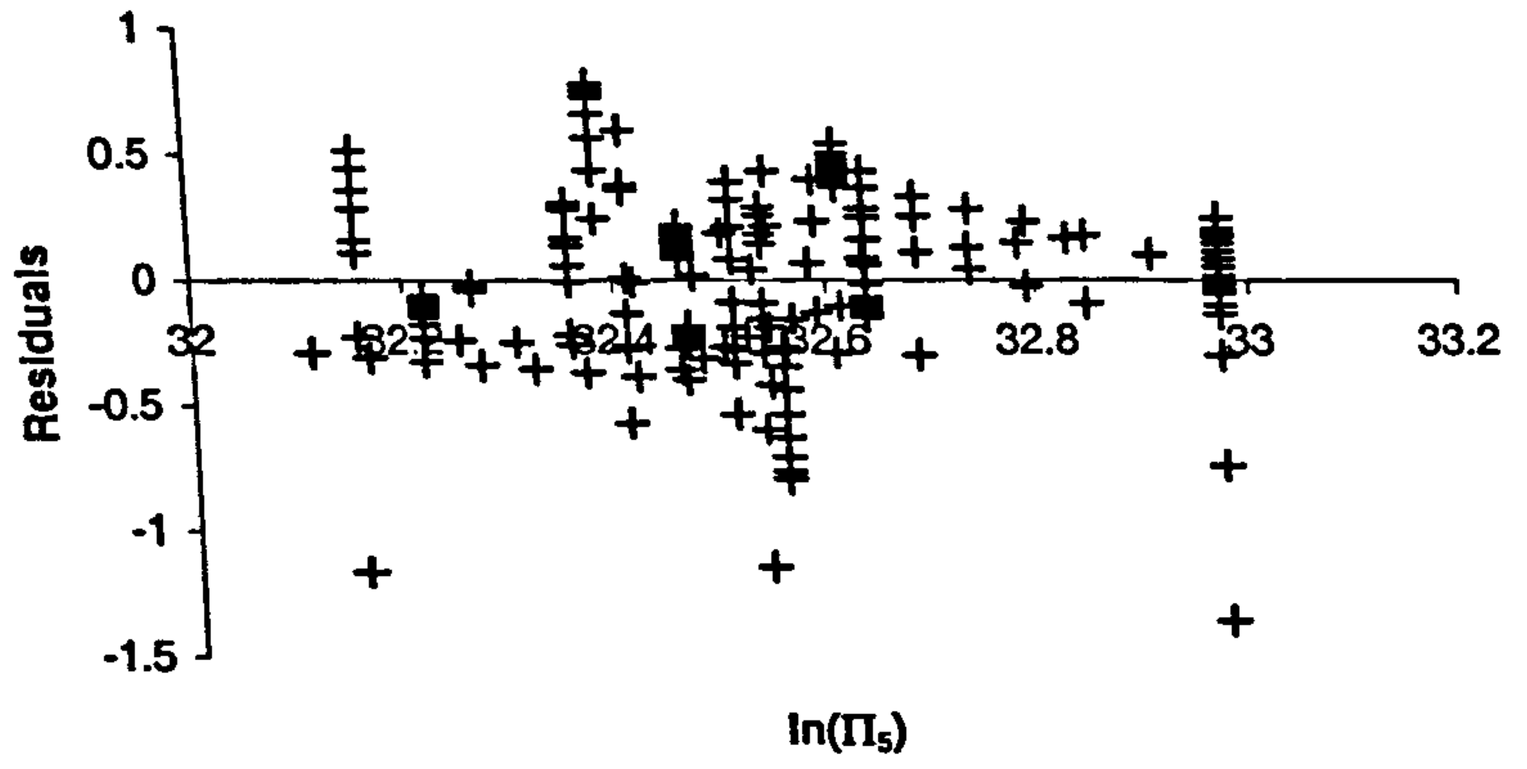

Figure 7.7.8a-d: Residual plots for the parameterisation of b_6

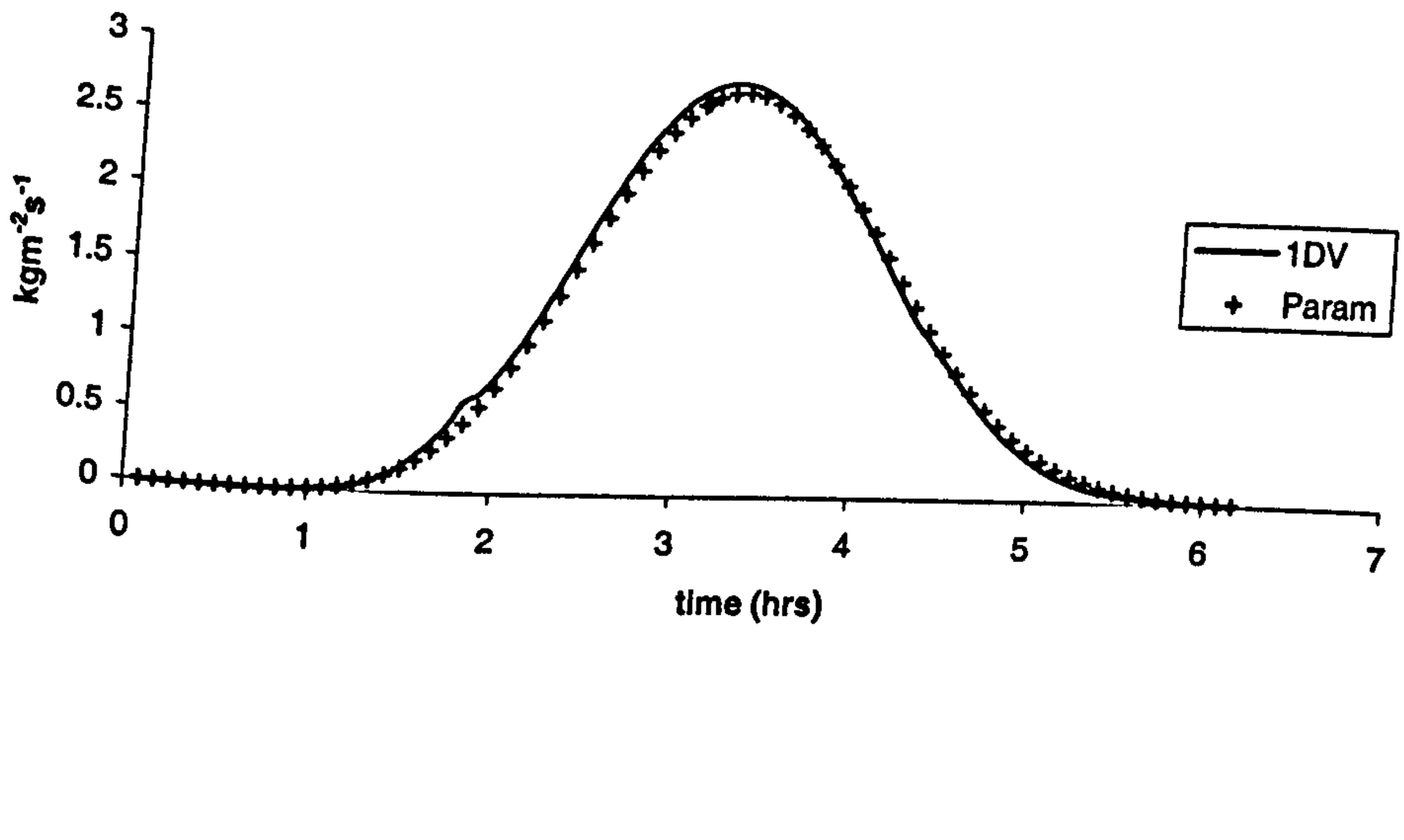

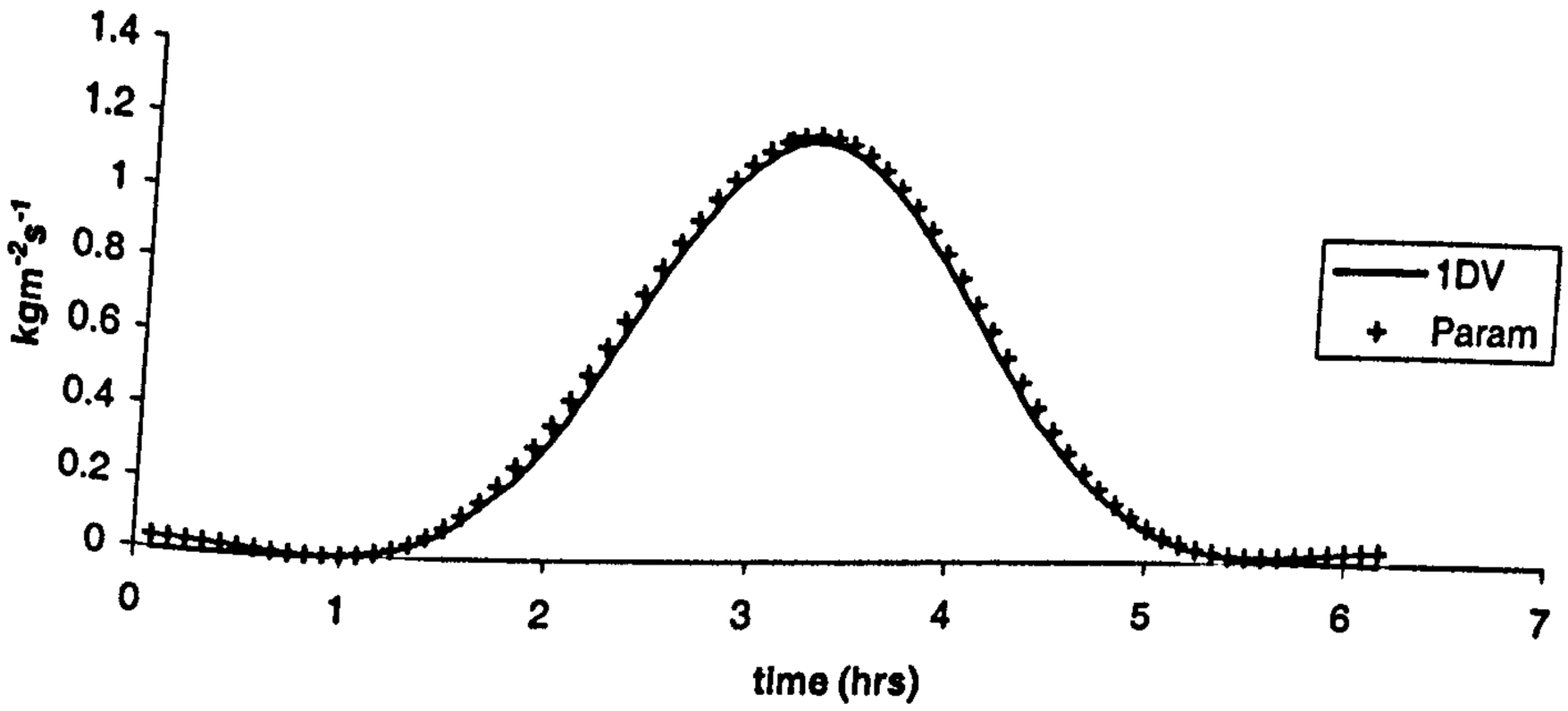

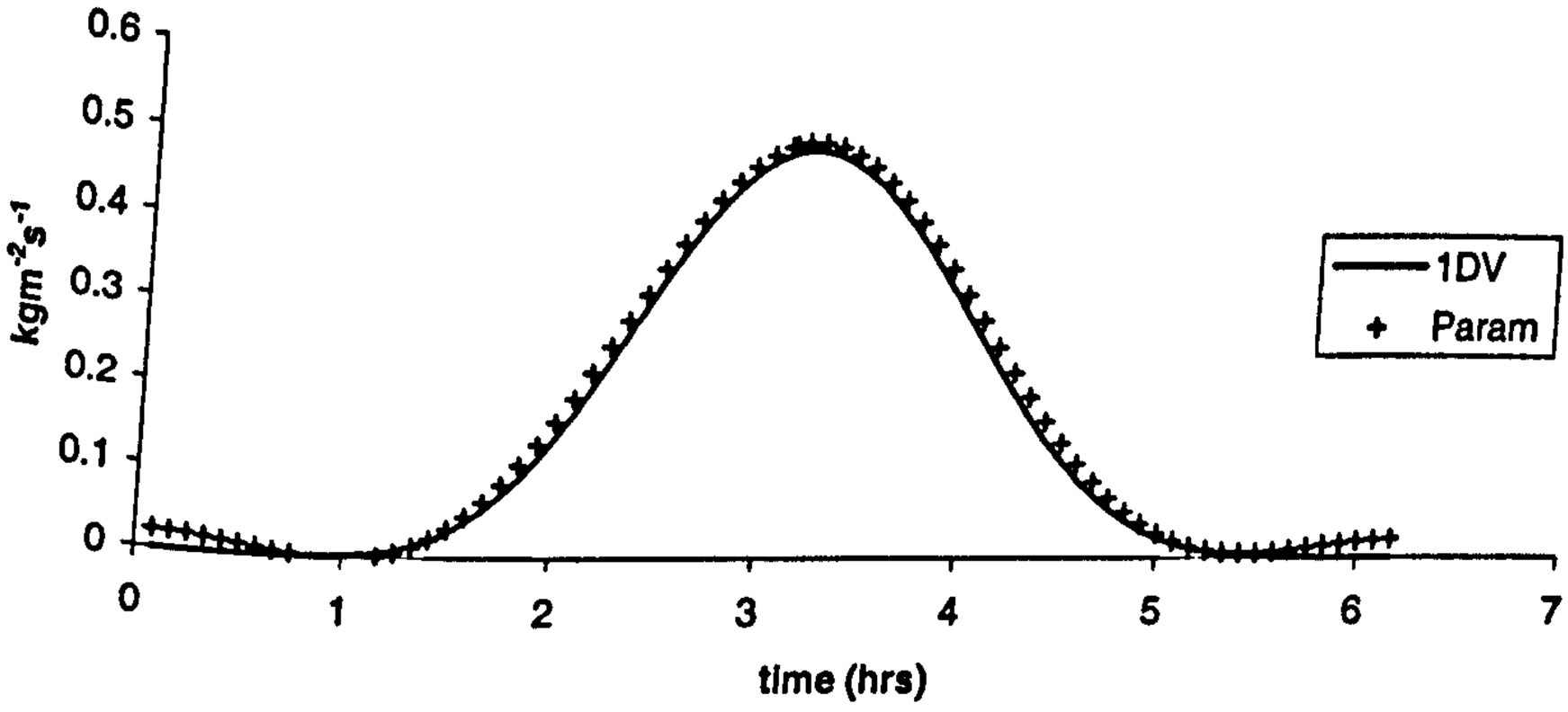

Figure 7.7.9a-c: Comparison of parameterised 1DV model (Param) and conventional 1DV model (1DV)

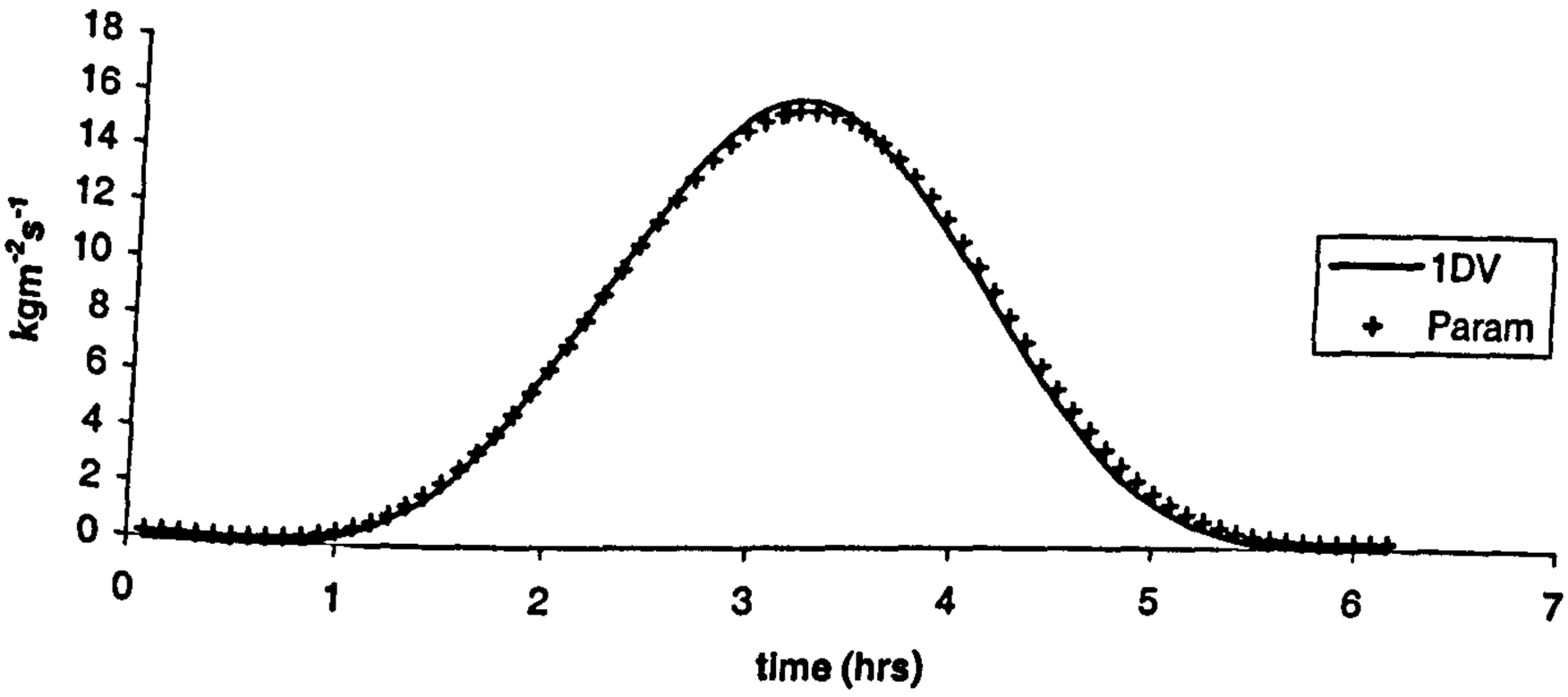

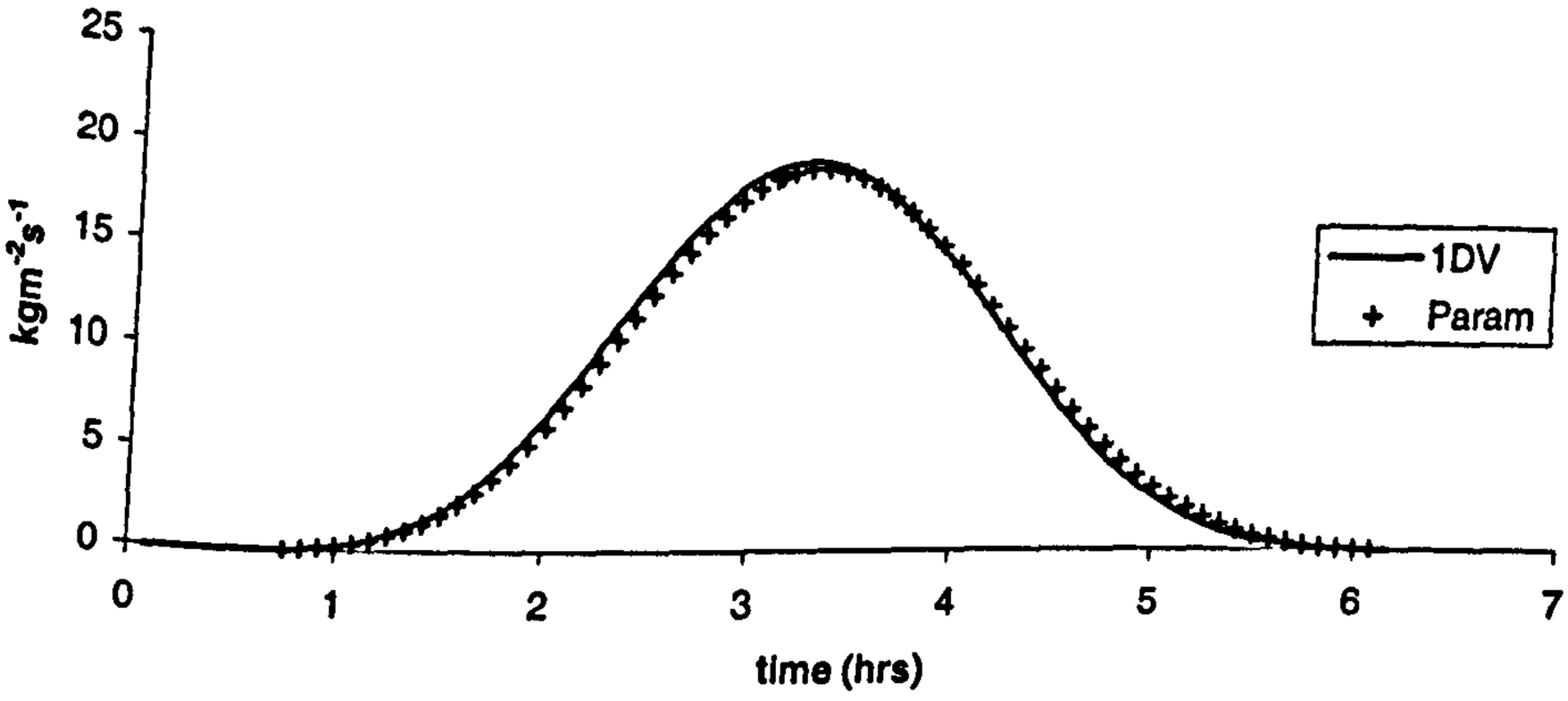

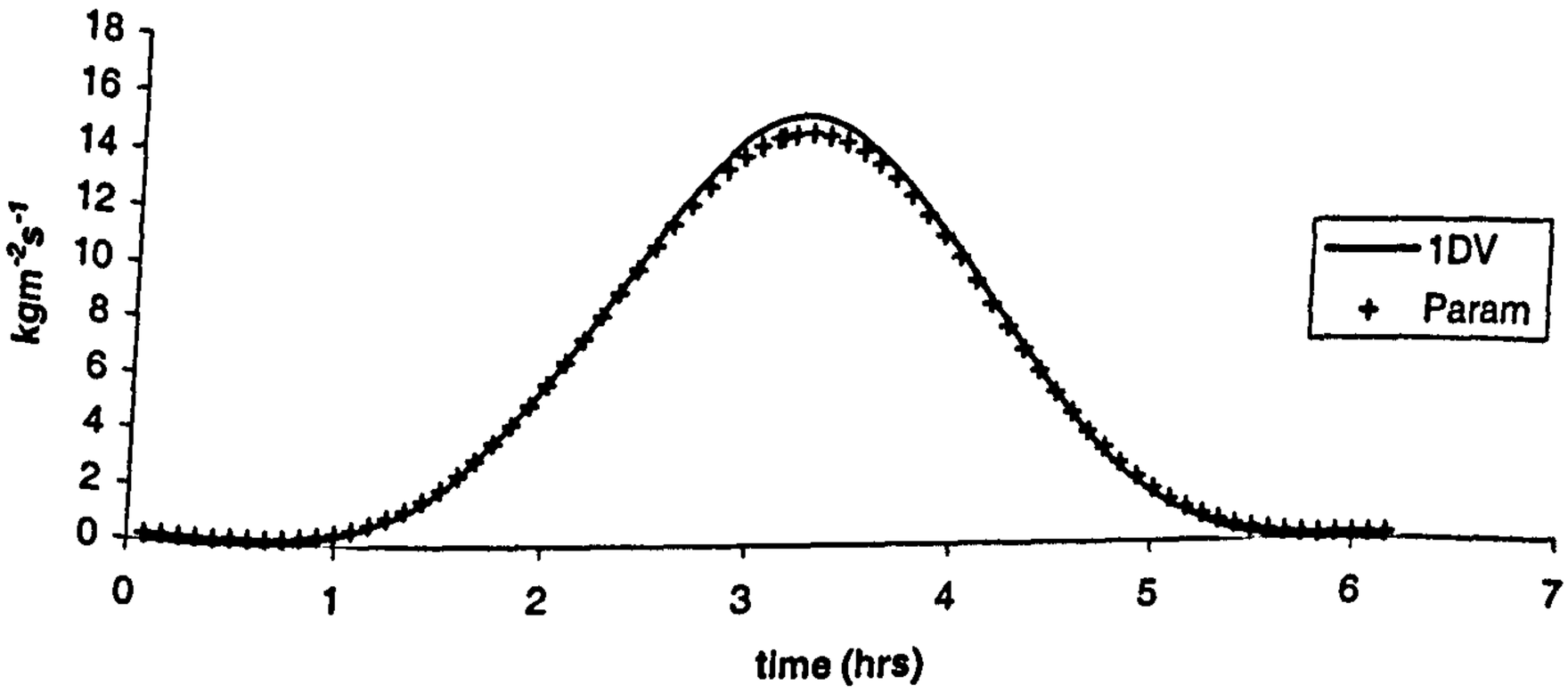

Figure 7.7.9d-f: Comparison of parameterised 1DV model (Param) and conventional 1DV model (1DV)

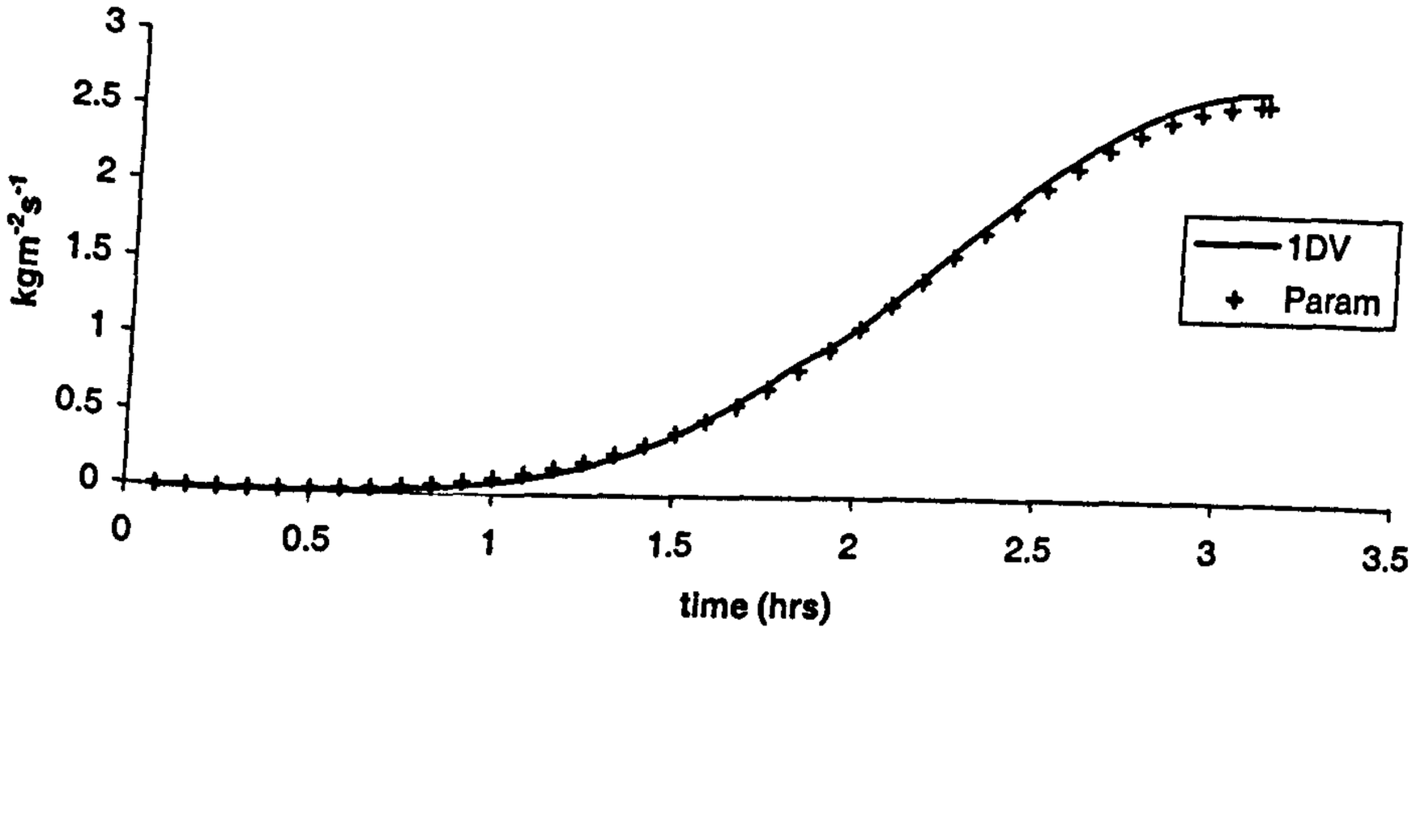

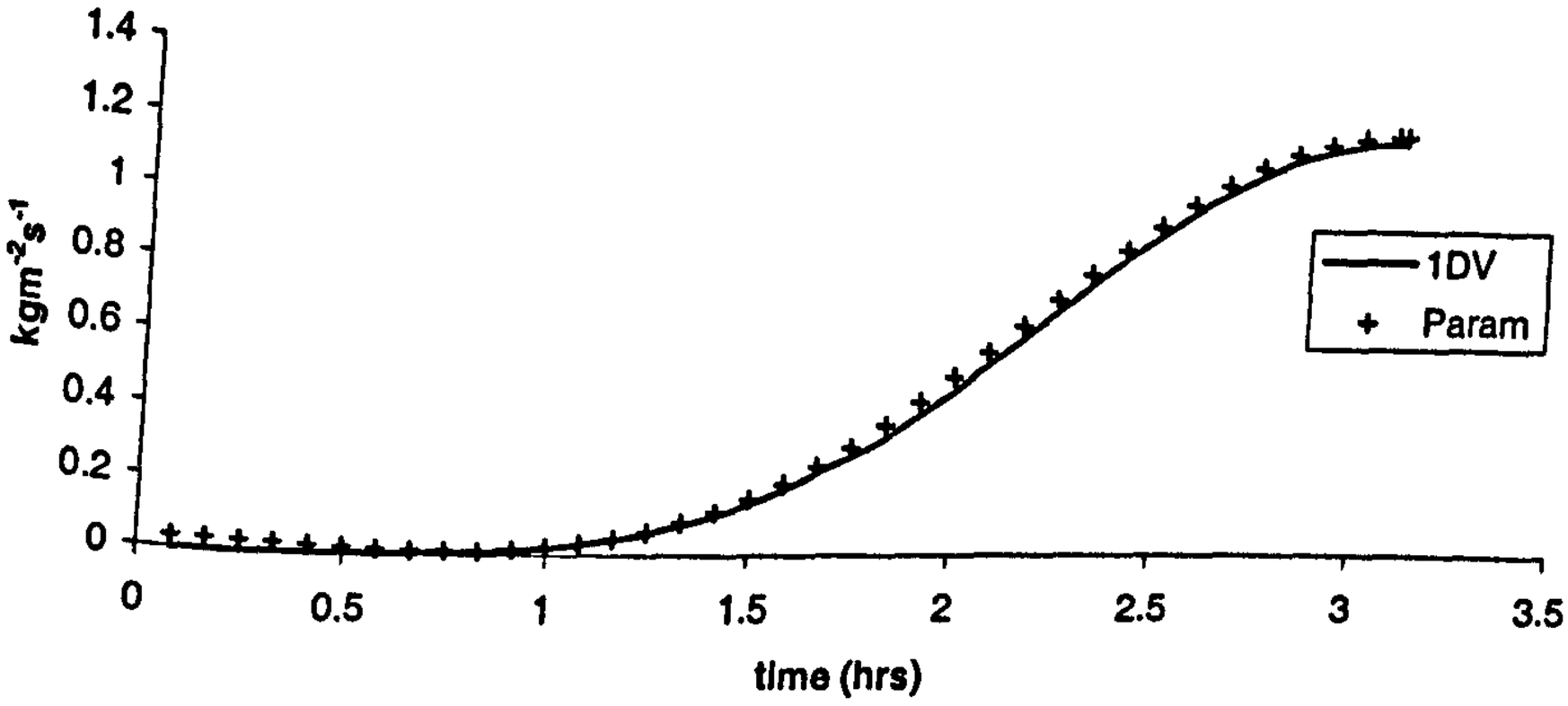

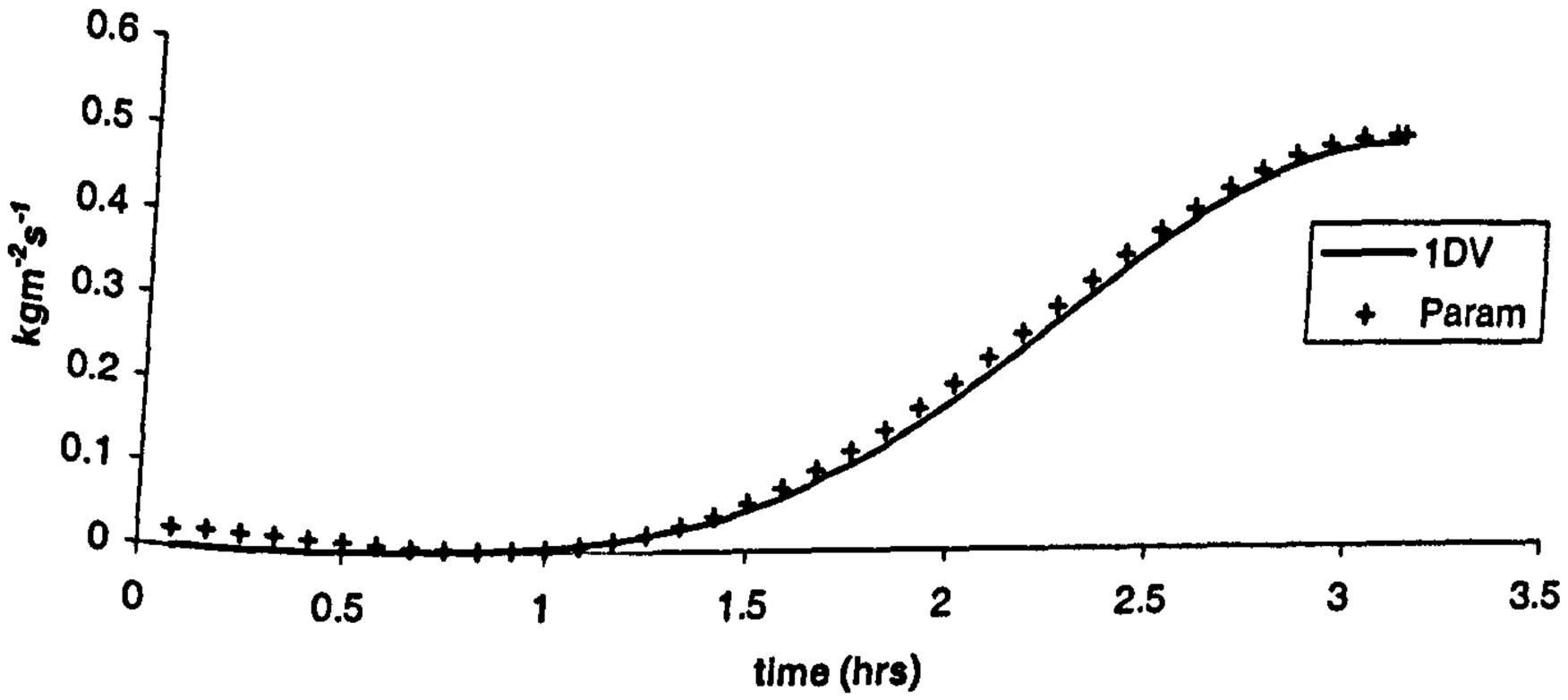

Figure 7.7.10a-c: Comparison of parameterised 1DV model (Param) and conventional 1DV model (1DV)

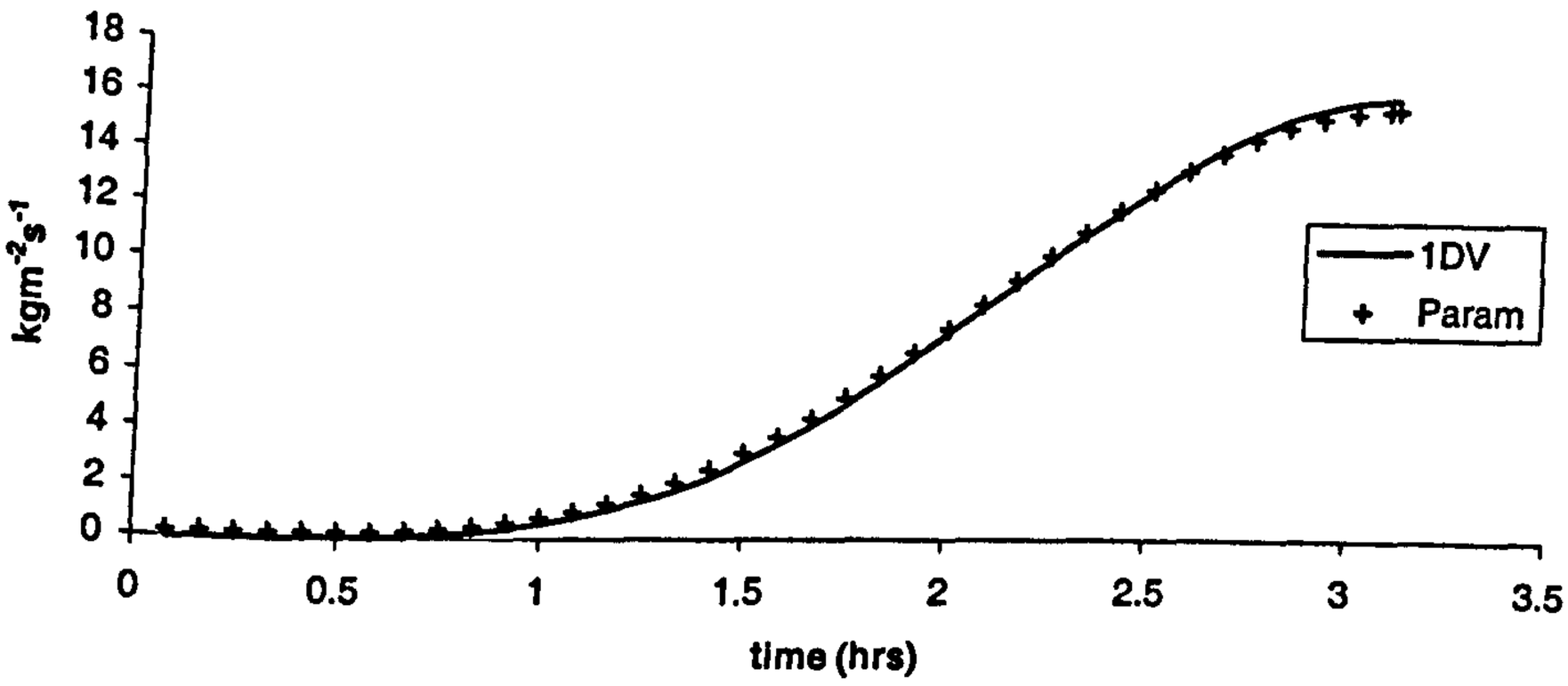

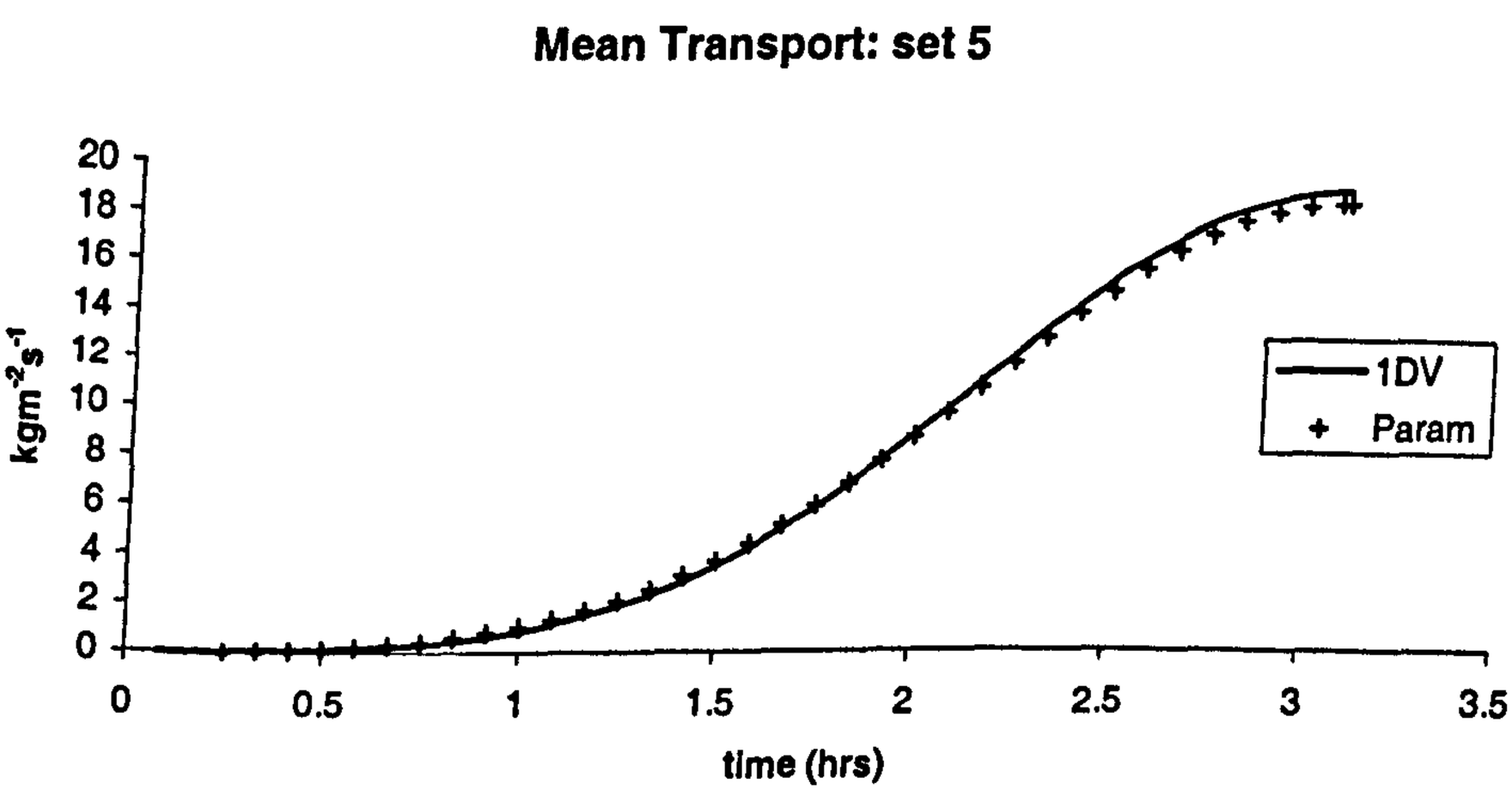

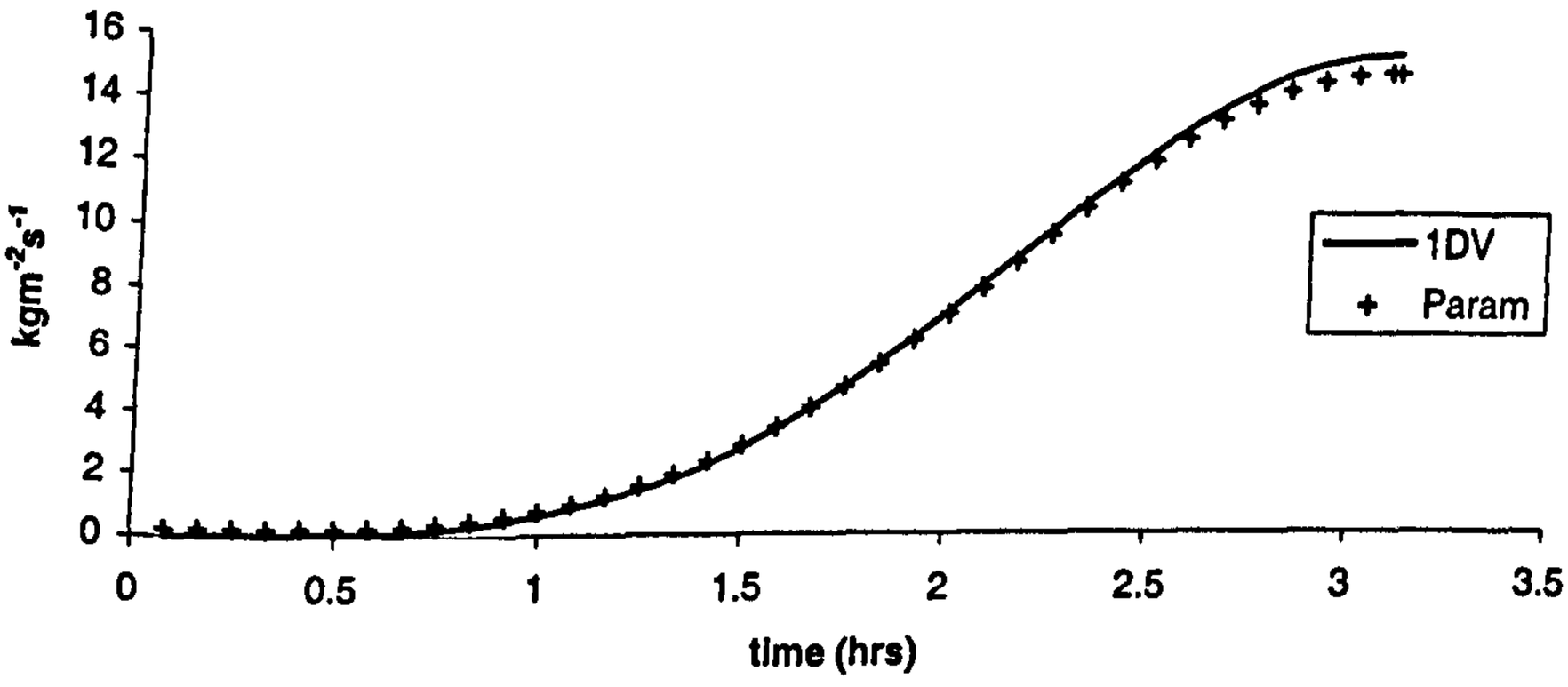

Figure 7.7.10d-f: Comparison of parameterised 1DV model (Param) and conventional 1DV model (1DV)

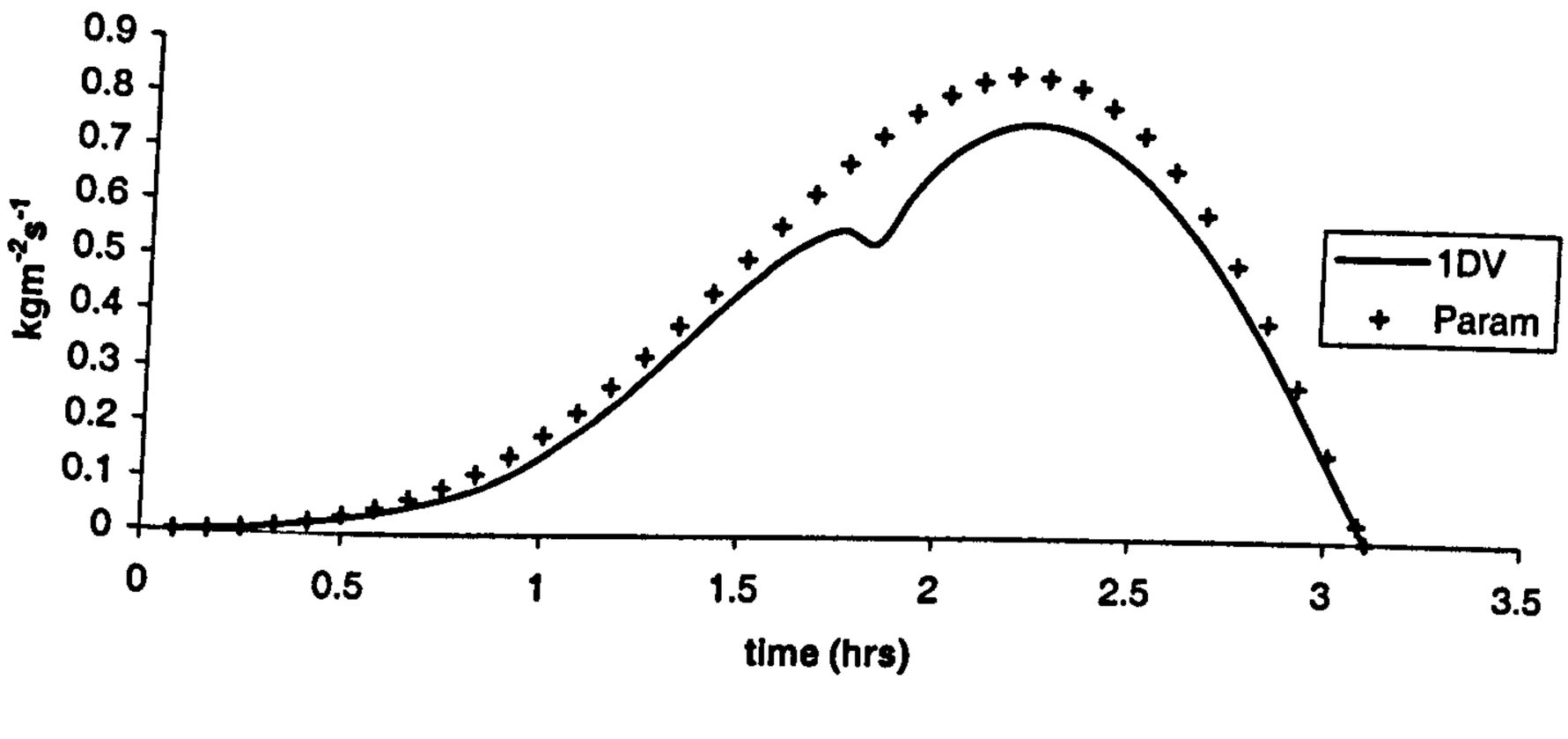

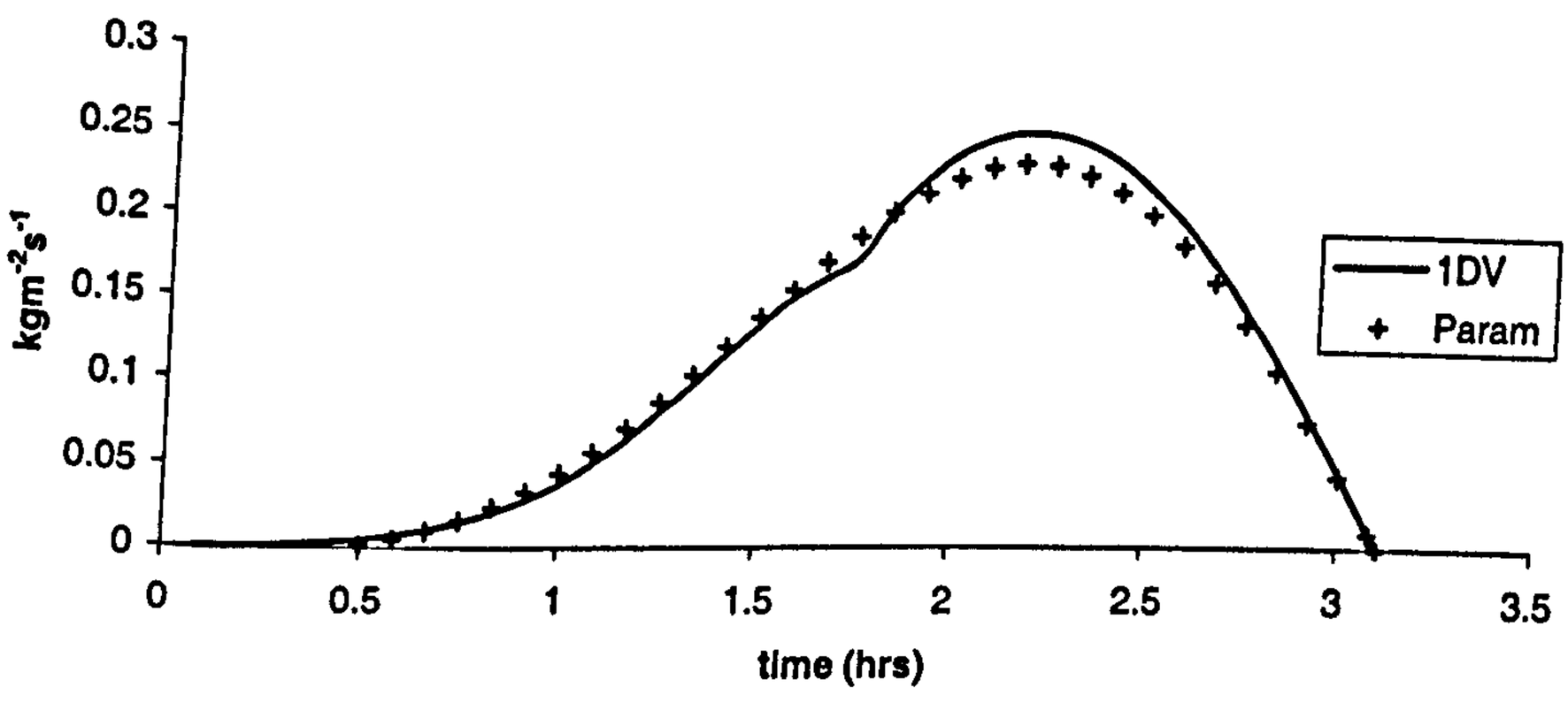

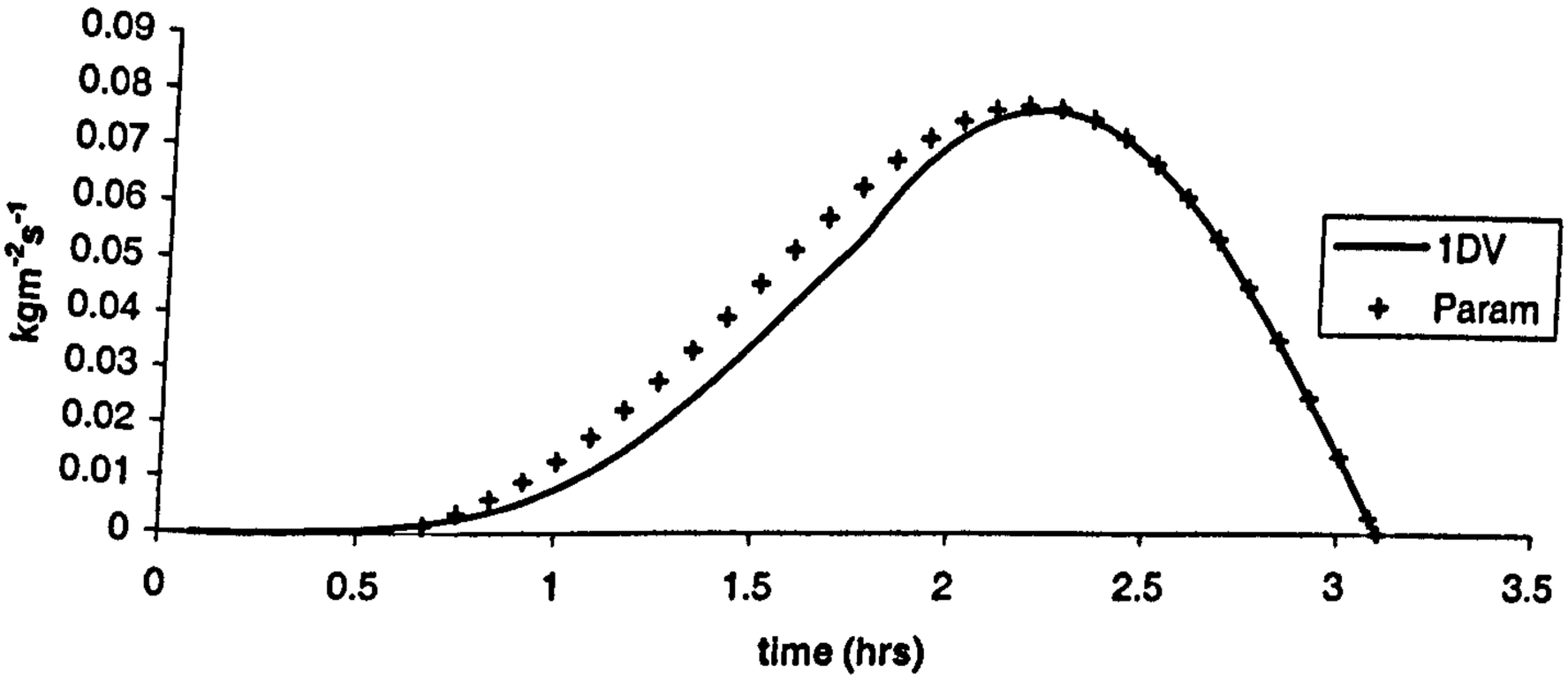

Figure 7.7.11a-c: Comparison of parameterised 1DV model (Param) and conventional 1DV model (1DV)

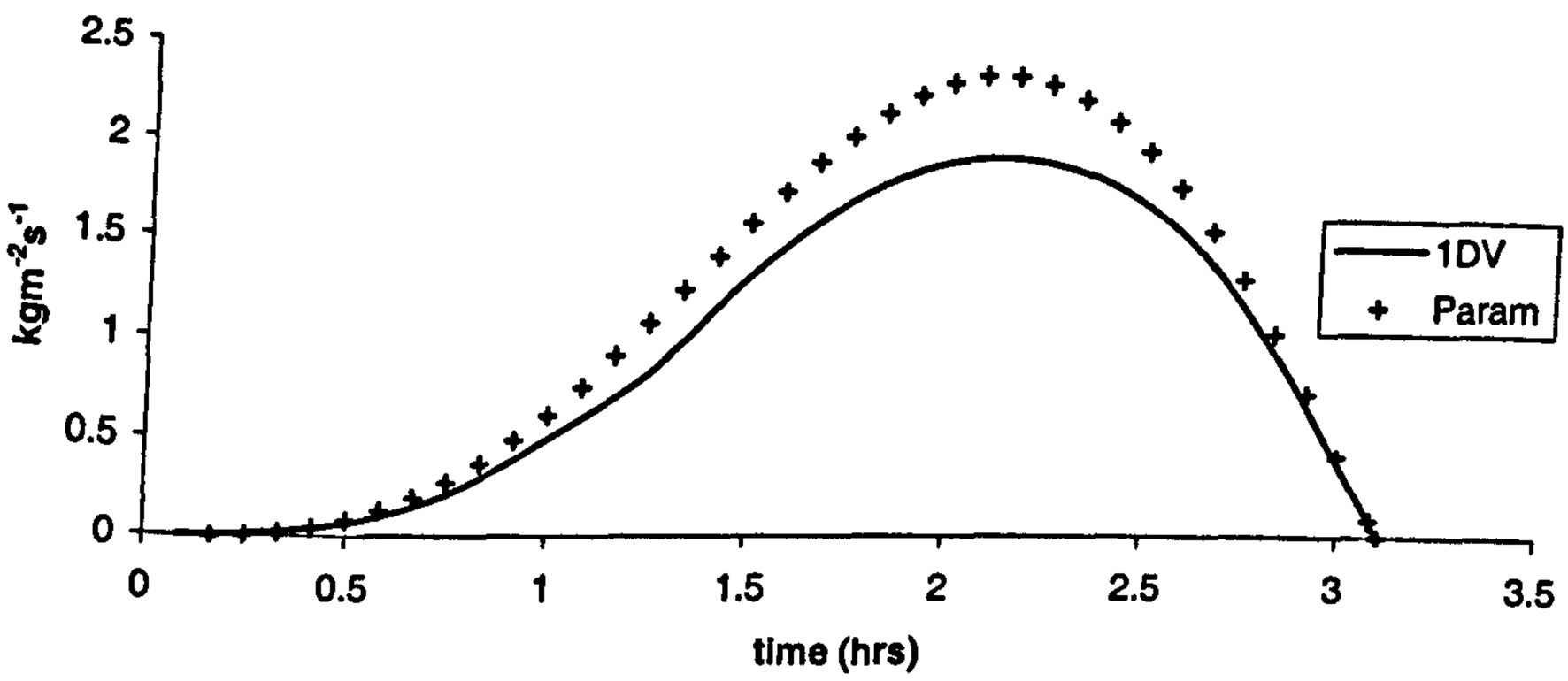

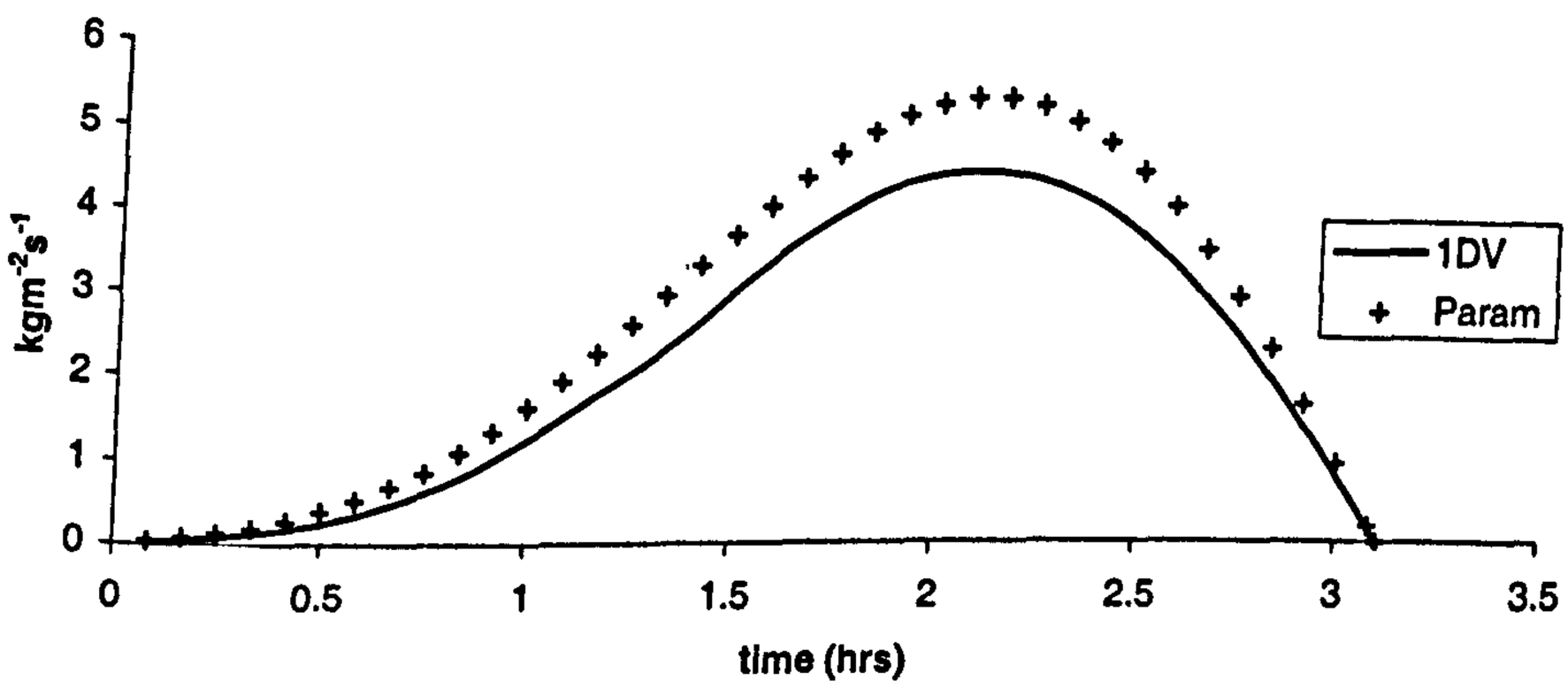

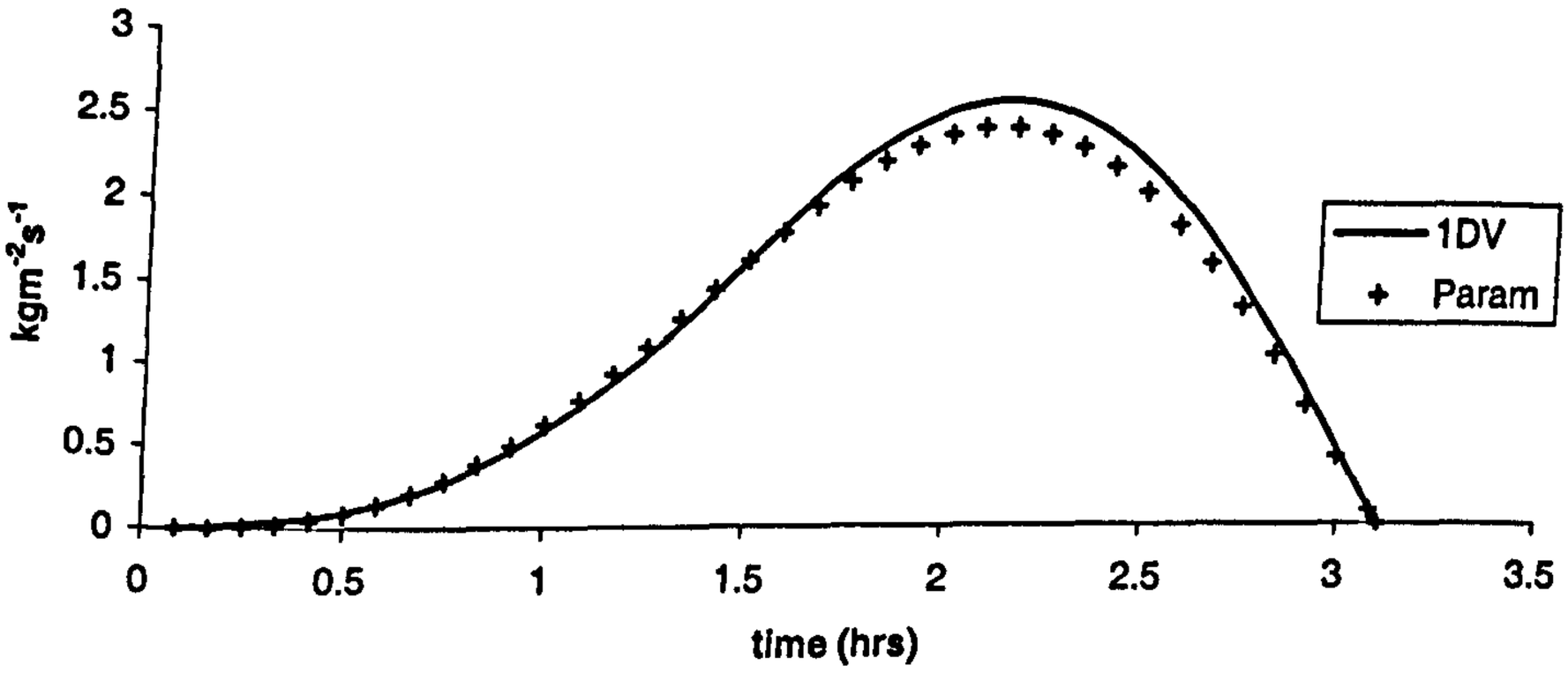

Figure 7.7.11d-f: Comparison of parameterised 1DV model (Param) and conventional 1DV model (1DV)

Chapter 8

Parameterised Corrector Method

8.1 Introduction

As stated in chapter 1, one aim of this thesis is to introduce a parameterised 1DV suspended sediment transport model into the new Corrector method proposed by O'Connor (1999). Having described the new Corrector method in chapter 2 and presented details of how it incorporates a numerical 1DV model in chapter 5, it now remains to show how the parameterised 1DV model is used in the new Corrector method.

Chapter 7 presented a parameterised 1DV model based on a set of ten characteristic parameters that defined the system. However, this model needs to be modified before it can be used in a 2DV system. Essentially, the 2DV system uses a different definition of the reference level for sediment calculations. This means that the reference level becomes an external factor defining the system and as such must be added to the list of characteristic parameters. Section 8.2 gives details of the new characteristic set and the extra non-dimensional parameter group that it creates.

Section 8.3 then describes the regression analysis used to fit the modified 1DV parameterisation to given data sets.

The new Corrector method also requires the parameterisation of both the depth-mean concentration and the transport due to fluctuations from the depth-mean values. Section 8.5 describes the methods used to parameterise these terms.

Finally, the new parameterised Corrector method is tested against eight independent data sets in order to assess the accuracy and computational speed of the new approach.

8.2 Modified 1DV Parameterisation

Although Chapter 7 described a parameterised model that can be used in place of a numerical 1DV model, it requires modification before it can be applied to a 2DV system.

8.2.1 Characteristic Parameters

The parameterisation described in chapter 7 assumes that the bed forms, and hence reference level, are calculated implicitly within the 1DV model. However, when considering a 2DV system, this is not the case. The reference level is defined as an average over the longitudinal scale (section 5.5.4) so that simplifications to the new Corrector method are justified, see section 2.4.2. It therefore differs from that predicted by the 1DV model. Effectively, the reference level is now an external parameter and as such must be added to the list of characteristic parameters defining the system. The set of characteristic parameters now becomes:-

$$\rho, \nu, \rho_s, d_{50}, \sigma, h_m, \gamma_s, u_{*m}, r, up, a \tag{8.2.1}$$

where a is the given reference level.

8.2.2 Parameter Groups

Since there are now eleven characteristic parameters, there must be eight non-dimensional groups produced by Buckingham's Pi Theorem.

Using the same set of basic quantities as used in chapter 7, i.e. ρ, γ_s and d_{50}, and following the same substitutions and manipulations, the same groups as

before are obtained with the addition of an extra group reflecting the influence of the reference level; i.e.:-

$$\Pi_1 = d_{50}\left(\frac{(s-1)g}{\nu^2}\right)^{1/3} \tag{7.5.5}$$

$$\Pi_2 = \frac{1}{\ln\sigma} \tag{7.5.6}$$

$$\Pi_3 = \frac{d_{50}}{h_m} \tag{7.5.7}$$

$$\Pi_4 = \frac{\bar{u}_m - \bar{u}_c}{\sqrt{d_{50}g(s-1)}} \tag{7.5.8}$$

$$\Pi_5 = \frac{up^2\gamma_s}{\rho d_{50}} \tag{7.5.9}$$

$$\Pi_6 = \frac{r}{d_{50}} \tag{7.5.10}$$

And now,

$$\Pi_7 = \frac{a}{d_{50}} \tag{8.2.2}$$

Note that again the density ratio is assumed constant and hence is omitted from further analysis thus leaving only seven groups.

8.2.3 Functional Form

In order to investigate the influence of the reference level, it is necessary to add some new data sets to those used in chapter 7. The twenty-seven new data sets are shown in table 8.2.1. The new sets are based on three sets of tidal conditions where the reference level has been fixed externally. The new reference levels vary as much as ten times that predicted by the 1DV model. This is used to reproduce conditions where there is change in the median grain diameter in the

longitudinal direction. This can produce different bed form dimensions, and hence reference level, for the same hydrodynamic conditions.

The effect of the reference level on each of the quantities to be parameterised is shown in figure 8.2.1. It can clearly be seen that group seven is influential for all quantities considered, indicated by the large variation in the values on the ordinate. It can also be seen that an exponential form similar to that seen in the previous chapter exists for the non-dimensional forms of the suspended transport at maximum velocity and the first two mean Fourier coefficients. Figure 8.2.1 also suggests a power law relationship for the remaining Fourier Coefficients. The functional form for the parameterisations are therefore given by:-

$$\frac{PT_m}{T_{me}} = 1 - \exp\left\{\alpha \Pi_1^{\beta_1} \Pi_2^{\beta_2} \Pi_3^{\beta_3} \Pi_7^{\beta_7}\right\} \tag{8.2.3}$$

$$\frac{Pa_2}{a_{2e}} = 1 - \exp\left\{\alpha \Pi_1^{\beta_1} \Pi_2^{\beta_2} \Pi_3^{\beta_3} \Pi_7^{\beta_7}\right\} \tag{8.2.4}$$

$$\frac{Pa_4}{a_{4e}} = 1 - \exp\left\{\alpha \Pi_1^{\beta_1} \Pi_2^{\beta_2} \Pi_3^{\beta_3} \Pi_7^{\beta_7}\right\} \tag{8.2.5}$$

$$\frac{-Pa_6}{\sqrt{\rho \gamma_s d_{50}}} = \alpha \Pi_1^{\beta_1} \Pi_3^{\beta_3} \Pi_4^{\beta_4} \Pi_7^{\beta_7} \tag{8.2.6}$$

$$\frac{-Pb_2}{\sqrt{\rho \gamma_s d_{50}}} = \alpha \Pi_1^{\beta_1} \Pi_2^{\beta_2} \Pi_3^{\beta_3} \Pi_4^{\beta_4} \Pi_5^{\beta_5} \Pi_7^{\beta_7} \tag{8.2.7}$$

$$\frac{Pb_4}{\sqrt{\rho \gamma_s d_{50}}} = \alpha \Pi_1^{\beta_1} \Pi_2^{\beta_2} \Pi_3^{\beta_3} \Pi_4^{\beta_4} \Pi_5^{\beta_5} \Pi_7^{\beta_7} \tag{8.2.8}$$

$$\frac{-Pb_6}{\sqrt{\rho \gamma_s d_{50}}} = \alpha \Pi_1^{\beta_1} \Pi_3^{\beta_3} \Pi_4^{\beta_4} \Pi_5^{\beta_5} \Pi_7^{\beta_7} \tag{8.2.9}$$

8.3 Regression Analysis

8.3.1 Data

As in chapter 7, regression analysis using a least squares estimator is applied to the one hundred and eighty-nine data sets given by table 7.6.1a and the new data

given in table 8.2.1. The values for the parameterisation quantities for the new data sets are given in table 8.3.1, equilibrium values in table 8.3.2 and non-dimensional group values in table 8.3.3. The values for the reference level and reference group, Π_7, for the data sets given in table 7.6.1a are given in table 8.3.4.

8.3.2 Analysis Variables

Again, the same analysis variables as used in chapter 7 are employed here.

(i). Percentage error:-

$$\%\,error = 100 \times \left| \frac{x - px}{x} \right|$$

where px is the parameterisation of the quantity x.

(ii). The absolute difference between the actual value of variable x and its parameterised value (units are those of transport):-

$$diff = |x - px|$$

(iii). r^2 value. A good correlation is shown by an r^2 value approaching unity.

(iv). The F-obs value. This should be significantly greater than the F_{cr} value if the fit of the proposed model is not due to chance.

The degrees of freedom of the F-distribution are given by:-

$$\nu_1 = k$$

$$\nu_2 = n - (k+1)$$

where,

k = the number of independent variables

n = the number of data sets used (216)

The value of F_{cr} for each of the parameterisations is therefore:-

$F_{cr} = 2.45$ for T_m, a_2, a_4 and a_6

$F_{cr} = 2.18$ for b_2 and b_4

$F_{cr} = 2.29$ for b_6

Again it should be noted that these values are taken for $\nu_2 = 120$ thus giving a larger value for F_{cr} than required.

8.3.3 Results

During the regression analysis, it became evident that a better parameterisation for b_6 could be obtained by excluding Π_5. Equation (8.2.9) therefore becomes:-

$$\frac{-Pb_6}{\sqrt{\rho\gamma_s d_{50}}} = \alpha\Pi_1^{\beta_1}\Pi_3^{\beta_3}\Pi_4^{\beta_4}\Pi_7^{\beta_7} \qquad (8.3.1)$$

It should be noted that $F_{cr} = 2.45$ for this version of the parameterisation of b_6.

The results of the regression analysis are given in table 8.3.6. Table 8.3.6a gives the values for all of the α's and β's used in the parameterisations whilst table 8.3.6b returns values for all of the analysis variables. The parameterisations are shown graphically in figure 8.3.1 where the bold line denotes a perfect fit.

It can be seen that the proposed parameterisation of the transport at maximum velocity shows good agreement with the actual values from the 1DV model. The high r^2 and F-obs values signify that the parameterisation is a good representation of the actual relationship. Both error variables return very small values, which

shows that the parameterisation is accurate. This is also supported by the difference variables; the maximum difference is only 0.030199 $kgm^{-2}s^{-1}$.

Results for the parameterisation of a_2 are very similar to those returned for T_m. Again, high values for both r^2 and F-obs imply that the functional form is valid. Low values for the error and difference variables show that the parameterisation is also accurate. The mean percentage error for all data sets is only 1.171%.

The parameterisation for a_4 also appears to be very good with errors of the same order as those obtained for the parameterisation of a_2.

Some scatter for the parameterisation for a_6 can be seen in figure 8.3.1. This is also evident in the analysis variables. The r^2 value has dropped to 0.832, which, combined with a low F-obs value, would seem to imply that the functional form used in the parameterisation may not be entirely adequate. However, the maximum difference in actual transport terms is only 0.002308 $kgm^{-2}s^{-1}$, which would seem to suggest that the error is insignificant in the overall transport calculation. The large values returned by the analysis variables are mainly due to set 175 where the contribution of a_6 can be seen to be negligible even though the error here is 1450.4%. (Removing this set would bring the maximum error down to a value of 211.8% and the average error to 24.63%.)

The parameterisation of the first lag coefficient, b_2, also returns favourable results. Again, the percentage error terms are low. The maximum difference, in terms of actual transport, is only 0.006417 $kgm^{-2}s^{-1}$.

Similar values are returned for the parameterisation of b_4, suggesting that the parameterisation is both valid and accurate.

The parameterisation for b_6 would appear to fall short of fully describing the actual relationship since the r^2 value is now only 0.866. This is supported by a low F-obs value; however, this is still greater than the critical value. The

maximum percentage error of 348.432% is somewhat misleading. The values for b_6 are smaller in magnitude than all other values so a large % error is actually only a small difference in transport terms, shown by the low value for the maximum difference in actual transport terms, 0.001154 $kgm^{-2}s^{-1}$.

Figure 8.3.2 shows the plot of residuals for Π_7. Again, the absence of any patterns supports the regression methods used here.

The proposed parameterisations are also tested against the same seven independent sets as used in chapter 7, see table 7.6.1b. The results are shown in table 8.3.7.

The results are, on the whole, only slightly worse than the regression results. The increase in mean values may be due to the fact that only 7 sets were used. An individual set is therefore more influential. The maximum variables provide a better test of the regression analysis. These are, in the most part, of the same order as those obtained by the regression analysis.

It is therefore concluded that the parameterisations suggested by equations (8.2.3) - (8.2.8) and (8.3.1), together with the values from table 8.3.6a, should be substituted into equation (7.7.3) to provide a model that can now be used in place of the numerical 1DV model in the new Corrector method; i.e.:-

$$PT_s(t) \approx PT_m + \sum_{n=1}^{3} Pa_{2n}\left\{\cos(2n\omega t) + (-1)^{n-1}\right\} + \sum_{n=1}^{3} Pb_{2n}\sin(2n\omega t) \quad (7.7.3)$$

8.4 New Corrector Method

Chapter 2 gives details of the derivation of the Corrector method whilst chapter 5 describes how it incorporates the use of a numerical 1DV model. If the parameterised version is substituted for the numerical 1DV model then problems arise in determining the value of certain terms in the Corrector model.

Consider:-

$$\frac{\partial T_{s,x}}{\partial t}+\overline{u}\frac{\partial T_{s,x}}{\partial x}=\overline{c}(h-a)\frac{\partial \overline{u}}{\partial t}+\frac{\partial T_{disp,x}}{\partial t} \qquad (5.4.1)$$

Chapter 5 also describes how the terms $\overline{c}$ and $T_{disp,x}$ are obtained from the 1DV equation. This is relatively simple since the 1DV concentration profile is calculated within the numerical 1DV model. If the parameterised version is used however, then the concentration profile is no longer calculated. Thus, a different method is required for evaluating these terms.

Consider:-

$$T_{s,x}=\int_a^h uc\partial z \qquad (8.4.1)$$

Split the velocity and concentration into their depth-average and fluctuating components:-

$$T_{s,x}=\int_a^h (\overline{u}+u')(\overline{c}+c')\partial z$$

Simplification gives,

$$T_{s,x}=\int_a^h \overline{u}\,\overline{c}\partial z+\int_a^h u'c'\partial z$$

i.e. $$T_{s,x}=T_{dm}+T_{disp,x} \qquad (8.4.2)$$

or $$T_{disp,x}=T_{s,x}-T_{dm}$$

where T_{dm} is the transport due to the depth-average components of the velocity and concentration.

Also,

$$T_{dm} = \int_a^h \overline{uc}\partial z$$

$$T_{dm} = (h-a)\overline{uc}$$

$$\text{i.e.} \qquad \overline{c} = \frac{T_{dm}}{(h-a)\overline{u}} \tag{8.4.3}$$

Therefore, if a parameterisation for T_{dm} can be determined then both $\overline{c}$ and $T_{disp,x}$ can be evaluated.

8.5 Parameterisation of Transport due to Depth-mean Values

Equation (8.4.2) suggests that a linear relationship may exist between the transport due to the depth-average values and the overall transport. In order to test this idea, the ratio of the two values (defined as the tidal ratio, α_r) is determined at a number of different stages in the tidal cycle for the data sets used in section 8.3. The results from two example sets are shown in figure 8.5.1. The bold line shows the fitted regression line. The absence of any significant scatter supports the linear model approach. Regression analysis is therefore performed on the model defined below.

$$\frac{T_{dm}}{T_{s,x}} = \alpha_r \tag{8.5.1}$$

Since $T_{s,x}$ has already been parameterised, it only remains to parameterise the tidal ratio ($P\alpha_r$). The parameterisation is based on those groups used in section 8.2.2; i.e. equations (7.5.5)-(7.5.10) and equation (8.2.2). However, during analysis it became evident that a better functional form could be achieved by using the exponential of Π_1; i.e.:-

$$\Pi_1 = \exp\left\{d_{50}\left(\frac{(s-1)g}{\nu^2}\right)^{1/3}\right\} \tag{8.5.2}$$

Figure 8.5.2 shows the effect of each group upon the ratio of equilibrium tidal ratio, α_{re}, over the tidal ratio, α_r. The equilibrium tidal ratio is defined by the following:-

$$\alpha_{re} = \frac{T_{dme}}{T_{se}} \tag{8.5.3}$$

where,

T_{dme} -Transport due to equilibrium depth-average values

T_{se} -Equilibrium transport

Again, equilibrium values are used so that limiting properties can be utilised. Figure 8.5.2 shows that the parameterisation should include Π_1, Π_2 and Π_7 since only these groups show significant variance in the ordinate. The parameterisation function used is therefore given by:-

$$\frac{P\alpha_r}{\alpha_{re}} = \frac{1}{\left(1-e^{\psi}\right)} \tag{8.5.4}$$

where,

$$\psi = -\alpha\Pi_1^{\beta_1}\Pi_2^{\beta_2}\Pi_7^{\beta_7}$$

The results of the regression analysis for the parameterised version of the tidal ratio (α_r) are shown in table 8.3.6. It is clear by the value of the analysis variables that the parameterisation is an excellent approximation. The mean % error indicates that the parameterisation is incredibly accurate, only 0.14% average error. The maximum % error is only 0.655%. The results from the independent sets (table 8.3.7) support the accuracy suggested by the regression analysis. The excellent agreement is shown graphically in figure 8.5.3; the bold line signifies perfect agreement. Figure 8.5.4 shows the residual plots for the proposed parameterisation. Again, the absence of any patterns validates the methods used in the regression analysis.

It is also clear that the parameterisation tends to its equilibrium value. Consider the following:-

$$d_{50} \to \infty \qquad \Rightarrow \qquad \Pi_1 \to \infty,\ \Pi_7 \to \frac{1}{\infty}.$$

$$\beta_1,\ \beta_7 > 0$$

$$\alpha < 0$$

Since Π_1 is an exponential function, it will dominate the effect of Π_7; therefore:-

$$\frac{P\alpha_r}{\alpha_{re}} \to \frac{1}{\left(1 - e^{-\infty}\right)} = 1$$

$$\text{i.e.} \qquad P\alpha_r \to \alpha_{re}$$

It is also clear that the parameterisation is only valid when the equilibrium value is non-zero. It is assumed that a zero value corresponds to zero transport, in which case the parameterisation is not applied.

The parameterisation for the transport due to depth-average contributions (PT_{dm}) is therefore given by:-

$$PT_{dm} = \frac{\alpha_{re}}{\left(1 - e^{\psi}\right)} PT_{s,x} \tag{8.5.3}$$

This then leads to the following parameterisation for the depth-average concentration:-

$$P\overline{c} = \frac{PT_{dm}}{(h-a)\overline{u}} \tag{8.5.4}$$

The parameterisation for the transport due to dispersive/fluctuating components is then given by:-

$$PT_{disp,x} = PT_{s,x} - PT_{dm} \tag{8.5.5}$$

Hence, the parameterised Corrector method is given by:-

$$\frac{\partial PT_{s,x}}{\partial t} + \overline{u}\frac{\partial PT_{s,x}}{\partial x} = P\overline{c}(h-a)\frac{\partial \overline{u}}{\partial t} + \frac{\partial PT_{disp,x}}{\partial t} \tag{8.5.6}$$

8.6 Results

8.6.1 Accuracy

The new parameterised Corrector model, equation (8.5.6), is compared against results from the conventional 2DV model for several test cases so that the accuracy of the new method can be assessed. In all cases the flow field is given a uniform depth-average value in the longitudinal direction but allowed to vary vertically according to the influence of the bed forms. Details of the data sets can be found in table 8.6.1.

Both models were run using the same machine so that computation time can be compared. The UNIX system provided by the University of Liverpool was used

in all tests. The system uses four 400MHz CPU's with 4Mb cache and 1Gb memory.

Nine horizontal grid points were used in all the test cases; $k = 1$ being the inflow grid with $k = 9$ as the outflow grid.

Table 8.6.2 shows the percentage error during the mid-tide phase, 2 - 4hrs, at each longitudinal grid point for each data set. Values for the full period are not given as errors of the order 1000% can occur during the beginning and end due to the small magnitude of transport being considered. It can be seen from the following test cases and accompanying figures that the interval containing the maximum tidal velocity produces the main error in terms of actual transport, rather than percentage error, and is therefore the main focus for analysis.

Test Case 1: data set 600

Figure 8.6.1 shows a comparison between the results obtained by the conventional model (2DV) and the new parameterised Corrector method (Param) at each of the nine horizontal grid points. It can be seen that the accuracy of the parameterised Corrector method is extremely good at each grid point. This is supported by figure 8.6.2, which shows the percentage error between the two models for the mid-tide region. Average error values during the mid-tide period are of the order of 1.5% for those grid points near the inflow boundary, whilst the error rises to 3% towards the outflow boundary.

Test Case 2: data set 601

This data set is essentially the same as set 600 except the sediment distribution has been altered. Here, the sediment particles are larger since the increment in the longitudinal direction is now ten microns rather than five. Again, the parameterised Corrector method is seen to give a good approximation to the conventional 2DV model as shown by figure 8.6.3. The main cause for the slight error would seem to occur near the outflow boundary where the sediment grain sizes are largest. This is supported by figure 8.6.4 where higher errors are shown for those grid points near the outflow boundary. Table 8.6.2 shows that the

average percentage error for the mid-tide region for each of the nine grid points is still remarkably low, in fact, errors are of order 1.5% near the inflow boundary.

Test Case 3: data set 602

This data set represents a change in standard deviation of the sediment grain distribution; otherwise it is the same as set 601. The parameterised Corrector method is seen to give a remarkably good agreement with the conventional 2DV model (figure 8.6.5). Table 8.6.2 shows that the average percentage error for each horizontal grid point is very low, ranging from 1.26% to 3.06%. It is interesting to note that the errors near the outflow boundary are considerably less than the corresponding errors for set 601. This would suggest that the wider range of particle size, due to the increase in standard deviation, causes the smaller grain particles to become more influential and hence negate the error incurred for larger grain sizes.

Test Case 4: data set 603

Data set 603 is identical to data set 602 except that now the mean water level has been increased.

Figure 8.6.7 shows that again the overall parameterisation is accurate. However, the parameterisation for the transport at maximum velocity seems to slightly over predict and also shows a slight error in the lag near the outflow boundary. This error seems to be due to the larger particle sizes near the outflow boundary rather than any influence of the change in mean water depth since this parameter is common to all parameterised quantities bar the tidal ratio.

Test Case 5: data set 604

This data set represents an increase in grain size from that used in set 603. Table 8.6.2 supports the theory that the parameterisation is less accurate for larger grain sizes. Near the outflow boundary it can be seen that the errors are slightly worse than the corresponding errors for set 603, although still less than 10%.

Test Case 6: data set 605

Data set 605 represents a bed that has a different spread of sediment sizes in each horizontal grid. The standard deviation of the sediment particle size in each grid increases in the longitudinal direction so that the spread of sediment fraction sizes also increases. This represents a more challenging situation and therefore shows the flexibility of the parameterisation.

It can be seen from figure 8.6.11 that the parameterised Corrector method produces a very good approximation for all of the nine horizontal grid points. Table 8.6.2 shows that the average percentage error during the mid-tide period is low for all computational grid points, as low as only 1.42% for grid point $k = 1$. The highest error occurs for the outflow boundary where both the standard deviation of grain size and median grain size are maximum; however, this is still very low (2.78%).

Test Case 7: data set 805

The parameterised Corrector method was also run for the data sets used to show the effect of the longitudinal component of the model, see chapter 6 and also table 6.4.1. It should be noted that both set 805 and set 807 are run with an increased maximum depth-average longitudinal tidal velocity, i.e. 2 ms^{-1}.

Figure 8.6.13 shows good agreement for all nine grid points of set 805. This is supported by the low values for the average error during the mid-tide phase as shown in table 8.6.2, only 1.86% for the last five grid points.

Test Case 8: data set 807

Figure 8.6.15 shows excellent agreement for set 807. Figure 8.6.16 shows that the parameterisation for the transport at maximum velocity is particularly good; typically only a 1.5% error. The overall error is also shown to very good for all computation points; table 8.6.2 shows values of the order 2%.

8.6.2 Computation Time

The testing shown in the previous section shows that the parameterised Corrector method gives a very good approximation to the tidal transport rates for a variety of simple situations. The real purpose of using the parameterised version of the Corrector method is to reduce computation time without significant loss in accuracy; it therefore remains to show that the computation time has been significantly reduced.

Table 8.6.3 gives the computation times for the data sets used in the previous section. [The efficiency is defined as the ratio of the Parameterised Corrector Method over the conventional method, expressed as a percentage.]

It can clearly be seen that the parameterised Corrector method is significantly faster than the conventional method. The new method requires approximately 60% of the computational time used by the conventional method in all test cases.

This is also a vast improvement on the non-parameterised Corrector method. Chapter 6 showed that the non-parameterised Corrector method requires 72% of the time used by the conventional 2DV approach, see table 6.5.1; this implies that the parameterised version provides a further reduction of approximately 10% in computation time for a system with only nine computation points.

8.7 Summary

The parameterised 1DV model presented in chapter 7 has been modified so that it may be used in a 2DV system. This has been achieved by including the reference level for sediment calculations as a characteristic parameter. The parameterisation is then based on the seven groups derived in chapter 7 plus a new group reflecting the influence of the reference level.

Regression analysis shows that the parameterised model is both valid and accurate for all quantities parameterised and therefore suitable to be used in a 2DV system.

One further parameterisation was performed in order to obtain values of the transport due to depth-mean values. The parameterisation is based on the fact that the ratio of transport due to depth-mean values and the actual transport rate remains approximately constant throughout the flood period. By parameterising this ratio and using the parameterised 1DV model described in section 8.2, it is possible to obtain the transport due to depth-mean values. From this, it is then possible to obtain both the depth-mean concentration and the transport due to fluctuations from depth-mean values.

All parameterisations are then combined to form a new parameterised Corrector method. Results from eight independent data sets indicate that the new parameterised Corrector method retains most of the accuracy shown by the non-parameterised method.

It has also been shown that the time required for computations is drastically reduced by using the new parameterised Corrector method, only 60% of the time taken by a conventional 2DV approach for nine computation points. It has also been shown that the new parameterised Corrector method requires 10% less computation time than the non-parameterised version for a system of nine longitudinal computation points.

Set	r (m)	h_m (m)	$\overline{u}_m$ (ms^{-1})	d_{50} (m)	up (s)	σ	a (m)
300	3	12	1	0.00015	44000	1.7044	0.00375
301	3	12	1	0.00015	44000	1.7044	0.01125
302	3	12	1	0.00015	44000	1.7044	0.01875
303	3	12	1	0.00015	44000	1.7044	0.02625
304	3	12	1	0.00015	44000	1.7044	0.03375
305	3	12	1	0.00015	44000	1.7044	0.04125
306	3	12	1	0.00015	44000	1.7044	0.04875
307	3	12	1	0.00015	44000	1.7044	0.05625
308	3	12	1	0.00015	44000	1.7044	0.06375
309	6	17	1.6	0.0002	44712	1.9	0.01631
310	6	17	1.6	0.0002	44712	1.9	0.048929
311	6	17	1.6	0.0002	44712	1.9	0.081549
312	6	17	1.6	0.0002	44712	1.9	0.114168
313	6	17	1.6	0.0002	44712	1.9	0.146788
314	6	17	1.6	0.0002	44712	1.9	0.179407
315	6	17	1.6	0.0002	44712	1.9	0.212027
316	6	17	1.6	0.0002	44712	1.9	0.244646
317	6	17	1.6	0.0002	44712	1.9	0.277265
318	9	20	2	0.00023	43500	1.8	0.069128
319	9	20	2	0.00023	43500	1.8	0.207383
320	9	20	2	0.00023	43500	1.8	0.345639
321	9	20	2	0.00023	43500	1.8	0.483895
322	9	20	2	0.00023	43500	1.8	0.62215
323	9	20	2	0.00023	43500	1.8	0.760406
324	9	20	2	0.00023	43500	1.8	0.898662
325	9	20	2	0.00023	43500	1.8	1.036917
326	9	20	2	0.00023	43500	1.8	1.175173

Table 8.2.1: Extra data sets used in the regression analysis due to the change in reference level for the parameterised Corrector method

Set	T_m ($kgm^{-2}s^{-1}$)	a_2 ($kgm^{-2}s^{-1}$)	a_4 ($kgm^{-2}s^{-1}$)	a_6 ($kgm^{-2}s^{-1}$)	b_2 ($kgm^{-2}s^{-1}$)	b_4 ($kgm^{-2}s^{-1}$)	b_6 ($kgm^{-2}s^{-1}$)
300	4.51489	-2.14747	0.721863	-0.09877	-0.5301	0.323492	-0.05837
301	2.11043	-1.0058	0.339146	-0.04435	-0.23143	0.140747	-0.0242
302	1.497396	-0.71439	0.241398	-0.03078	-0.1575	0.095716	-0.01606
303	1.199025	-0.57248	0.193748	-0.02424	-0.12218	0.074245	-0.01224
304	1.01767	-0.48619	0.164757	-0.0203	-0.10104	0.061403	-0.00999
305	0.893857	-0.42726	0.144944	-0.01763	-0.08679	0.05276	-0.00849
306	0.803029	-0.384	0.130383	-0.01569	-0.07644	0.046485	-0.00741
307	0.732992	-0.35066	0.119153	-0.01419	-0.06854	0.041697	-0.00659
308	0.677036	-0.324	0.110171	-0.013	-0.06229	0.037908	-0.00595
309	21.59592	-10.5028	3.030974	-0.26838	-2.43634	1.259797	-0.12334
310	10.21238	-4.97559	1.444189	-0.11942	-1.04129	0.538208	-0.04938
311	7.293583	-3.55711	1.035525	-0.08226	-0.69976	0.362078	-0.03213
312	5.86592	-2.8628	0.835089	-0.06439	-0.53762	0.278568	-0.02418
313	4.99416	-2.4389	0.712384	-0.0536	-0.44096	0.228801	-0.01953
314	4.39646	-2.14802	0.628089	-0.04628	-0.37603	0.195391	-0.01645
315	3.956111	-1.9337	0.565879	-0.04094	-0.32905	0.171218	-0.01426
316	3.615417	-1.76784	0.517682	-0.03684	-0.2933	0.152828	-0.01261
317	3.342282	-1.63485	0.478989	-0.03357	-0.26507	0.138311	-0.01132
318	19.08044	-9.38229	2.630829	-0.13749	-1.86648	0.948347	-0.0487
319	9.755364	-4.80625	1.355179	-0.06217	-0.8165	0.4176	-0.02068
320	7.201704	-3.55205	1.003304	-0.04253	-0.55178	0.284135	-0.01419
321	5.902659	-2.91346	0.823545	-0.03289	-0.42442	0.219994	-0.01122
322	5.085568	-2.51173	0.710145	-0.027	-0.34789	0.181476	-0.00952
323	4.511429	-2.22926	0.630288	-0.02298	-0.29621	0.155477	-0.00841
324	4.079473	-2.01666	0.57011	-0.02003	-0.2587	0.136614	-0.00763
325	3.738996	-1.84898	0.522616	-0.01776	-0.23009	0.122232	-0.00706
326	3.461452	-1.71231	0.483862	-0.01595	-0.20748	0.110864	-0.00661

Table 8.3.1: Transport at maximum velocity and Fourier coefficients for the extra sets used in regression analysis due to change in reference level

Set	T_{me} ($kgm^{-2}s^{-1}$)	a_{2e} ($kgm^{-2}s^{-1}$)	a_{4e} ($kgm^{-2}s^{-1}$)
300	8.179933	-3.82422	1.524708
301	3.522309	-1.65413	0.650823
302	2.399394	-1.1293	0.441367
303	1.869022	-0.88102	0.342739
304	1.553492	-0.73312	0.284185
305	1.341657	-0.63375	0.24494
306	1.188366	-0.56182	0.216582
307	1.071614	-0.50697	0.195009
308	0.97932	-0.4636	0.177971
309	37.09372	-17.9423	6.050641
310	15.94194	-7.73186	2.570501
311	10.8713	-5.27991	1.742394
312	8.478848	-4.12208	1.353105
313	7.055212	-3.43236	1.122136
314	6.098681	-2.96884	0.967248
315	5.405748	-2.63278	0.855267
316	4.877308	-2.37649	0.769995
317	4.458986	-2.17357	0.702583
318	27.25887	-13.356	4.309312
319	12.77811	-6.27587	1.986278
320	9.071454	-4.46089	1.397438
321	7.253374	-3.56999	1.110208
322	6.139037	-3.02347	0.934989
323	5.371736	-2.64699	0.814767
324	4.803966	-2.36829	0.726099
325	4.362744	-2.15161	0.657369
326	4.007468	-1.97707	0.602181

Table 8.3.2: Equilibrium values for the extra data set used in the regression analysis due to change in reference level

Set	Π_1	Π_2	Π_3	Π_4	Π_5	Π_6	Π_7
300	3.02	1.875423	1.25E-05	12.25685	2.03E+14	20000	25
301	3.02	1.875423	1.25E-05	12.25685	2.03E+14	20000	75
302	3.02	1.875423	1.25E-05	12.25685	2.03E+14	20000	125
303	3.02	1.875423	1.25E-05	12.25685	2.03E+14	20000	175
304	3.02	1.875423	1.25E-05	12.25685	2.03E+14	20000	225
305	3.02	1.875423	1.25E-05	12.25685	2.03E+14	20000	275
306	3.02	1.875423	1.25E-05	12.25685	2.03E+14	20000	325
307	3.02	1.875423	1.25E-05	12.25685	2.03E+14	20000	375
308	3.02	1.875423	1.25E-05	12.25685	2.03E+14	20000	425
309	4.02	1.557987	1.18E-05	21.54792	1.57E+14	30000	81.55
310	4.02	1.557987	1.18E-05	21.54792	1.57E+14	30000	244.645
311	4.02	1.557987	1.18E-05	21.54792	1.57E+14	30000	407.745
312	4.02	1.557987	1.18E-05	21.54792	1.57E+14	30000	570.84
313	4.02	1.557987	1.18E-05	21.54792	1.57E+14	30000	733.94
314	4.02	1.557987	1.18E-05	21.54792	1.57E+14	30000	897.035
315	4.02	1.557987	1.18E-05	21.54792	1.57E+14	30000	1060.135
316	4.02	1.557987	1.18E-05	21.54792	1.57E+14	30000	1223.23
317	4.02	1.557987	1.18E-05	21.54792	1.57E+14	30000	1386.325
318	4.62	1.701298	1.15E-05	26.56607	1.29E+14	39130.43	300.5565
319	4.62	1.701298	1.15E-05	26.56607	1.29E+14	39130.43	901.6652
320	4.62	1.701298	1.15E-05	26.56607	1.29E+14	39130.43	1502.778
321	4.62	1.701298	1.15E-05	26.56607	1.29E+14	39130.43	2103.891
322	4.62	1.701298	1.15E-05	26.56607	1.29E+14	39130.43	2705
323	4.62	1.701298	1.15E-05	26.56607	1.29E+14	39130.43	3306.113
324	4.62	1.701298	1.15E-05	26.56607	1.29E+14	39130.43	3907.226
325	4.62	1.701298	1.15E-05	26.56607	1.29E+14	39130.43	4508.335
326	4.62	1.701298	1.15E-05	26.56607	1.29E+14	39130.43	5109.448

Table 8.3.3: Values of the non-dimensional groups for the extra sets used in the regression analysis due to change in reference level

Set	a (m)	Π_7
100	0.0075	50
101	0.008	50
102	0.010158	59.75294
103	0.012887	71.59444
104	0.016127	84.87895
105	0.020144	100.72
106	0.024501	116.6714
107	0.0295	134.0909
108	0.035189	152.9957
109	0.016082	94.6
110	0.020364	113.1333
111	0.025437	133.8789
112	0.031546	157.73
113	0.038393	182.8238
114	0.046251	210.2318
115	0.055192	239.9652
116	0.065285	272.0208
117	0.076589	306.356
118	0.103304	491.9238
119	0.112529	523.3907
120	0.122296	555.8909
121	0.132615	589.4
122	0.143498	623.9043
123	0.154954	659.3787
124	0.166988	695.7833
125	0.179608	733.0939
126	0.192818	771.272
127	0.03968	180.3636
128	0.0398	180.9091
129	0.03991	181.4091
130	0.040014	181.8818
131	0.040111	182.3227
132	0.040203	182.7409
133	0.04029	183.1364
134	0.040372	183.5091
135	0.040451	183.8682
136	0.084536	338.144
137	0.084682	338.728
138	0.084818	339.272
139	0.084946	339.784
140	0.085066	340.264
141	0.08518	340.72
142	0.089222	356.888
143	0.095211	380.844
144	0.10051	402.04
145	0.100756	438.0696
146	0.102851	447.1783
147	0.104634	454.9304
148	0.106168	461.6
149	0.107504	467.4087
150	0.108681	472.5261

Set	a (m)	Π_7
151	0.109725	477.0652
152	0.110662	481.1391
153	0.111505	484.8043
154	0.0075	50
155	0.0075	50
156	0.007923	52.82
157	0.008853	59.02
158	0.00977	65.13333
159	0.010679	71.19333
160	0.011582	77.21333
161	0.012478	83.18667
162	0.020529	136.86
163	0.016571	82.855
164	0.018644	93.22
165	0.020691	103.455
166	0.022718	113.59
167	0.024731	123.655
168	0.026731	133.655
169	0.038164	190.82
170	0.057079	285.395
171	0.066765	333.825
172	0.022378	101.7182
173	0.026037	118.35
174	0.029574	134.4273
175	0.03303	150.1364
176	0.036426	165.5727
177	0.039775	180.7955
178	0.043084	195.8364
179	0.04636	210.7273
180	0.073488	334.0364
181	0.01122	66
182	0.010802	63.54118
183	0.010441	61.41765
184	0.010123	59.54706
185	0.009841	57.88824
186	0.009587	56.39412
187	0.009358	55.04706
188	0.00915	53.82353
189	0.00896	52.70588
190	0.02946	155.0526
191	0.02841	149.5263
192	0.027492	144.6947
193	0.02668	140.4211
194	0.025956	136.6105
195	0.025303	133.1737
196	0.024711	130.0579
197	0.02417	127.2105
198	0.023675	124.6053
199	0.096971	461.7667
200	0.096181	458.0048
201	0.095482	454.6762

Table 8.3.4: Extra data used in regression analysis due to change in reference level

Set	a (m)	Π_7
202	0.094849	451.6619
203	0.094267	448.8905
204	0.093723	446.3
205	0.093208	443.8476
206	0.092712	441.4857
207	0.09223	439.1905
208	0.008	50
209	0.008	50
210	0.008	50
211	0.008	50
212	0.008	50
213	0.008	50
214	0.008	50
215	0.008	50
216	0.008	50
217	0.024101	120.505
218	0.024755	123.775
219	0.025409	127.045
220	0.026061	130.305
221	0.026713	133.565
222	0.027364	136.82
223	0.028014	140.07
224	0.028663	143.315
225	0.029773	148.865
226	0.114379	497.3
227	0.117418	510.513
228	0.12045	523.6957
229	0.123475	536.8478
230	0.126493	549.9696
231	0.129505	563.0652
232	0.132508	576.1217
233	0.135504	589.1478
234	0.140618	611.3826
235	0.0075	50
236	0.0075	50
237	0.0075	50
238	0.0075	50
239	0.0075	50
240	0.0075	50
241	0.0075	50
242	0.0075	50
243	0.0075	50
244	0.025952	129.76
245	0.026415	132.075

Set	a (m)	Π_7
246	0.026876	134.38
247	0.027335	136.675
248	0.027792	138.96
249	0.028246	141.23
250	0.028698	143.49
251	0.029149	145.745
252	0.029598	147.99
253	0.101166	459.8455
254	0.101446	461.1182
255	0.101829	462.8591
256	0.102283	464.9227
257	0.102788	467.2182
258	0.103333	469.6955
259	0.103908	472.3091
260	0.104507	475.0318
261	0.105128	477.8545
262	0.0075	50
263	0.008	50
264	0.009273	54.54706
265	0.012385	68.80556
266	0.01626	85.57895
267	0.021184	105.92
268	0.026911	128.1476
269	0.033772	153.5091
270	0.04191	182.2174
271	0.013506	79.44706
272	0.017919	99.55
273	0.023387	123.0895
274	0.030213	151.065
275	0.038239	182.0905
276	0.047812	217.3273
277	0.059114	257.0174
278	0.085473	356.1375
279	0.116113	464.452
280	0.009001	60.00667
281	0.012385	77.40625
282	0.016694	98.2
283	0.028708	159.4889
284	0.044213	232.7
285	0.065045	325.225
286	0.08432	401.5238
287	0.10726	487.5455
288	0.134314	583.9739

Table 8.3.4 contd: Extra data used in regression analysis due to change in reference level

	α	β_1	β_2	β_3	β_4	β_5	β_6	β_7
T_m	6.648	0.470	0.932	0.337	----------	----------	----------	0.159
a_2	7.273	0.453	0.969	0.343	----------	----------	----------	0.158
a_4	43.645	0.320	0.904	0.518	----------	----------	----------	0.188
a_6	1.839e-11	-0.768	----------	-1.270	2.931	----------	----------	-0.715
b_2	0.000163	-0.687	-1.753	-1.239	3.458	-0.432	----------	-0.74332
b_4	4.0415e-5	-0.692	-1.434	-1.093	3.287	-0.350	----------	-0.726
b_6	3.958e-13	-1.091	----------	-1.672	2.583	----------	----------	-0.744
α_r	-2.02	0.015	0.244					0.07

Table 8.3.5a: Results of parameterisation

	r^2	F-obs	Mean % error	Max % error	Mean diff ($kgm^{-2}s^{-1}$)	Max diff ($kgm^{-2}s^{-1}$)
T_m	0.985	3492.8	1.052	4.484	0.007363	0.030199
a_2	0.981	2741.9	1.171	5.786	0.008271	0.046093
a_4	0.979	2434.0	1.709	6.892	0.010585	0.03259
a_6	0.832	261.4	30.893	1450.404	0.000317	0.002308
b_2	0.997	10003.17	4.472	30.220	0.000675	0.006417
b_4	0.997	10821.2	4.339	17.628	0.000319	0.002055
b_6	0.866	338.8	25.736	348.432	0.000124	0.001154
α_r	0.936	1026.8	0.140	0.655	0.00136	0.00629

Table 8.3.5b: Analysis of parameterisation

	Mean % error	Max % error	Mean diff ($kgm^{-2}s^{-1}$)	Max diff ($kgm^{-2}s^{-1}$)
T_m	2.435	5.904	0.017608	0.044163
a_2	2.802	5.948	0.02031	0.044783
a_4	2.712	7.681	0.017983	0.05385
a_6	36.610	70.156	0.000609	0.001746
b_2	6.308	23.653	0.000712	0.003853
b_4	9.297	25.994	0.000554	0.002488
b_6	34.267	59.983	0.000175	0.000596
α_r				

Table 8.3.6: Effect of parameterisation on independent sets

Set	r (m)	h_m (m)	$\overline{u}_m$ (ms^{-1})	up (s)
600	3	10	1.0	44712
601	3	10	1.0	44712
602	3	10	1.0	44712
603	3	20	1.0	44712
604	3	20	1.0	44712
605	3	10	1.0	44712

Table 8.6.1a: Tidal information for the data sets used to compare the parameterised Corrector method with the conventional 2DV model

Set	d_{50} (μm)									σ								
	k=1	k=2	k=3	k=4	k=5	k=6	k=7	k=8	k=9	k=1	k=2	k=3	k=4	k=5	k=6	k=7	k=8	k=9
600	150	155	160	165	170	175	180	185	190	1.5	1.5	1.5	1.5	1.5	1.5	1.5	1.5	1.5
601	150	160	170	180	190	200	210	220	230	1.5	1.5	1.5	1.5	1.5	1.5	1.5	1.5	1.5
602	150	160	170	180	190	200	210	220	230	1.7044	1.7044	1.7044	1.7044	1.7044	1.7044	1.7044	1.7044	1.7044
603	150	160	170	180	190	200	210	220	230	1.7044	1.7044	1.7044	1.7044	1.7044	1.7044	1.7044	1.7044	1.7044
604	210	215	220	225	230	235	240	245	250	1.7044	1.7044	1.7044	1.7044	1.7044	1.7044	1.7044	1.7044	1.7044
605	150	155	160	165	170	175	180	185	190	1.5	1.6	1.7044	1.7044	1.8	1.8	1.9	1.9	2.0

Table 8.6.1b: Spatial information for the data sets used to compare the parameterised Corrector method with the conventional 2DV model

Set	Average % error								
	$k=1$	$k=2$	$k=3$	$k=4$	$k=5$	$k=6$	$k=7$	$k=8$	$k=9$
600	1.42	1.52	1.67	1.84	2.06	2.32	2.64	3.10	3.64
601	1.38	1.58	1.85	2.18	2.65	3.65	4.60	5.71	6.88
602	1.26	1.40	1.77	2.08	2.32	2.62	2.72	2.88	3.06
603	7.57	6.99	6.57	6.49	6.73	6.90	7.59	8.66	9.83
604	5.85	6.26	6.72	7.21	7.72	8.24	8.81	9.39	9.99
605	1.42	1.52	1.74	1.88	2.10	2.21	2.43	2.54	2.78
805	6.96	6.96	6.96	2.86	1.86	1.86	1.86	1.86	1.86
807	2.65	1.26	1.82	1.82	1.82	1.82	1.82	1.82	1.82

Table 8.6.2: Average percentage error during mid-tide period for test data sets

Input Set	Conventional 2DV Hrs:min:s	Parameterisation Hrs:min:s	Efficiency (%)
600	1:26:10.07	0:46:84.51	55
601	1:23:04.05	0:47:01.39	56
602	1:23:53.02	0:47:56.79	57
603	1:23:17.66	0:47:98.81	58
604	1:23:38.87	0:50:68.35	61
605	1:23:40.05	0:47:01.39	56
805	1:29:26.25	0:49:53.22	56
807	1:29:09.26	0:49:56.92	58

Table 8.6.3: Comparison of computational time required for the 2DV methods

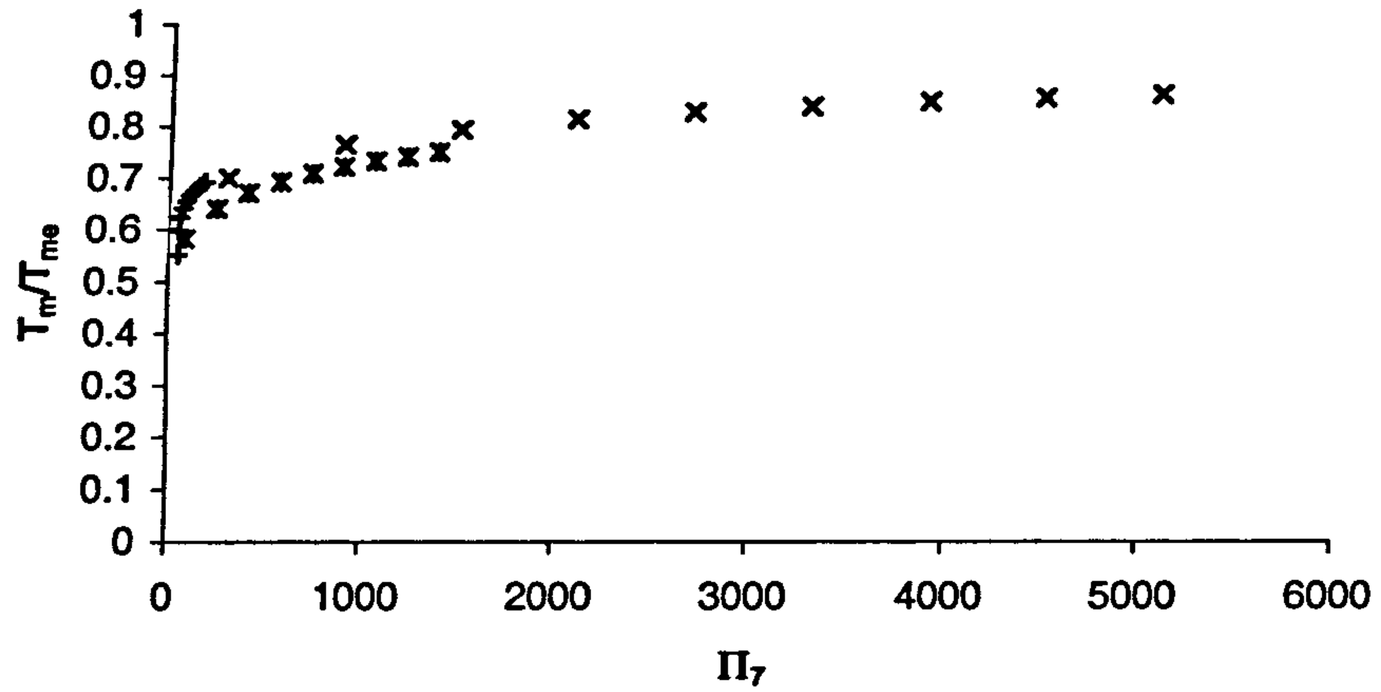

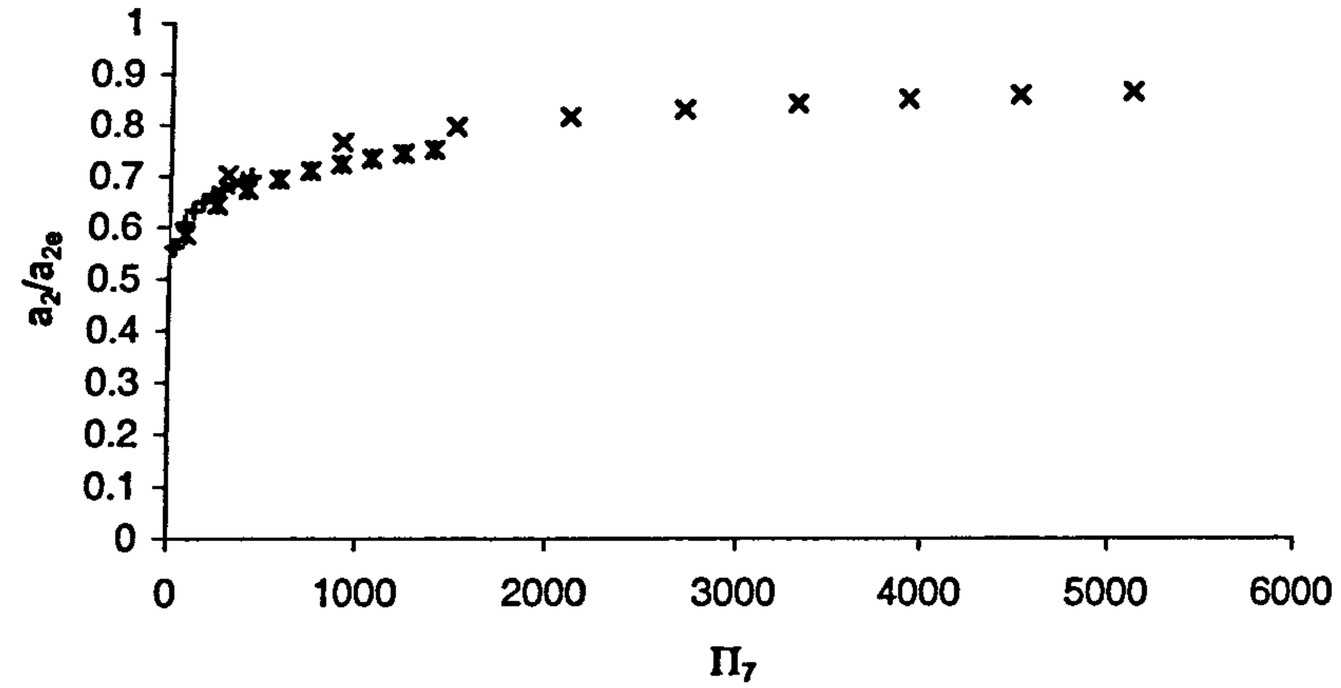

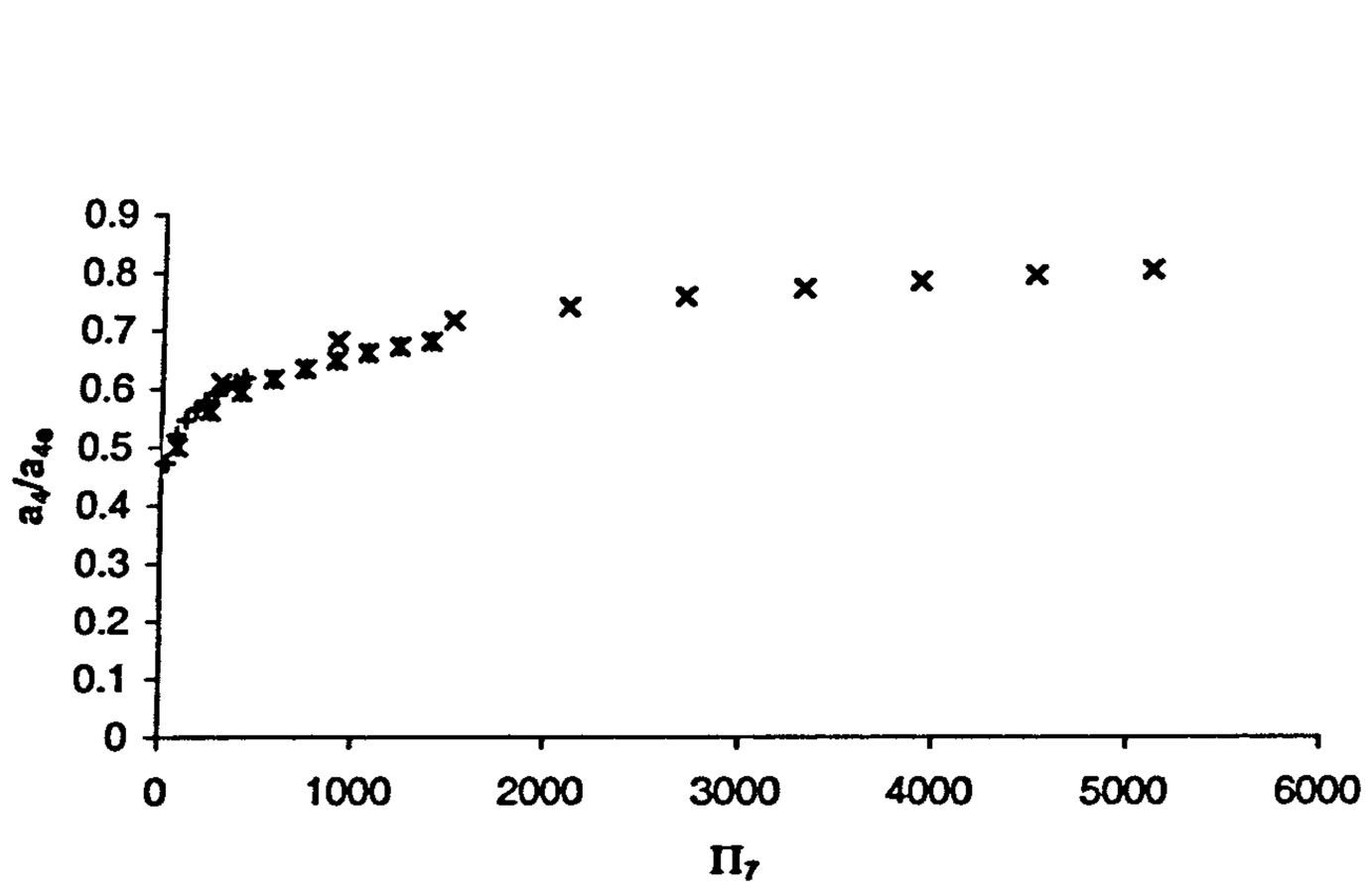

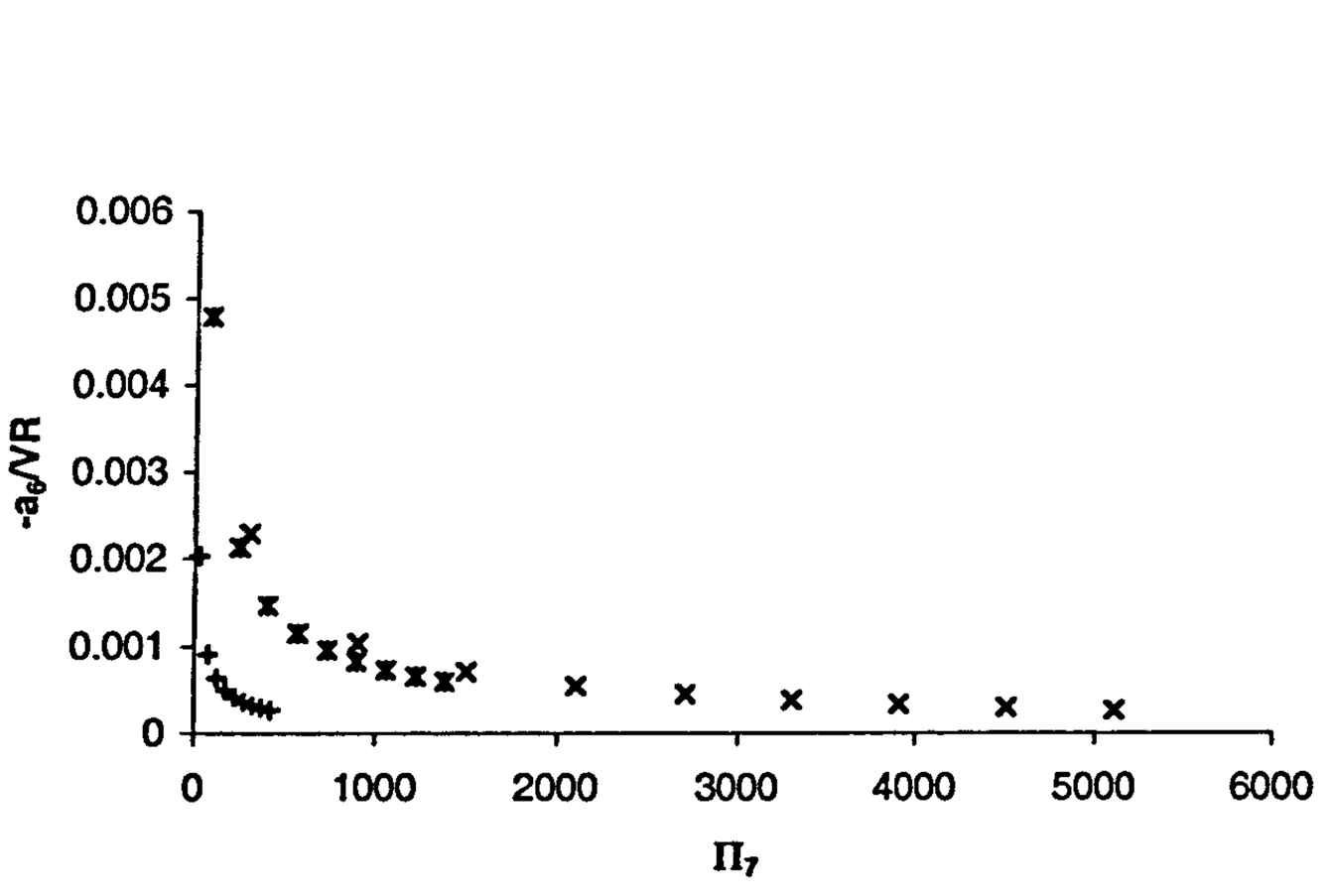

Figure 8.2.1a-d: Parameterisation quantity versus non-dimensional group values for the data sets used in the regression analysis
(Symbols represent the three sets of nine for each group)

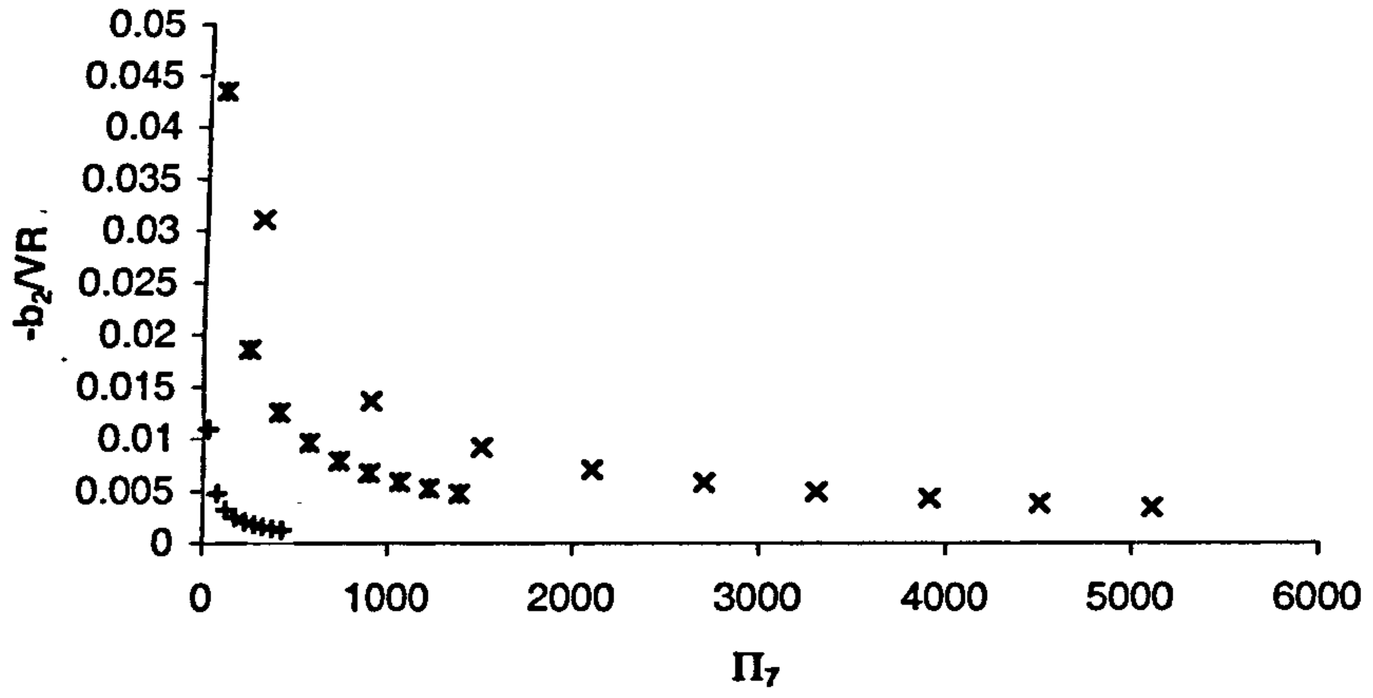

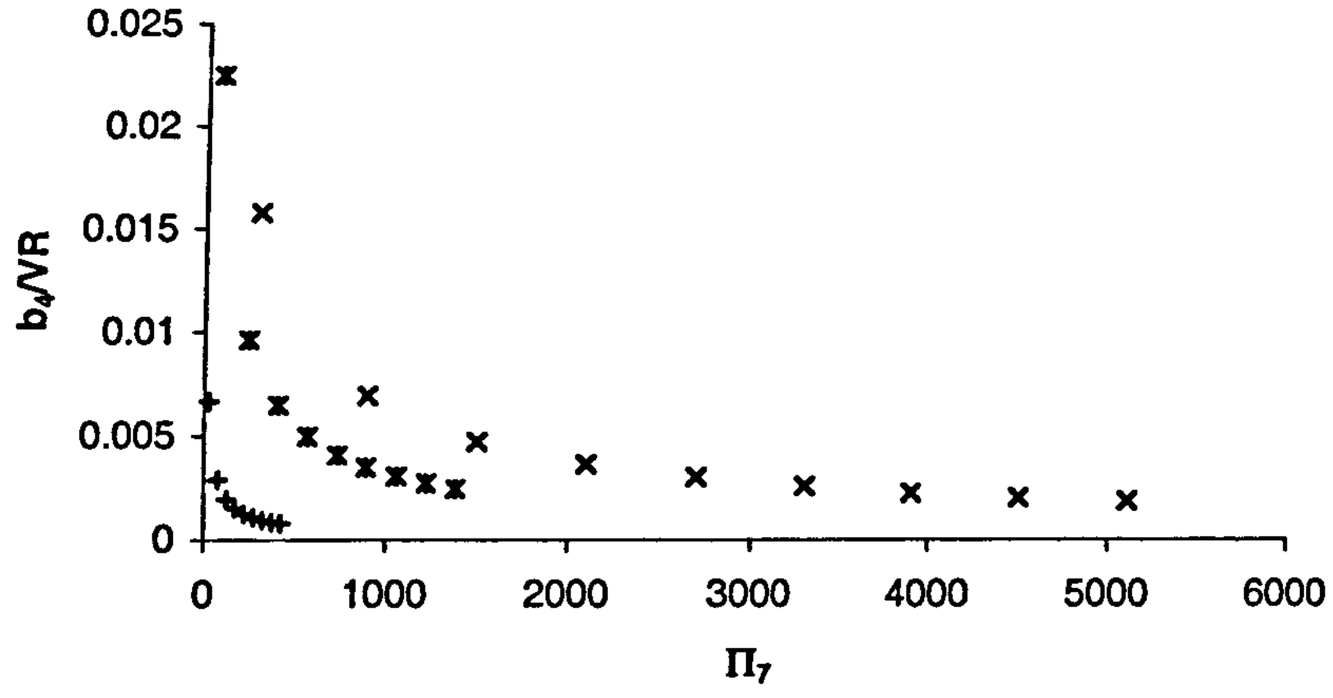

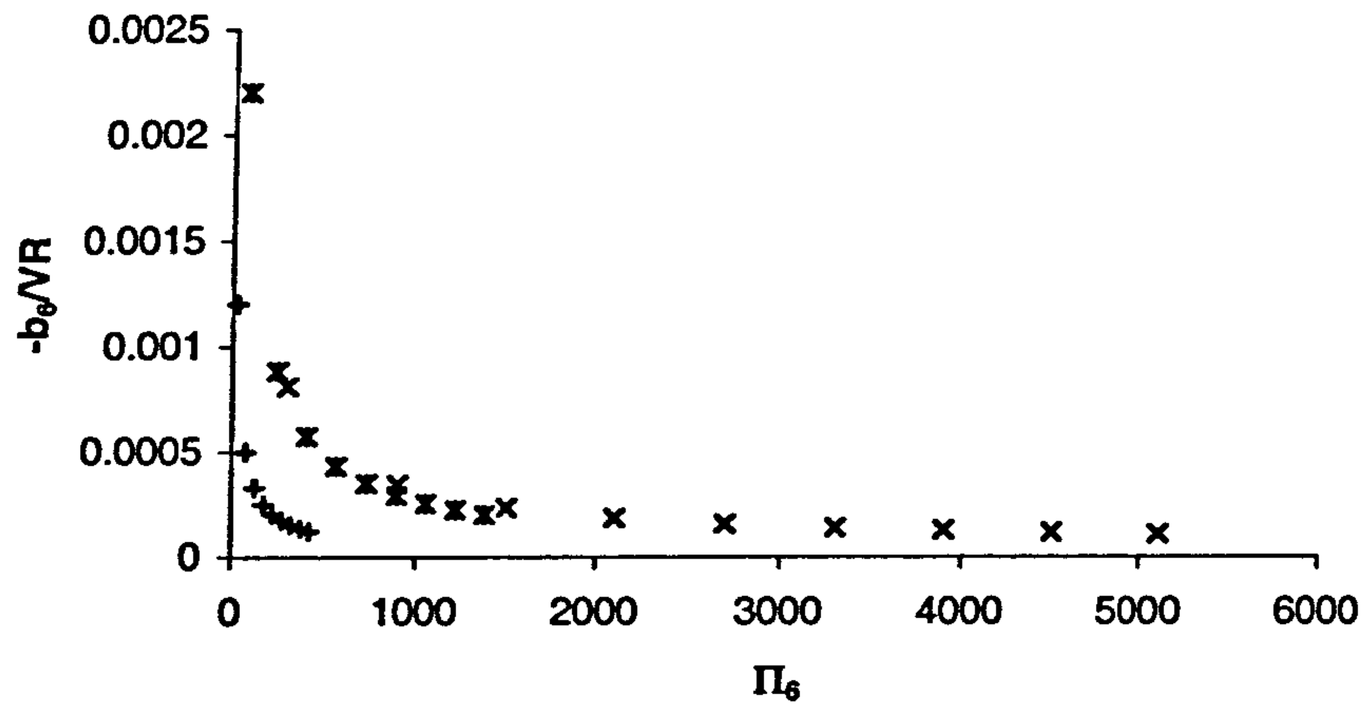

Figure 8.2.1e-g: Parameterisation quantity versus non-dimensional group values for the data sets used in the regression analysis
(Symbols represent the three sets of nine for each group)

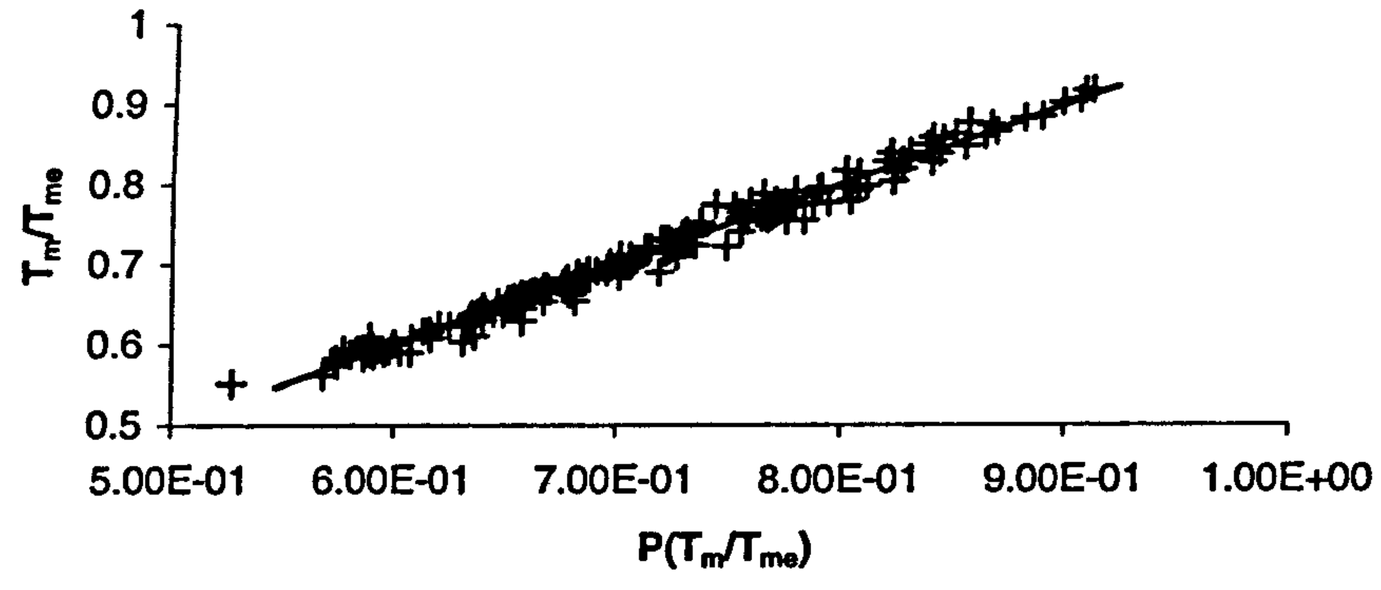

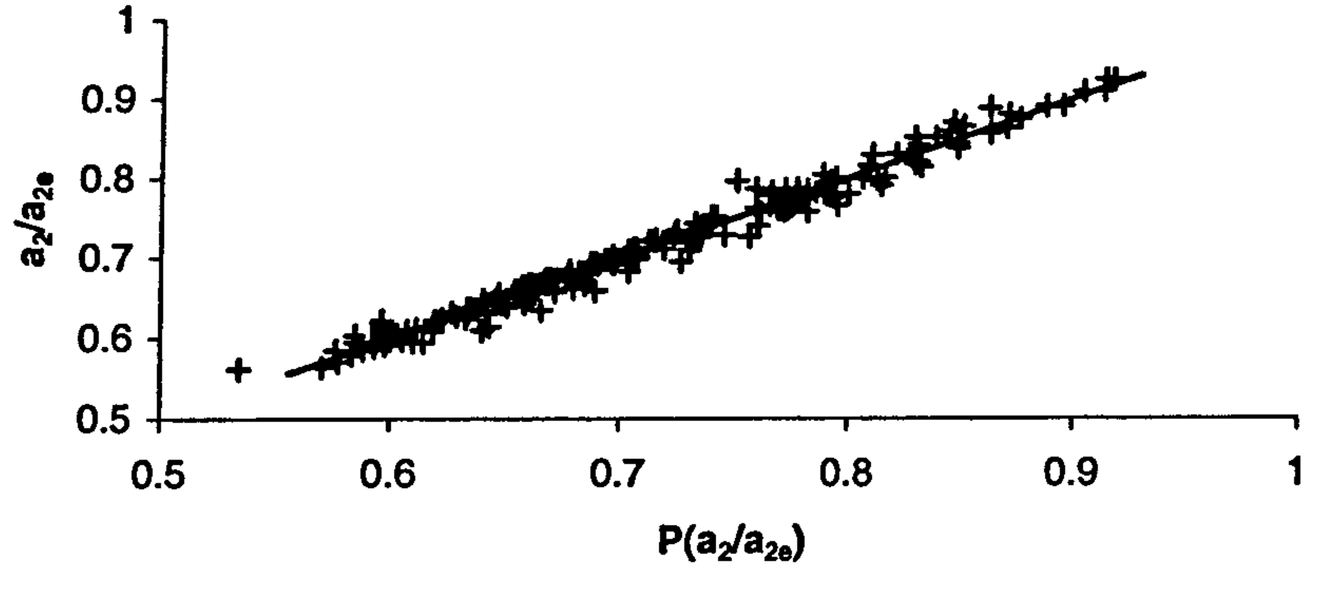

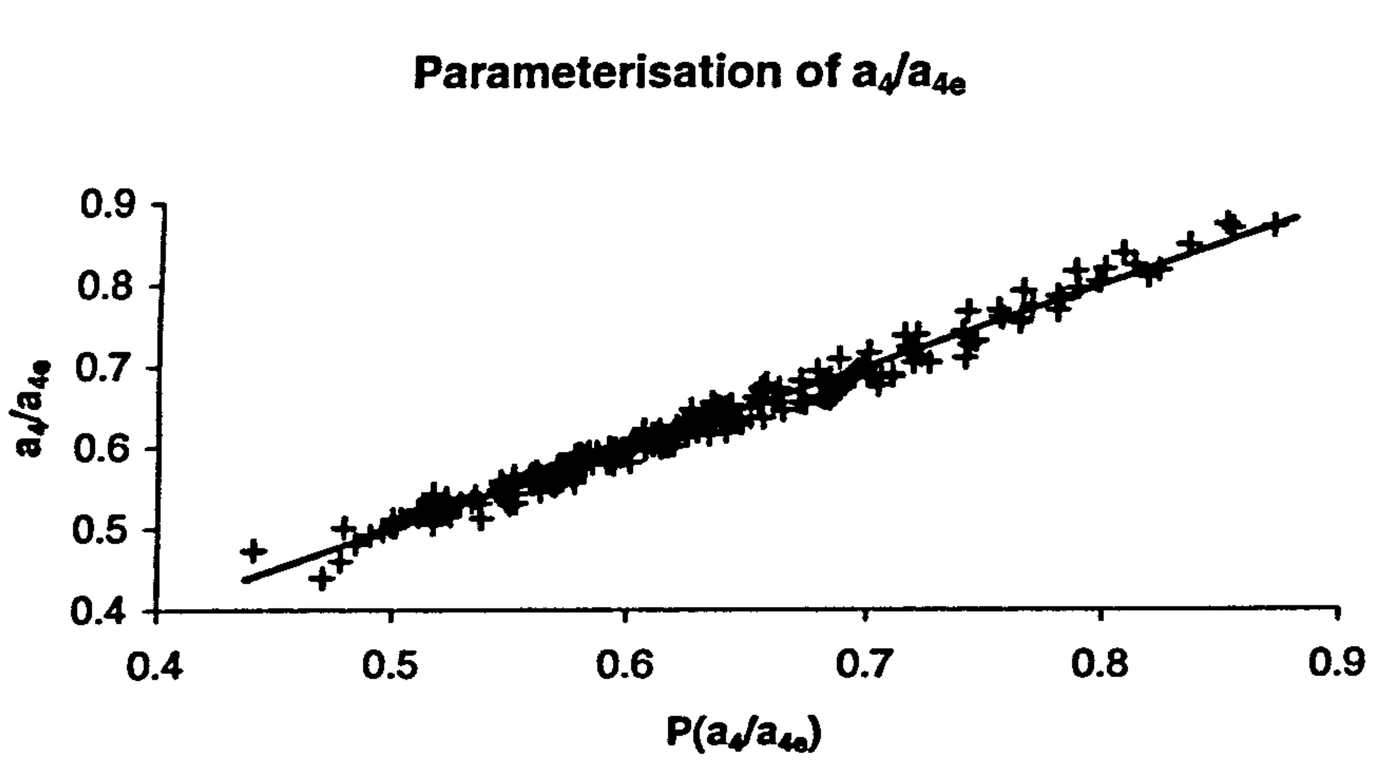

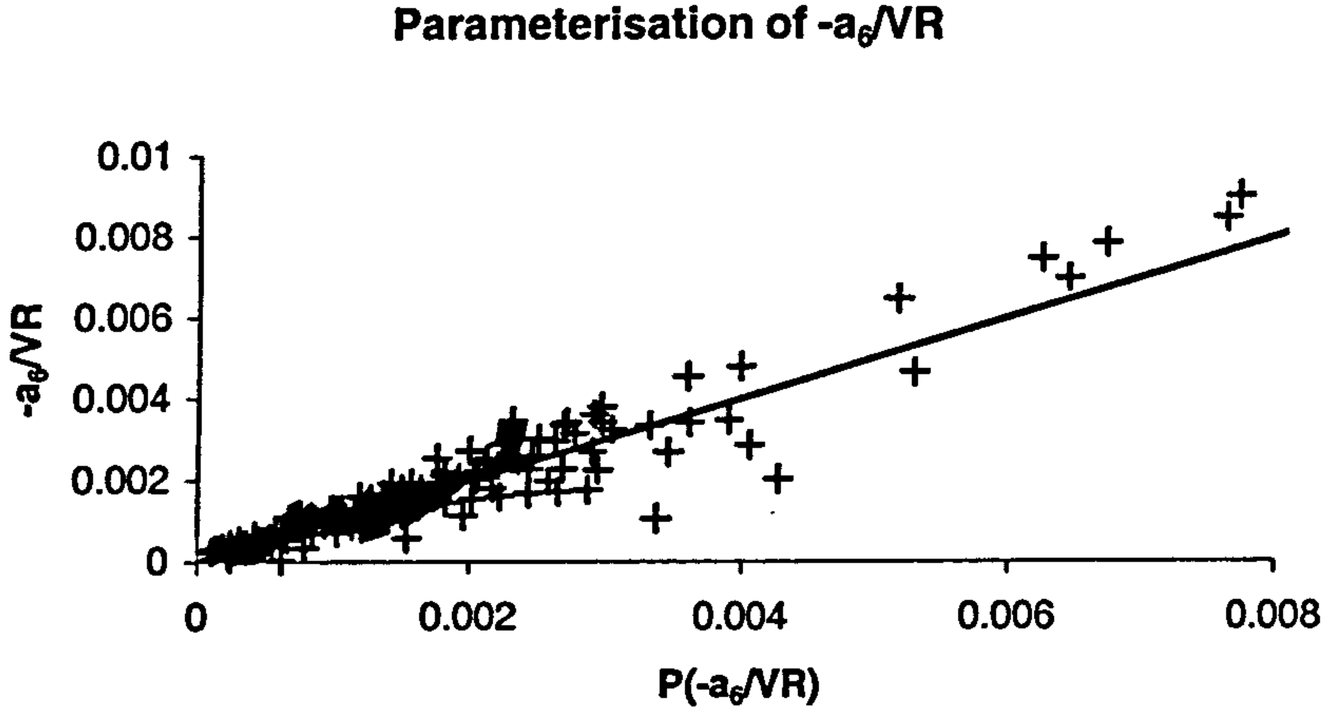

Figure 8.3.1a-d:Parameterised 1DV quantities versus values from the numerical model

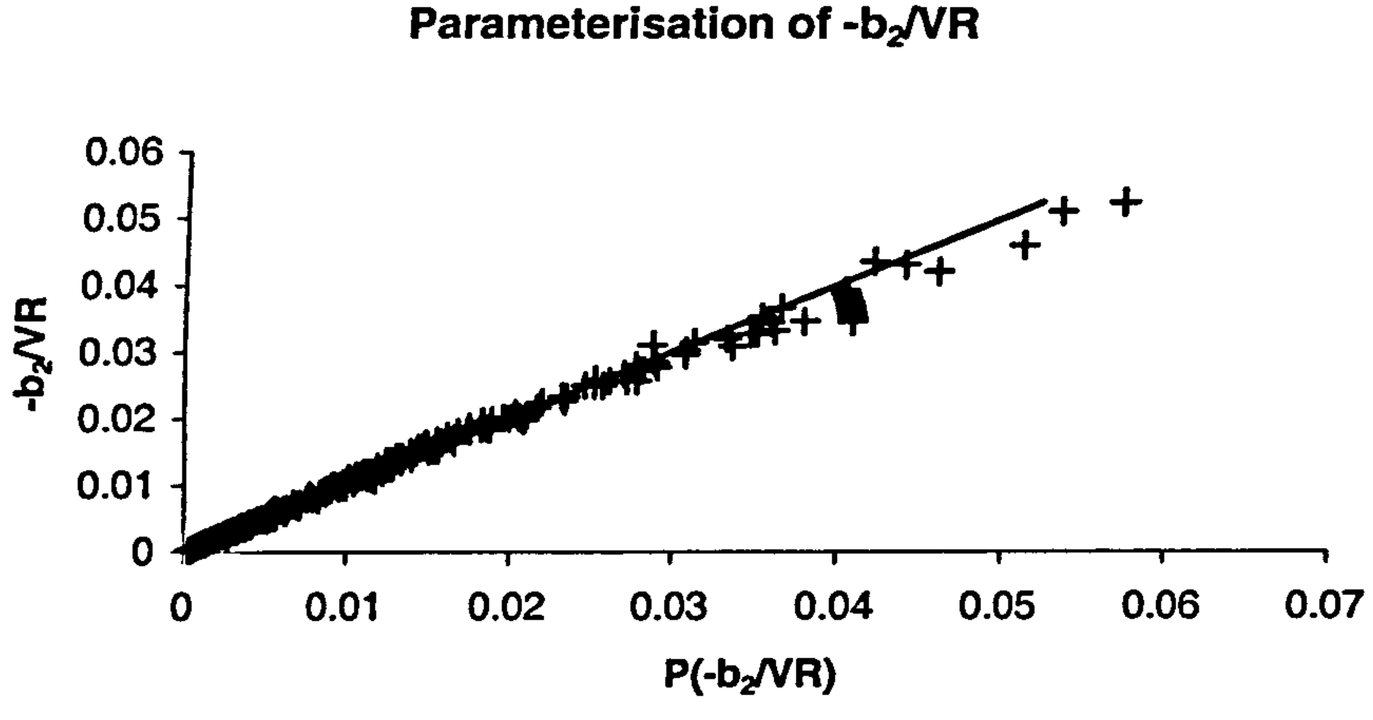

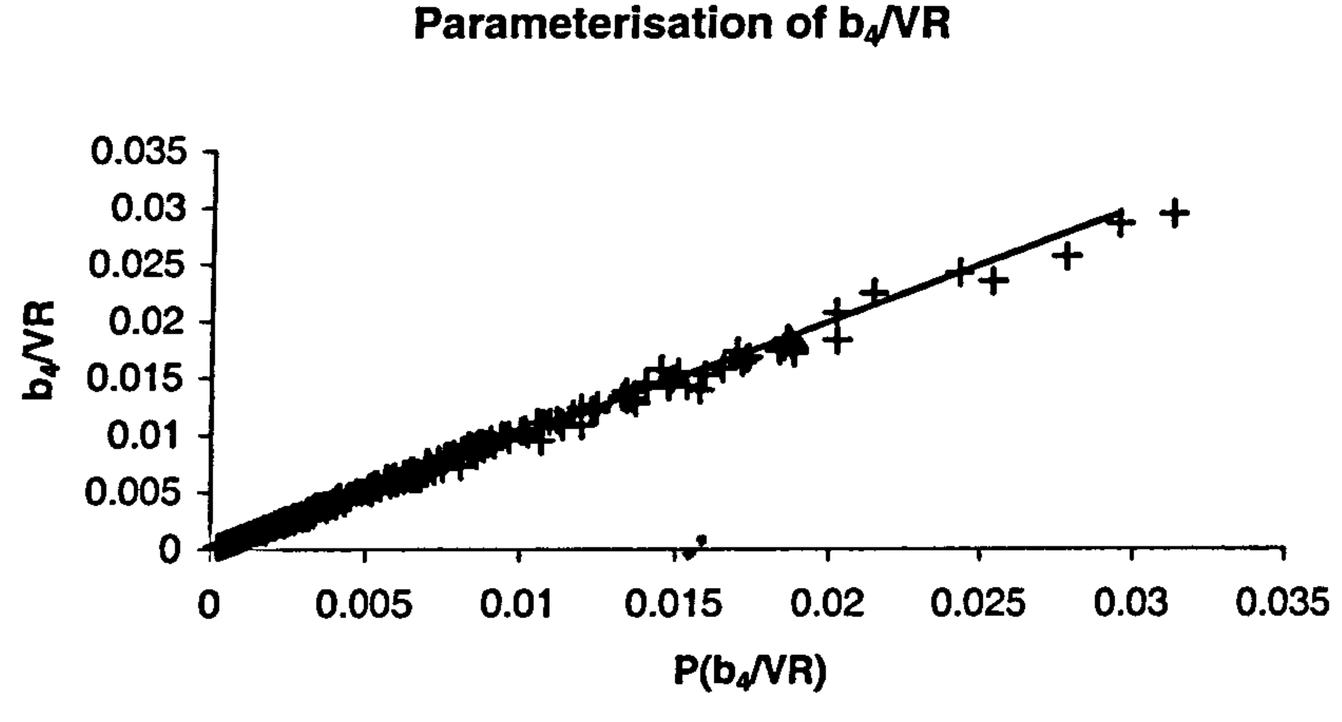

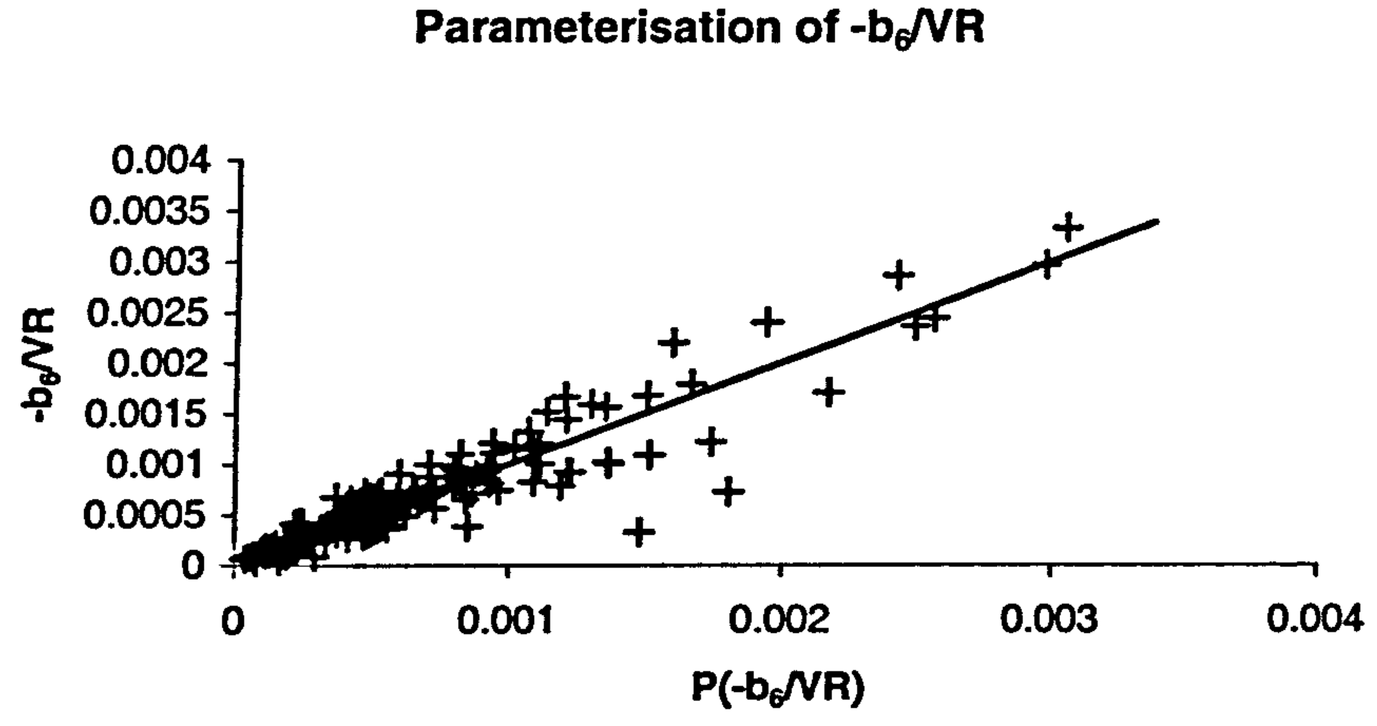

Figure 8.3.1e-g:Parameterised 1DV quantities versus values from the numerical model

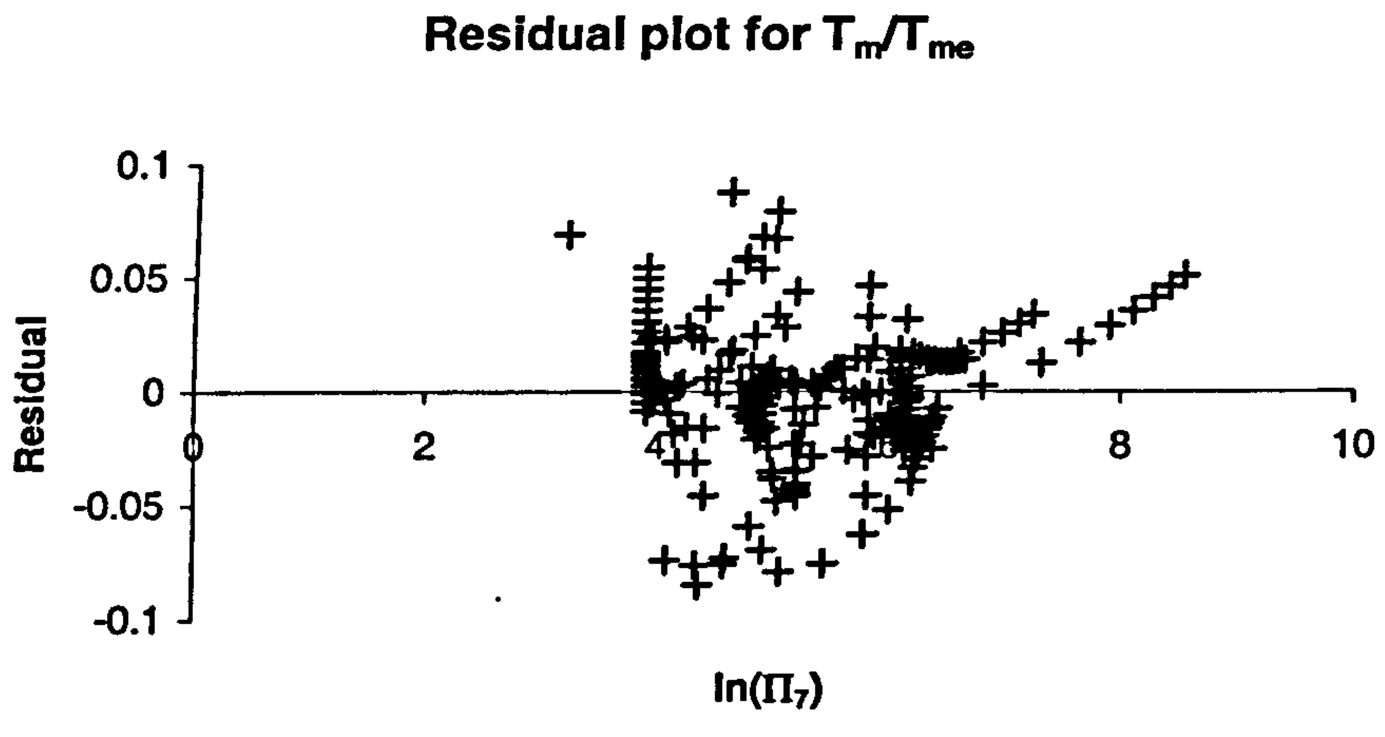

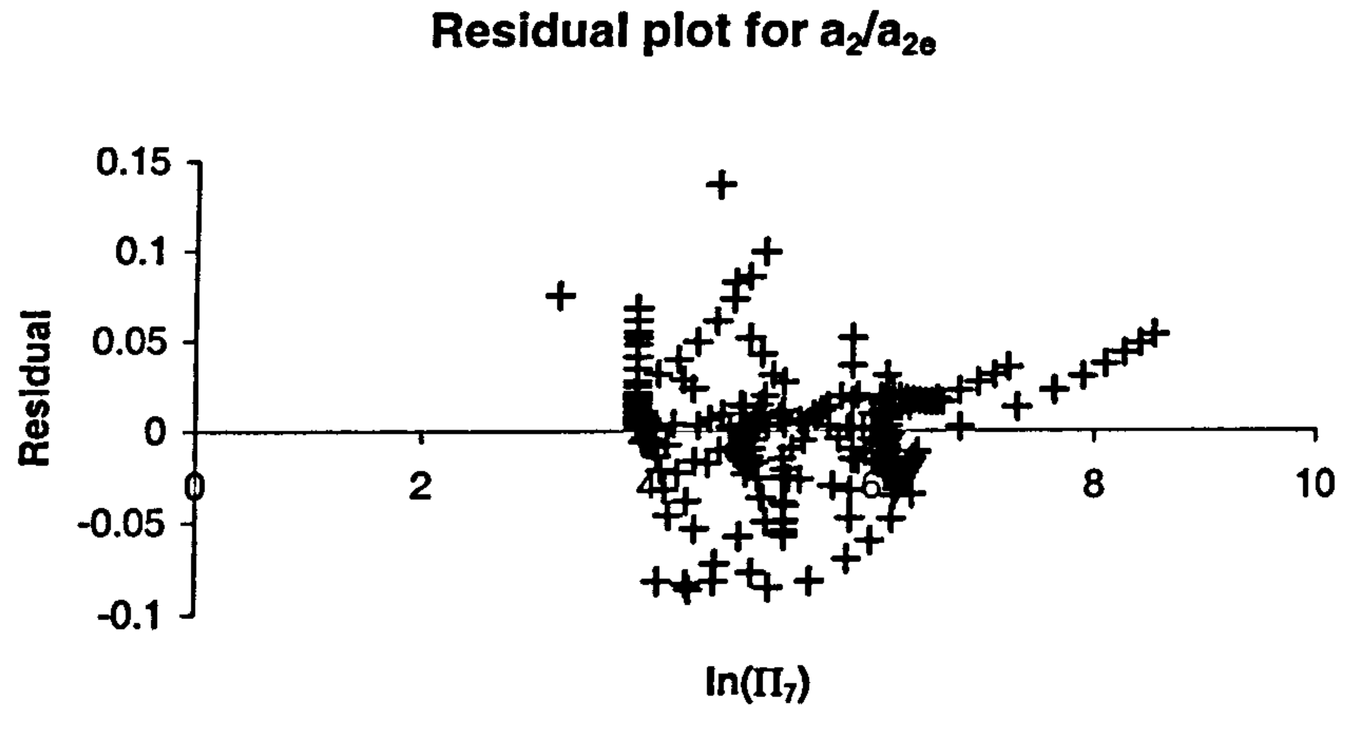

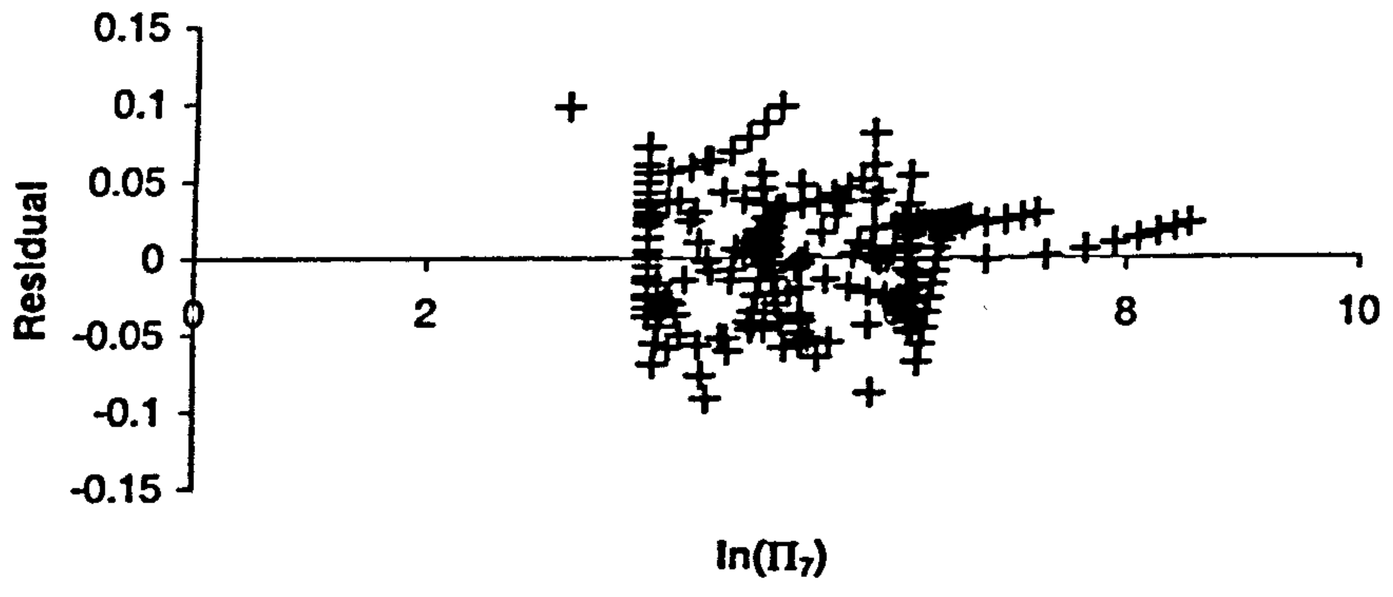

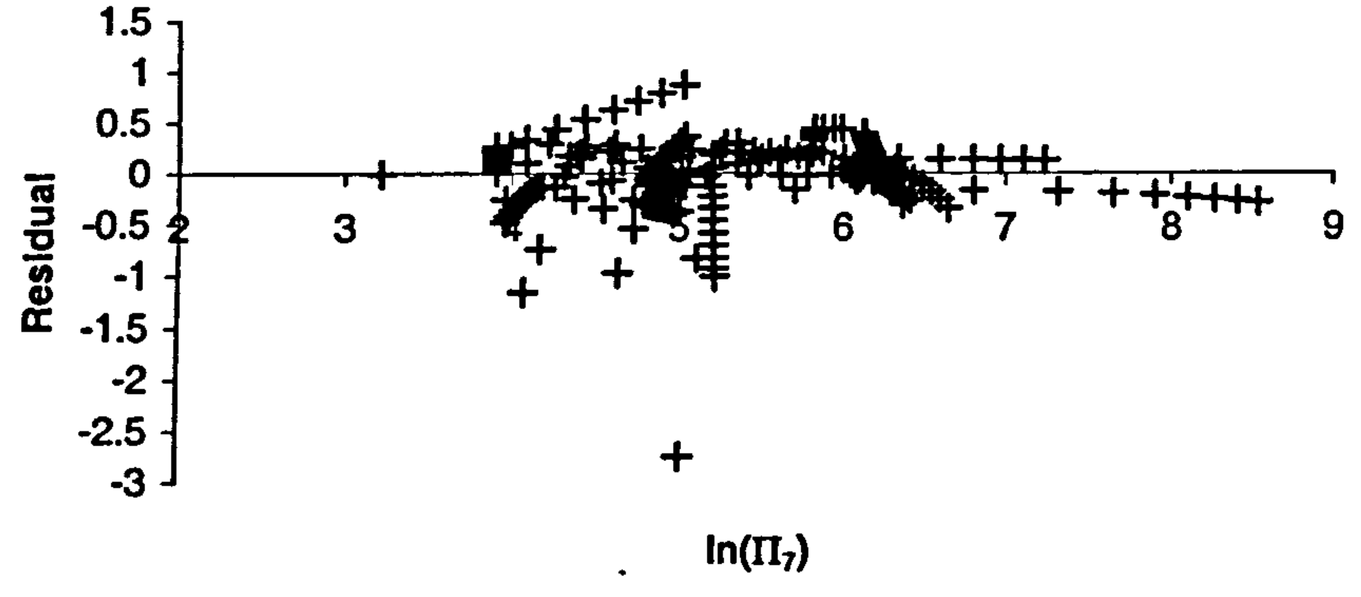

Figure 8.3.2a-d: Residual plots for regression analysis

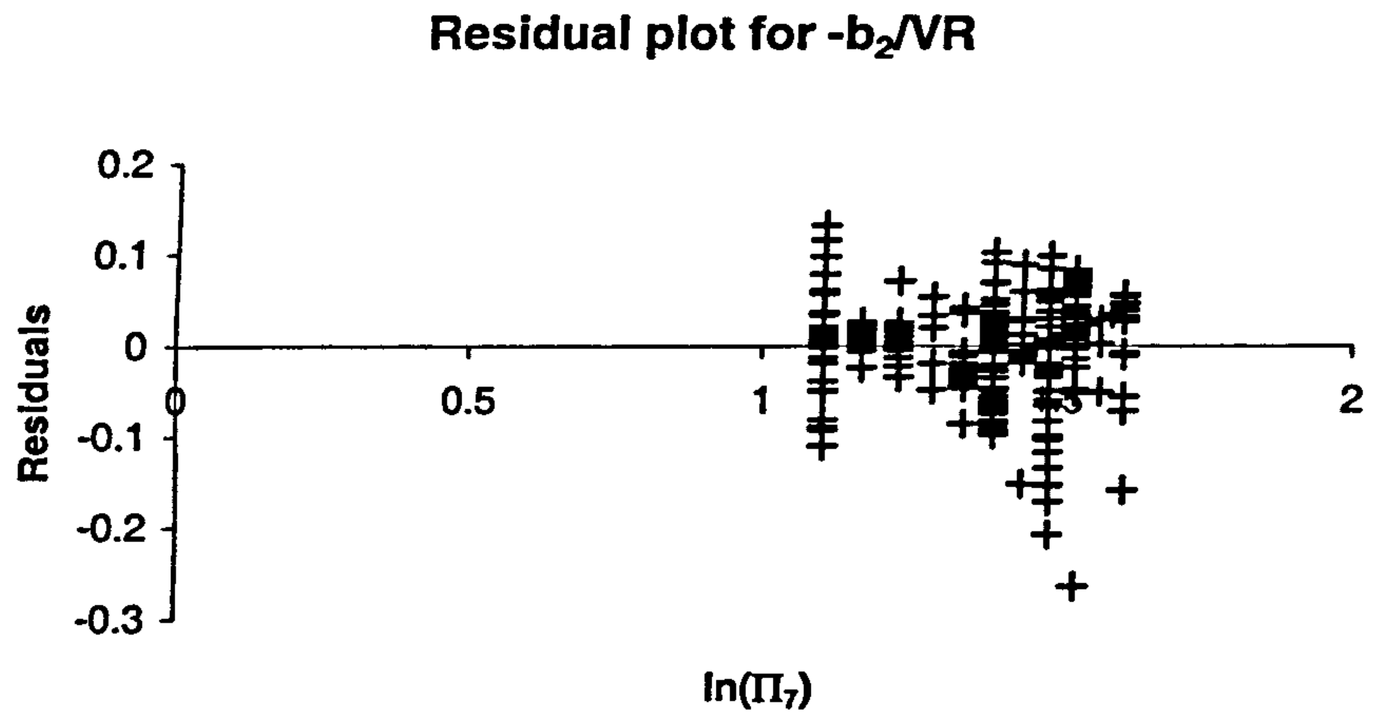

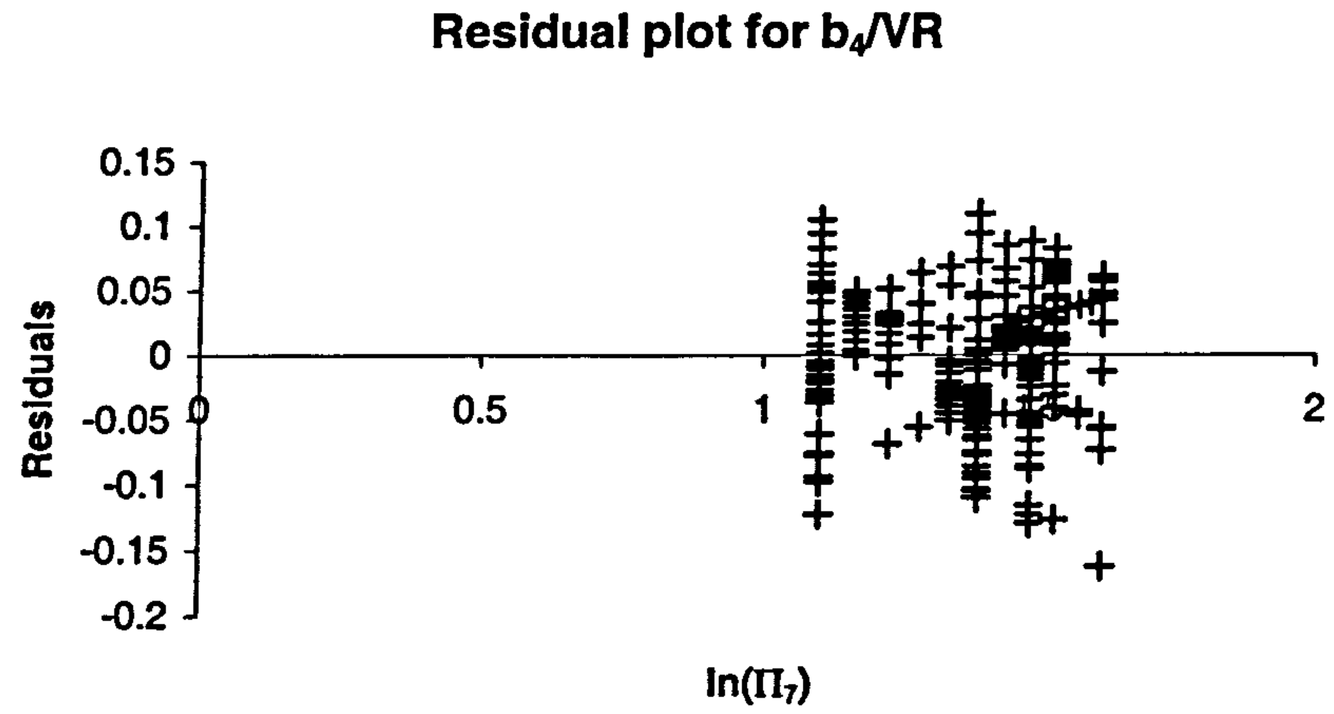

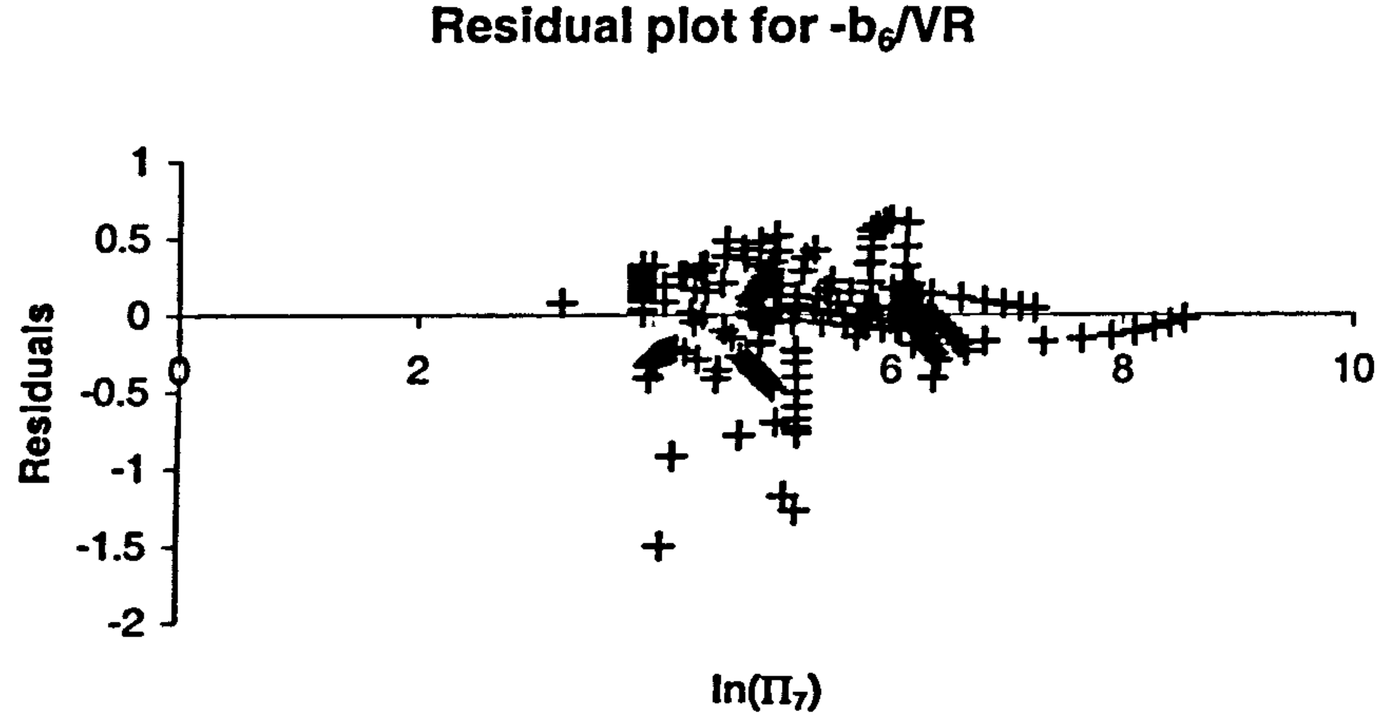

Figure 8.3.2e-g: Residual plots for regression analysis

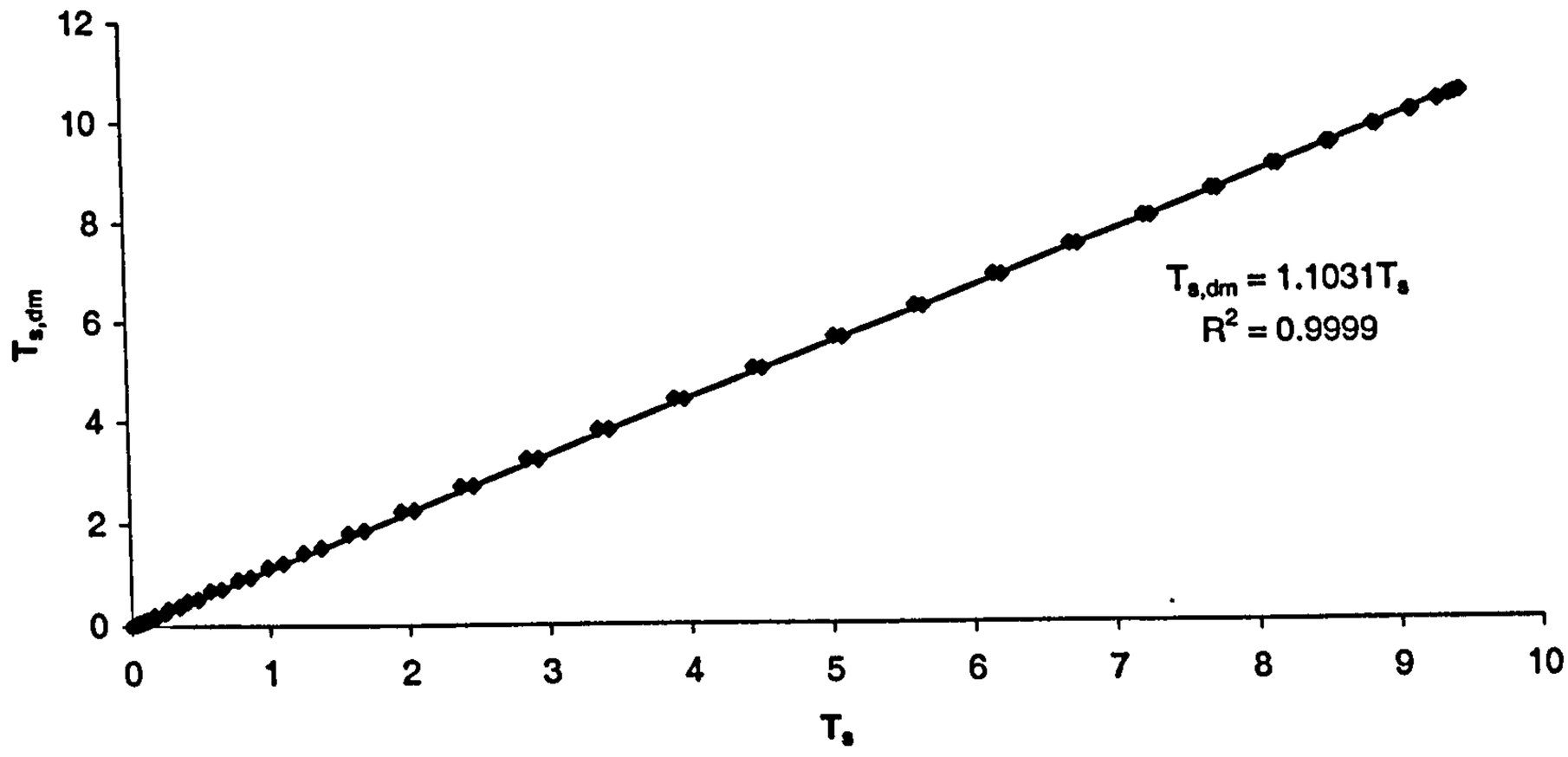

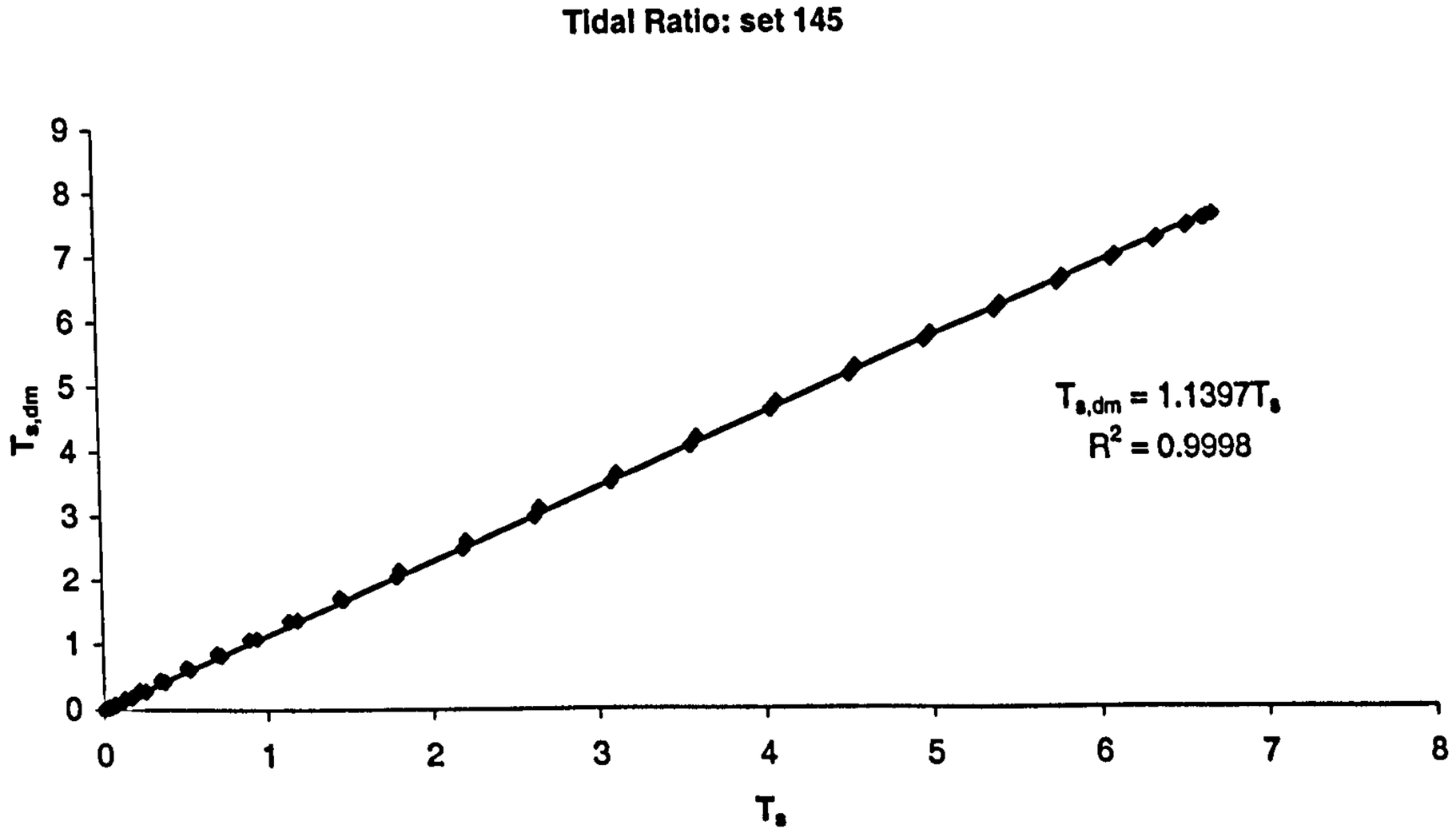

Figure 8.5.1a&b: Relational test of transport (T_s) against transport due to depth-average values (T_{dm}).

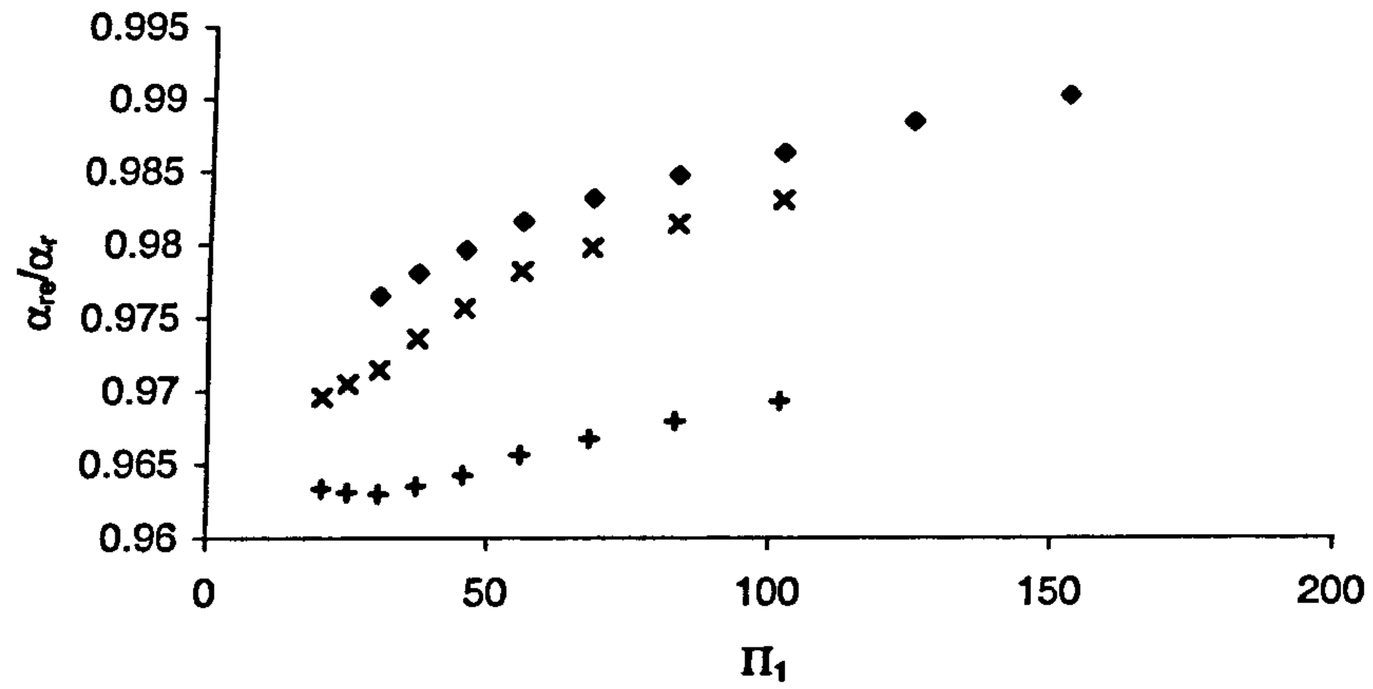

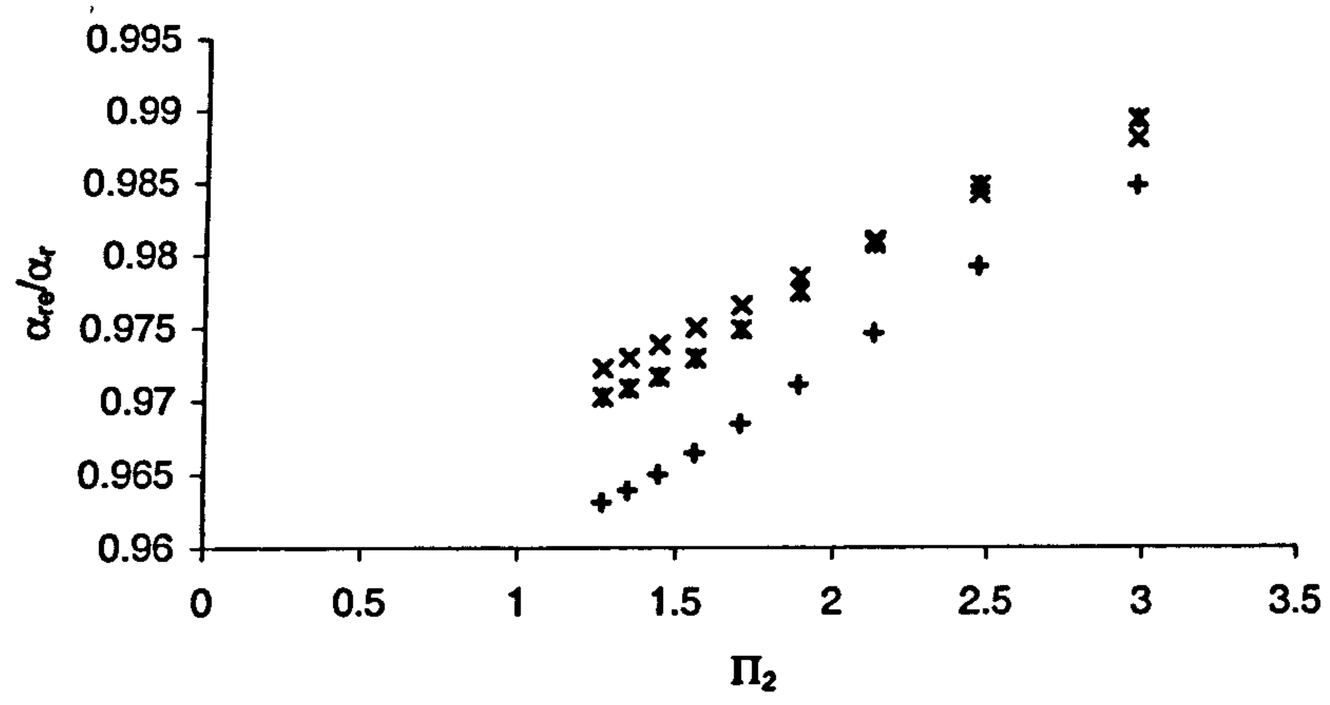

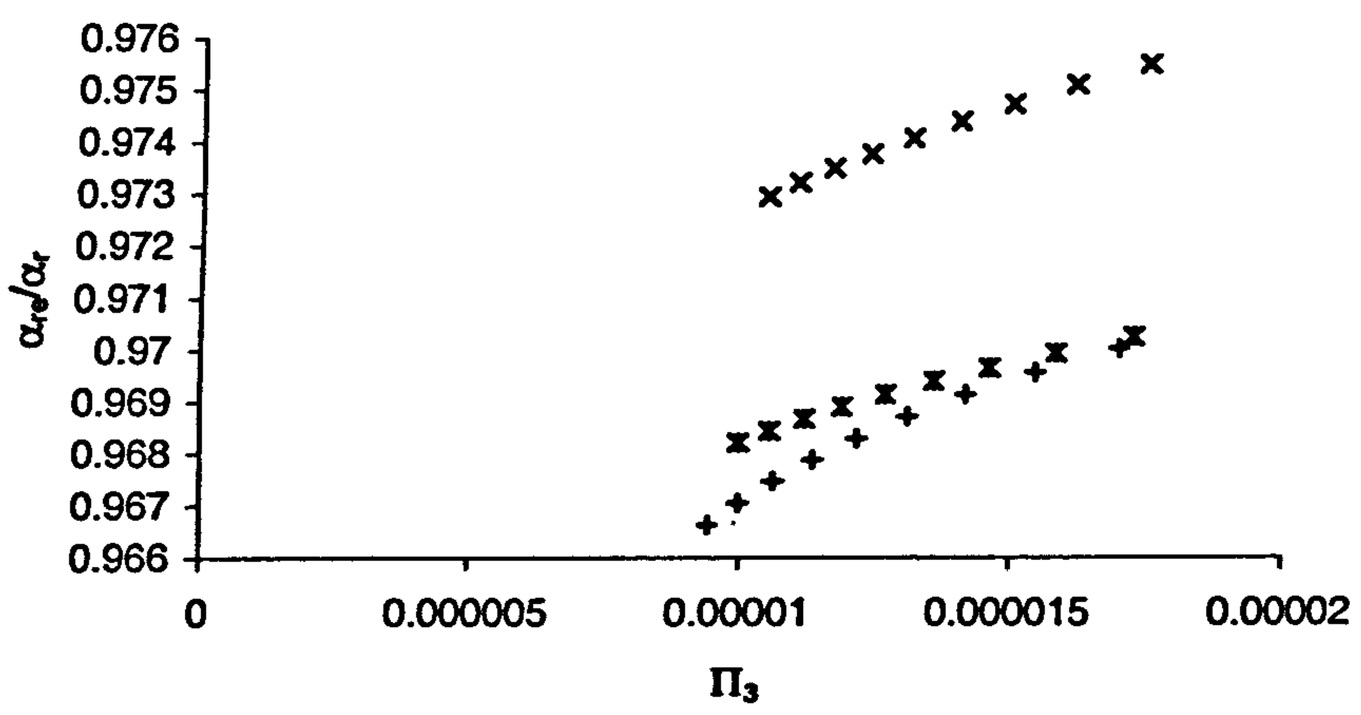

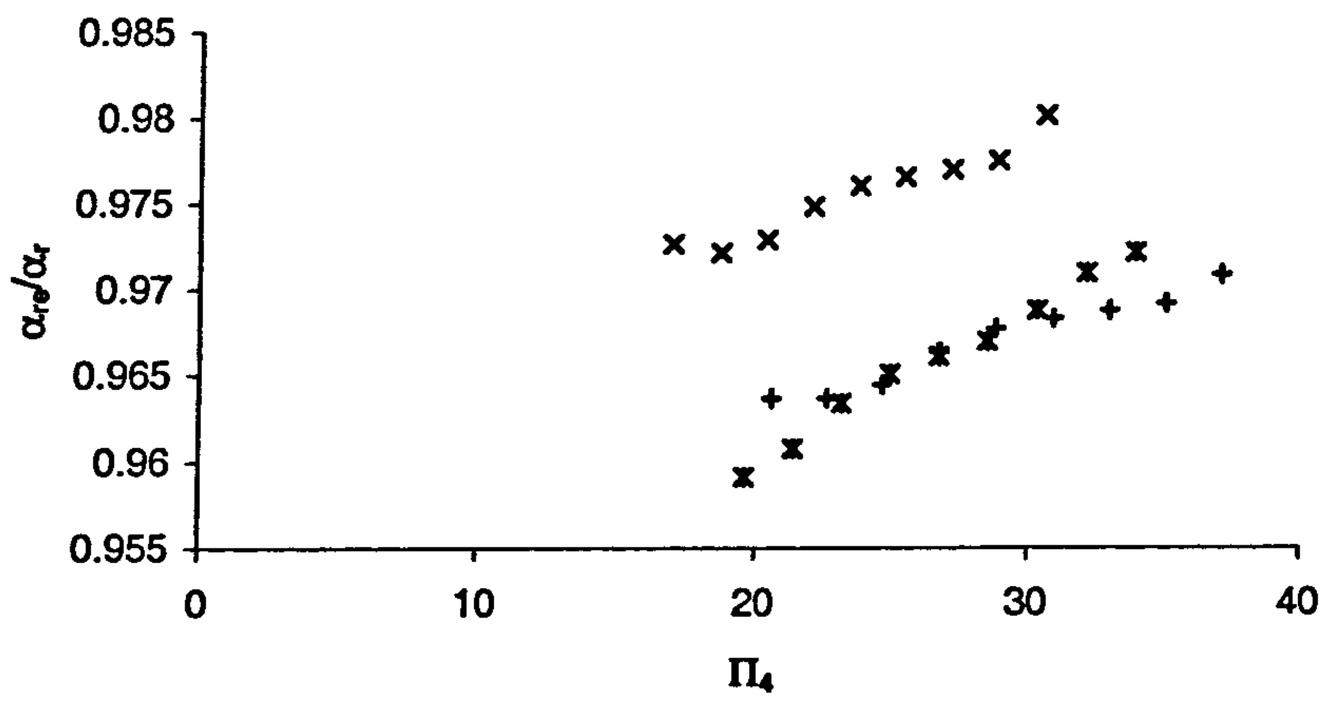

Figure 8.5.2a-d: Parameterisation quantity versus non-dimensional group values for the data sets used in the regression analysis
(Symbols represent the three sets of nine for each group)

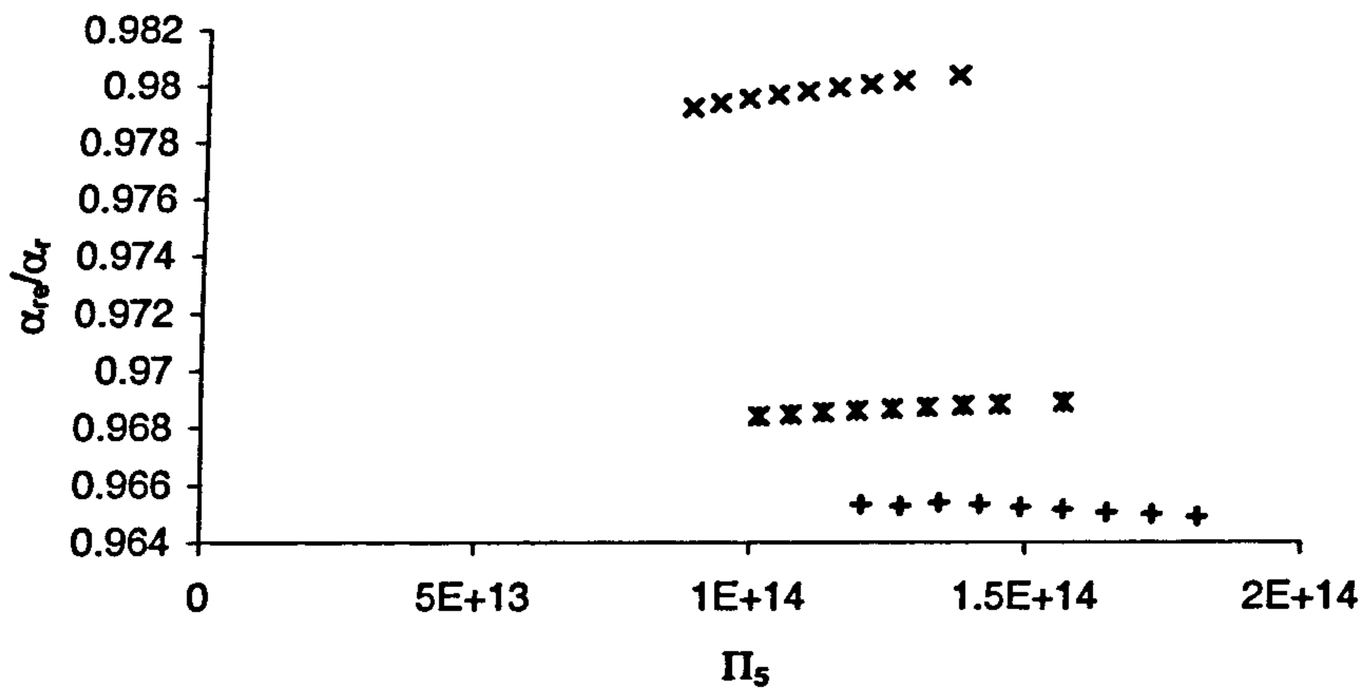

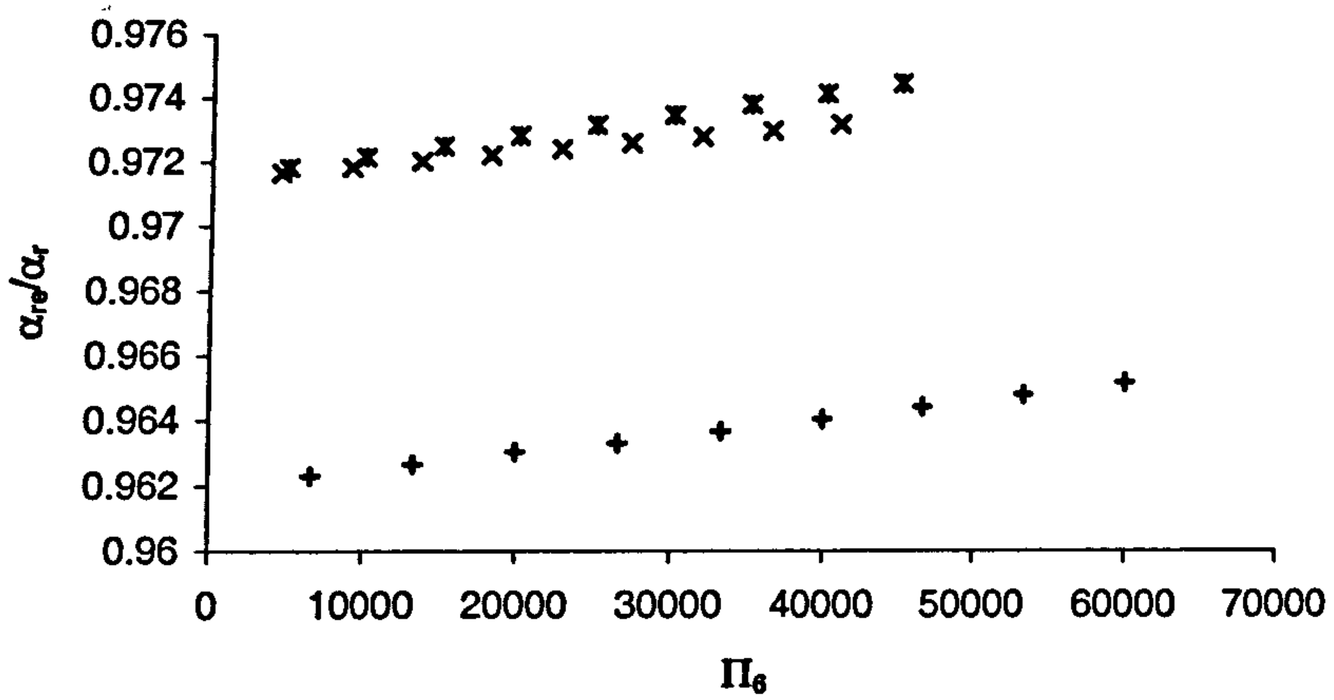

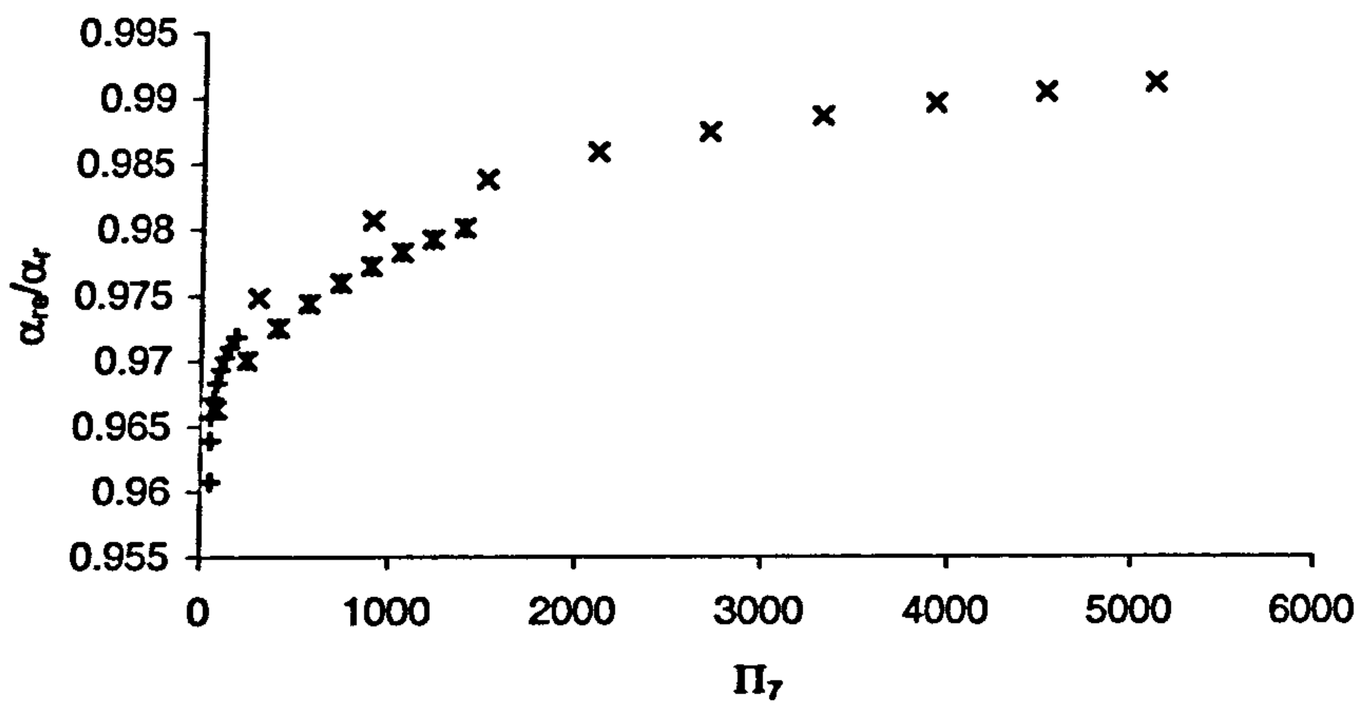

Figure 8.5.2e-g: Parameterisation quantity versus non-dimensional group values for the data sets used in the regression analysis
(Symbols represent the three sets of nine for each group)

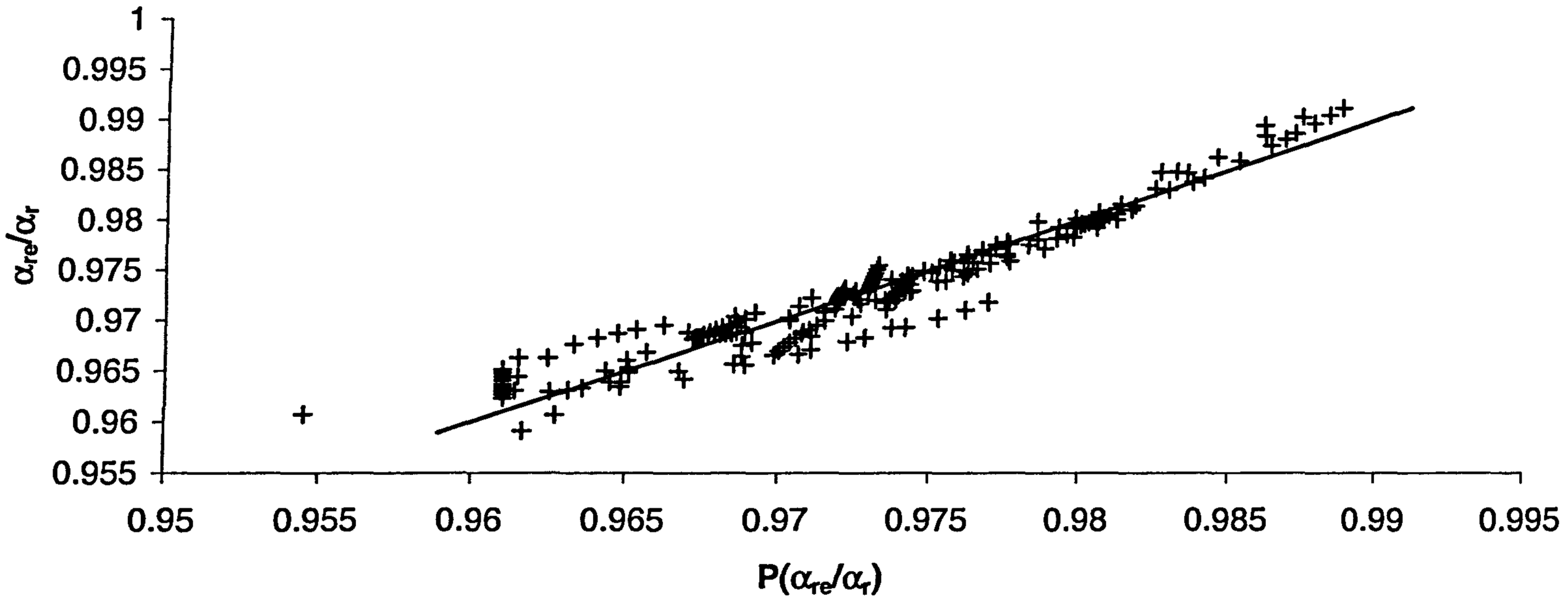

Figure 8.5.3: Parameterised tidal ratio versus values from the numerical 1DV model

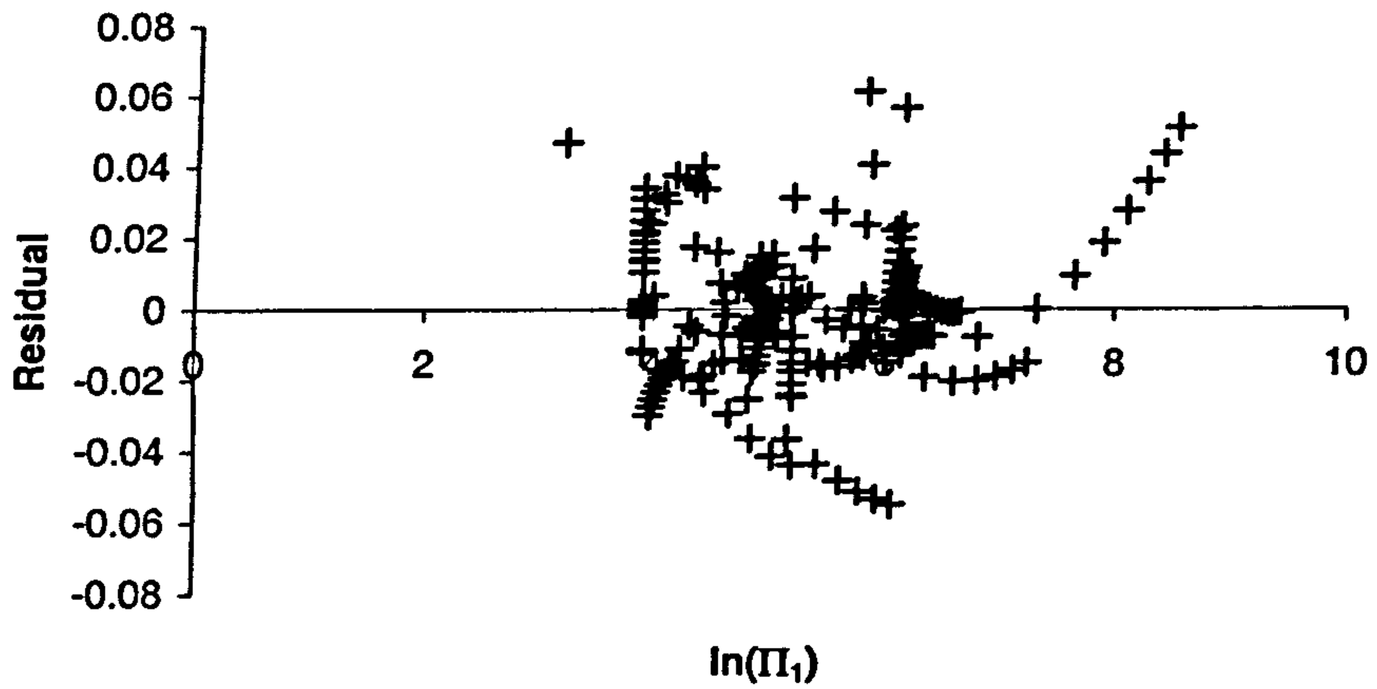

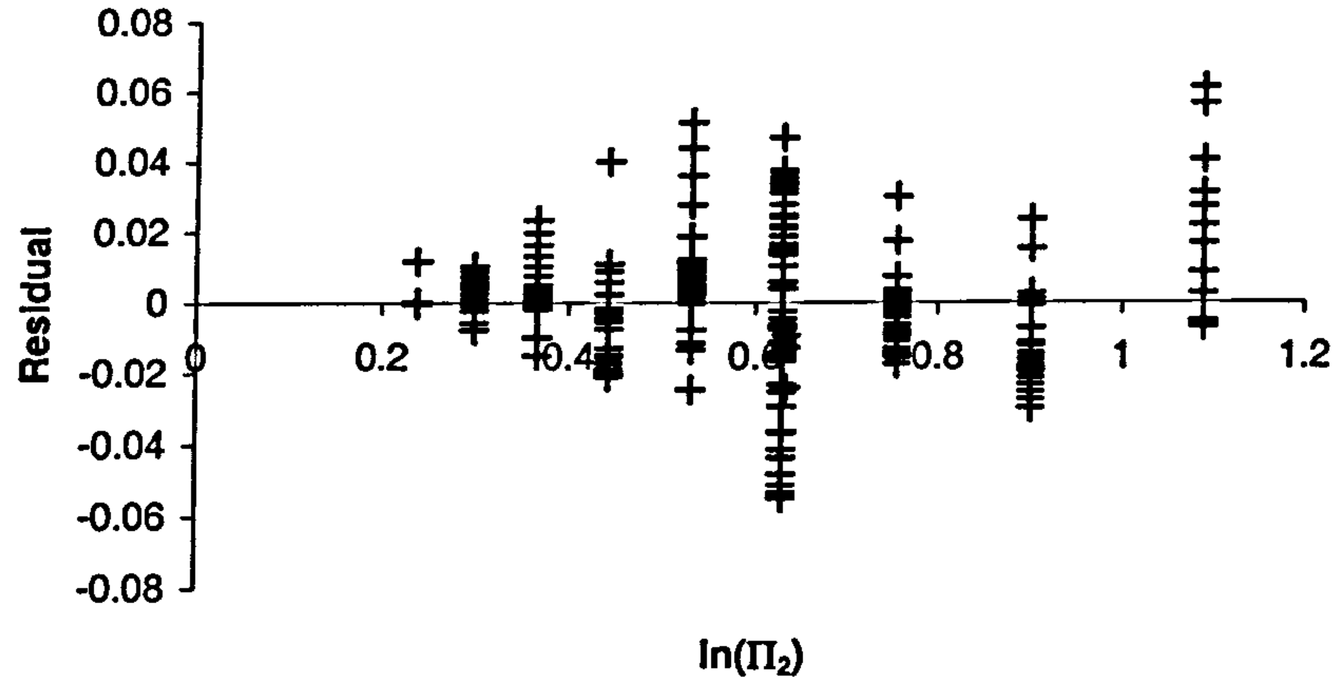

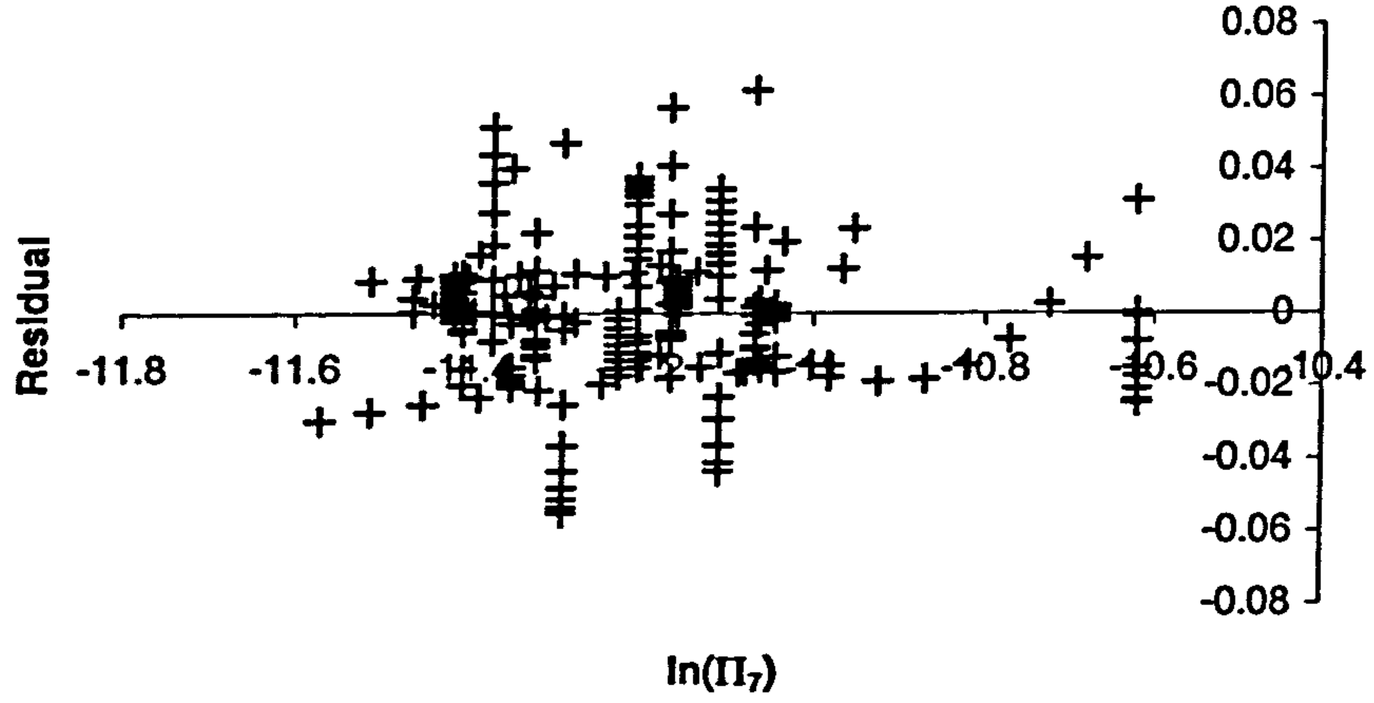

Figure 8.5.4a-c: Residual plots for the parameterisation of the Tidal Ratio

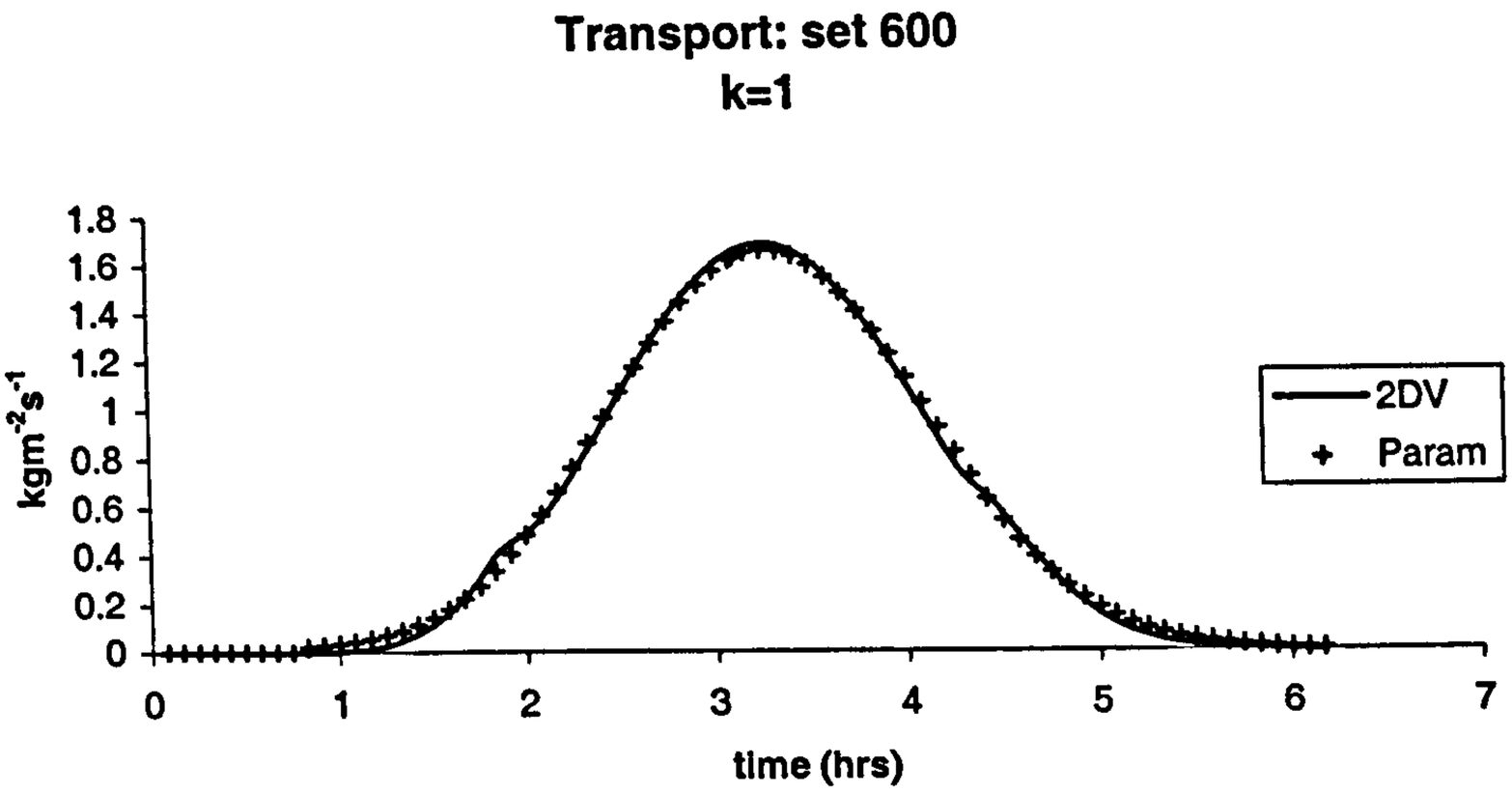

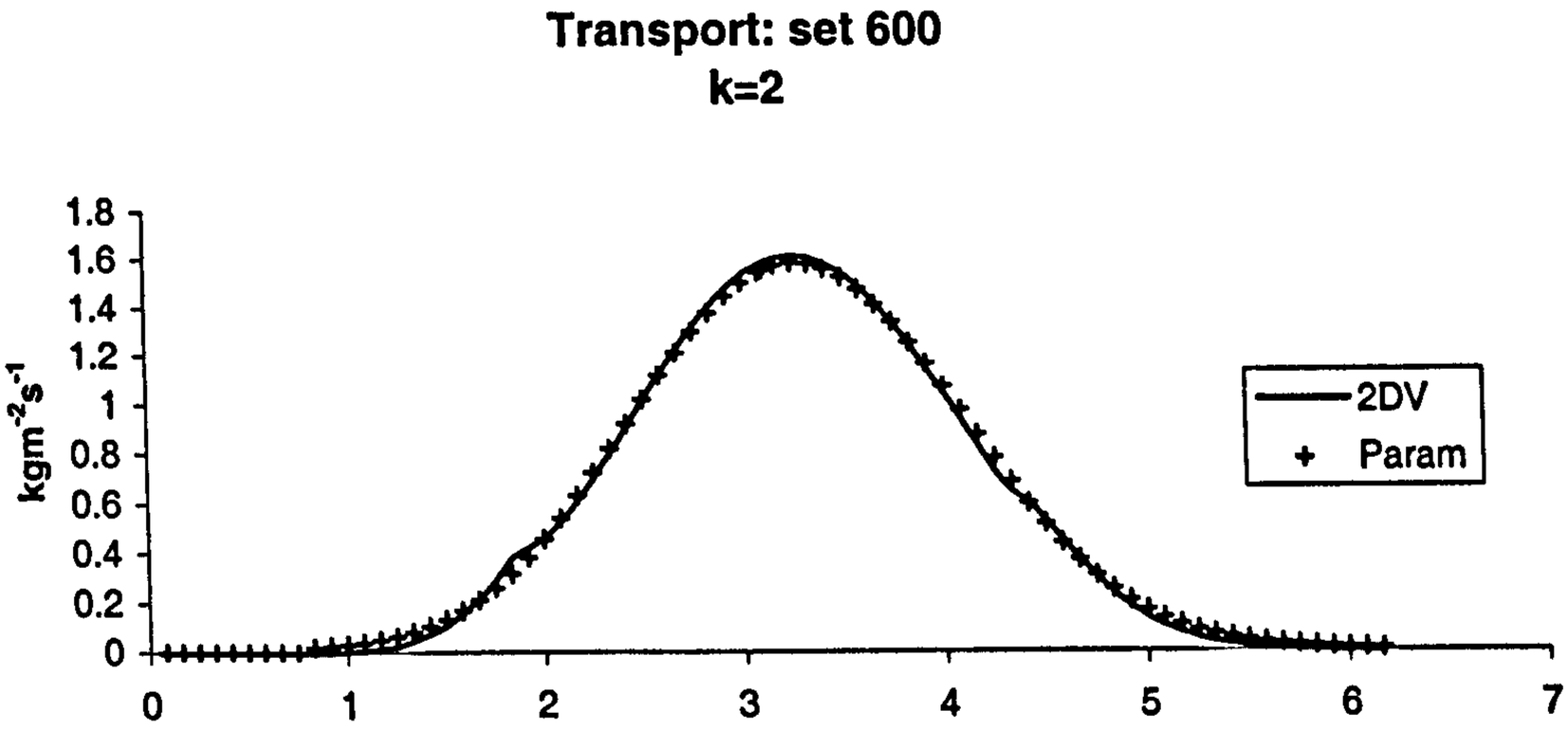

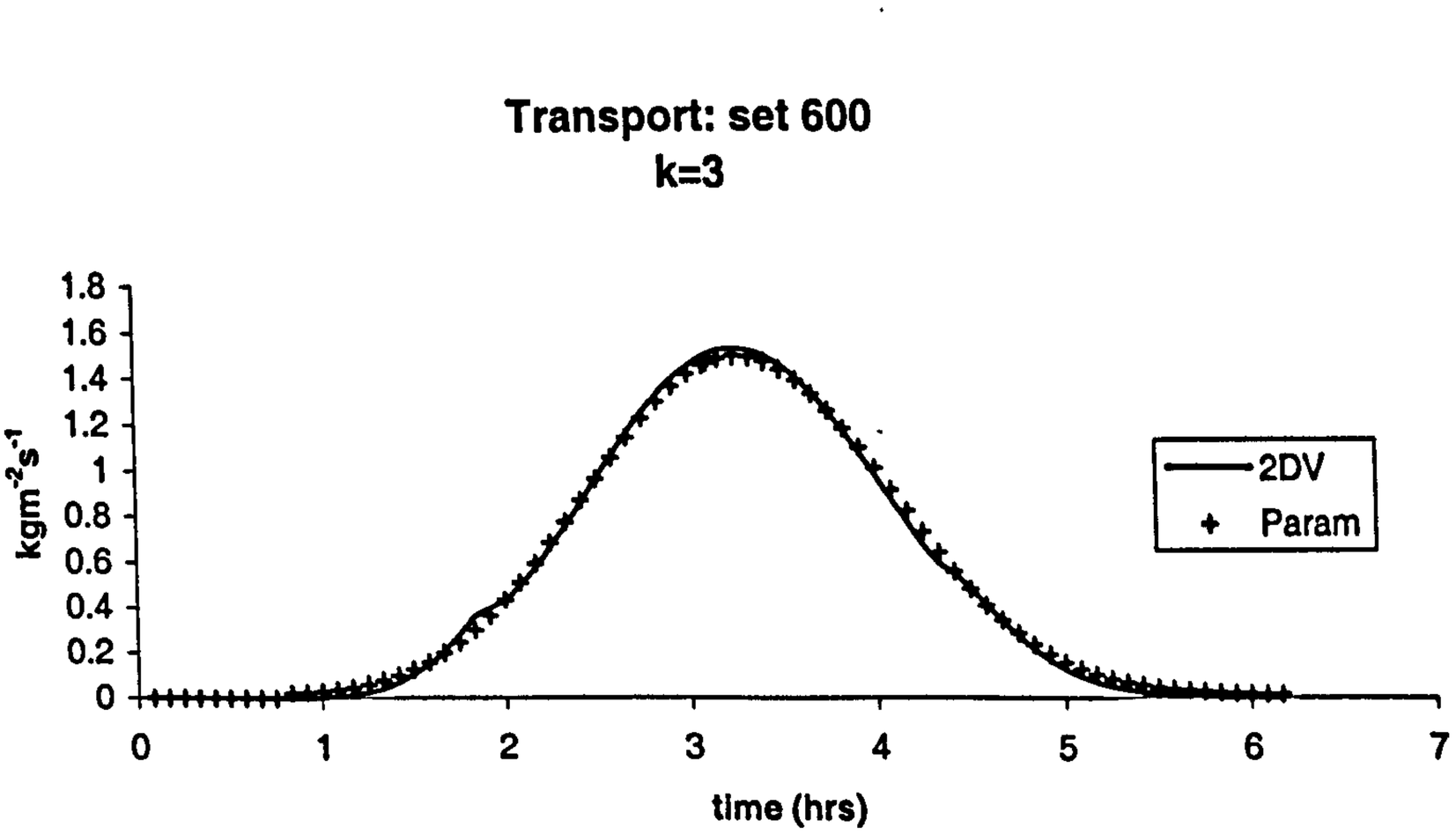

Figure 8.6.1a-c: Comparison between parameterised Corrector (Param) and conventional 2DV (2DV)

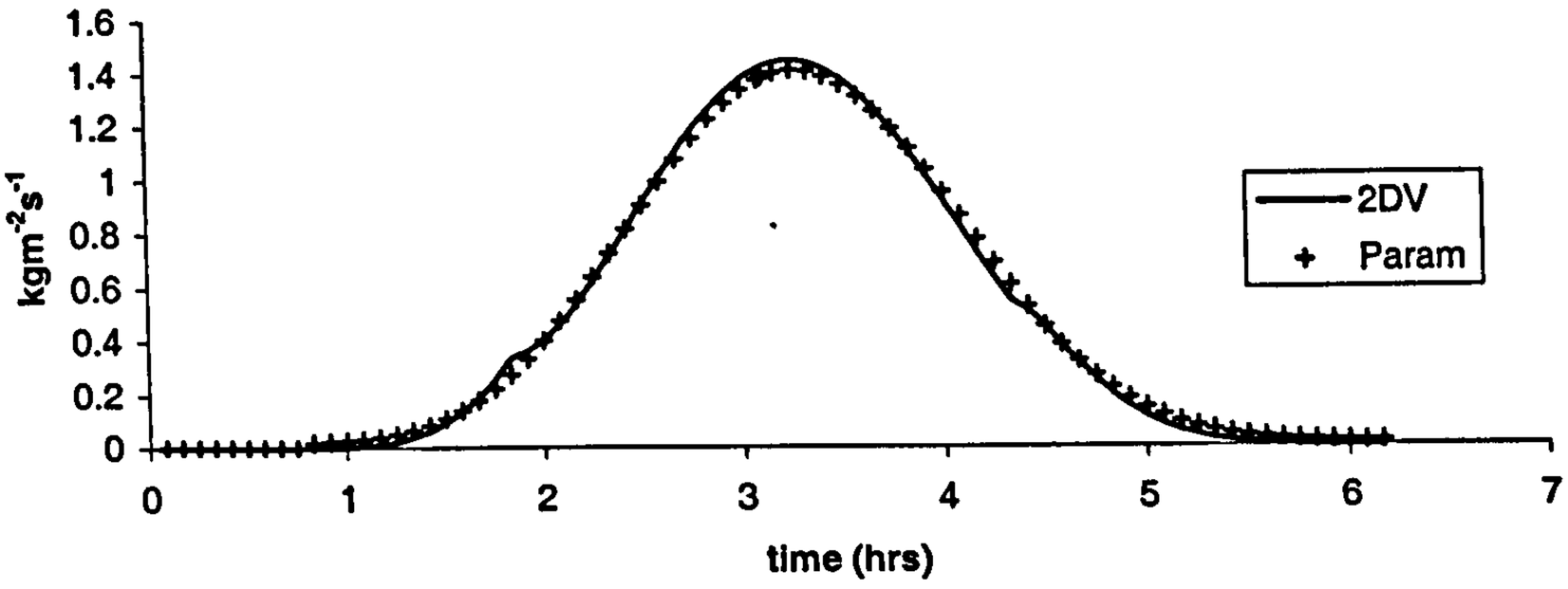

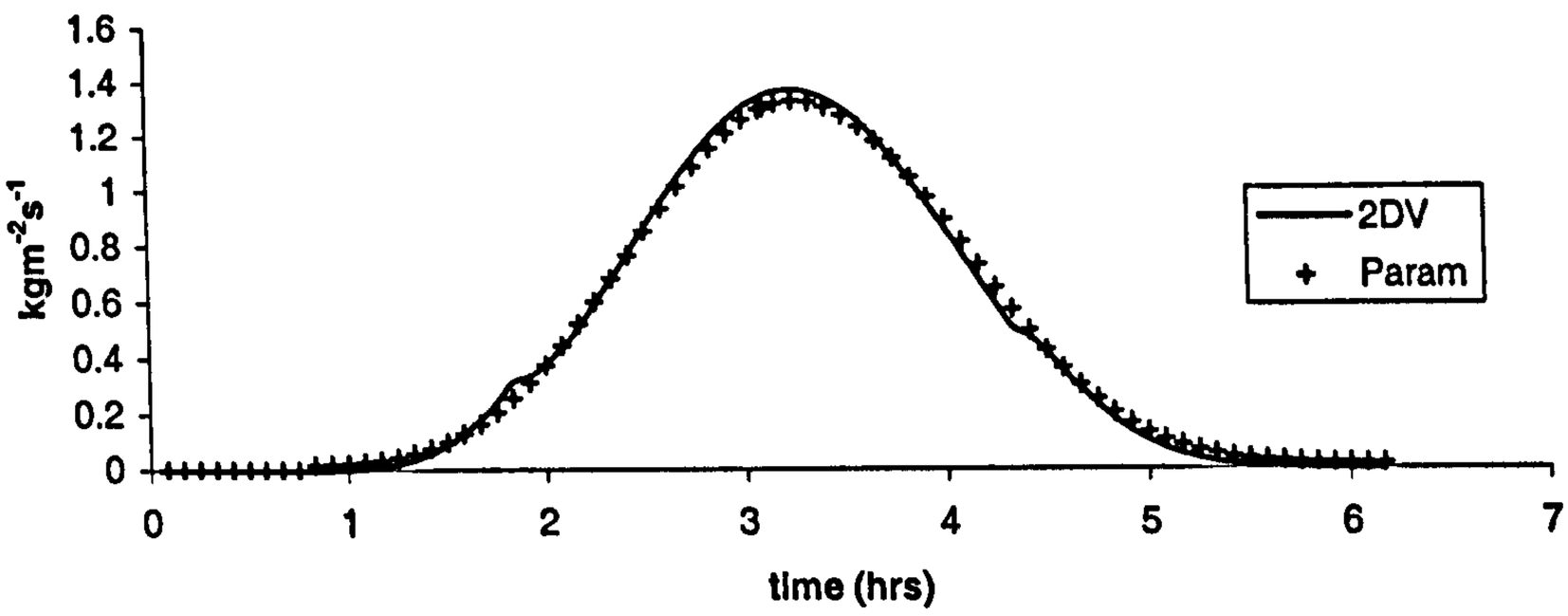

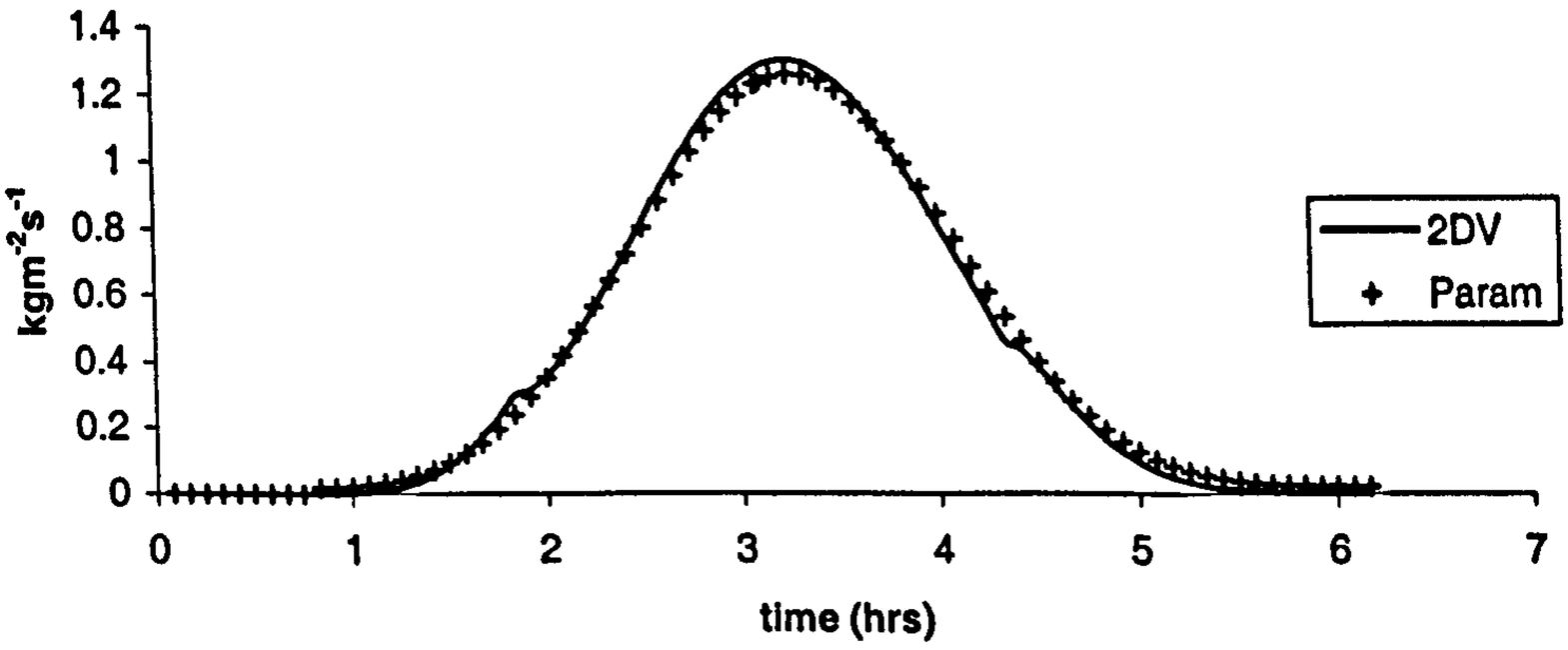

Figure 8.6.1d-f: Comparison between parameterised Corrector (Param) and conventional 2DV (2DV)

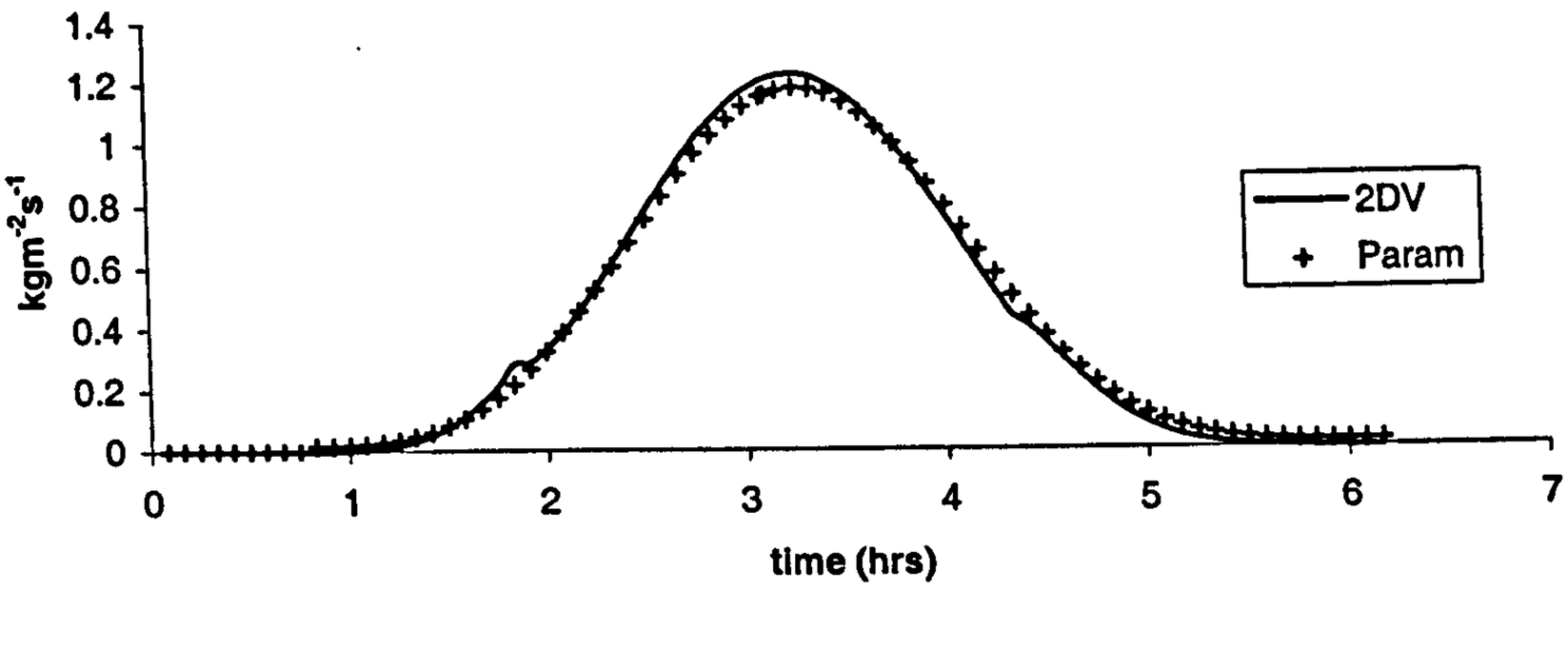

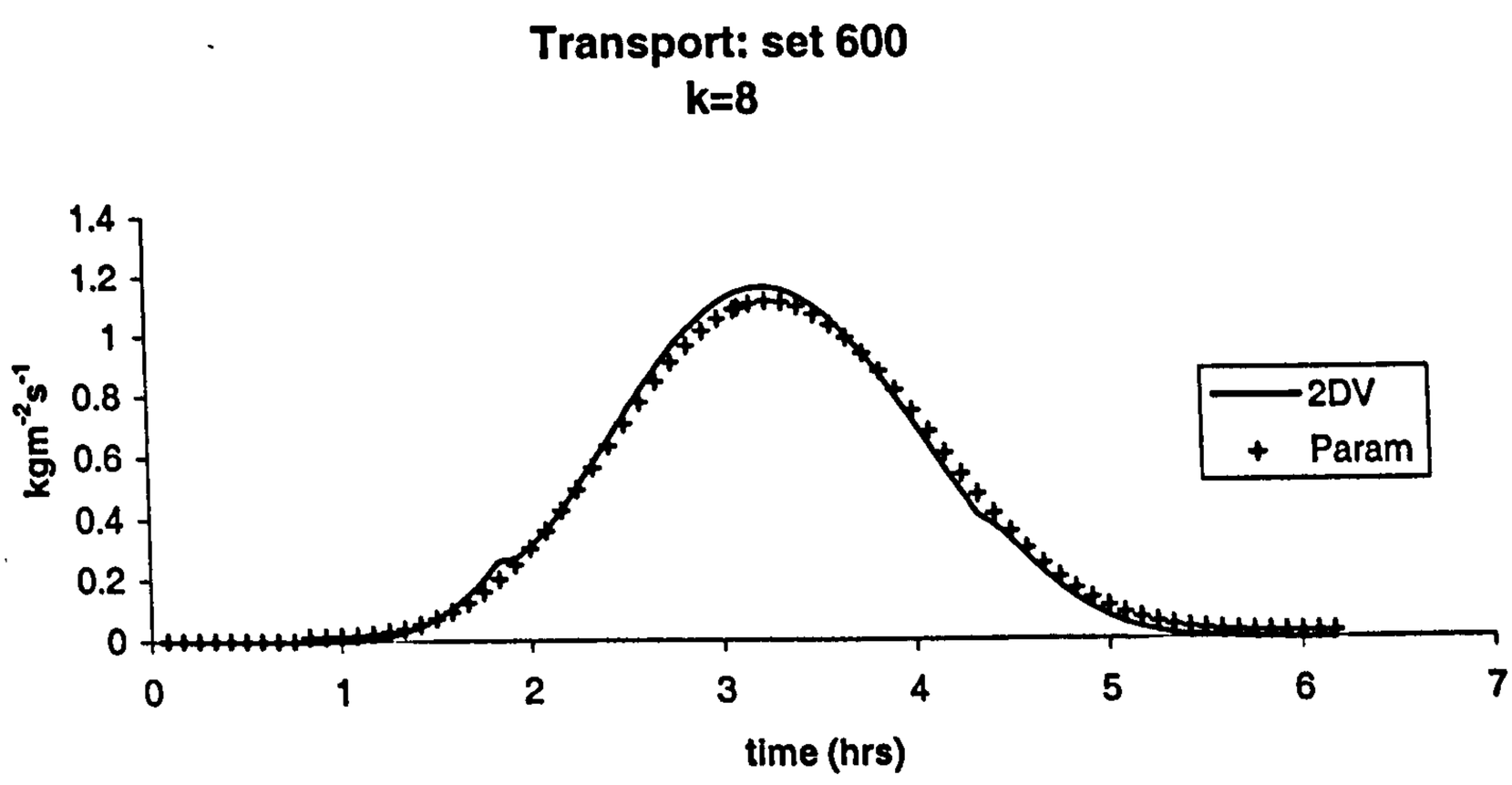

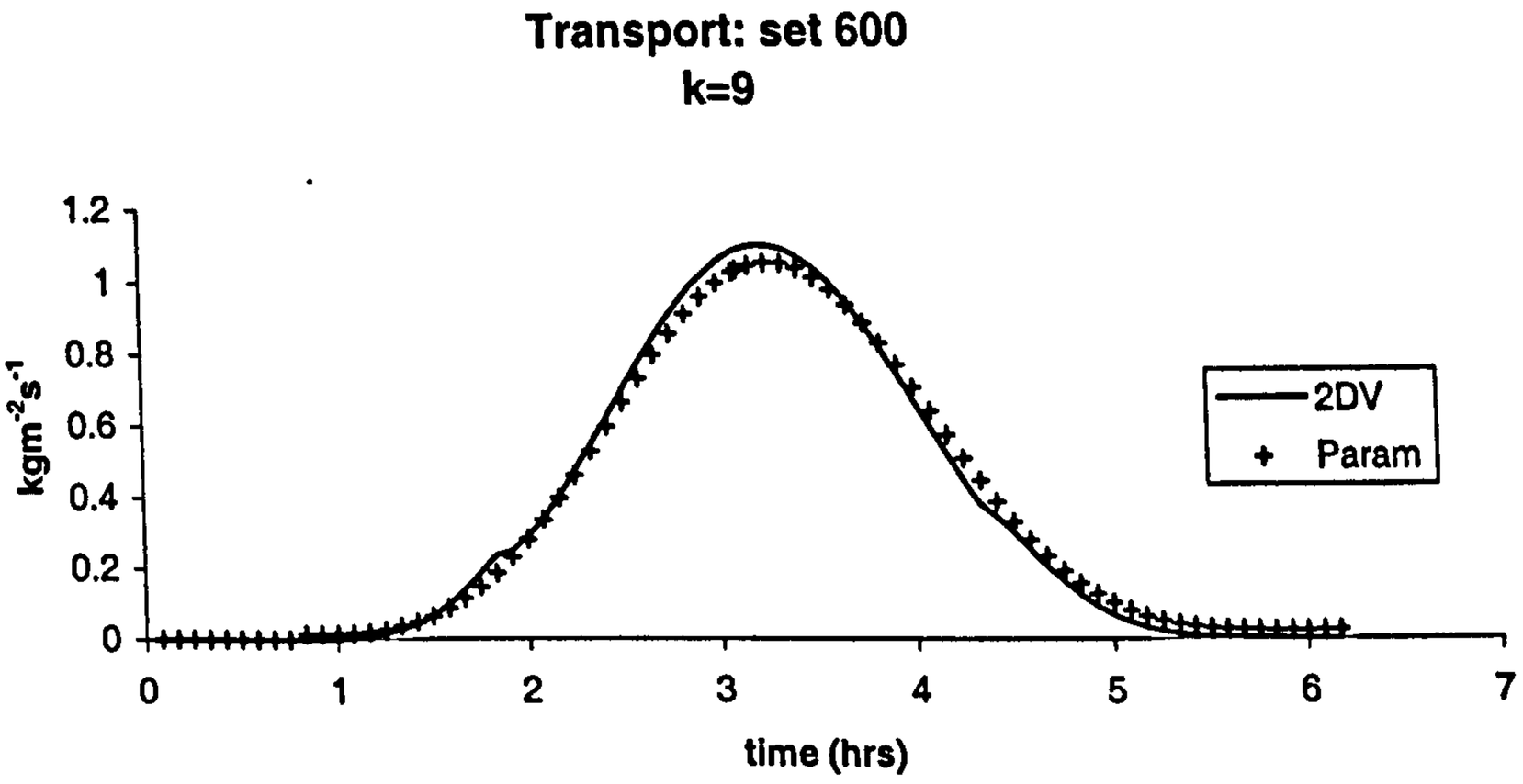

Figure 8.6.1g-i: Comparison between parameterised Corrector (Param) and conventional 2DV (2DV)

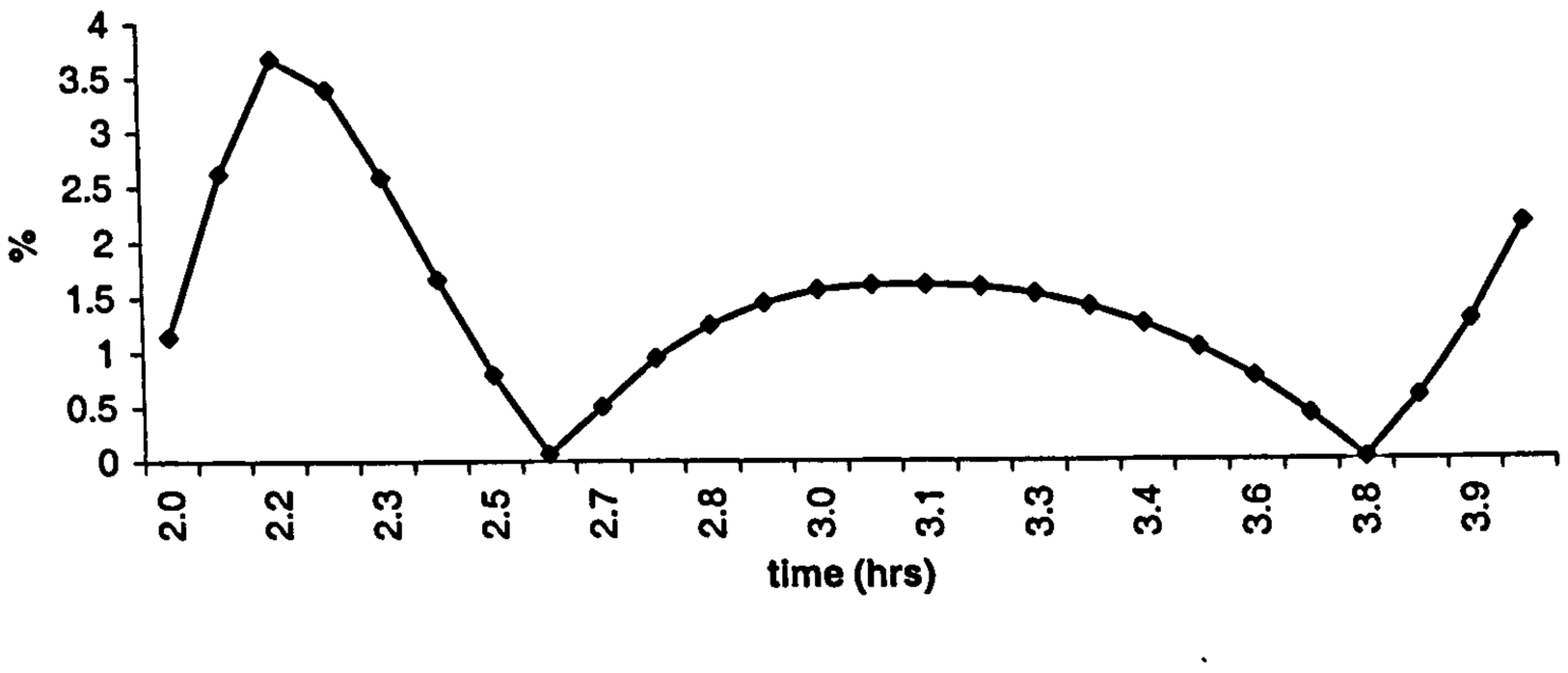

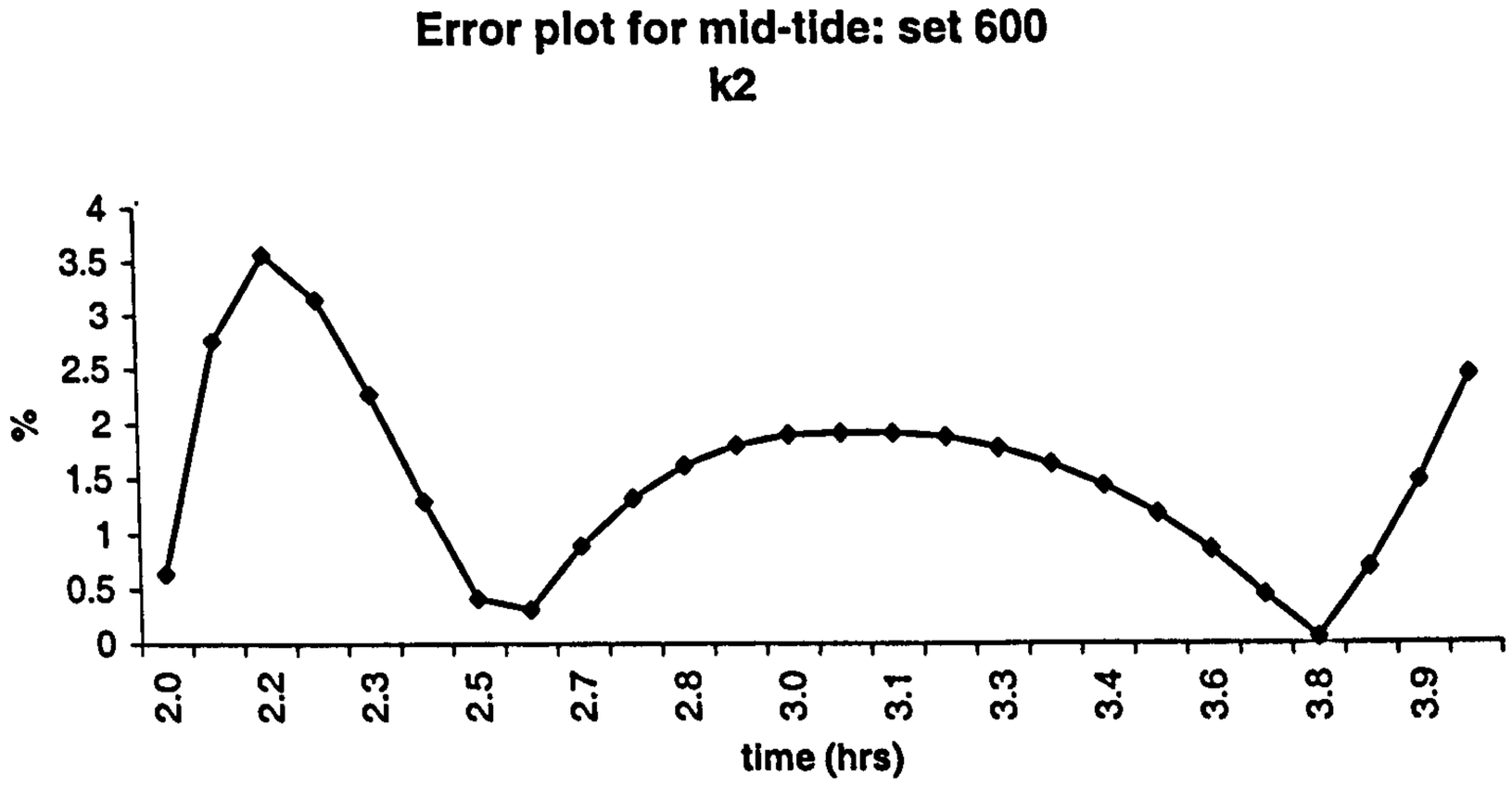

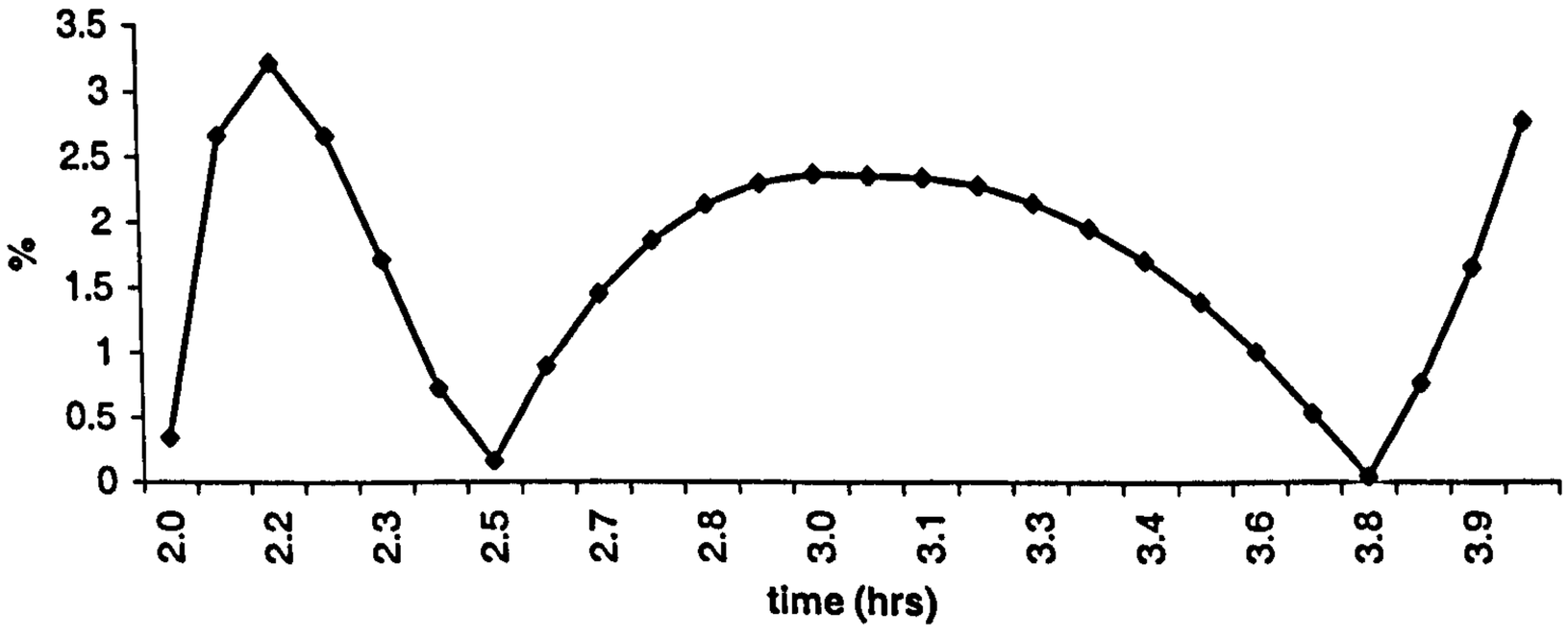

Figure 8.6.2a-c: Error between conventional 2DV method and parameterised Corrector method during the mid-tide phase.

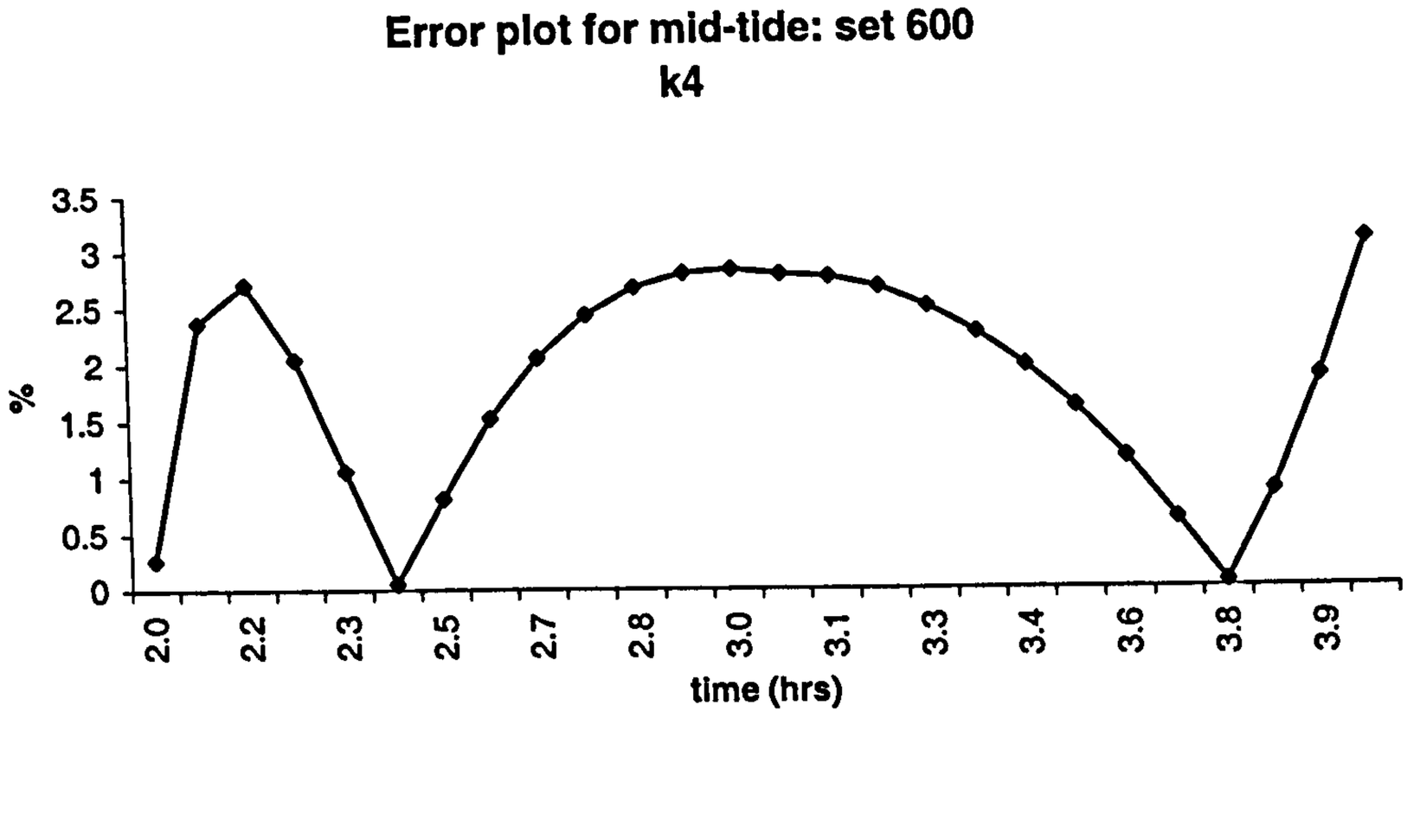

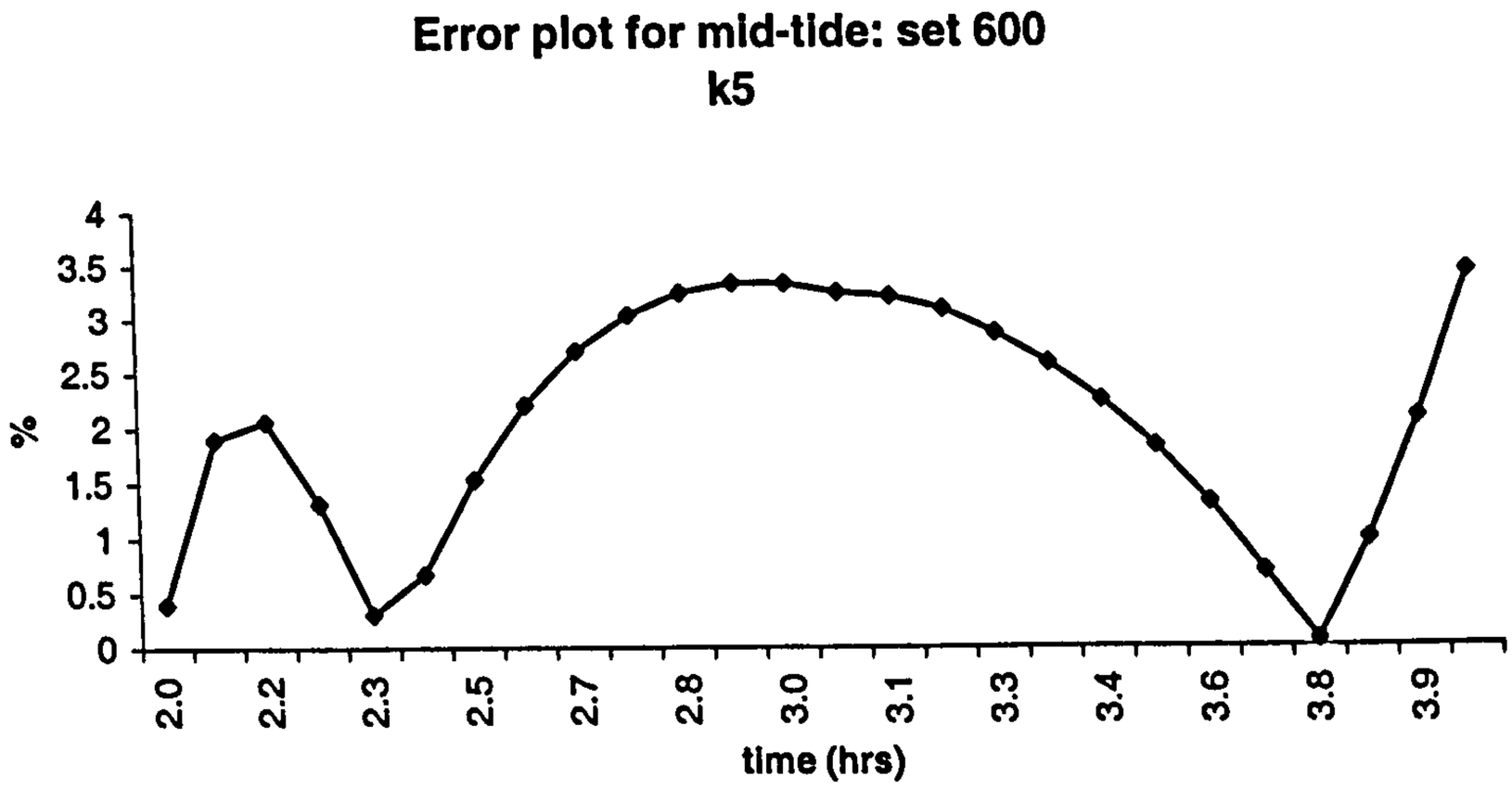

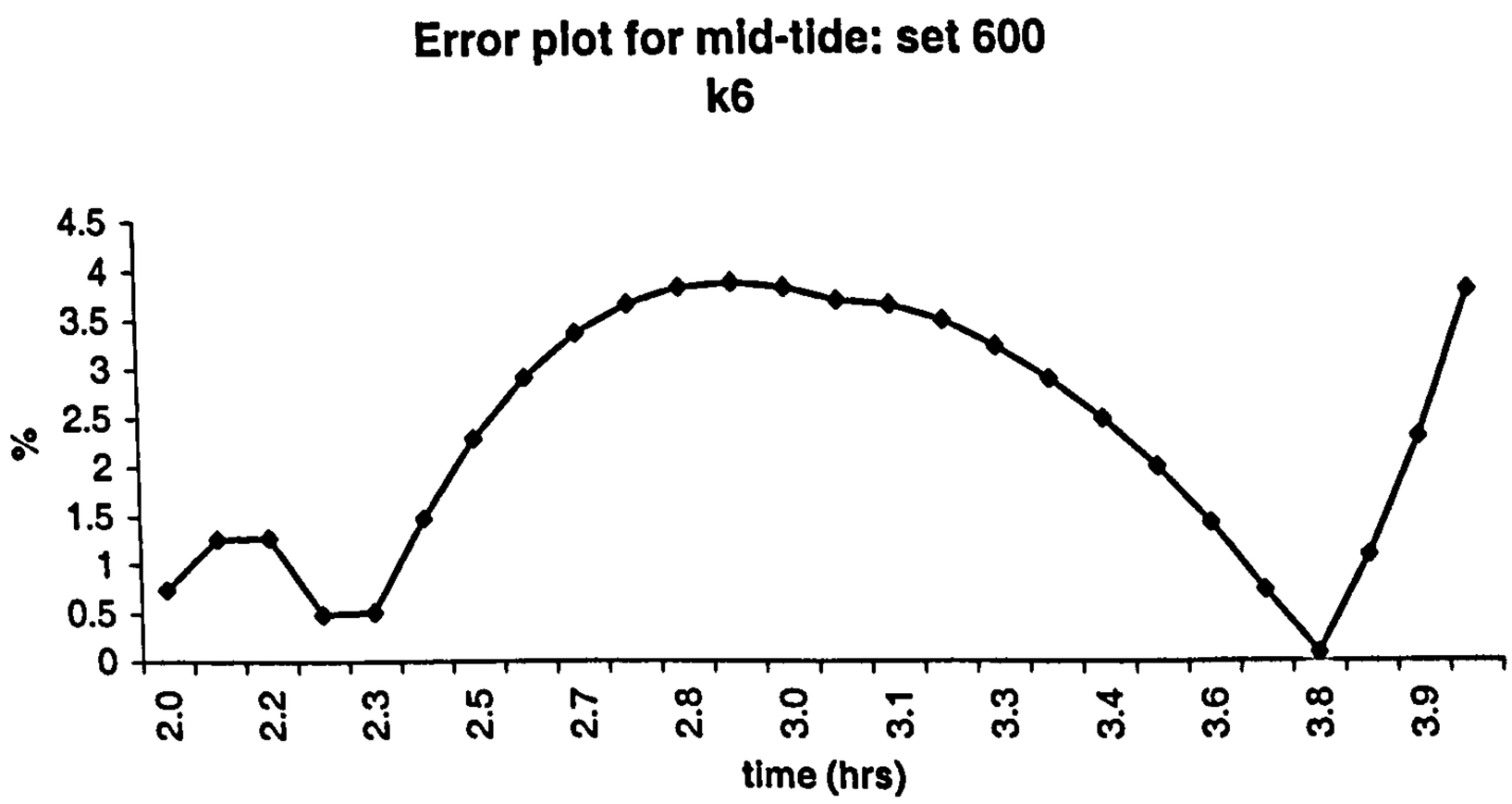

Figure 8.6.2d-f: Error between conventional 2DV method and parameterised Corrector method during the mid-tide phase.

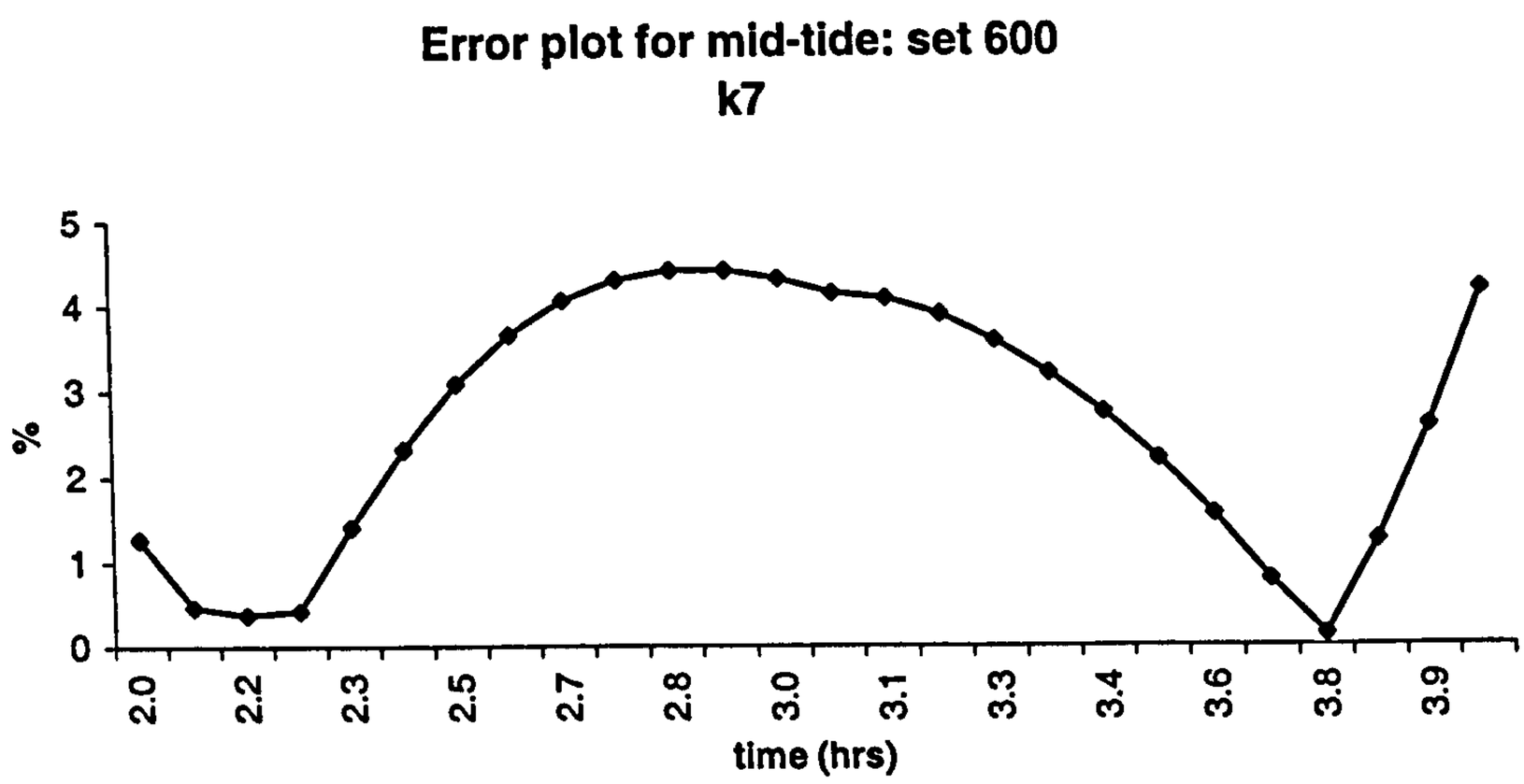

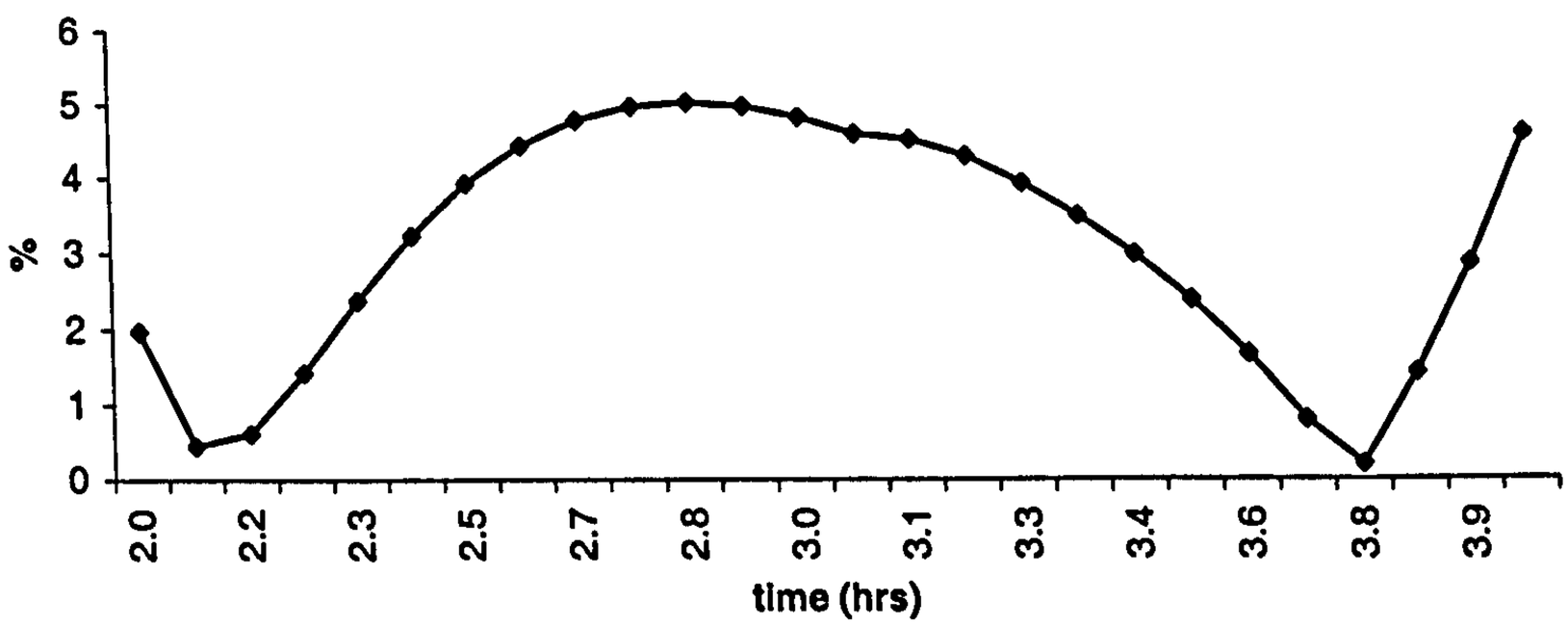

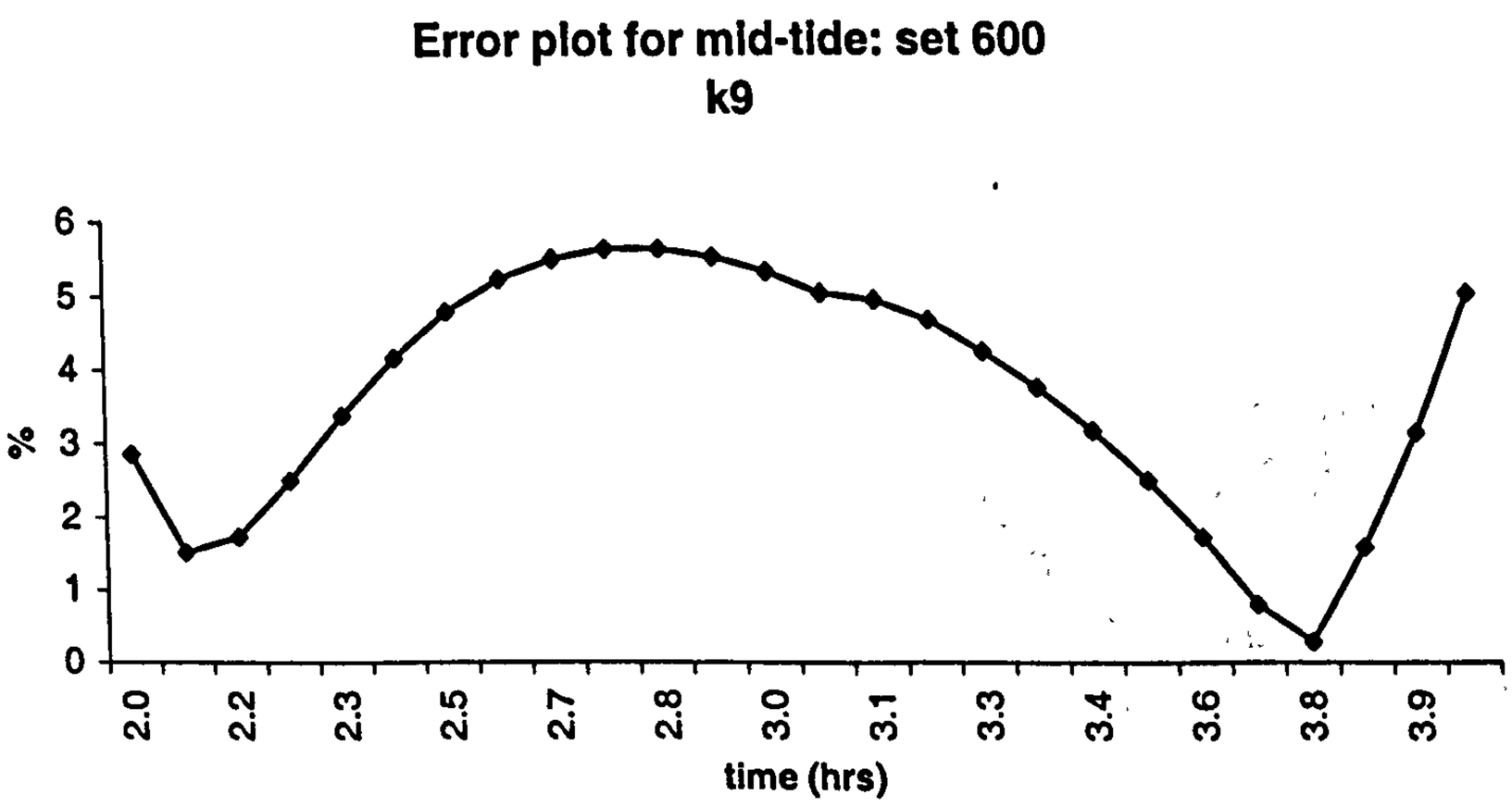

Figure 8.6.2g-i: Error between conventional 2DV method and parameterised Corrector method during the mid-tide phase.

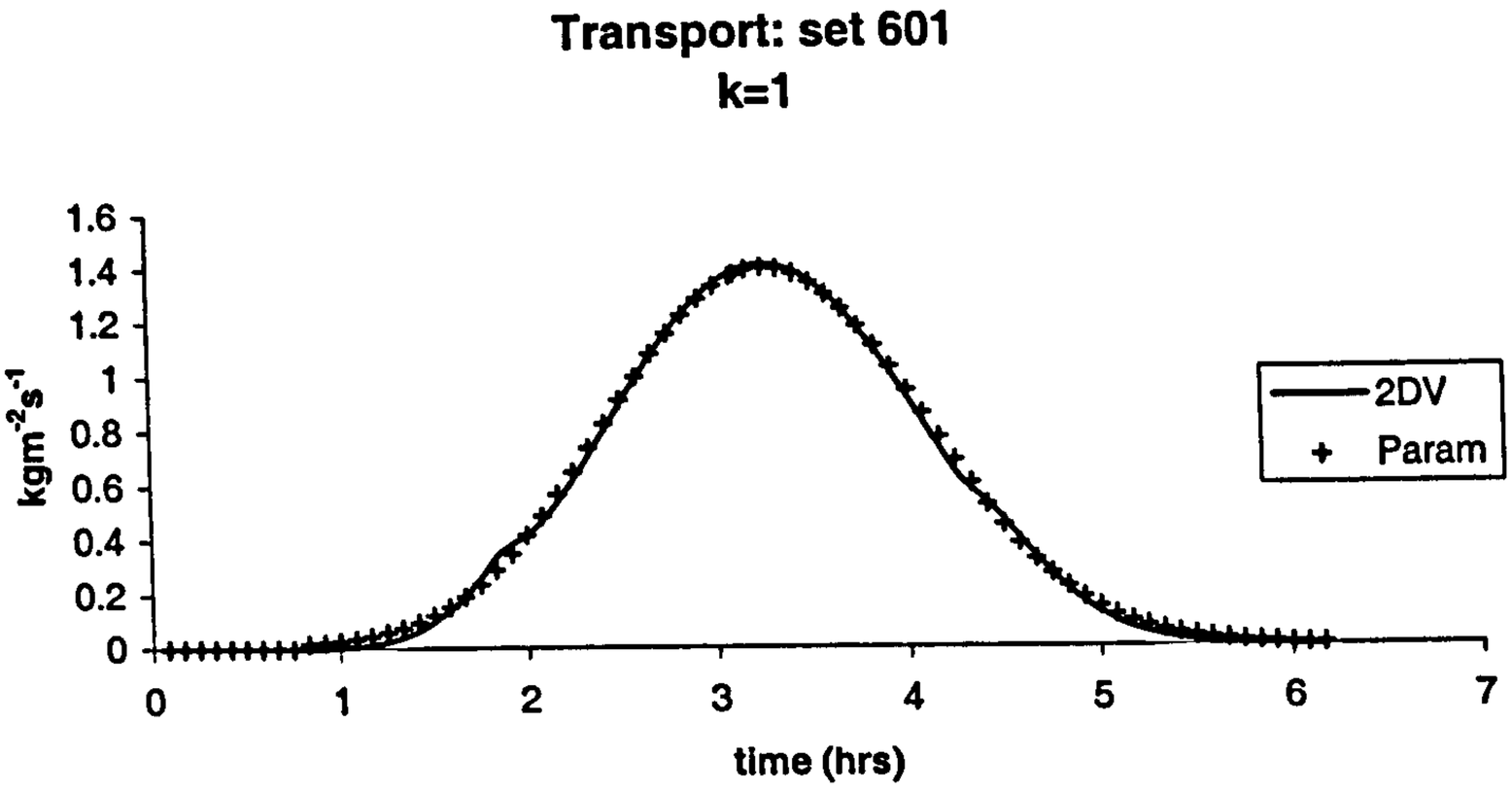

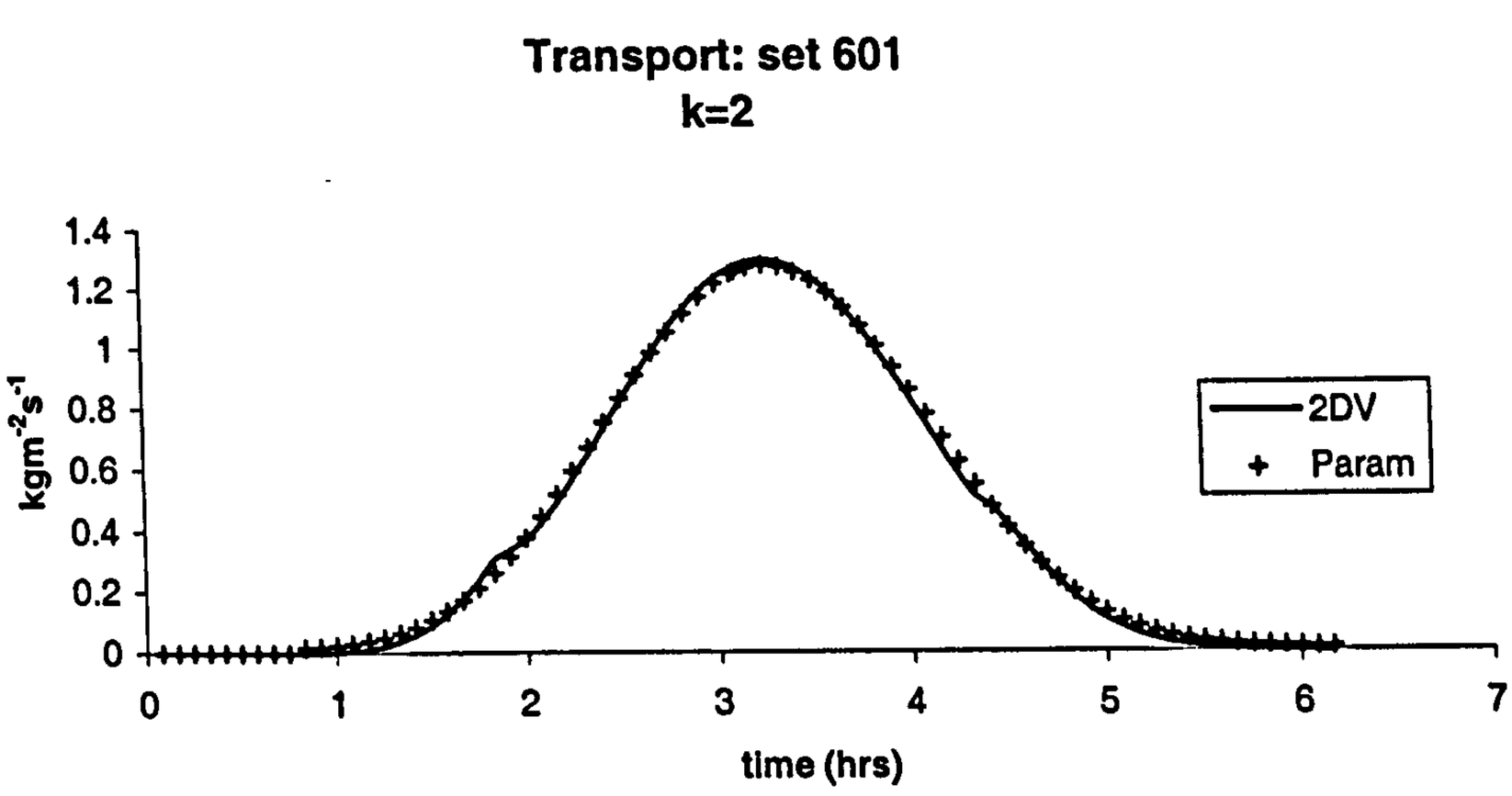

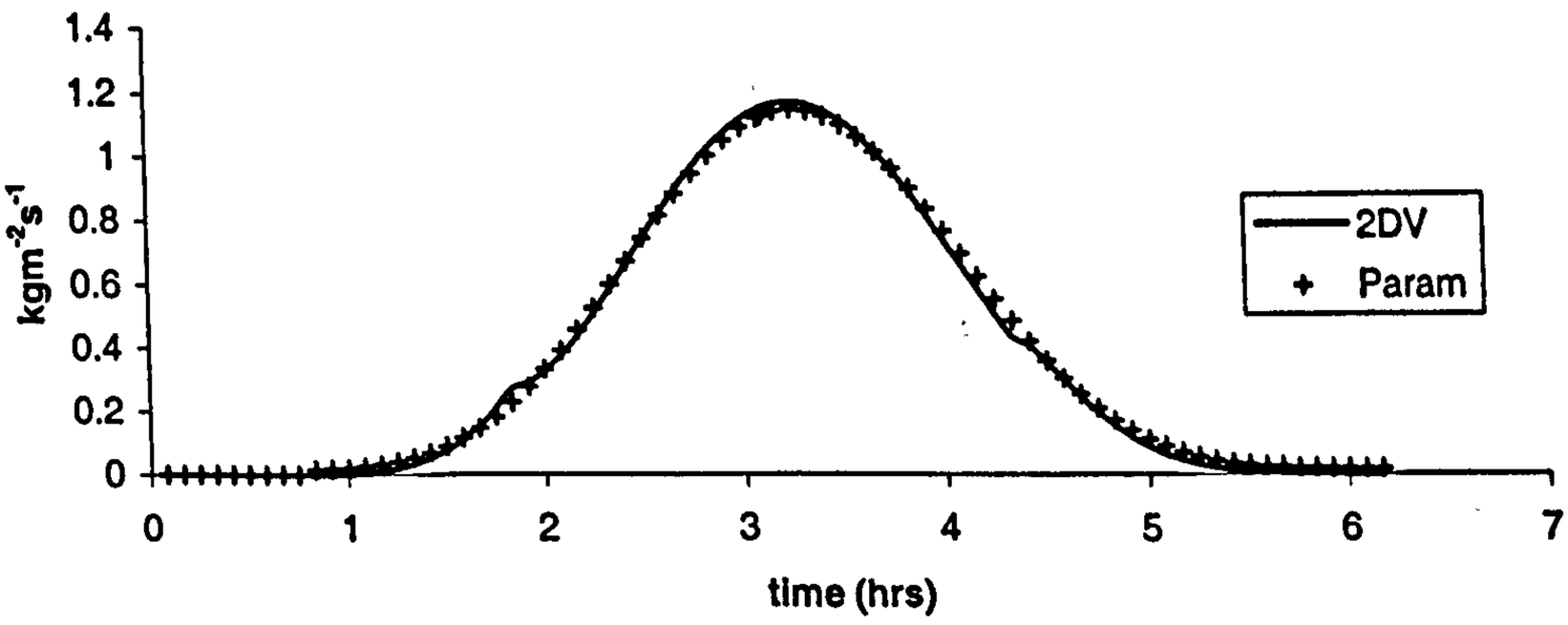

Figure 8.6.3a-c: Comparison between parameterised Corrector method (Param) and conventional 2DV (2DV)

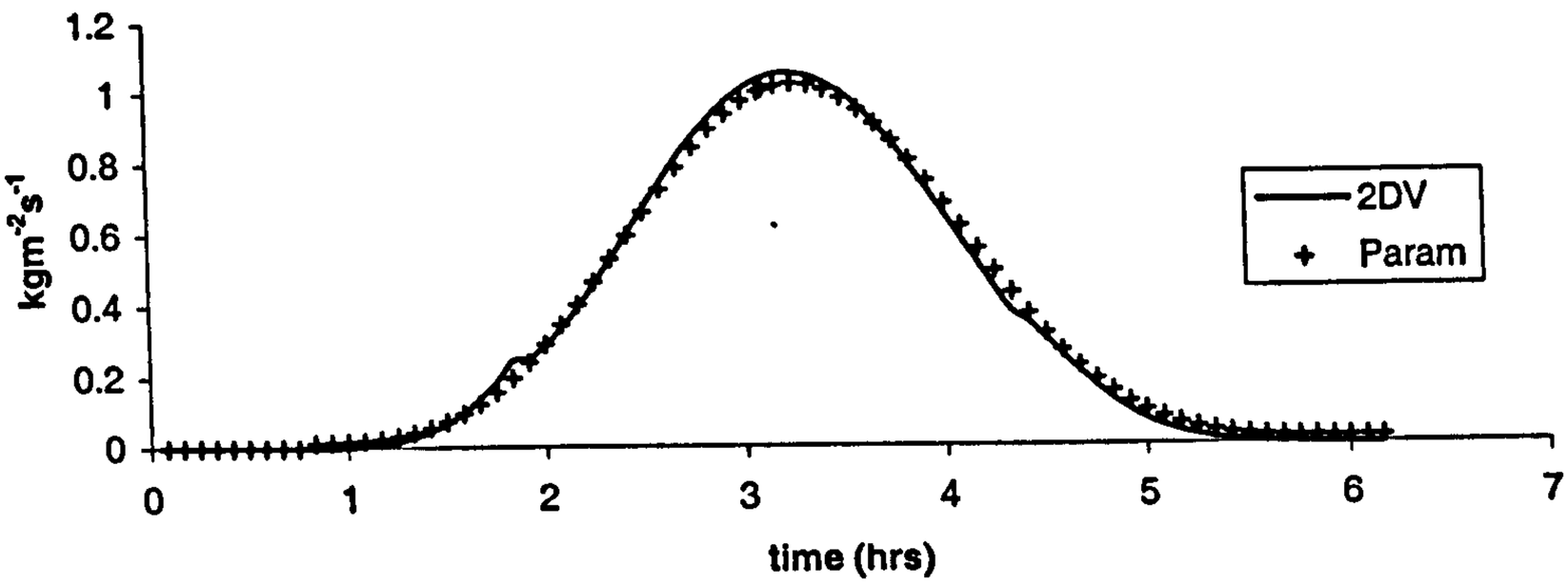

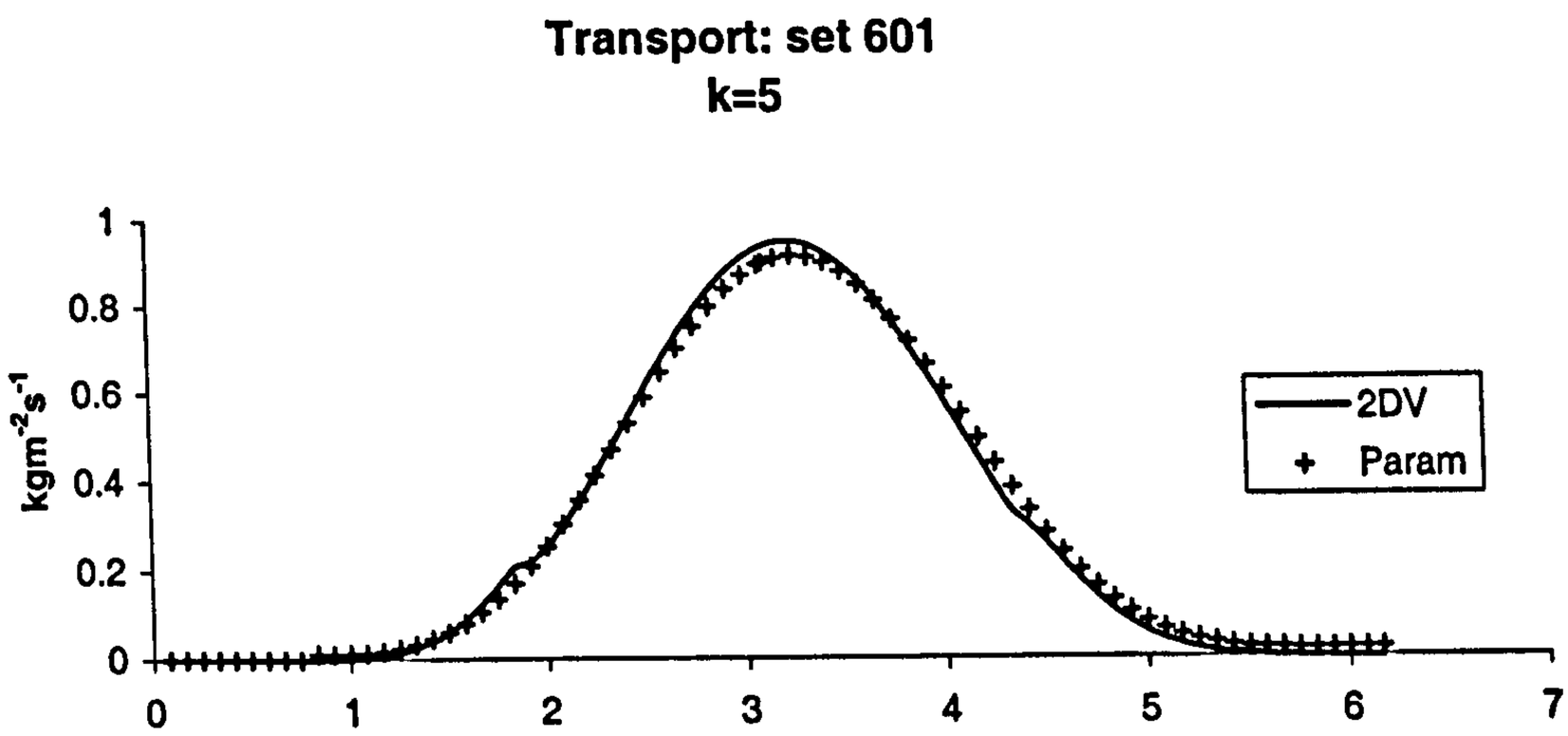

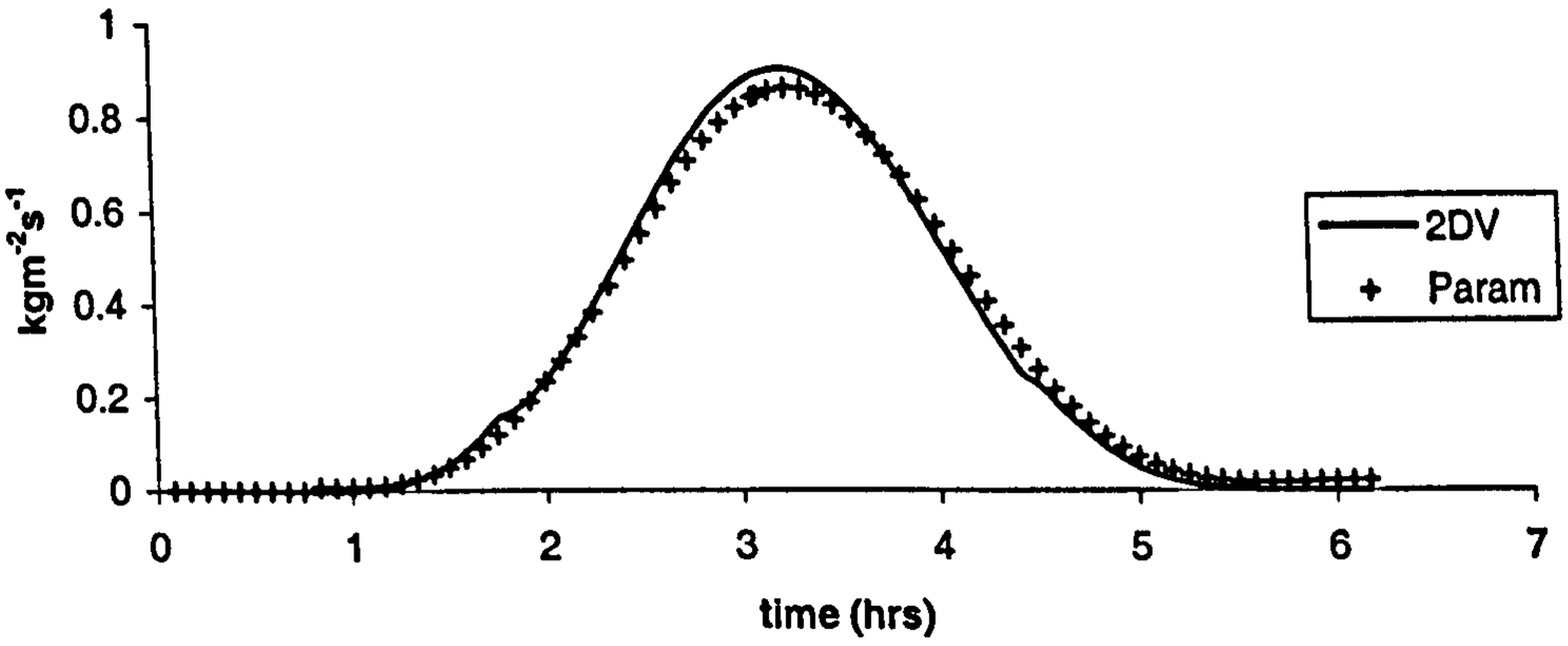

Figure 8.6.3d-f: Comparison between parameterised Corrector method (Param) and conventional 2DV (2DV)

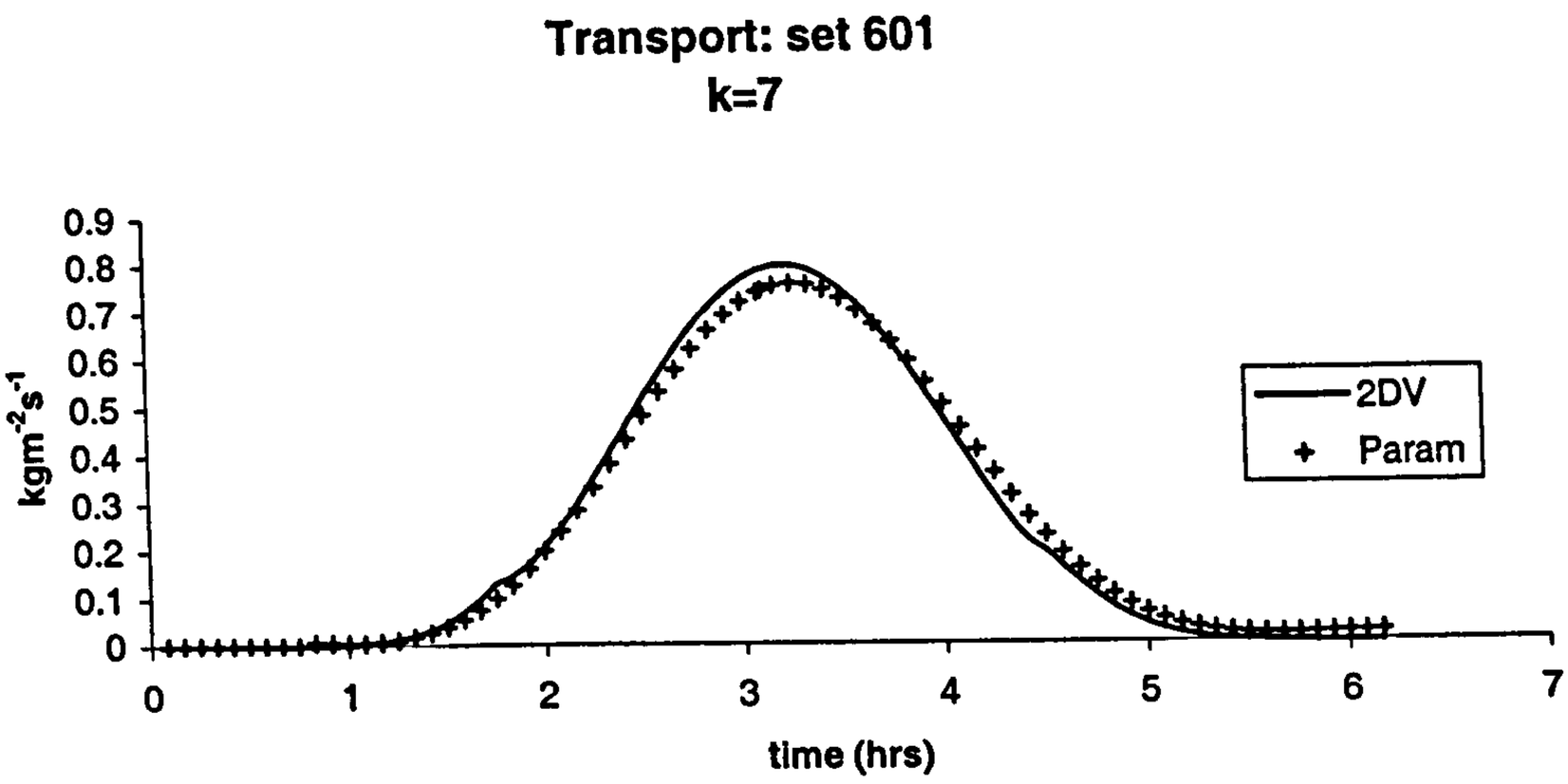

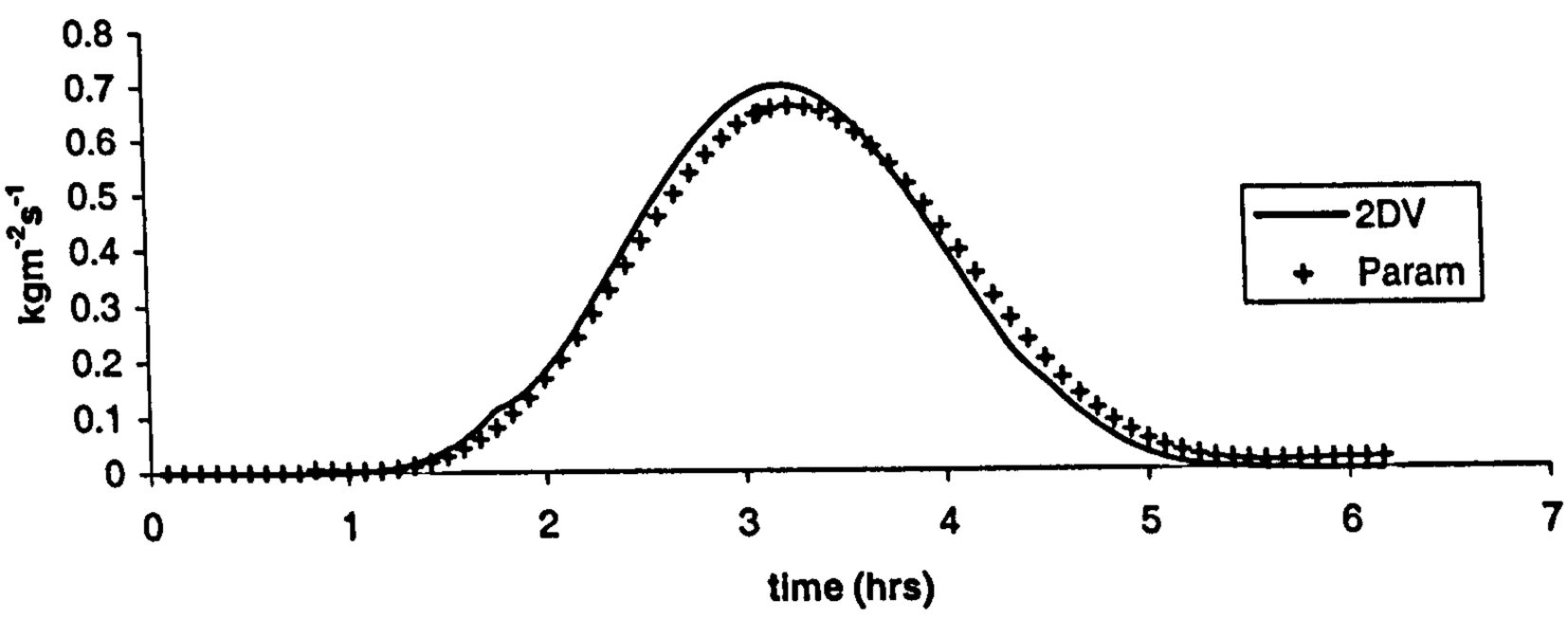

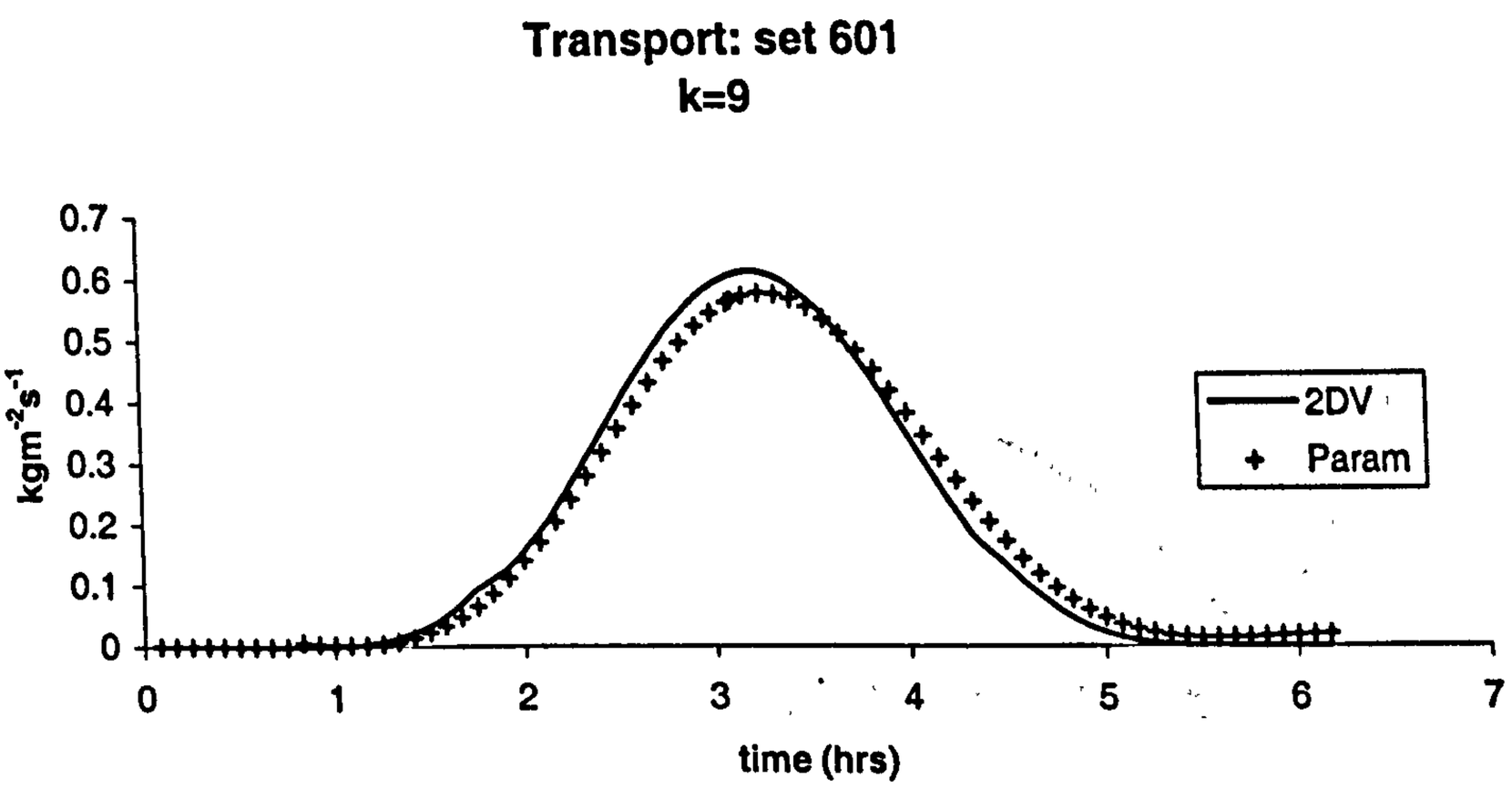

Figure 8.6.3g-i: Comparison between parameterised Corrector method (Param) and conventional 2DV (2DV)

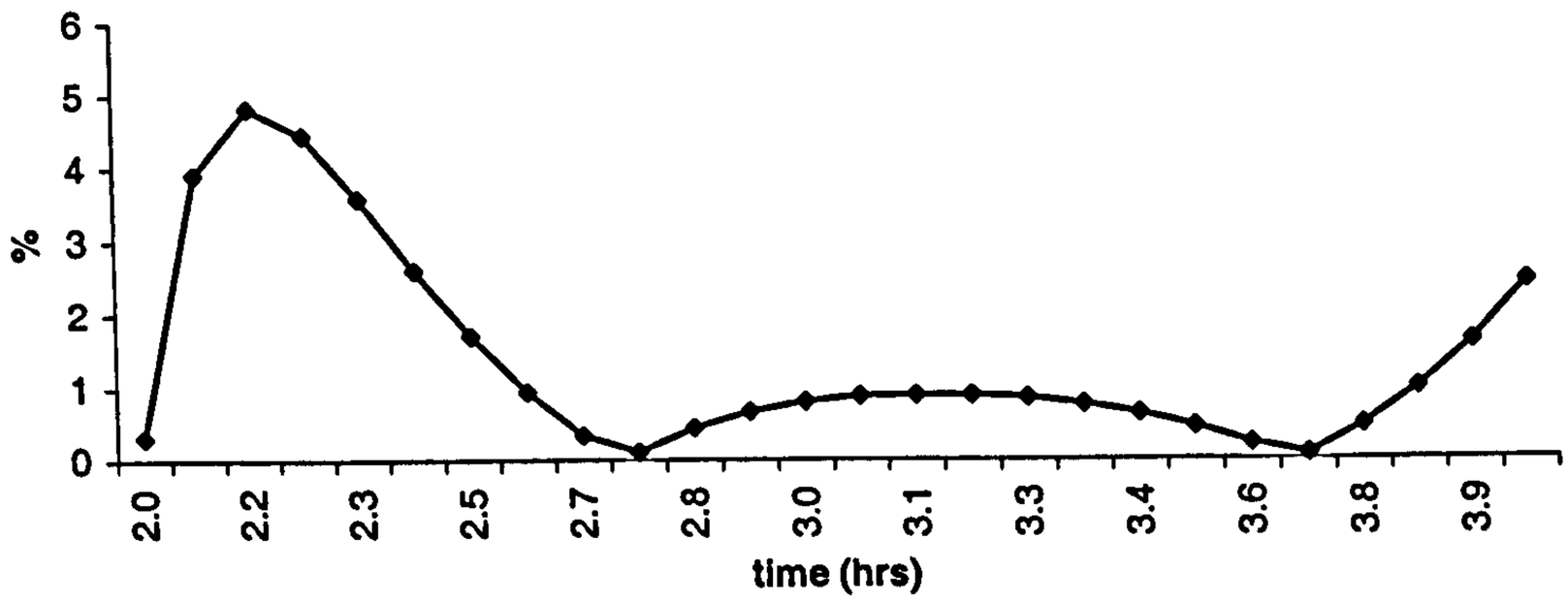

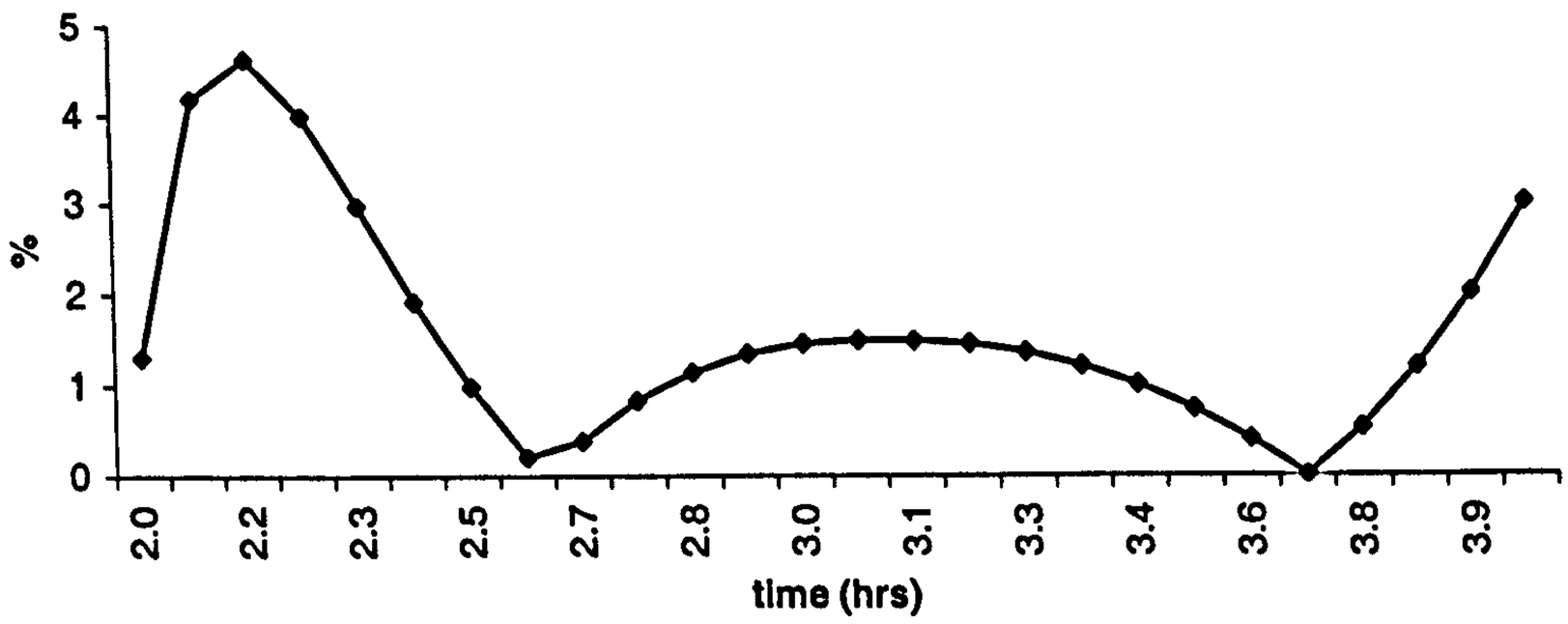

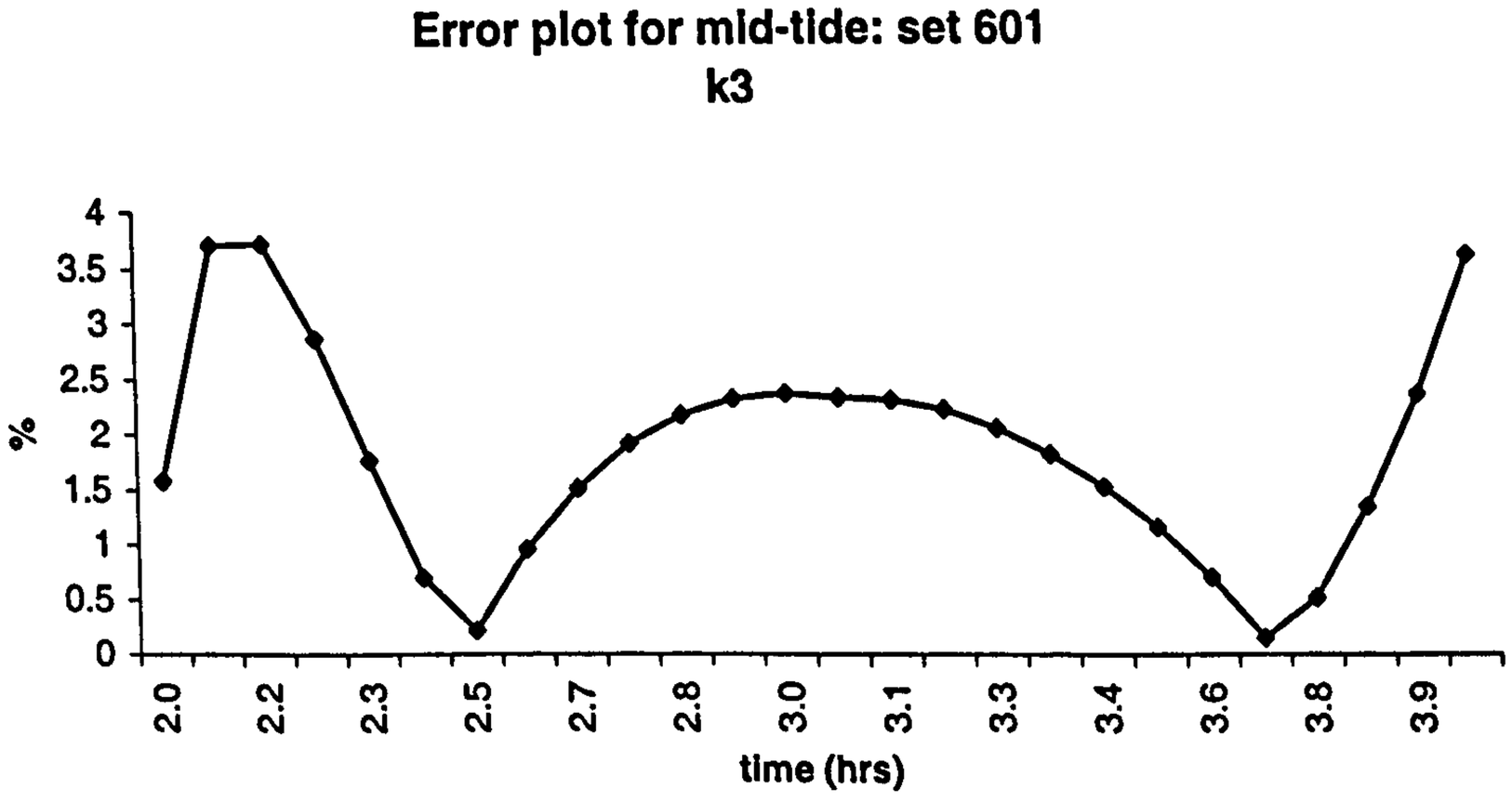

Figure 8.6.4a-c: Error between conventional 2DV method and parameterised Corrector method during the mid-tide phase.

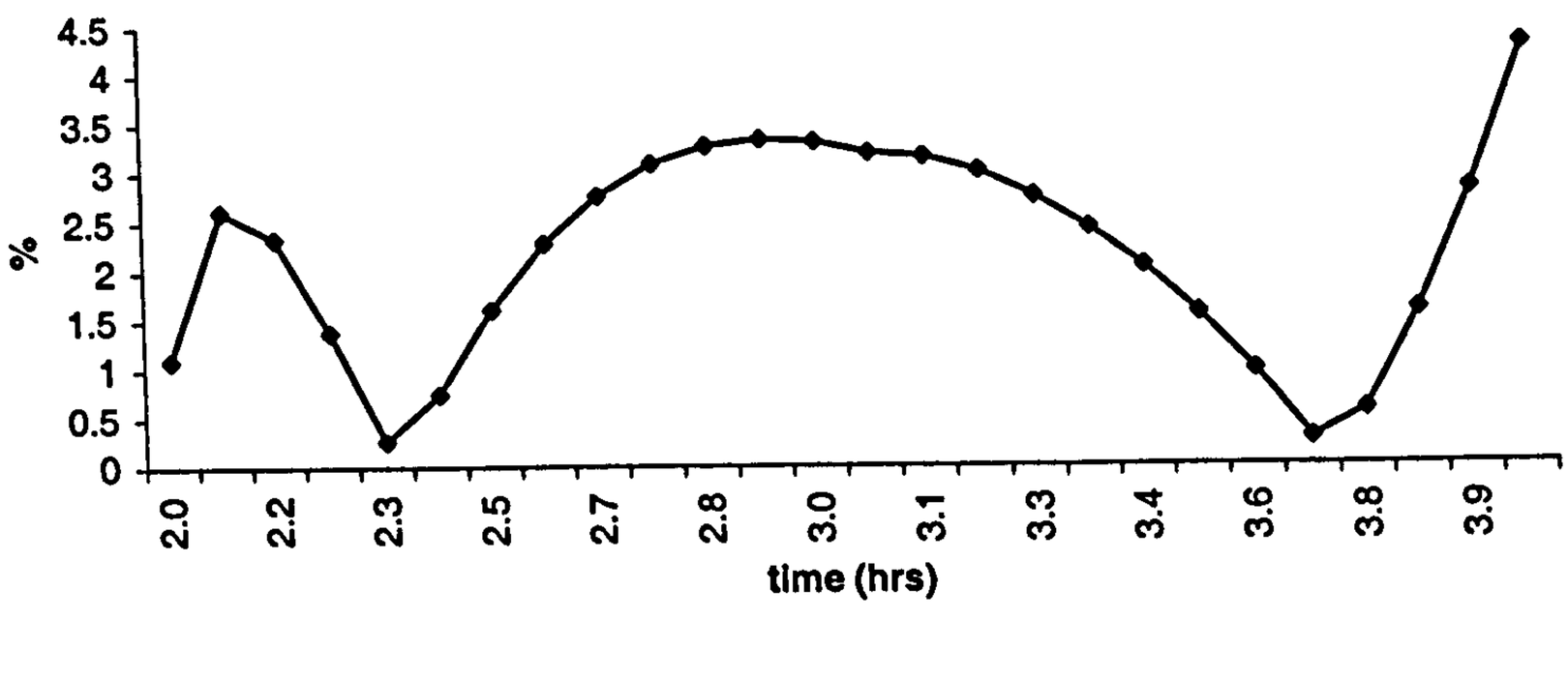

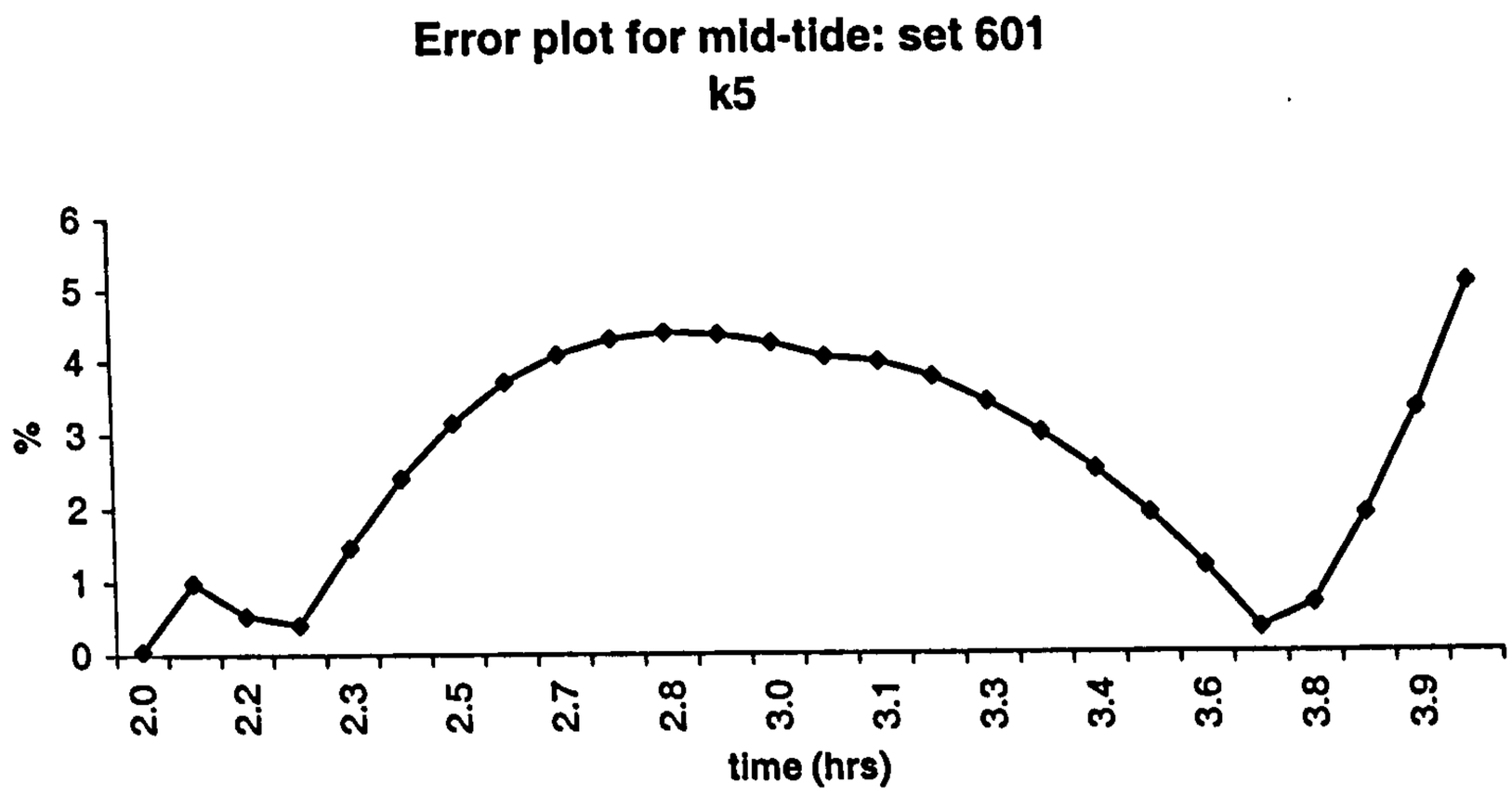

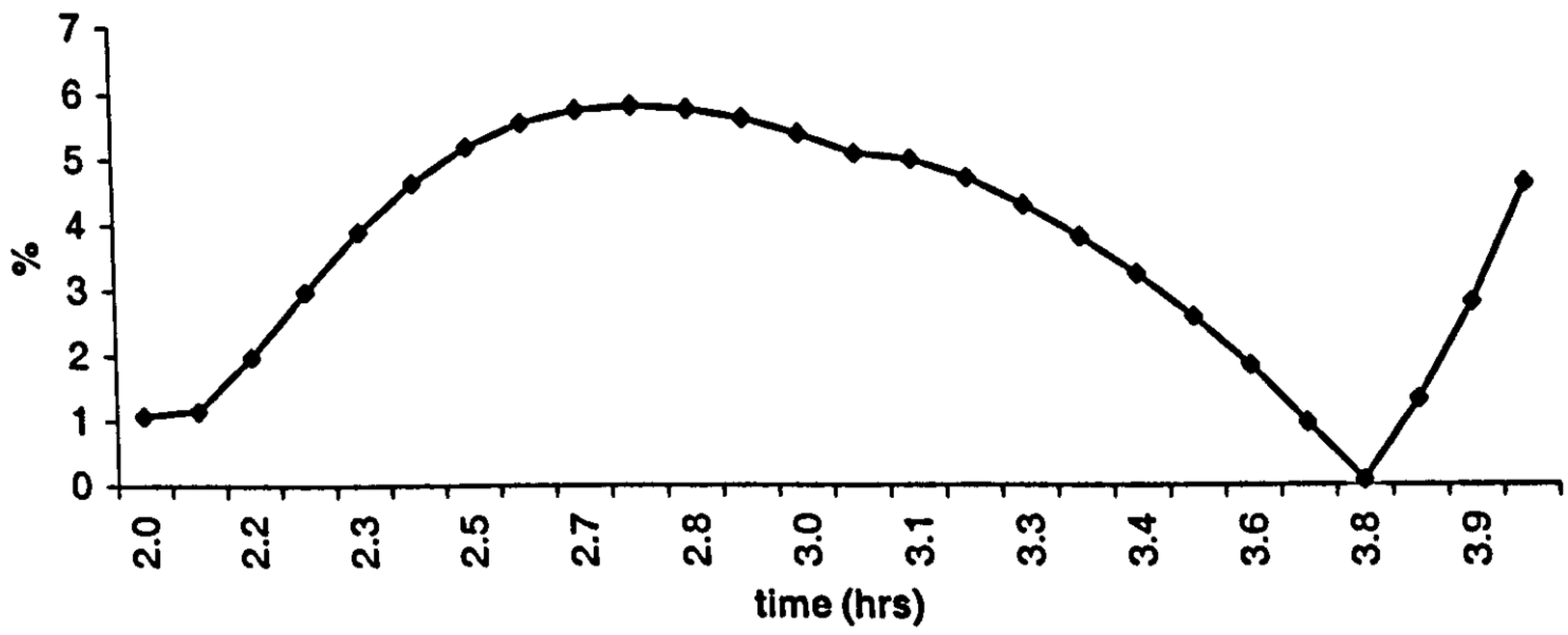

Figure 8.6.4d-f: Error between conventional 2DV method and parameterised Corrector method during the mid-tide phase.

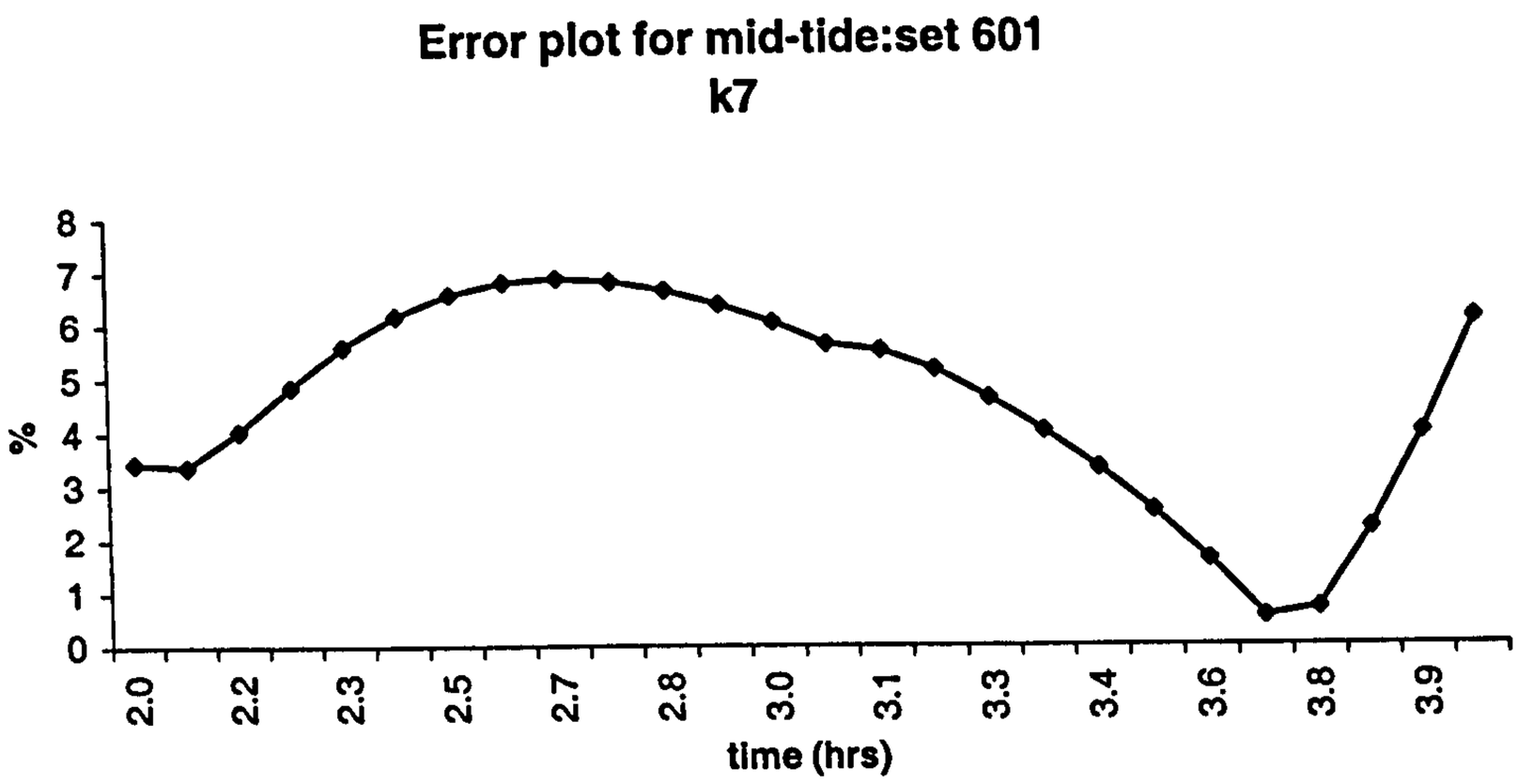

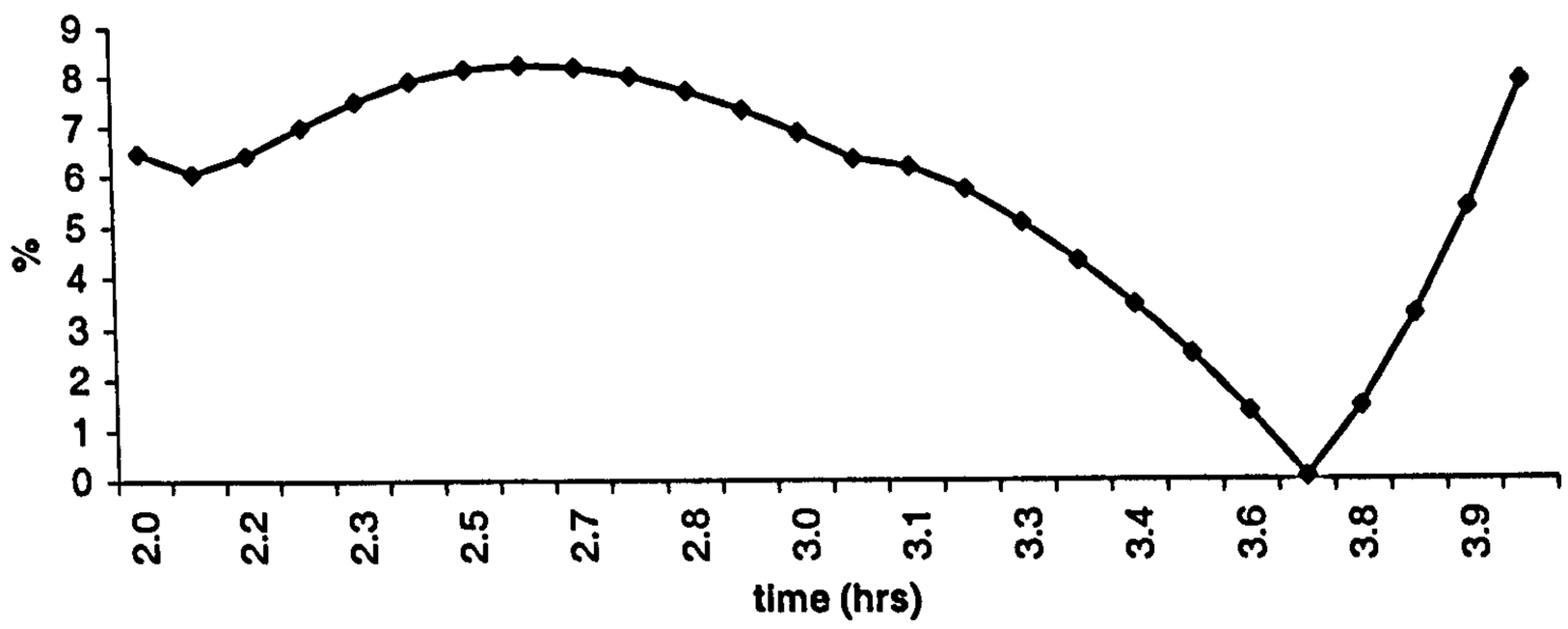

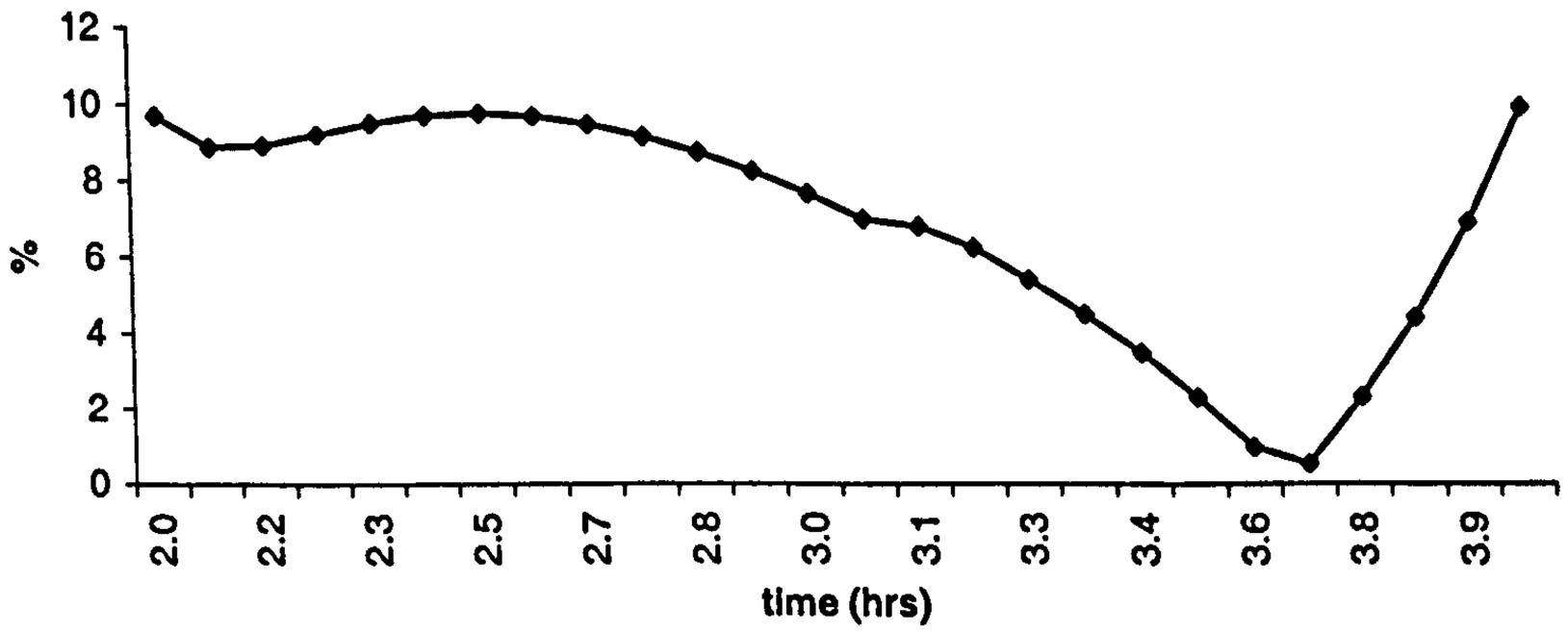

Figure 8.6.4g-i: Error between conventional 2DV method and parameterised Corrector method during the mid-tide phase.

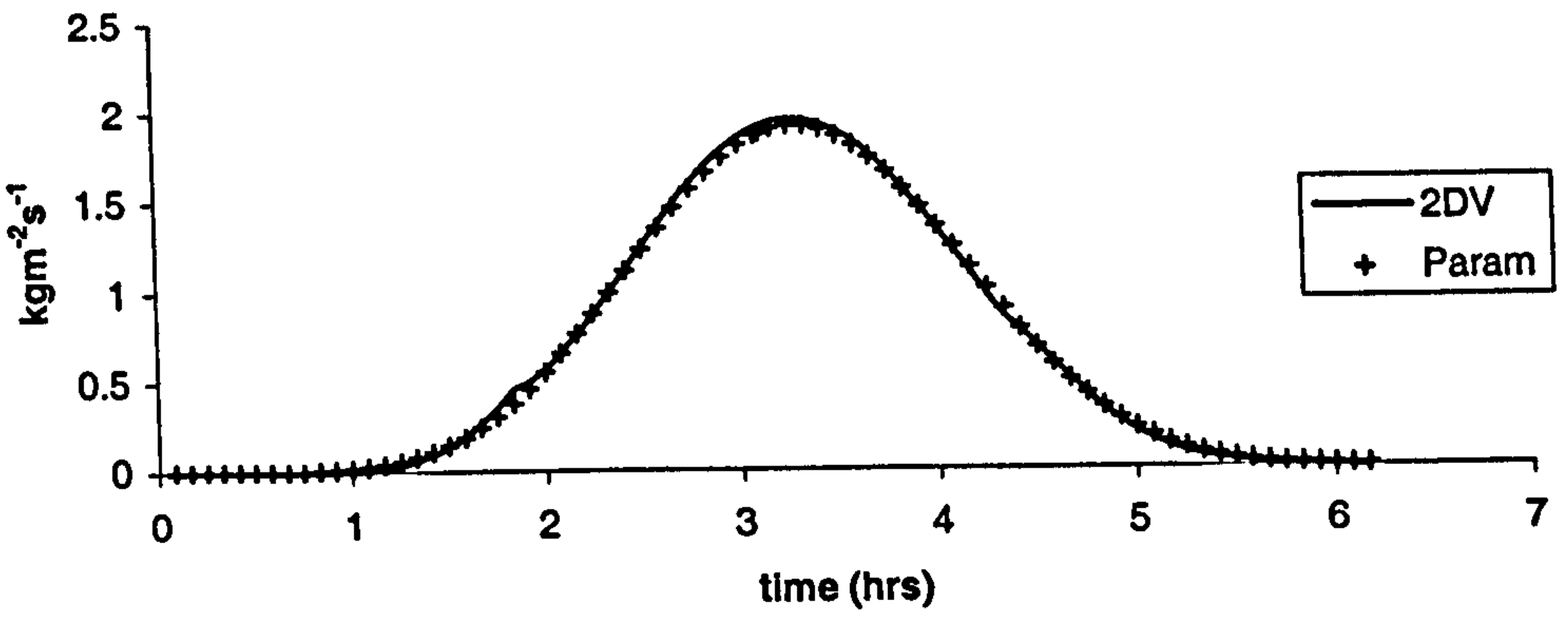

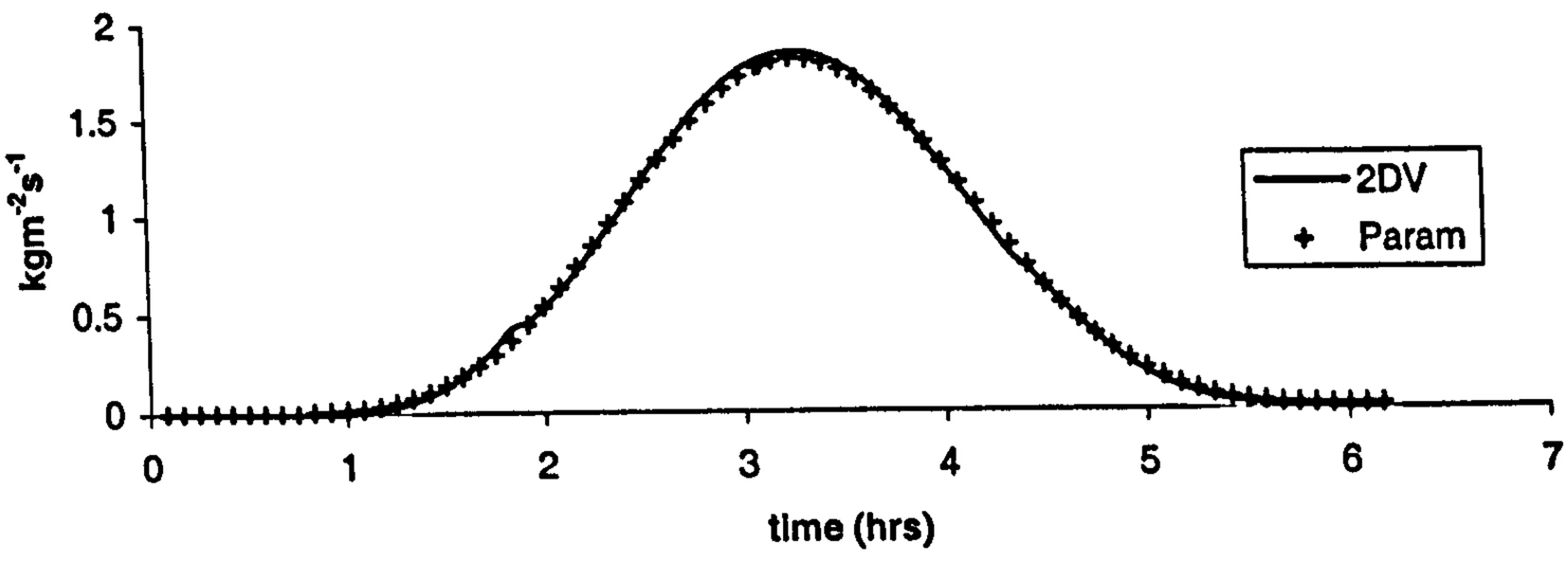

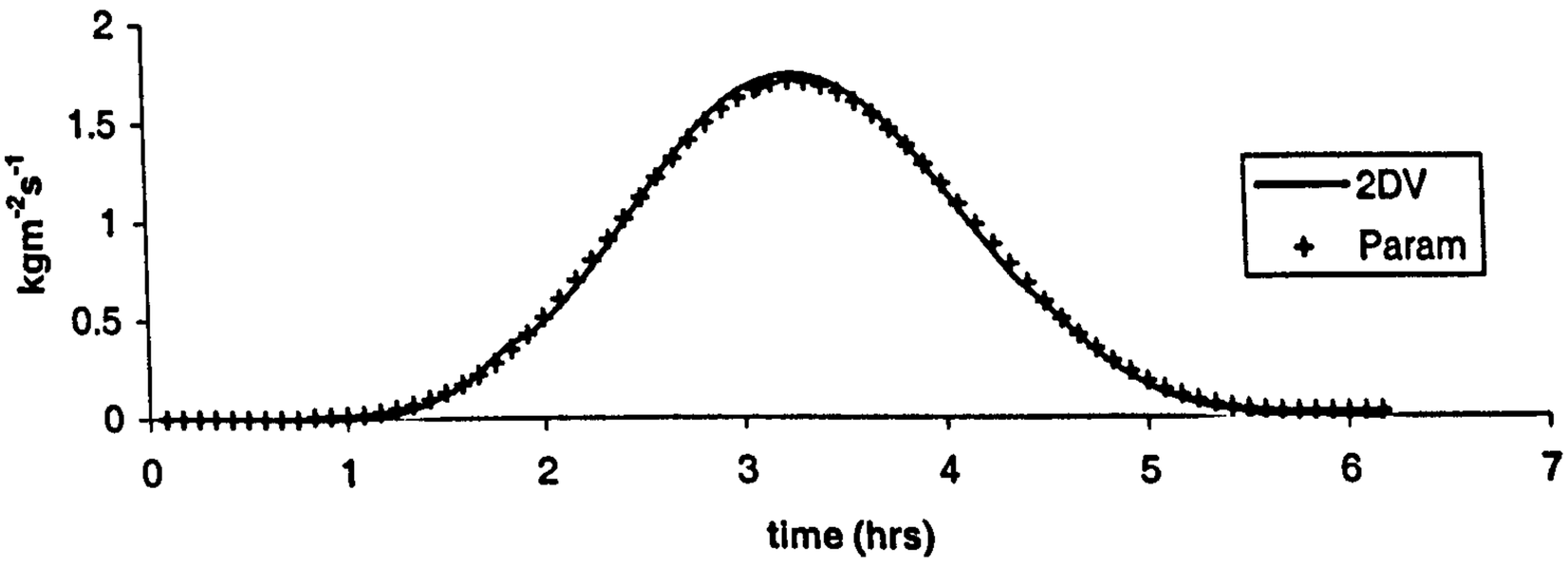

Figure 8.6.5a-c: Comparison between parameterised Corrector (Param) and conventional 2DV (2DV)

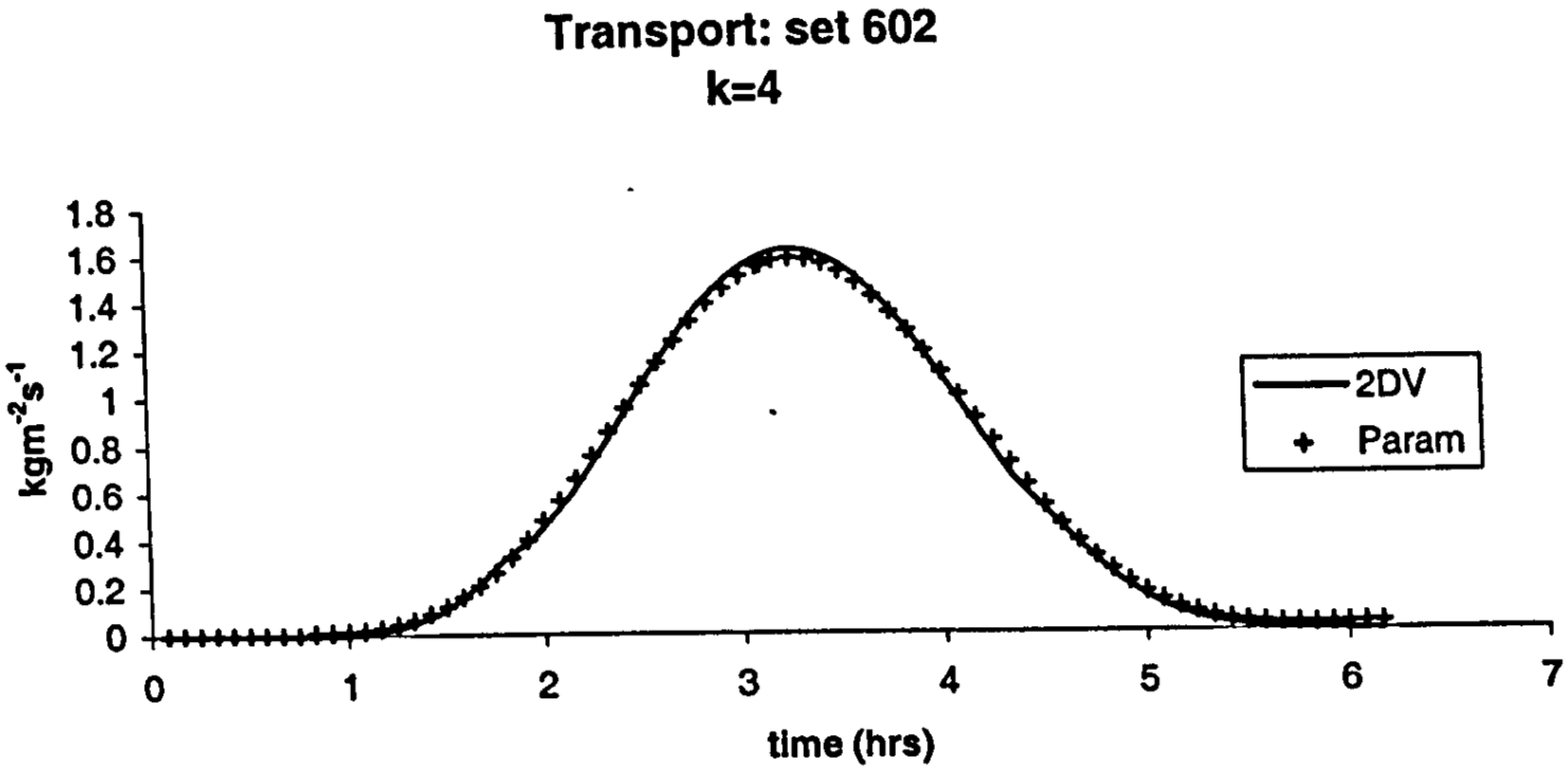

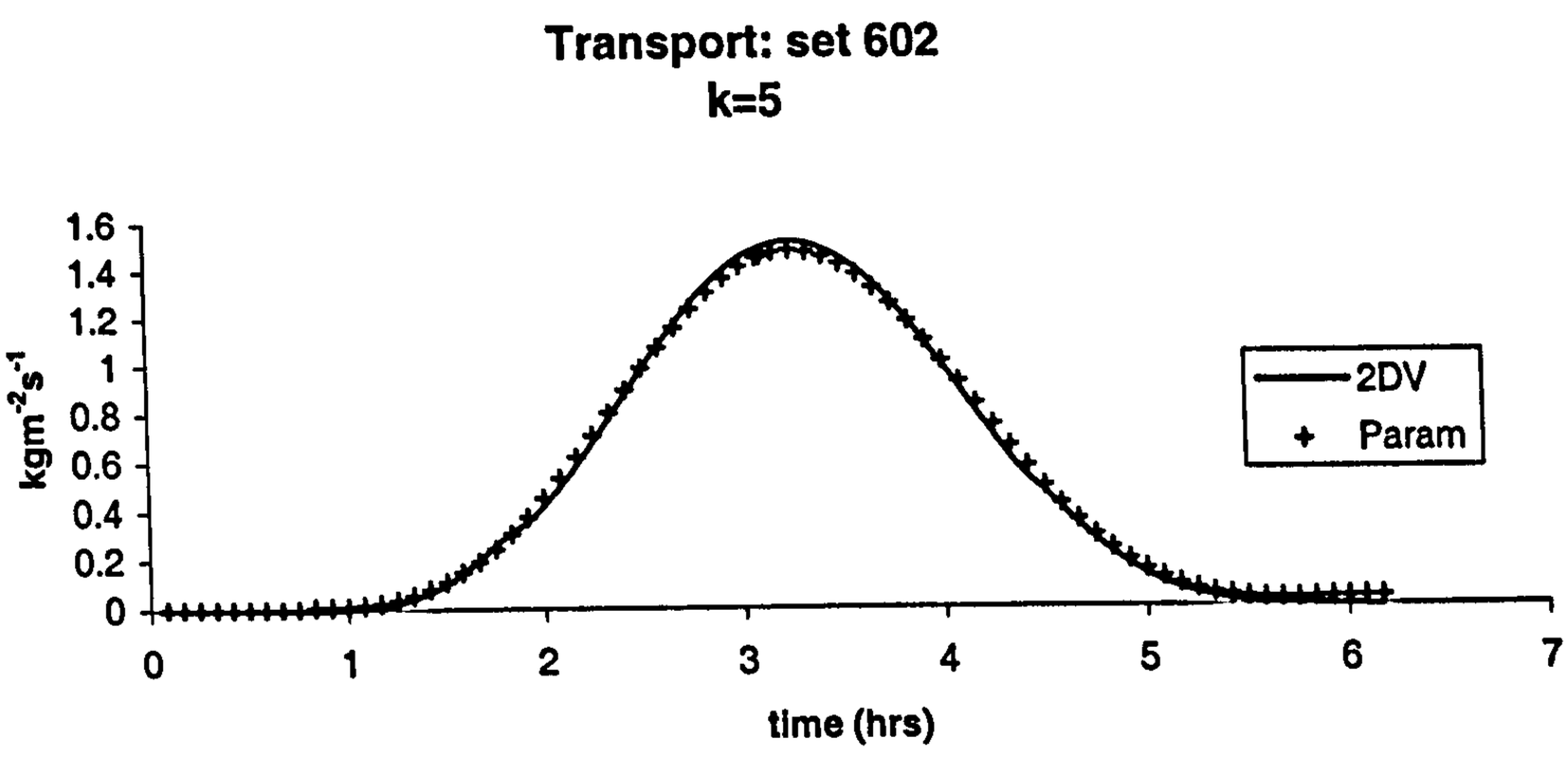

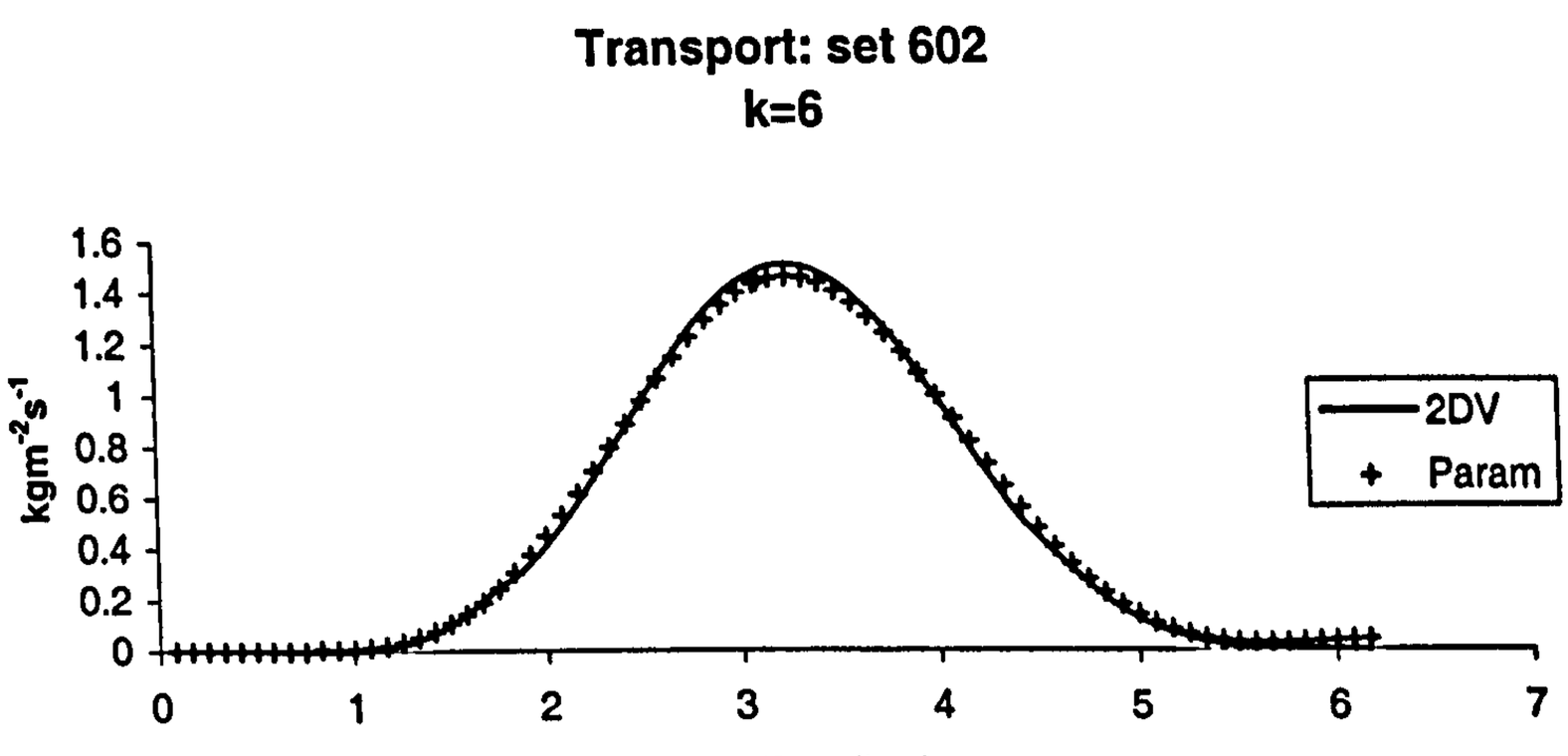

Figure 8.6.5d-f: Comparison between parameterised Corrector (Param) and conventional 2DV (2DV)

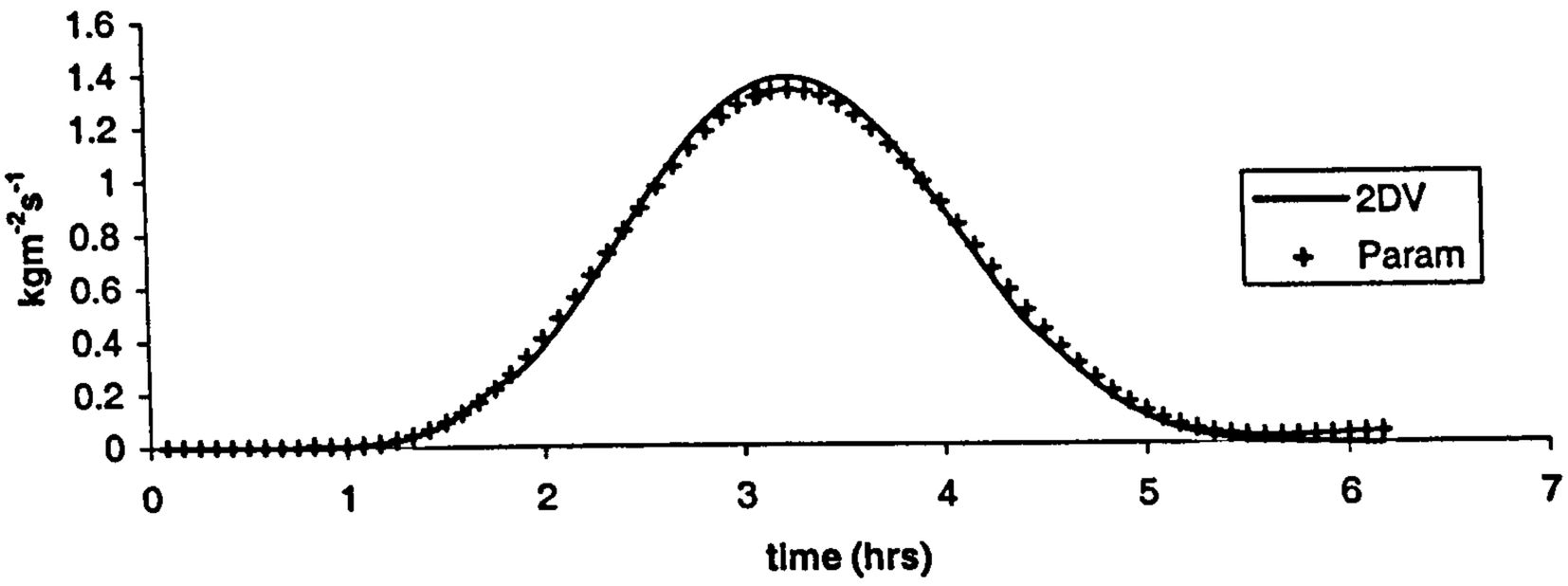

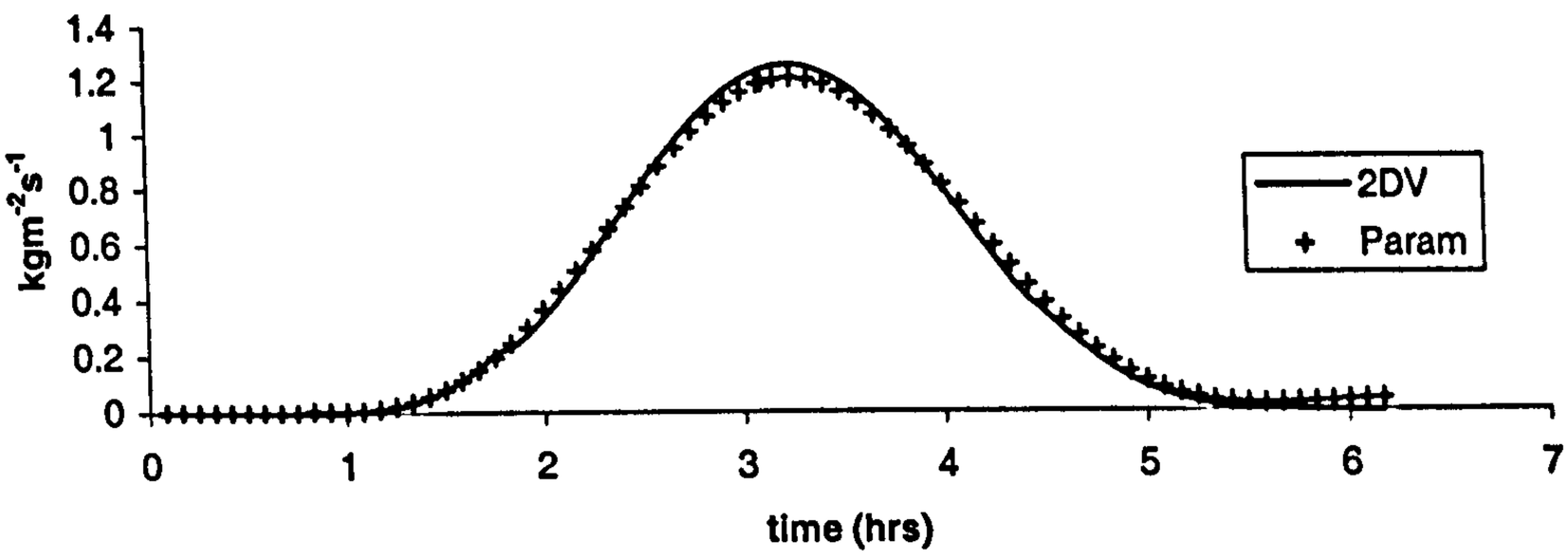

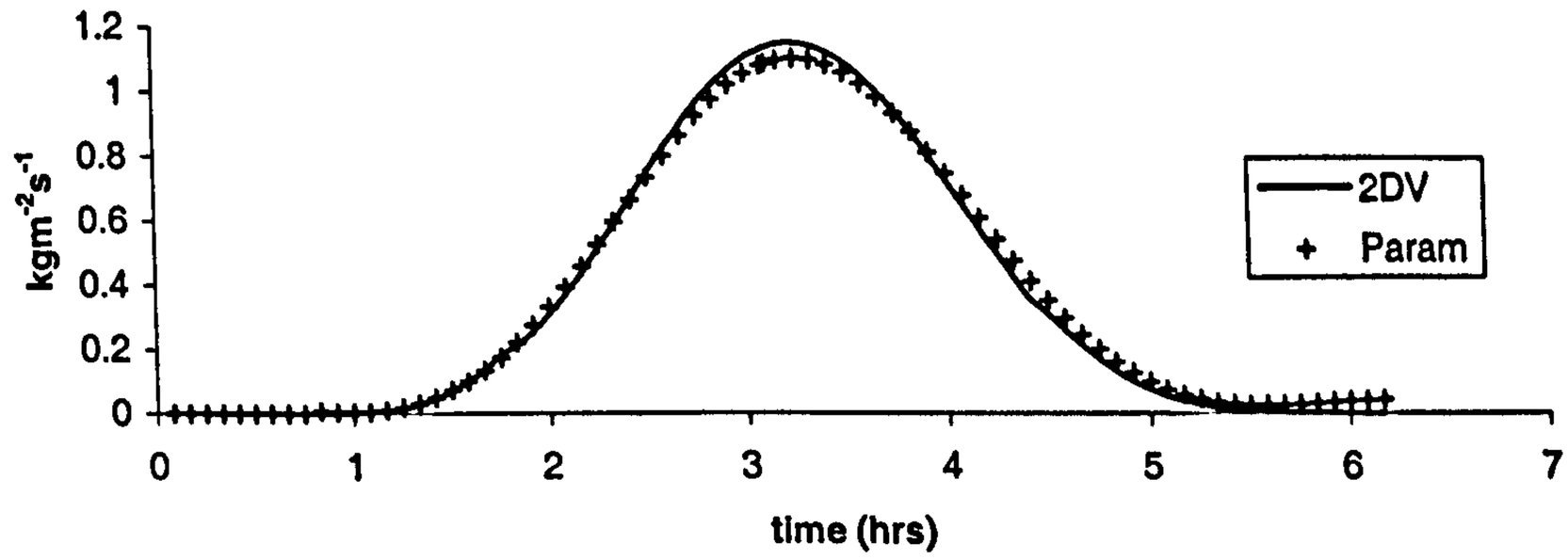

Figure 8.6.5g-i: Comparison between parameterised Corrector (Param) and conventional 2DV (2DV)

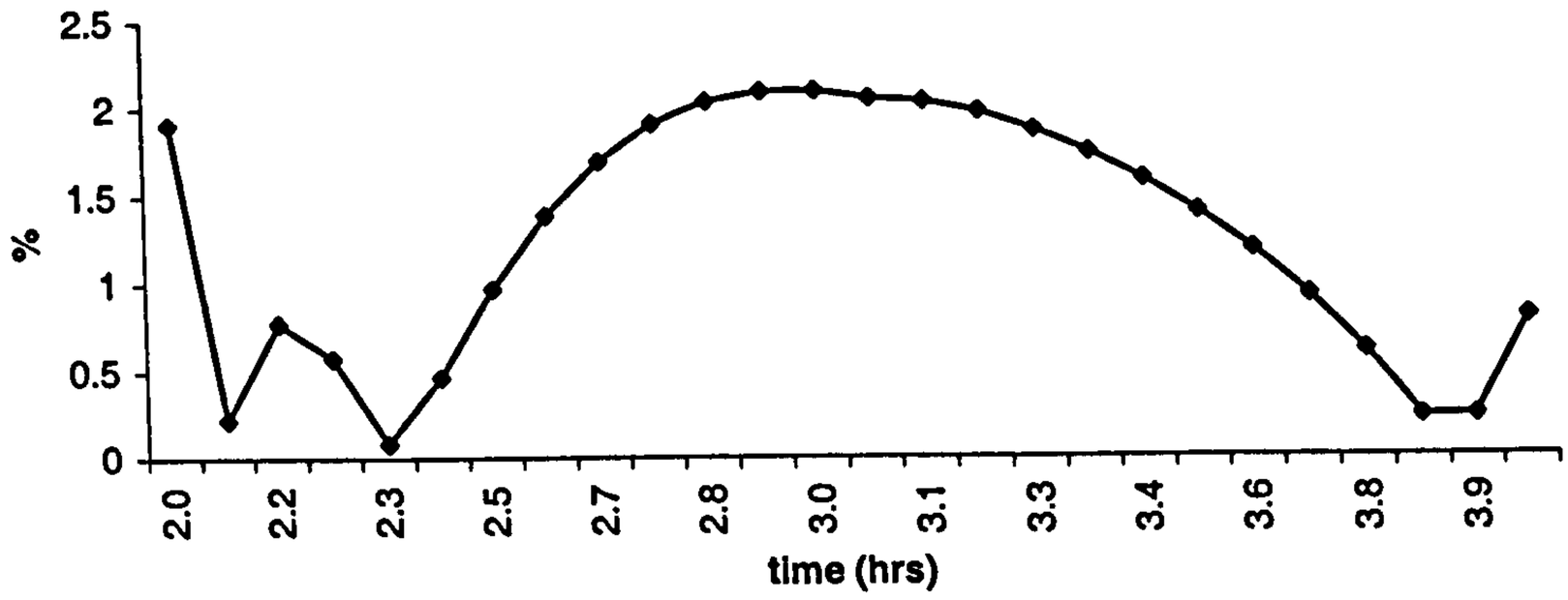

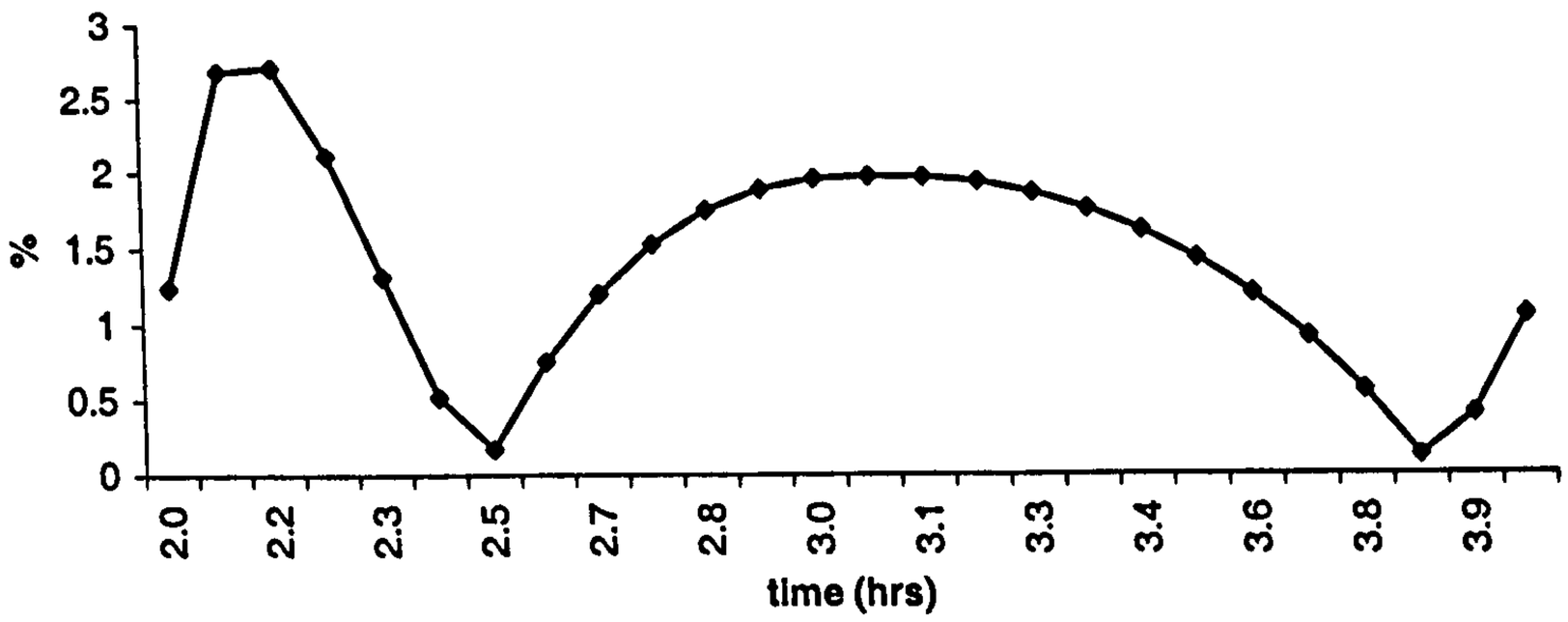

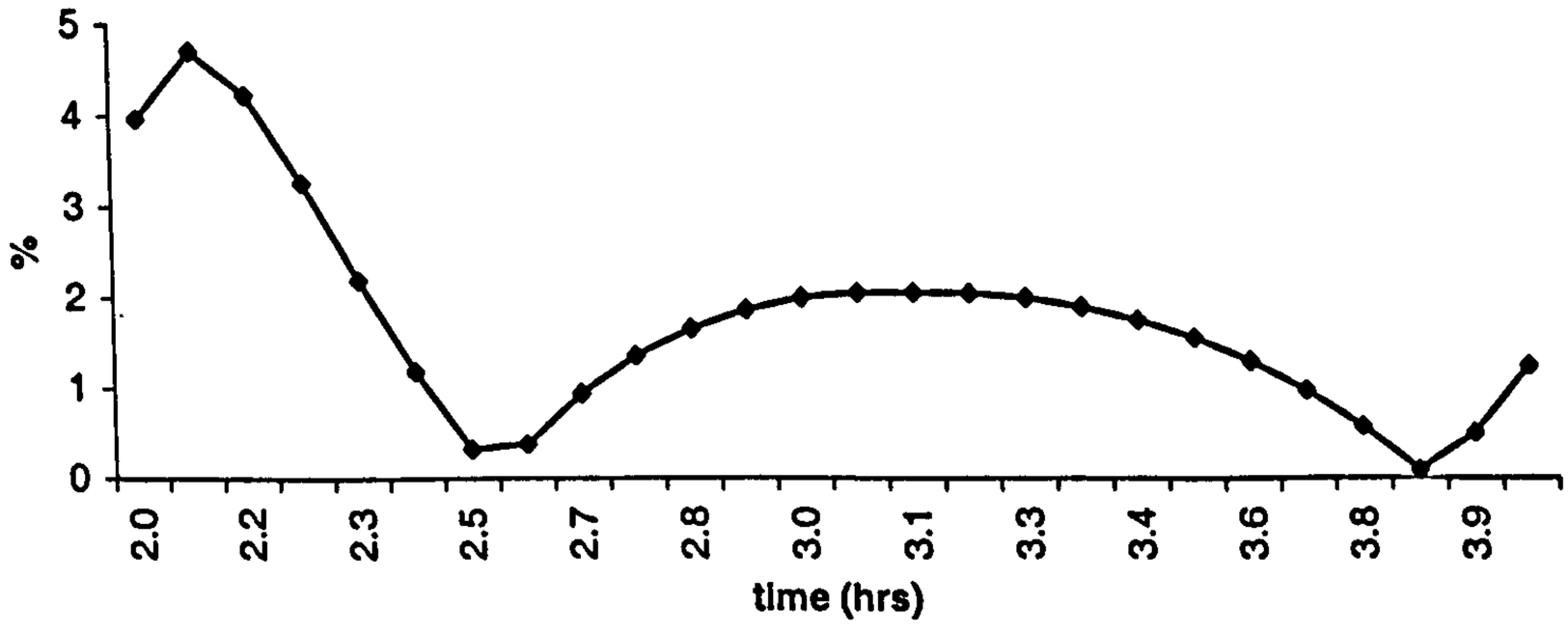

Figure 8.6.6a-c: Error between conventional 2DV method and parameterised Corrector method during the mid-tide phase.

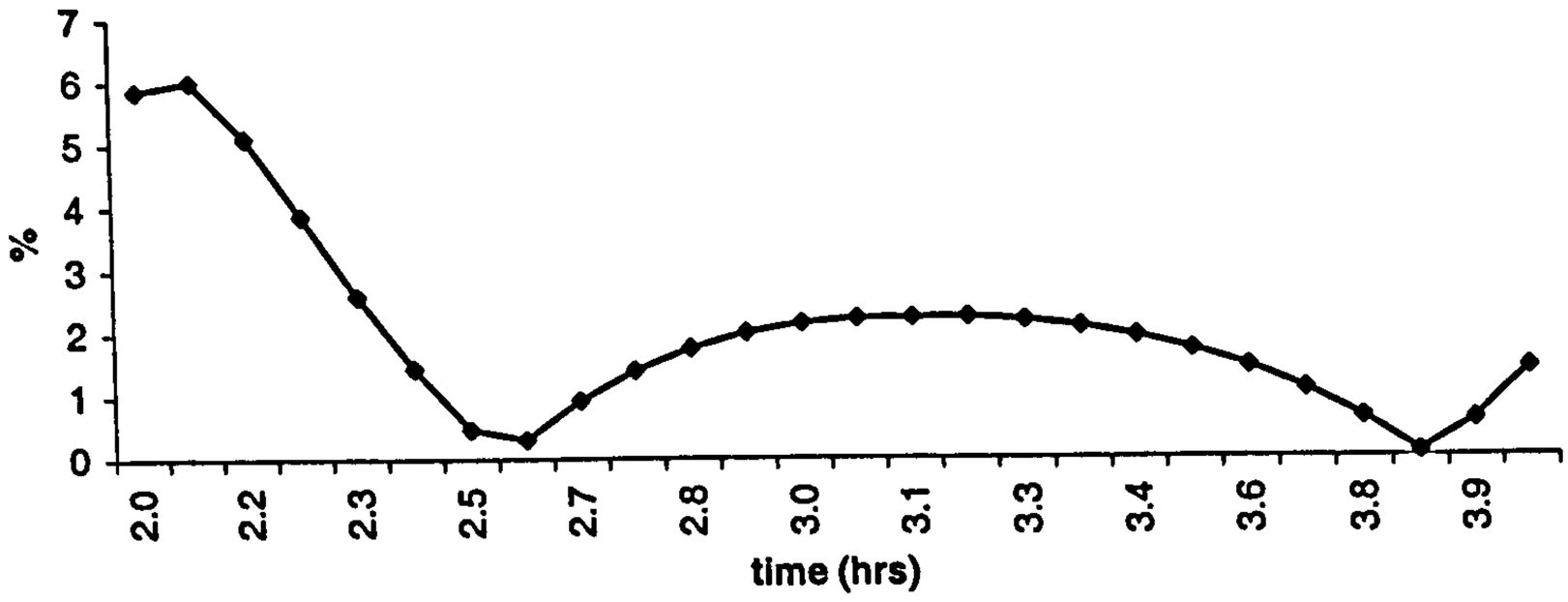

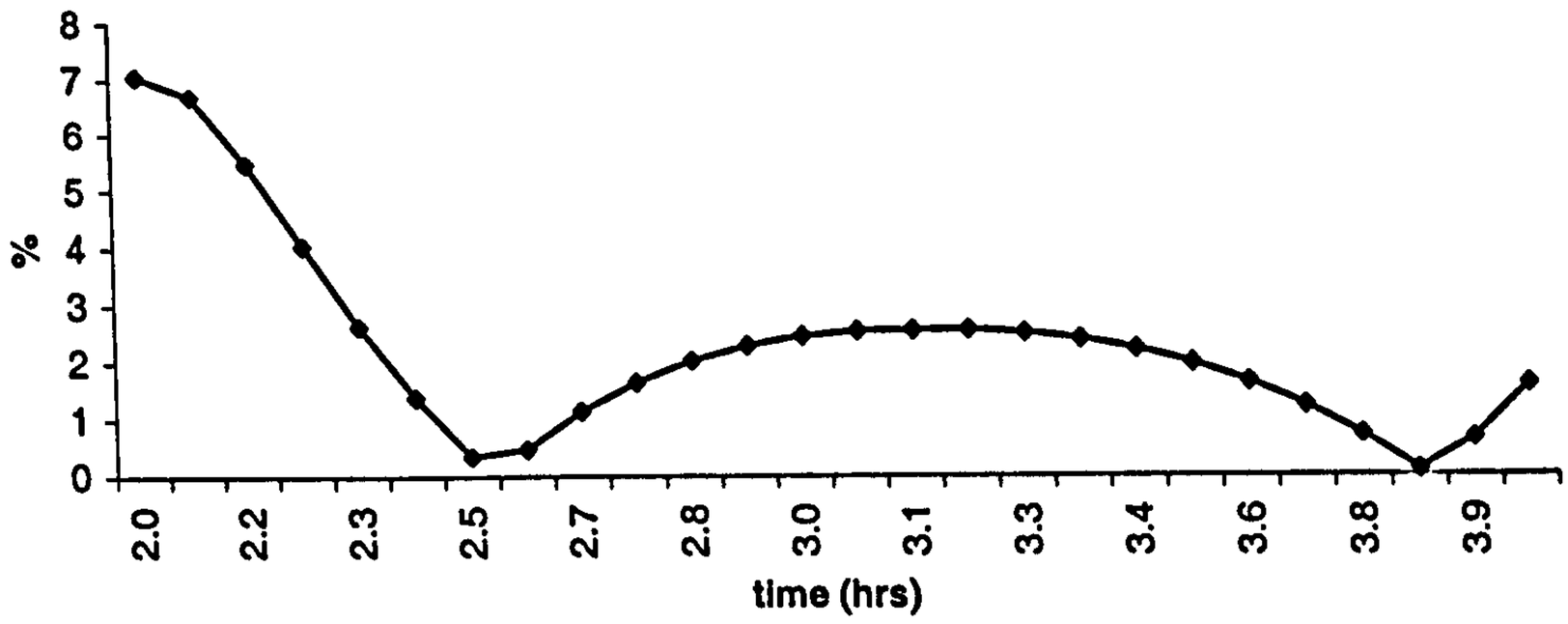

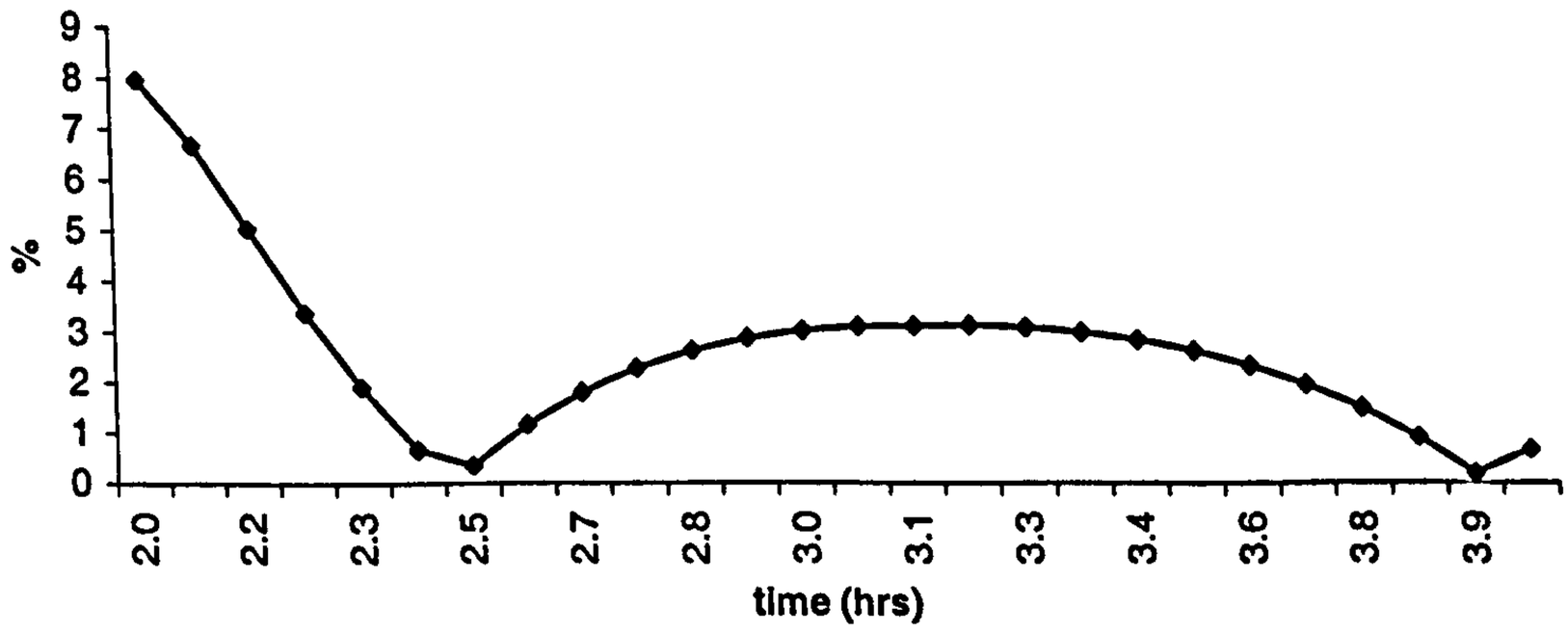

Figure 8.6.6d-f: Error between conventional 2DV method and parameterised Corrector method during the mid-tide phase.

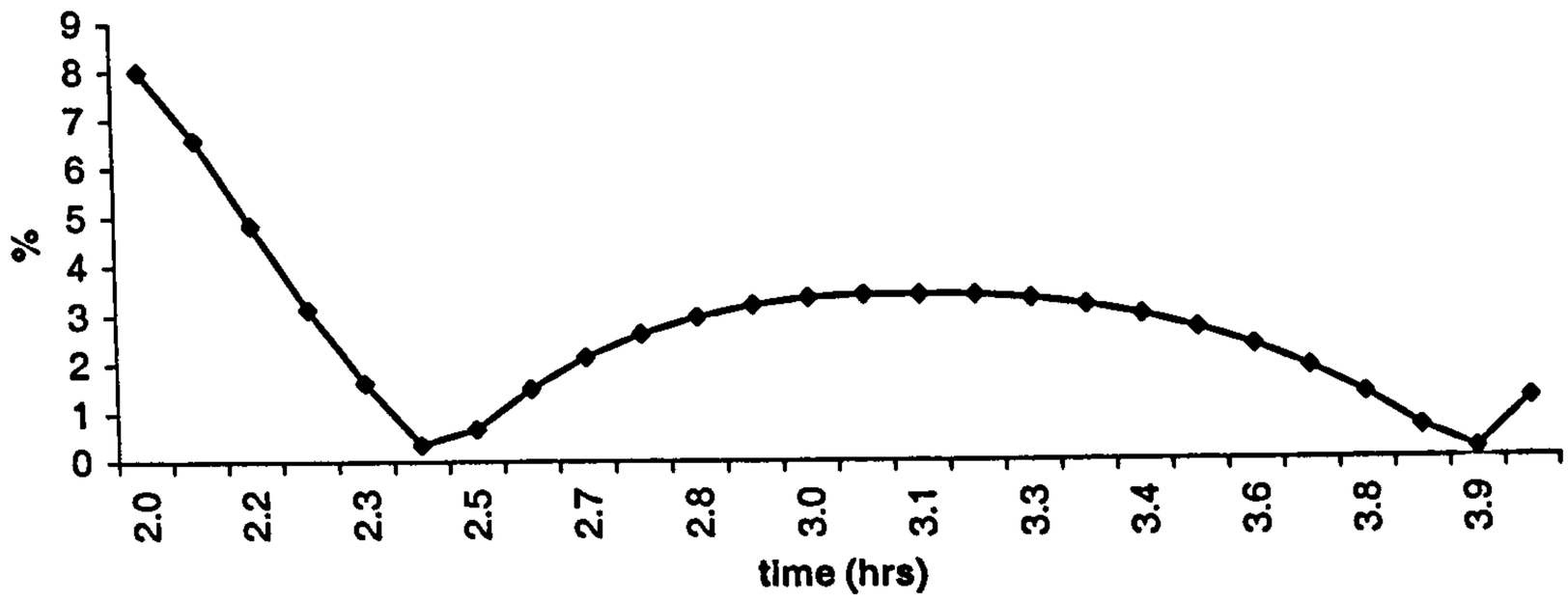

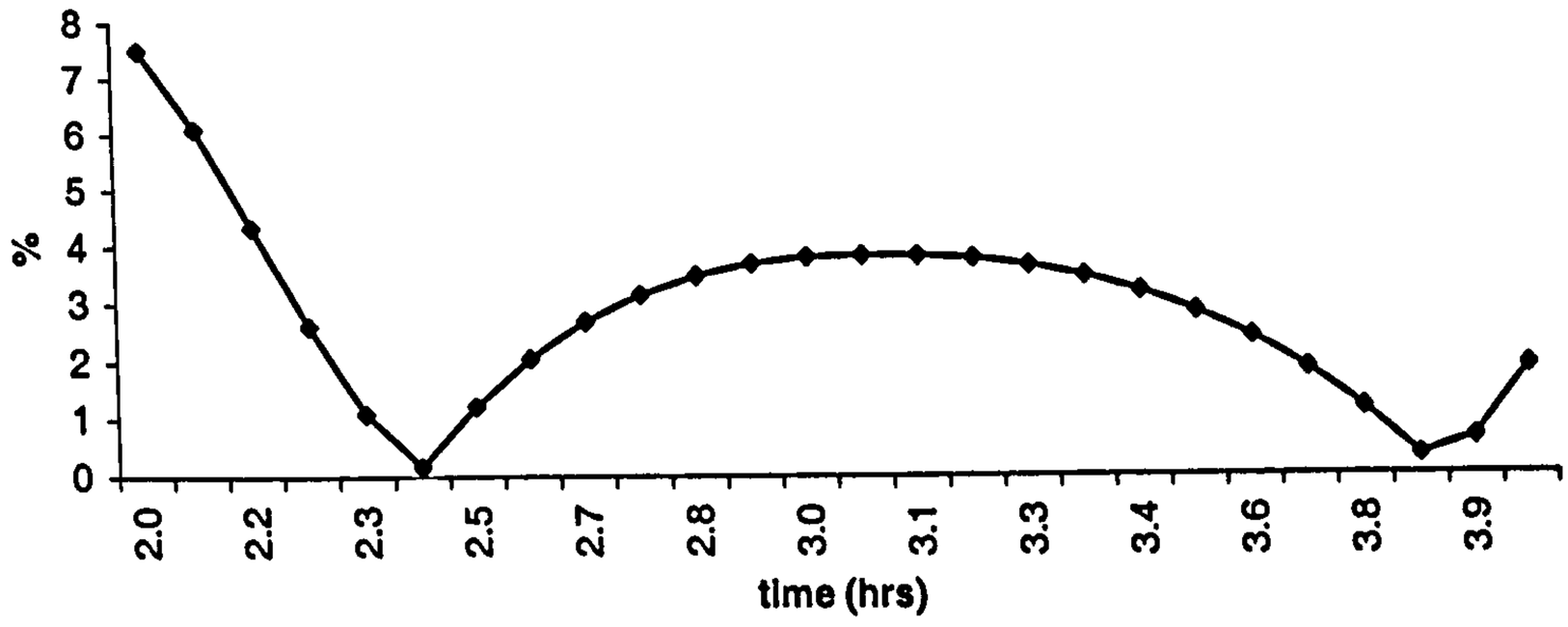

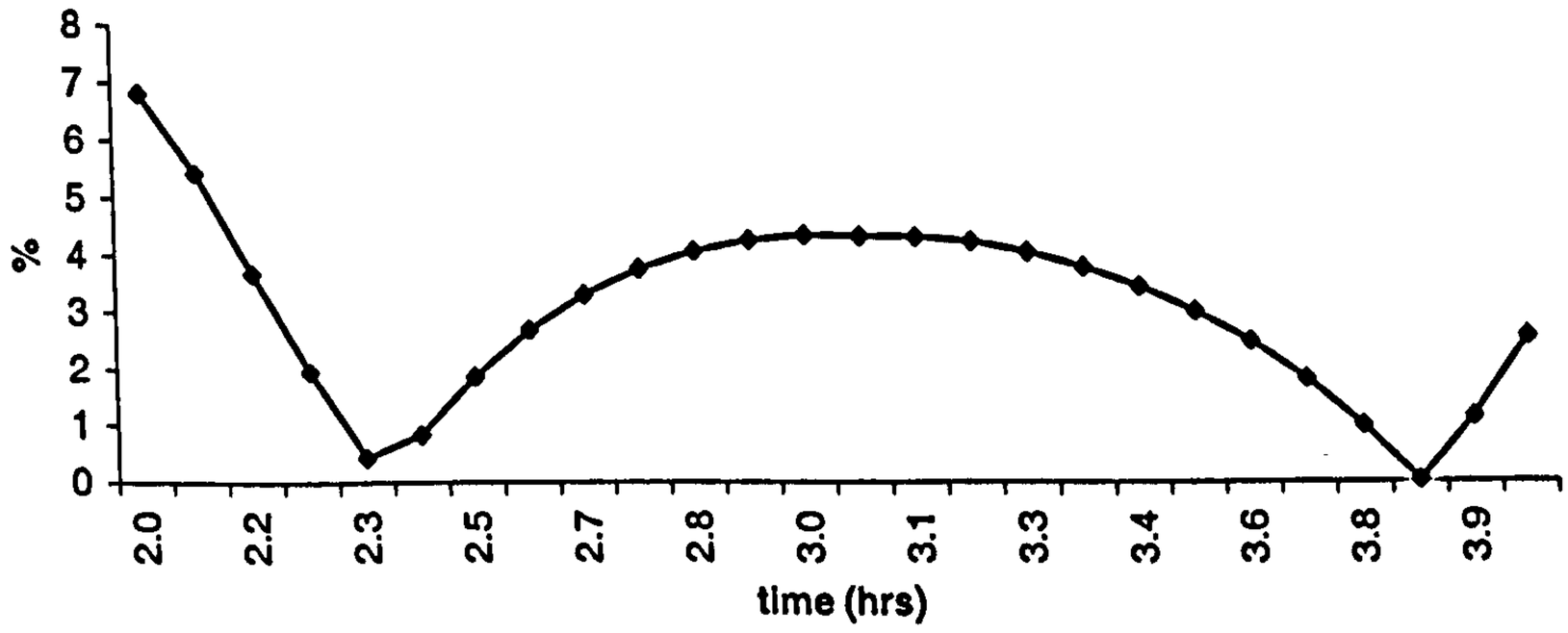

Figure 8.6.6g-i: Error between conventional 2DV method and parameterised Corrector method during the mid-tide phase.

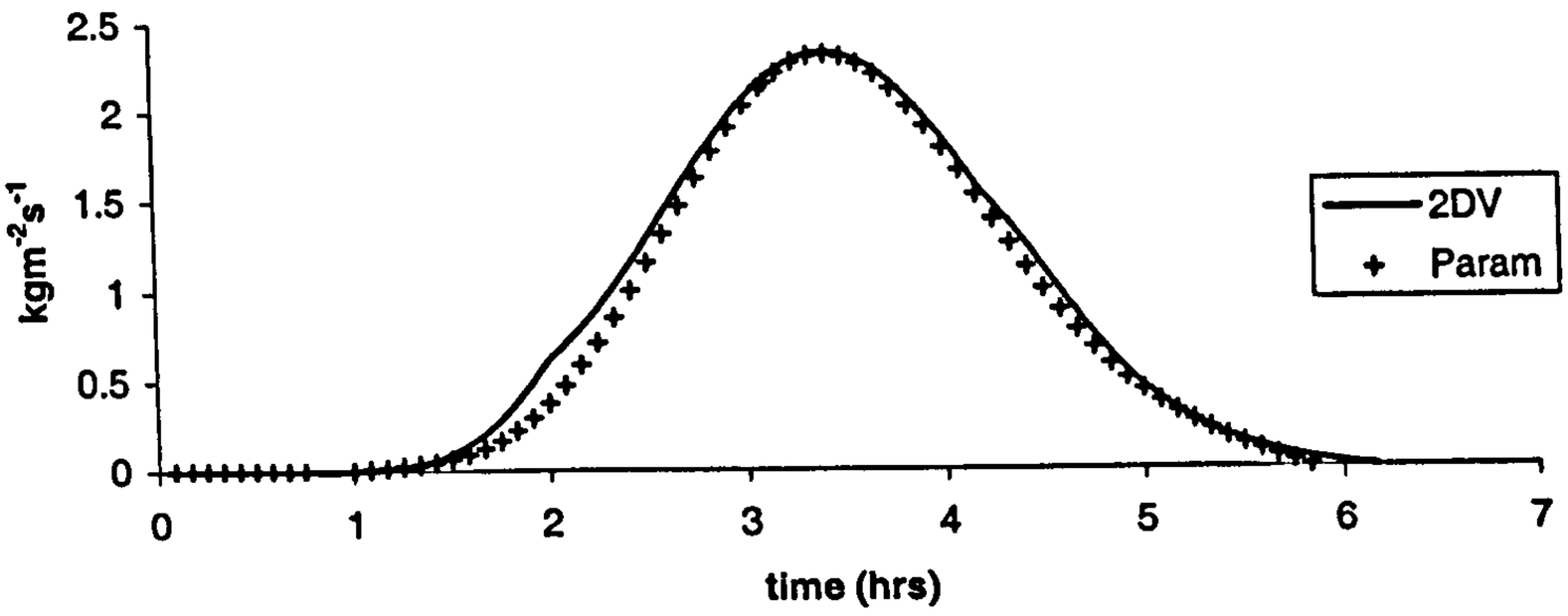

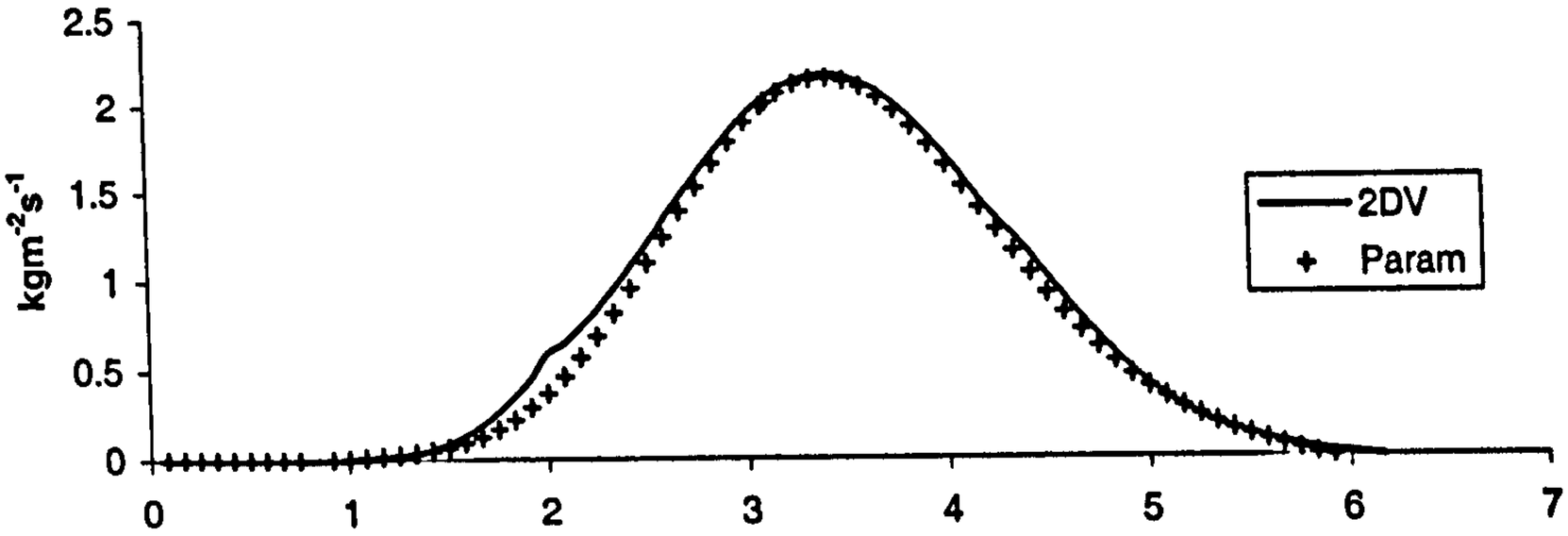

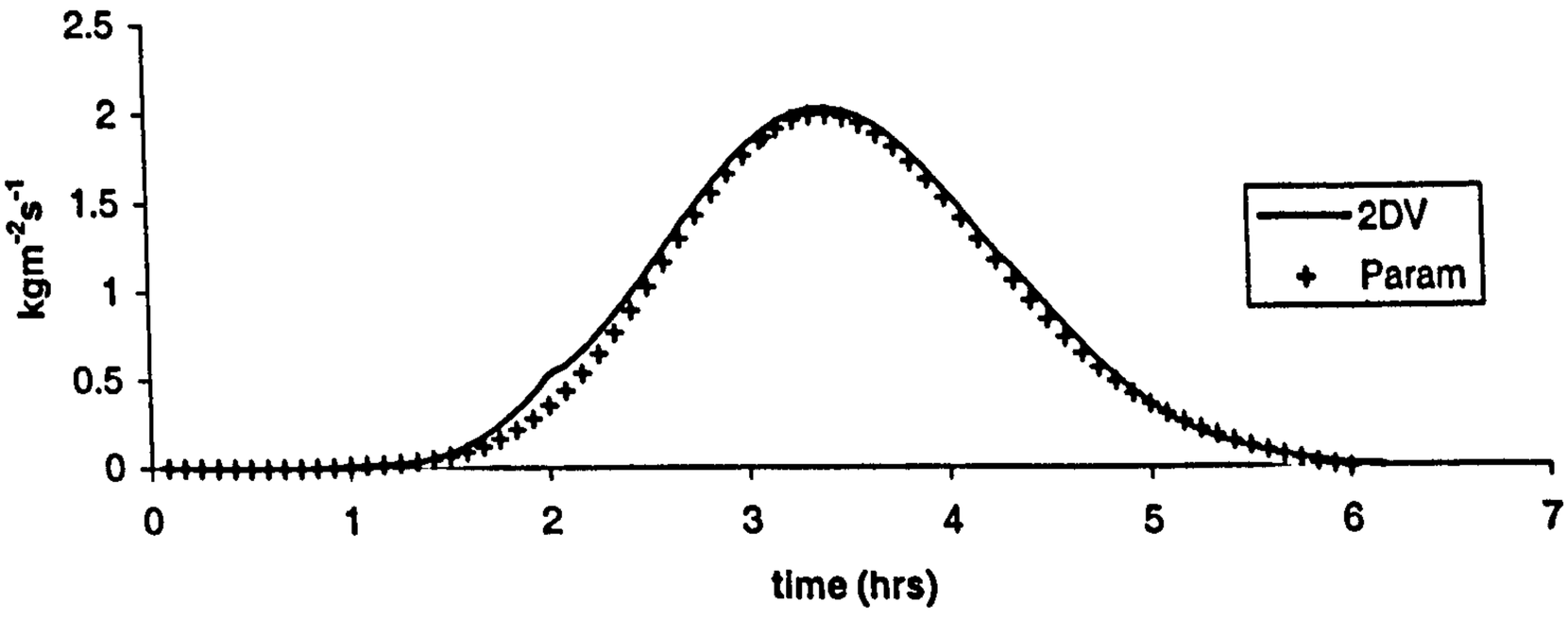

Figure 8.6.7a-c: Comparison between parameterised Corrector (Param) and conventional 2DV (2DV)

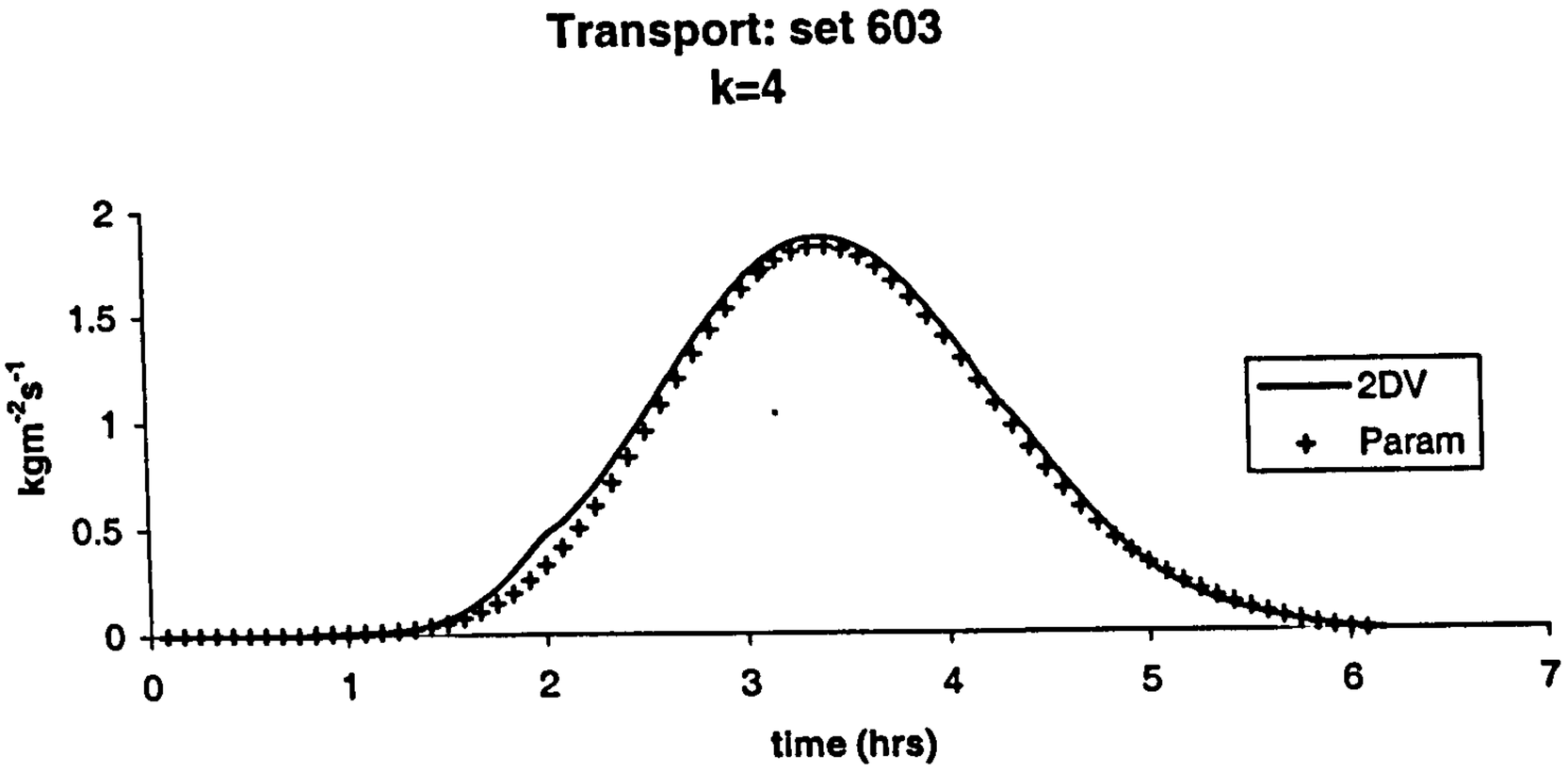

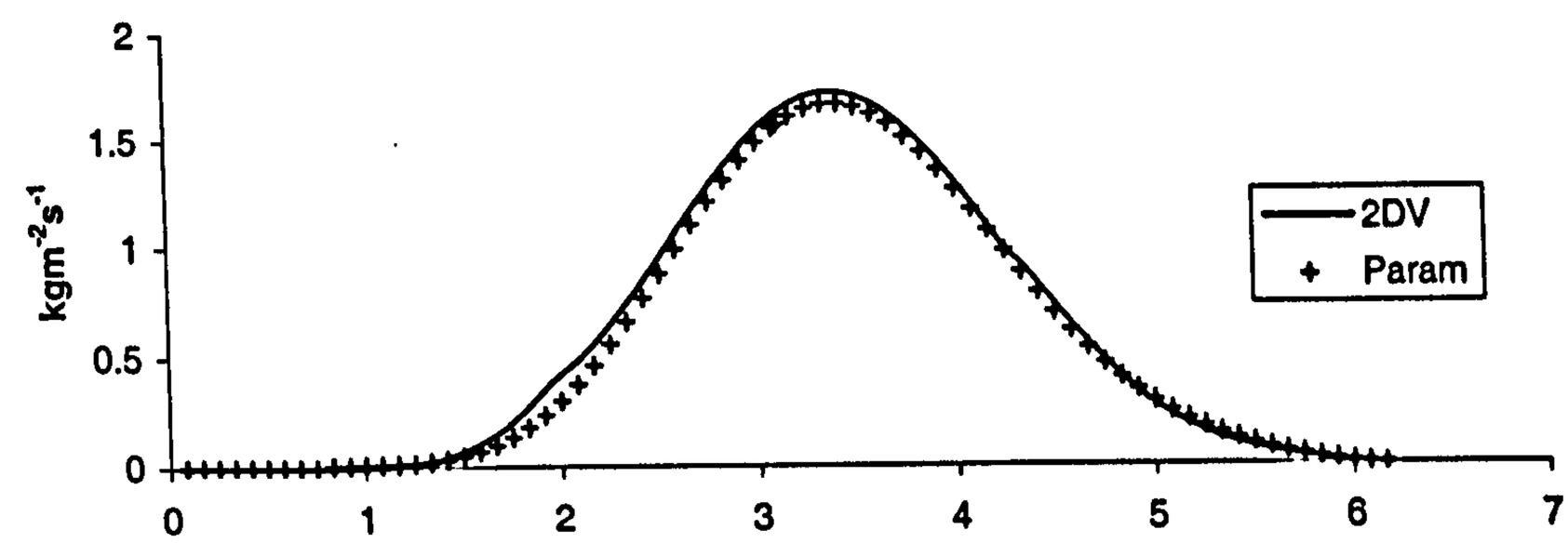

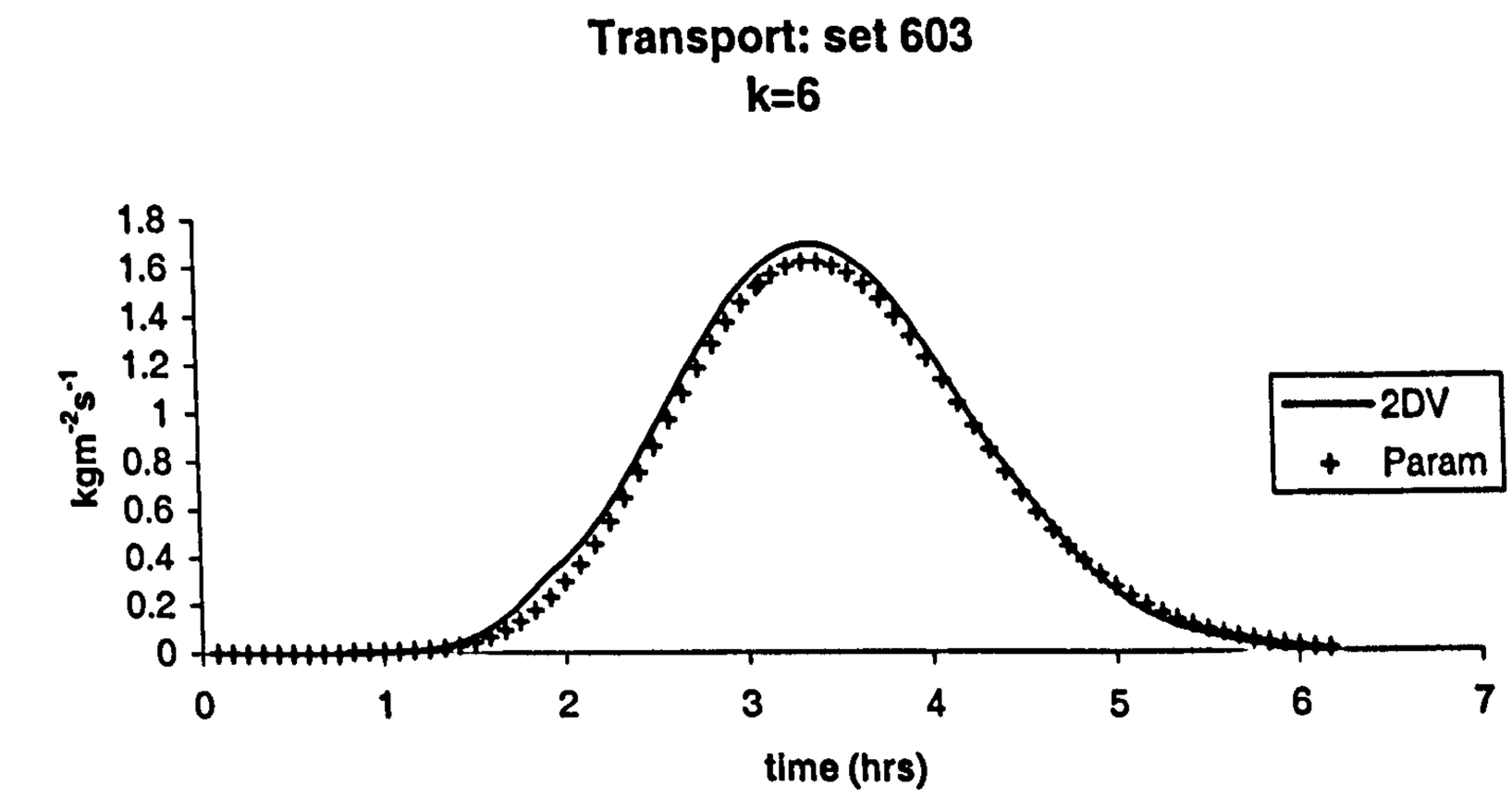

Figure 8.6.7d-f: Comparison between parameterised Corrector (Param) and conventional 2DV (2DV)

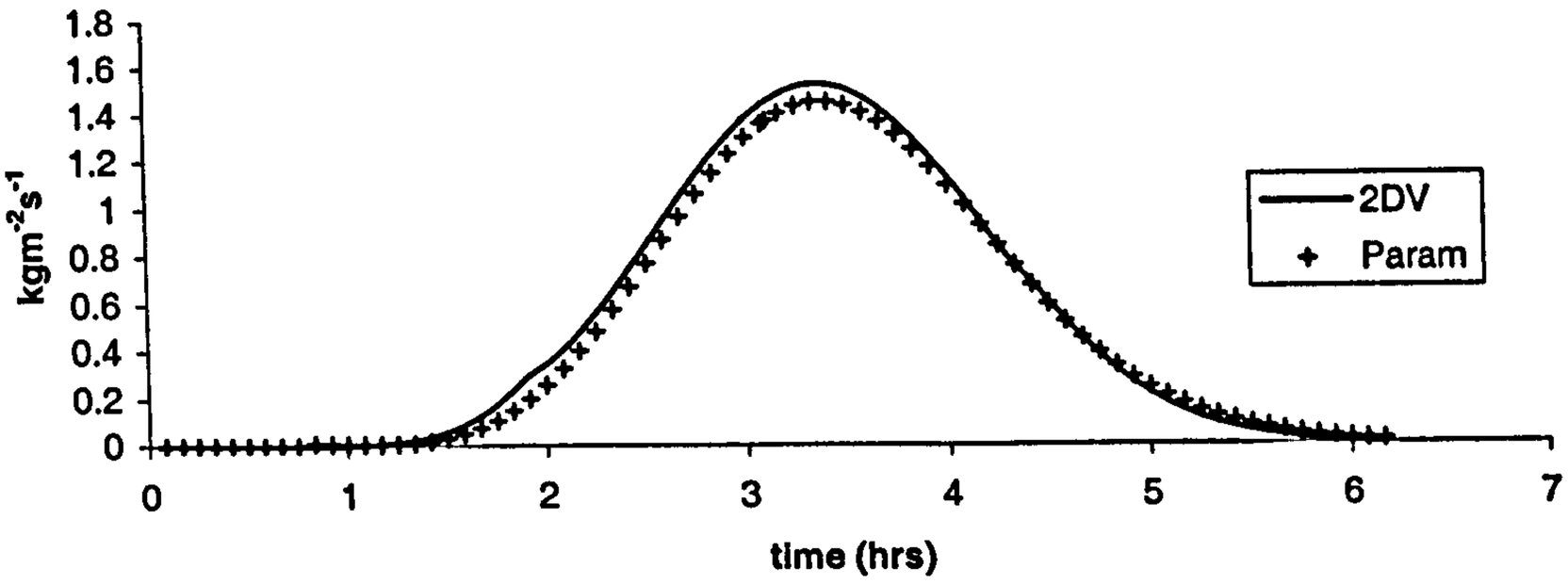

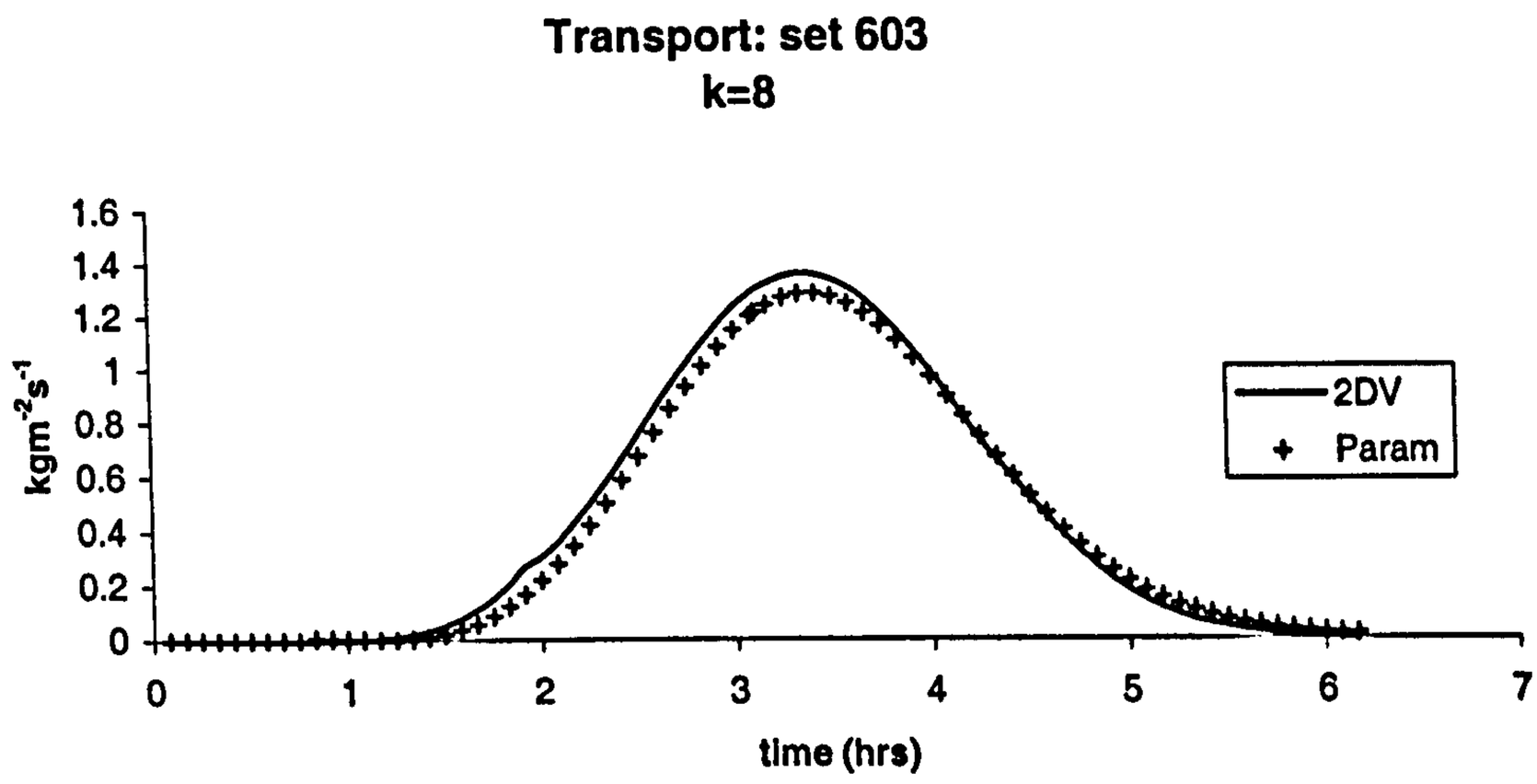

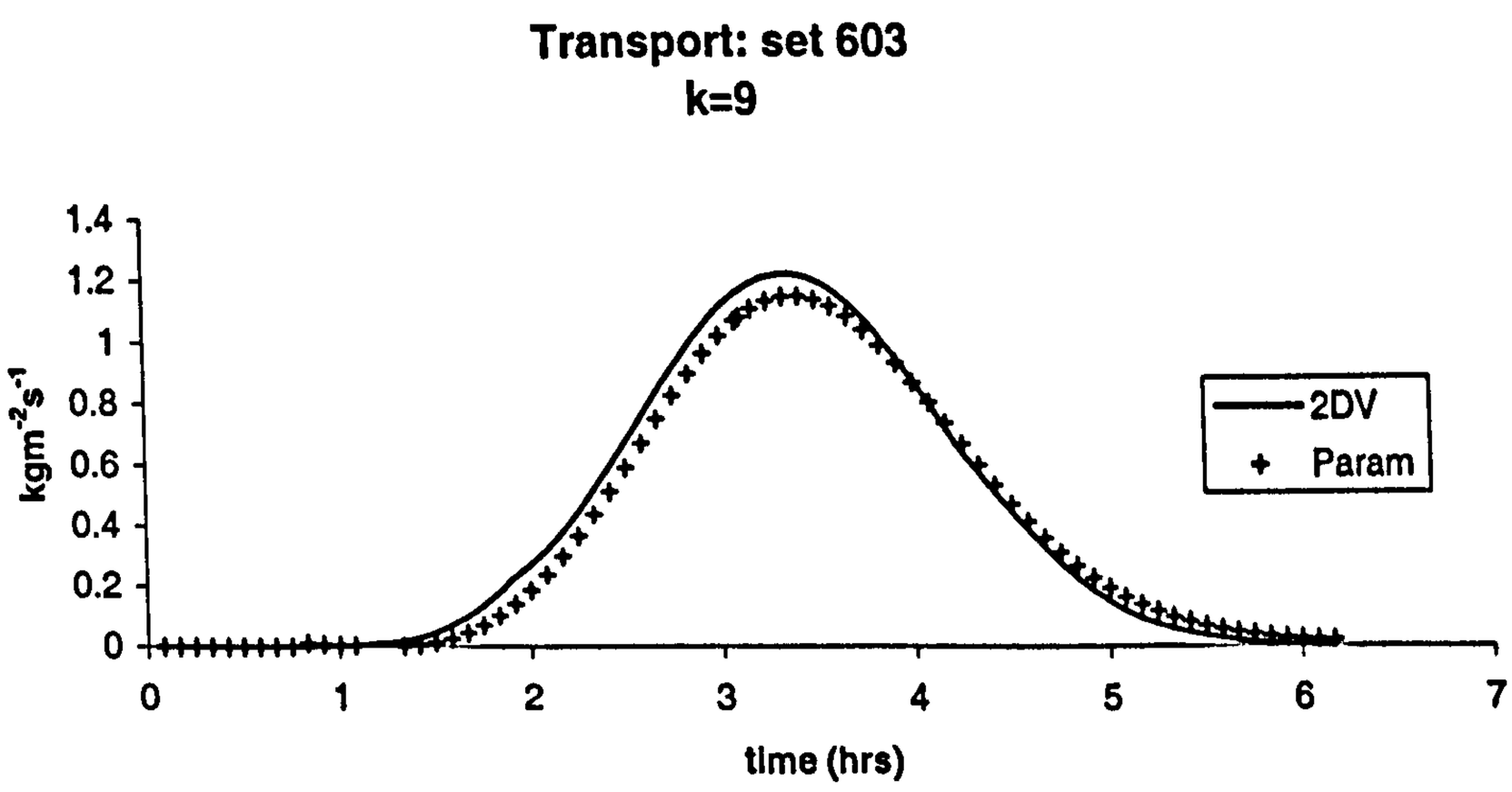

Figure 8.6.7g-i: Comparison between parameterised Corrector (Param) and conventional 2DV (2DV)

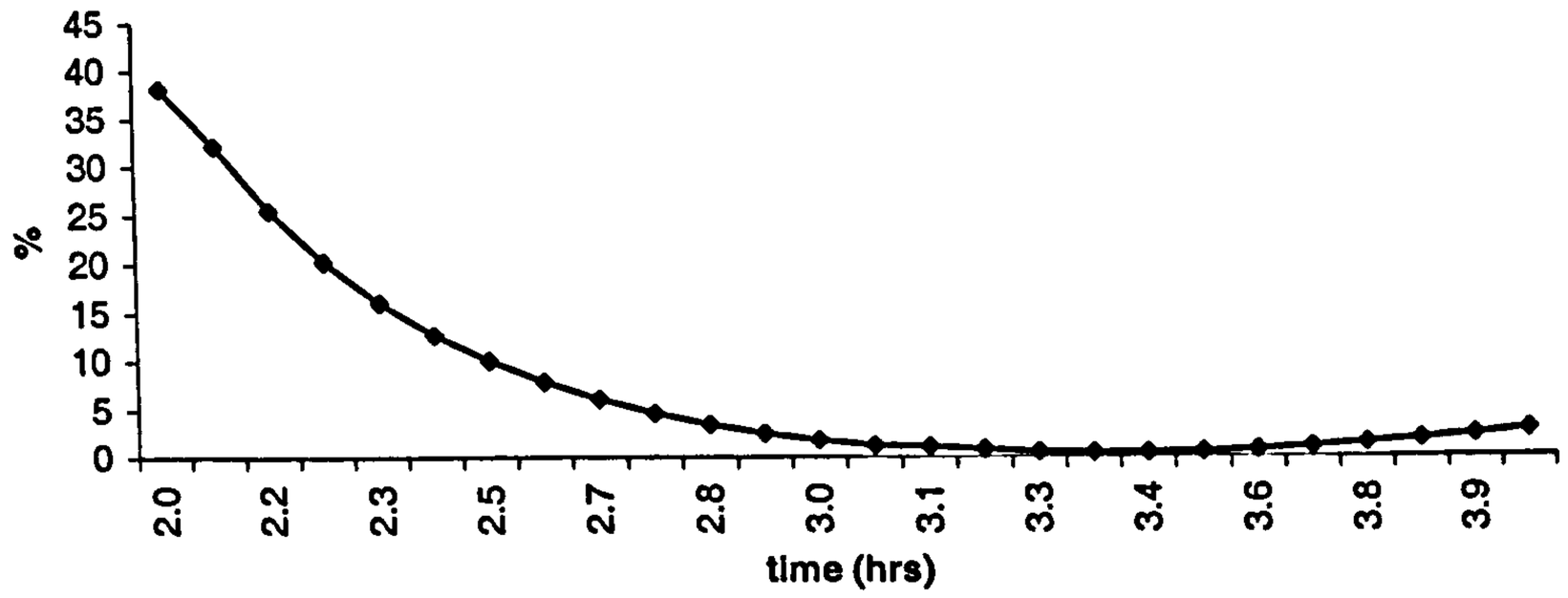

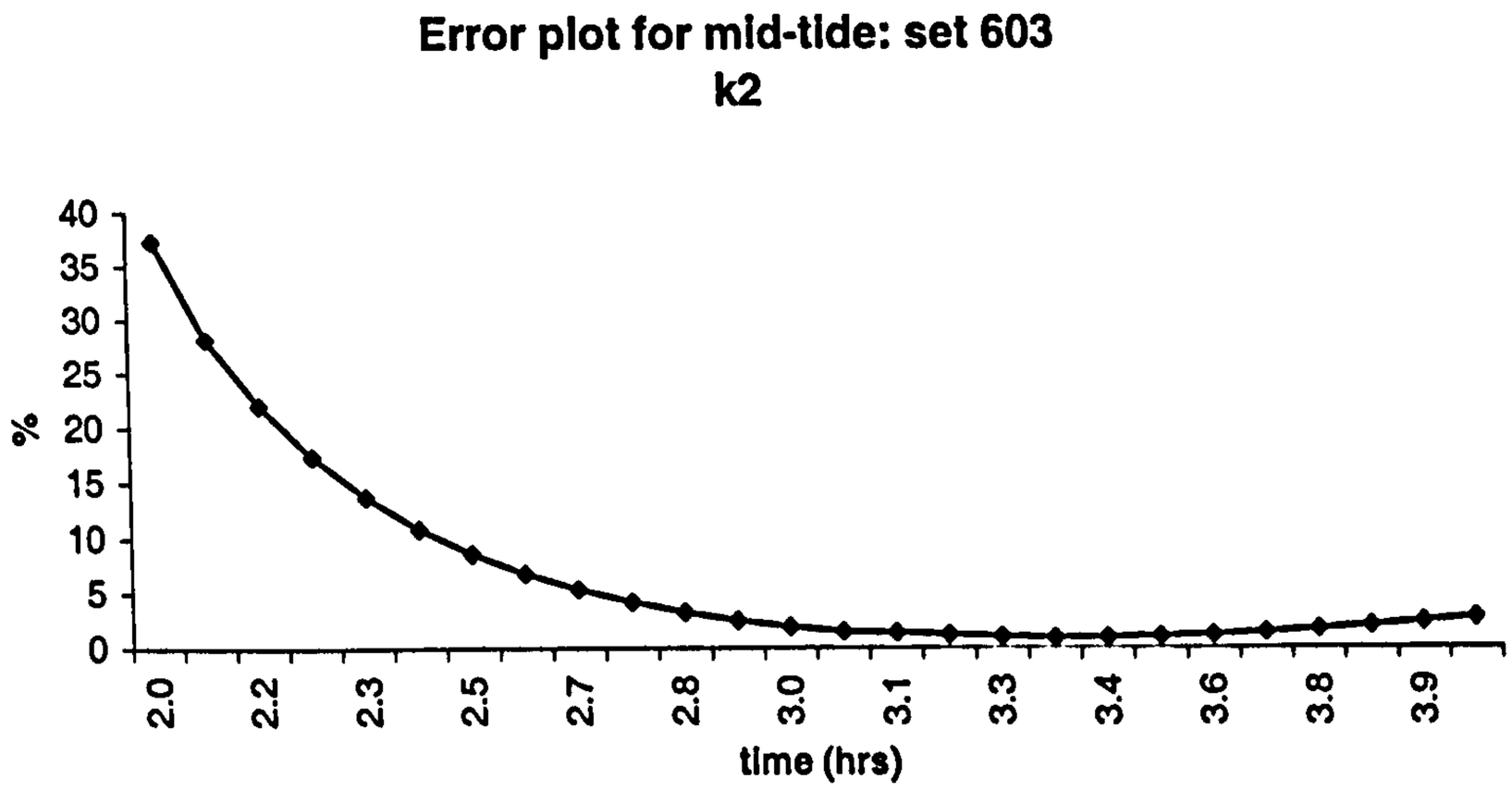

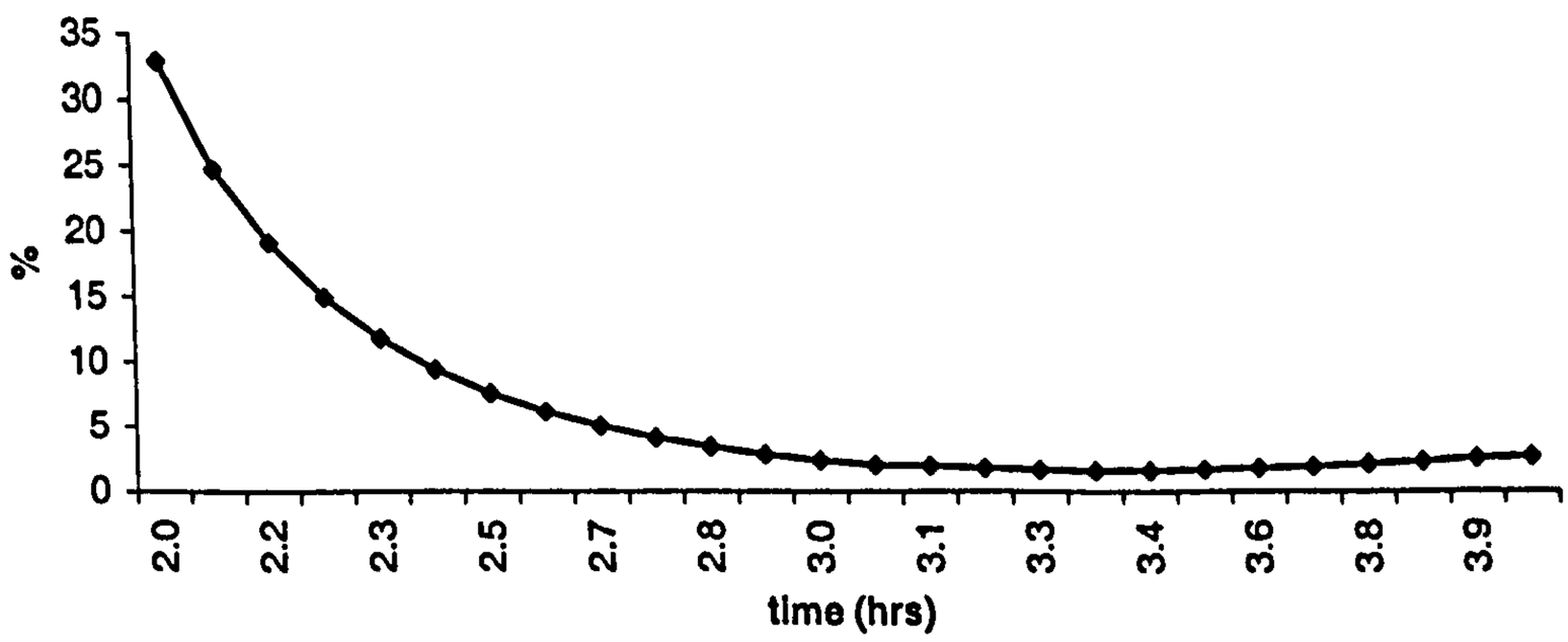

Figure 8.6.8a-c: Error between conventional 2DV method and parameterised Corrector method during the mid-tide phase.

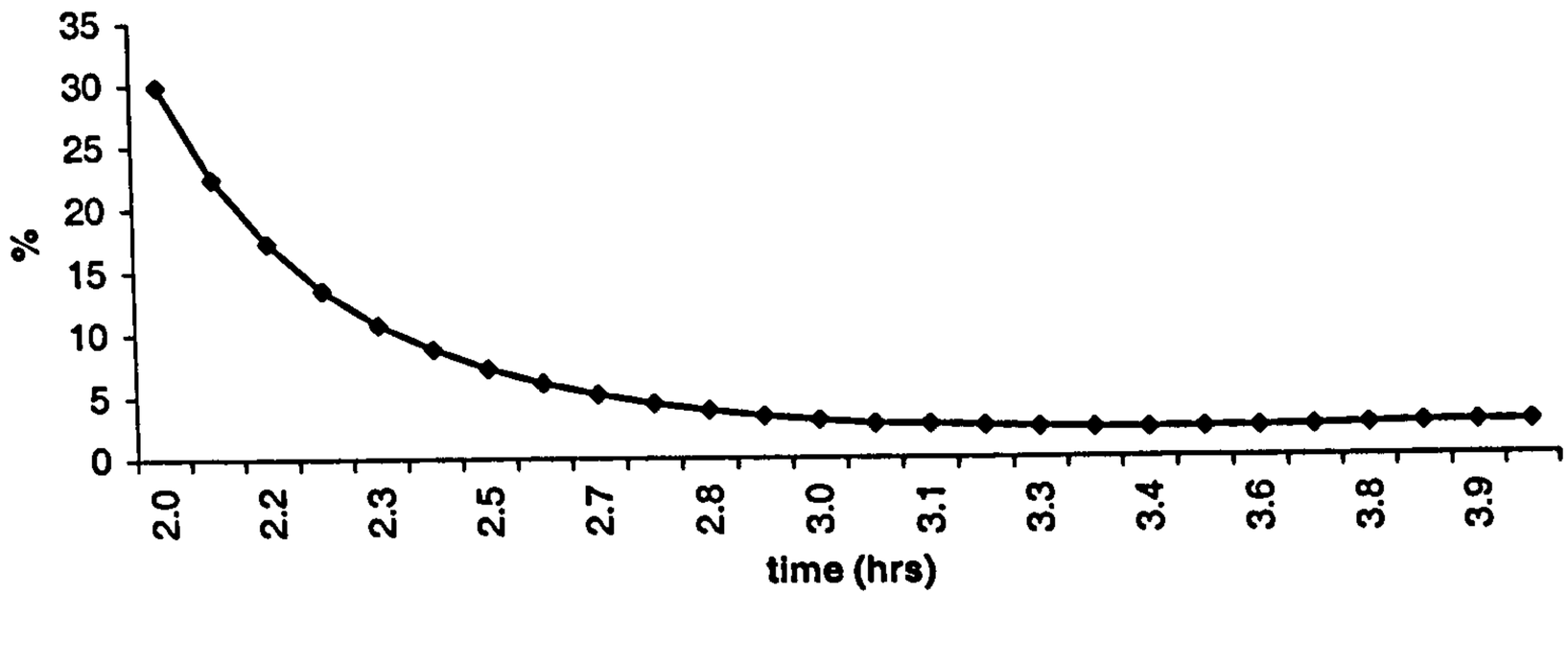

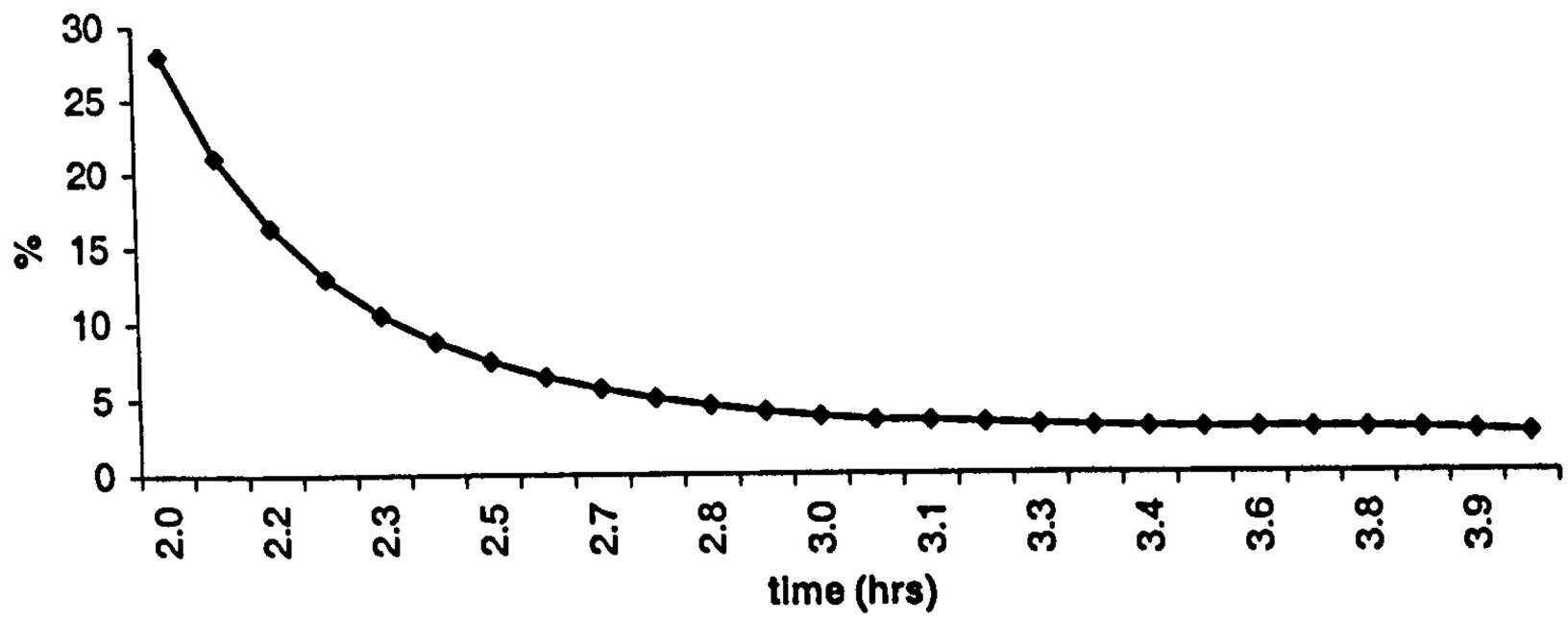

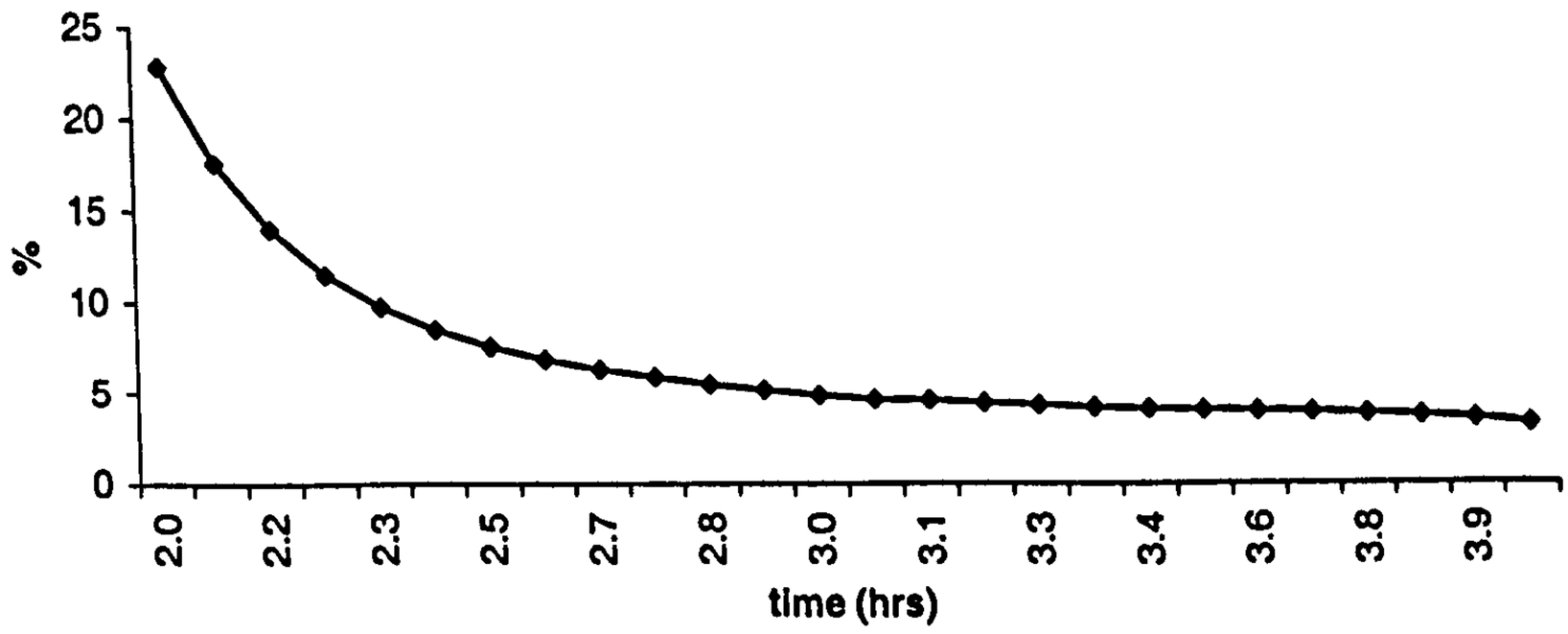

Figure 8.6.8d-f: Error between conventional 2DV method and parameterised Corrector method during the mid-tide phase.

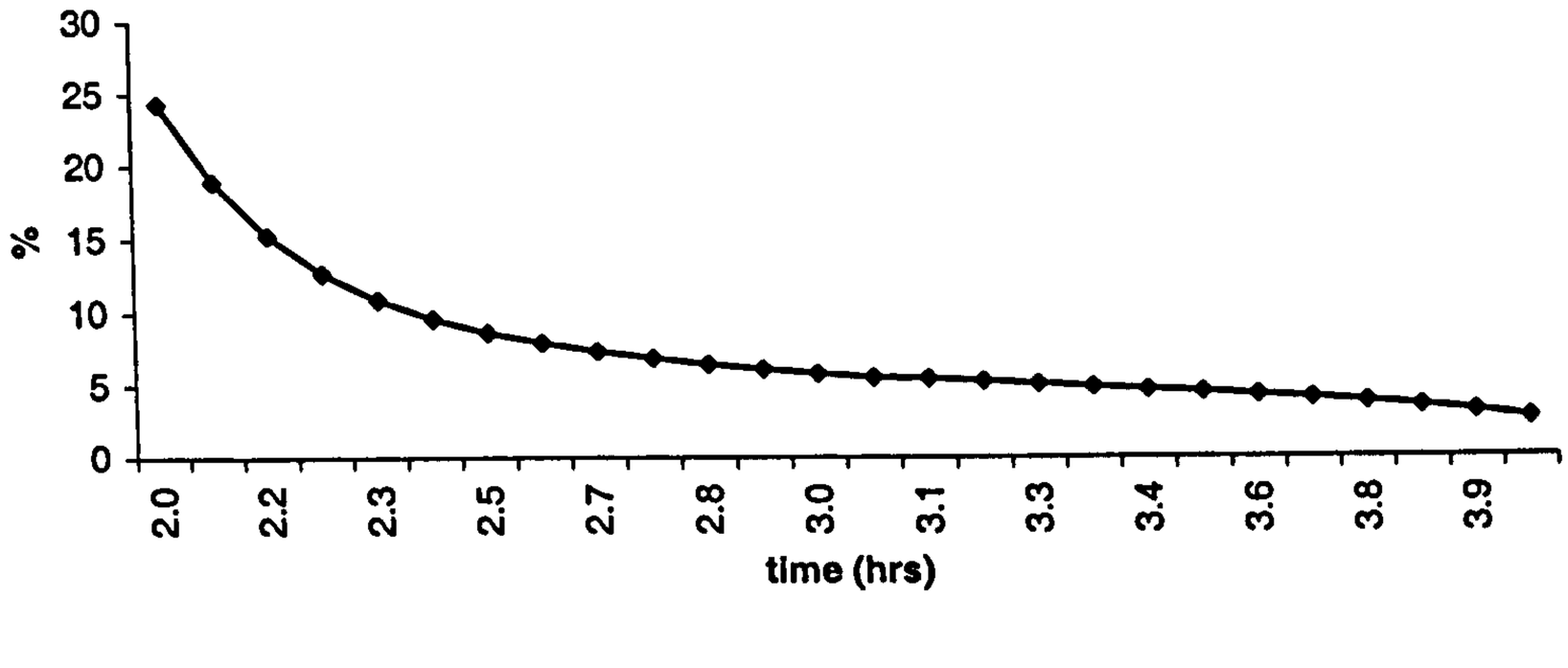

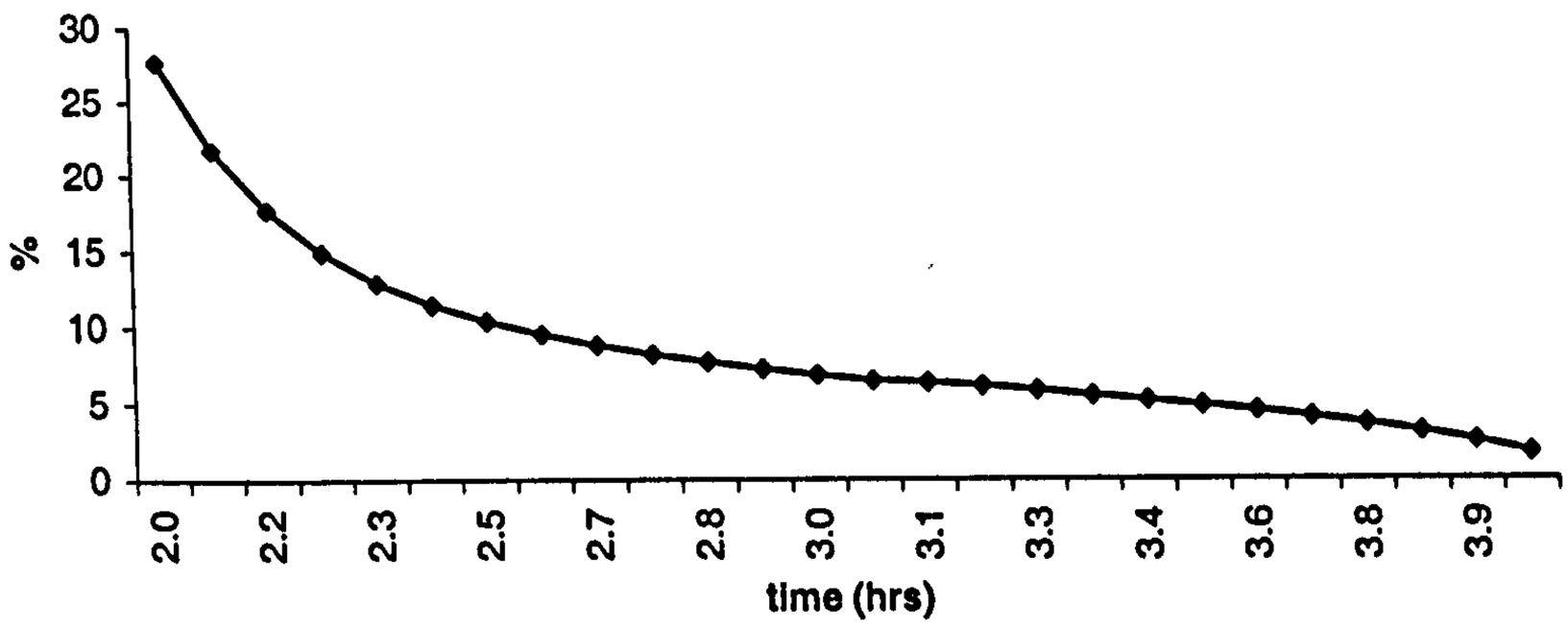

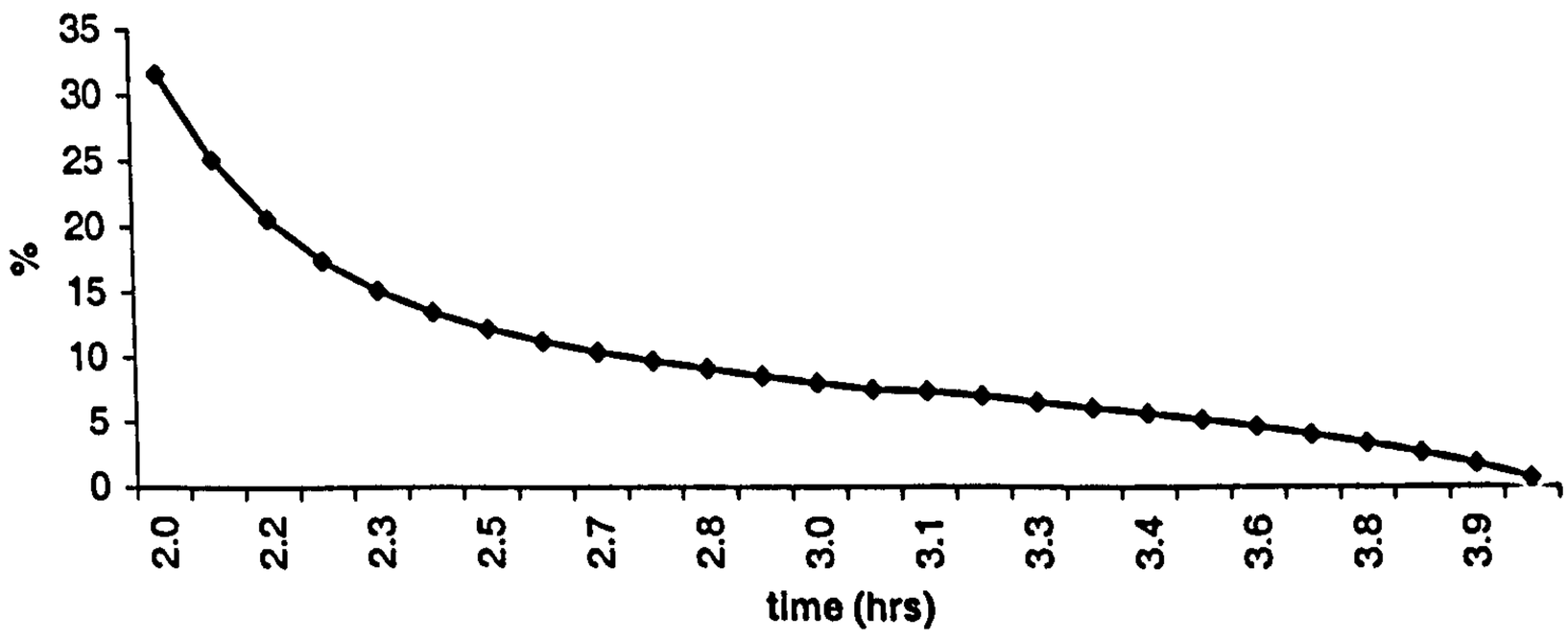

Figure 8.6.8g-i: Error between conventional 2DV method and parameterised Corrector method during the mid-tide phase.

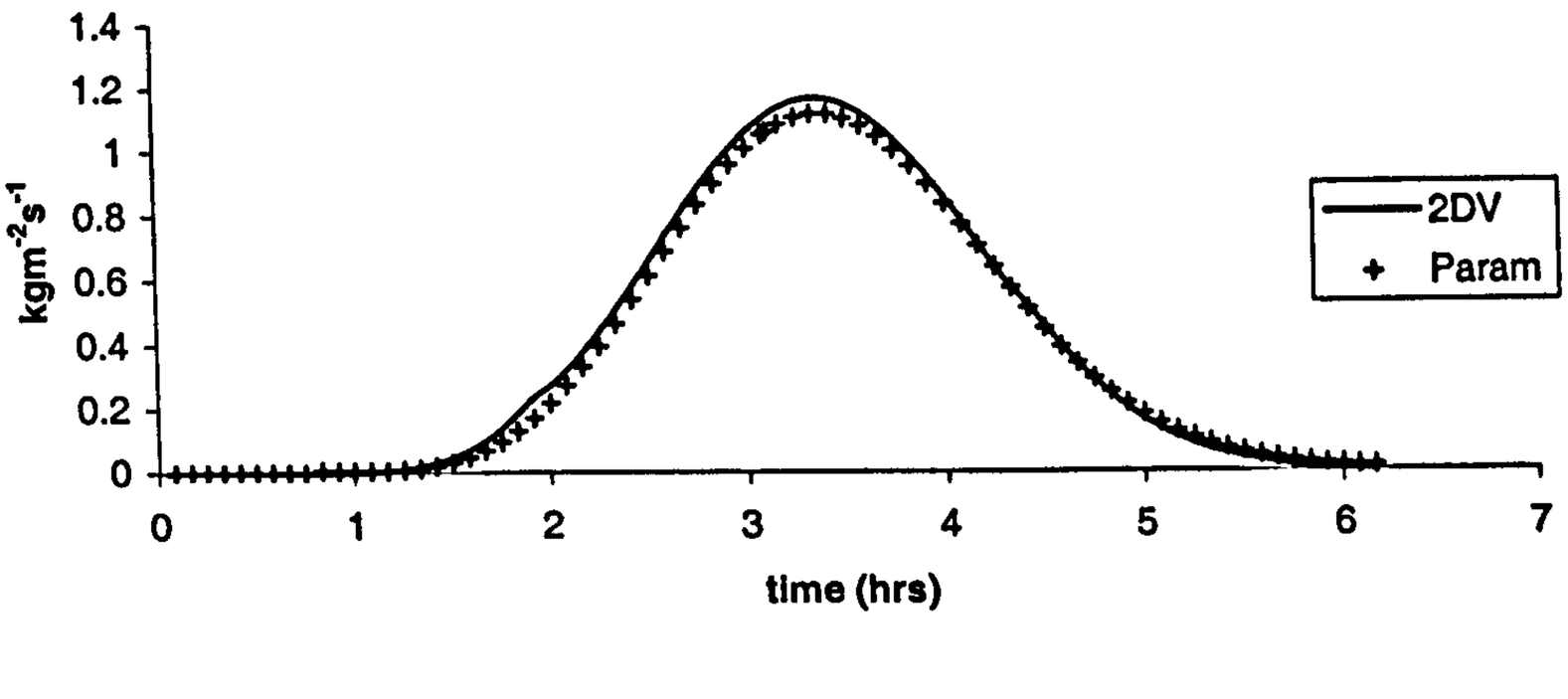

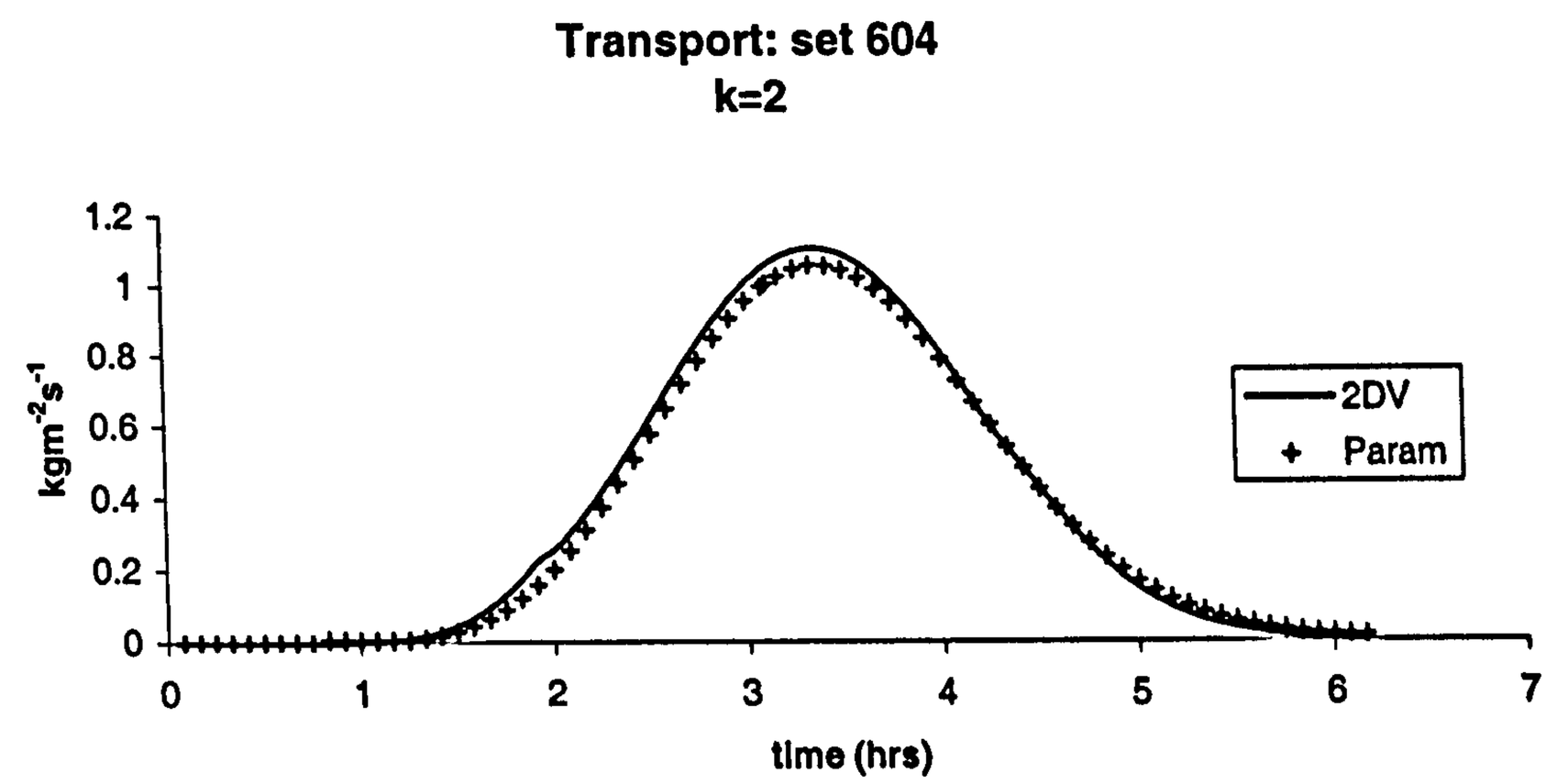

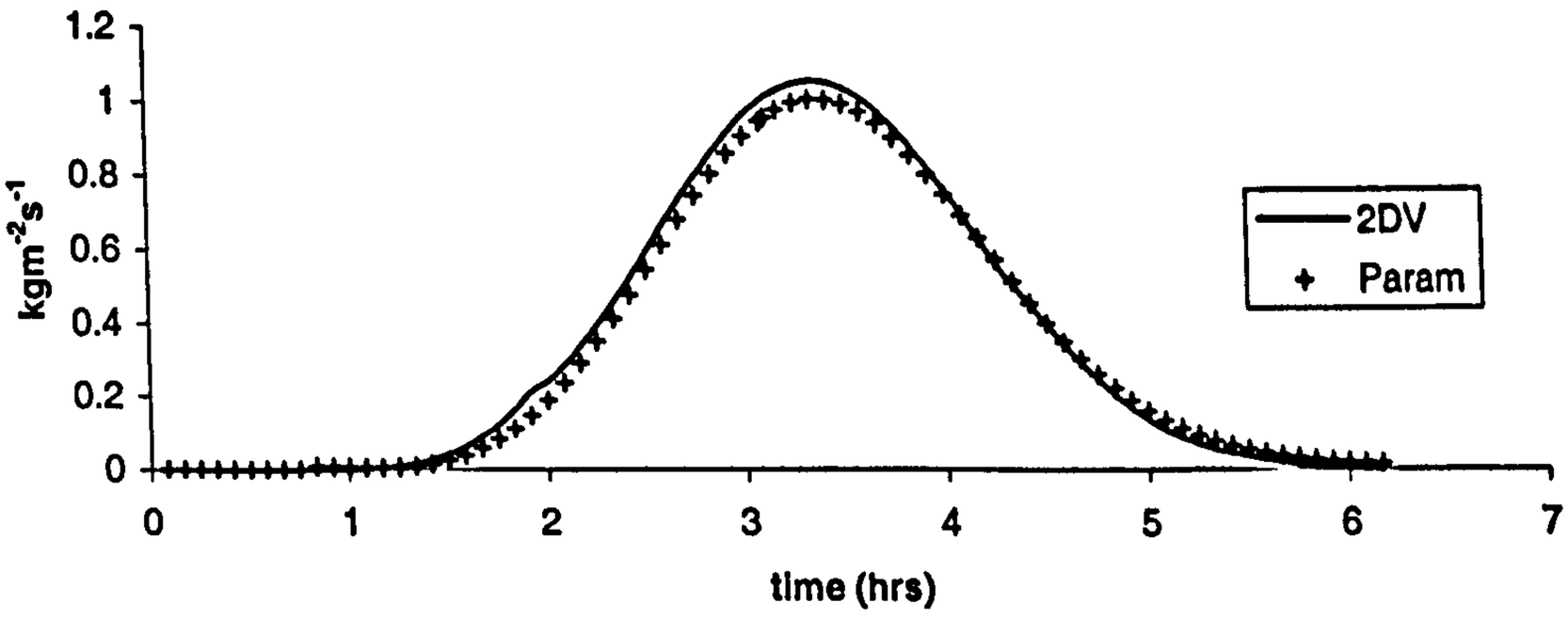

Figure 8.6.9a-c: Comparison between parameterised Corrector (Param) and conventional 2DV (2DV)

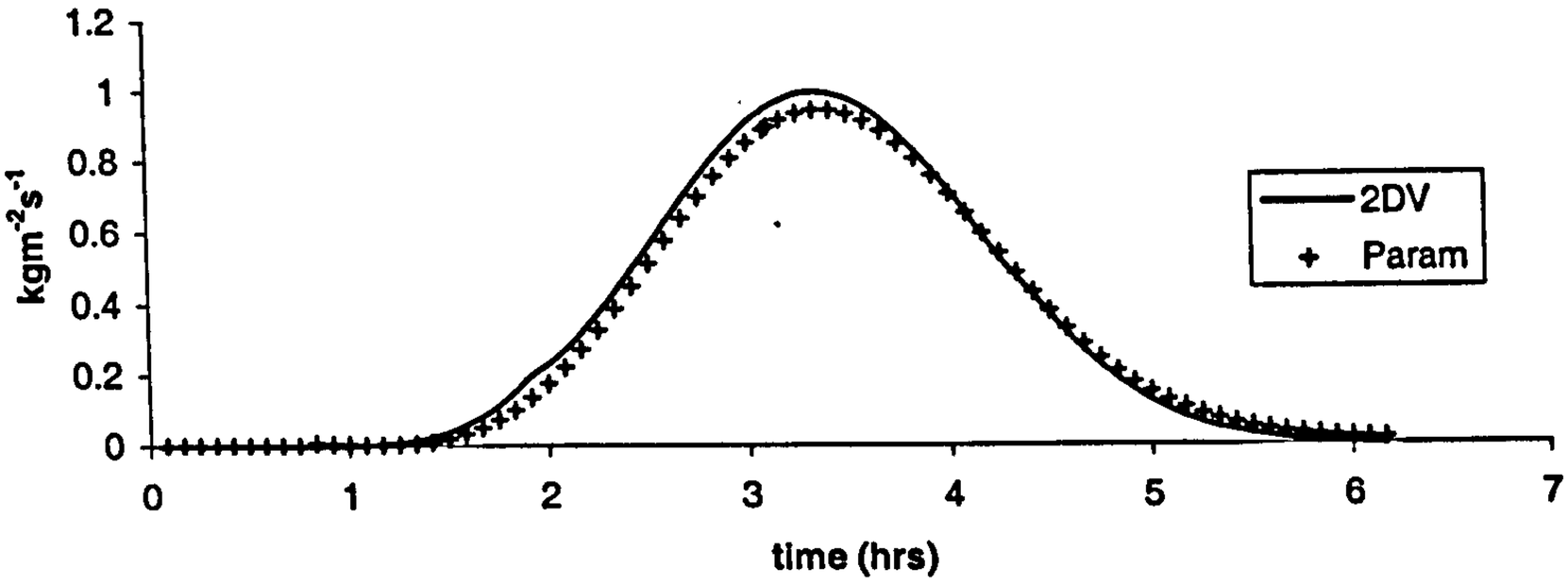

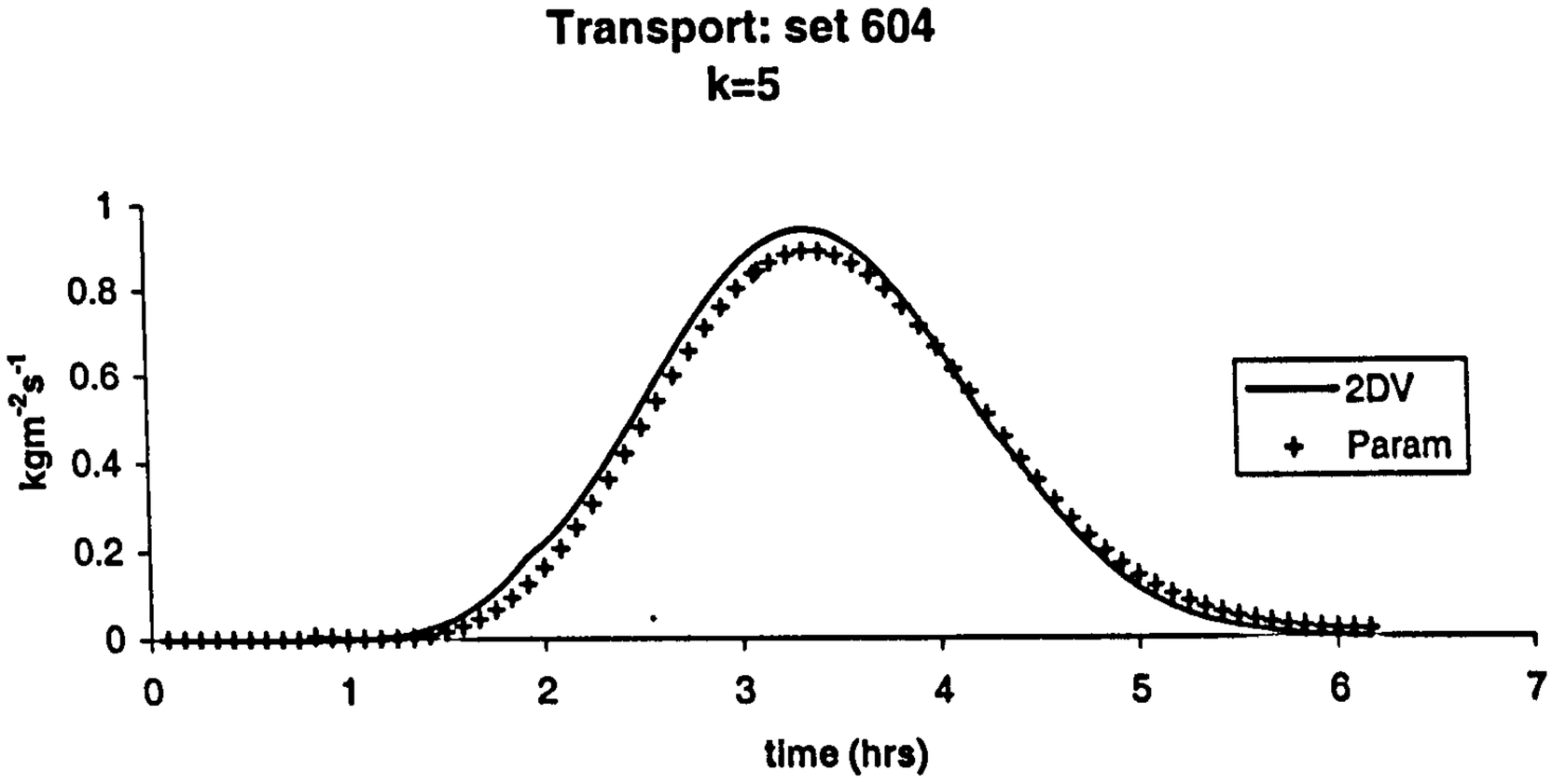

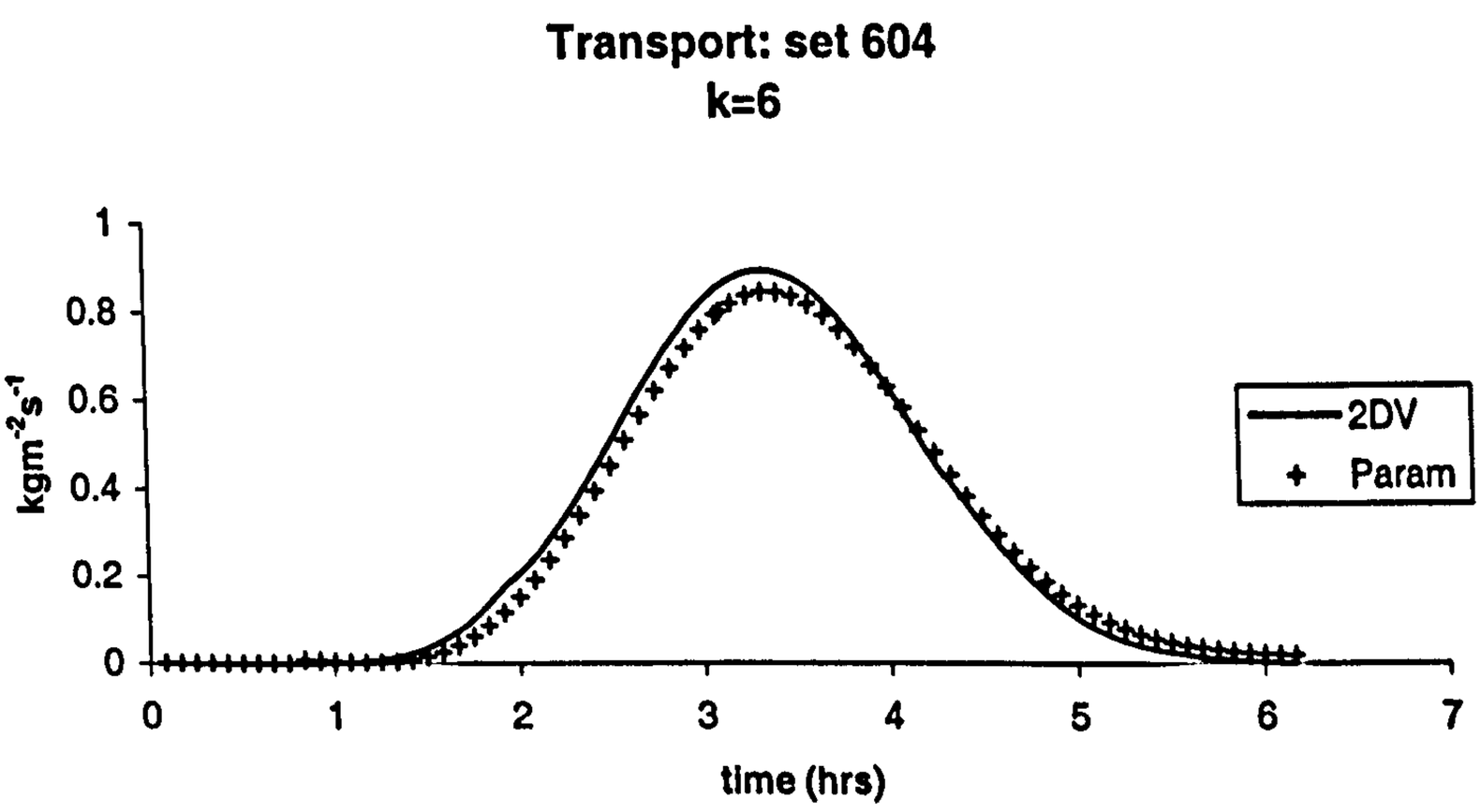

Figure 8.6.9d-f: Comparison between parameterised Corrector (Param) and conventional 2DV (2DV)

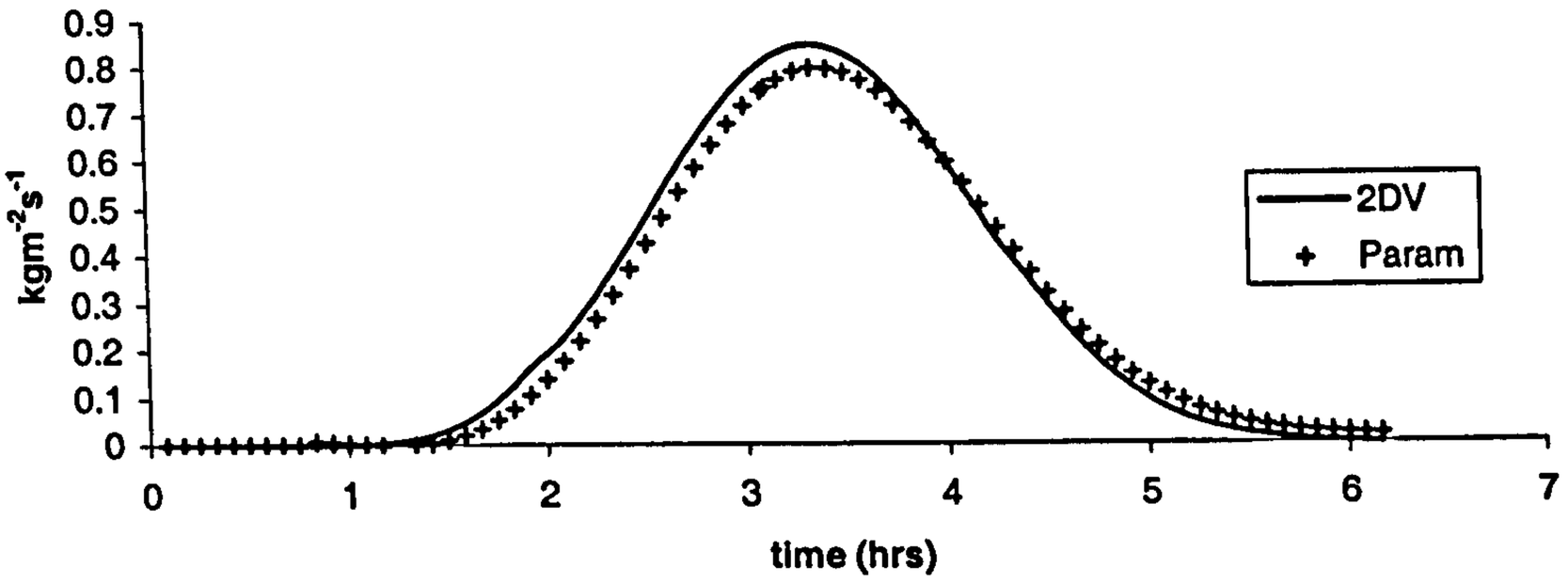

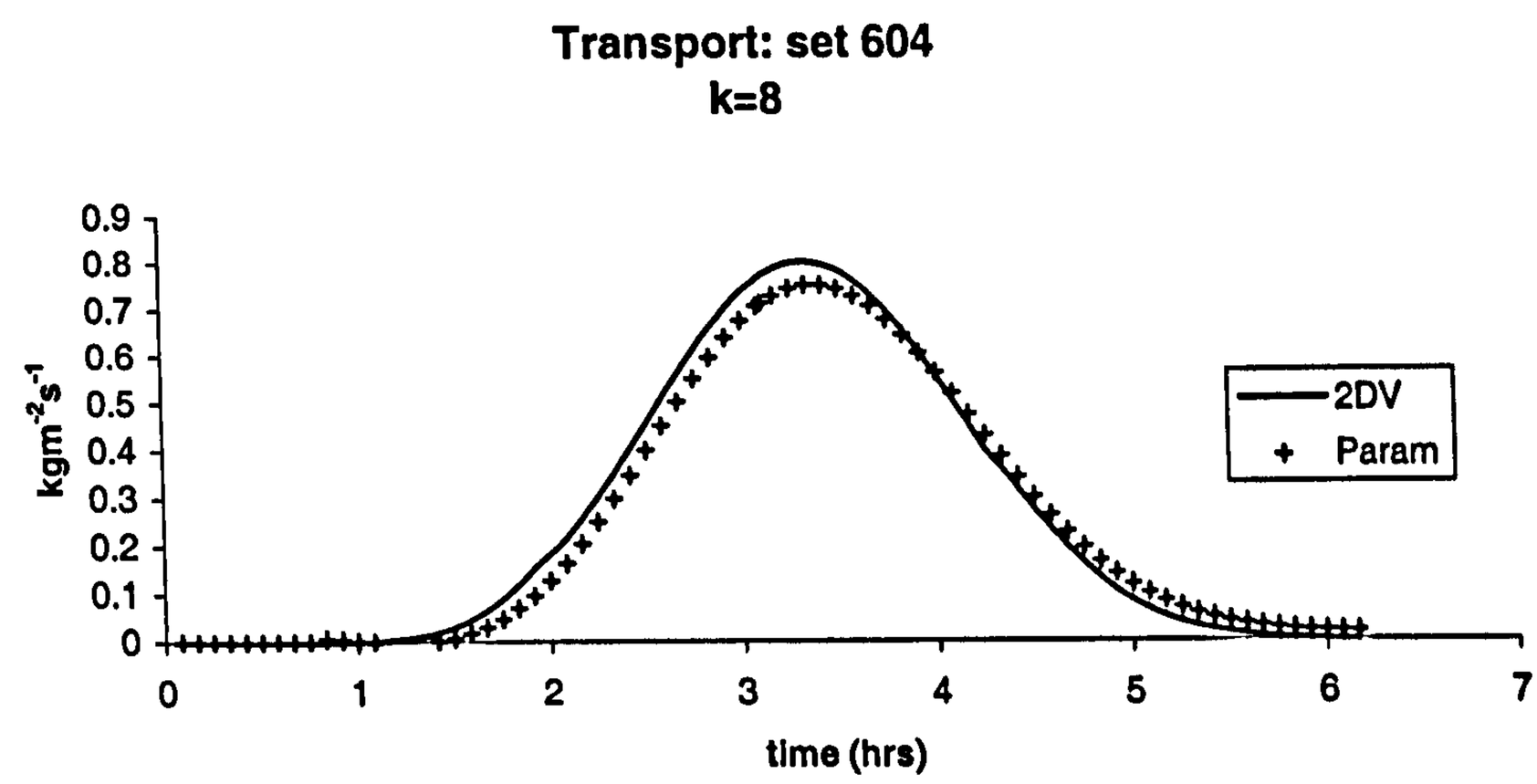

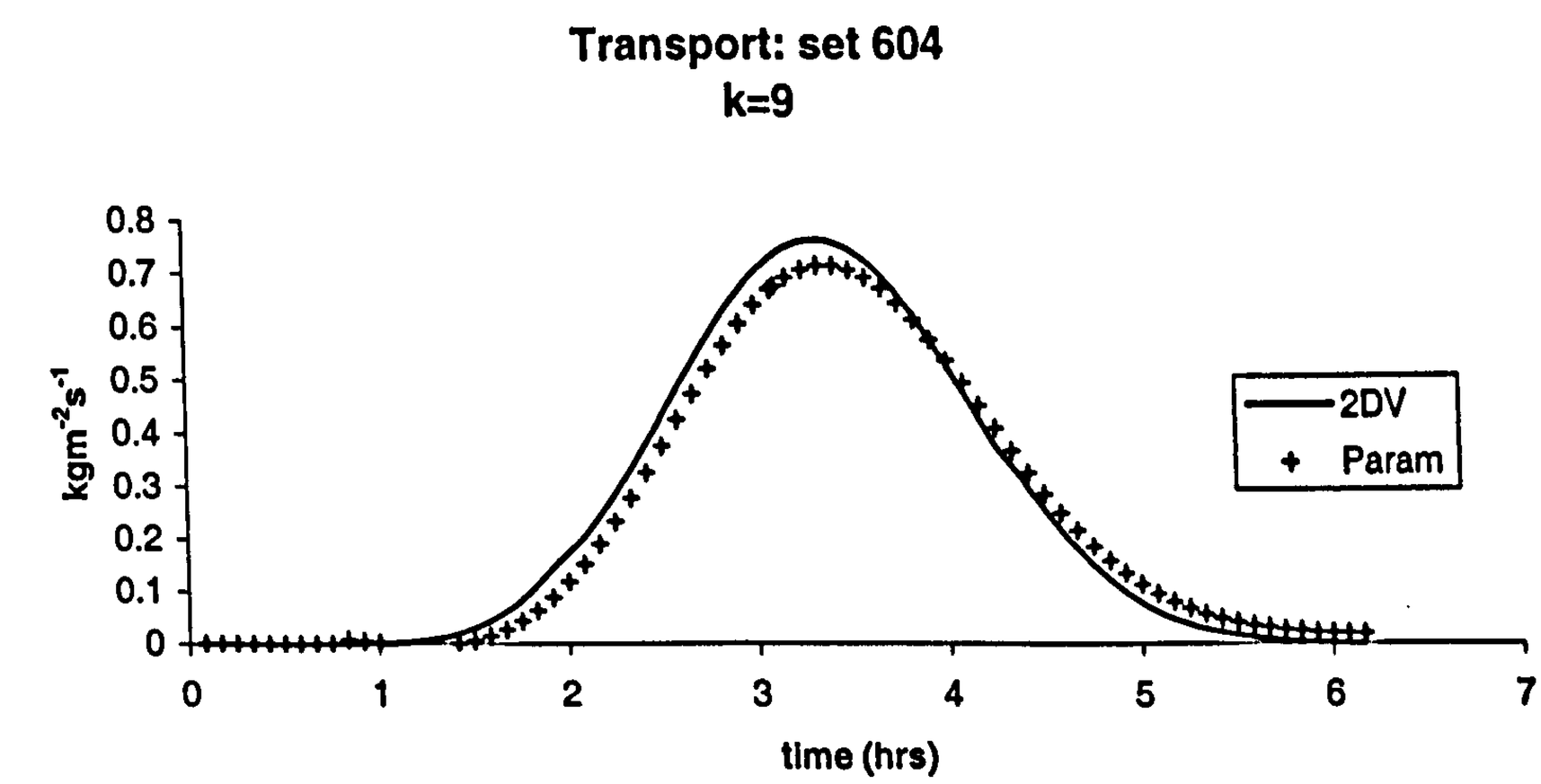

Figure 8.6.9g-i: Comparison between parameterised Corrector (Param) and conventional 2DV (2DV)

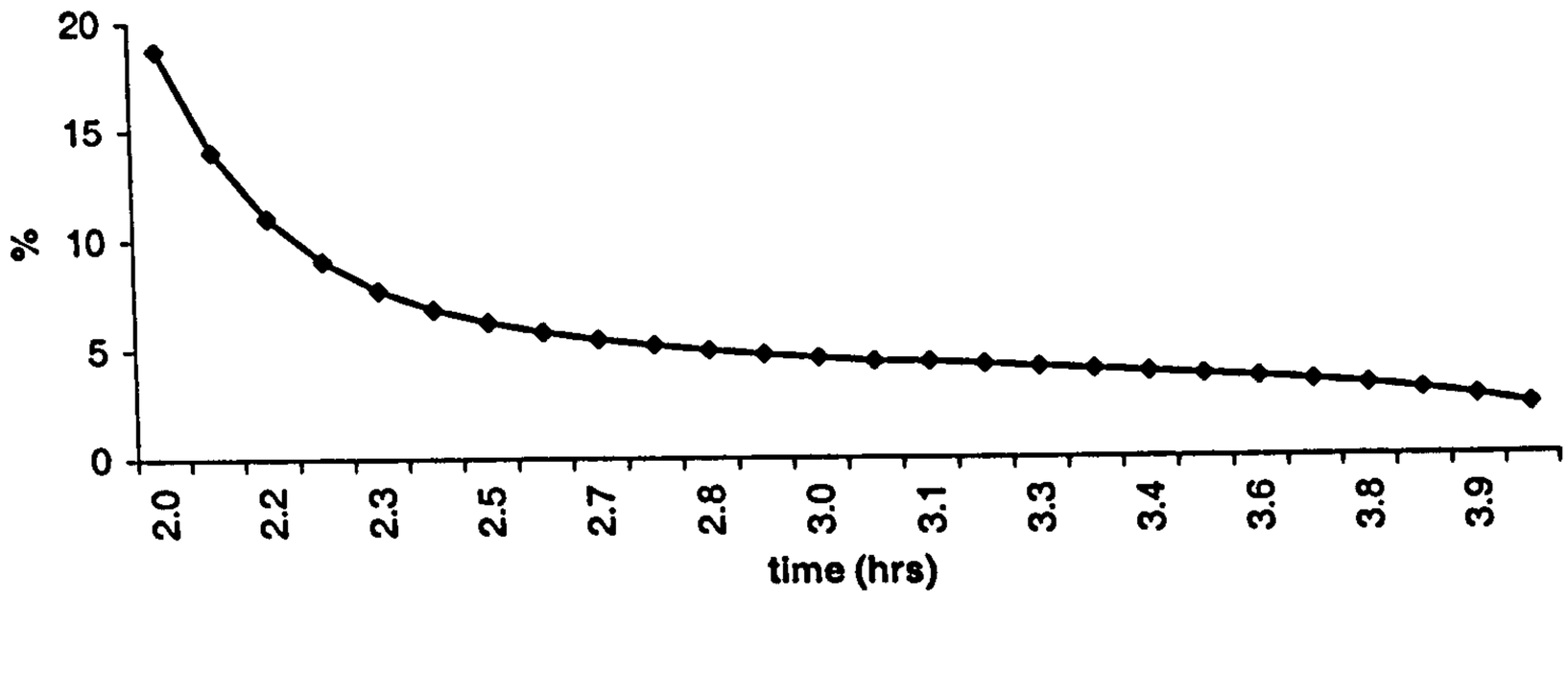

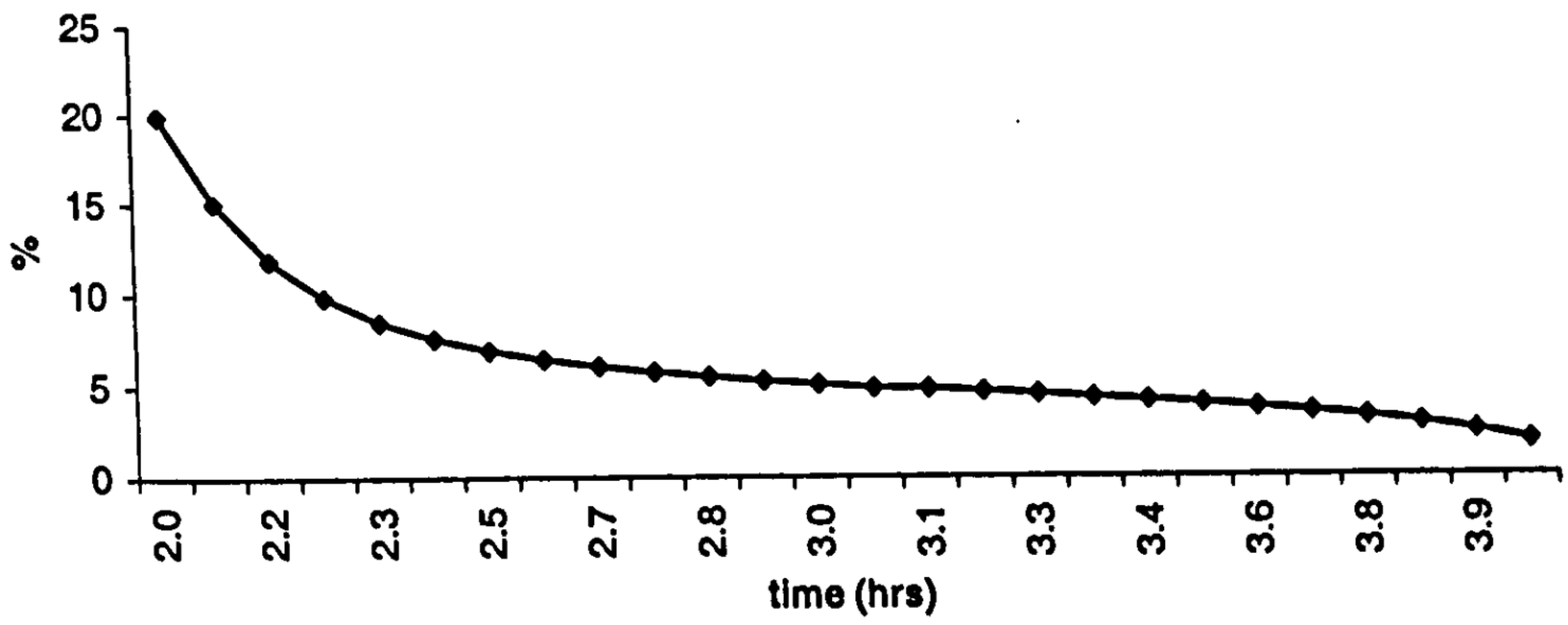

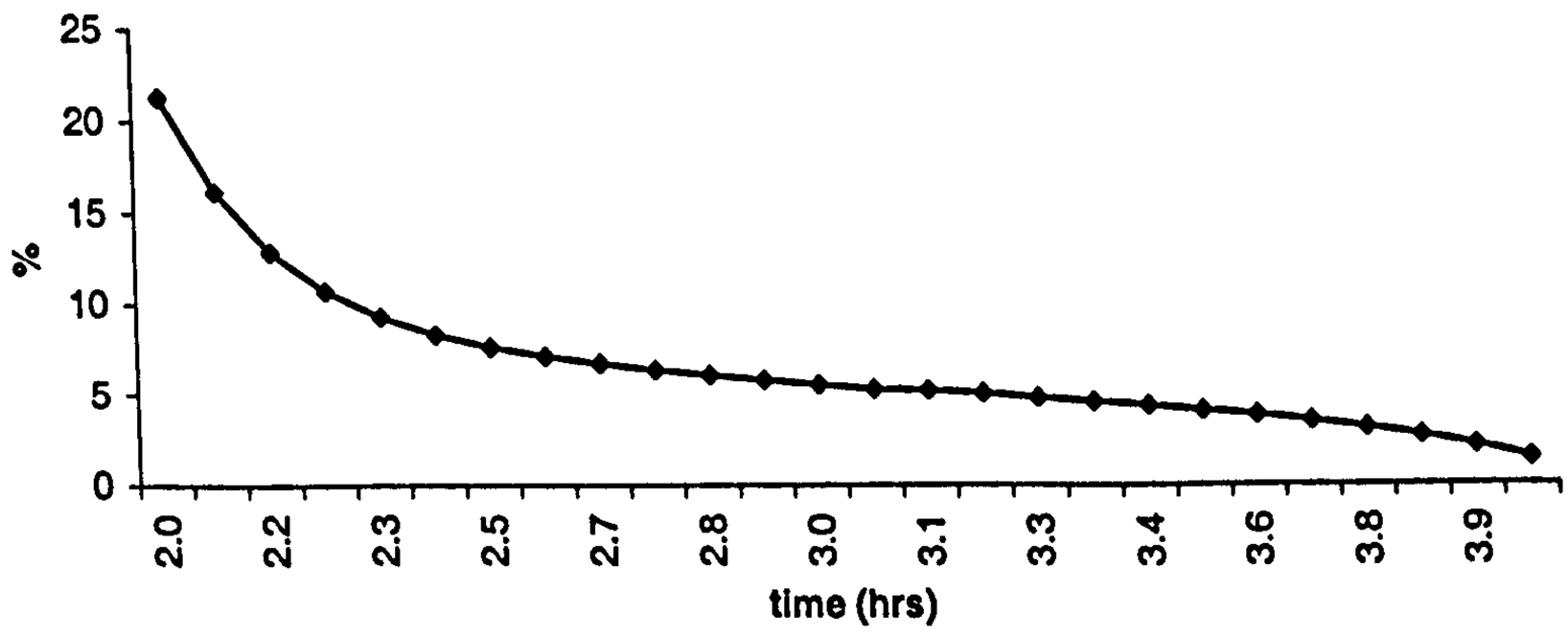

Figure 8.6.10a-c: Error between conventional 2DV method and parameterised Corrector method during the mid-tide phase.

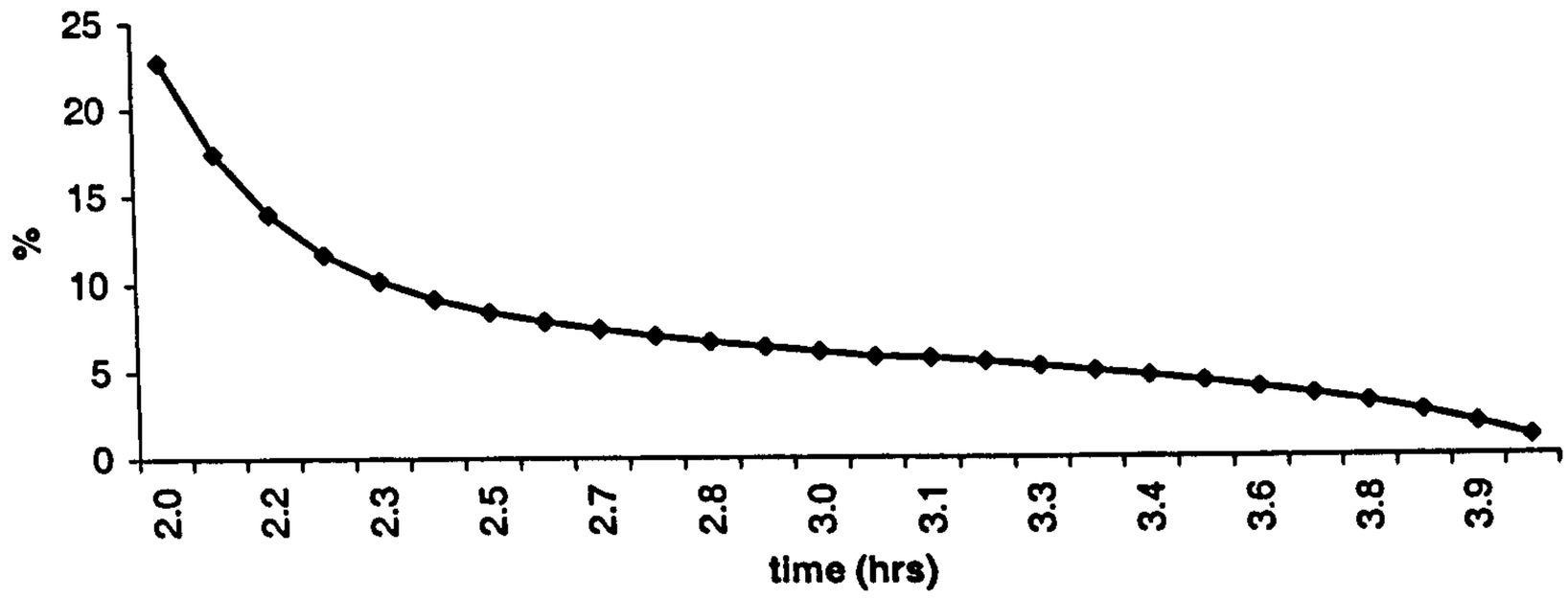

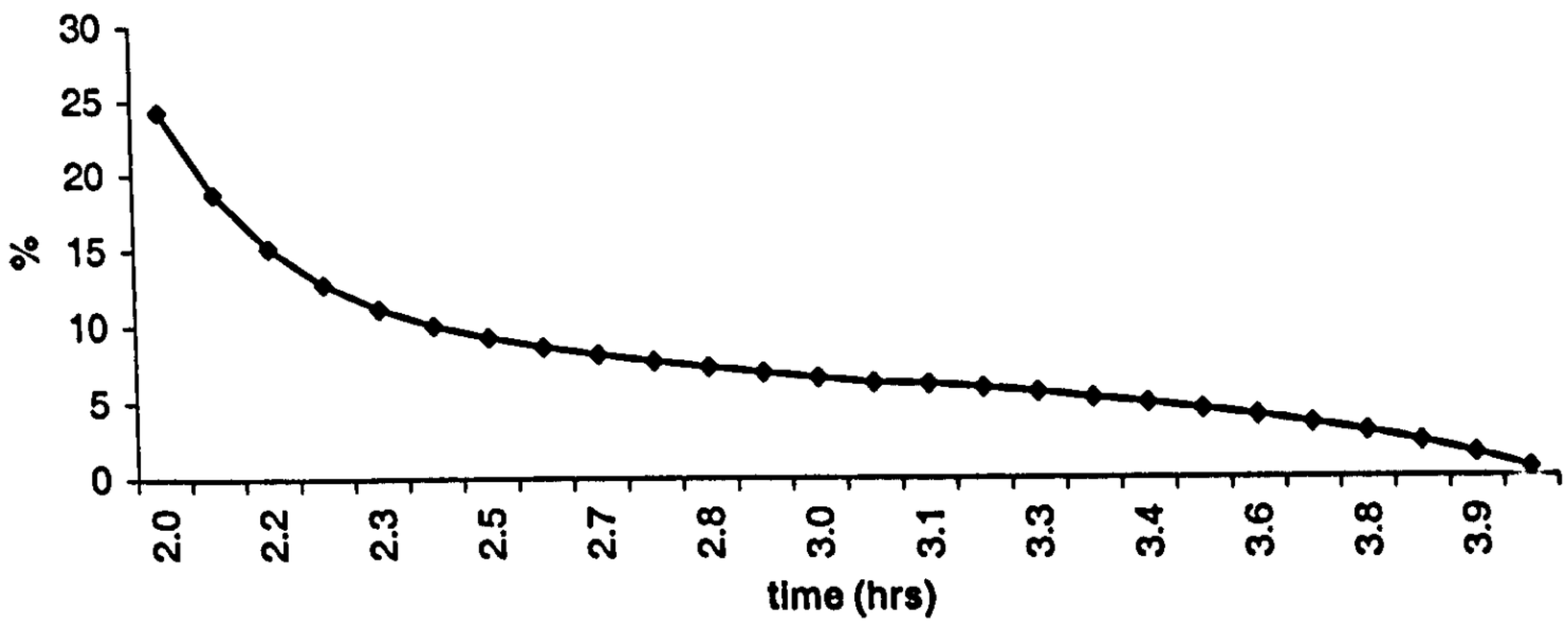

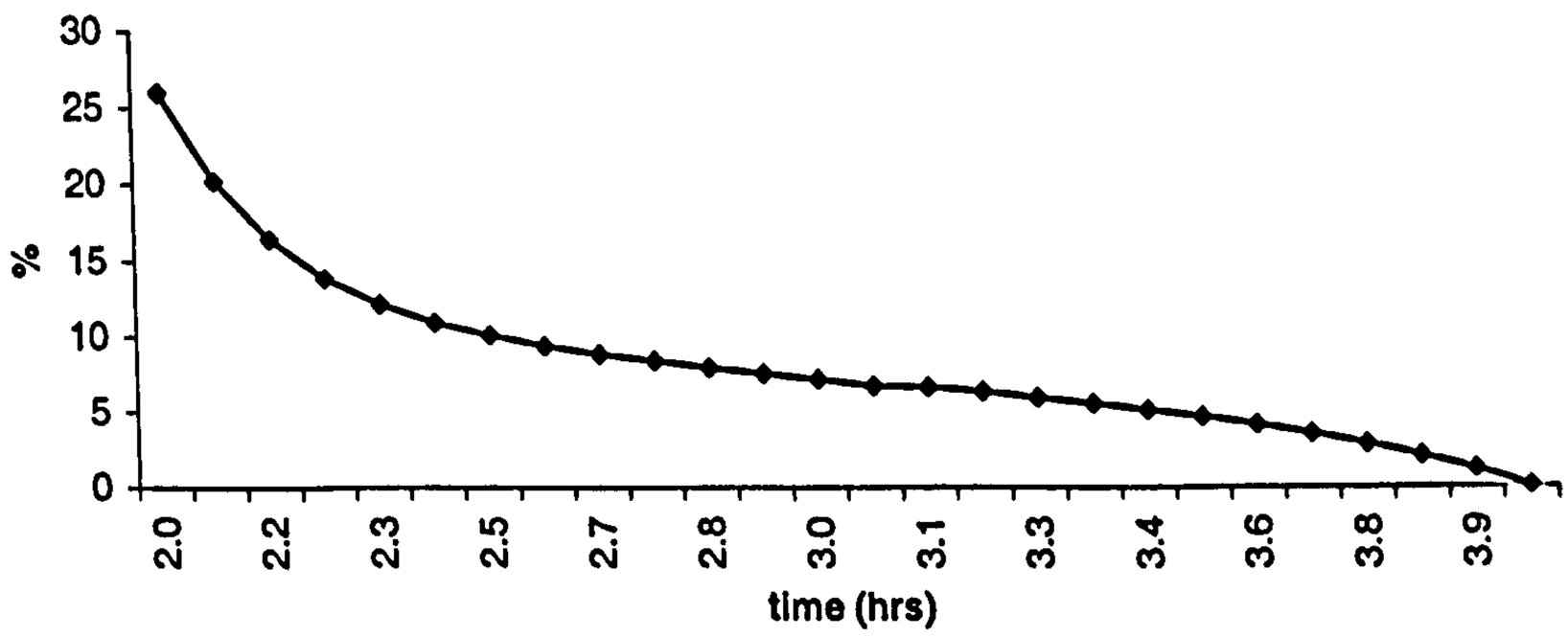

Figure 8.6.10d-f: Error between conventional 2DV method and parameterised Corrector method during the mid-tide phase.

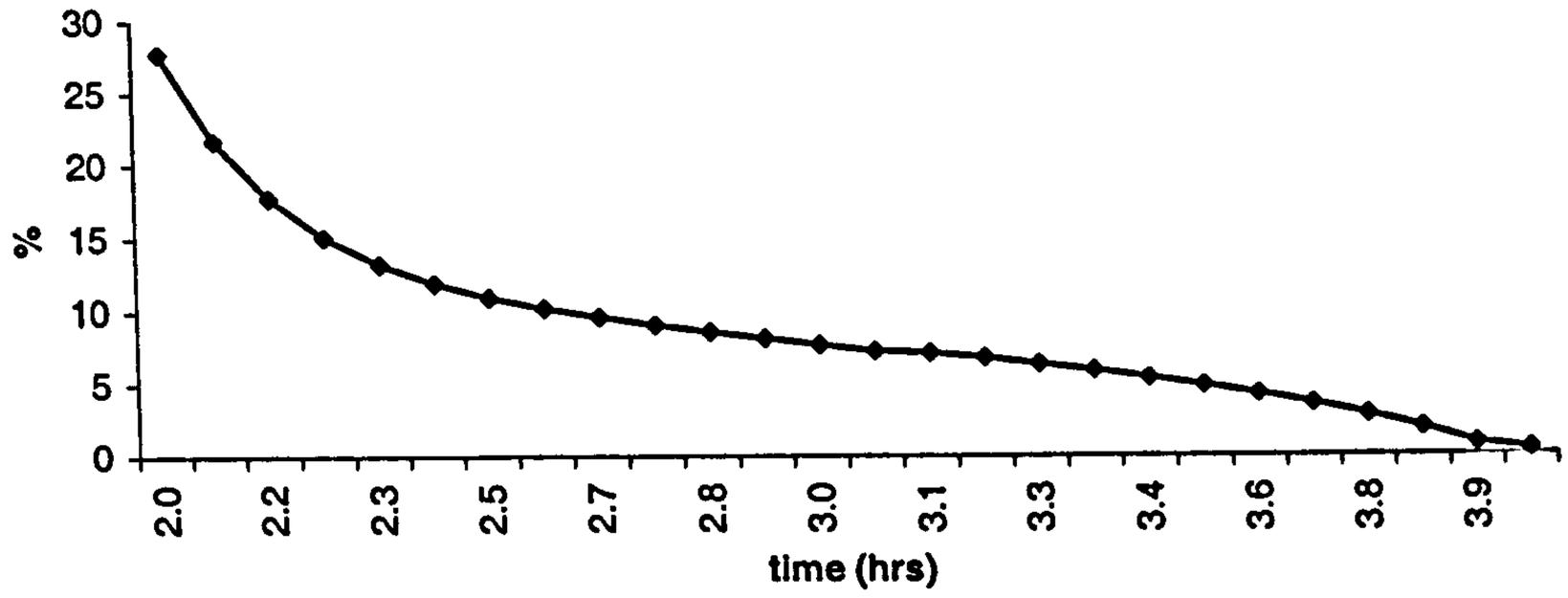

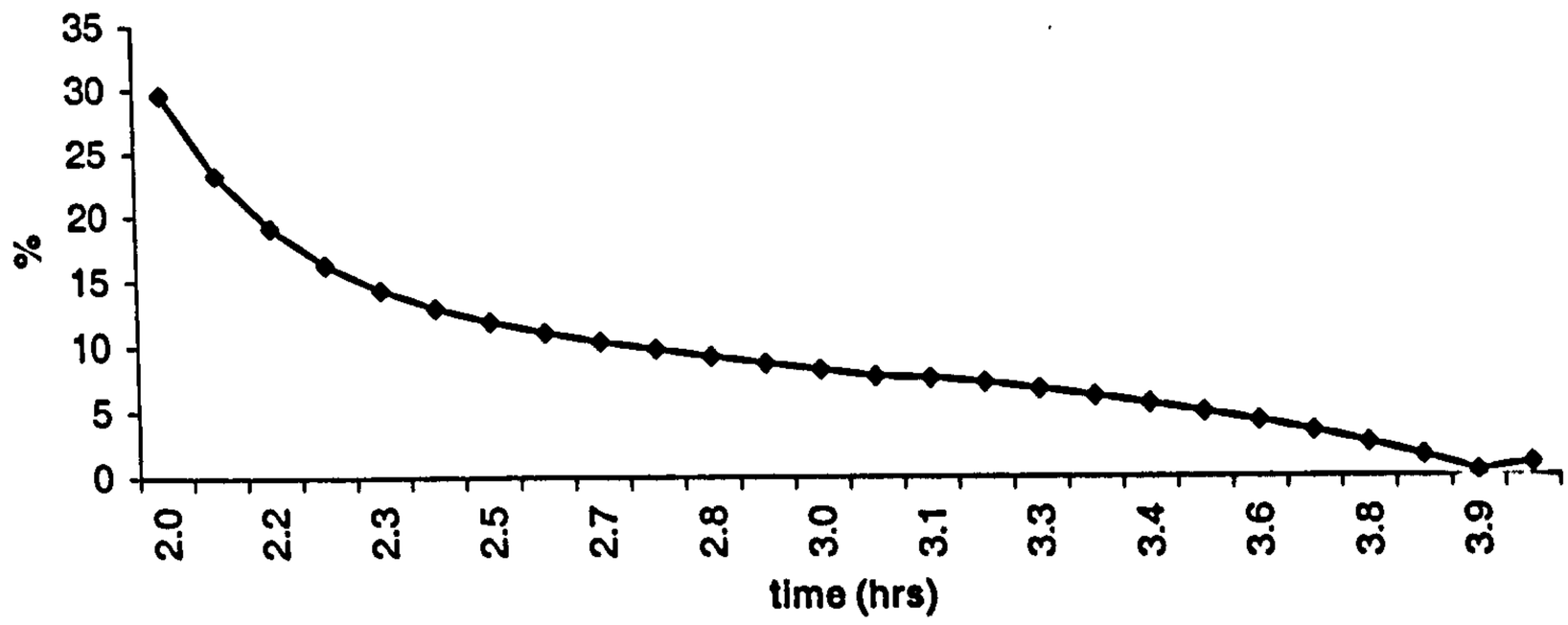

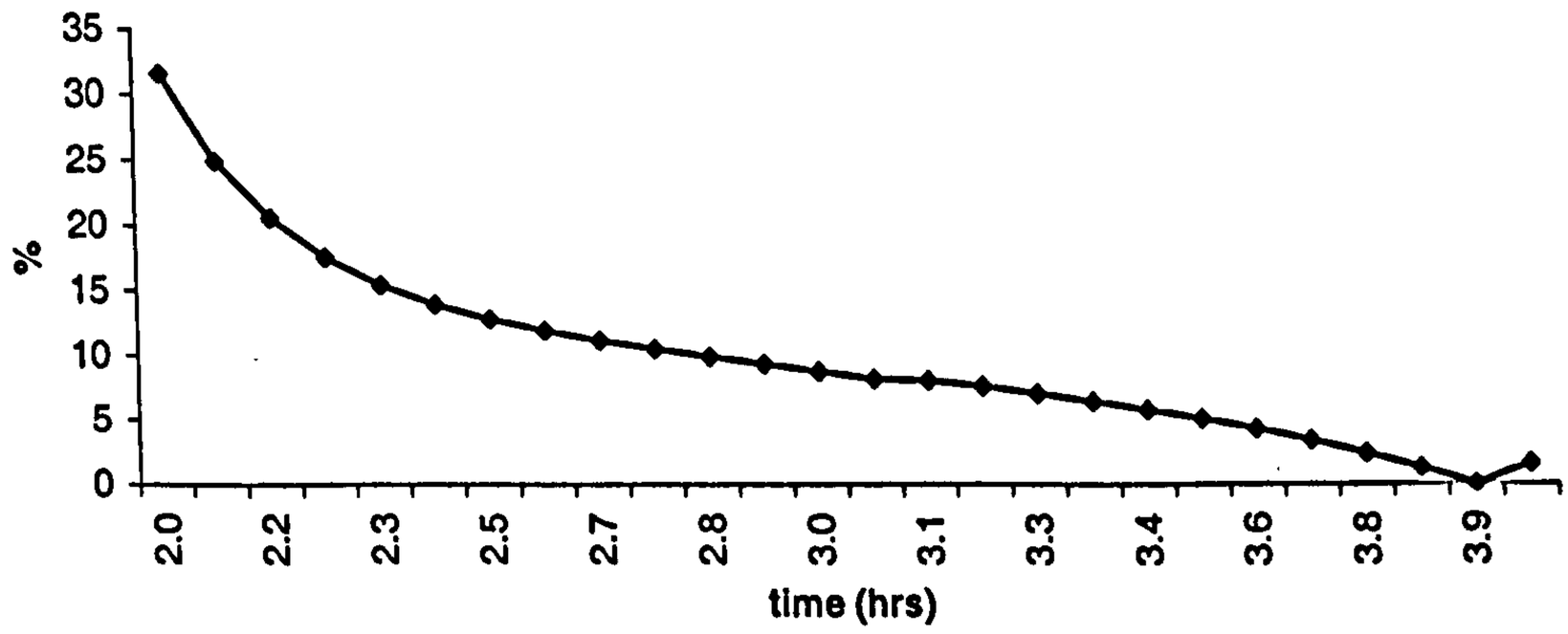

Figure 8.6.10g-i: Error between conventional 2DV method and parameterised Corrector method during the mid-tide phase.

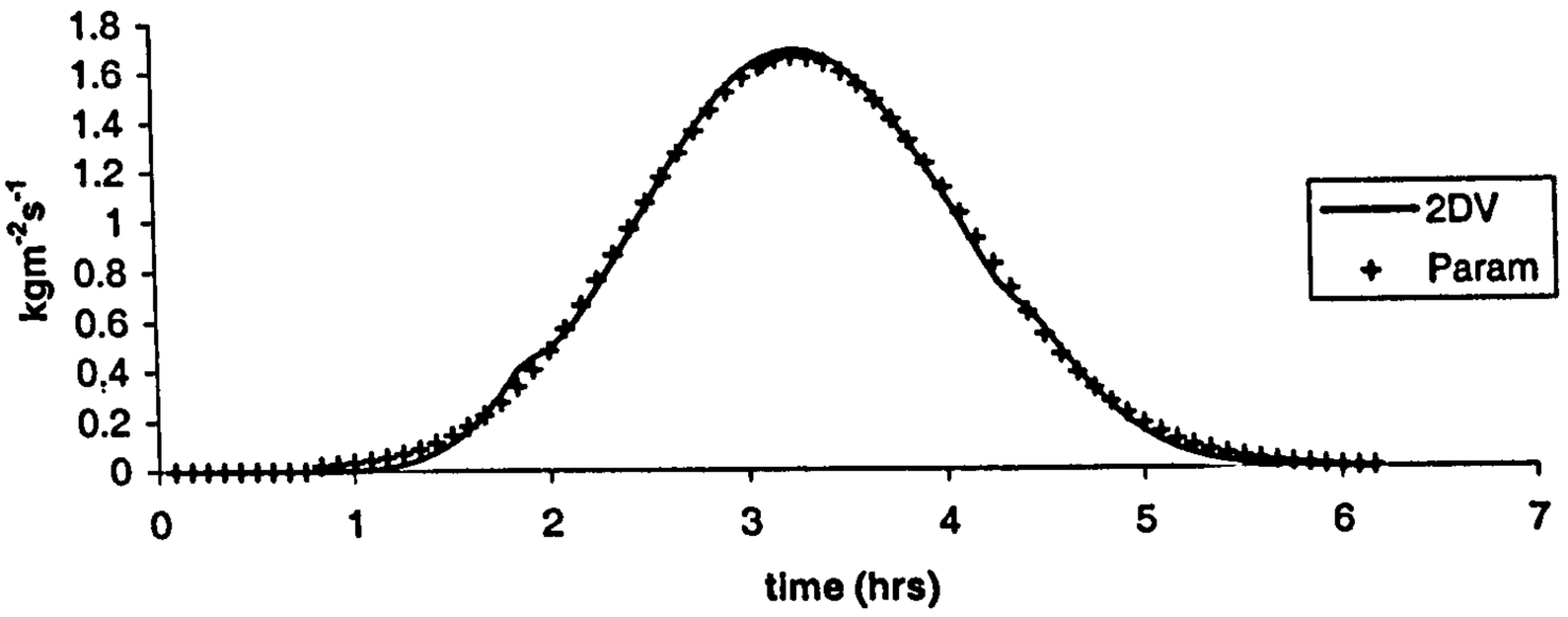

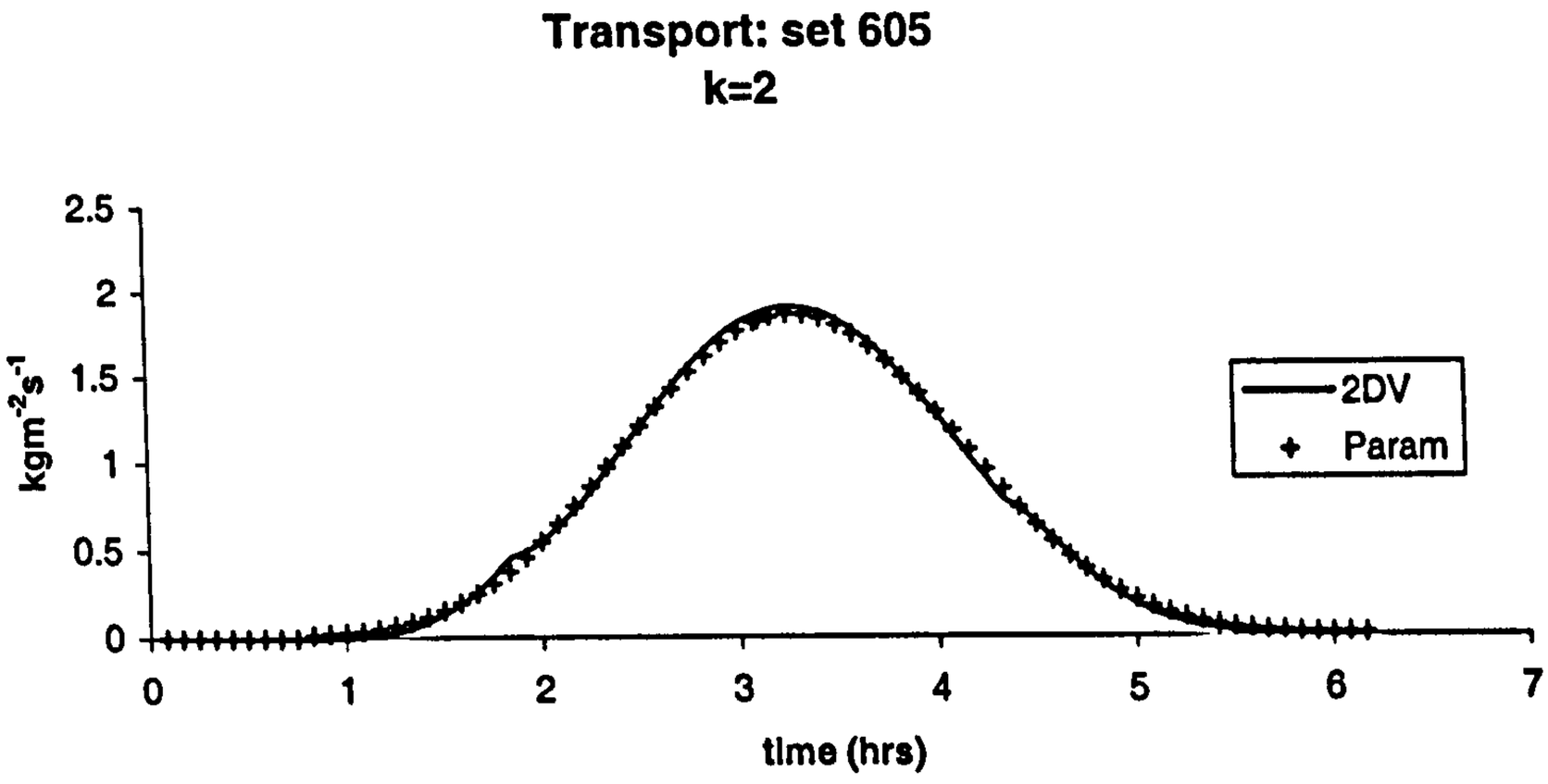

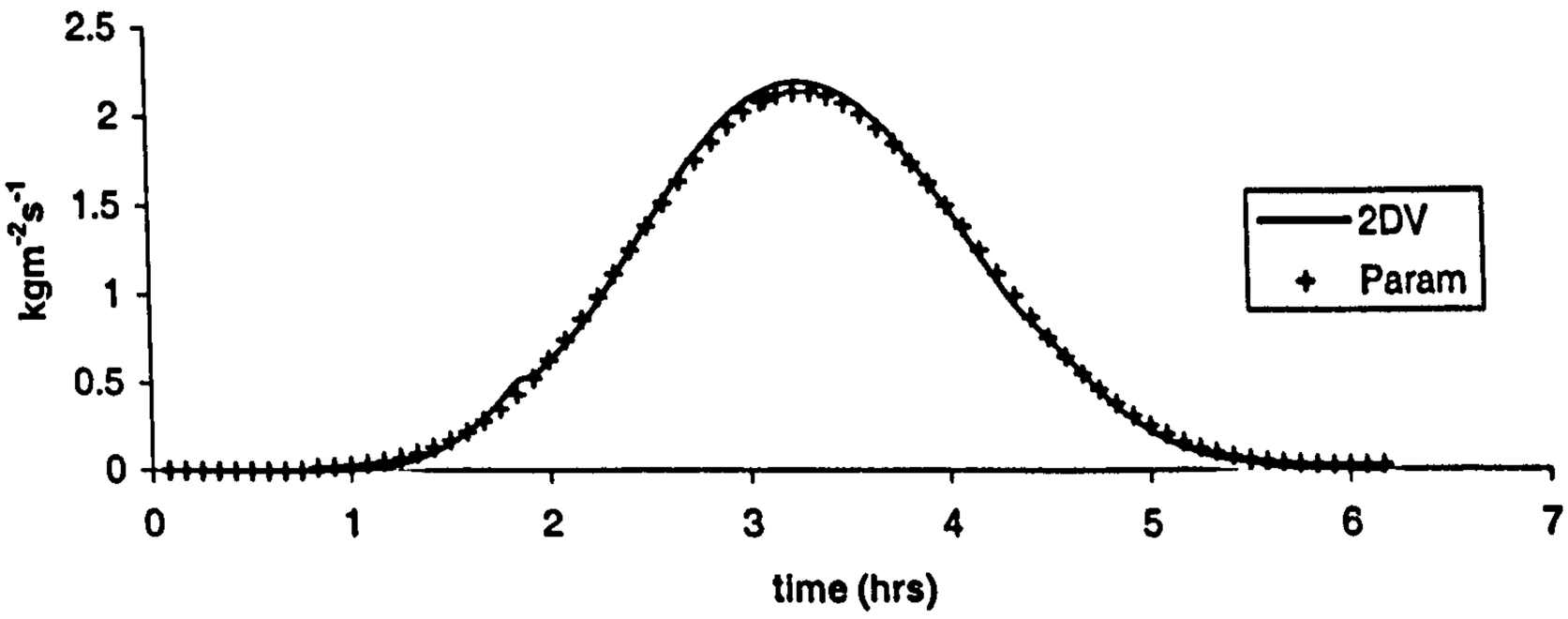

Figure 8.6.11a-c: Comparison between parameterised Corrector (Param) and conventional 2DV (2DV)

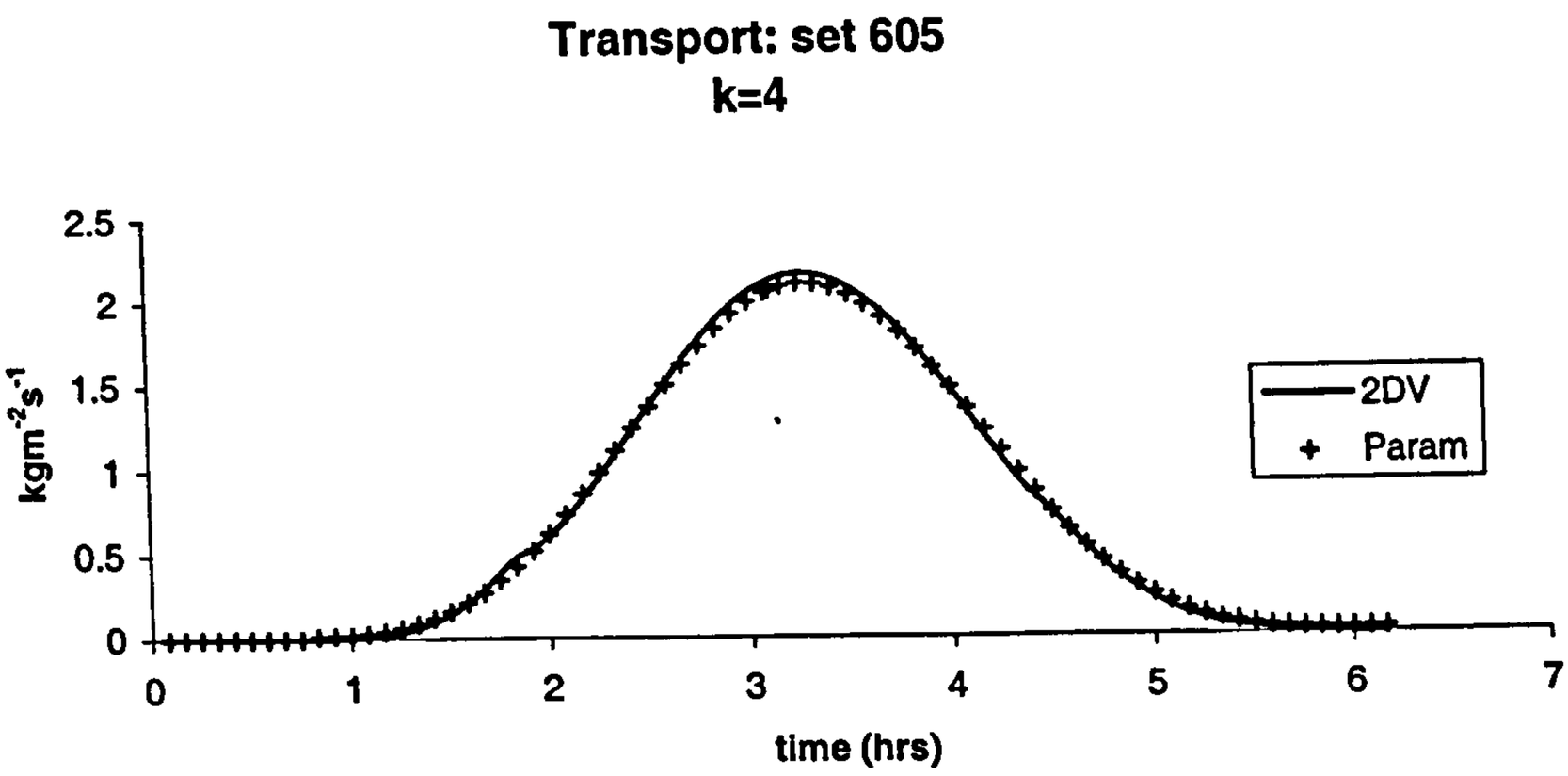

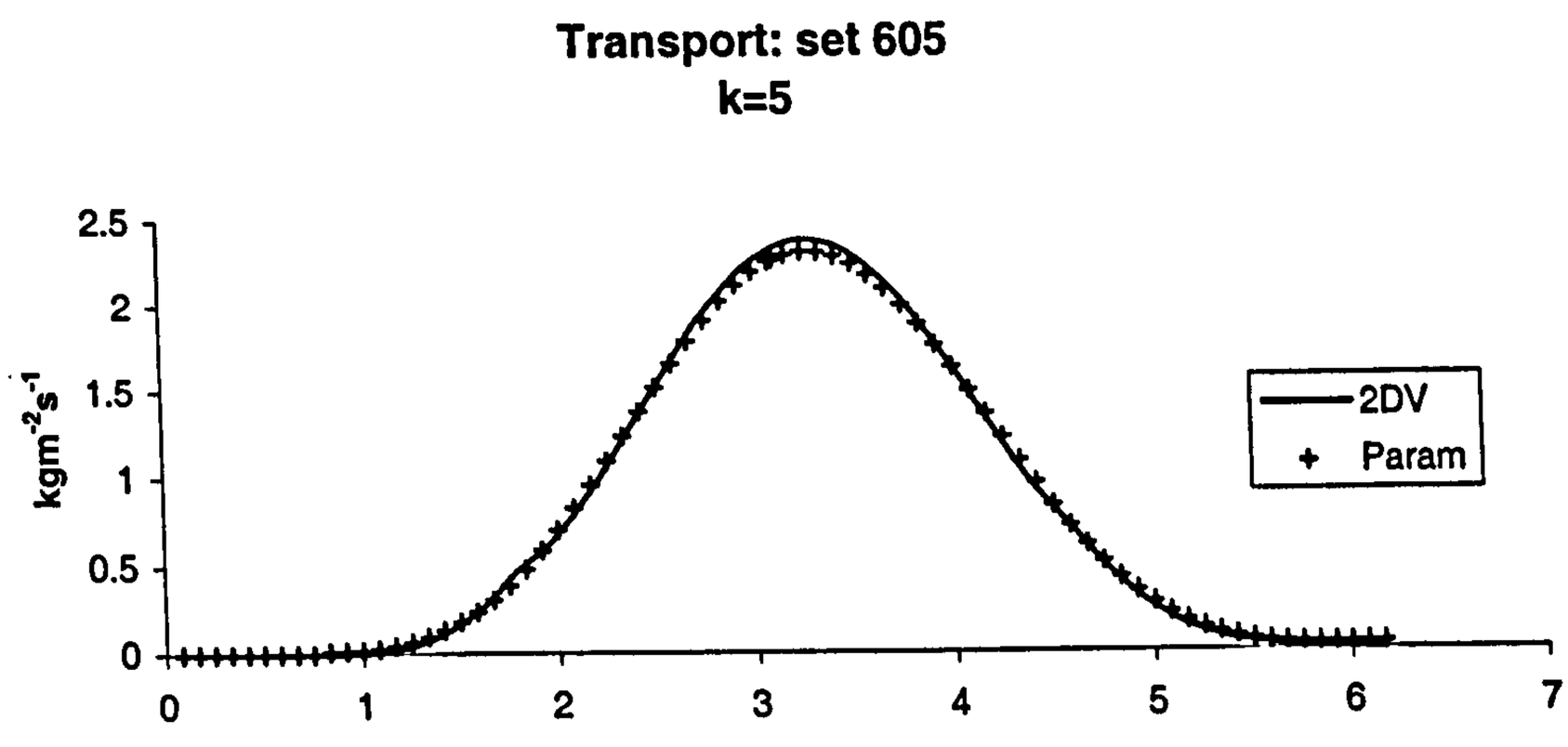

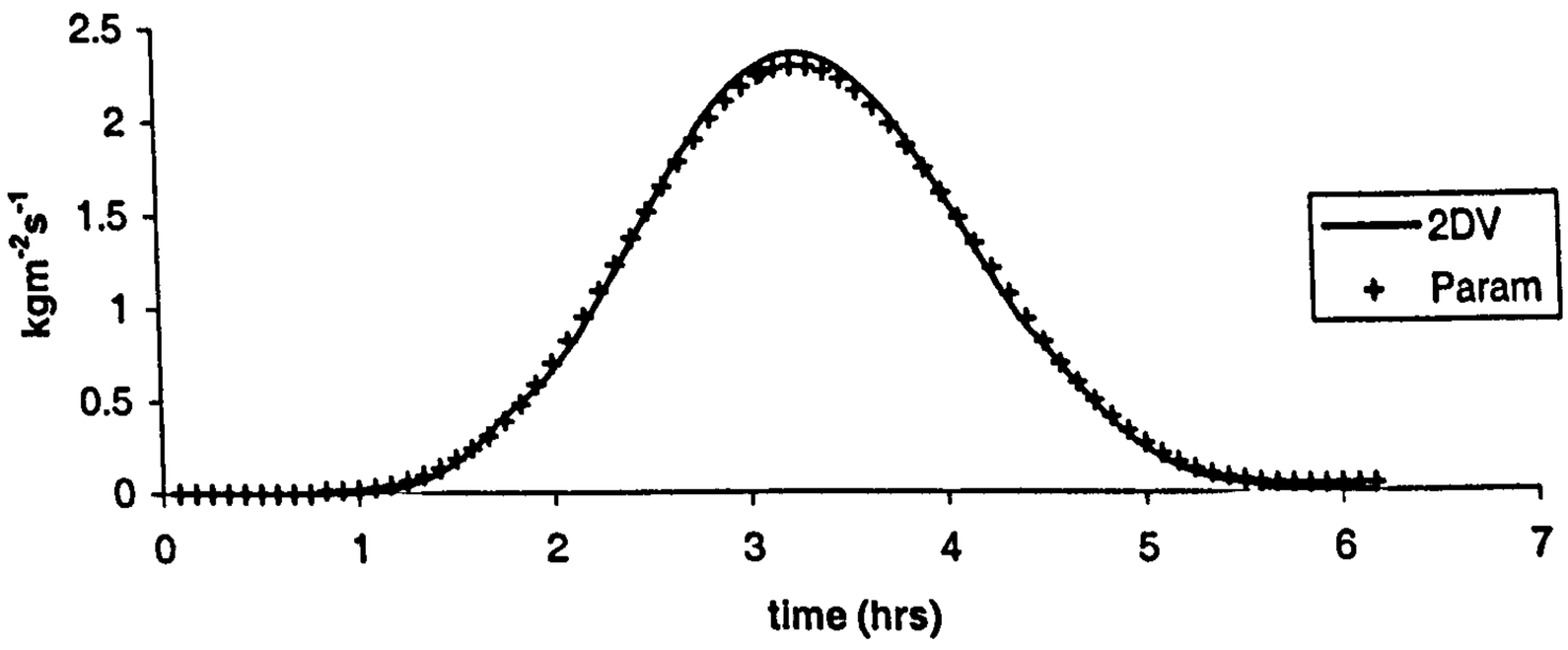

Figure 8.6.11d-f: Comparison between parameterised Corrector (Param) and conventional 2DV (2DV)

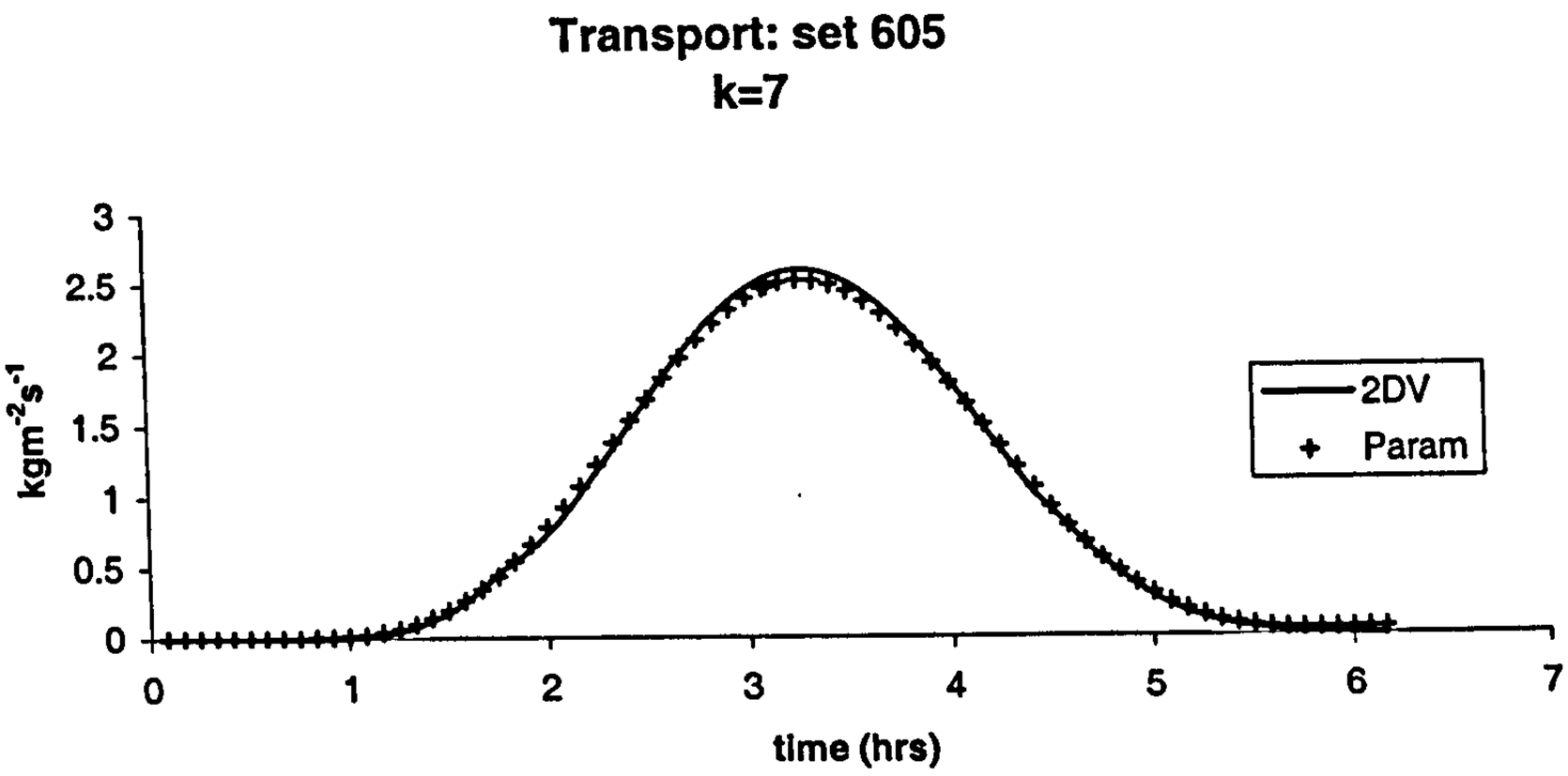

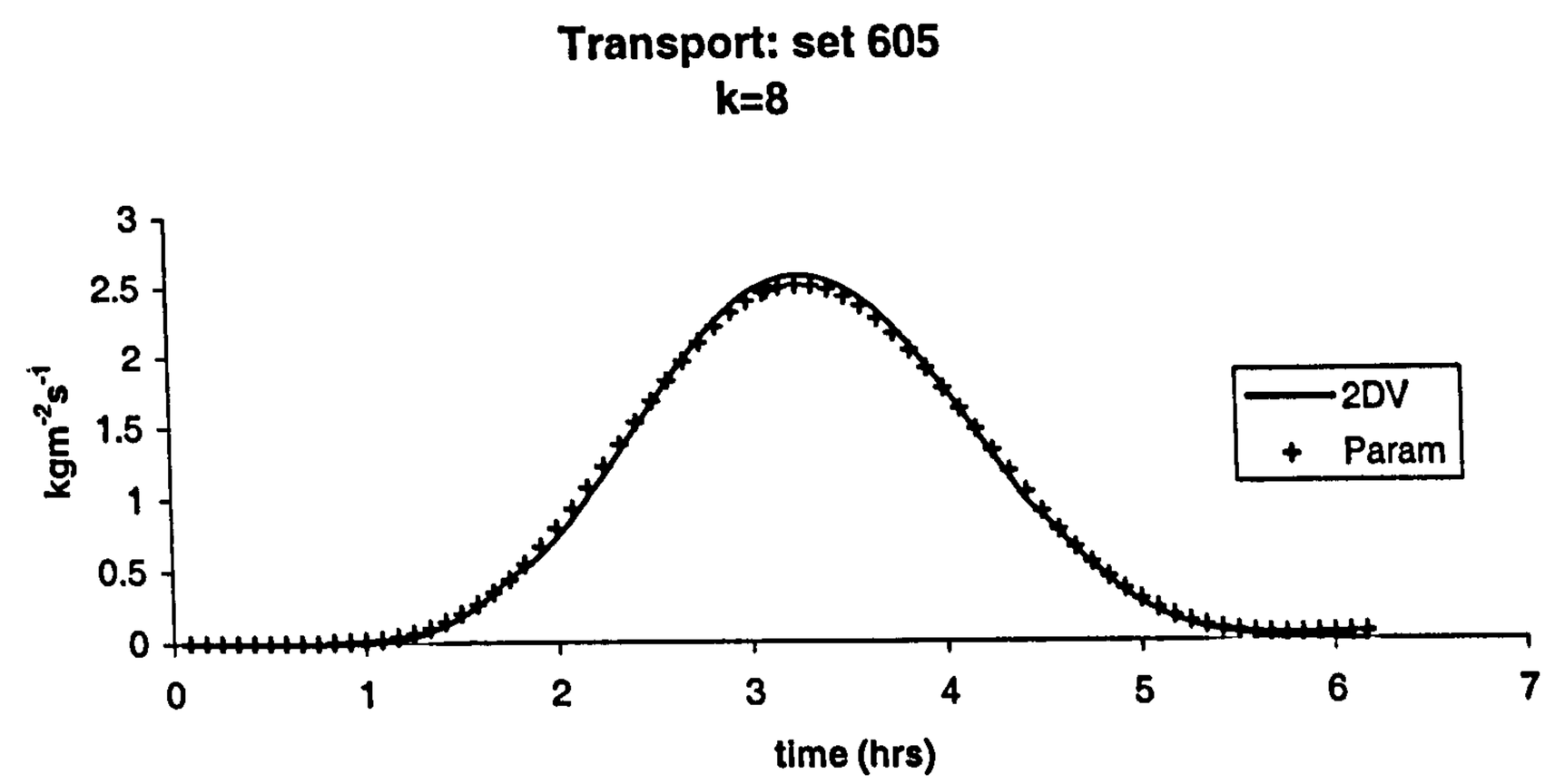

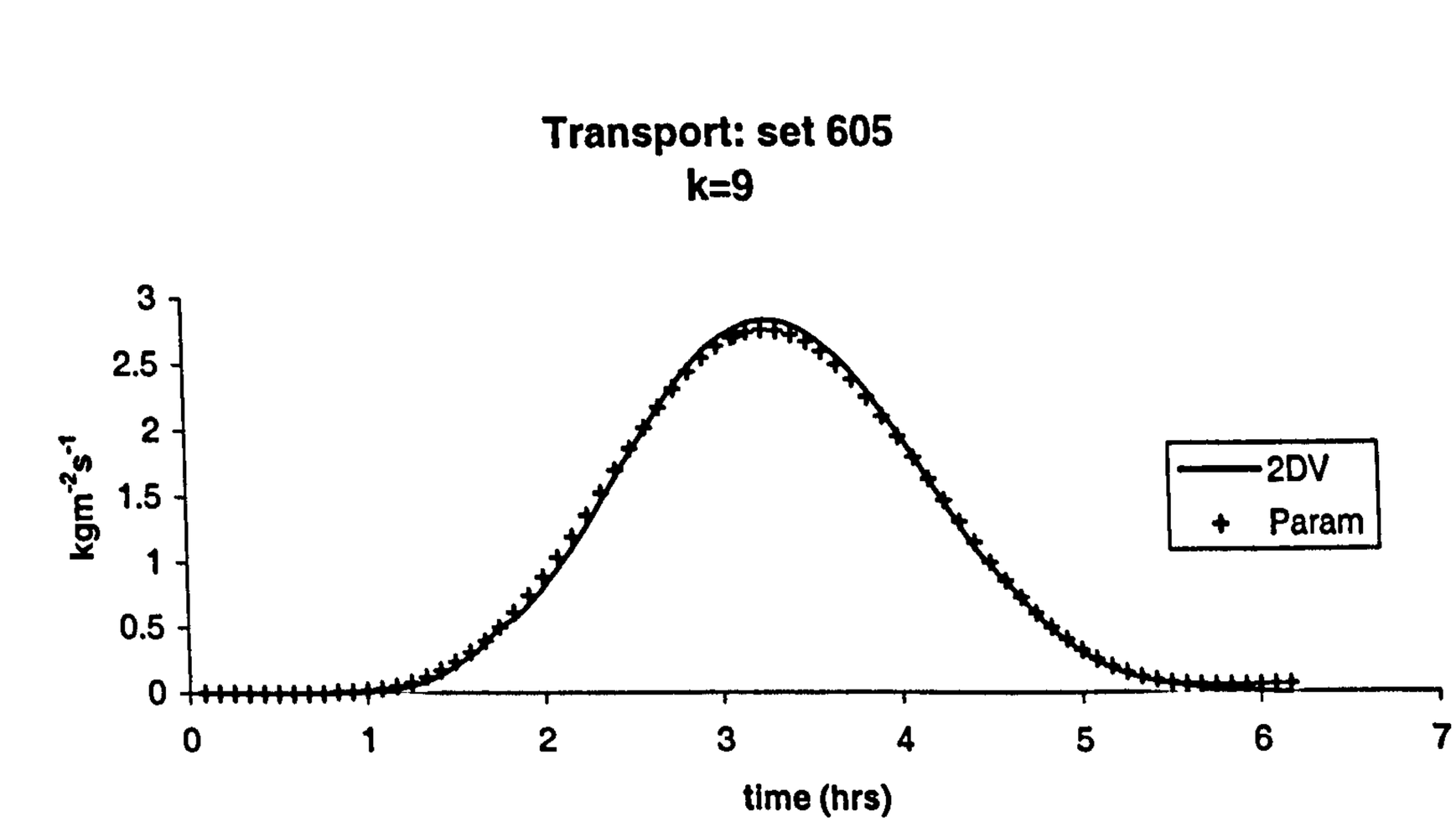

Figure 8.6.11g-i: Comparison between parameterised Corrector (Param) and conventional 2DV (2DV)

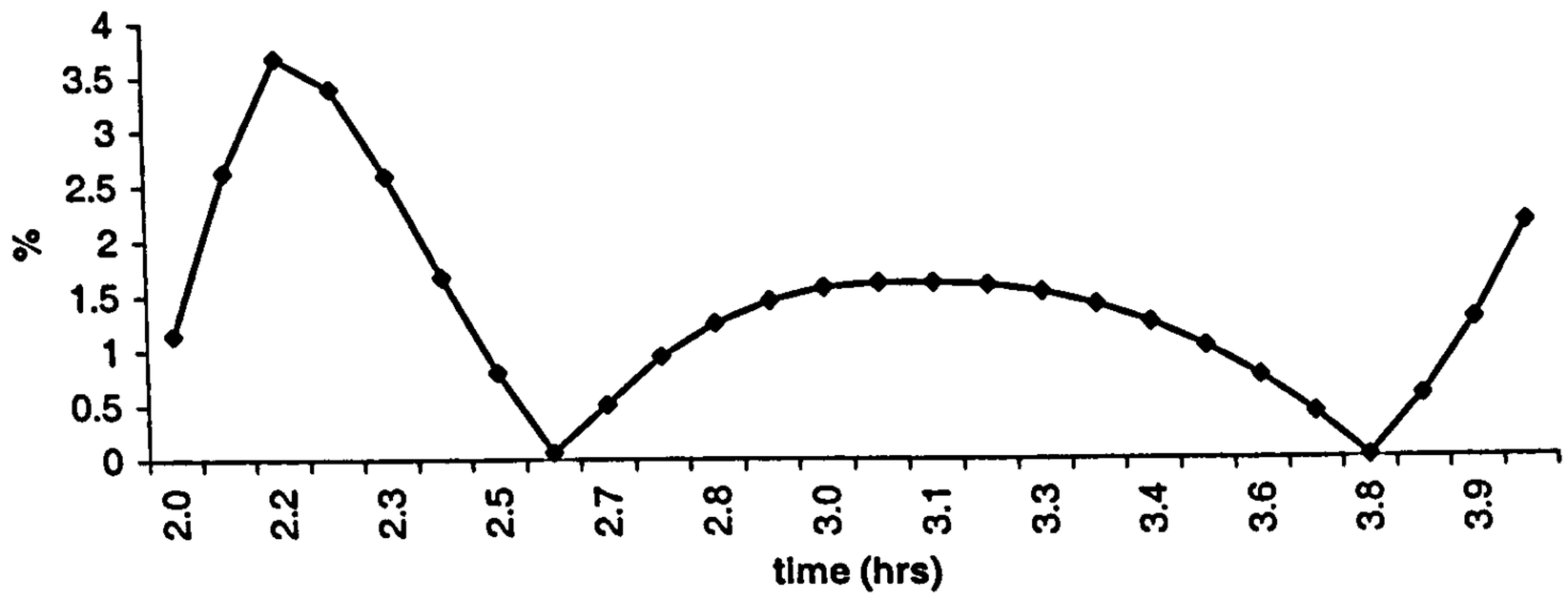

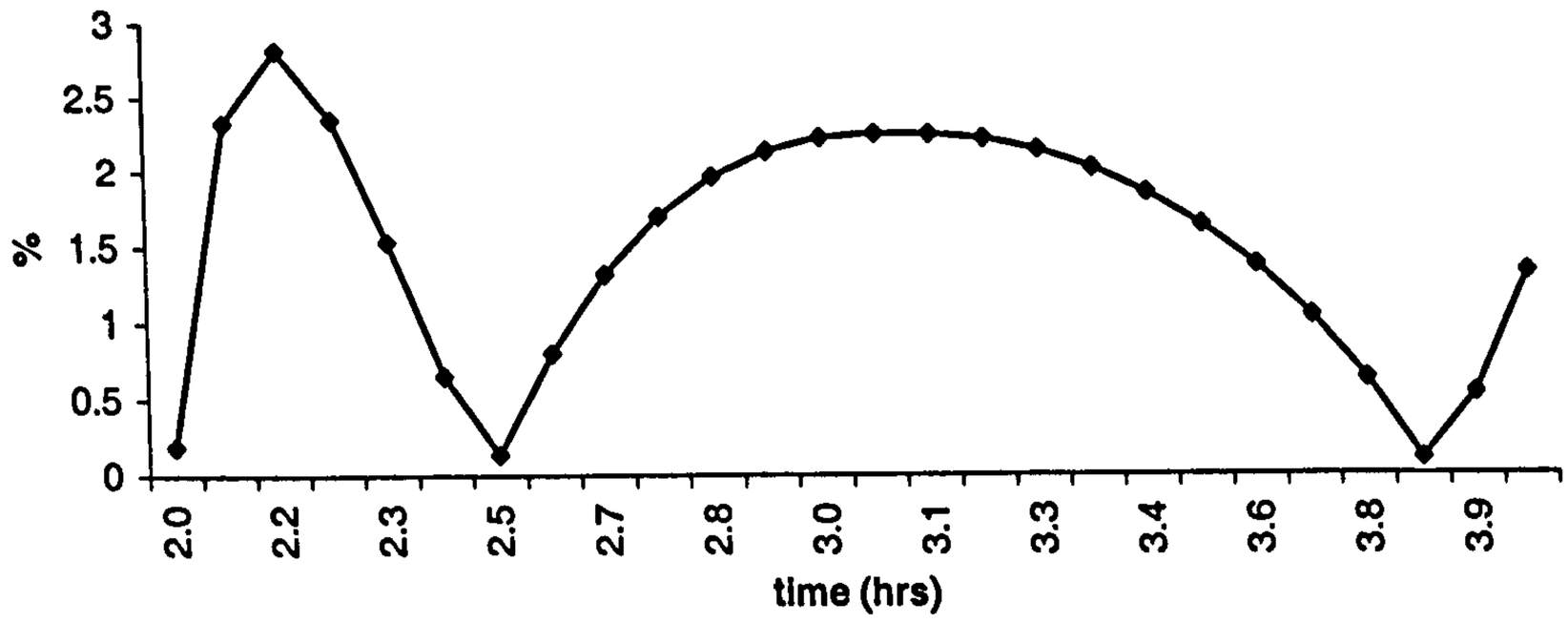

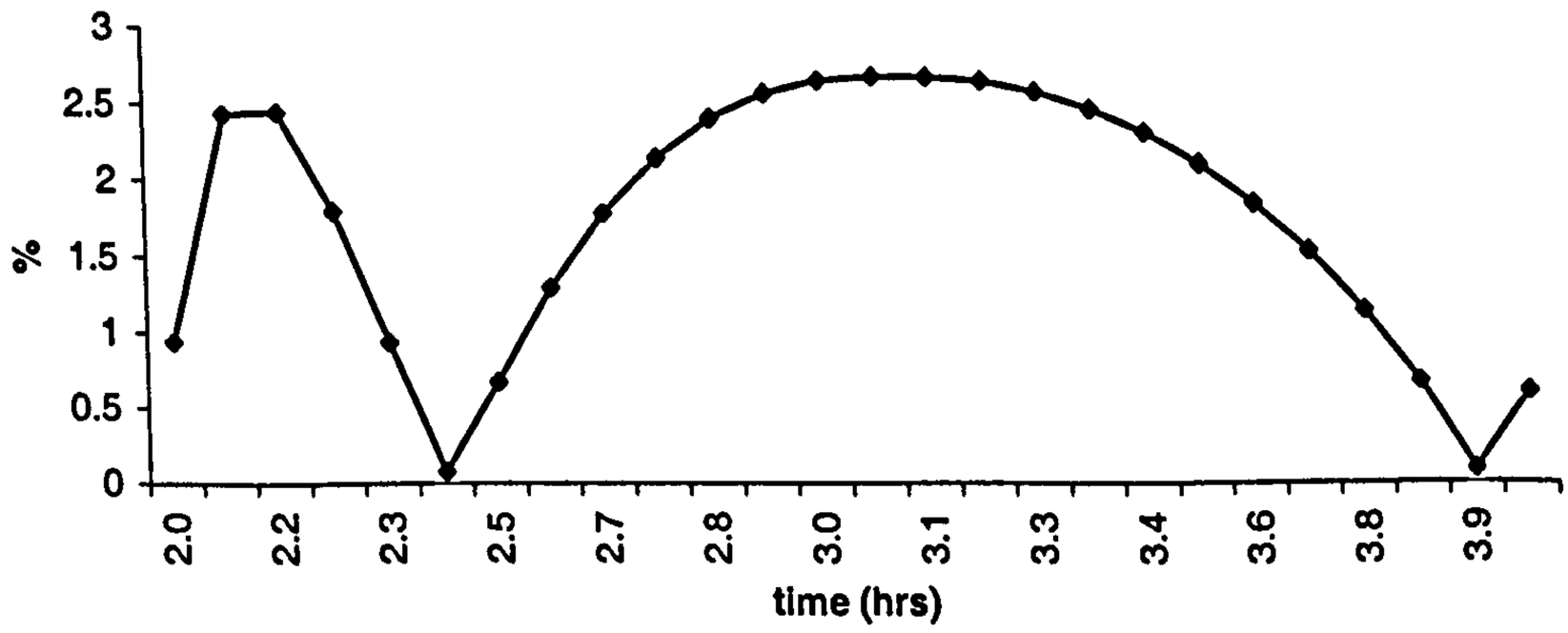

Figure 8.6.12a-c: Error between conventional 2DV method and parameterised Corrector method during the mid-tide phase.

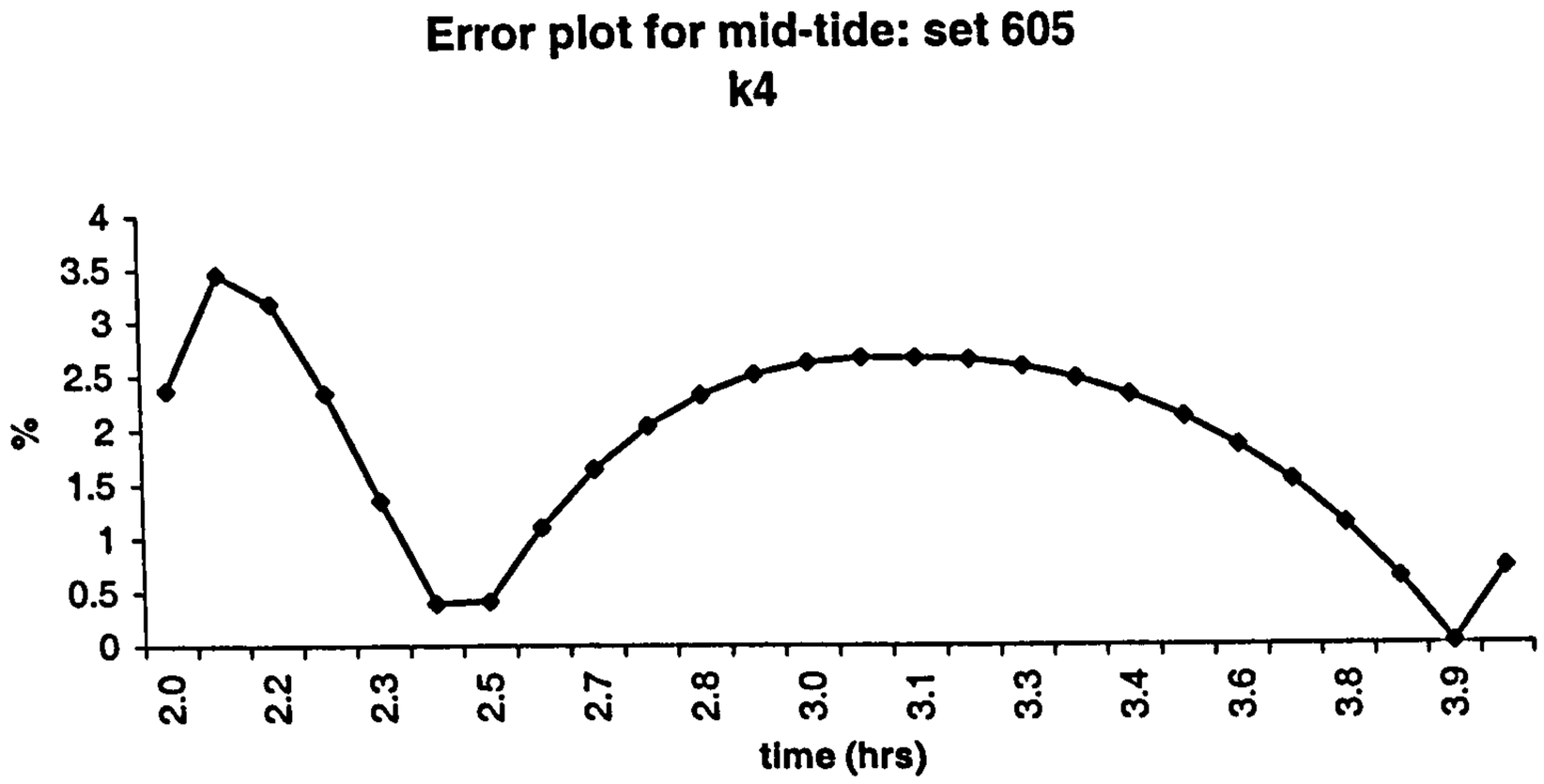

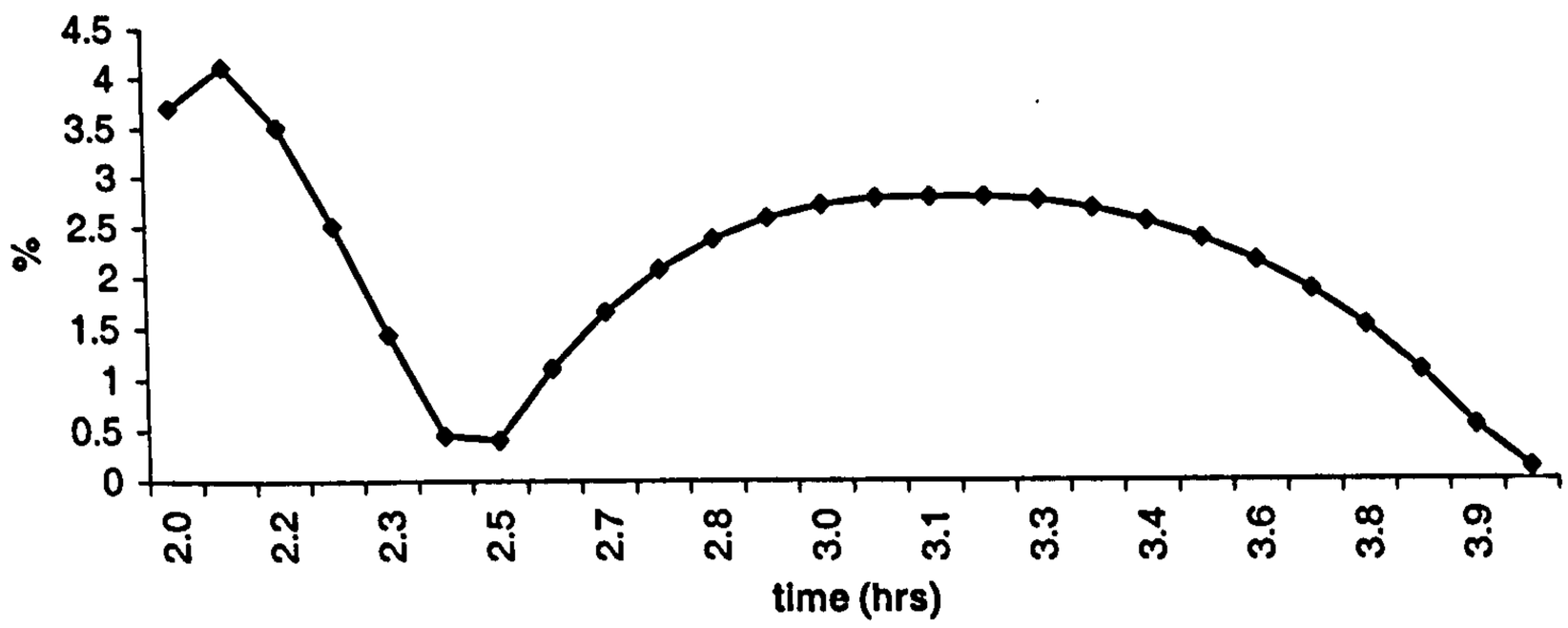

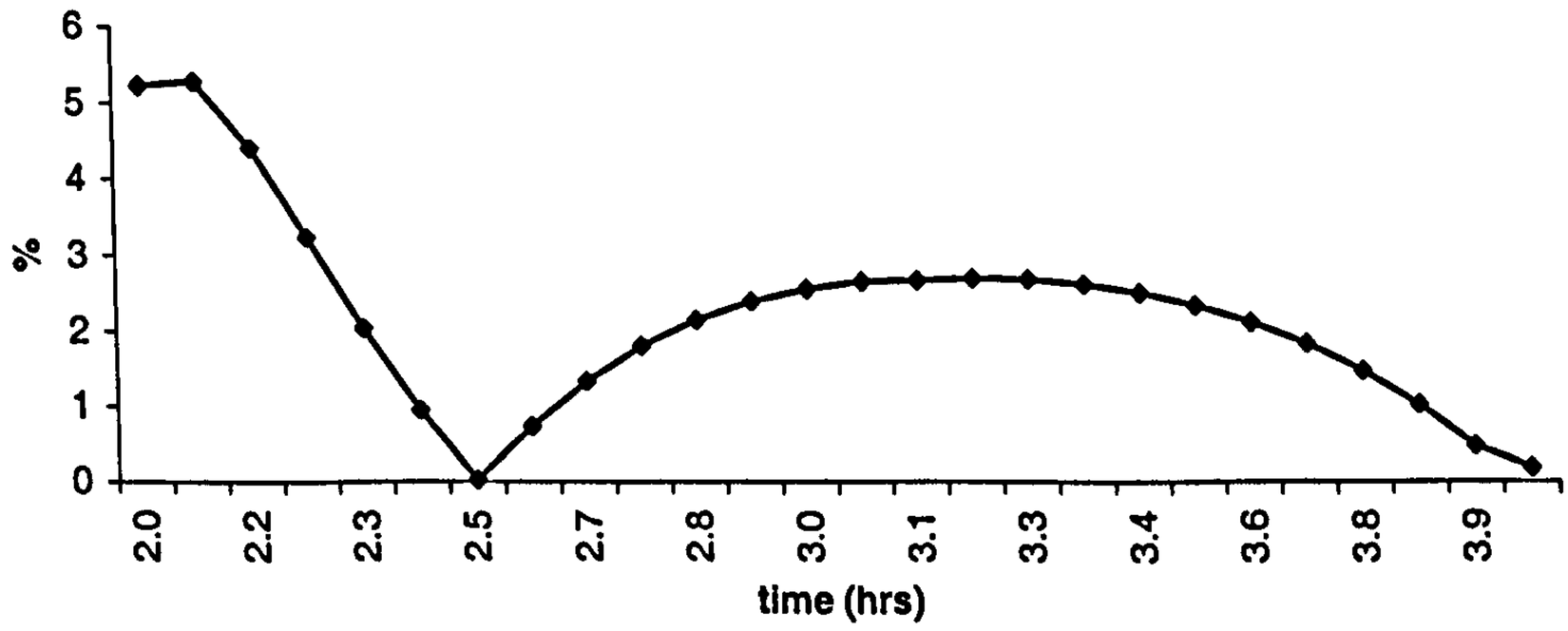

Figure 8.6.12d-f: Error between conventional 2DV method and parameterised Corrector method during the mid-tide phase.

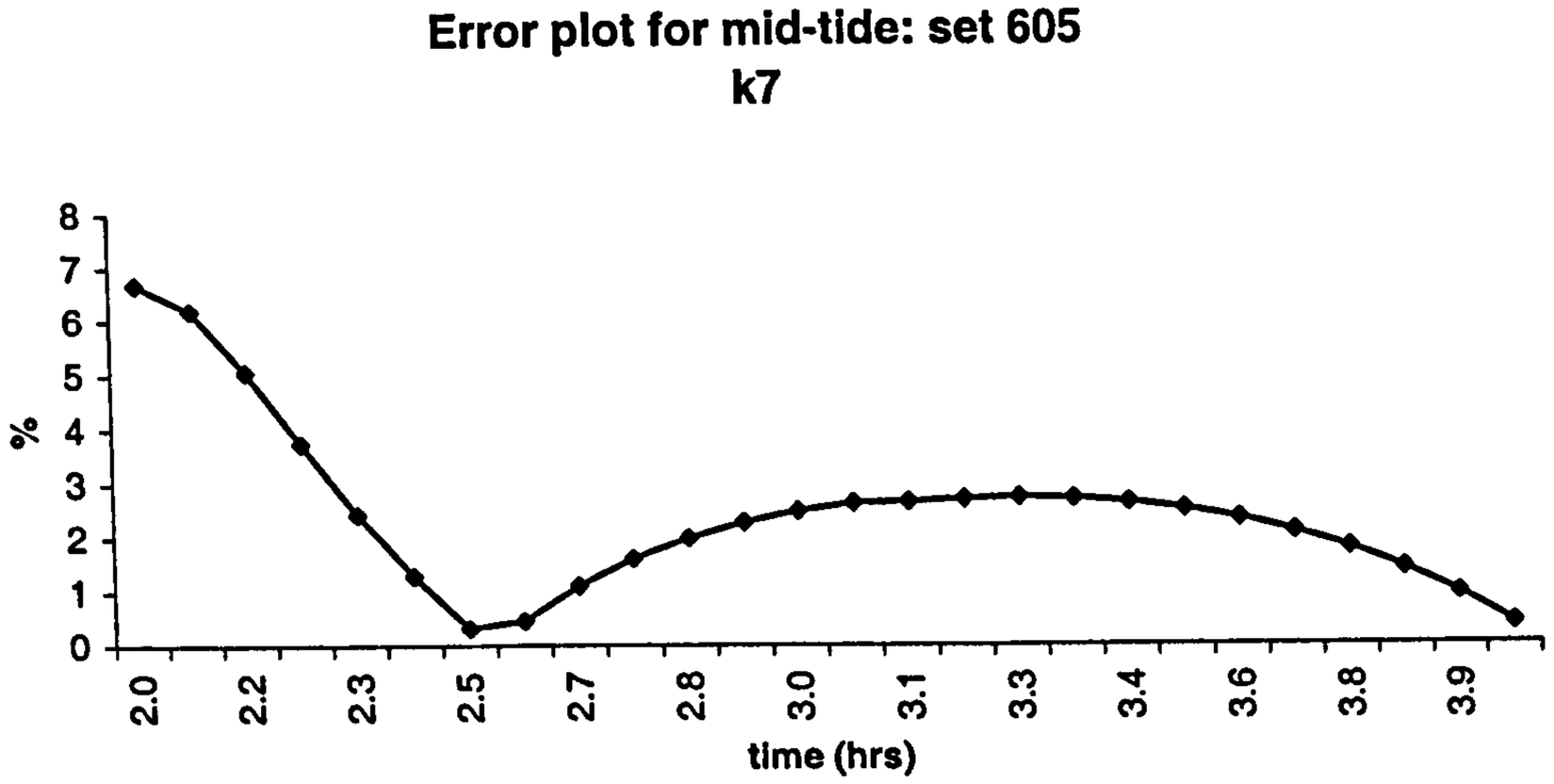

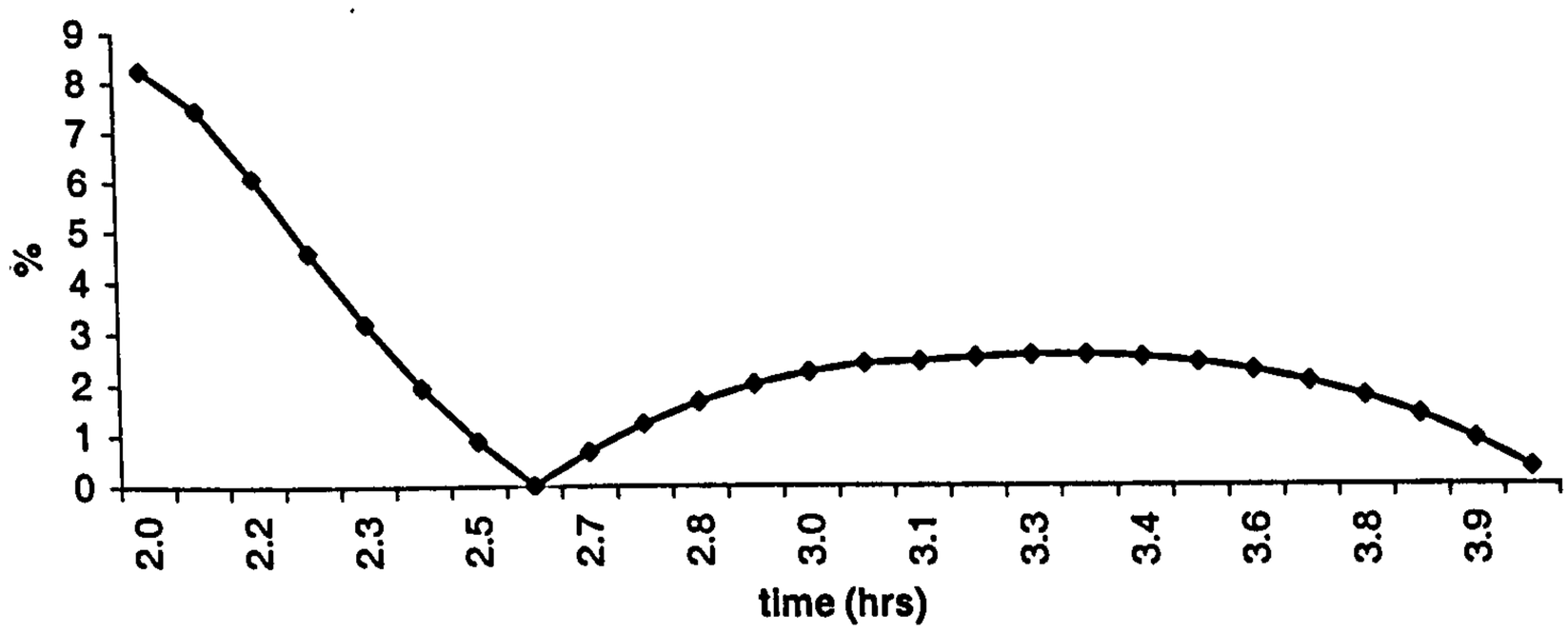

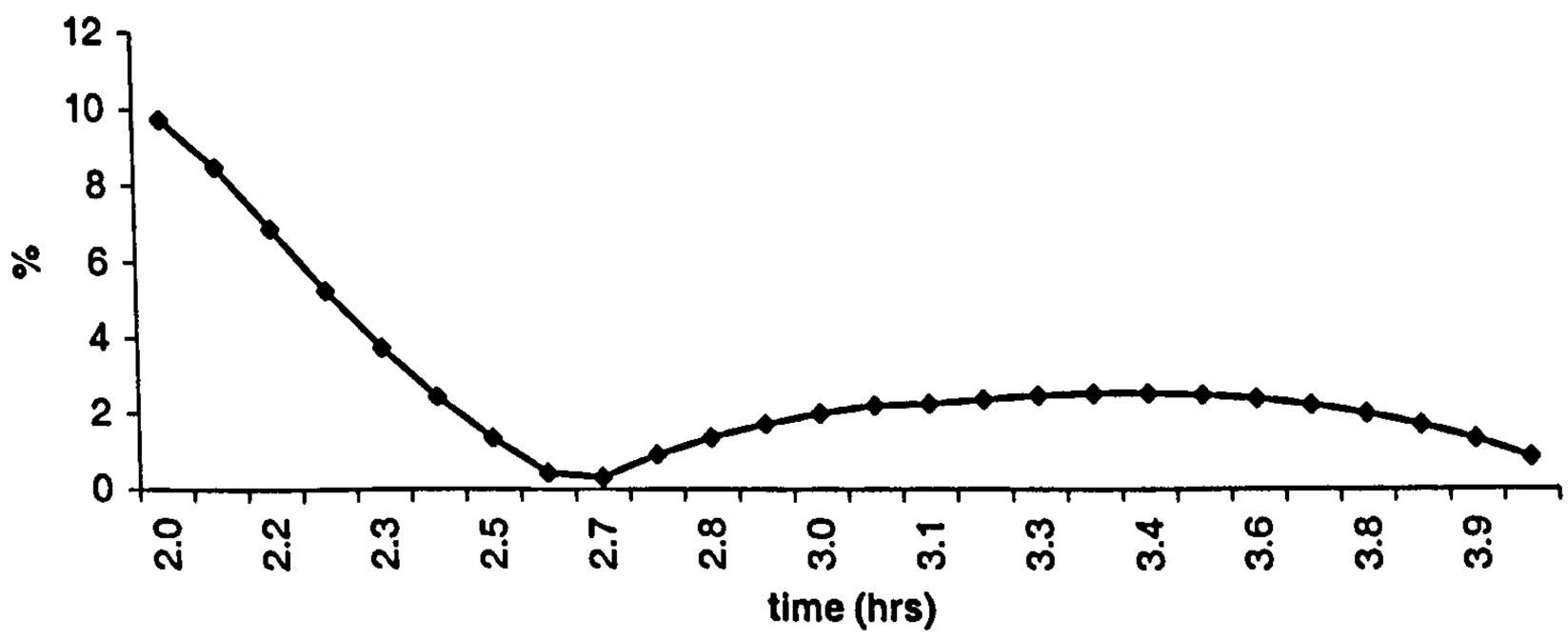

Figure 8.6.12g-i: Error between conventional 2DV method and parameterised Corrector method during the mid-tide phase.

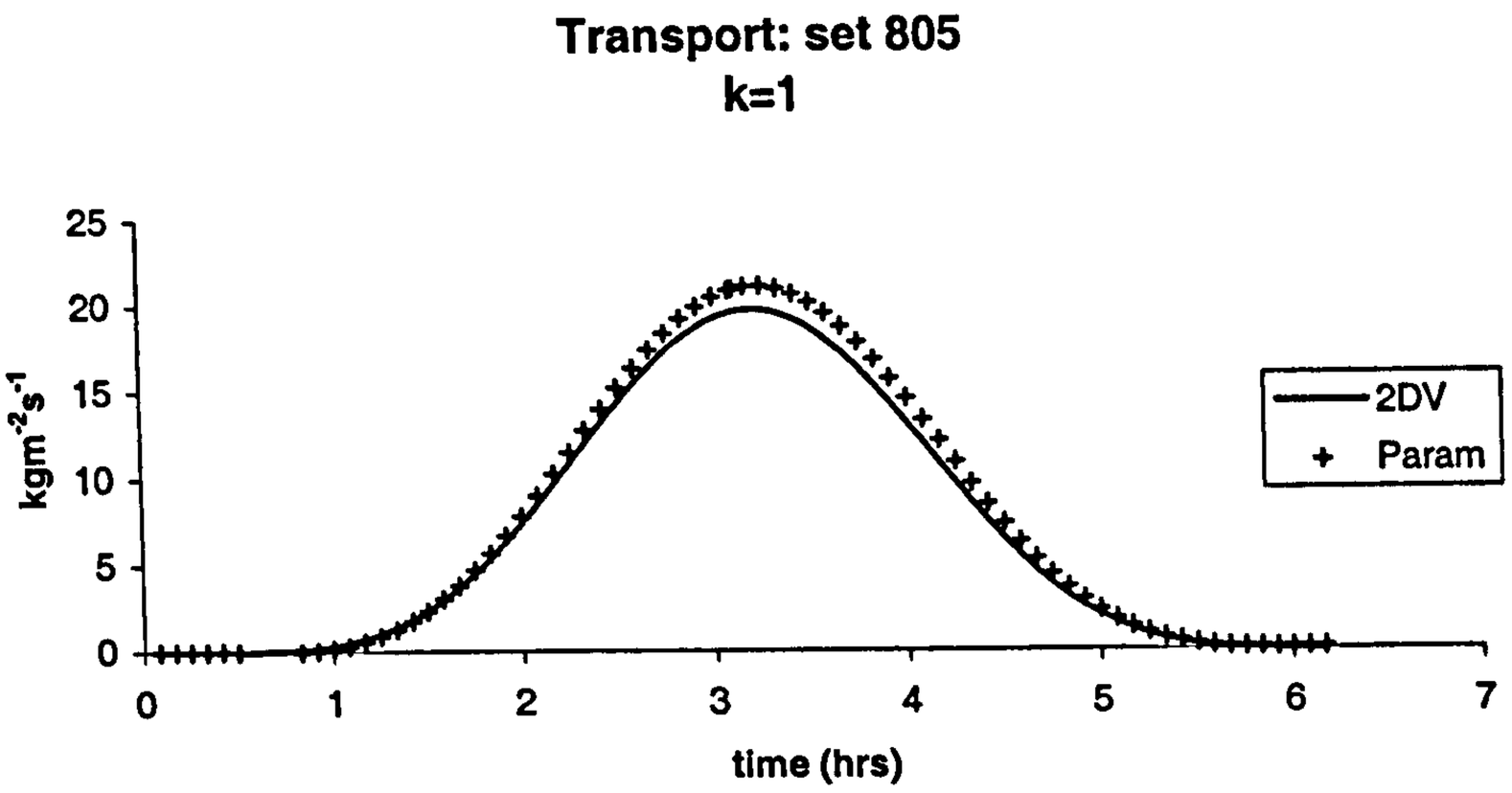

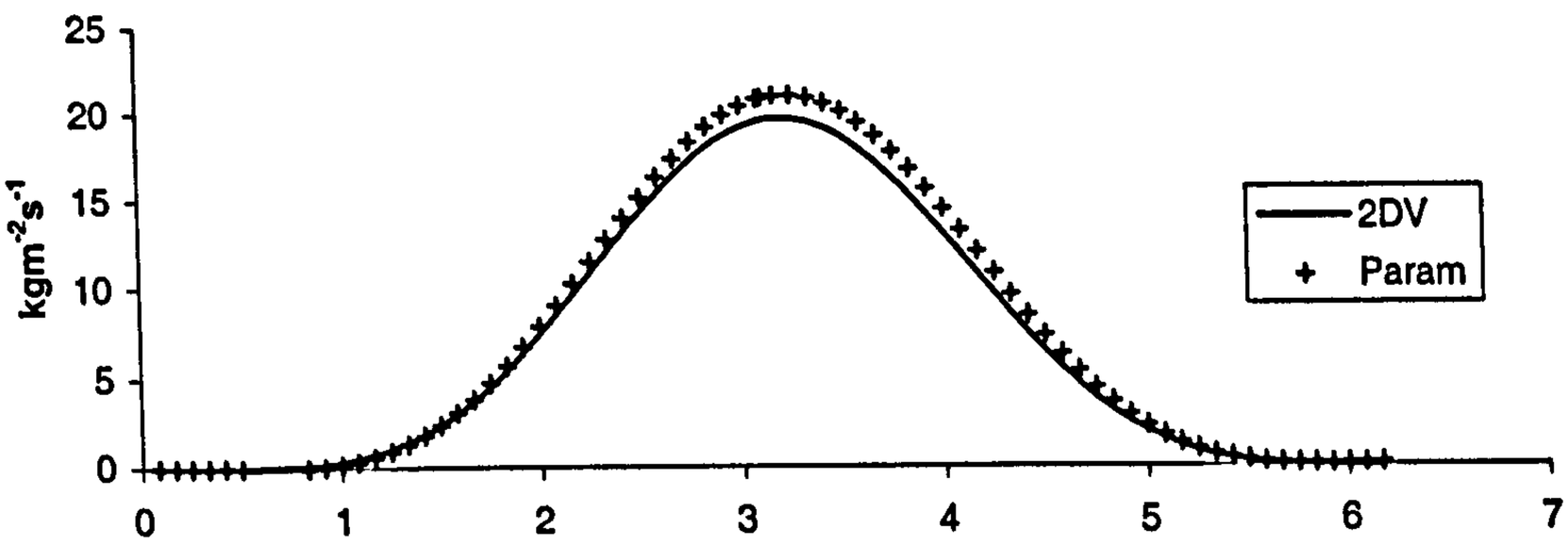

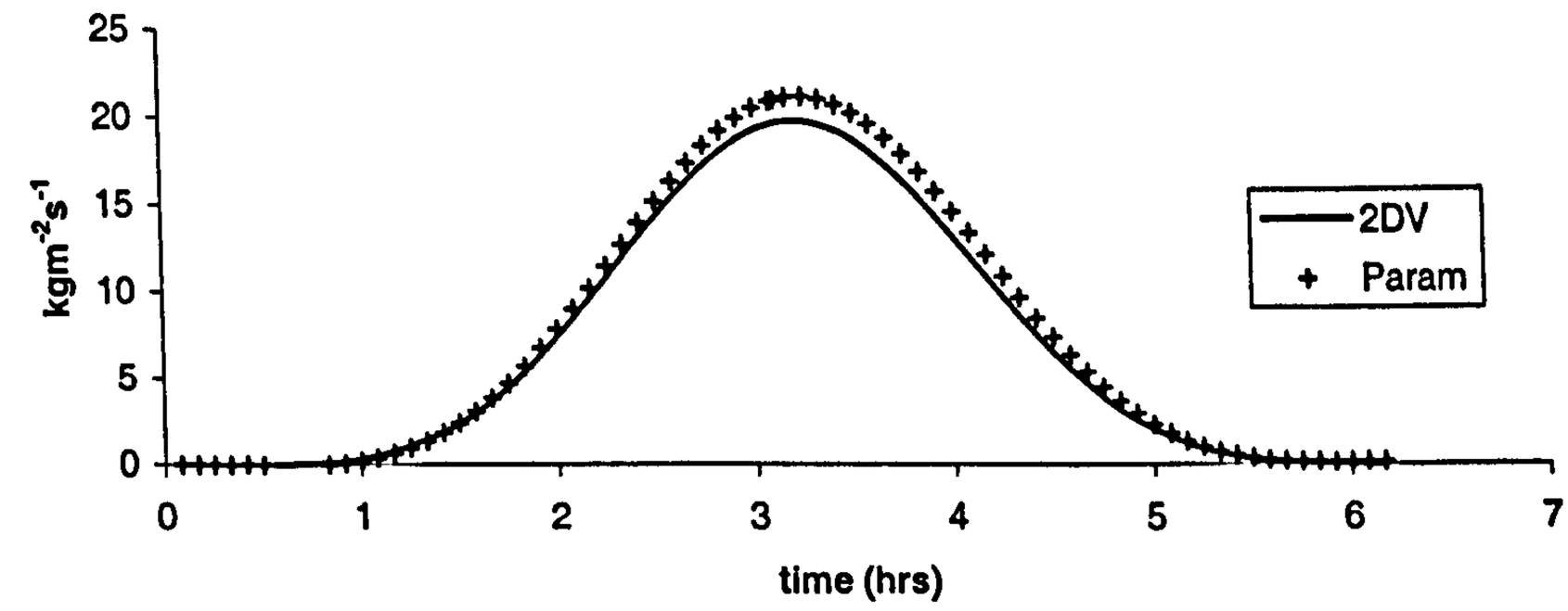

Figure 8.6.13a-c: Comparison between parameterised Corrector (Param) and conventional 2DV (2DV)

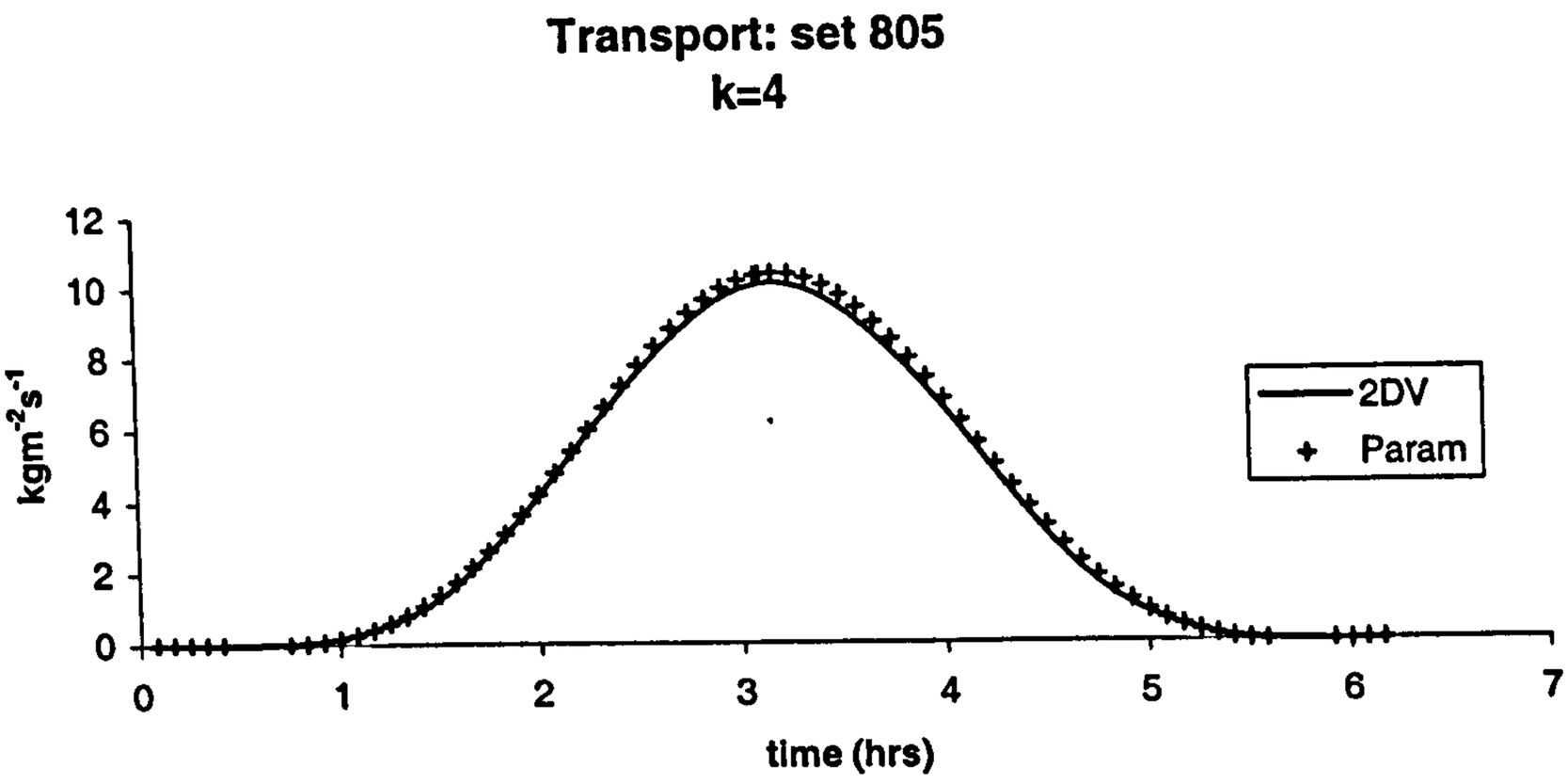

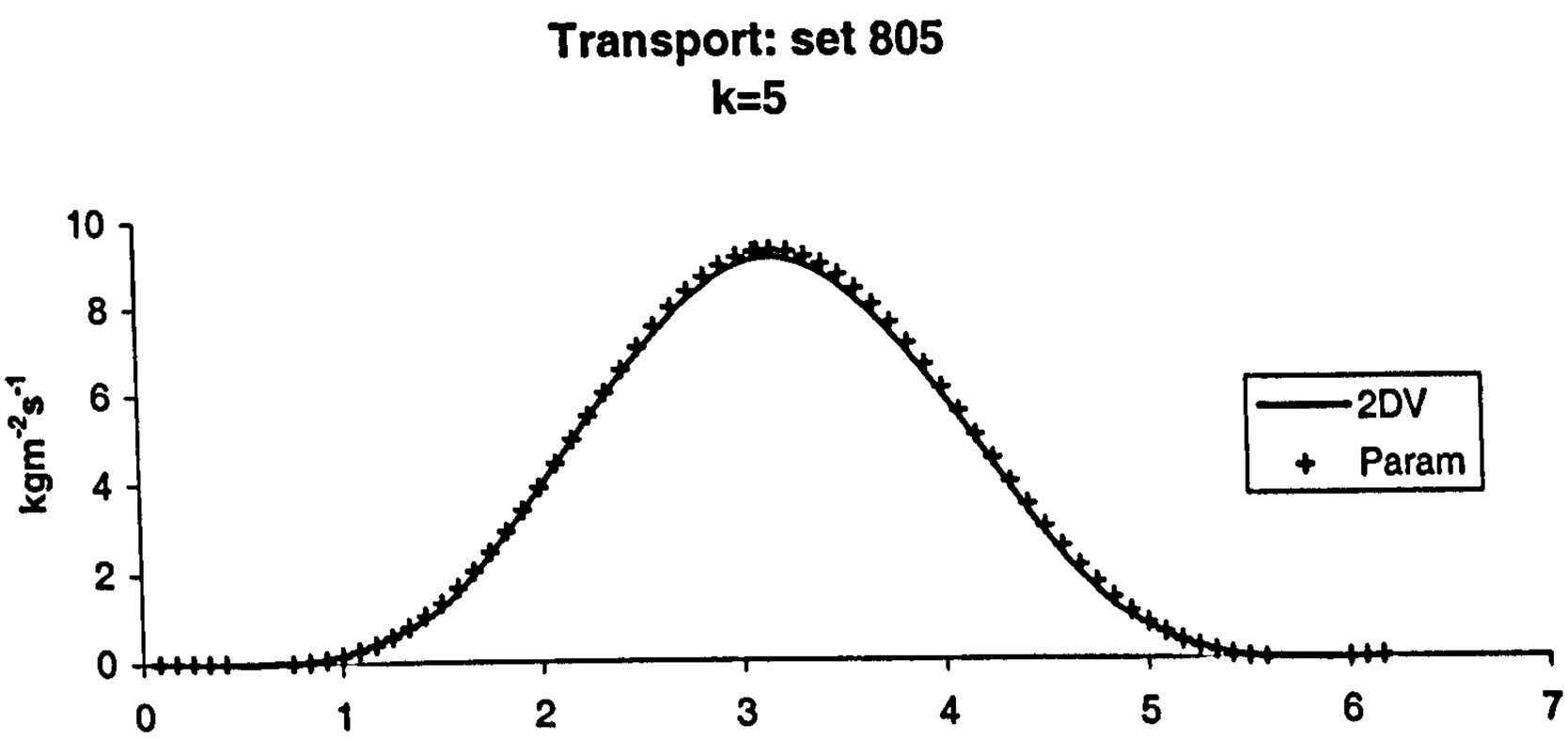

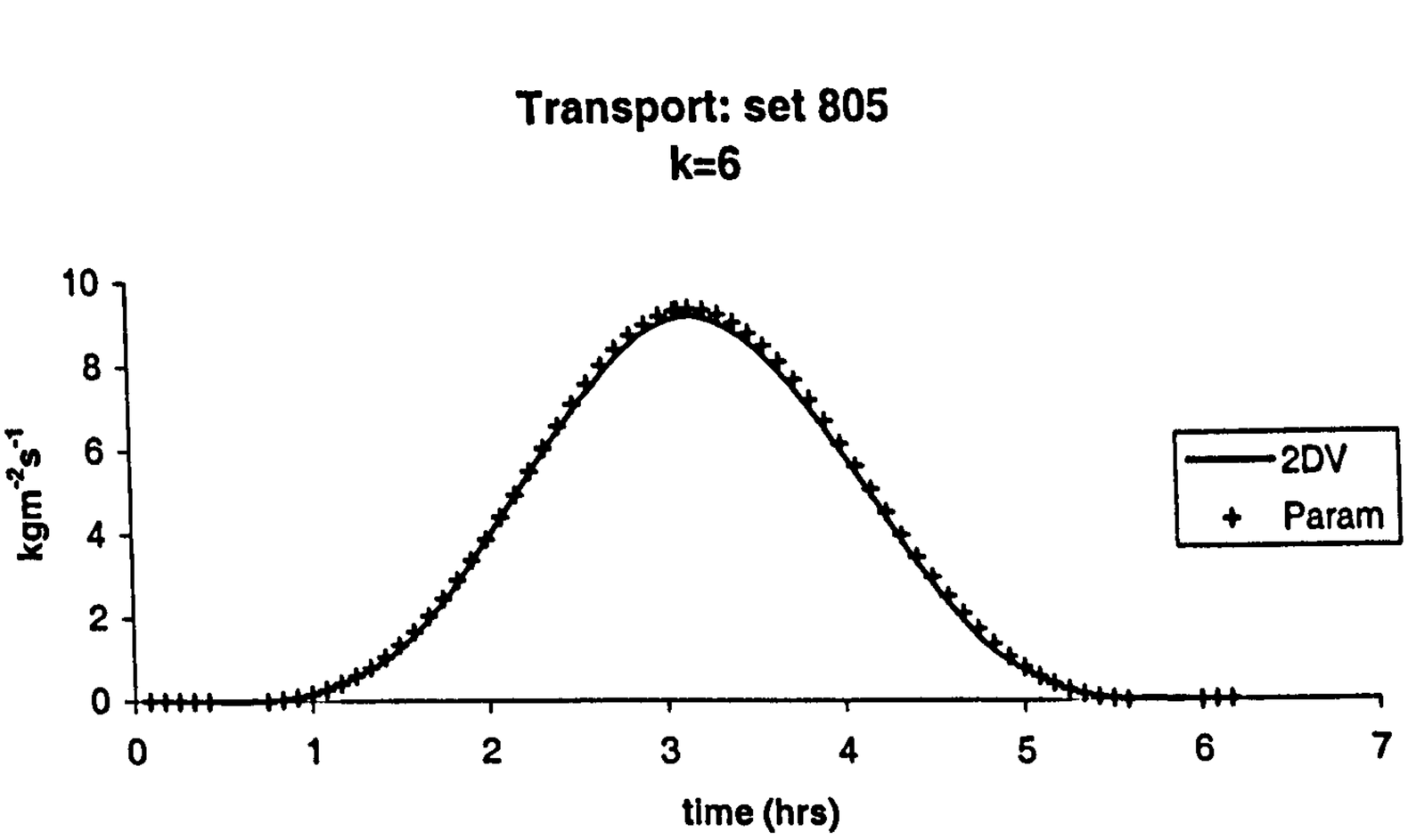

Figure 8.6.13d-f: Comparison between parameterised Corrector (Param) and conventional 2DV (2DV)

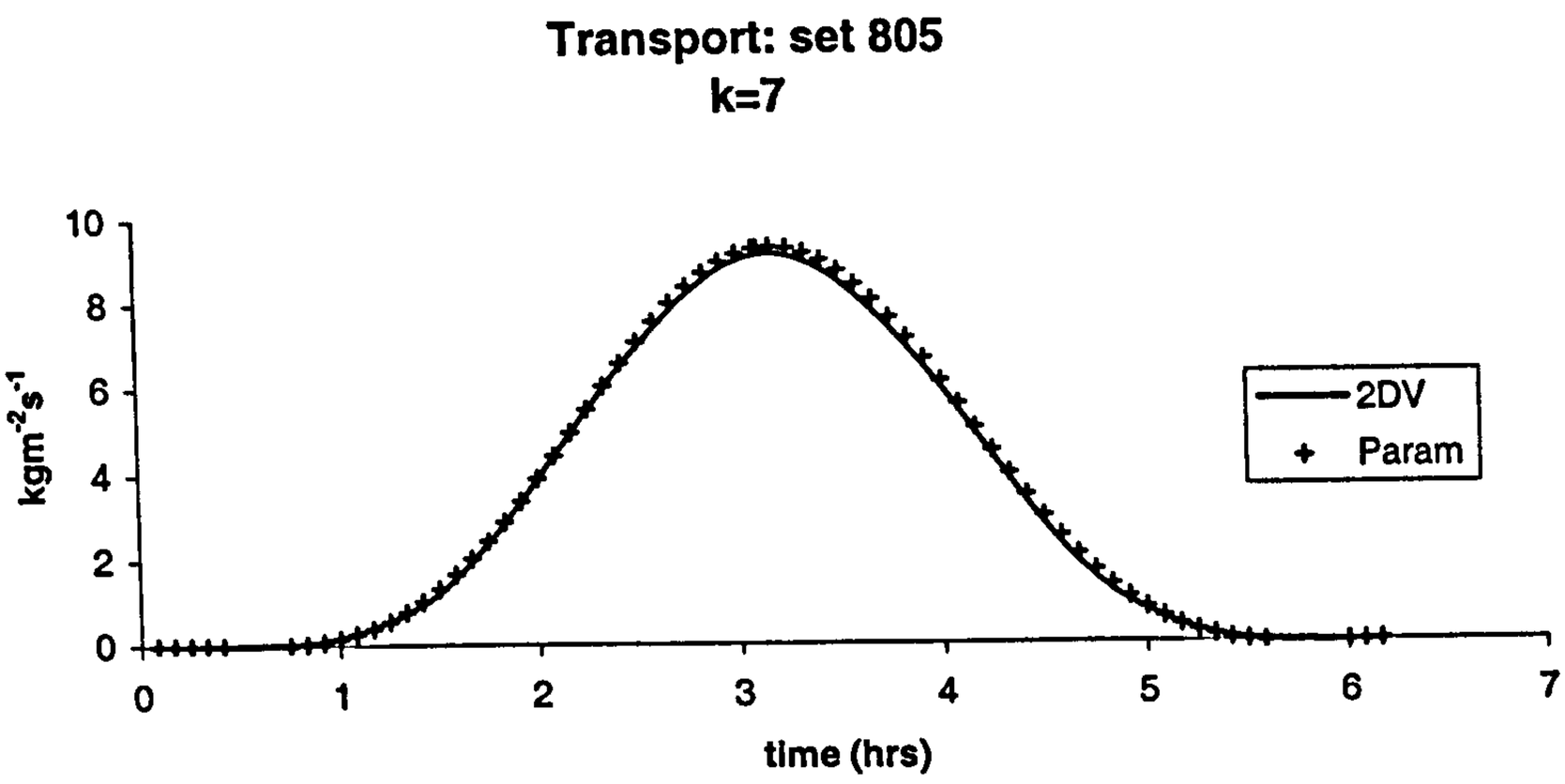

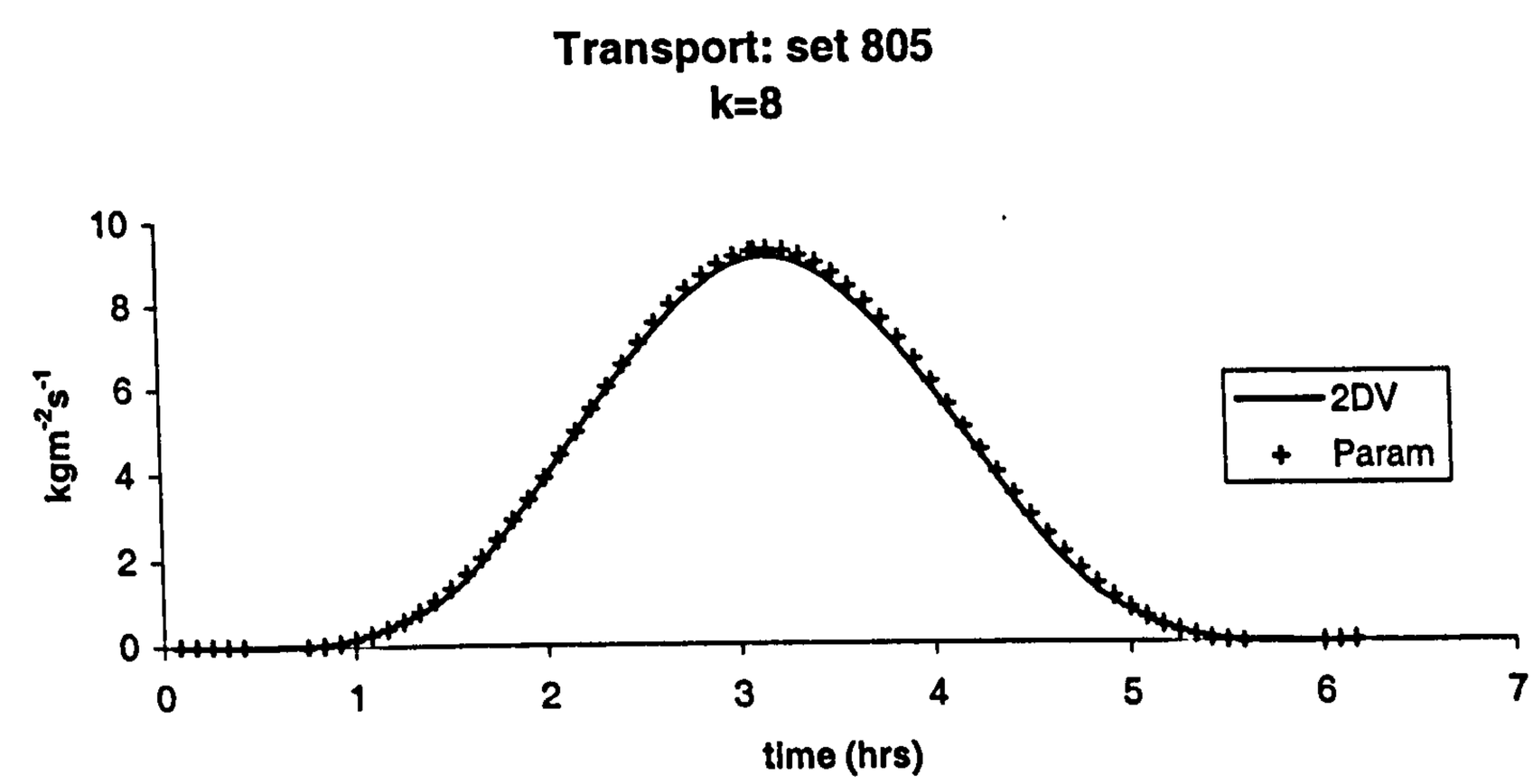

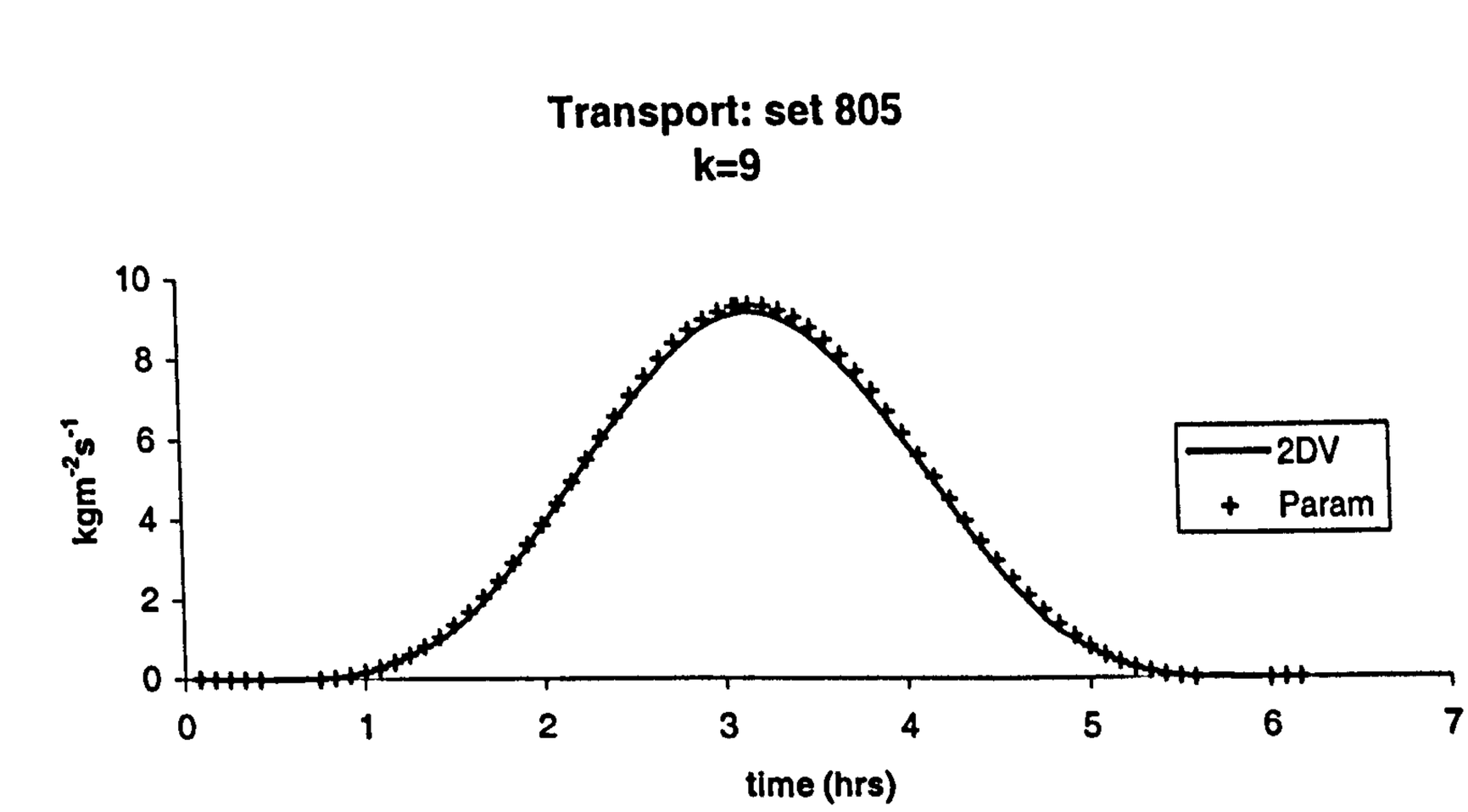

Figure 8.6.13g-i: Comparison between parameterised Corrector (Param) and conventional 2DV (2DV)

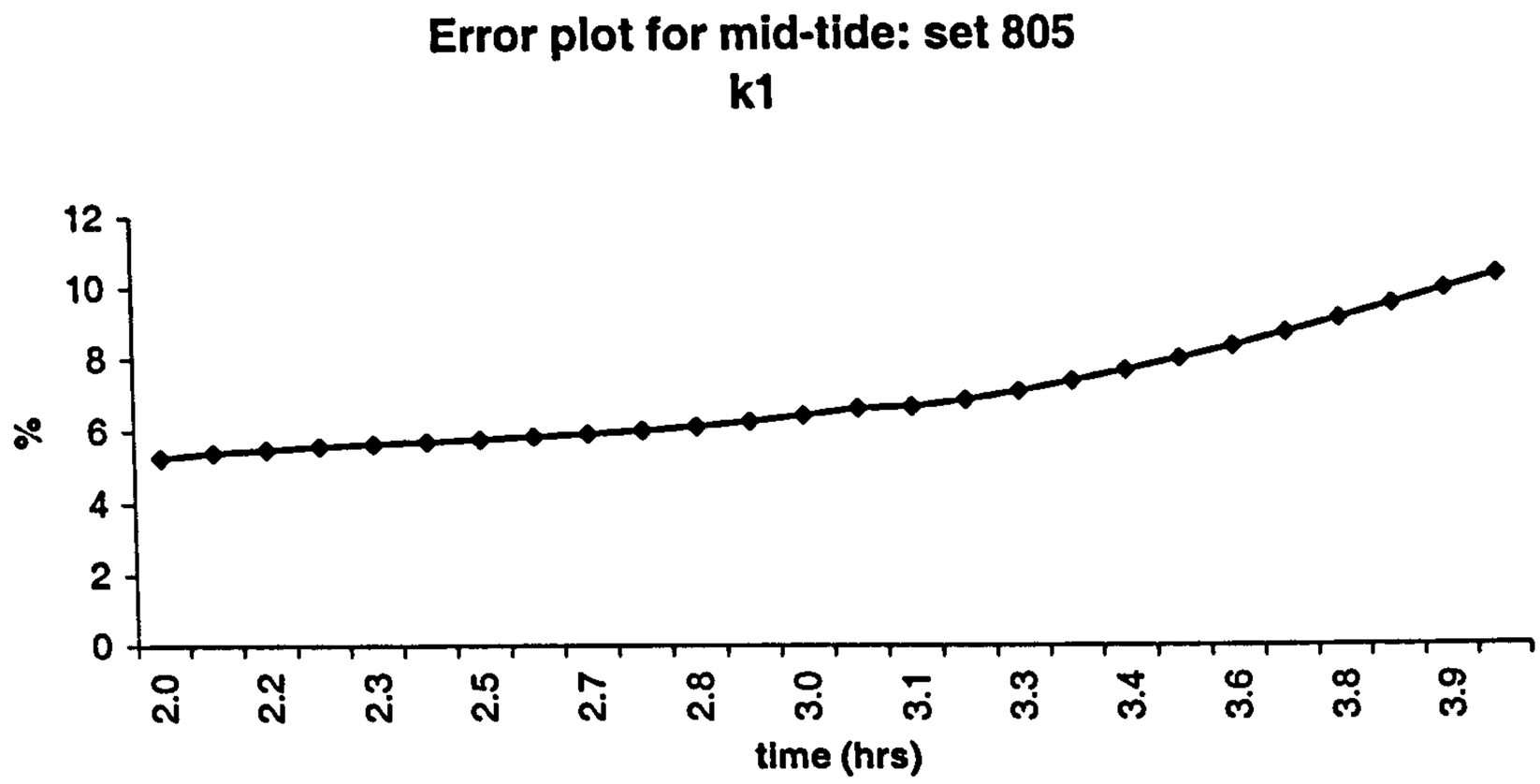

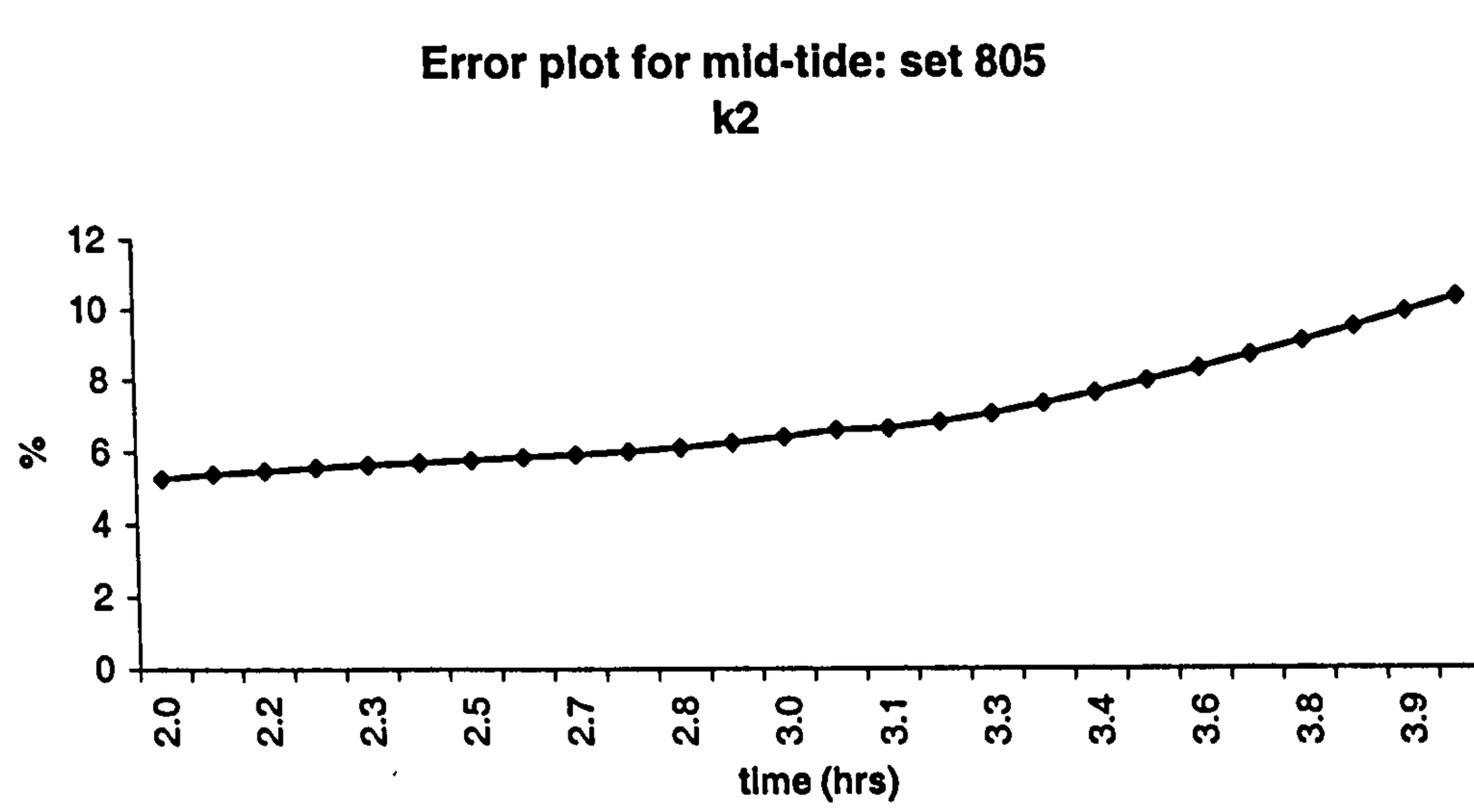

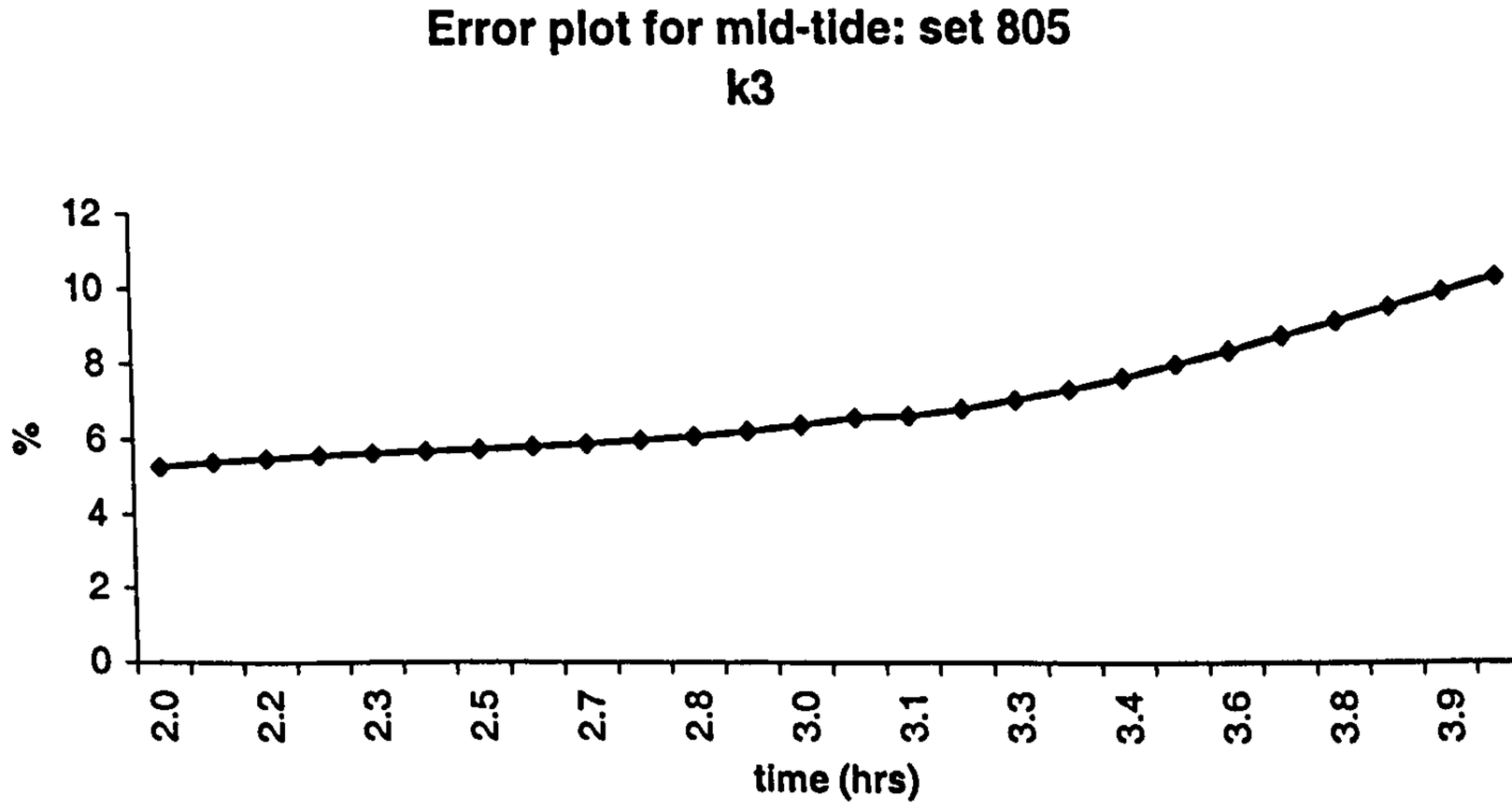

Figure 8.6.14a-c: Error between conventional 2DV method and parameterised Corrector method during the mid-tide phase.

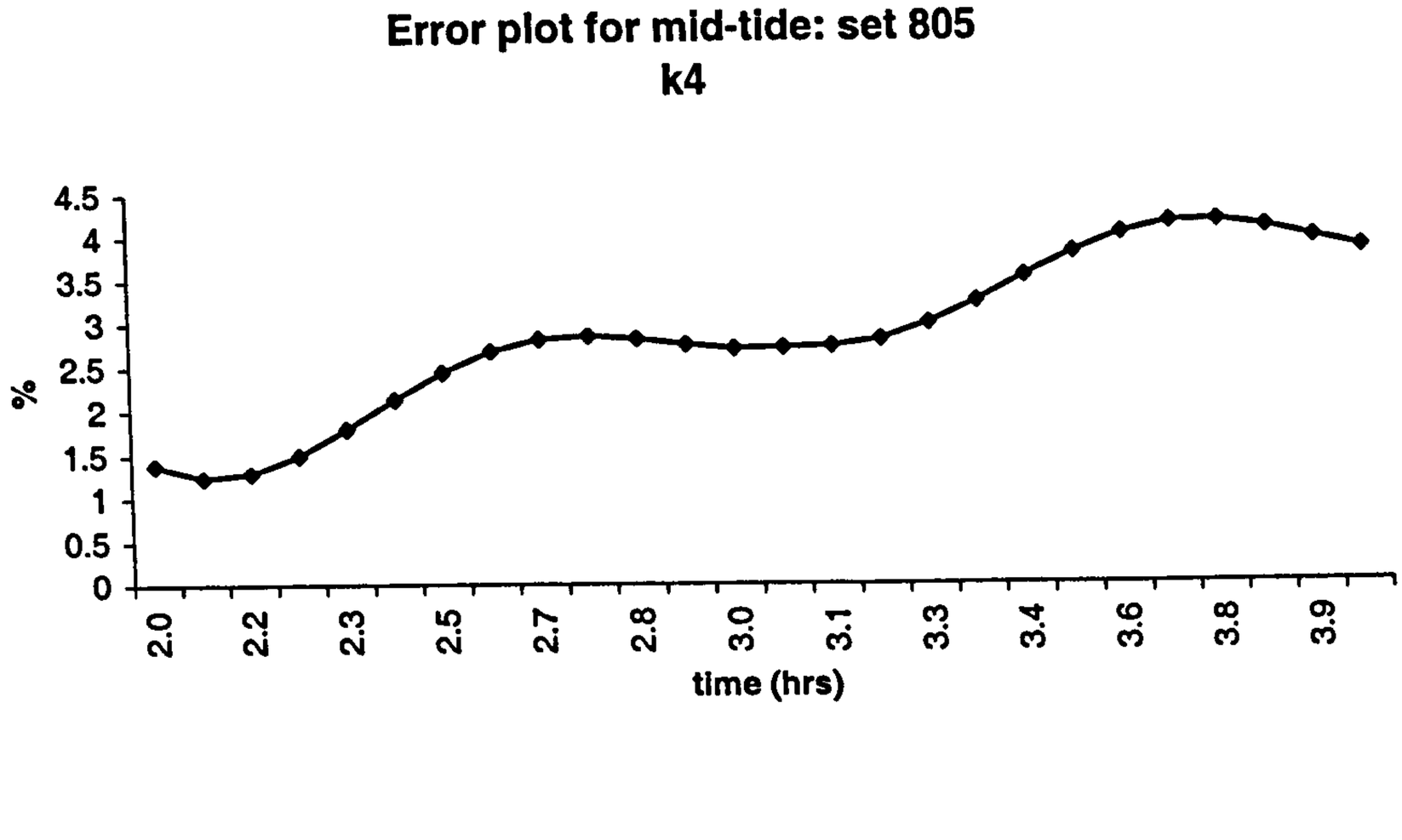

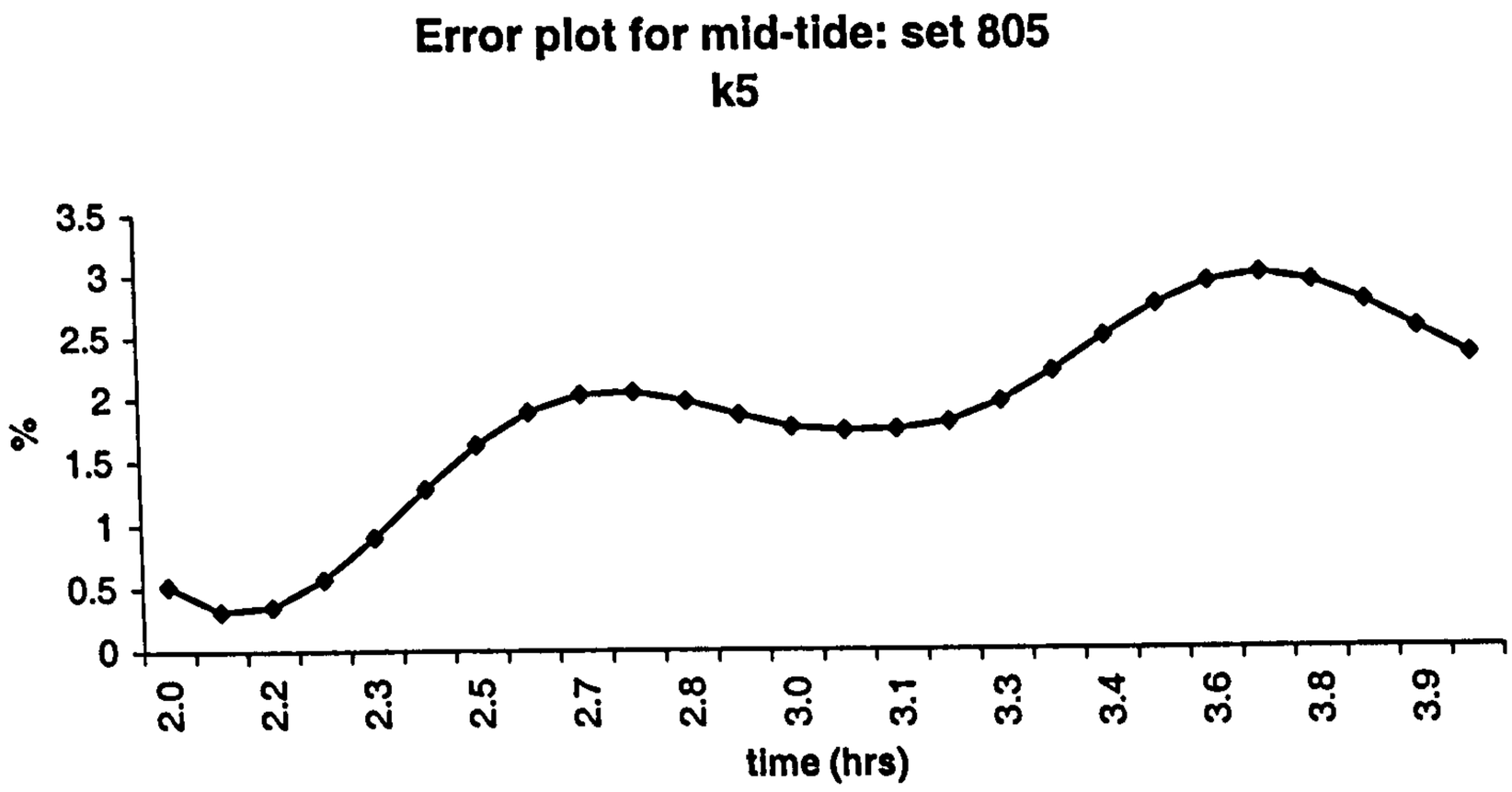

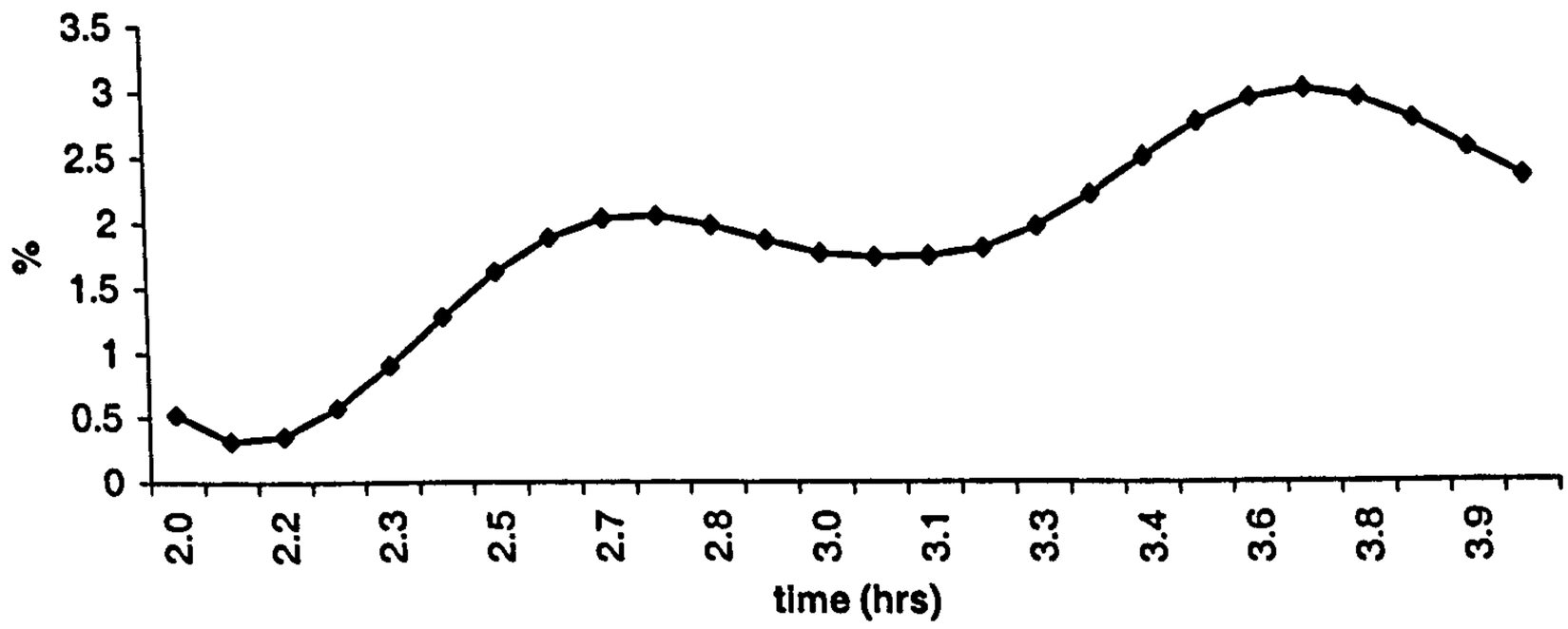

Figure 8.6.14d-f: Error between conventional 2DV method and parameterised Corrector method during the mid-tide phase.

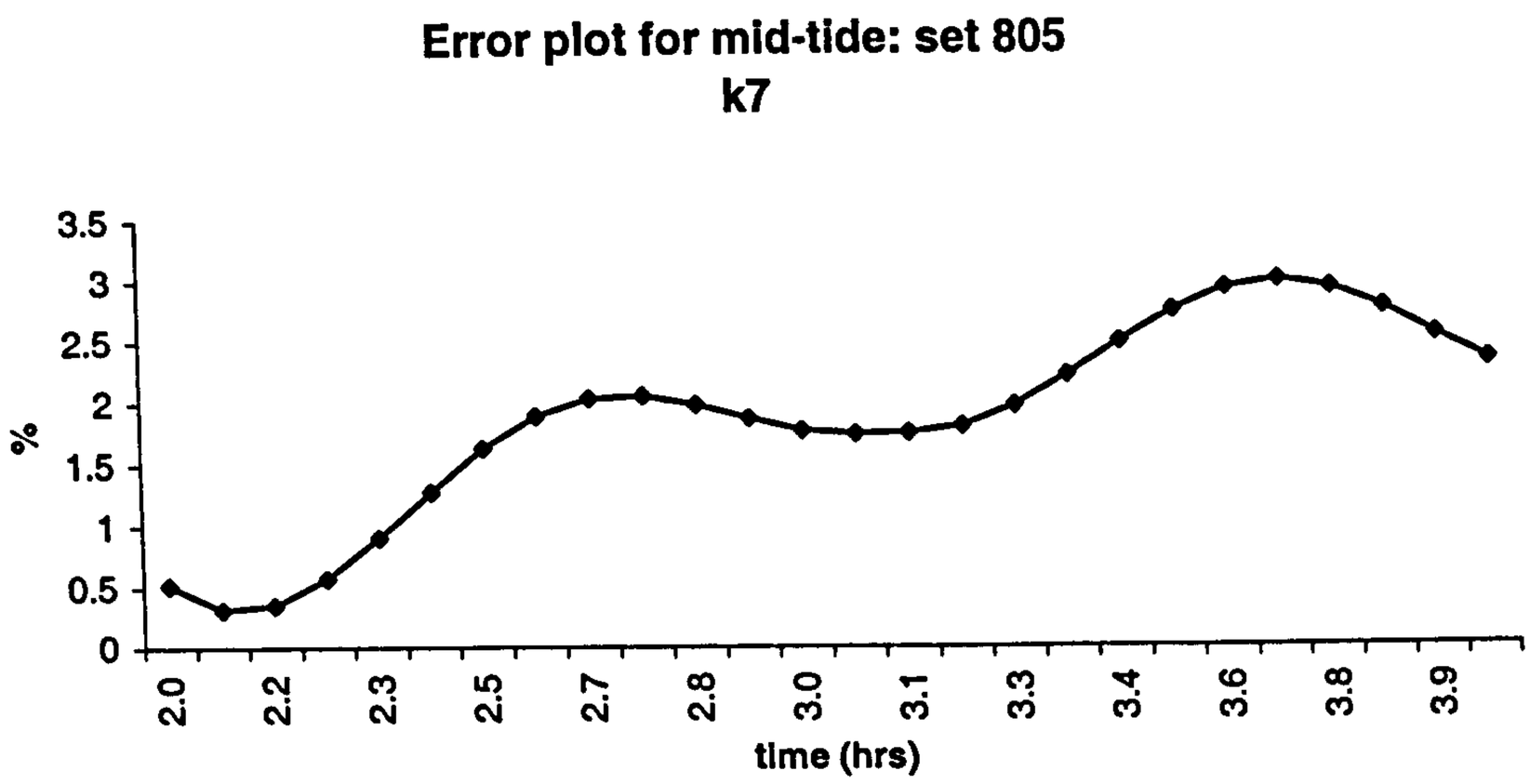

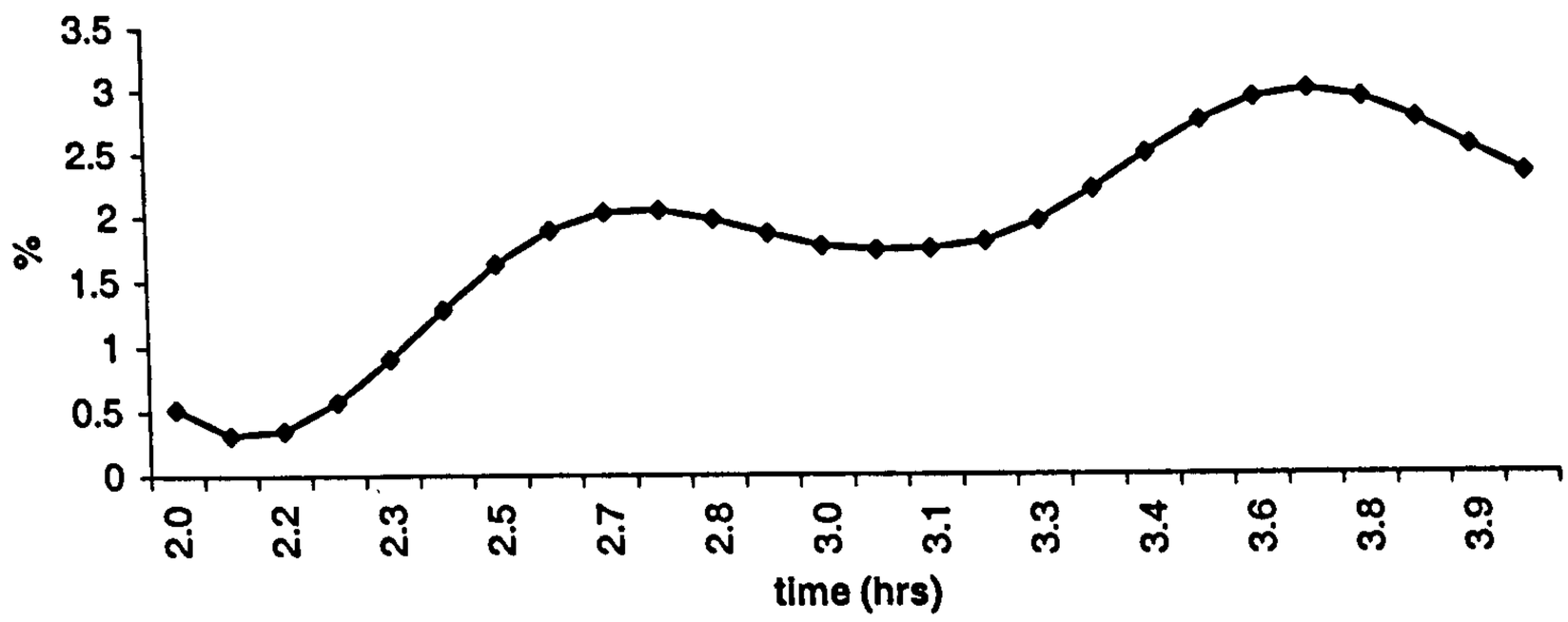

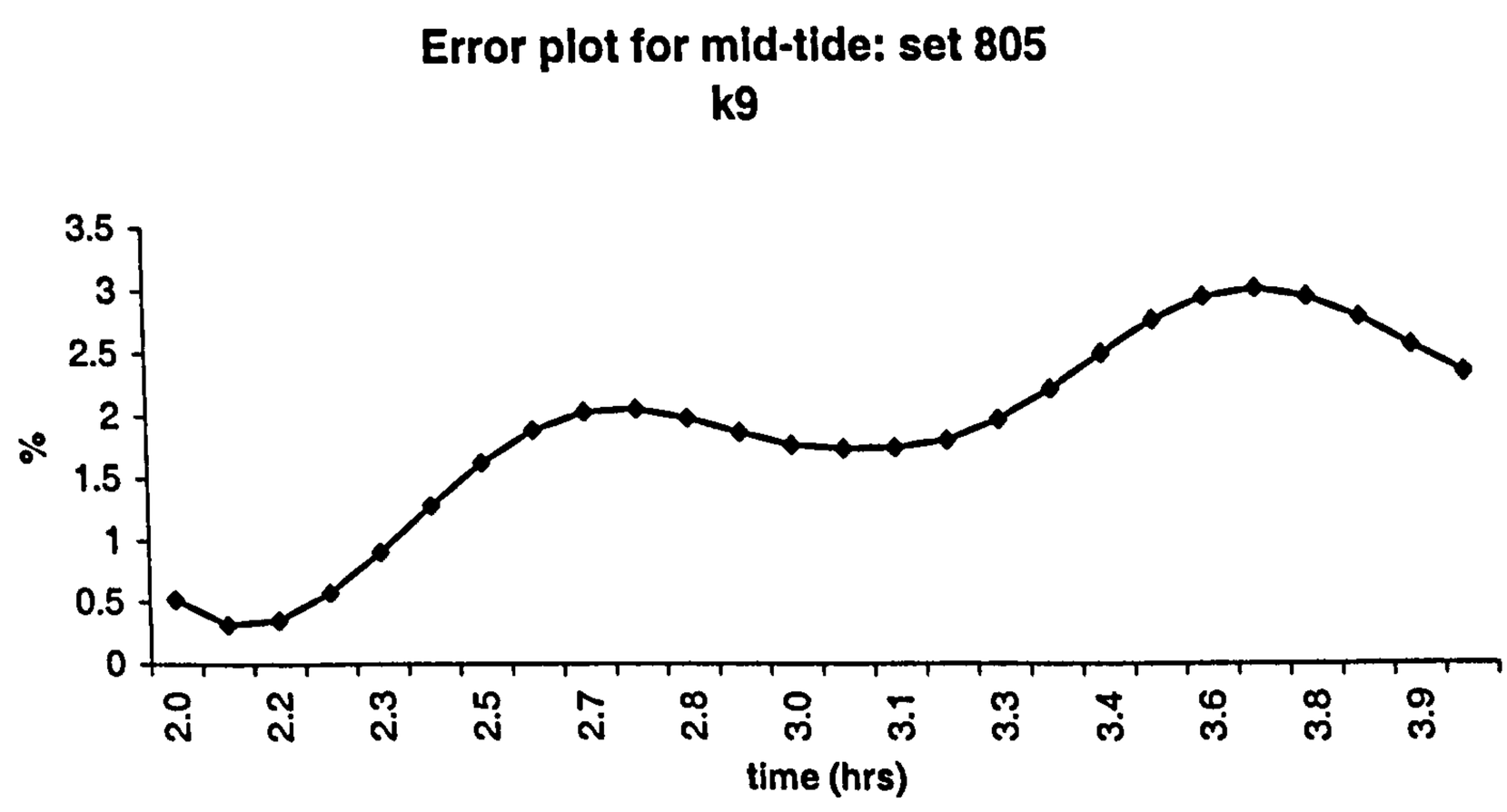

Figure 8.6.14g-i: Error between conventional 2DV method and parameterised Corrector method during the mid-tide phase.

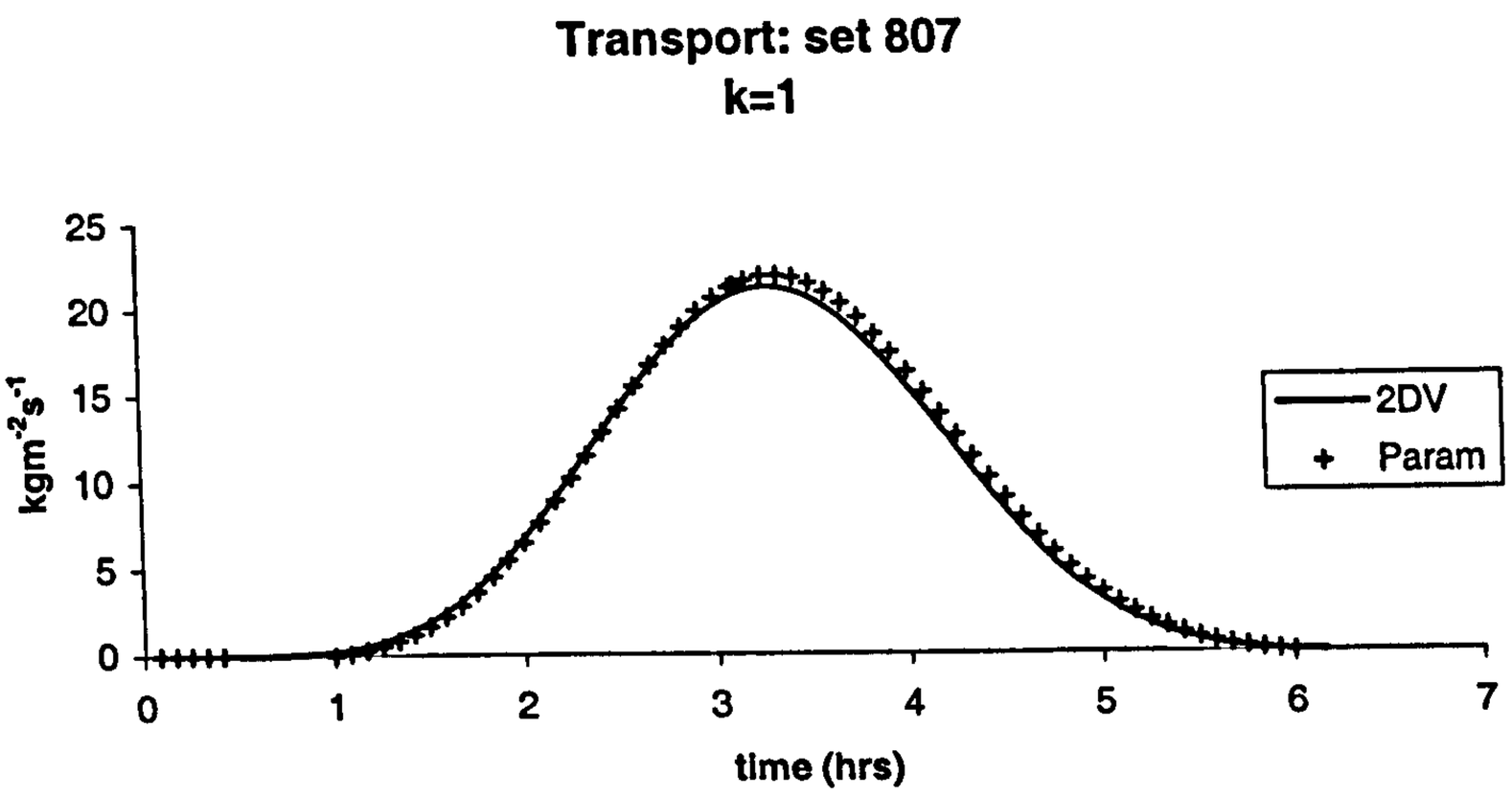

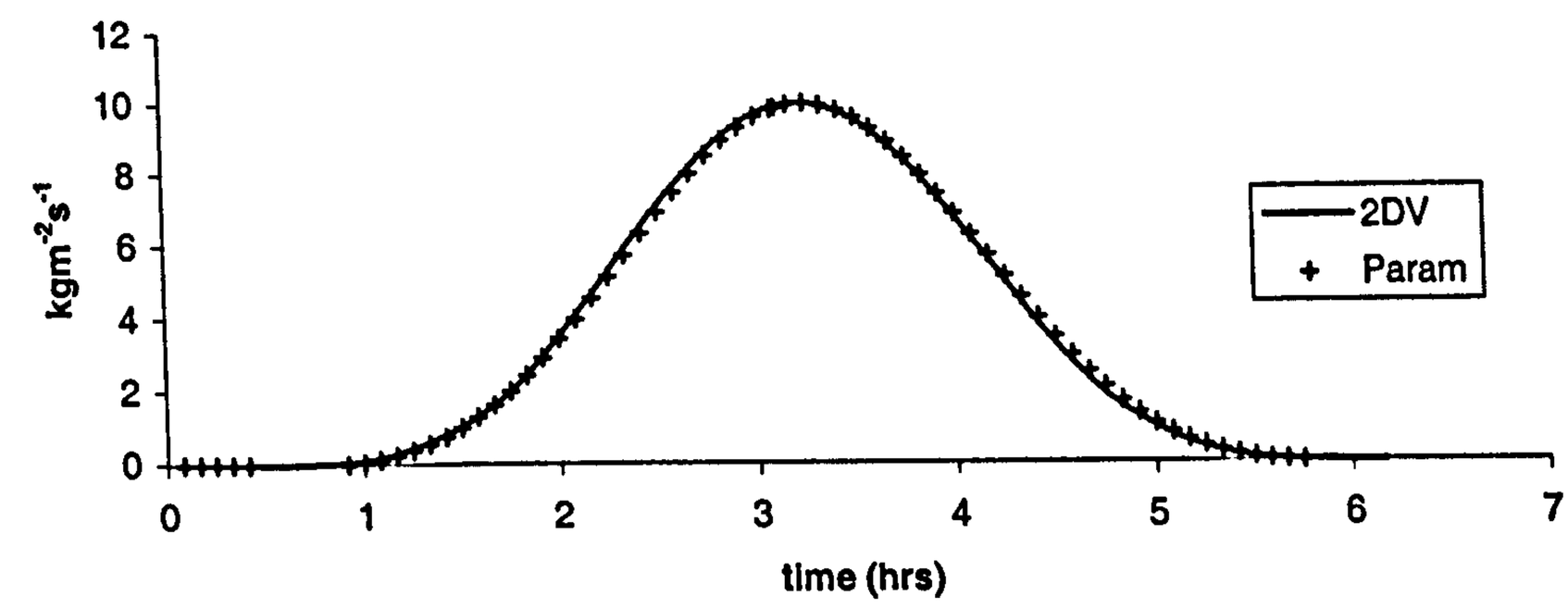

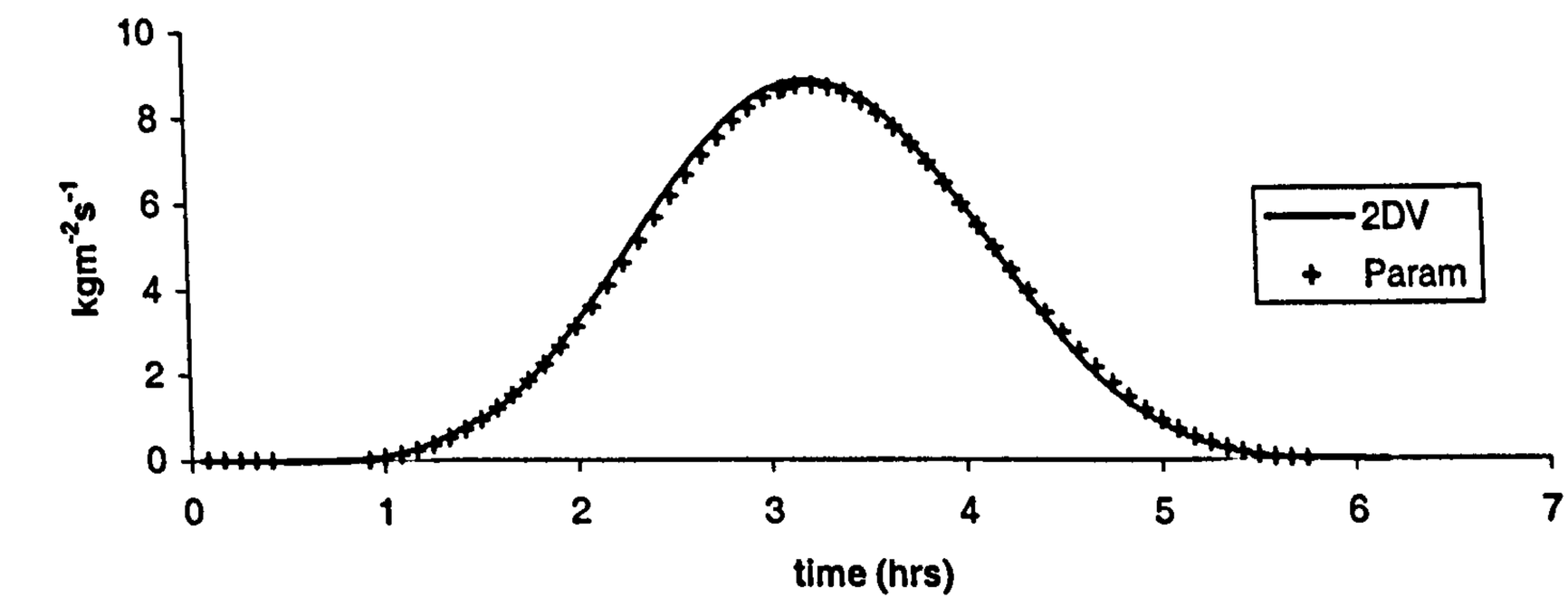

Figure 8.6.15a-c: Comparison between parameterised Corrector (Param) and conventional 2DV (2DV)

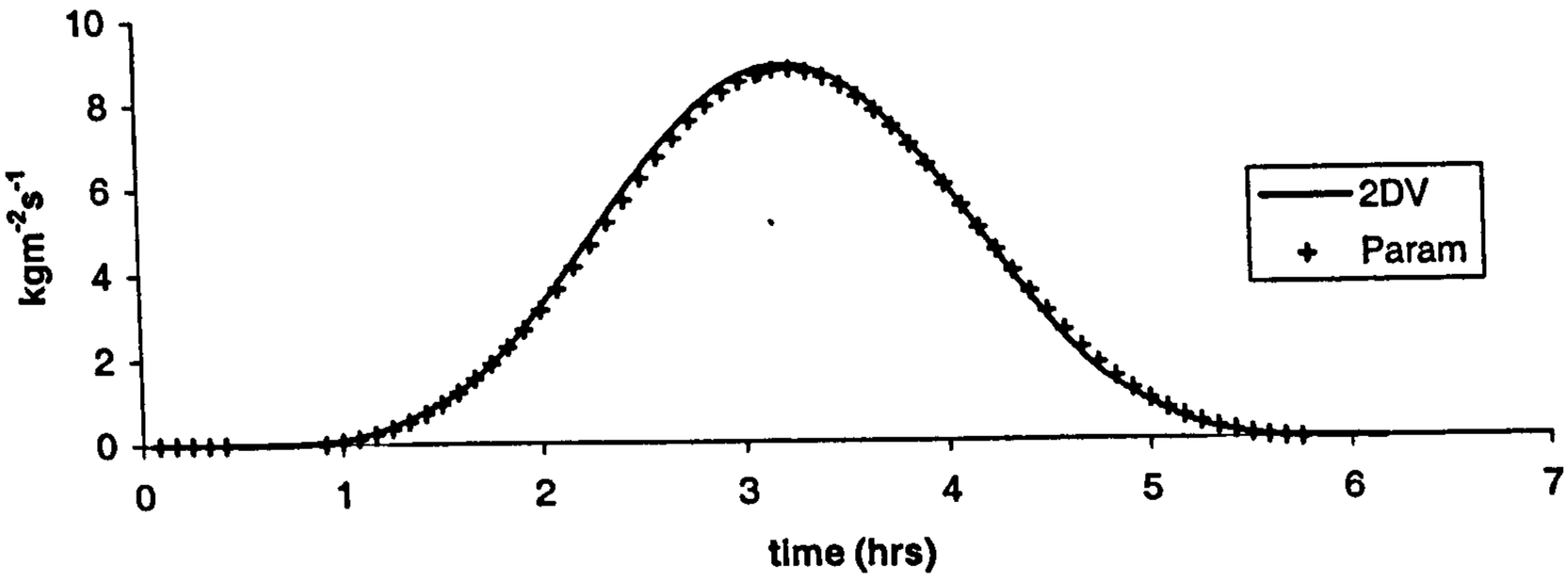

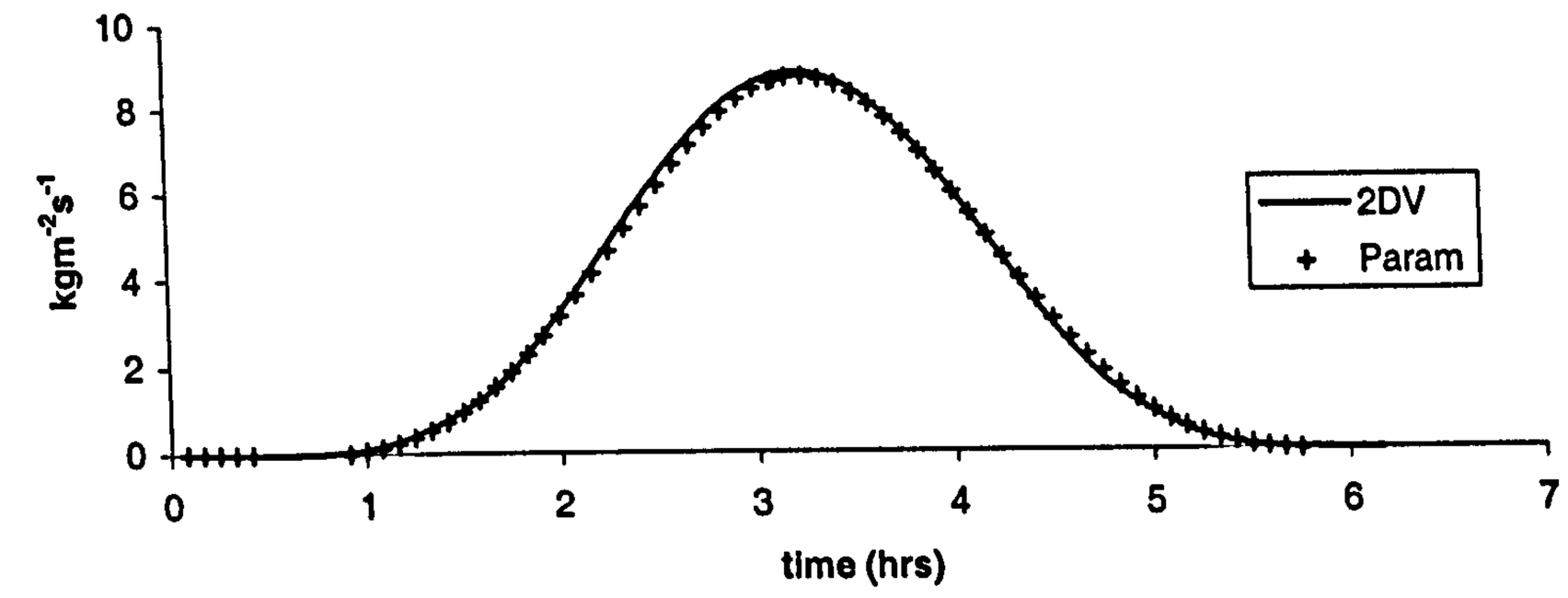

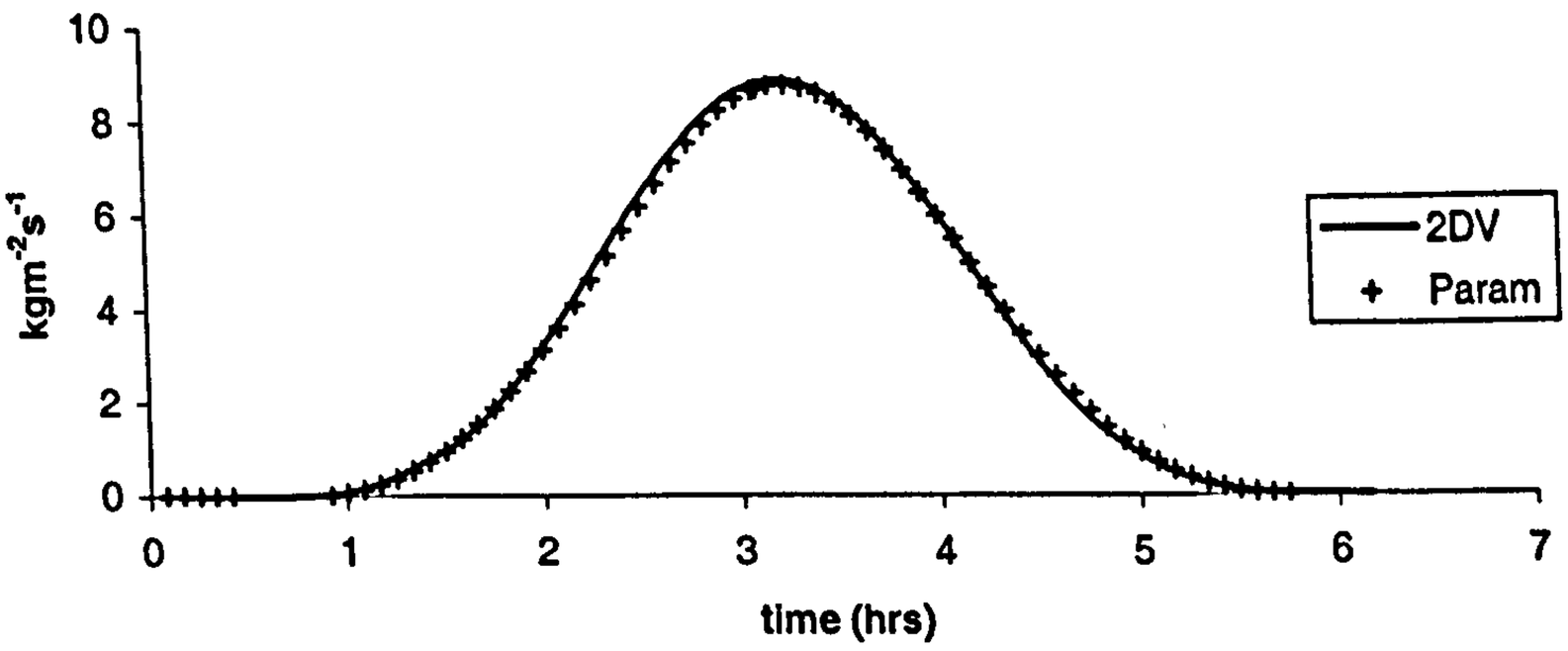

Figure 8.6.15d-f: Comparison between parameterised Corrector (Param) and conventional 2DV (2DV)

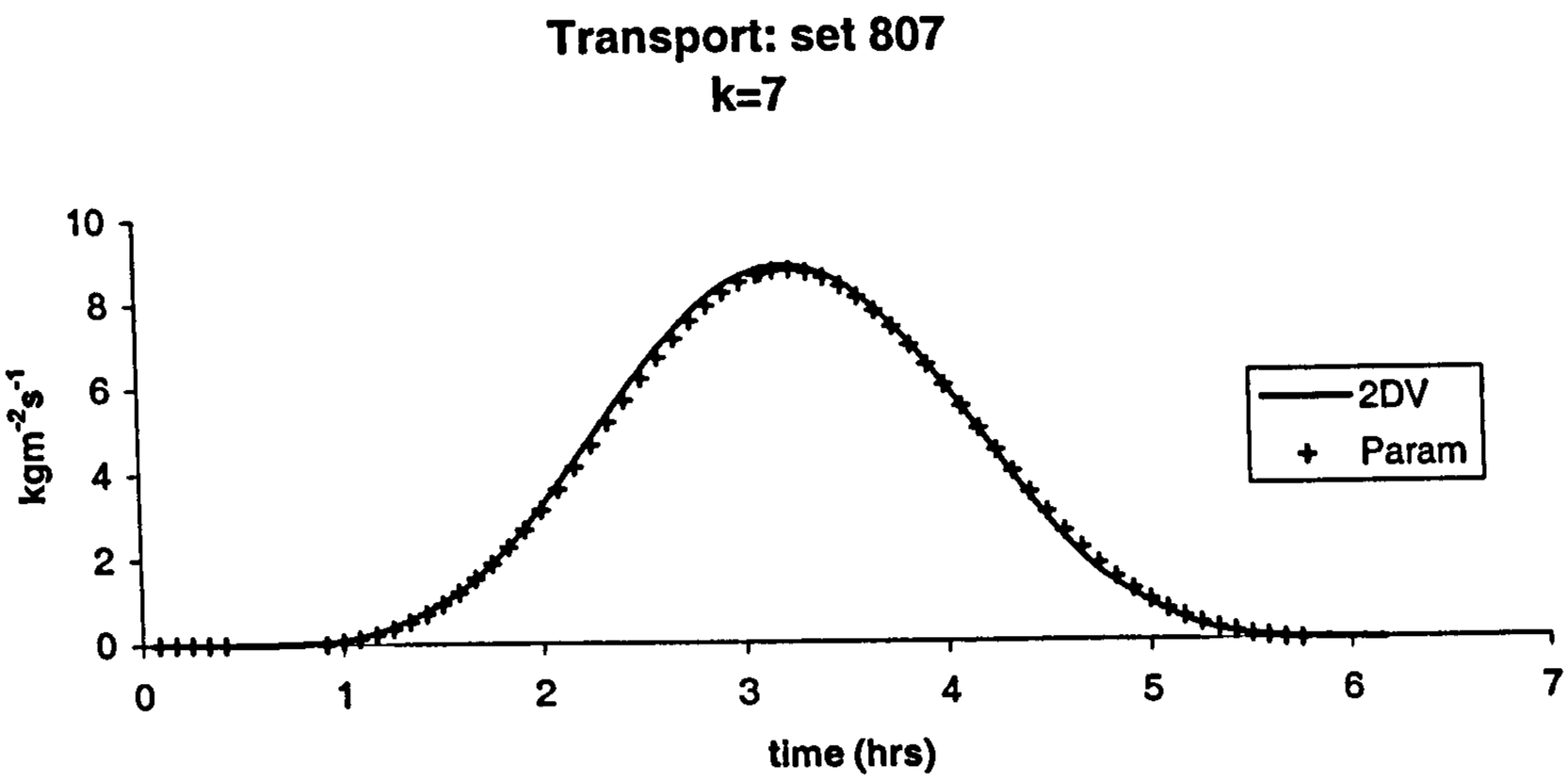

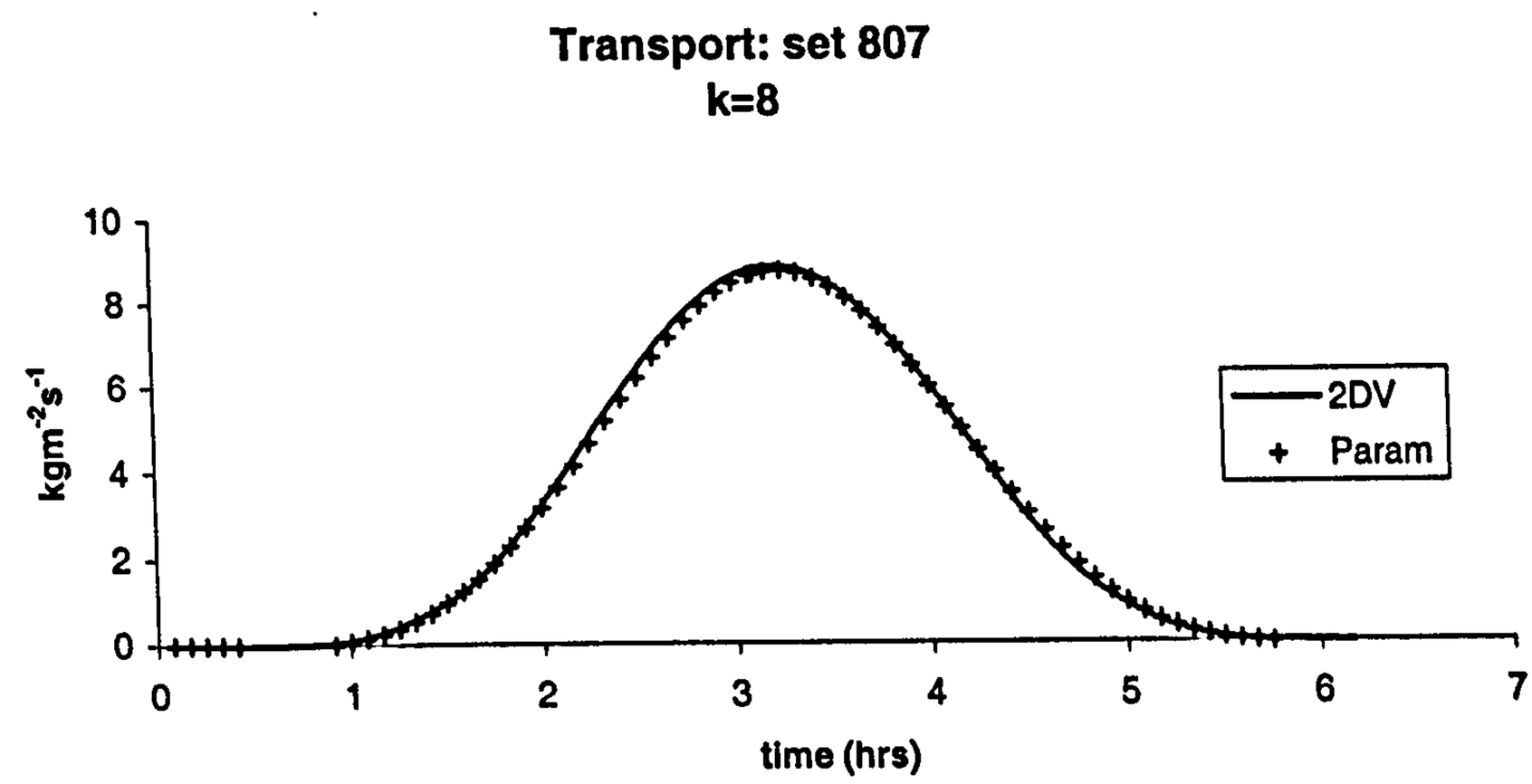

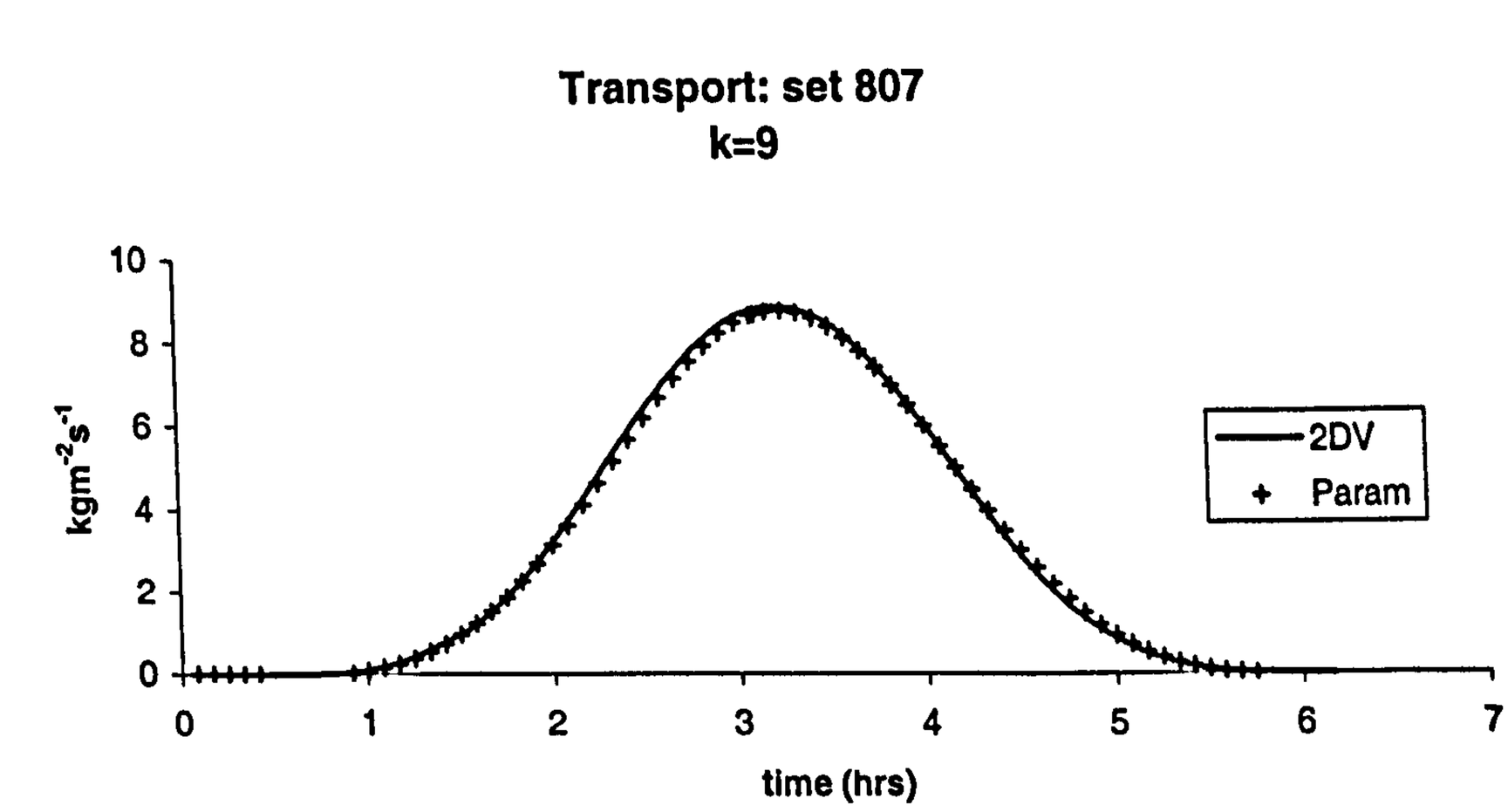

Figure 8.6.15g-i: Comparison between parameterised Corrector (Param) and conventional 2DV (2DV)

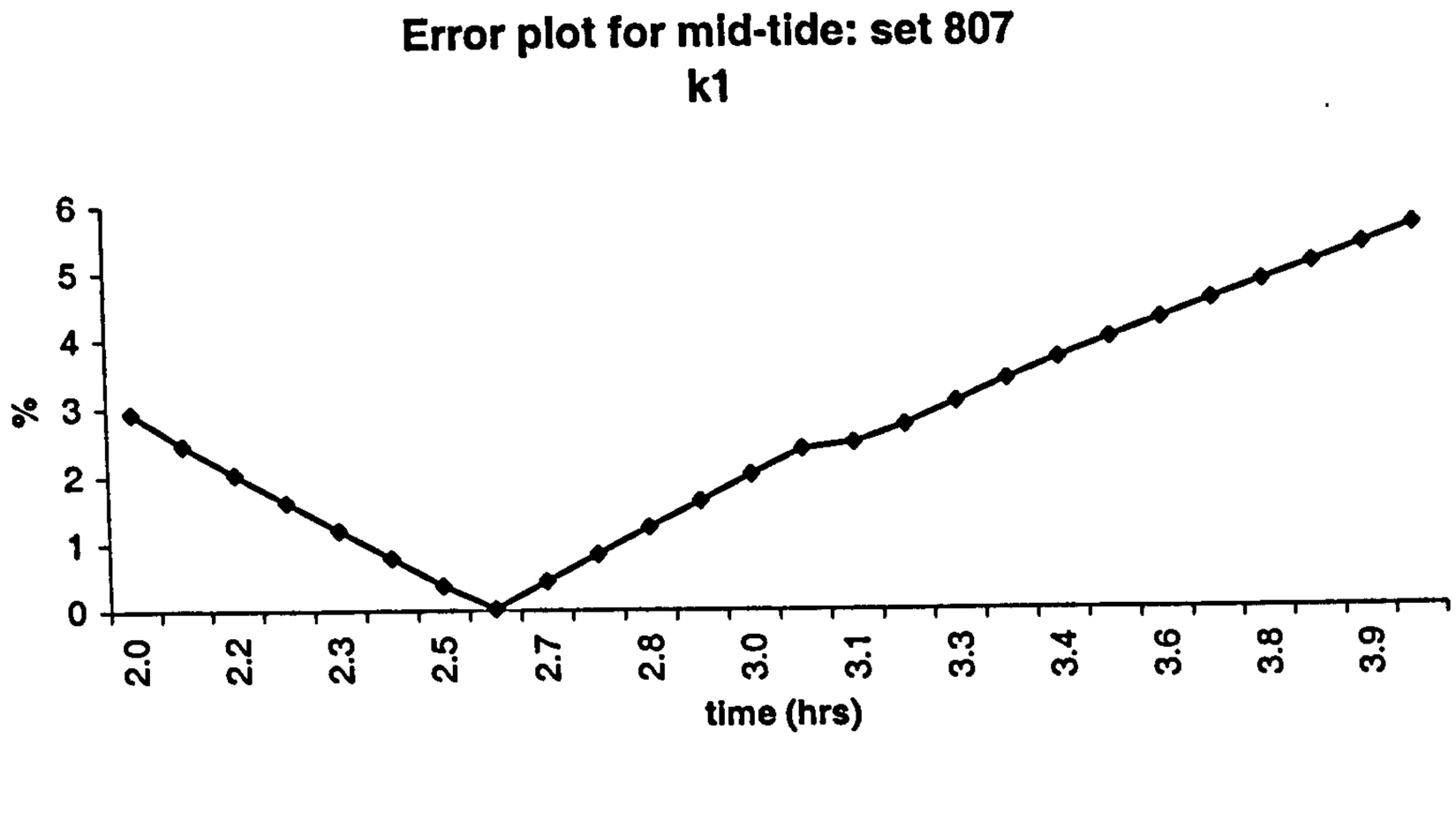

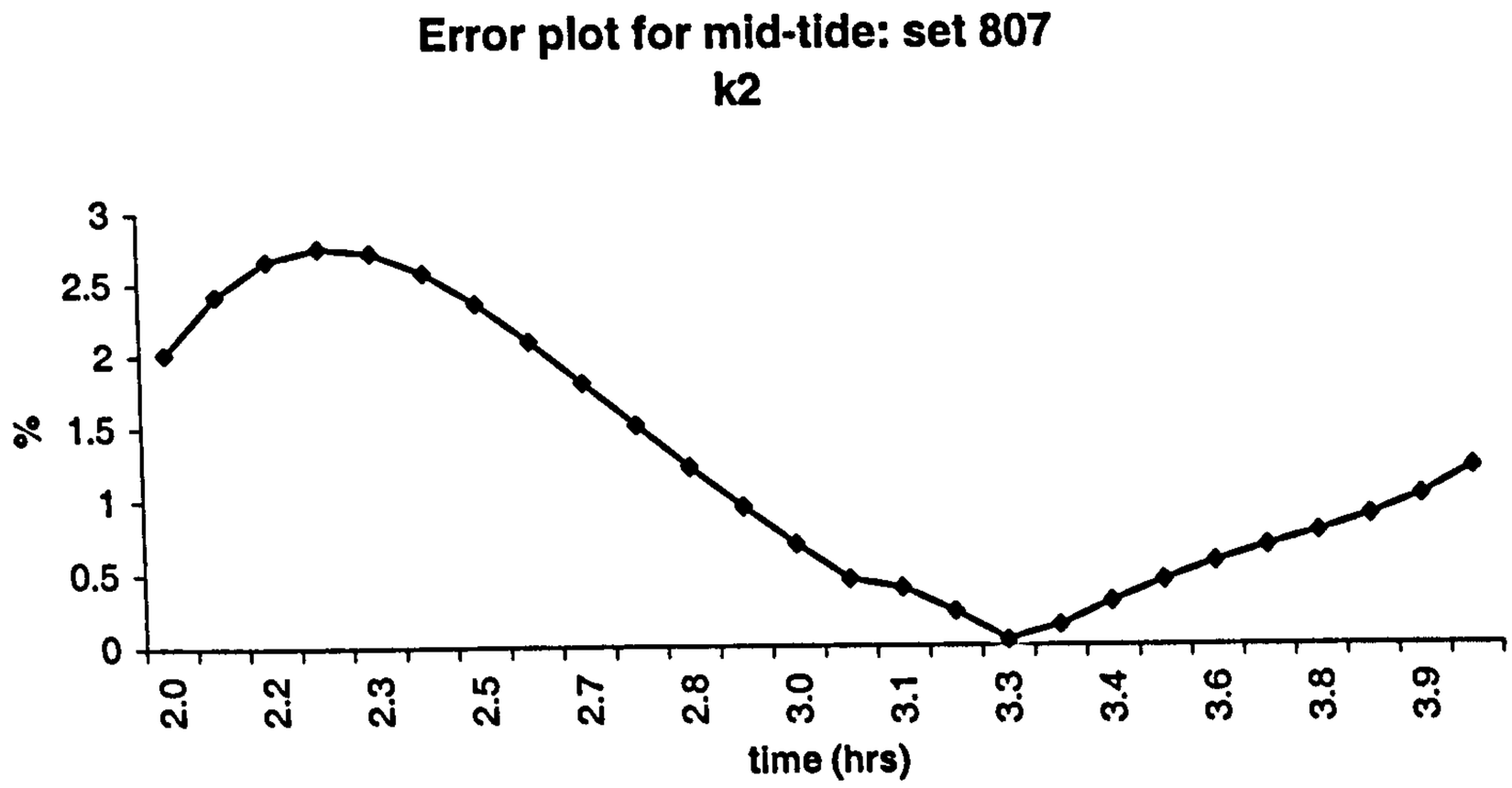

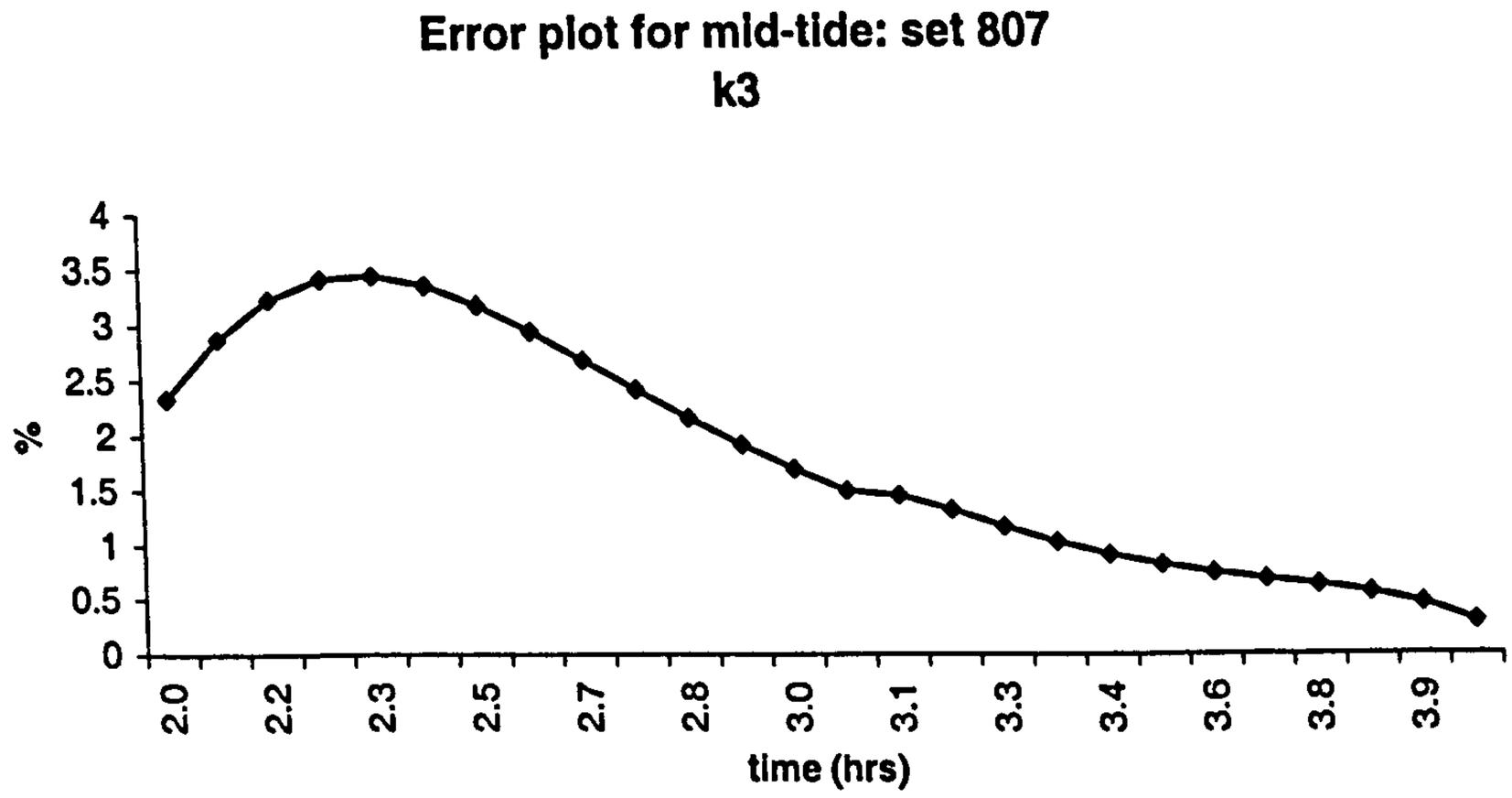

Figure 8.6.16a-c: Error between conventional 2DV method and parameterised Corrector method during the mid-tide phase.

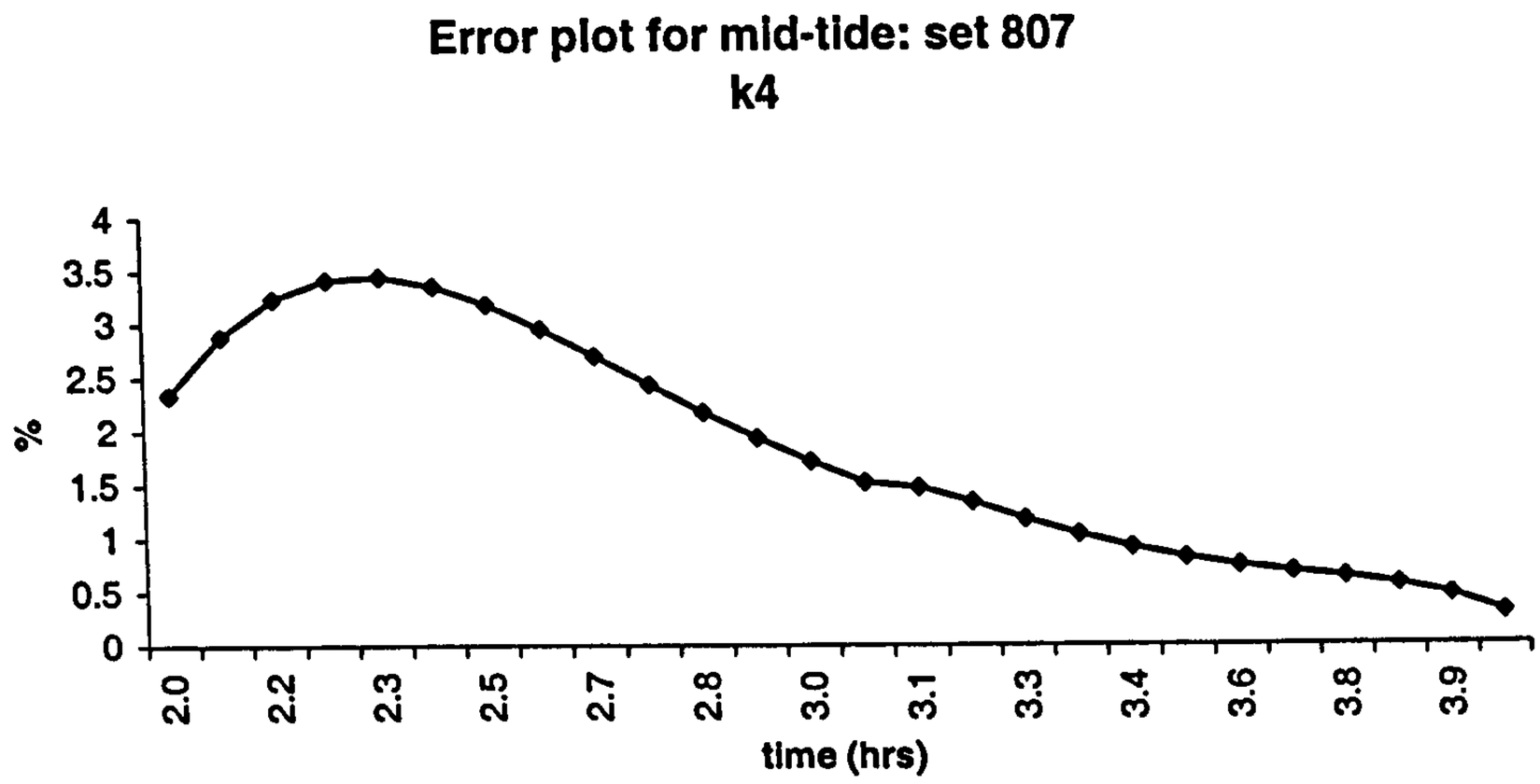

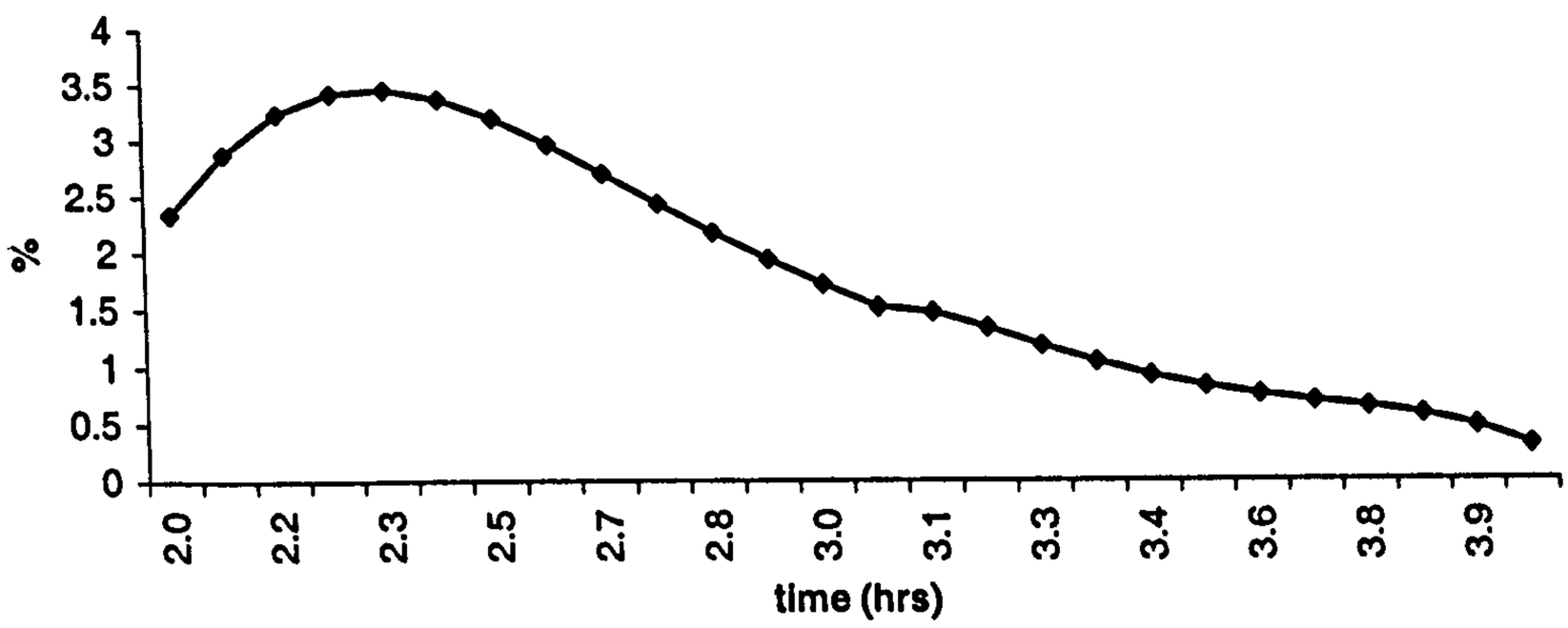

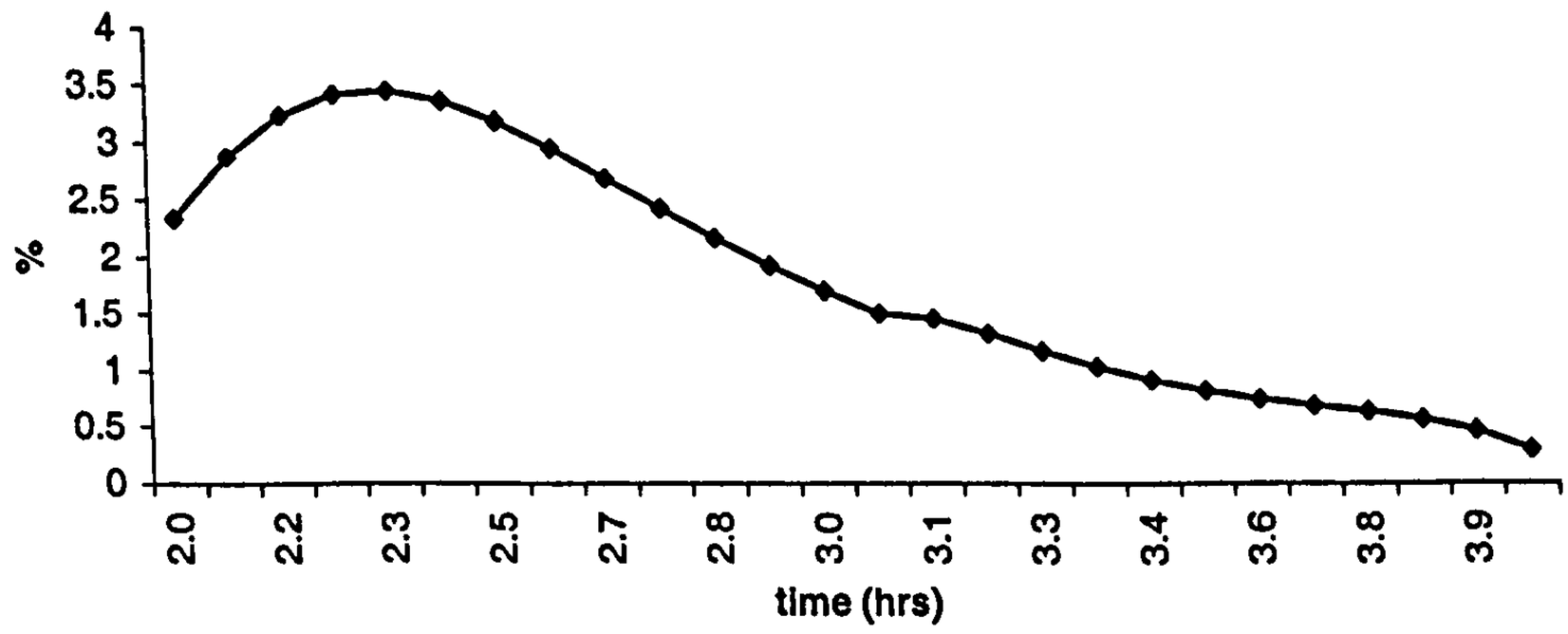

Figure 8.6.16d-f: Error between conventional 2DV method and parameterised Corrector method during the mid-tide phase.

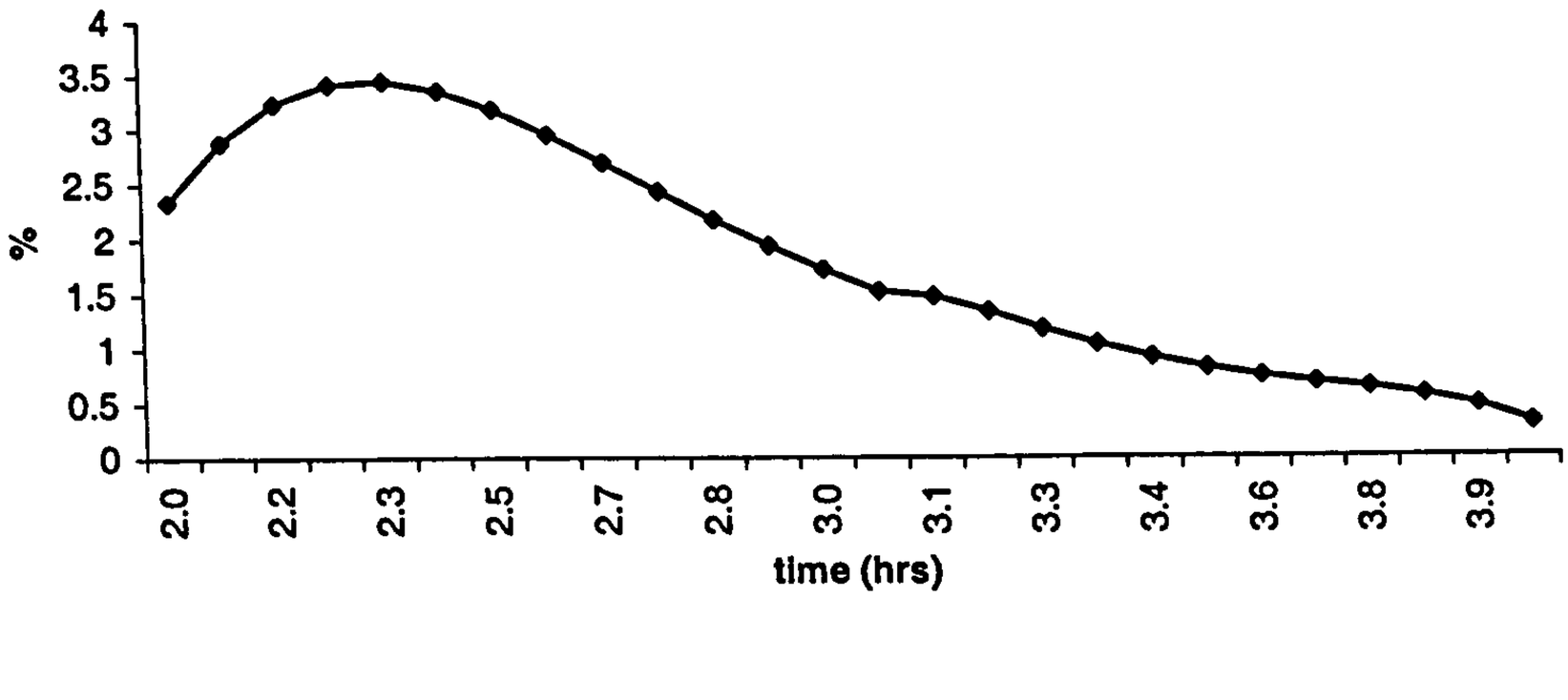

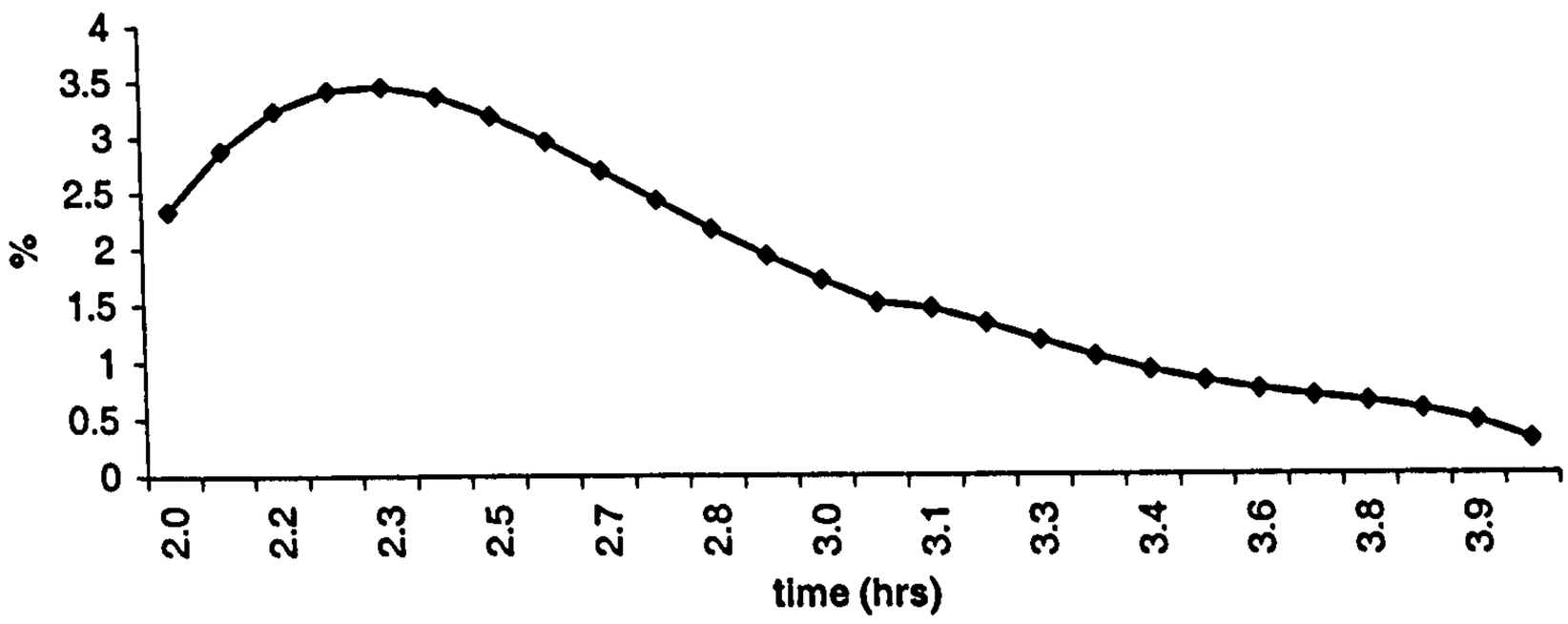

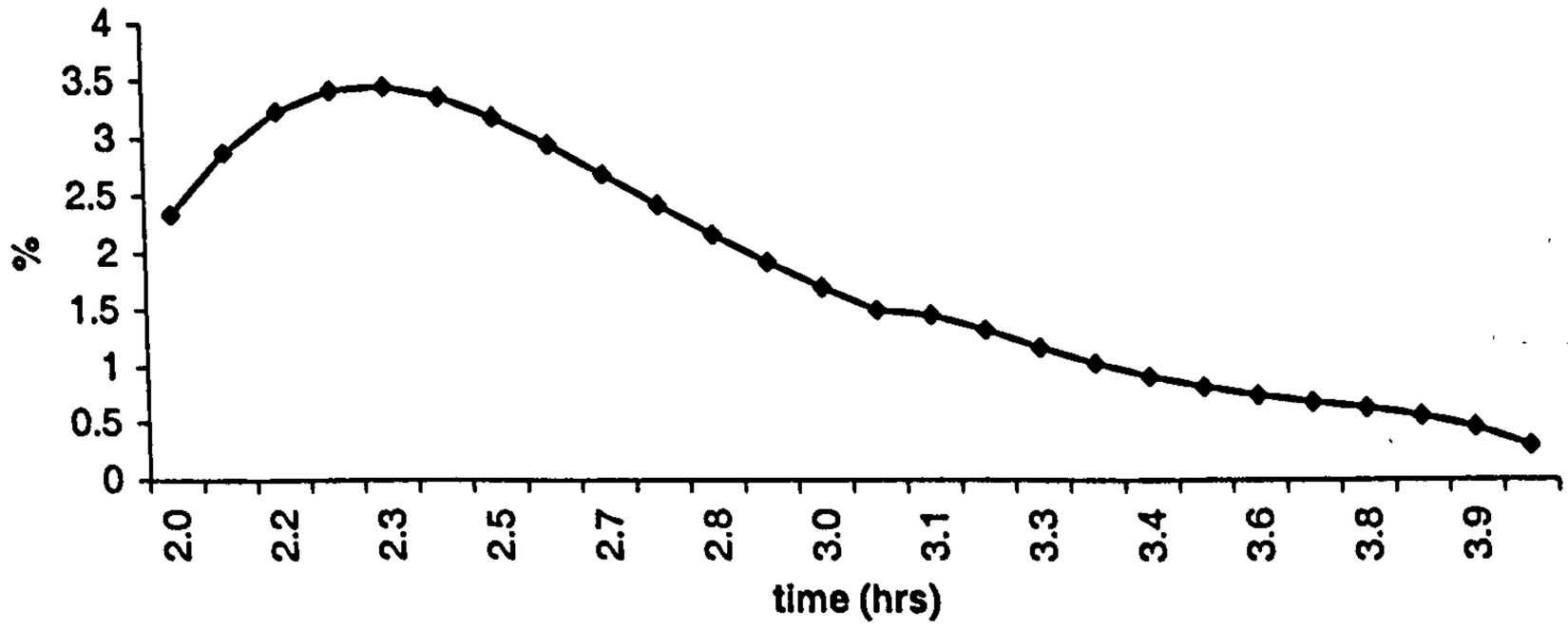

Figure 8.6.16g-i: Error between conventional 2DV method and parameterised Corrector method during the mid-tide phase.

Chapter 9

Conclusions and Recommendations

9.1 Introduction

The work presented within this thesis has been undertaken in order to satisfy the aims set out in chapter 1; i.e.:-

1) To present the details of a new theory proposed by O'Connor (1999) for a Predictor-Corrector method for calculating tidal suspended sediment transport rates.
2) To produce a parameterised 1DV model that can be used in place of a numerical 1DV model in the new Corrector method.
3) To investigate the accuracy and computational cost of the new Corrector method

These aims are based on the limitations faced by present methods when considering a large number of spatial computation points. If the area of study is considered uniform then only a 1DV model is required to calculate transport rates; however, spatial non-uniformity requires a 2DV or fully 3D approach. Standard methods for solving 2DV and 3D models are based on numerical solutions, which can be very demanding in computer run time if applied to a large number of computation points. It is necessary therefore to consider new methods for calculating sediment transport rates that reduce the computational cost without losing accuracy.

Both the new parameterised Corrector method and the non-parameterised version can be seen to be such models. Their construction involved the use of several

other models, detailed in their respective chapters. This chapter begins by summarising those models used throughout the thesis.

Attention is then focused on the main aims of the thesis. Section 9.3 presents a discussion of the final results and draws conclusions concerning the accuracy and computational cost of both the new parameterised Corrector method and the non-parameterised version.

The results from both the new parameterised Corrector method and the non-parameterised version have raised the possibility that the methods might be improved still further and applied to more complicated situations. Ideas for further research are therefore discussed in section 9.4.

9.2 Summary of Methods

The new parameterised Corrector method is based on the results of several other models, all of which are described within this thesis.

The process begins with the construction of a model that predicts bed form dimensions for tidal conditions, see chapter 3. The model applies a tidal limit, suggested by O'Connor and Duckett (1989), to the steady state predictions of Van Rijn (1993). The bed form dimensions are then used to calculate the hydraulic roughness of the system.

Chapter 4 describes how the roughness values are then incorporated into a 1DV numerical model that predicts tidal suspended sediment transport rates. The 1DV model is given by the integral of the product of concentration and velocity values up through the water column. The concentration component uses a parabolic vertical sediment diffusion coefficient, the grain fall velocity of Soulsby (1994), the reference level and reference concentration of Van Rijn (1993) and a simple model for the vertical flow velocity based on the rate of change of the water depth. The concentration model is then discretised using the scheme proposed by Stone and Brian (1963) for the temporal derivative and a Crank-Nicholson

scheme for the spatial derivatives. The resulting set of simultaneous equations is solved using the method of Gaussian Elimination. The longitudinal velocity is given by a simple logarithmic profile. The model also incorporates a modified version of the coordinate transform suggested by O'Connor (1997). The integration is then performed using Simpson's rule for numerical integration.

The 1DV model is of paramount importance since it provides the first component of both the conventional 2DV model and the new Corrector method. The details of the new Corrector method are given in chapter 2, thus satisfying the first aim of the thesis. Chapter 5 then describes how the new Corrector method incorporates the numerical 1DV model. The method consists of two components; the first is the predictor step, which is simply the 1DV model for suspended sediment transport rates. The second component is the new Corrector step. The new Corrector step is derived from a 1DH model obtained when the 2DV system is split into its vertical and longitudinal components. The equation defining the Corrector step is obtained by multiplying the 1DH equation by the depth-average longitudinal flow velocity, then integrating over the depth.

The new Corrector method is then tested against a conventional 2DV model to assess its accuracy and computational cost. Essentially, the conventional 2DV model is the 1DV model with an added component that adjusts results for longitudinal advection. Details of both the construction of the 2DV conventional model and the test conditions are given in chapter 6.

Parameterisation of the 1DV model is then based on the Fourier series approximation to the tidal suspended sediment transport rates. Chapter 7 shows how a parameterised 1DV model is constructed from ten characteristic parameters that define the system. The parameterisation fits a functional form to five non-dimensional parameter groups using regression analysis on the results from the 1DV numerical model.

Chapter 8 then describes how this 1DV parameterised model is modified so that it may be used in place of the numerical 1DV model in the new Corrector method. Essentially, the modification takes the form of the addition of an extra

characteristic parameter, or the associated non-dimensional group to be more precise, that accounts for the change in reference level for the 2DV system.

Chapter 8 also presents details of the parameterisation for the transport rate due to depth-average values and how it is used, together with the modified parameterisation of the 1DV model, to produce a new parameterised Corrector method.

It is seen therefore, that the thesis describes a number of models, i.e.:-

i). A tidal bed form model.
ii). A 1DV tidal suspended sediment transport model.
iii). A conventional 2DV model for calculating tidal suspended sediment transport rates.
iv). A new Corrector method.
v). A Fourier series approximation to tidal suspended sediment transport rates.
vi). A parameterised 1DV model.
vii). A parameterised 1DV model that can be used in a 2DV system.
viii). A new parametric Corrector method.

9.3 Conclusions

The main aim of the thesis is to reduce computational costs by using a parameterised 1DV model in a new Corrector method for calculating 2DV tidal suspended sediment transport rates. The conclusions are therefore split into two sections; the first concerns the accuracy of the new approach, the second concerns the time required for computations.

9.3.1 Accuracy

New Corrector Method

Chapter 6 presents the results of comparison tests between the conventional 2DV model and the new Corrector method. It is shown that the two methods are

almost indistinguishable for the two data sets used in the test. The difference between the predicted values of transport rates is shown graphically by figures 6.5.6 and 6.5.7. It is clearly seen that the two methods are in good agreement. It is concluded therefore, that the accuracy of the new Corrector method is of the same order as the conventional approach to 2DV suspended sediment transport modelling for the range of conditions tested.

Parameterised 1DV Models

The regression analysis performed in chapter 7 shows the results of fitting exponential and power functions to the five non-dimensional groups obtained from the set of characteristic parameters. It is shown that most of the parameterised quantities are adequately reproduced. However, a_6 and b_6 both ask questions of the validity of the functional form suggested. The error in terms of actual transport rate is shown to be insignificant since these quantities are small in magnitude and are therefore not very influential in the overall parameterisation.

Testing of the combined parameterisations, in the form of the parameterised Fourier series, shows good agreement with the results from the numerical 1DV model. All six of the test sets shown in figure 7.7.9 show good agreement. It is shown therefore that the accuracy of the parameterised 1DV model is only slightly less than that of the numerical approach.

The modified parameterised 1DV model returns similar regression results as the non-modified approach. Again, only the parameterisations for a_6 and b_6 are questionable. However, the same order of magnitude argument applies. It is seen therefore that the error in the parameterised Fourier series due to these quantities is negligible.

Parameterised Corrector Method

The accuracy of the parameterised Corrector method relies upon the accuracy of each of the parameterised terms used in the method. It has already been stated that the accuracy of the parameterised 1DV model is slightly less than its numerical counterpart. However, the parameterised Corrector method also uses

parameterisations for both the depth-average concentration and the transport due to fluctuations from depth-mean values. These in turn depend upon the parameterisations for the 1DV transport rates and the parameterisation of the tidal ratio.

Regression analysis for the parameterisation of the tidal ratio returns excellent results such that the maximum error between predicted and actual values is only 0.655% for the data sets used in the analysis. This suggests that error incurred by the parameterisation for the tidal ratio is practically negligible.

Tests described in chapter 8, comparing the new parameterised Corrector method with results from the conventional 2DV model, show that the two models are in reasonable agreement. For the eight test cases considered, the worst margin of error during the mid-tide phase is of the order 10%. This occurs for data set 604, which considers larger particle sizes. The overall margin of error is excellent with values as low as 1.26% for data set 807. It is shown therefore, that the error incurred by using the new parameterised Corrector method is of the order 10% or less for those situations considered.

The error incurred by the parameterised Corrector method is predominately due to the parameterisation of the 1DV model since it has been shown that both the parameterisation for the tidal ratio and the new approach to 2DV transport rates do not produce significant error.

9.3.2 Computational Cost

The Corrector method has been constructed so that the number of calculations required to predict 2DV tidal suspended sediment transport rates is reduced. Essentially, the conventional approach calculates 1DV sediment concentration values at each longitudinal computation point. These values are then corrected for longitudinal effects at each vertical computation point. The new Corrector method begins with the same calculation for the vertical sediment concentration values at each longitudinal computation point. However, the next step is to

calculate the 1DV transport rate at each longitudinal computation point. The 1DV transport rates are then corrected for longitudinal effects. Thus, only one calculation is required to correct for longitudinal effects rather than one calculation per vertical computation level as used by the conventional approach.

New Corrector Method

Chapter 6 compares the time required for both the conventional 2DV model and the new Corrector method for two simple test cases. It is shown that for the situation where only nine longitudinal computation points are used, the new Corrector method requires only 72% of the time used by the conventional model. Although this is significant in itself, if the model were expanded to include the lateral dimension and a larger number of horizontal computation points, then the reduction in the computational cost would be considerable.

New parameterised Corrector Method

Similar tests have been performed on the new parameterised Corrector method. Since the numerical solution procedure has been replaced by simple analytic expressions, the computational cost in calculating the 1DV tidal suspended sediment transport rates is greatly reduced.

This is shown in the tests performed in chapter 8 where the computation time required for both the new parameterised Corrector method and the conventional 2DV model are compared for eight data sets. It is shown that the new parameterised Corrector method requires only 60% of the computation time used by the conventional approach.

It can be seen therefore, that the new Corrector method predicts 2DV tidal suspended sediment transport rates to the same degree of accuracy as the conventional approach but requires only 72% of the computation time for a simple situation. The parameterised Corrector method reduces the computation time still further, 60% of that required by the conventional approach and 10% less than that used by the non-parameterised version. However, this reduction in computation time is offset by an error of the order 10% or less.

9.4 Recommendations for Further Research

Although the work presented in this thesis has satisfied all of the aims set out, it has also raised the possibility of further topics for research and indeed, further improvement to the presented work; ideas which, due to time constraints, were unable to be investigated in the present thesis.

Further improvements to the accuracy and computational cost of the new parameterised Corrector method may be achieved by considering the following points:-

1. A better insight into the functional relationship between the parameterisation quantities and the non-dimensional parameters groups, listed in chapter 8, may be achieved by the use of additional data sets. It should be noted however, that care must be taken when choosing data sets for the regression analysis since it is easy to produce a bias in the analysis. It is essential therefore that all combinations are represented proportionally.

2. The parameterisation presented in this thesis requires the use of equilibrium values for the transport at maximum velocity and for the mean Fourier coefficients. Obviously, this requires the calculation of the equilibrium transport for each time step during the tidal cycle and then calculation of the Fourier series approximating the equilibrium tidal transport rates. If the parameterisation could be carried out without these values, perhaps using the basic quantities instead, then the time required for computation would be reduced still further. It is unclear how this would affect the accuracy of the parameterisation since the equilibrium values are used so that an exponential functional form may be considered.

It should be remembered that the work presented in this thesis is designed as a preliminary investigation into the accuracy and computational cost of a new parameterised Corrector method for predicting 2DV tidal suspended sediment transport rates. It remains therefore to test the method for more complex situations. Possible areas for expansion are given as follows:-

1. The parameterisation should be expanded for more extreme tidal conditions, such as larger values for the median grain diameter and depth-average longitudinal flow velocity.
2. Although flood or ebb dominated tides have been considered in the parameterisation, this should be expanded to include those tides where the flood phase, or ebb phase, is dominated by either the accelerating or decelerating stage.
3. The model should also be expanded to account for flow reversal.
4. As stated earlier, the reduction in computational cost would be even more dramatic if the lateral dimension was also considered. This appears to be obvious but still needs to be quantified.
5. Only a simple flow field has been considered thus far. The validity of the new parameterised Corrector method should now be tested using a more complex flow pattern.
6. Having shown the usefulness of the new parameterised Corrector method for tidal currents, the method should now be expanded to include the effects of waves.
7. It should also be noted that a higher order interpolation scheme might be required for actual field application of either the new parameterised Corrector method or the non-parameterised version. A simple linear method was sufficient to show theoretically the relative accuracy between the new methods and the conventional 2DV approach. However, it may not be sufficient for field application.

References

Aguirre-Pe, J. and Fuentes, R., (1990), *Resistance to flow in Steep Rough Streams*, Journal of Hydraulic Engineering, A.S.C.E., Vol.90, No. HY4

Akiyama, J. and Fukushima, Y., (1986), *Entrainment of Non-cohesive Sediment into Suspension*, 3rd Int. Symp. On River Sedimentation, S. Y. Wang, H. W. Shen, and L. Z. Ding, eds., Univ. of Mississippi, pp 804-813

Allen, J.R.L., (1968), *Current Ripples*, North-Holland Publishing Company, Amsterdam

Apmann, R.P., and Rumer, R.R.Jr., (1967), *Diffusion of Sediment in a Non-uniform Flow Field*, Civil Engineering Report No. 16, State University of New York at Buffalo, December, 1967

Carstens, M.R., (1952), *Accelerated Motion of a Spherical Particle*, Transactions of the American Geophysical Union, Vol. 33, No. 5, October, pp 713-720

Celik, I., and Rodi, W., (1984), *A Deposition Entrainment model for Suspended Sediment Transport*, Report SFB 210/T/6, Universitat Karlsruhe, Karlsruhe, Germany

Coleman, N.L., (1970), *Flume Studies of the Sediment Transfer Coefficient*, Water Resources Research, Vol. 6, No. 3, June, 1970, pp 801-809

Duckett, F.J.L., (1984), *A Study of Friction in Unsteady Flows*, M.Sc. Thesis, University of Manchester

Einstein, H. A., (1950), *The Bed-Load Function for Sediment Transportation in Open Channel Flows*, Technical Bulletin No. 1026, U.S. Dep. of Agriculture, Washington, D.C.

Einstein, H.A. and Chien, N., (1955), *Effects of Heavy Sediment Concentration near the Bed on Velocity and Sediment Distribution*, Inst. Of Eng. Research, University of California, Berkely, California, USA

Engelund, F. and Hansen, E., (1967), *A Monograph on Sediment Transport*, Technisk Forlag, Copenhagen, Denmark

Engelund, F. and Fredsøe, J., (1976), *A Sediment Transport Model for Straight Alluvial Channels*, Nordic Hydrology, 7, pp 293-306

Fredsøe, J., (1980), *The Formation of Dunes*, Int. Symp. On River Sedimentation, Beijing, China

Fredsøe, J., (1982), *Shape and Dimensions of Stationary Dunes in rivers*, Journal of the Hydraulics Division, A.S.C.E., HY8

Fredsøe, J. and Deigaard, R. (1992), *Mechanics of Coastal Sediment Transport*, World Scientific, London

Garcia, M. and Parker, G., (1991), *Entrainment of Bed Sediment into Suspension*, Journal of Hydraulic Engineering, A.S.C.E., Vol. 117, No. 4, April, pp 414-435

Gibbs, R.J., Matthews, M.D., and Link D.A. (1971), *The relationship between sphere size and settling velocity*, Journal of Sedimentary Petrology, Vol 41, No. 1,pp 7-18

Gladki, H., (1975), *Discussions of Determination of Sand Roughness for Fixed Beds*, Journal of Hydraulic Research, Vol. 13, No.2

Hallermeier, R.J., (1981), *Terminal settling velocity of commonly occurring sand grains*, Sedimentology, 28, 859-865

Hey, R.D., (1979), *Flow Resistance in Gravel-bed Rivers*, Journal of Hydraulic Division, A.S.C.E., No. HY4

Ippen, A.T., (1966), *Estuary and Coastline Hydrodynamics*, McGraw-Hill Book Company, Inc. New York

Itakura, T. and Kishi, T., (1980), *Open Channel Flow with Suspended Sediments*, Journal of the Hydraulic Division, A.S.C.E, Vol. 106, No. 8, pp 1325-1343

Jain, S.C. and Kennedy, J.F., (1971), *The Growth of Sand Waves*, In. Proc. Intern. Symposium on Stochastic Hydraulics (Pittsburgh, USA), p449-471

James, G., (1992), *Modern Engineering Mathematics*, Addison-Wesley

Jobson, H.E. and Sayre, W.W., (1970), *Vertical Transfer in Open Channel Flow*, Journal of the Hydraulics Division, A.S.C.E., Vol. 96, No. HY3, March, pp 703-724

Kamphuis, J.W., (1975), *Friction Factor under Oscillatory Waves*, Journal of the Waterway, Port, Coastal and Ocean Div., A.S.C.E, Vol, 101, No. WW2, p 135-144

Katopodi, I. And Ribberink, J.S., (1992), *Quasi-3D modelling of suspended sediment transport by currents and waves*, Coastal Engineering, Vol.18, (1992), pp 83-110

Kim, H., (1993), *Three-dimensional sediment transport model*, Ph.D. Thesis at the University of Liverpool

Kerssens, P.M.J., Prins, A. and Van Rijn, L.C, (1979), *Model for Suspended Sediment Transport*, Journal of the Hydraulics Division, A.S.C.E, Vol. 105, No.HY5, 1979, pp 461-476

Lin, B.L. and Falconer, R.A., (1997), *Numerical modelling of three-dimensional suspended sediment for estuarine and coastal waters*, Journal of Hydraulic Research, Vol. 34, 1996, N0.4, pp 435-456

Lui, H.K., (1957), *Mechanics of Sediment-Ripple Formation*, Journal of Hydraulics Division, A.S.C.E., Vol. 83, HY2, p1-21

Lyn, D.A., (1991), *Resistance in Flat-bed Sediment-laden Flows*, Journal of Hydraulic Engineering, A.S.C.E., Vol. 117, No.1

Mahmood, K., (1971), *Flow in Sand Bed Channels*, Water Management Technical Report No. 11, Colorado State University, Fort Collins, Colorado, USA

McDowell, D.M. and O'Connor, B.A., (1977), *Hydraulic Behaviour of Estuaries*, Macmillan, London.

Mei, C.C., (1969), *Nonuniform Diffusion of Suspended Sediment*, Journal of the Hydraulics Division, Proc. A.S.C.E, Vol.95, No. HY1, 1969, pp 581-584

Muir Wood, A.M. and Fleming, C.A. (1981), *Coastal Hydraulics*, Macmillian Press Ltd, London.

Nicholson J., (1983), *Three-dimensional models of particluate and cohesive suspended sediment transport*, Ph.D. Thesis at the University of Manchester.

Nielsen, P., (1986), *Suspended Sediment Concentrations under Waves*, Coastal Engineering, Vol.10., (1986), pp 23-31

O'Connor, B.A. (1971), *Mathematical model of sediment distribution*, Proc. 14th IAHR Conf., Paris, September 1971, 4, D23, 195-202

O'Connor, B.A. and Nicholson J., (1988), *A Three-dimensional Model of Suspended Particulate Sediment Transport*, Coastal Engineering, Vol. 12, pp 157-174

O'Connor, B.A. and Duckett, F. J. L., (1989), *Bed Friction in Tidal Flows*, Advances in Water Modelling and Measurement, M.H. Palmer (ed.), BHRA, Cranfield

O'Connor, B.A., (1992), *Prediction of Seabed Sand Waves*, Computer Modelling of Seas and Coastal Regions (ed. P.W. Partridge), Int. Conf. On Computer Modelling of Seas and Coastal Regions and Boundary Elements and Fluid Dynamics, Southampton, U.K, Computational Mechanics Pubs., Southampton

O'Connor, B.A. and Nicholson J., (1997), *Tidal Sediment Transport*, Proceedings of International Conference on Computer Modelling of Seas and Coastal Regions, COASTAL, (1997), p 367-379

O'Connor, B.A., (1999), *Personal communication*

O'Connor, B.A., Pan, S., Li, M. and Nicholson J., (2001), *Quantification of Sediment Entrainment Processes in the Coastal Zone*, COSMOD Project, Departmental Report, University of Liverpool, Department of Civil Engineering, Report No. CE/05/01, July (2001)

Oliver, D.R., (1961), *The Sedimentation Suspension of Closely-Sized Spherical Particles*. Chem. Eng. Science, Vol. 15, p230-242

Richardson, Y.F. and Zaki, W.N., (1954), *Sedimentation and Fluidisation, Part 1*, Trans. Inst. Chem. Eng., Vol. 32, p35-53

Ranga Raju, K.G. and Soni, J.P., (1976), *Geometry of Ripples and Dunes in Alluvial Channels*, Journal of Hydraulic Research, Vol. 14, No. 3, The Netherlands

Simons, D.B. and Richardson, E.V., (1961), *Forms of Bed Roughness in Alluvial Channels*, Journal of Hydraulics Division, A.S.C.E., Vol. 87, HY3, p 87-105

Singamsetti, S.R., (1966), *Diffusion of Sediment in a Submerged Jet*, Journal of the Hydraulics Division, A.S.C.E, Vol.92, No.Hy2, Proc. Paper4726, March, pp153-168

Smith, G.D., (1998), *Numerical Solution of Partial Differential Equations*, Third Edition, Clarendon Press, Oxford

Smith, J.D. and McLean, S.R., (1977), *Spatially Averaged Flow over a Wavy Surface*, Journal of Geophysical Research, Vol. 82, No. 12, pp 1735-1746

Soulsby, R.L., (1994), *Manual of Marine Sands*, Report SR 351, October 1994, HR Wallingford.

Sternberg, R.W., Kranck, K, Cacchione, D.A. and Drake, D.E., (1988), *Suspended Sediment Transport under Estuarine Tidal Channel Conditions*, Sedimentary Geology, 57, pp 257-272

Stone, H.L. and Brian, P.L.T., (1963), *Numerical Solution of Convective Transport Problems*, Journal Am. Inst. Chem. Engrs., Vol. 9, No. 5, 1963.

Terwindt, J.H.J., (1970), *Sand Waves in the Southern Bight of the North Sea*, Marine Geology, 10, p 51-67

Tsubaki, T. and Shinohara, K., (1954), *On the Characteristics of Sand Waves Formed upon the Beds of Open Channels and Rivers*, Reports of Research Institute for Applied Mechanics, Vol. VII, No. 25, 1959

Van Rijn, L.C., (1982), *Equivalent Roughness of Alluvial Bed*, Journal of the Hydraulic Division, A.S.C.E., Vol, 108, No. HY10

Van Rijn, L.C., (1984), *Sediment Transport, Part II: Suspended Load Transport*, Journal of Hydraulic Engineering, A.S.C.E, Vol. 110, No. 11.

Van Rijn, L. C., (1993), *Principles of Sediment Transport in Rivers, Estuaries and Coastal Seas*, Aqua Publications, Amsterdam.

Velikanov, M.A., (1955), *Dynamics of Alluvial Streams, Vol. II (Sediment and Bed Flow)*, State Publishing House for Theor. and Techn. Literature, Moscow, 1955

Velikanov, M.A., (1958), *Alluvial Process (Fundamental Principles)*, State Publishing House for Physical and Mathematical Literature, Moscow, 1958

Verboom, G.K., (1975), *The advection-dispersion equation for an an-isotropic medium solved by fractional-step method*, Proc. Int. Conf. On Math. Models for Environmental Problems, Southampton, U.K. (ed. Breddia, C.A.)

White, W., Paris, E. and Bettess, R., (1979), *A New General Method for Predicting the Frictional Characteristics of Alluvial Streams*, H.R.S. Wallingford, Report No. IT 187, England

Wilson, K.C., (1988), *Frictional Behaviour of Sheet Flow*, Progress Report 67, p 11-12

Wilson, K.C., (1989), *Friction of Wave-Induced Sheet Flow*, Coastal Engineering, 12

Winterwerp, J.C., De Groot, M.B., Mastbergen, D.R. and Verwoert, H., (1990), *Hyper-concentrated Sand-water Mixture Flows over Flat Bed*, Journal of Hydraulic Engineering, A.S.C.E., Vol. 116, No.1

Winyu, R. and Shibayama, T., (1994), *Suspended Sediment Concentration Profiles under Non-breaking and Breaking Waves*, Coastal Engineering, Vol. 3, pp 2813-2827

Yalin, M.S., (1977), *Mechanics of Sediments Transport*, Pergamon Press

Yalin, M.S., (1985), *On the Determination of Ripple Geometry*, Journal of Hydraulic Engineering, Vol. 3, No. 8.

Yotsukura, N. and Fiering, M.B., (1964), *Numerical Solution to a Dispersion Equation*, Proc. ASCE, Vol. 90, No. HY5, 1964.

Appendix A

Structure of Computer Models

A.1 Introduction

The diagrams shown in this Appendix are designed to help clarify the models described in the thesis. The models concerned are:-

1. The conventional 2DV model as described in chapter 6.
2. The new Corrector method as described in chapter 5.
3. The new parameterised Corrector method as described in chapter 8.

All models are coded using FORTRAN 90 and are run on the UNIX system provided by the University of Liverpool.

A.2 Conventional 2DV Model

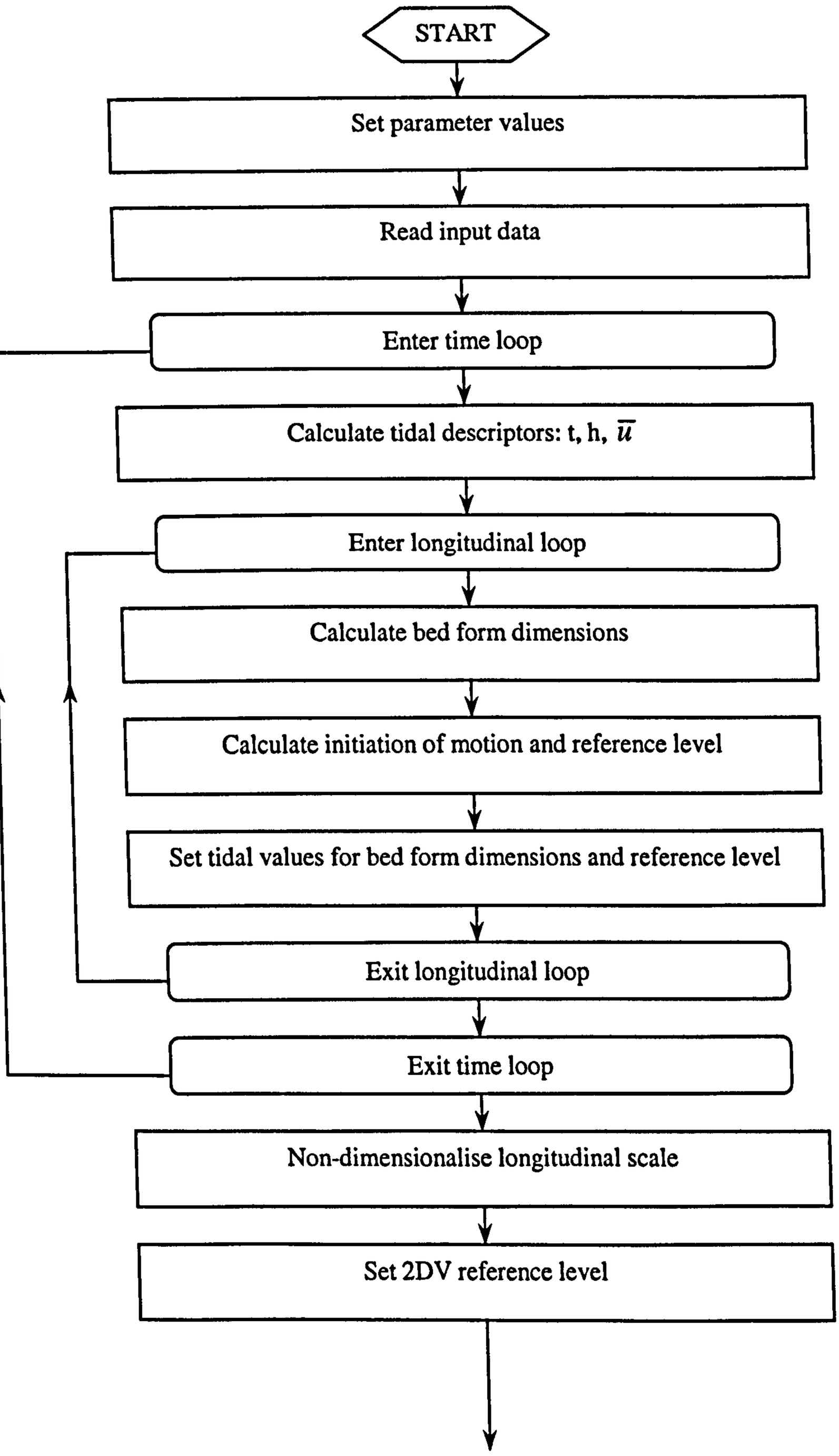

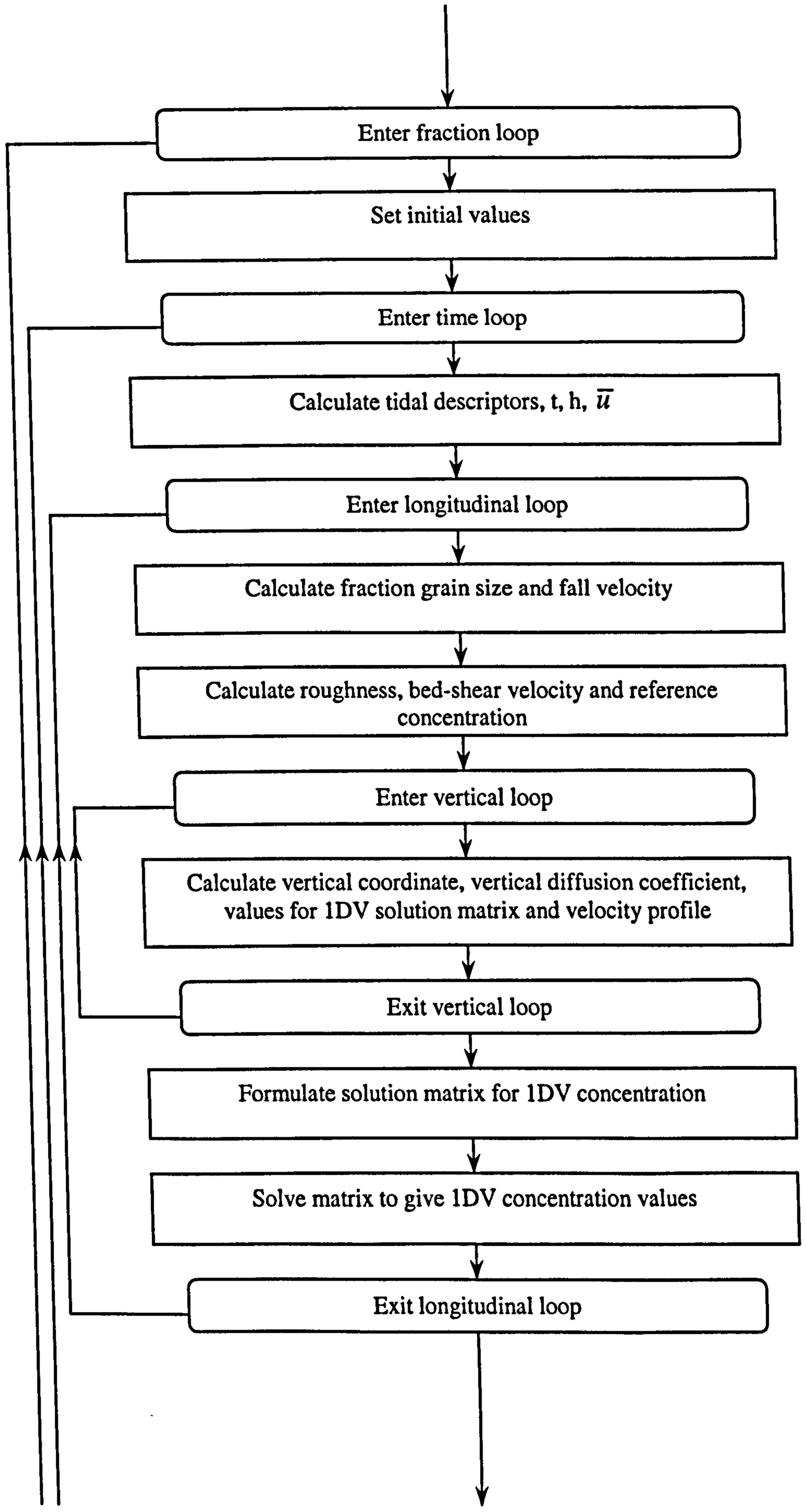
Enter fraction loop
Set initial values
Enter time loop
Calculate tidal descriptors, t, h, $\bar{u}$
Enter longitudinal loop
Calculate fraction grain size and fall velocity
Calculate roughness, bed-shear velocity and reference concentration
Enter vertical loop
Calculate vertical coordinate, vertical diffusion coefficient, values for 1DV solution matrix and velocity profile
Exit vertical loop
Formulate solution matrix for 1DV concentration
Solve matrix to give 1DV concentration values
Exit longitudinal loop

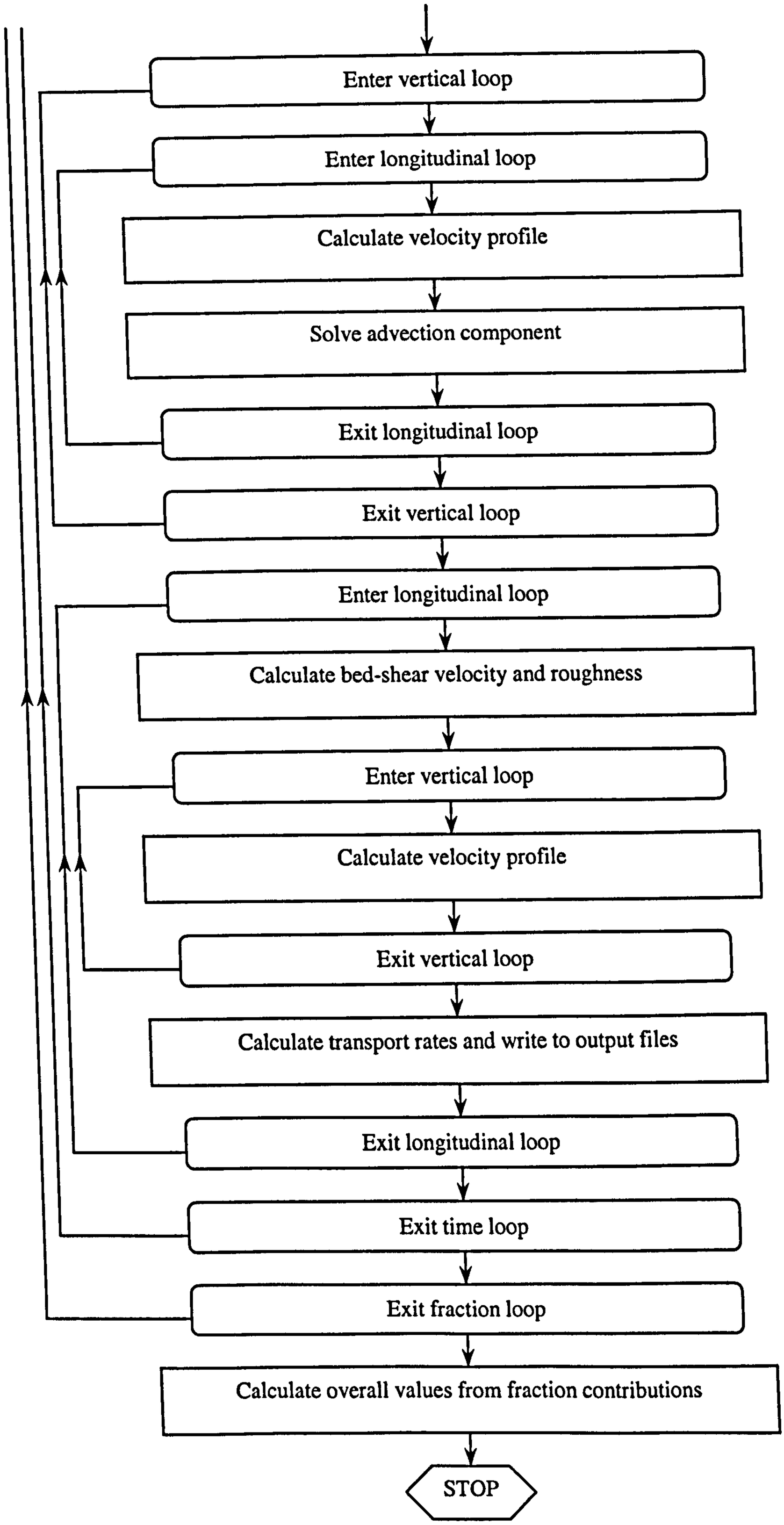
Enter vertical loop
Enter longitudinal loop
Calculate velocity profile
Solve advection component
Exit longitudinal loop
Exit vertical loop
Enter longitudinal loop
Calculate bed-shear velocity and roughness
Enter vertical loop
Calculate velocity profile
Exit vertical loop
Calculate transport rates and write to output files
Exit longitudinal loop
Exit time loop
Exit fraction loop
Calculate overall values from fraction contributions
STOP

A.3 New Corrector Method

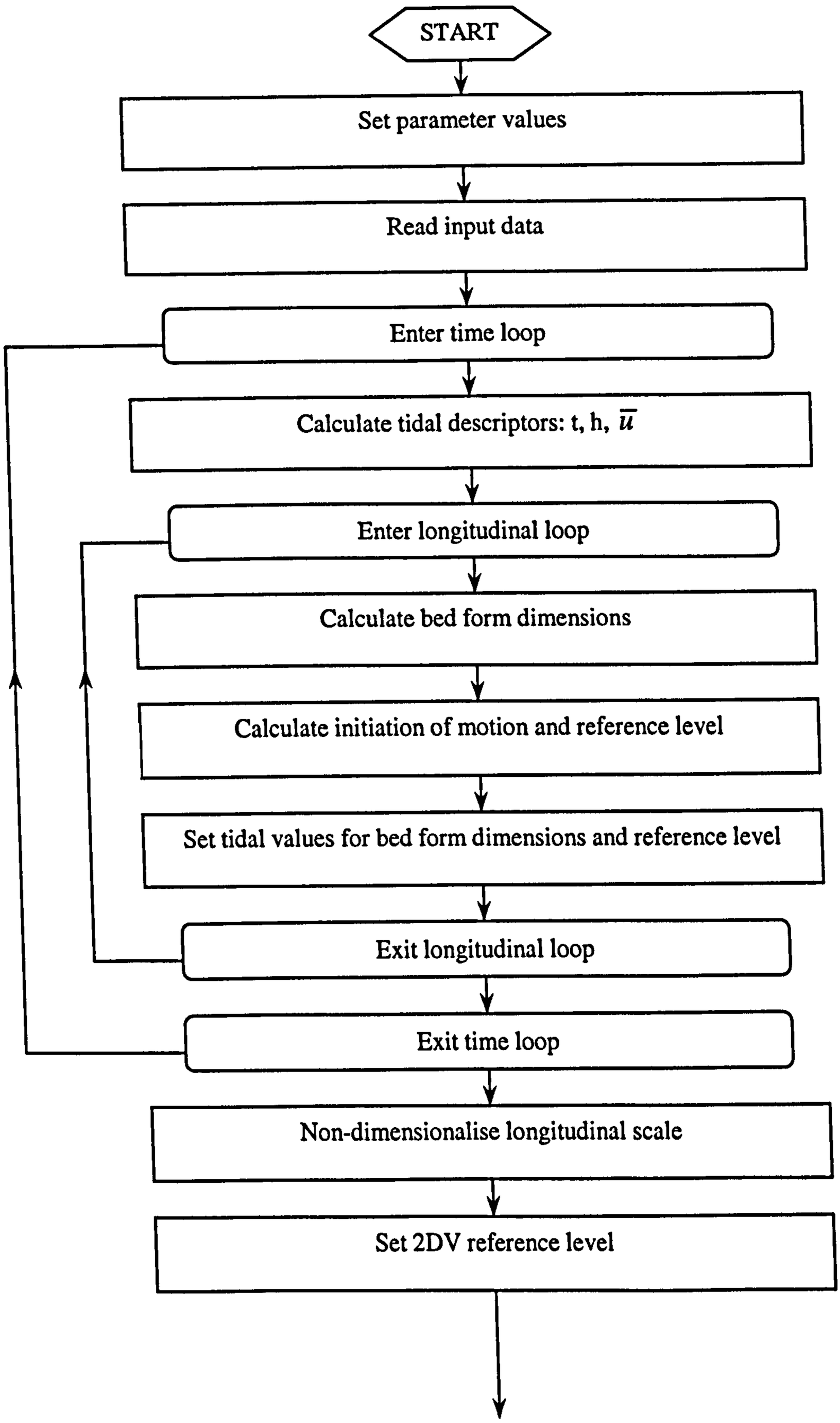

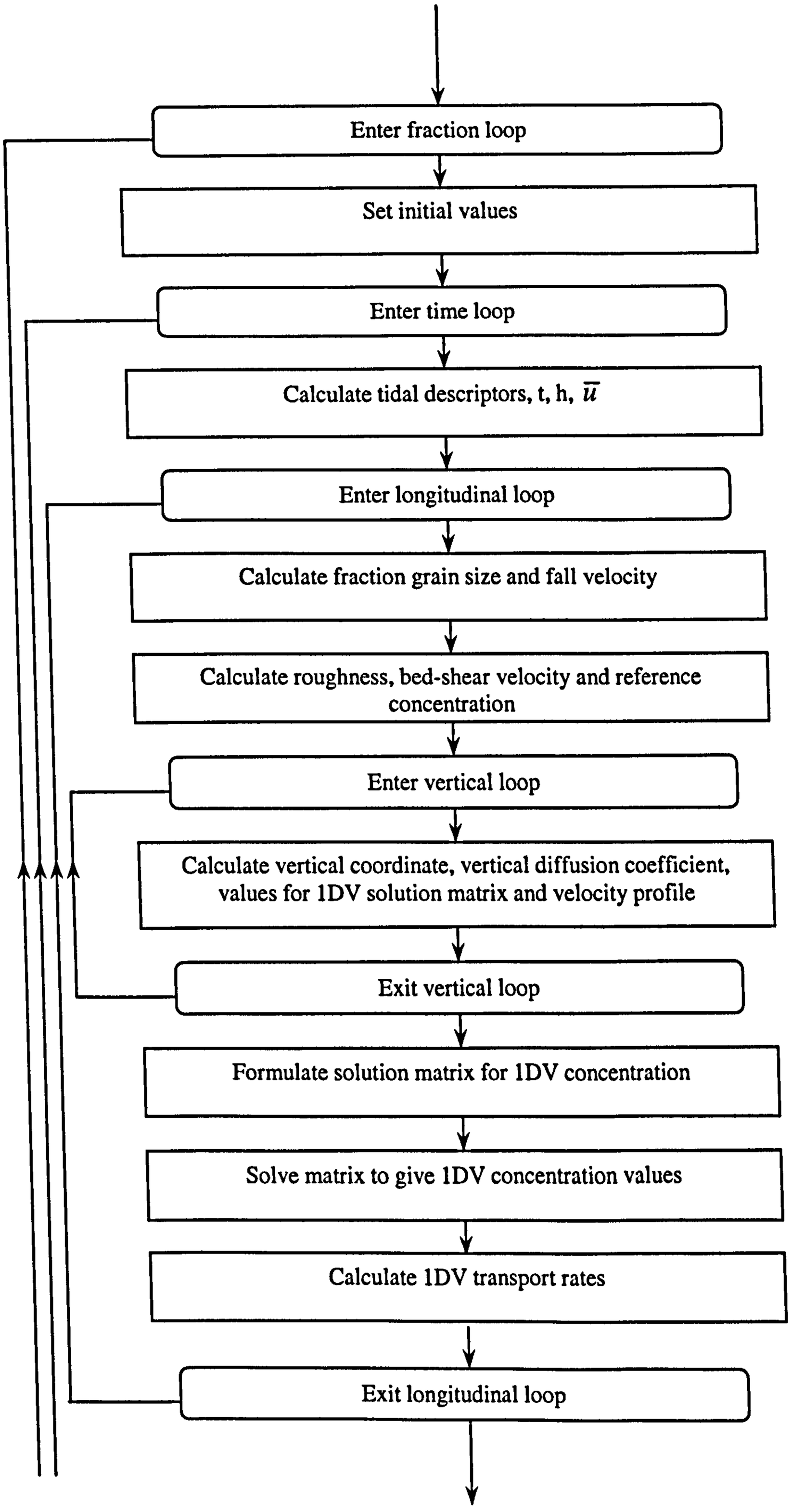
Enter fraction loop
Set initial values
Enter time loop
Calculate tidal descriptors, t, h, $\overline{u}$
Enter longitudinal loop
Calculate fraction grain size and fall velocity
Calculate roughness, bed-shear velocity and reference concentration
Enter vertical loop
Calculate vertical coordinate, vertical diffusion coefficient, values for 1DV solution matrix and velocity profile
Exit vertical loop
Formulate solution matrix for 1DV concentration
Solve matrix to give 1DV concentration values
Calculate 1DV transport rates
Exit longitudinal loop

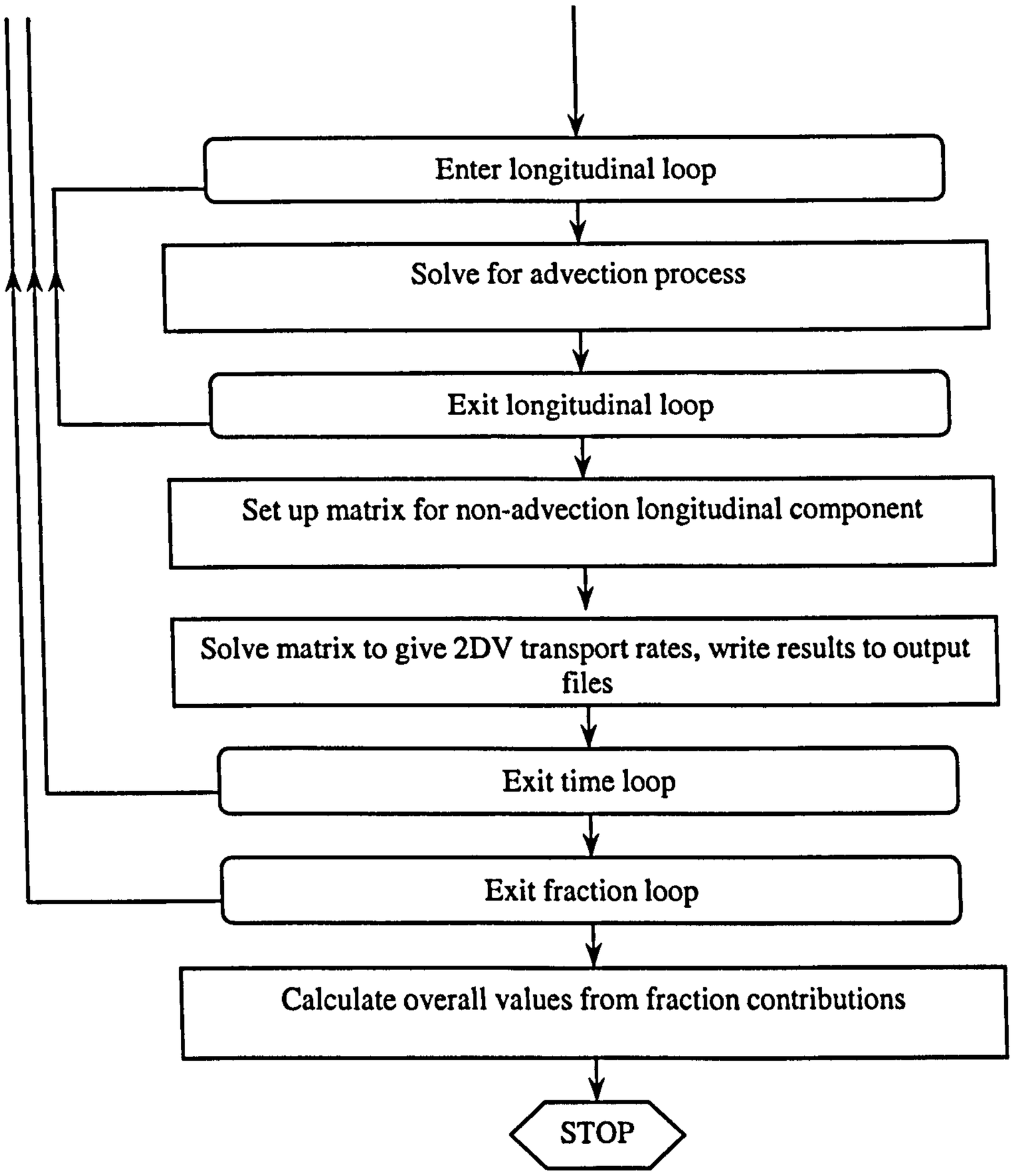
Enter longitudinal loop
Solve for advection process
Exit longitudinal loop
Set up matrix for non-advection longitudinal component
Solve matrix to give 2DV transport rates, write results to output files
Exit time loop
Exit fraction loop
Calculate overall values from fraction contributions
STOP

A.4 New Parameterised Corrector Method

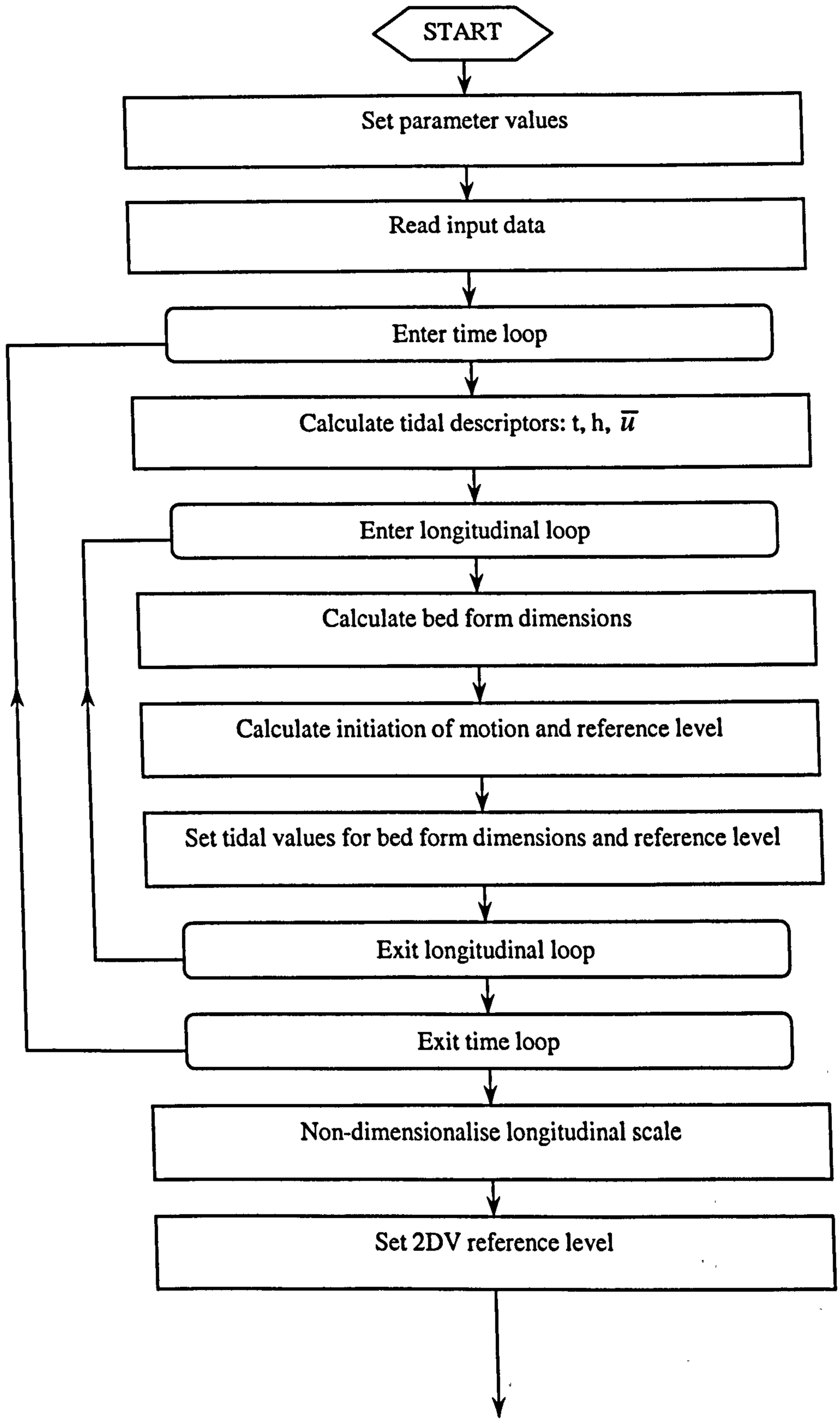

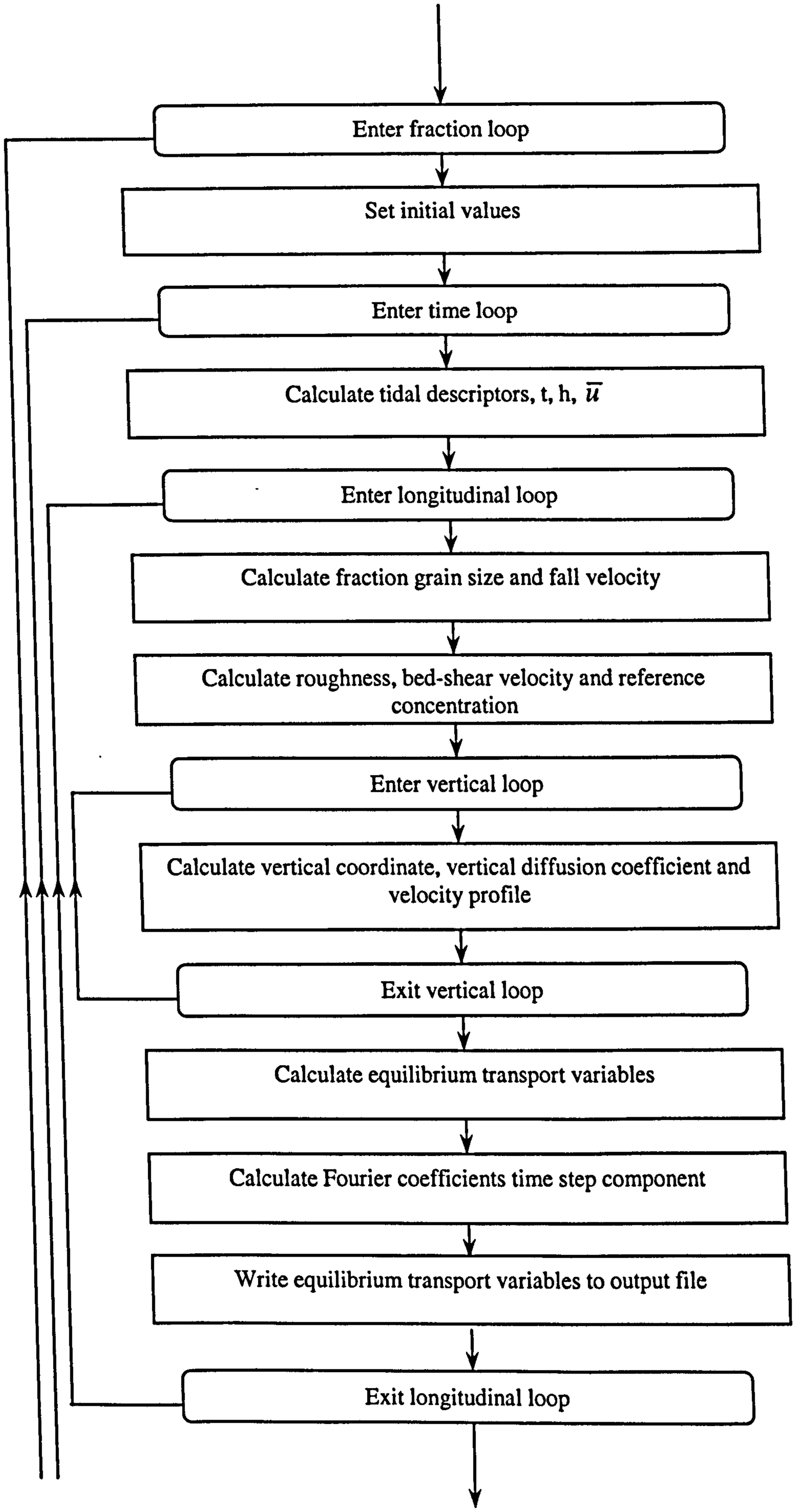
Enter fraction loop
Set initial values
Enter time loop
Calculate tidal descriptors, t, h, $\overline{u}$
Enter longitudinal loop
Calculate fraction grain size and fall velocity
Calculate roughness, bed-shear velocity and reference concentration
Enter vertical loop
Calculate vertical coordinate, vertical diffusion coefficient and velocity profile
Exit vertical loop
Calculate equilibrium transport variables
Calculate Fourier coefficients time step component
Write equilibrium transport variables to output file
Exit longitudinal loop

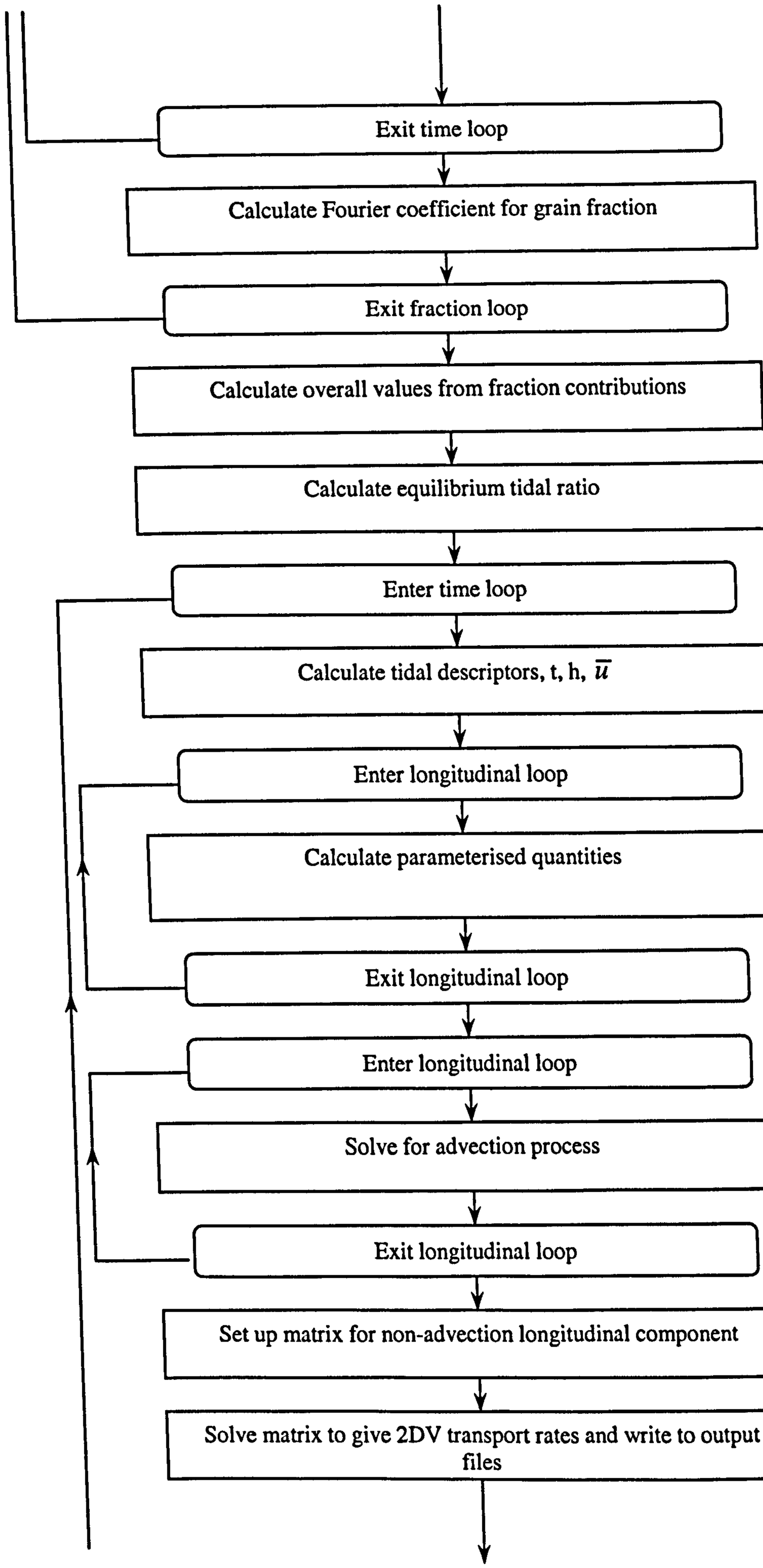
Exit time loop
Calculate Fourier coefficient for grain fraction
Exit fraction loop
Calculate overall values from fraction contributions
Calculate equilibrium tidal ratio
Enter time loop
Calculate tidal descriptors, t, h, $\bar{u}$
Enter longitudinal loop
Calculate parameterised quantities
Exit longitudinal loop
Enter longitudinal loop
Solve for advection process
Exit longitudinal loop
Set up matrix for non-advection longitudinal component
Solve matrix to give 2DV transport rates and write to output files

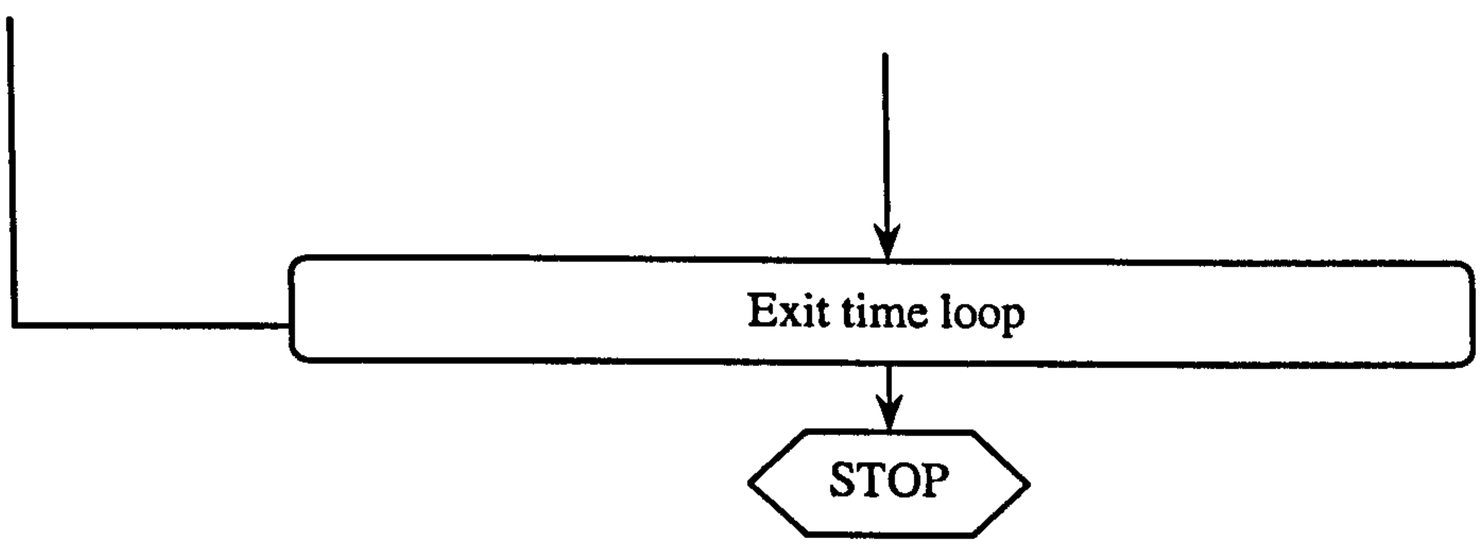
Exit time loop
STOP

Appendix B

Numerical Solution of the 1DV Concentration Model

B.1 Introduction

Chapter 4 described how the three-dimensional advection-diffusion model for the sediment concentration profile was derived from the principle of continuity. By considering only the vertical dimension and simplifying, the following equation was determined for the 1DV concentration:-

$$\frac{\partial c}{\partial t} = \varepsilon_{s,z}\frac{\partial^2 c}{\partial z^2} + \left(\frac{\partial \varepsilon_{s,z}}{\partial z} - \mathrm{w} + w_f\right)\frac{\partial c}{\partial z} \qquad (4.2.1)$$

The corresponding boundary conditions are given by:-

$c = 0$ at $z = h$

$c = c_a$ at $z = a$

After applying the coordinate transform described in section 4.9, equation (4.2.1) becomes:-

$$\frac{\partial c}{\partial t} = A\frac{\partial^2 c}{\partial z_*^2} + B\frac{\partial c}{\partial z_*} \qquad (4.9.2)$$

where,

$$A = \frac{\varepsilon_{s,z}}{\xi_a^2 \eta^2 h^2}$$

$$B = \frac{\varepsilon_{s,z}}{\xi_a h^2 \eta^2} - \left(\frac{\dfrac{\partial \varepsilon_{s,z}}{\partial z} - \mathrm{w} + w_f + \eta z_* \dfrac{\partial h}{\partial t}}{\xi_a \eta h} \right)$$

The corresponding boundary conditions are now:-

Surface: $c = 0$ at $z_* = 1$ (4.9.3)

Bed: $c = c_a$ at $z_* = 0$ (4.9.4)

The concentration profile is found by first discretising equation (4.9.2), then using finite difference techniques to approximate the derivatives. An implicit Crank-Nicholson scheme based on central differences is used to approximate both the first and second order spatial derivatives whilst the weighted-average approach of Stone and Brian (1963) is used to approximate the temporal derivative.

The resulting tri-diagonal solution matrix is solved using Gaussian Elimination, as described by Smith (1998).

The discretisation of the solution domain consists of dividing the transformed vertical dimension into equal sized computation grids, $i = 1 \cdots ii$. The bed boundary is denoted by $i = 1$ whilst the surface boundary is denoted by $i = ii$.

B.2 Spatial Derivatives

Both first and second order spatial derivatives are approximated using an implicit Crank-Nicholson scheme, therefore the stability of the scheme is assumed to be satisfactory. The implicit scheme uses values from both present and previous time steps, equally weighted, to approximate the concentration gradients. The approximations for the spatial derivatives are therefore given by:-

$$\frac{\partial c}{\partial z_*} \approx \frac{1}{2}\left(\frac{c_{i+1}^{n} - c_{i-1}^{n}}{2\Delta z_*} + \frac{c_{i+1}^{n-1} - c_{i+1}^{n-1}}{2\Delta z_*} \right) \qquad \text{(B.2.1)}$$

$$\frac{\partial^2 c}{\partial z_*^2} \approx \frac{1}{2}\left(\frac{c_{i+1}^n - 2c_i^n + c_{i-1}^n}{\Delta z_*^2} + \frac{c_{i+1}^{n-1} - 2c_i^{n-1} + c_{i-1}^{n-1}}{\Delta z_*^2}\right) \qquad \text{(B.2.2)}$$

B.3 Temporal Derivative

The temporal derivative is approximated using the finite difference scheme proposed by Stone and Brian (1963). The scheme uses values for both the present and previous time steps and then applies spatial weighting. The temporal derivative is therefore approximated by the following scheme:-

$$\frac{\partial c}{\partial t} \approx \frac{1}{6}\left(\frac{c_{i+1}^n - c_{i+1}^{n-1}}{\Delta t}\right) + \frac{2}{3}\left(\frac{c_i^n - c_i^{n-1}}{\Delta t}\right) + \frac{1}{6}\left(\frac{c_{i-1}^n - c_{i-1}^{n-1}}{\Delta t}\right) \qquad \text{(B.3.1)}$$

B.4 Numerical Scheme

Substituting the finite difference approximations for the derivative terms and discretising the coefficients, equation (4.9.2) becomes:-

$$\frac{1}{6\Delta t}\left(c_{i+1}^n - c_{i+1}^{n-1} + 4c_i^n - 4c_i^{n-1} + c_{i-1}^n - c_{i-1}^{n-1}\right)$$

$$= \frac{A_i}{2\Delta z_*^2}\left(c_{i+1}^n - 2c_i^n + c_{i-1}^n + c_{i+1}^{n-1} - 2c_i^{n-1} + c_{i-1}^{n-1}\right) + \frac{B_i}{4\Delta z_*}\left(c_{i+1}^n - c_{i-1}^n + c_{i+1}^{n-1} - c_{i-1}^{n-1}\right)$$

(B.4.1)

If $r = \frac{\Delta t}{\Delta z_*^2}$, then:-

$$c_{i+1}^n\left(1 - 3rA_i - \frac{3}{2}r\Delta z_* B_i\right) + c_i^n\left(4 + 6rA_i\right) + c_{i-1}^n\left(1 - 3rA_i + \frac{3}{2}r\Delta z_* B_i\right)$$

$$=$$

$$c_{i+1}^{n-1}\left(1 + 3rA_i + \frac{3}{2}r\Delta z_* B_i\right) + c_i^{n-1}\left(4 - 6rA_i\right) + c_{i-1}^{n-1}\left(1 + 3rA_i - \frac{3}{2}r\Delta z_* B_i\right)$$

(B.4.2)

Let:-

$$\alpha_i = 1 - 3rA_i - 1.5r\Delta z_* B_i \quad ; \quad \alpha 2_i = 1 + 3rA_i + 1.5r\Delta z_* B_i$$

$$\beta_i = 1 - 3rA_i + 1.5r\Delta z_* B_i \quad ; \quad \beta 2_i = 1 + 3rA_i - 1.5r\Delta z_* B_i$$

$$\gamma_i = 4 + 6rA_i \quad ; \quad \gamma 2_i = 4 - 6rA_i$$

Then equation (B.4.2) reduces to:-

$$\alpha_i c_{i+1}^n + \gamma_i c_i^n + \beta_i c_{i-1}^n = \alpha 2_i c_{i+1}^{n-1} + \gamma 2_i c_i^{n-1} + \beta 2_i c_{i-1}^{n-1} \qquad \text{(B.4.3)}$$

for $i = 1 \ldots ii$.

B.5 Boundary Conditions

B.5.1 Surface Boundary

Since a zero concentration is applied at the water surface, the calculation at $i = ii$ is not required. This also simplifies the scheme for the calculation at $i = ii - 1$, i.e.:-

$$\alpha_{ii-1} c_{ii}^n + \gamma_{ii-1} c_{ii-1}^n + \beta_{ii-1} c_{ii-2}^n = \alpha 2_{ii-1} c_{ii}^{n-1} + \gamma 2_{ii-1} c_{ii-1}^{n-1} + \beta 2_{ii-1} c_{ii-2}^{n-1} \quad \text{(B.5.1)}$$

But $c_{ii}^n = c_{ii}^{n-1} = 0$, therefore equation (B.7) reduces to:-

$$\gamma_{ii-1} c_{ii-1}^n + \beta_{ii-1} c_{ii-2}^n = \gamma 2_{ii-1} c_{ii-1}^{n-1} + \beta 2_{ii-1} c_{ii-2}^{n-1} \qquad \text{(B.5.2)}$$

B.5.2 Bed Boundary

Applying condition (4.9.4) to equation (B.4.3) dispenses with the need for the calculation at $i = 1$; it also simplifies the calculation for $i = 2$, i.e.:-

$$\alpha_2 c_3^n + \gamma_2 c_2^n + \beta_2 c_1^n = \alpha 2_2 c_3^{n-1} + \gamma 2_2 c_2^{n-1} + \beta 2_2 c_1^{n-1} \qquad \text{(B.5.3)}$$

Since $c_1^n = c_a^n$ and similarly $c_1^{n-1} = c_a^{n-1}$, equation (B.5.3) reduces to:-

$$\alpha_2 c_3^n + \gamma_2 c_2^n + \beta_2 c_a^n = \alpha 2_2 c_3^{n-1} + \gamma 2_2 c_2^{n-1} + \beta 2_2 c_a^{n-1}$$

Thus, since the reference concentration for each time step is known, the numerical scheme for the calculation at $i = 2$ is given by:-

$$\alpha_2 c_3^n + \gamma_2 c_2^n = \alpha 2_2 c_3^{n-1} + \gamma 2_2 c_2^{n-1} + \beta 2_2 c_a^{n-1} - \beta_2 c_a^n \qquad \text{(B.5.4)}$$

where the terms on the right hand side are all known.

B.6 Solution Matrix

Combining equations (B.4.3), (B.5.2) and (B.5.4) gives the following solution matrix:-

$$\begin{bmatrix} \gamma_2 & \alpha_2 & & & & & & \\ \beta_3 & \gamma_3 & \alpha_3 & & & & & \\ & \ddots & \ddots & \ddots & & & & \\ & & \beta_i & \gamma_i & \alpha_i & & & \\ & & & \ddots & \ddots & \ddots & & \\ & & & & \beta_{ii-2} & \gamma_{ii-2} & \alpha_{ii-2} & \\ & & & & & \beta_{ii-1} & \gamma_{ii-1} \end{bmatrix} \begin{bmatrix} c_2^n \\ c_3^n \\ \vdots \\ c_i^n \\ \vdots \\ c_{ii-2}^n \\ c_{ii-1}^n \end{bmatrix} = \begin{bmatrix} rhs_2 \\ rhs_3 \\ \vdots \\ rhs_i \\ \vdots \\ rhs_{ii-2} \\ rhs_{ii-1} \end{bmatrix} \qquad \text{(B.6.1)}$$

where,

$$rhs_2 = \alpha 2_2 c_3^{n-1} + \gamma 2_2 c_2^{n-1} + \beta 2_2 c_a^{n-1} - \beta_2 c_a^n$$

$$rhs_{i=3..ii-2} = \alpha 2_i c_{i+1}^{n-1} + \gamma 2_i c_i^{n-1} + \beta 2_i c_{i-1}^{n-1}$$

$$rhs_{ii-1} = \gamma 2_{ii-1} c_{ii-1}^{n-1} + \beta 2_{ii-1} c_{ii-2}^{n-1}$$

B.7 Gaussian Elimination

Since the solution matrix (B.6.1) is tri-diagonal, it is possible to use a simple iterative process to solve for the concentration values. The method of Gaussian Elimination, described by Smith (1998), is shown below.

Step1

$$\eta_1 = \gamma_1$$

$$\eta_{i=2..ii-1} = \gamma_i - \frac{\alpha_{i-1}\beta_i}{\eta_{i-1}}$$

Step 2

$$s_2 = rhs_2$$

$$s_{i=2..ii-1} = rhs_i - \frac{\beta_i s_{i-1}}{\eta_{i-1}}$$

Step 3

$$c_{ii-1} = \frac{s_{ii-1}}{\eta_{ii-1}}$$

$$c_{i=ii-2..2} = \frac{s_i - \alpha_i c_{i+1}}{\eta_i}$$

It should also be noted that the Gaussian elimination technique must satisfy the following stability criteria:-

(i) $\alpha_i > 0$, $\beta_i > 0$ and $\gamma_i > 0$

(ii) $\gamma_i > \alpha_{i-1} + \beta_{i+1}$

(iii) $\gamma_i > \alpha_i + \beta_i$

Appendix C

Numerical Solution of the Corrector Method

C.1 Introduction

This appendix contains details of the numerical techniques used to solve the new Corrector method proposed by O'Connor (1999). The solution builds upon the 1DV sediment transport rates, which are solved by techniques described in appendix B.

It must be noted that the diffusive transport is neglected so that the new Corrector method is given by the equation described below.

$$\frac{\partial T_{s,x}}{\partial t}+\bar{u}\frac{\partial T_{s,x}}{\partial x}=\bar{c}(h-a)\frac{\partial \bar{u}}{\partial t}+\frac{\partial T_{disp,x}}{\partial t} \qquad (5.4.1)$$

First, the operator splitting technique is applied to equation (5.4.1) to give:-

$$\frac{\partial T_{s,x}}{\partial t}+\bar{u}\frac{\partial T_{s,x}}{\partial x}=0 \qquad (5.6.1)$$

$$\frac{\partial T_{s,x}}{\partial t}=\bar{c}(h-a)\frac{\partial \bar{u}}{\partial t}+\frac{\partial T_{disp,x}}{\partial t} \qquad (5.6.2)$$

The method of characteristic projection is used to solve the advection component, equation (5.6.1), whilst a Stone and Brian (1963) finite difference scheme is used to solve equation (5.6.2).

The tri-diagonal matrix obtained by the finite difference approximation to equation (5.6.2) is solved by the method of Gaussian Elimination described in appendix B.

The discretisation of the solution domain consists of dividing the longitudinal direction into equal sized computation grids, $k = 1 \cdots kk$. The inflow boundary is denoted by $k = 1$ whilst the outflow boundary is denoted by $k = kk$.

C.2 Method of Characteristic Projection

C.2.1 Characteristic Solution

Equation (5.6.1) can be solved by first determining its characteristics. By following the method described by Smith (1998), the following equation is obtained for the characteristic solution of equation (5.6.1):-

$$x = \bar{u}t \qquad \text{(C.2.1)}$$

C.2.2 Projection

Since equation (5.6.1) is purely advection, the solution can be found by simply reversing the advection process. The transport value for the present time level at grid point k, $T^n_{s,k}$, is projected backwards along the characteristic solution to the previous time level, denoted by the superscript $n-1$, see figure C.1. It should be noted that the previous time level refers to the previous split, i.e. the 1DV transport values.

The new transport rate is then calculated by considering the point at which the characteristic intercepts the previous time line. This value is simply the 1DV transport that is then advected to the grid point k by equation (5.6.1).

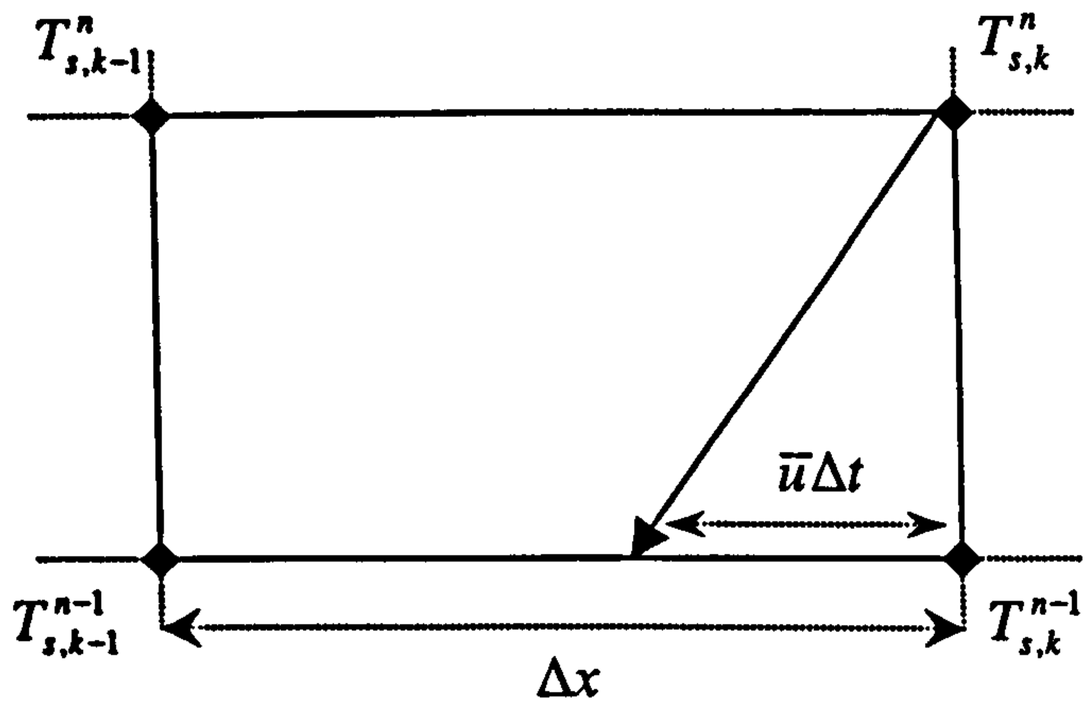

Figure C.1: Projection method used in the solution of the Corrector method

If the distance of the intercept from the point $T^{n-1}_{s,k-1}$ is given by:-

$$\Delta x - \overline{u}\Delta t$$

Then the percentage of the whole distance between $T^{n-1}_{s,k-1}$ and $T^{n-1}_{s,k}$ where the intercept occurs, is given by:-

$$r_x = \frac{\Delta x - \overline{u}\Delta t}{\Delta x} \qquad \text{(C.2.2)}$$

The new value of transport can now be given by considering the percentage difference between the actual values of $T^{n-1}_{s,k-1}$ and $T^{n-1}_{s,k}$, i.e.:-

$$T^{n}_{s,k} = T^{n-1}_{s,k-1} + r_x\left(T^{n-1}_{s,k} - T^{n-1}_{s,k-1}\right) \qquad \text{(C.2.3)}$$

The projection method can be seen to calculate the new transport rate by using a weighted-average approach.

C.2.3 Boundary Conditions

Inflow Boundary

When $k=1$, the transport rate is given by:-

$$T_{s,1}^{n} = T_{s,0}^{n-1} + r_x\left(T_{s,1}^{n-1} - T_{s,0}^{n-1}\right)$$

But the inflow boundary has been chosen such that the 1DV transport rates at the inflow boundary, $k=1$, are the same as those in the upstream grid, i.e. $k=0$. Therefore, the transport rate at the inflow boundary is simply:-

$$T_{s,1}^{n} = T_{s,0}^{n-1} = T_{s,1}^{n-1} \qquad \text{(C.2.4)}$$

Outflow Boundary

Since flow reversal is not considered in the Corrector method, the flow is always in the same direction. The outflow boundary therefore, does not pose a problem, i.e.:-

$$T_{s,kk}^{n} = T_{s,kk-1}^{n-1} + r_x\left(T_{s,kk}^{n-1} - T_{s,kk-1}^{n-1}\right) \qquad \text{(C.2.5)}$$

It must be noted however that these equations only hold if the advection does not continue for more than one grid size. Therefore, the following condition is applied:-

$$\Delta x - \bar{u}\Delta t > 0 \qquad \text{(C.2.6)}$$

Since the spatial step, Δx, and the time step, Δt, have already been set, then this places a restriction on the depth-mean velocity, i.e.:-

$$\bar{u} < \frac{\Delta x}{\Delta t} \qquad \text{(C.2.7)}$$

C.3 Finite Difference Scheme

As stated earlier, a Stone and Brian (1963) finite difference scheme is used to approximate the time derivatives in equation (5.6.2). The discretisation of the time derivatives gives the following approximations:-

$$\frac{\partial T_{s,x}}{\partial t} \approx \frac{1}{6}\left(\frac{T^{n}_{s,k+1} - T^{n-1}_{s,k+1}}{\Delta t}\right) + \frac{2}{3}\left(\frac{T^{n}_{s,k} - T^{n-1}_{s,k}}{\Delta t}\right) + \frac{1}{6}\left(\frac{T^{n}_{s,k-1} - T^{n-1}_{s,k-1}}{\Delta t}\right) \quad \text{(C.3.1)}$$

$$\frac{\partial T_{disp,x}}{\partial t} \approx \frac{1}{6}\left(\frac{T^{n}_{disp,k+1} - T^{n-1}_{disp,k+1}}{\Delta t}\right) + \frac{2}{3}\left(\frac{T^{n}_{disp,k} - T^{n-1}_{disp,k}}{\Delta t}\right) + \frac{1}{6}\left(\frac{T^{n}_{disp,k-1} - T^{n-1}_{disp,k-1}}{\Delta t}\right) \text{(C.3.2)}$$

It should be noted that the derivative of the depth-mean longitudinal flow with respect to time does not require a finite difference approximation since it can be solved analytically, as given below.

$$\frac{\partial \bar{u}}{\partial t} = \frac{2\bar{u}_m \pi}{up}\cos\left(\frac{2\pi}{up}t\right) \quad \text{(C.3.3)}$$

The finite difference approximation to equation (5.6.2) is therefore given by:-

$$\frac{1}{6}\left(\frac{T^{n}_{s,k+1} - T^{n-1}_{s,k+1}}{\Delta t}\right) + \frac{2}{3}\left(\frac{T^{n}_{s,k} - T^{n-1}_{s,k}}{\Delta t}\right) + \frac{1}{6}\left(\frac{T^{n}_{s,k-1} - T^{n-1}_{s,k-1}}{\Delta t}\right)$$

$$\approx \bar{c}_k (h-a)\frac{2\bar{u}_m \pi}{up}\cos\left(\frac{2\pi}{up}t\right) +$$

$$+\frac{1}{6}\left(\frac{T^{n}_{disp,k+1} - T^{n-1}_{disp,k+1}}{\Delta t}\right) + \frac{2}{3}\left(\frac{T^{n}_{disp,k} - T^{n-1}_{disp,k}}{\Delta t}\right) + \frac{1}{6}\left(\frac{T^{n}_{disp,k-1} - T^{n-1}_{disp,k-1}}{\Delta t}\right) \text{(C.3.4)}$$

Rearranging terms gives:-

$$\left(T^{n}_{s,k+1} - T^{n-1}_{s,k+1} + 4T^{n}_{s,k} - 4T^{n-1}_{s,k} + T^{n}_{s,k-1} - T^{n-1}_{s,k-1}\right)$$

$$\approx 6\Delta t A_k + \left(T^{n}_{disp,k+1} - T^{n-1}_{disp,k+1} + 4T^{n}_{disp,k} - 4T^{n-1}_{disp,k} + T^{n}_{disp,k-1} - T^{n-1}_{disp,k-1}\right) \text{(C.3.5)}$$

where,

$$A_k = \bar{c}_k (h-a)\frac{2\bar{u}_m \pi}{up}\cos\left(\frac{2\pi}{up}t\right)$$

It must be noted that the terms $T_{s,k+1}^{n-1}$, $T_{s,k}^{n-1}$ and $T_{s,k-1}^{n-1}$ refer to values given in the previous split. These values are the transport values after applying equation (5.6.1) and hence, are known. Equation (C.3.5) can now be arranged so that all known values are given on the right hand side:-

$$T_{s,k+1}^{n} + 4T_{s,k}^{n} + T_{s,k-1}^{n} = r_k \qquad \text{(C.3.6)}$$

where,

$$r_k = T_{s,k+1}^{n-1} + 4T_{s,k}^{n-1} + T_{s,k-1}^{n-1} + 6\Delta t A_k + \left(T_{disp,k+1}^{n} - T_{disp,k+1}^{n-1} + 4T_{disp,k}^{n} - 4T_{disp,k}^{n-1} + T_{disp,k-1}^{n} - T_{disp,k-1}^{n-1}\right)$$

The terms involving T_{disp} are obtained from the 1DV stage of the model and so are also known.

C.3.1 Boundary Conditions

Inflow Boundary

The finite difference scheme at the inflow boundary is found by substituting $k = 1$ into equation (C.3.6).

$$T_{s,2}^{n} + 4T_{s,1}^{n} + T_{s,0}^{n} = r_1$$

where,

$$r_1 = T_{s,2}^{n-1} + 4T_{s,1}^{n-1} + T_{s,0}^{n-1} + 6\Delta t A_1 + \left(T_{disp,2}^{n} - T_{disp,2}^{n-1} + 4T_{disp,1}^{n} - 4T_{disp,1}^{n-1} + T_{disp,0}^{n} - T_{disp,0}^{n-1}\right)$$

Since the 1DV values are the same for $k = 1$ as $k = 0$ then r_1 simplifies to give:-

$$r_1 = T_{s,2}^{n-1} + 4T_{s,1}^{n-1} + T_{s,0}^{n-1} + 6\Delta t A_1 + \\ + \left(T_{disp,2}^{n} - T_{disp,2}^{n-1} + 5T_{disp,1}^{n} - 5T_{disp,1}^{n-1}\right)$$

There still remain terms on both sides of the equation which refer to the upstream grid, i.e. $k = 0$. It is therefore necessary to introduce the following conditions:-

(i) $$T_{s,1}^{n} = \theta T_{s,0}^{n} + (1-\theta) T_{s,2}^{n}$$

$$\rightarrow \quad T_{s,0}^{n} = \frac{1}{\theta} T_{s,1}^{n} - \frac{(1-\theta)}{\theta} T_{s,2}^{n}$$

(ii) $$T_{s,1}^{n-1} = \theta T_{s,0}^{n-1} + (1-\theta) T_{s,2}^{n-1}$$

$$\rightarrow \quad T_{s,0}^{n-1} = \frac{1}{\theta} T_{s,1}^{n-1} - \frac{(1-\theta)}{\theta} T_{s,2}^{n-1}$$

By applying (i) and (ii), the value at the inflow boundary is found by taking the weighted-average of the values to either side. If $\theta = 0.5$ then the value at the inflow boundary is simply the mean of the values at grid points $k = 0$ and $k = 2$. However, the boundary condition is such that the sediment and flow characteristics are the same for both $k = 0$ and $k = 1$; it would seem reasonable therefore to assume that the transport rate at $k = 1$ will be closer to that at $k = 0$ than the value at $k = 2$ since the 1DV effects are dominant. Hence, a value of $\theta = 0.7$ is used to produce the necessary bias.

The finite difference scheme at the inflow boundary is therefore given by:-

$$T_{s,2}^{n}\left(1 - \frac{1-\theta}{\theta}\right) + T_{s,1}^{n}\left(4 + \frac{1}{\theta}\right) = r_1 \qquad \text{(C.3.7)}$$

where,

$$r_1 = T_{s,2}^{n-1}\left(1 - \frac{1-\theta}{\theta}\right) + T_{s,1}^{n-1}\left(4 + \frac{1}{\theta}\right) + 6\Delta t A_1 +$$

$$+\left(T^{n}_{disp,2}-T^{n-1}_{disp,2}+5T^{n}_{disp,1}-5T^{n-1}_{disp,1}\right).$$

Outflow Boundary

The finite difference scheme at the outflow boundary is found by substituting $k=kk$ into equation (C.3.6).

$$T^{n}_{s,kk+1}+4T^{n}_{s,kk}+T^{n}_{s,kk-1}=r_{kk}$$

where,

$$r_{kk}=T^{n-1}_{s,kk+1}+4T^{n-1}_{s,kk}+T^{n-1}_{s,kk-1}+6\Delta tA_{kk}+$$
$$+\left(T^{n}_{disp,kk+1}-T^{n-1}_{disp,kk+1}+4T^{n}_{disp,kk}-4T^{n-1}_{disp,kk}+T^{n}_{disp,kk-1}-T^{n-1}_{disp,kk-1}\right)$$

Again, since the 1DV values are the same for $k=kk+1$ as $k=kk$ then r_{kk} simplifies to give:-

$$r_{kk}=T^{n-1}_{s,kk+1}+4T^{n-1}_{s,kk}+T^{n-1}_{s,kk-1}+6\Delta tA_{kk}+$$
$$+\left(5T^{n}_{disp,kk}-5T^{n-1}_{disp,kk}+T^{n}_{disp,kk-1}-T^{n-1}_{disp,kk-1}\right)$$

The following conditions, similar to those used for the inflow boundary, are now imposed on the outflow boundary.

(i) $$T^{n}_{s,kk}=\theta T^{n}_{s,kk+1}+(1-\theta)T^{n}_{s,kk-1}$$

$$\rightarrow \quad T^{n}_{s,kk+1}=\frac{1}{\theta}T^{n}_{s,kk}-\frac{(1-\theta)}{\theta}T^{n}_{s,kk-1}$$

(ii) $$T^{n-1}_{s,kk}=\theta T^{n-1}_{s,kk+1}+(1-\theta)T^{n-1}_{s,kk-1}$$

$$\rightarrow \quad T^{n-1}_{s,kk+1}=\frac{1}{\theta}T^{n-1}_{s,kk}-\frac{(1-\theta)}{\theta}T^{n-1}_{s,kk-1}$$

Applying conditions (i) and (ii) gives the following finite difference scheme at the outflow boundary:-

$$T^n_{s,kk}\left(4+\frac{1}{\theta}\right)+T^n_{s,kk-1}\left(1-\frac{1-\theta}{\theta}\right)+=r_{kk} \qquad \text{(C.3.8)}$$

where,

$$r_{kk}=T^{n-1}_{s,kk}\left(4+\frac{1}{\theta}\right)+T^{n-1}_{s,kk-1}\left(1-\frac{1-\theta}{\theta}\right)+6\Delta tA_{kk}+$$
$$+\left(5T^n_{disp,kk}-5T^{n-1}_{disp,kk}+T^n_{disp,kk-1}-T^{n-1}_{disp,kk-1}\right)$$

C.3.2 Solution Matrix

Combining equations (C.3.6), (C.3.7) and (C.3.8) gives the following matrix:-

$$\begin{bmatrix} \left(4+\frac{1}{\theta}\right) & \left(1-\frac{1-\theta}{\theta}\right) & & & & & \\ 1 & 4 & 1 & & & & \\ & \ddots & \ddots & \ddots & & & \\ & & 1 & 4 & 1 & & \\ & & & \ddots & \ddots & \ddots & \\ & & & & 1 & 4 & 1 \\ & & & & & \left(1-\frac{1-\theta}{\theta}\right) & \left(4+\frac{1}{\theta}\right) \end{bmatrix} \begin{bmatrix} T^n_{s,1} \\ T^n_{s,2} \\ \vdots \\ T^n_{s,k} \\ \vdots \\ T^n_{s,kk-1} \\ T^n_{s,kk} \end{bmatrix} = \begin{bmatrix} r_1 \\ r_2 \\ \vdots \\ r_k \\ \vdots \\ r_{kk-1} \\ r_{kk} \end{bmatrix} \qquad \text{(C.3.9)}$$

This is now solved using the method of Gaussian Elimination for a tri-diagonal matrix, as described in appendix B.